AD-A219956

UNITED STATES AIR FORCE

SUMMER FACULTY RESEARCH PROGRAM

1989

PROGRAM TECHNICAL REPORT

UNIVERSAL ENERGY SYSTEMS, INC.

VOLUME I of IV

Program Director, UES
Rodney C. Darrah

Program Administrator, UES
Susan K. Espy

Program Manager, AFOSR
Lt. Col. Claude Cavender

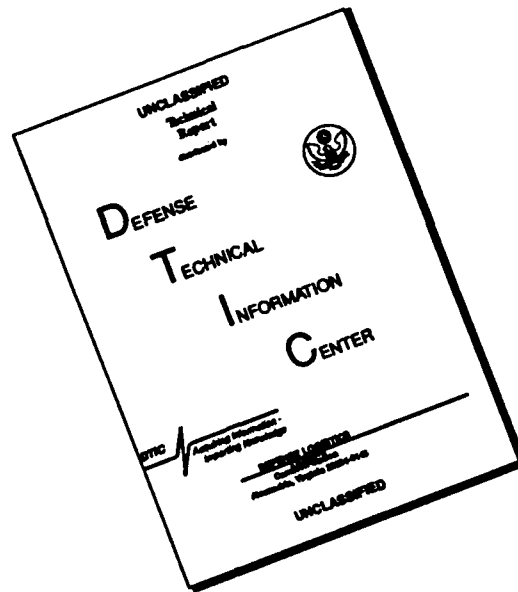Submitted to

Air Force Office of Scientific Research

Bolling Air Force Base

Washington, DC

December 1989

Accesion For		
NTIS CRA&I		☑
DTIC TAB		☐
Unannounced		☐
Justification		
By		
Distribution /		
Availability Codes		
Dist	Avail and / or Special	
A-1		

DISCLAIMER NOTICE

THIS DOCUMENT IS BEST QUALITY AVAILABLE. THE COPY FURNISHED TO DTIC CONTAINED A SIGNIFICANT NUMBER OF PAGES WHICH DO NOT REPRODUCE LEGIBLY.

REPORT DOCUMENTATION PAGE

1a. REPORT SECURITY CLASSIFICATION UNCLASSIFIED		1b. RESTRICTIVE MARKINGS		
2a. SECURITY CLASSIFICATION AUTHORITY		3. DISTRIBUTION/AVAILABILITY OF REPORT APPROVED FOR PUBLIC RELEASE; Distribution Unlimited		
2b. DECLASSIFICATION/DOWNGRADING SCHEDULE				
4. PERFORMING ORGANIZATION REPORT NUMBER(S)		5. MONITORING ORGANIZATION REPORT NUMBER(S) AFOSR-TR 90-0366		
6a. NAME OF PERFORMING ORGANIZATION Universal Energy Systems, INc	6b. OFFICE SYMBOL (If applicable)	7a. NAME OF MONITORING ORGANIZATION AFOSR/XOT		
6c. ADDRESS (City, State and ZIP Code) 4401 Dayton-Xenia Road Dayton, OH 45432		7b. ADDRESS (City, State and ZIP Code) Building 410 Bolling AFB, DC 20332		
8a. NAME OF FUNDING/SPONSORING ORGANIZATION AFOSR	8b. OFFICE SYMBOL (If applicable) XOT	9. PROCUREMENT INSTRUMENT IDENTIFICATION NUMBER F49620-85-C-0013		

8c. ADDRESS (City, State and ZIP Code) Building 410 Bolling AFB, DC 20332	10. SOURCE OF FUNDING NOS.			
	PROGRAM ELEMENT NO. 61102F	PROJECT NO. 3396	TASK NO. D5	WORK UNIT NO.

11. TITLE *(Include Security Classification)*
USAF Summer Faculty Research Program - Management Report - Vol 1 of 4

12. PERSONAL AUTHOR(S)
Rodney C. Darrah, Susan K. Espy

TYPE OF REPORT Annual	13b. TIME COVERED FROM _____ TO _____	14. DATE OF REPORT (Yr., Mo., Day) Dec 89	15. PAGE COUNT

16. SUPPLEMENTARY NOTATION

17.	COSATI CODES		18. SUBJECT TERMS *(Continue on reverse if necessary and identify by block number)*
FIELD	GROUP	SUB. GR.	

19. ABSTRACT *(Continue on reverse if necessary and identify by block number)*

See Attached

20. DISTRIBUTION/AVAILABILITY OF ABSTRACT UNCLASSIFIED/UNLIMITED XX SAME AS RPT. ☐ DTIC USERS ☐	21. ABSTRACT SECURITY CLASSIFICATION UNCLASSIFIED	
22a. NAME OF RESPONSIBLE INDIVIDUAL Lt Col Claude Cavender	22b. TELEPHONE NUMBER (Include Area Code) 202-767-4970	22c. OFFICE SYMBOL XOT

TABLE OF CONTENTS

PREFACE

The United States Air Force Summer Faculty Research Program (USAF-SFRP) is designed to introduce university, college, and technical institute faculty members to Air Force research. This is accomplished by the faculty members being selected on a nationally advertised competitive basis for a ten-week assignment during the summer intersession period to perform research at Air Force laboratories/centers. Each assignment is in a subject area and at an Air Force facility mutually agreed upon by the faculty members and the Air Force. In addition to compensation, travel and cost of living allowances are also paid. The USAF-SFRP is sponsored by the Air Force Office of Scientific Research, Air Force Systems Command, United States Air Force, and is conducted by Universal Energy Systems, Inc.

The specific objectives of the 1989 USAF-SFRP are:

(1) To provide a productive means for U.S. faculty members to participate in research at Air Force Laboratories/Centers;

(2) To stimulate continuing professional association among the faculty and their professional peers in the Air Force;

(3) To further the research objectives of the United States Air Force; and

(4) To enhance the research productivity and capabilities of the faculty especially as these relate to Air Force technical interests.

During the summer of 1989, 168-faculty members participated. These researchers were assigned to 23 USAF laboratories/centers across the country. This four volume document is a compilation of the final reports written by the assigned faculty members about their summer research efforts.

LIST OF 1989 PARTICIPANTS

NAME/ADDRESS	DEGREE, SPECIALTY, LABORATORY ASSIGNED

Thomas Abraham
Instructor
Saint Paul's College
Sci. & Math. Dept.
Lawrenceville, VA 23868
804\848-3111

Degree: MS
Specialty: Mathematics
Assigned: School of Aerospace Medicine

Charles Alajajian
Assistant Prof.
West Virginia University
PO Box 6101
Morgantown, WV 26506
304\293-6371

Degree: PhD
Specialty: Electrical Eng.
Assigned: Rome Air Development Center

Barbara Alvin
Associate Prof.
Eastern Washington Univ.
Math Dept. #32
Cheney, WA 99004
509\359-2203

Degree: PhD
Specialty: Biostatistics
Assigned: Occupational & Environmental
Health Laboratory

Jon Anderson
Assistant Prof.
Texas Tech. University
PO Box 4200
Lubbock, TX 79409
806\742-3538

Degree: PhD
Specialty: Civil Engineering
Assigned: Engineering & Services Center

Peter Armendarez
Professor
Brescia College
7th at Frederica
Owensboro, KY 42301
502\686-4285

Degree: PhD
Specialty: Physical Chemistry
Assigned: Armament Laboratory

Pradip Bakshi
Professor
Boston College
Physics Dept.
Chestnut Hill, MA 02167
617\552-3585

Degree: PhD
Specialty: Theoretical Physics
Assigned: Geophysics Laboratory

NAME/ADDRESS	DEGREE, SPECIALTY, LABORATORY ASSIGNED	
William Bannister Professor Lowell, University of Dept. of Chemistry Lowell, MA 01854 508\452-5000	Degree: Specialty: Assigned:	PhD Organic Chemistry Engineering & Services Center
Beryl Barber Assistant Prof. Oregon Institute of Tech. 3201 Campus Dr. Klamath Falls, OR 97601 503\882-3899	Degree: Specialty: Assigned:	MS Electronic Engineering Electronic Systems Division
Brian Beecken Assistant Prof. Bethel College 3900 Bethel Dr. St. Paul, MN 55112 612\638-6334	Degree: Specialty: Assigned:	PhD Physics Arnold Engineering Development Center
Christopher Bell Assistant Prof. Illinois State Univ. 133 Stevenson Normal, IL 61761 309\438-8338	Degree: Specialty: Assigned:	PhD Psychology Human Resources Laboratory: Manpower & Personnel Div.
Kevin Bennett Assistant Prof. Wright State University 309 Oelman Hall Dayton, OH 45435 513\873-2444	Degree: Specialty: Assigned:	PhD Applied Psychology Human Resources Laboratory: Logistics & Human Factors
Emerson Besch Professor Florida, University of Box J-144 JHMHSC Gainesville, FL 32610 904\392-1841	Degree: Specialty: Assigned:	PhD Animal Physiology Engineering & Services Center

NAME/ADDRESS	DEGREE, SPECIALTY, LABORATORY ASSIGNED

Robert Blystone
Professor
Trinity University
715 Stadium Dr.
San Antonio, TX 78284
512\736-7231

<u>Degree:</u> PhD
<u>Specialty:</u> Zoology
<u>Assigned:</u> School of Aerospace Medicine

Karren Brito
Research Chem.
Dayton, University of
300 College Park
Dayton, OH 45469
513\229-3118

<u>Degree:</u> PhD
<u>Specialty:</u> Chemistry
<u>Assigned:</u> Materials Laboratory

Lee Britt
Instructor
Grambling State University
Dept. of Physics
Grambling, LA 71245
318\274-2575

<u>Degree:</u> MS
<u>Specialty:</u> Physics
<u>Assigned:</u> Arnold Engineering Development Center

Joseph Brown
Professor
Mississippi State Univ.
PO Brawer ME
Mississippi State, MS 39762
601\325-7310

<u>Degree:</u> PhD
<u>Specialty:</u> Mechanical Engineering
<u>Assigned:</u> Armament Laboratory

Roger Bunting
Professor
Illinois State University
Dept. of Chemistry
Normal, IL 61761
309\438-7661

<u>Degree:</u> PhD
<u>Specialty:</u> Inorganic Chemistry
<u>Assigned:</u> Armament Laboratory

Larry Byrd
Assistant Prof.
Arkansas State University
PO Box 1080
State University, AR 72467
501\972-2088

<u>Degree:</u> PhD
<u>Specialty:</u> Mechanical Engineering
<u>Assigned:</u> Flight Dynamics Laboratory

NAME/ADDRESS	DEGREE, SPECIALTY, LABORATORY ASSIGNED	

Anthony Carlisle
Assistant Prof.
Huntingdon College
1500 E. Fairview Ave.
Montgomery, AL 36194
205\265-0511

Degree: MS
Specialty: Computer Science
Assigned: Engineering & Services Center

Carolyn Caudle-Alexander
Assistant Prof.
Tennessee State University
3500 John A. Merritt Blvd.
Nashville, TN 37209
615\320-3115

Degree: PhD
Specialty: Microbiology
Assigned: School of Aerospace Medicine

James Chambers
Associate Prof.
Texas-San Antonio, Univ.
Brain Research Lab. of
  Biochemistry
San Antonio, TX 78285
512\691-5477

Degree: PhD
Specialty: Biochemistry
Assigned: School of Aerospace Medicine

Satish Chandra
Assistant Prof.
Kansas State Univ.
Dept. of Elec. and Comp. Eng.
Manhattan, KS 66506
913\532-5600

Degree: PhD
Specialty: Electrical Engineering
Assigned: Armament Laboratory

Chi Chen
Professor
Southeastern Mass. Univ.
Dept. of Elect. & Comp. Eng.
North Dartmouth, MA 02747
508\999-8475

Degree: PhD
Specialty: Electrical Engineering
Assigned: Geophysics Laboratory

David Choate
Assistant Prof.
Transylvania University
Dept. of Mathematics
Lexington, KY 40508
606\233-8237

Degree: PhD
Specialty: Mathematics
Assigned: Avionics Laboratory

NAME/ADDRESS	DEGREE, SPECIALTY, LABORATORY ASSIGNED

Ajit Choudhury
Associate Prof.
Howard University
Dept. of Electrical Eng.
Washington, DC 20059
202\636-6593

Degree: PhD
Specialty: Electrical Engineering
Assigned: Electronic Systems Division

Derald Chriss
Assistant Prof.
Southern University
PO Box 10572
Baton Rouge, LA 70813
504\771-3990

Degree: MS
Specialty: Chemistry
ssigned: Engineering & Services Center

Donald Chung
Associate Prof.
San Jose State Univ.
Dept. of Mat. Eng.
San Jose, CA 95192
408\924-3873

Degree: PhD
Specialty: Material Science
Assigned: Materials Laboratory

Mingking Chyu
Assistant Prof.
Carnegie Mellon University
Dept. of Mechanical Eng.
Pittsburgh, PA 15213
412\268-3658

Degree: PhD
Specialty: Mechanical Engineering
Assigned: Aero Propulsion Laboratory

David Cicci
Assistant Prof.
Auburn University
162 Wilmore Laboratories
Auburn, AL 36849
205\826-4874

Degree: PhD
Specialty: Aerospace Engineering
Assigned: Armament Laboratory

Brian Circelli
Assistant Prof.
Mississippi, Univ. of
Dept. of Chemical Eng.
University, MS 38677
601\232-5347

Degree: PhD
Specialty: Chemical Engineering
Assigned: Arnold Engineering Development Ctr.

NAME/ADDRESS	DEGREE, SPECIALTY, LABORATORY ASSIGNED

Jerry Clark
Assistant Prof.
Wright State Univ.
Dept. of Physics
Dayton, OH 45435
513\873-2954

Degree: PhD
Specialty: Physics
Assigned: Aero Propulsion Laboratory

Stephen Cobb
Assistant Prof.
Murray State University
Dept. of Physics
Murray, KY 42071
502\762-6186

Degree: PhD
Specialty: Physics
Assigned: Arnold Engineering Development Ctr.

Kathryn Cochran
Assistant Prof.
Northern Colorado, University
Div. of Res., Eval., & Devel.
Greeley, CO 80639
303\351-2807

Degree: PhD
Specialty: Educational Psychology
Assigned: Human Resources Laboratory:
Manpower & Personnel Division

R. H. Cofer
Professor
Florida Institute
150 W. University Blvd.
Melbourne, FL 32901
407\984-5689

Degree: PhD
Specialty: Electrical Eng.
Assigned: Avionics Laboratory

George Coleman
Instructor
Elizabeth City St. University
Dept. of Mathematics
Elizabeth City, NC 27909
919\335-3487

Degree: MS
Specialty: Applied Mathematics
Assigned: Armament Laboratory

Kenneth Cornelius
Assistant Prof.
Wright State Univ.
Dept. of Mechanical Eng.
Dayton, OH 45435
513\873-3682

Degree: PhD
Specialty: Fluid Mechanics
Assigned: Flight Dynamics Laboratory

NAME/ADDRESS	DEGREE, SPECIALTY, LABORATORY ASSIGNED	
Mark Cornwall Assistant Prof. Northern Arizona Univ. POB 15105 Flagstaff, AZ 86011 602\523-1606	Degree: Specialty: Assigned:	PhD Human Performance School of Aerospace Medicine
Larry Crum Professor Wright State University Dept. of Comp. Sci. & Eng. Dayton, OH 45435 513\259-1342	Degree: Specialty: Assigned:	PhD Electrical Engineering Avionics Laboratory
Kenneth Currie Assistant Prof. Kansas State Univ. 228 Durland Hall Manhattan, KS 66506 913\532-5606	Degree: Specialty: Assigned:	PhD Industrial Engineering Materials Laboratory
Phanindramohan Das Professor Texas A&M University Dept. of Meteorology College Station, TX 77843 409\845-0633	Degree: Specialty: Assigned:	PhD Geophysical Science Geophysics Laboratory
Vito DelVecchio Chairman Scranton, University of Biology Dept. Scranton, PA 18510 717\961-6117	Degree: Specialty: Assigned:	PhD Biochemical Engineering School of Aerospace Medicine
Avery Demond Assistant Prof. Massachusetts, University of Dept. of Civil Eng. Amherst, MA 01003 413\545-0685	Degree: Specialty: Assigned:	PhD Civil Engineering Engineering & Services Center

NAME/ADDRESS	DEGREE, SPECIALTY, LABORATORY ASSIGNED

Walter Drost-Hansen
Professor
Miami, University of
Dept. of Chemistry
Coral Gables, FL 33124
305\284-5842

Degree: PhD
Specialty: Physical Chemical
Assigned: Wilford Hall Medical Center

Thomas Dwyer
Professor
Illinois, University of
104 South Mathews Ave.
Urbana, IL 61801
217\244-0720

Degree: PhD
Specialty: Mathematics
Assigned: Weapons Laboratory

Wayne Eckerle
Associate Prof.
Clarkson University
MIE Dept.
Clarkson University, NY 13676
315\268-2203

Degree: PhD
Specialty: Fluid Mechanics
Assigned: Aero Propulsion Laboratory

Dennis Farrell
Associate Prof.
Cincinnati, University of
Mail Location 103
Cincinnati, OH 45210
513\556-6558

Degree: MS
Specialty: Electrical Engineering
Assigned: Flight Dynamics Laboratory

William Filippone
Associate Prof.
Arizona, University of
Group X6, MS B226
Los Alamos, NM 87545
505\665-2307

Degree: PhD
Specialty: Nuclear Engineering
Assigned: Weapons Laboratory

John Francis
Professor
Oklahoma, University of
865 Asp, Room 210
Norman, OK 73019
405\325-5011

Degree: PhD
Specialty: Mechanical Engineering
Assigned: Arnold Engineering Development Ctr.

NAME/ADDRESS	DEGREE, SPECIALTY, LABORATORY ASSIGNED	

Frank Gerner
Assistant Prof.
Cincinnati, University of
756 Baldwin Hall Mail Loc. #72
Cincinnati, OH 45221
513\566-2646

Degree: PhD
Specialty: Mechanical Engineering
Assigned: Aero Propulsion Laboratory

Robert Granger
Professor
US Naval Academy
Dept. of Mechanical Engineering
Annapolis, MD 21402
301\267-3186

Degree: PhD
Specialty: Mechanical Engineering
Assigned: Frank J. Seiler Research Lab.

William Grissom
Assistant Prof.
Morehouse College
830 Westview Dr. SW
Atlanta, GA 30314
404\681-2800

Degree: MS
Specialty: Mechanical Eng.
Assigned: Weapons Laboratory

Ian Grosse
Assistant Prof.
Massachusetts, University of
ELAB 213
Amherst, MA 01003
413\545-1350

Degree: PhD
Specialty: Mechanical Eng.
Assigned: Rome Air Development Center

J⸄hn Hadjilogiou
Professor
Florida Instit.Tech.
150 West University Blvd.
Melbourne, FL 32901
407\768-8000

Degree: PhD
Specialty: Electrical Eng.
Assigned: Rome Air Development Center

Ernest Hallford
Assistant Prof.
Moorhead State Univ.
Dept. of Psychology
Moorhead, MN 56560
218\236-4077

Degree: PhD
Specialty: Psychology
Assigned: Aerospace Medical Research Lab.

NAME/ADDRESS	DEGREE, SPECIALTY, LABORATORY ASSIGNED

Orlando Hankins
Assistant Prof.
North Carolina State Univ.
NCSU Box 7909
Raleigh, NC 27695
919\737-3292

Degree: PhD
Specialty: Nuclear Eng.
Assigned: Arnold Engineering Development Center

Patrick Hannon
Associate Prof.
Northern Arizona University
Box 6012
Flagstaff, AZ 86011
602\523-4331

Degree: PhD
Specialty: Exercise Science
Assigned: School of Aerospace Medicine

Cynthia Hardy
Associate Prof.
Jackson State Univ.
1400 Lynch St.
Jackson, MS 39217
601\968-2371

Degree: PhD
Specialty: Education Psychology
Assigned: School of Aerospace Medicine

Kirk Hatfield
Assistant Prof.
Florida, University of
346 Weil Hall
Gainesville, FL 32611
904\392-0956

Degree: PhD
Specialty: Civil Engineering
Assigned: Engineering & Services Center

Kim Hayes
Assistant Prof.
Michigan, University of
Dept. of Civil Engineering
Ann Arbor, MI 48109
313\763-9661

Degree: PhD
Specialty: Environmental Eng.
Assigned: Engineering & Services Center

Henry Helmken
Professor
Florida Atlantic University
PO Box 3091
Boca Raton, FL 33431
407\367-3452

Degree: PhD
Specialty: Physics
Assigned: Rome Air Development Center

NAME/ADDRESS	DEGREE, SPECIALTY, LABORATORY ASSIGNED		

Peter Henriksen
Associate Prof.
Akron, University
Dept. of Physics
Akron, OH 44325
216\375-6054

Degree: PhD
Specialty: Physics
Assigned: Materials Laboratory

Lloyd Hillman
Assistant Prof.
Cornell University
215 Phillips Hall
Ithaca, NY 14853
607\255-8212

Degree: PhD
Specialty: Optical Engineering
Assigned: Frank J. Seiler Research Lab.

Jeffrey Himm
Assistant Prof.
North Dakota State University
Dept. of Physics
Fargo, ND 58105
701\237-7048

Degree: PhD
Specialty: Physics
Assigned: School of Aerospace Medicine

Stuart Hirshfield
Associate Prof.
Hamilton College
Dept. of Math. & Comp. Sci.
Clinton, NY 13323
315\859-4136

Degree: PhD
Specialty: Computer Science
Assigned: Rome Air Development Center

Harry Hogan
Assistant Prof.
Texas A&M University
Eng./Physics Bldg.
College Station, TX 77843
409\845-1538

Degree: PhD
Specialty: Mechanical Eng.
Assigned: Weapons Laboratory

Gwendolyn Howze
Associate Prof.
Texas Southern Univ.
3100 Cleburne
Houston, TX 77004
713\527-7095

Degree: PhD
Specialty: Molecular Biology
Assigned: School of Aerospace Medicine

NAME/ADDRESS	DEGREE, SPECIALTY, LABORATORY ASSIGNED	

Carl Ingling
Associate Prof.
Ohio State Univ.
1314 Kinnear Rd.
Columbus, OH 43212
614\292-6424

Degree: PhD
Specialty: Psychology
Assigned: Aerospace Medical Research Lab.

Alan Kafka
Associate Prof.
Boston College
Weston Observatory
Weston, MA 02193
617\899-0950

Degree: PhD
Specialty: Geophysics
Assigned: Geophysics Laboratory

Mohammad Karim
Associate Prof.
Dayton, University of
300 College Park
Dayton, OH 45469
513\229-3611

Degree: PhD
Specialty: Electrical Eng.
Assigned: Avionics Laboratory

John Kenney
Assistant Prof.
Eastern New Mexico University
Station #33
Portales, NM 88130
505\562-2152

Degree: PhD
Specialty: Physical Chemistry
Assigned: Astronautics Laboratory

M. Kenney
Instructor
Eastern New Mexico University
Station #33
Portales, NM 88130
505\562-2152

Degree: MS
Specialty: Physical Chemistry
Assigned: Astronautics Laboratory

Charles Kincaid
Lecturer
Florida, University of
477 Little Hall
Gainesville, FL 32611
904\392-1941

Degree: MS
Specialty: Statistics
Assigned: Aerospace Medical Research Lab.

NAME/ADDRESS	DEGREE, SPECIALTY, LABORATORY ASSIGNED

Lynn Kirms
Assistant Prof.
Southern Oregon St. College
Chemistry Dept.
Ashland, OR 97520
503\482-6471

Degree: PhD
Specialty: Organic Chemistry
Assigned: Astronautics Laboratory

Mark Kirms
Assistant Prof.
Southern Oregon St. College
Dept. of Chemistry
Ashland, OR 97520
503\482-6471

Degree: PhD
Specialty: Organic Chemistry
Assigned: Astronautics Laboratory

Michael Klein
Professor
Worcester Poly Inst
100 Institute Rd.
Worcester, MA 01609
508\831-5527

Degree: PhD
Specialty: Physics
Assigned: Rome Air Development Center

Faysal Kolkailah
Professor
California Polytec.
Dept. of Aero. Eng.
San Luis Obispo, CA 93407
805\786-2393

Degree: PhD
Specialty: Mechanical Eng.
Assigned: Astronautics Laboratory

William Kuriger
Professor
Oklahoma, University of
EECS Dept.
Norman, OK 73019
405\325-4721

Degree: PhD
Specialty: Electrical Eng.
Assigned: Rome Air Development Center

Thomas Lalk
Associate Prof.
Texas A&M Univ.
Dept. of Mechanical Eng.
College Station, TX 77843
409\845-4734

Degree: PhD
Specialty: Mechanical Eng.
Assigned: Aero Propulsion Laboratory

NAME/ADDRESS	DEGREE, SPECIALTY, LABORATORY ASSIGNED

John Lanning
Associate Prof.
Colorado-Denver, University
Box 144, 1200 Larimer St.
Denver, CO 80204
303\556-2557

Degree: PhD
Specialty: Analytical Chemistry
Assigned: Frank J. Seiler Research Lab.

Jay Lee
Assistant Prof.
Syracuse University
Link Hall
Syracuse, NY 13244
315\443-4395

Degree: PhD
Specialty: Electrical Engineering
Assigned: Rome Air Development Center

Lang-Wah Lee
Professor
Wisconsin-Plattevil.
Dept. of Mechanical Eng.
Platteville, WI 53818
608\342-1534

Degree: PhD
Specialty: Mechanical Eng.
Assigned: Arnold Engineering Development Center

Tze San Lee
Assistant Prof.
Western Illinois University
Dept. of Mathematics
Macomb, IL 61455
309\298-1485

Degree: PhD
Specialty: Applied Mathematics
Assigned: School of Aerospace Medicine

Baruch Lieber
Assistant Prof.
New York, State Univ. of
Dept. of Mech. & Aero. Eng.
Buffalo, NY 14260
716\636-2391

Degree: PhD
Specialty: Aerospace Engineering
Assigned: Aero Propulsion Laboratory

Charles Lishawa
Assistant Prof.
Utica College
Burstone Rd.
Utica, NY 13502
315\792-3139

Degree: PhD
Specialty: Physical Chemistry
Assigned: Geophysics Laboratory

NAME/ADDRESS	DEGREE, SPECIALTY, LABORATORY ASSIGNED	

Dar-Biau Liu
Professor
California State University
Dept. of Comp. Sci. and Eng.
Long Beach, CA 90840
213\985-1594

Degree: PhD
Specialty: Applied Math
Assigned: Avionics Laboratory

Thomas Lockwood
Associate Prof.
Wright State Univ.
3640 Col. Glenn Hwy.
Dayton, OH 45435
513\873-3060

Degree: PhD
Specialty: Toxicology
Assigned: Aerospace Medical Research Lab.

Harold Longbotham
Assistant Prof.
Texas-San Antonio, University
7000 Loop 1604 NW
San Antonio, TX 78285
512\691-5518

Degree: PhD
Specialty: Electrical Eng.
Assigned: School of Aerospace Medicine

Lewis Lutton
Associate Prof.
Mercyhurst College
Glenwood Hills
Erie, PA 16546
814\825-0372

Degree: PhD
Specialty: Envir. Physiology
Assigned: Aerospace Medical Research Lab.

Ethel Matin
Professor
Long Island Univ.
CW Post Campus/LIU
Brookville, NY 11548
516\299-2063

Degree: PhD
Specialty: Exper. Psychology
Assigned: Aerospace Medical Research Lab.

Stewart Maurer
Associate Prof.
New York Inst. Tech.
1855 Bway
New York, NY 10023
212\399-9698

Degree: PhD
Specialty: Electrical Eng.
Assigned: Occupational and Environmental
Health Laboratory

NAME/ADDRESS	DEGREE, SPECIALTY, LABORATORY ASSIGNED	

Amy Miller
Assistant Prof.
Oklahoma, Univ. of
620 Parrington Oval
Norman, OK 73019
405\325-4836

Degree:	PhD
Specialty:	Chemistry
Assigned:	Geophysics Laboratory

Thomas Miller
Professor
Oklahoma, Univ. of
Dept. of Physics & Astronomy
Norman, OK 73019
405\325-3961

Degree:	PhD
Specialty:	Physics
Assigned:	Geophysics Laboratory

Deborah Mitta
Assistant Prof.
Texas A&M Univ.
Dept. of Industrial Eng.
College Station, TX 77843
409\845-3299

Degree:	PhD
Specialty:	Industrial Eng.
Assigned:	Human Resources Laboratory: Logistics & Human Factors

Augustus Morris
Assistant Prof.
Central State Univ.
Dept. of Manufacturing Eng.
Wilberforce, OH 45384
513\376-6435

Degree:	PhD
Specialty:	Biomedical Engineering
Assigned:	Flight Dynamics Laboratory

Rex Moyer
Professor
Trinity Univ.
715 Stadium Dr.
San Antonio, TX 78284
512\736-7242

Degree:	PhD
Specialty:	Microbiology
Assigned:	School of Aerospace Medicine

Sundaram Natarajan
Associate Prof.
Tennessee Tech Univ.
Box 5004
Cookeville, TN 38505
615\372-3450

Degree:	PhD
Specialty:	Electrical Eng.
Assigned:	Electronic Systems Division

NAME/ADDRESS	DEGREE, SPECIALTY, LABORATORY ASSIGNED		
Henry Nebel Associate Prof. Alfred University Physics Dept. Alfred, NY 14802 607\871-2208	Degree: Specialty: Assigned:	PhD Physics Geophysics Laboratory	
Joseph Newkirk Assistant Prof. Missouri-Rolla, University 282 McNutt Hall Rolla, MO 65401 314\341-4725	Degree: Specialty: Assigned:	PhD Materials Science Materials Laboratory	
Duc Nguyen Assistant Prof. Old Dominion Univ. Civil Eng. Dept. Norfolk, VA 23529 804\683-3761	Degree: Specialty: Assigned:	PhD Civil Engineering Weapons Laboratory	
James Noyes Associate Prof. Wittenberg Univ. Box 720 Springfield, OH 45501 513\327-7858	Degree: Specialty: Assigned:	PhD Computer Science Avionics Laboratory	
Hugh Nutley Professor Seattle Pacific University 3307 3rd Ave. W. Seattle, WA 98119 206\281-2954	Degree: Specialty: Assigned:	PhD Physics Geophysics Laboratory	
Robert O'Connell Associate Prof. Missouri, Univ. of ECE Dept. Columbia, MO 65211 314\882-8373	Degree: Specialty: Assigned:	PhD Electrical Eng. Rome Air Development Center	

NAME/ADDRESS	DEGREE, SPECIALTY, LABORATORY ASSIGNED

Bipin Pai
Associate Prof.
Purdue Univ.
Dept. of Eng.
Hammond, IN 46323
219\989-2694

Degree: PhD
Specialty: Mechanical Eng.
Assigned: Astronautics Laboratory

Harvey Paige
Associate Prof.
Alfred University
PO Box 546
Alfred, NY 14802
607\871-2201

Degree: PhD
Specialty: Inorganic Chem.
Assigned: Materials Laboratory

Arnold Polak
Professor
Cincinnati, University of
M.L. #70
Cincinnati, OH 45221
513\556-3550

Degree: PhD
Specialty: Aerospace Eng.
Assigned: Flight Dynamics Laboratory

Randy Pollack
Assistant Prof.
Wright State Univ.
Computer Sci. Dept.
Dayton, OH 45435
513\873-2491

Degree: PhD
Specialty: Anthropology
Assigned: Aerospace Medical Research Lab.

Raymond Quock
Professor
Univ. of Illinois at Rockford
604 N. 16th St.
Milwaukee, WI 53233
414\224-7251

Degree: PhD
Specialty: Pharmacology
Assigned: School of Aerospace Medicine

Vittal Rao
Professor
Missouri-Rolla, University
Dept. of Electrical Eng.
Rolla, MO 65401
314\341-4508

Degree: PhD
Specialty: Control Systems
Assigned: Astronautics Laboratory

NAME/ADDRESS	DEGREE, SPECIALTY, LABORATORY ASSIGNED	
Craig Rasmussen Assistant Prof. Utah State Univ. CASS UMC 4405 Logan, UT 84322 801\750-2967	<u>Degree:</u> <u>Specialty:</u> <u>Assigned:</u>	PhD Physics Geophysics Laboratory
Michael Resch Assistant Prof. Nebraska-Lincoln, University of 212 Bancroft Hall Lincoln, NE 68588 402\472-2354	<u>Degree:</u> <u>Specialty:</u> <u>Assigned:</u>	PhD Materials Science Materials Laboratory
Richard Robertson Professor California State Univ. 3801 W. Temple Ave. Pomona, CA 91768 714\869-3488	<u>Degree:</u> <u>Specialty:</u> <u>Assigned:</u>	MS Mathematics Astronautics Laboratory
Larry Roe Assistant Prof. Virginia Poly Institute Dept. of Mech. Eng. Blacksburg, VA 24061 703\231-7295	<u>Degree:</u> <u>Specialty:</u> <u>Assigned:</u>	PhD Mechanical Eng. Aero Propulsion Laboratory
Deborah Ross Assistant Prof. Indiana-Purdue, University of 2101 Coliseum Blvd. East Fort Wayne, IN 46805 219\481-6313	<u>Degree:</u> <u>Specialty:</u> <u>Assigned:</u>	PhD Microbiology Engineering & Services Center
Duane Sanders Assistant Prof Texas A&M Univ. Dept. of Civil Eng. College Station, TX 77843 409\845-9566	<u>Degree:</u> <u>Specialty:</u> <u>Assigned:</u>	PhD Civil Engineering Weapons Laboratory

NAME/ADDRESS	DEGREE, SPECIALTY, LABORATORY ASSIGNED

John Sanders
Assistant Prof.
Northwestern State University
Fournet Hall
Natchitoches, LA 71497
318\357-5501

Degree: PhD
Specialty: Chemistry
Assigned: Frank J. Seiler Research Lab.

Paul Scheie
Professor
Texas Lutheran Coll
1000 West Court
Seguin, TX 78155
512\379-4161

Degree: PhD
Specialty: Biophysics
Assigned: School of Aerospace Medicine

William Schulz
Professor
Eastern Kentucky University
Moore 337
Richmond, KY 40475
606\622-1463

Degree: PhD
Specialty: Analytical Chemistry
Assigned: Aero Propulsion Laboratory

Ronald Seaman
Associate Prof.
Louisiana Tech University
PO Box 3185
Ruston, LA 71272
318\257-4562

Degree: PhD
Specialty: Biomedical Eng.
Assigned: School of Aerospace Medicine

Sally Sedelow
Professor
Arkansas-Little Rock, Univ.
33rd and University
Little Rock, AR 72204
501\569-8130

Degree: PhD
Specialty: Computer Science
Assigned: Rome Air Development Center

Nisar Shaikh
Assistant Prof.
Nebraska-Lincoln, University
212 Bancroft Hall
Lincoln, NE 68588
402\472-6692

Degree: PhD
Specialty: Applied Math.
Assigned: Flight Dynamics Laboratory

NAME/ADDRESS	DEGREE, SPECIALTY, LABORATORY ASSIGNED

Clay Sharts
Professor
San Diego State University
Dept. of Chemistry
San Diego, CA 92182
619\594-5576

Degree: PhD
Specialty: Chemistry
Assigned: Frank J. Seiler Research Lab.

Edmund Shearer
Professor
Fort Hays State University
600 Park St.
Hays, KS 67601
913\628-4506

Degree: PhD
Specialty: Chemistry
Assigned: Occupational and Environmental
Health Laboratory

James Sherwood
Assistant Prof.
New Hampshire, University of
Kingsbury Hall
Durham, NH 03824
603\862-2624

Degree: PhD
Specialty: Aero. Mechanics
Assigned: Materials Laboratory

Robert Shock
Associate
Wright State Univ.
Dept. of CEG and CS
Dayton, OH 45435
513\259-8402

Degree: PhD
Specialty: Mathematics
Assigned: Avionics Laboratory

Hugh Siefken
Chairman
Greenville College
Dept. of Physics
Greenville, IL 62246
618\664-4081

Degree: PhD
Specialty: Nuclear Physics
Assigned: Weapons Laboratory

John Silvestro
Assistant Prof.
Clemson Univ.
Riggs Hall
Clemson, SC 29634
803\656-5921

Degree: PhD
Specialty: Electrical Eng.
Assigned: Weapons Laboratory

NAME/ADDRESS	DEGREE, SPECIALTY, LABORATORY ASSIGNED	

Miles Simpson
Associate Prof.
North Carolina Cent. Univ.
Dept. of Sociology
Durham, NC 27707
919\560-6420

<u>Degree:</u> PhD
<u>Specialty:</u> Sociology
<u>Assigned:</u> Human Resources Laboratory:
Manpower and Personnel Division

Boghos Sivazlian
Professor
Florida, Univ. of
303 Weil Hall
Gainesville, FL 32611
904\392-1464

<u>Degree:</u> PhD
<u>Specialty:</u> Operations Research
<u>Assigned:</u> Armament Laboratory

William Smith
Associate Prof.
Pittsburgh, Univ. of
526 C.L.
Pittsburgh, PA 15260
412\624-6559

<u>Degree:</u> PhD
<u>Specialty:</u> Linguistics
<u>Assigned:</u> Human Resources Laboratory:
Training Systems

Michael Stanisic
Assistant Prof.
Notre Dame, University of
Dept. of Aero/Mech Eng.
Notre Dame, IN 46556
219\239-7897

<u>Degree:</u> PhD
<u>Specialty:</u> Robotics
<u>Assigned:</u> Aerospace Medical Research Lab.

Stanley Stephenson
Associate Prof.
Southwest Texas State University
CIS/ADS Dept.
San Marcos, TX 78666
512\245-2291

<u>Degree:</u> PhD
<u>Specialty:</u> Psychology
<u>Assigned:</u> Human Resources Laboratory:
Training Systems

Chun Fu Su
Assistant Prof.
Mississippi State University
Dept. of Physics
Mississippi State, MS 39762
601\325-2931

<u>Degree:</u> PhD
<u>Specialty:</u> Physics
<u>Assigned:</u> Arnold Engineering Development
Center

NAME/ADDRESS	DEGREE, SPECIALTY, LABORATORY ASSIGNED

Khaja Subhani
Associate Prof.
Lawrence Tech. Univ.
21000 West Ten Mile
Southfield, MI 48075
313\356-0200

Degree: PhD
Specialty: Electrical Eng.
Assigned: Rome Air Development Center

Larry Swanson
Assistant Prof.
Denver, Univ. of
2390 S. York St.
Denver, CO 80208
303\871-3816

Degree: PhD
Specialty: Mechanical Eng.
Assigned: Astronautics Laboratory

Michael Sydor
Professor
Minnesota-Duluth, University of
Dept. of Physics
Duluth, MN 55812
218\726-7205

Degree: PhD
Specialty: Physics
Assigned: Materials Laboratory

Joseph Szucs
Associate Prof.
Texas A&M Univ.
GACD PO Box 1675
Galveston, TX 77553
409\740-4463

Degree: PhD
Specialty: Functional Analytics
Assigned: Aerospace Medical Research Lab.

Chi-Ming Tang
Associate Prof.
New York, State Univ. of
Dept. of Math
Geneseo, NY 14454
716\245-5386

Degree: PhD
Specialty: Mathematics
Assigned: Aerospace Medical Research Lab.

Richard Tankin
Professor
Northwestern Univ.
Mechanical Eng. Dept.
Evanston, IL 60201
312\491-3532

Degree: PhD
Specialty: Mechanical Eng.
Assigned: Aero Propulsion Laboratory

NAME/ADDRESS	DEGREE, SPECIALTY, LABORATORY ASSIGNED	

Teresa Taylor
Assistant Prof.
Missouri-Columbia, University of
600 West Mechanic
Independence, MO 64050
816\276-1285

Degree: PhD
Specialty: Civil Eng.
Assigned: Engineering & Services Center

Ebo Tei
Professor
Arkansas-Pine Bluff, Univ. of
Social & Behavioral Sci.
Pine Bluff, AR 71601
501\541-6787

Degree: PhD
Specialty: Psychology
Assigned: Aerospace Medical Research Lab.

Roger Thompson
Assistant Prof.
Pennsylvania St. University
233 Hammond Bldg.
University Park, PA 16802
814\863-0968

Degree: PhD
Specialty: Eng. Mechanics
Assigned: Astronautics Laboratory

Richard Tipping
Professor
Alabama, University
Dept. of Physics
Tuscaloosa, AL 35487
205\348-3799

Degree: PhD
Specialty: Physics
Assigned: Arnold Engineering Development Ctr.

Phillip Tomporowski
Assistant Prof.
Alabama, University of
Box 870348
Tuscaloosa, AL 35487
205\348-1936

Degree: PhD
Specialty: Psychology
Assigned: Human Resources Laboratory:
Operations Training Division

Ram Tripathi
Professor
Texas-San Antonio, Univ. of
Dept. of Mathematics
San Antonio, TX 78285
512\691-5549

Degree: PhD
Specialty: Statistics
Assigned: School of Aerospace Medicine

NAME/ADDRESS	DEGREE, SPECIALTY, LABORATORY ASSIGNED

Steven Trogdon
Associate Prof.
Minnesota-Duluth, University of
108 Heller Hall
Duluth, MN 55812
218\726-6173

<u>Degree:</u> PhD
<u>Specialty:</u> Mechanics
<u>Assigned:</u> Armament Laboratory

Timothy Troutt
Associate Prof.
Washington State University of
Mech. & Mat. Eng. Dept.
Pullman, WA 99164
509\335-4375

<u>Degree:</u> PhD
<u>Specialty:</u> Mechanical Eng.
<u>Assigned:</u> Frank J. Seiler Research Lab.

Donald Ucci
Associate Prof.
Illinois Inst.Tech.
3300 S. Federal St.
Chicago, IL 60616
312\567-3405

<u>Degree:</u> PhD
<u>Specialty:</u> Electrical Eng.
<u>Assigned:</u> Rome Air Development Center

George Veyera
Assistant Prof.
Rhode Island, University of
Dept. of Civil Eng.
Kingston, RI 02881
401\792-2692

<u>Degree:</u> PhD
<u>Specialty:</u> Civil Eng.
<u>Assigned:</u> Engineering & Services Center

Hung Vu
Assistant Prof.
California State University
Mech. Eng. Dept.
Long Beach, CA 90840
213\985-1524

<u>Degree:</u> PhD
<u>Specialty:</u> Applied Mechanics
<u>Assigned:</u> Frank J. Seiler Research Lab.

Bonnie Walker
Assistant Prof.
Central State Univ.
Psychology Dept.
Wilberforce, OH 45384
513\376-6516

<u>Degree:</u> PhD
<u>Specialty:</u> Experimental Psychology
<u>Assigned:</u> Aerospace Medical Research Lab.

NAME/ADDRESS	DEGREE, SPECIALTY, LABORATORY ASSIGNED

William Wallace
Professor
Rensselaer Poly. Inst
CII Room 5117
Troy, NY 12180
518\276-6452

Degree: PhD
Specialty: Management Science
Assigned: Rome Air Development Center

Ji Wang
Professor
San Jose State Univ.
S. 7 St.
San Jose, CA 95192
408\924-4299

Degree: PhD
Specialty: Mechanical Eng.
Assigned: Astronautics Laboratory

Phillip Wapner
Associate Prof.
Southern Illinois University
Dept. of Mech. Eng.
Carbondale, IL 62901
618\453-7021

Degree: PhD
Specialty: Chemical Eng.
Assigned: Astronautics Laboratory

Robert Wheasler
Professor
Wyoming, Univ. of
Box 3295 University Station
Laramie, WY 82071
307\766-5126

Degree: PhD
Specialty: Engineering
Assigned: Aero Propulsion Laboratory

D. Wilkes
Assistant Prof.
Vanderbilt Univ.
Box 1649 Station B
Nashville, TN 37235
615\343-6016

Degree: PhD
Specialty: Electrical Eng.
Assigned: Arnold Engineering Development Center

Robert Willis
Associate Prof.
Mercer University
1400 Coleman Ave.
Macon, GA 31207
912\744-2704

Degree: PhD
Specialty: Physics
Assigned: Geophysics Laboratory

NAME/ADDRESS	DEGREE, SPECIALTY, LABORATORY ASSIGNED	

John Wills
Professor
Indiana Univ.
Physics Dept.
Bloomington, IN 47405
812\855-1479

Degree:	PhD
Specialty:	Physics
Assigned:	Geophysics Laboratory

David Woehr
Assistant Prof.
Texas A&M Univ.
Dept. of Psychology
College Station, TX 77843
409\845-2097

Degree:	PhD
Specialty:	Industrial Psychology
Assigned:	Human Resources Laboratory: Manpower and Personnel Division

Michael Wolfe
Assistant Prof.
West Virginia Univ.
PO Box 6025
Morgantown, WV 26506
304\293-4495

Degree:	PhD
Specialty:	Management Science
Assigned:	Human Resources Laboratory: Logistics & Human Factors

William Wolfe
Associate Prof.
Ohio State Univ.
470 Hitchcock Hall
Columbus, OH 43210
614\292-0790

Degree:	PhD
Specialty:	Engineering
Assigned:	Flight Dynamics Laboratory

James Wolper
Assistant Prof.
Hamilton College
Dept. of Math. & Comp. Sci.
Clinton, NY 13323
315\859-4417

Degree:	PhD
Specialty:	Mathematics
Assigned:	Rome Air Development Center

Asad Yousuf
Assistant Prof.
Savannah State College
PO Box 20089
Savannah, GA 31404
912\356-2154

Degree:	MS
Specialty:	Electrical Eng.
Assigned:	Armament Laboratory

NAME/ADDRESS	DEGREE, SPECIALTY, LABORATORY ASSIGNED

Juin Yu
Professor
West Virginia Tech.
Mechanical Eng. Dept.
Montgomery, WV 25136
304\442-3248

Degree: PhD
Specialty: Mechanical Engineering
Assigned: Flight Dynamics Laboratory

Gregory Zagursky
Assistant Prof.
Morris College
Div. General Studies
Sumter, SC 29150
803\775-9371

Degree: MS
Specialty: Biology
Assigned: Occupational and Environmental
Health Laboratory

Lawrence Zavodney
Assistant Prof.
Ohio State Univ.
209 Boyd Lab.
Columbus, OH 43210
614\292-2209

Degree: PhD
Specialty: Mechanical Eng.
Assigned: Flight Dynamics Laboratory

Yehoshua Zeevi
Professor
Harvard Univ.
Applied Sciences
Cambridge, MA 02138
617\495-2850

Degree: PhD
Specialty: Electrical Eng.
Assigned: Human Resources Laboratory:
Operations Training Division

Robert Zerwekh
Assistant Prof.
Northern Illinois University
Dept. of Comp. Sci.
DeKalb, IL 60115
815\753-6949

Degree: PhD
Specialty: Philosophy
Assigned: Human Resources Laboratory:
Training Systems

Henry Zmuda
Assistant Prof.
Stevens Inst Tech
Dept. of Electrical Eng.
Hoboken, NJ 07030
201\420-5507

Degree: PhD
Specialty: Electrical Eng.
Assigned: Rome Air Development Center

PARTICIPANT LABORATORY ASSIGNMENT

C. PARTICIPANT LABORATORY ASSIGNMENT (Page 1)

1989 USAF/UES SUMMER FACULTY RESEARCH PROGRAM

AERO PROPULSION LABORATORY (WRDC/APL)
(Wright-Patterson Air Force Base)

1.	Mingking Chyu	6.	Baruch Lieber
2.	Jerry Clark	7.	Larry Roe
3.	Wayne Eckerle	8.	William Schulz
4.	Frank Gerner	9.	Richard Tankin
5.	Thomas Lalk	10.	Robert Wheasler

ARMAMENT LABORATORY (ATL)
(Eglin Air Force Base)

1.	Peter Armandarez	6.	George Coleman
2.	Joseph Brown	7.	Boghos Sivazlian
3.	Roger Bunting	8.	Steven Trogdon
4.	Satish Chandra	9.	Asad Yousuf
5.	David Cicci		

HARRY G. ARMSTRONG AEROSPACE MEDICAL RESEARCH LABORATORY (AAMRL)
(Wright-Patterson AFB)

1.	Ernest Hallford	7.	Randy Pollack
2.	Carl Ingling	8.	Michael Stanisic
3.	Charles Kincaid	9.	Joseph Szucs
4.	Thomas Lockwood	10.	Chi-Ming Tang
5.	Lewis Lutton	11.	Ebo Tei
6.	Ethel Matin	12.	Bonnie Walker

ARNOLD ENGINEERING DEVELOPMENT CENTER (AEDC)
(Arnold Air Force Base)

1.	Brian Beecken	6.	Orlando Hankins
2.	Lee Britt	7.	Lang-Wah Lee
3.	Brian Circelli	8.	Chun Fu Su
4.	Stephen Cobb	9.	Richard Tipping
5.	John Francis	10.	D. Mitchell Wilkes

ASTRONAUTICS LABORATORY (AL)
Edwards Air Force Base)

1.	John Kenney	7.	Vittal Rao
2.	M. Inga Kenney	8.	Richard Robertson
3.	Lynn Kirms	9.	Larry Swanson
4.	Mark Kirms	10.	Roger Thompson
5.	Faysal Kolkailah	11.	Ji Wang
6.	Bipin Pai	12.	Phillip Wapner

AVIONICS LABORATORY (WRDC/AL)
(Wright-Patterson Air Force Base)

1.	David Choate	5.	Dar-Biau Liu
2.	R. H. Cofer	6.	James Noyes
3.	Larry Crum	7.	Robert Shock
4.	Mohammad Karim		

ELECTRONIC SYSTEMS DIVISION (ESD)
(Hanscom Air Force Base)
1. Beryl Barber
2. Ajit Choudhury
3. S. Natarajan

ENGINEERING AND SERVICES CENTER (ESC)
(Tyndall Air Force Base)
1. Jon Anderson
2. William Bannister
3. Emerson Besch
4. Anthony Carlisle
5. Derald Chriss
6. Avery Demond
7. Kirk Hatfield
8. Kim Hayes
9. Deborah Ross
10. Teresa Taylor
11. George Veyera

FLIGHT DYNAMICS LABORATORY (WRDC/FDL)
(Wright-Patterson Air Force Base)
1. Larry Byrd
2. Kenneth Cornelius
3. Dennis Farrell
4. Augustus Morris
5. Arnold Polak
6. Nisar Shaikh
7. William Wolfe
8. Juin Yu
9. Lawrence Zavodney

FRANK J. SEILER RESEARCH LABORATORY (FJSRL)
(USAF Academy)
1. R. Granger
2. L. Hillman
3. John Lanning
4. John Sanders
5. Clay Sharts
6. Timothy Troutt
7. Hung Vu

GEOPHYSICS LABORATORY (AFGL)
(Hanscom Air Force Base)
1. Pradhip Bakshi
2. Chi Chen
3. P. Das
4. Alan Kafka
5. Charles Lishawa
6. Amy Miller
7. Thomas Miller
8. Henry Nebel
9. Hugh Nutley
10. Craig Rasmussen
11. Robert Willis
12. John Wills

HUMAN RESOURCES LABORATORY (HRL)
(Brooks, Williams, and Wright-Patterson Air Force Bases)
1. Christopher Bell
2. Kevin Bennett
3. Kathryn Cochran
4. Deborah Mitta
5. Miles Simpson
6. William Smith
7. Stanley Stephensen
8. P. Tomporowski
9. David Woehr
10. Michael Wolfe
11. Yehoshua Zeevi
12. Robert Zerwekh

C. PARTICIPANT LABORATORY ASSIGNMENT (Page 3)

MATERIALS LABORATORY (ML)
(Wright-Patterson Air Force Base)
1. Karren Brito
2. Donald Chung
3. Kenneth Currie
4. Peter Henrisken
5. Joseph Newkirk
6. Harvey Paige
7. Michael Resch
8. James Sherwood
9. Michael Sydor

OCCUPATIONAL AND ENVIRONMENTAL HEALTH LABORATORY (OEHL)
(Brooks Air Force Base)
1. Barbara Alvin
2. Stewart Maurer
3. Edmund Shearer
4. Gregory Zagursky

ROME AIR DEVELOPMENT CENTER (RADC)
(Griffiss Air Force Base)
1. Charles Alajajian
2. Ian Grosse
3. John Hadjilogiou
4. Henry Helmken
5. Stuart Hirshfield
6. Michael Klein
7. William Kuriger
8. Jay Lee
9. Robert O'Connell
10. Sally Sedelow
11. Khaja Subhani
12. Donald Ucci
13. William Wallace
14. James Wolper
15. Henry Zmuda

SCHOOL OF AEROSPACE MEDICINE (SAM)
(Brooks Air Force Base)
1. Thomas Abraham
2. Robert Blystone
3. Carolyn Caudle-Alexander
4. James Chambers
5. Mark Cornwall
6. Vito DelVecchio
7. Patrick Hannon
8. Cynthia Hardy
9. Jeffrey Himm
10. Gwendolyn Howze
11. Tze San Lee
12. Harold Longbotham
13. Rex Moyer
14. Raymond Quock
15. Paul Scheie
16. Ronald Seaman
17. Ram Tripathi

WEAPONS LABORATORY (WL)
(Kirtland Air Force Base)
1. Thomas Dwyer
2. William Filippone
3. William Grissom
4. Harry Hogan
5. Duc Nguyen
6. Duane Sanders
7. Hugh Siekfen
8. John Silvestro

WILFORD HALL MEDICAL CENTER (WHMC)
(Lackland Air Force Base)
1. Walter Drost-Hansen

RESEARCH REPORTS

RESEARCH REPORTS

1989 SUMMER FACULTY RESEARCH PROGRAM

Technical Report Number	Title	Professor
Volume I		
Armament Laboratory		
1	Reactive Compositions Using Light Metals and Metal Alloys	Dr. Peter Armendarez
2	Maneuvering Hard Target Penetrators	Dr. Joseph Brown
3	A Study of Ionic Polymer Membranes for Application as Capacitor Electrolytes and Preliminary Investigations on Photo-Activated Stripline Switches	Dr. Roger Bunting
4	Multisensor Seeker for Medium Range Air-to-Air Missiles	Dr. Satish Chandra
5	Extended Kalman Filter Tuning and Alternative Techniques	Dr. David Cicci
6	Statistical Analysis of Blast Loading in Concrete	Dr. George Coleman
7	A Methodology for Evaluating the Effectiveness of Smart Submunition Systems	Dr. Boghos Sivazlian
8	Shock Wave Initiated Detonation of an Explosive	Dr. Steven Trogdon
9	Distributed Filter Architecture Implementation with VLSI and Expert Systems	Dr. Asad Yousuf
Arnold Engineering Development Center		
10	Response of Infrared Detectors to Pulsed Radiation	Dr. Brian Beecken
11	An Analysis of Focal Plane Irradiance Effects on IR Detectors	Dr. Lee Britt
12	Code Development for Design of a High Temperature Hypersonic Facility Mixer	Dr. Brian Circelli

Arnold Engineering Development Center (continued)

Astronautics Laboratory

Astronautics Laboratory (continued)

27	A Neural Network Approach to the Adaptive Control of Large Space Structures	Dr. Richard Robertson
28	Cryogenic Heat Pipes	Dr. Larry Swanson
29	Design and Development of a Flexible Multi-Body Dynamics Experiment	Dr. Roger Thompson
30	Synthesis of Active Space Structure Vibration Control Systems for an Astrex Test Article	Dr. Ji Wang
31	Dynamic Mechanical Response of Carbon/ Carbon Composites by Vibrating Reed Measurements	Dr. Phillip Wapner

Electronics Systems Division

32	Carrier Free Radar	Dr. Beryl Barber
33	Detection Performance for Over Resolved Targets with Varying Energy Level in Cells	Dr. Ajit Choudhury
34	Analysis of Testability Concepts and its Application to RSIP	Dr. S. Natarajan

Engineering and Services Center

35	Proposed Innovative Semi-Hard Aircraft Shelter	Dr. Jon Anderson
36	JP-8 Ignitability	Dr. William Bannister
37	Effect of Jet Aircraft Noise on Domestic Goats	Dr. Emerson Besch
38	An Algorithmic System for Subjective Comparisons	Dr. Anthony Carlisle
39	The Study of Alkali-Enhanced Cements and Concretes	Dr. Derald Chriss
40	Prediction of the Capillary Pressure-Saturation Relationships for Aquifers Contaminated with Jet Fuels	Dr. Avery Demond
41	Contaminant Flux Reduction Through In Situ Solubility Modification	Dr. Kirk Hatfield

Geophysics Laboratory (continued)

56	Estimating Characteristics of Chemical Explosions in New England and Eastern Kazakhstan Using Local and Regional Seismic Data	Dr. Alan Kafka
57	A Study of the Water Vapor Cation-Neutral Reactions	Dr. Randal Lishawa
58	Acidities of Iron Hydride and Various Transition-Metal Compounds; Reactions of Iron and Iron Carbonyl Anions	Dr. Amy Miller
59	Acidities of Iron Hydride and Various Transition-Metal Compounds; Reactions of Iron and Iron Carbonyl Anions (Same Report as Dr. Amy Miller)	Dr. Thomas Miller
60	CO_2(4.3μm) Vibrational Temperatures and Limb Radiances Under Sunlit Conditions in the 50-120 KM Altitude Range	Dr. Henry Nebel
61	Estimating Solar Flare Proton Fluences From 1850 with Tritium Data	Dr. Hugh Nutley
62	Electric Fields in the Middle-and Low-Latitude Ionosphere and Plasmasphere	Dr. Craig Rasmussen
63	Review and Assessment of Carbon Dioxide Pressure Broadening Data	Dr. Robert Willis
64	Non-Uniform Clouds	Dr. John Wills

Rome Air Development Center

65	Design Considerations in the Implementation of ACT Programmable Transversal Filters	Dr. Charles Alajajian
66	Automating Finite Element Reliability Assessment of Microelectronic Components	Dr. Ian Grosse
67	Design for Testability: From Components to Systems	Dr. John Hadjilogiou
68	Development of a High Resolution Research Facility	Dr. Henry Helmken
69	Iterative V&V: A Model for Verification and Validation in the Rapid Prototyping Life Cycle	Dr. Stuart Hirshfield

Rome Air Development Center (continued)

70 Capable Neural Networks for   Dr. Oleg Jakubowicz
    Applications in Data Analysis
    (1988 Participant)

71 A Study of Interacting Tunneling Dr. Michael Klein
    Units with Possible Application to
    High Temperature Superconductors

72 Design of a Practical Binary Phase- Dr. William Kuriger
    Only Optical Correlator

73 A Computer for Temporal Frequency Dr. Jay Lee
    Spectrum of Vegetation Clutter Return

74 Material Effects in Photoconductive Dr. Robert O'Connell
    Frozen Wave Generators

75 Parallel Processing for Associative Dr. Sally Sedelow
    Semantic Space Analysis

76 Characterization of an Optical Switch Dr. Khaja Subhani

77 Study of a Communication Receiver Dr. Donald Ucci
    for Spread Spectrum Signals

78 Tactical Command and Control: A Group Dr. William Wallace
    Problem Solving and Decision Making
    Process

79 Neural Networks for Invariant Pattern Dr. James Wolper
    Recognition: A Survey of the State of
    the Art

80 Optical Beamforming for Phased Array Dr. Henry Zmuda
    Antennas

Weapons Laboratory

81 An Experimental Protocol for Line- Dr. Thomas Dwyer
    of-Sight Slewing, Optical Alignment
    and AFT Body Station Keeping Control
    Emulation

82 Linking the Twodant S_N Code and the Dr. William Filippone
    MCNP Monte Carlo Code

83 Simulation of a Spray Reactor for Dr. William Grissom
    Generating Excited Oxygen

84 Modeling the Response of Pressurized Dr. Harry Hogan
    Composite Cylinders to Laser Damage

Weapons Laboratory (continued)

Volume III
(Wright Research Development Center)
Aero Propulsion Laboratory

Avionics Laboratory

99	A Theoretical Resolution of Multiple Frequencies	Dr. David Choate
100	Ladar Target Detection and Recognition	Dr. R. H. Cofer
101	Toolbox for Image Processing using Distributed Computing	Dr. Larry Crum
102	Analytical Model of a Unique E-O Beam Scanner	Dr. Mohammad Karim
103	Dynamic Task Scheduling for the "ADA Distributed System Evaluation Testbed (ADSET)"	Dr. Dar-Biau Liu
104	Ada Compiler Efficiency Evaluation	Dr. James Noyes
105	Towards a Course-Grained Test Suite for VHDL Validation	Dr. Robert Shock

Flight Dynamics Laboratory

106	Parametric Study of Combined Boiling and Partial Dryout in Liquid Metal Heat Pipe Wicks	Dr. Larry Byrd
107	3-D Analysis of Laser Measurements of Vortex Bursting on Chined Forebody Fighter Configuration	Dr. Kenneth Cornelius
108	Robust Design Using Internal Model Control	Dr. Dennis Farrell
109	Neural Networks and their Role in Visual Object Recognition	Dr. Augustus Morris
110	A Study of Surface Roughness Effects in Hypersonic Flow	Dr. Arnold Polak
111	Life Prediction of Aircraft Transparencies by Accelerated Crazing Tests	Dr. Nisar Shaikh
112	Strain Distribution in Composite Coupons in Tension	Dr. William Wolfe
113	Characteristics of an Osmotically Driven Thermal Transfer Cycle	Dr. Juin Yu
114	The Influence of Viscoelastically Damped Members on the Dynamic Response of Flexible Elastic Structures	Dr. Lawrence Zavodney

Materials Laboratory

Volume IV
Human Systems Division Laboratories
Harry G. Armstrong Aerospace Medical Research Laboratory

Harry G. Armstrong Medical Research Laboratory (continued)

Human Resources Laboratory

Human Resources Laboratory

Occupational and Environmental Health Laboratory

School of Aerospace Medicine

School of Aerospace Medicine (continued)

156	The Effects of Three Reputed Carboxyesterase Inhibitors Upon Rat Serum Esterase Activity Using Paranitrophenyl and Naphthyl Esters as Substrates	Dr. James Chambers
157	Anti-G Suit Inflation Influence on Lower Extremity Muscle Performance during Sustained +G$_z$ Acceleration	Dr. Mark Cornwall
158	PCR Analysis and in situ Detection of Ureaplasma urealyticum and Mycoplasma hominis	Dr. Vito DelVecchio
159	The Influence of Broad Spectrum Illumination on Circadian Neuroendocrine Responses and Performance	Dr. Patrick Hannon
160	The relationship between locus of control, performance on cognitive tasks, and affective states after the consumption of antihistamines in hi- and low-workload conditions among aircrew personnel	Dr. Cynthia Ford Hardy
161	Aspects of the Diffusion of Inert Gases in Biological Systems	Dr. Jeffrey Himm
162	Studies of Interactions Between Microwaves, Melanin and Melanocytes	Dr. Gwendolyn Howze
163	Two-Phase Regression Model with Application	Dr. Tze-San Lee
164	System and Signal Analysis of VEP Data and Joystick Error Analysis	Dr. Harold Longbotham
165	Higher Plant Hormones Effect Upon Chlamydomonas Phototaxis	Dr. Rex Moyer
166	Influence of Radio Frequency Radiation on Psychotropic Drug Effects	Dr. Raymond Quock
167	Porous Glass as Bed Material in a Pressure Swing Adsorption Unit Used for Air Purification	Dr. Paul Scheie
168	Models for RFR Biological Effects	Dr. Ronald Seaman

School of Aerospace Medicine (continued)

Wilford Hall Medical Center

1989 USAF-UES SUMMER FACULTY RESEARCH PROGRAM

Sponsored by the

AIR FORCE OFFICE OF SCIENTIFIC RESEARCH

Conducted by the

Universal Energy Systems, Inc.

FINAL REPORT

REACTIVE COMPOSITIONS USING LIGHT METALS AND METAL ALLOYS

Prepared by: Peter X. Armendarez

Academic Rank: Professor of Chemistry

College: Chemistry, Brescia College,Owensboro, KY, 42301

Research Location: Armament Laboratory,
                   AFATL/MNW
                   Eglin AFB, FL, 32542-5000

USAF Researcher: Mr. A.L. Weimorts

Date: August 11, 1989

Contract No: F49620-88-C-0053

Reactive Compositions Using Light Metals and Metal Alloys

Peter Armandarez

ABSTRACT

The explosive nature of ammonium perchlorate is studied. Its
use in high energy compositions involving light metals and
their alloys is investigated. Thermodynamic calculations
using the Tiger Code were carried out to predict the perfor-
mance of several reactive compositions.

The use of metal alloying reactions to boost the output of
reactive compositions is examined. A reactive warhead design
is proposed using metal alloying systems.

ACKNOWLEDGEMENTS

I. INTRODUCTION

Reactive compositions involving use of light metals, and metal alloys for warhead and reactive fragment uses have been the subject of interest and investigation at the Armament Laboratory(AFATL/MNW) at Eglin Air Force Base.

My research experience includes service with the USAF as a nuclear research officer(1954-1957) at the Research Directorate(Warheads Branch) at Kirtland AFB, and one year (1983-84) as a research chemist with the Naval Weapons Support Center at Crane, Indiana. The latter research included work which involved the formulation and testing of reactive compositions for use in flares.

.II. OBJECTIVES OF RESEARCH EFFORT

The chief objective of this study was to investigate the use of reactive compositions using light metals and their alloys.

This study is concerned with the use of ammonium perchlorate(AP) as oxidant and reactant in combination with highly reducible species, e.g., the light metals of Groups I, II, III of the periodic table. Several calculations on the explosion thermodynamics of AP/metal mixtures were made to give information on explosive characteristics in order to assess various compositions using ammonium perchlorate.

This study also deals with the use of alloying reactions to boost and achieve greater energy output of reactive

compositions. A reactive warhead design is proposed using metal alloys and hydrogen-containing metal systems.

III. ANALYSIS OF REACTIVE SYSTEMS

1. <u>Ammonium Perchlorate:Decomposition Chemistry</u>.

Ammonium perchlorate(AP) is a versatile reagent having application to various high energy uses. This includes use in reactive compositions in flares, incendiaries, igniters, explosives and rocket propellants[1]. Thermal initiation of detonation occurs at 435° C., and its detonation velocity is 3400 meters/sec.[2].

There have been several studies on the thermal decomposition of ammonium perchlorate[3,4,5]. This salt is stable to 130° C., begins to sublime beyond this point with decomposition beginning at 260° C. AP utilizes 75% of its available oxygen(54.5 %) in self-oxidation to produce mostly water and nitrogen oxides. It also produces chlorine which increases its oxidizing potential.

The decomposition of AP at 350° C. is described by the chemical equation:

$$2 \ NH_4ClO_4(s) \longrightarrow 4 \ H_2O(g) + 2 \ O_2(g) + Cl_2(g) + 2 \ NO(g) \quad (1)$$
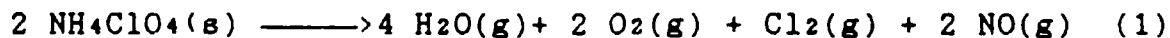
The rate-determining step involves a proton-transfer occuring on the surface of the crystal to form initial transitory products of ammonia and perchloric acid:

$$NH_4ClO_4 \longrightarrow NH_3(g) + HClO_4(liq.,AP \ surface) \quad (2)$$
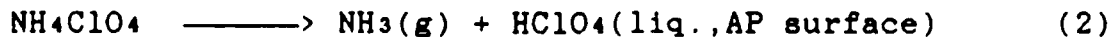
The latter is a vigorous oxidant especially when hot. It leads to violent reaction with organic materials, and may be expected to attack light metals readilly.

2. Explosion Thermodynamics.

The Tiger Code[6], which has been applied extensively to estimate explosion thermodynamics, was used to calculate the explosion point and the Chapman-Jouguet (C-J) point for AP.

Table I presents information on these calculations for initial densities near the optimum(rho =1.2-1.3 gm./cc.) as found from experiment[7] on this explosive. The Becker-

Table I.   Explosion Point and C-J Point Description of
           Ammonium Perchlorate Detonation.

density(gm/cc.) rho	0.80	1.0	1.2	1.4
1. Explosion point.				
temperature(°C.)	1237	1121	1001	880
pressure(atm)	14,051	20,889	29,251	39,229
2. C-J point.				
temperature(°C.)	1457	1279	1145	1008
pressure(atm)	30,022	44,869	63,075	84,865
detonation velocity(met./sec)	3605	4029	4446	4860
particle velocity (met/sec)	1055	1128	1198	1264
moles of gases/ Kg. of explosive	34.05	34.04	34.04	34.04
principle products(all runs): H_2O, O_2, Cl_2, N_2				

Kistiakowsky-Wilson(BKW) equation of state was used in these calculations. It is seen that the temperatures at the explosion and the C-J point are relatively low(about 1200° C.). The detonation velocities are about those determined experimentally[8] . In comparison, a high order detonation for an explosive such as TNT, for example, has a detonation velocity of 6900 meters/sec and a calculated explosion temperature of the order of 2000° C.[9]. According to Mader[10], to obtain the best explosive performance at the C-J point requires high particle and energy densities. One way to increase the energy density of ammonium perchlorate is to add a highly reducible light metal such as magnesium or aluminum.

3. Ignition of Light Metals.

Table II gives the ignition temperatures and other thermodynamic properties for several light metals. The ignition temperature is a sensitive function of the particle size and the availability of the oxidizer at the reaction site. The lower ignition temperatures for a given metal occurs for very finely divided powders(10 microns or less) and where there is a large supply of oxygen or other oxidizer. Magnesium and lithium are very reactive metals and may be ignited with a match. Beryllium and boron are difficult to ignite, requiring relatively large temperatures for ignition. Boron, for example, although a promising candidate as a metal additive due to its high energy of oxidation(16.2 kcal/gm.), ignites at about 700° C. It burns well but only superficially.

Table II. Ignition Temperatures and Other Properties of
Light Metals[11,12].

	Al	Mg	Li	Be	B
Metal					
ign. temp.(°C.)	645-2340	475-618	200	2400	1900
melt.pt.(°C.)	660	650	179	1283	2300
boil. pt.(°C.)	2050	1105	1370	2970	2550
density(g/cc.)	2.71	1.74	0.534	1.85	2.33
Metal Oxide	Al_2O_3	MgO	Li_2O	BeO	B_2O_3
melt.pt.(°C.)	2050	2823	1570	2547	450
boil. pt.(°C.)	3547	3193	2563	3787	2043
density(gm./cc.)	4.0	3.2	2.02	3.0	1.8
heat of form. (kcal./gm.)	7.4	5.9	10.2	16.2	14.0

Similarly, aluminum powders may be ignited over a large
temperature range(650-2300° C.).The lower ignition temperatures occur for very fine powders in an oxygen-rich ambient.

4. Effect of Nature of Metal Oxide on Ignition.

Attack by oxygen of a fresh metal surface is relatively
rapid, but as the oxide layers accumulate the oxidation rate
decreases. The oxide layer becomes impervious to further
oxidation as in aluminum, or it may form a non-protective
layer as in the case of the alkali metals and magnesium. The
latter metals ignite and sustain oxidation readilly. Berylium, boron and aluminum, on the other hand, form protective

oxide layers. Reaction at the metal surface is therefore impeded until sufficiently high temperatures are obtained. Then diffusion of metal and oxygen can occur across the oxide layers. The oxidation of aluminum increases slowly as the temperature rises near to the melting point of aluminum. At the higher temperatures, aluminum vapor begins to diffuse through the oxide layers permitting greater reaction to occur. The diffusion rate increases with temperature and at or near the melting point of the oxide($2050°$ C.). At this point reaction rates increase more rapidly.

5. Reaction of Ammonium Perchlorate and Aluminum Particles.

The ignition of aluminum particles alone and in the presence of ammonium perchlorate has been studied by Friedman and Macek[13]. The experiments were carried out under optimum conditions of oxygen availability and included the use of fuels(trioxymethylene and plastisol-type polyvinyl chloride) to augment flame temperatures.

These observations indicate that a successful reaction between ammonium perchlorate and aluminum requires very fine powders(10 microns or less) and a sufficiently high temperature($>2050°$ C.) so that ignition and a sustained reaction may occur.

The reaction between ammonium perchlorate and aluminum may be summarized by the reaction:

$$2\ NH_4ClO_4(s) + 4\ Al(s) \longrightarrow$$
$$N_2(g) + 2\ H_2O(g) + 3\ H_2(g) + 2HCl(g) + 2\ Al_2O_3(s)\ (3)$$
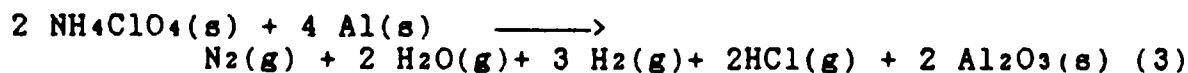
The standard heat of reaction(enthalpy change) is - 820.7 kcal(2334 cal/gm of reactant mixture). Tiger Code calculations for explosion and C-J conditions are given in Table III for a few loading densities of AP/Al and an aluminum metal content of 27.6%. The high temperatures, pressures and detonation velocities shown in this table suggest the high potential for energy release for AP/Al compositions. The bottleneck for successful explosive performance lies in the initiation process. The relatively low explosion temperature

Table III. Explosion Point and C-J Point Description of Ammonium Perchlorate/Aluminum Mixture(27.6% Al).

Density(gm/cc.)/rho	1.2	1.4	1.6	1.8
1. Explosion point.				
temperature(°C.)	6003	5918	5814	5701
pressure(atm)	35,199	46,876	60,809	77,379
2. C-J point.				
temperature(°C.)	6304	6209	6102	5986
pressure(atm)	74,638	98,995	127,800	162,410
detonation velocity(met./sec)	4562	5000	5477	6009
particle velocity (met/sec)	1381	1433	1477	1521
moles of gases/ Kg. of explosive	18.76	18.63	18.52	18.42
principle products(all runs): H_2O, HCl, N_2, H_2, Cl_2, Al_2O_3.				

of AP(1200° C.) and the mechanics of aluminum particle

burning described above act to frustrate the realization of

a large energy release expected from the explosion ther-

modynamics.

Table IV presents the explosion thermodymanics for

a mixture of ammonium perchlorate, TNT and aluminum. The

result expected is that the higher temperature of the TNT-

initiating explosion will ignite the aluminum particles to a

sufficiently high temperature so that the aluminum oxidation

Table IV. Explosion Point and C-J Point Description of
          Ammonium Perchlorate,TNT, Aluminum Mixtures
          (AP/TNT/Al = 50/20/30 by weight)

Density(gm/cc.)/rho	1.0	1.2	1.4	1.6
1. Explosion point.				
temperature(°C.)	5496	5403	5294	5357
pressure(atm)	30,595	42,943	57,668	72,057
2. C-J point.				
temperature(°C.)	5826	5946	5895	5821
pressure(atm) detonation	66,000	92,226	119,150	150,430
velocity(met./sec)	4642	5040	5397	5813
particle velocity (met/sec)	1440	1556	1598	1639
moles of gases/ Kg. of explosive	22.56	22.32	22.02	20.86

principle
products(all runs): H_2, CO, N_2, HCl, Cl_2, Al_2O_3.

process is facilated. Although the results of the calculations are comparable to those of Table III, the pressures, temperatures and detonation velocities are generally lower for the aluminized explosive. The latter may be explained by the endothermic effect of the aluminum which lowers the detonation velocity, pressure and temperature of the explosive composition.

6. <u>Lithium/Ammonium Perchlorate Compositions</u>.

The use of lithium as the reductant with ammonium perchlorate removes the difficulty with oxide layer formation, since lithium oxide does not form a protective layer about the metal. Lithium is a very reactive metal with a low melting and ignition point (melt. pt. 179° C. and ign. pt.. 200° C., Table III). Lithium is best handled in an inert atmosphere such as argon. The explosion characteristics of ammonium perchlorate and lithium are presented in Table V(AP/Al = 70/30 by weight).

The explosive performance is not as marked as that for aluminum-containing mixtures. Due to the easy ignitability of lithium it is probable that thermodynamic predictions may be more readilly realized in practice. The high reactivity of this element, however, may preclude its use except for possible special applications.

8. <u>Use of Aluminum Alloys in Reactive Compositions</u>.

Aluminum alloys of lithium and magnesium may be prepared having 4 and 15% content of these metals, respectively[14].

1-12

Table V. Explosion Point and C-J Point Description of
Ammonium Perchlorate/Lithium Mixtures
(AP/Li = 70/30 by weight)

Density(gm/cc.)/rho	0.8	1.0	1.2	1.4
1. Explosion point.				
temperature($^\circ$C.)	4689	4649	4552	4465
pressure(atm)	16,470	26,695	40,801	60,964
2. C-J point.				
temperature($^\circ$C.)	4779	4713	4645	4557
pressure(atm)	22,936	57,342	86,435	125,260
detonation velocity(met./sec)	3953	4713	5597	6786
particle velocity 1639(met/sec)	1135	1234	1304	1336
moles of gases/ Kg. of explosive	17.79	17.39	16.40	15.66

principle
products(all runs): H_2, HCl, N_2, H_2O, Li_2O.

Mg-Li alloys having a composition of 9/1 by weight
also are stable at room temperature[15]. Properties of these
materials, including hydrogen-containing aluminum, are given
in table VI.

The presence of hydrogen in aluminum is a problem in
the production of aluminum, since it causes structural
unsoundness in the metal. Table VII gives the per cent
of hydrogen soluble in aluminum at one atmosphere pressure
of hydrogen. Information on the the solubility of hydrogen in

aluminum at higher pressures was not found.

The use of these alloys in reactive compositions with AP and other oxidizing systems may be expected to produce quick energy release from the easy oxidation of the alloying additives. The ignition temperatures of lithium and magnesium are relatively low. At the melting point of the alloy, the vapor pressure of these elements will be larger than that of aluminum and oxidation will occur more rapidly. The higher temperatures obtained from this quick release of energy may be expected to promote the oxidation of aluminum particles.

Table VI. Properties of Aluminum Alloys with Magnesium, Lithium and Hydrogen.

Alloy or Mixture	Al/Li	Al/Mg	Al/H2	Al/Mg/Li
Properties				
Weight ratios	96/4	85/15	99+/.000624	90/9/1
Density(gm/cc.) (calc.).	2.62	2.18	2.71	2.60
Energy release as oxide(kcal/ 100 gm./Al)	40.8	88.5	.036	95.7
Melting point (°C.)	600	450	660	660/590*

*lithium/magnesium alloy

8. Metal-alloying Reactions.

An alloying reaction occurs when a 3/1 mixture of Al/Pd is heated to a temperature of 640° C.[16]. The exothermic process produces 3.23 kcal/cc. of mixture. Tests to study

the damage due to this energy release were made by shooting
palladium fragments against aluminum targets[17]. The results
indicated that some alloying reaction did occur, although not
sufficiently to markedly enhance the effects of damage as
compared to steel fragments. In order to improve the alloying
reaction so that it would occur under more favorable con-
ditions, cubical fragments composed of Al/Pd were tested
against simulated fuel tank targets[18]. Again some alloying
reaction was noted, but the damage results were not con-
clusive when compared to steel fragment damage.

One of the problems noted with the Pd/Al experiments
was the difficulty of producing the necessary chemical
intimacy between the two metal reactants for efficient
chemical reaction. Attempts to weld or roll the sheet
metal components to achieve bonding between the Al/Pd
components failed due to premature ignition.

Besides the Al/Pd system, the use of alloys in reactive
compositions involving Ni/Al and Pd/H$_2$ is also considered.
Table VII presents the relevant properties of metals, Mg,
Al, Pd and Ni, particular combinations of which are con-
sidered below as potential candidates for alloying reactions
for explosive devices.

9. __Alloying Reactions and Energy Release__.

Table VIII gives data on the the two alloy systems, Pd/Al and
Ni/Al. It also gives some properties of the compound, Pd/H$_2$.
A brief description of these systems is given below.

Table VII. Physical Properties of the metals Mg, Al, Pd, and Ni[19].

| Property | Metal | | | |
	Mg	Al	Ni	Pd
Atomic weight	24.3	26.98	58.71	106.4
density(g/cc)	1.738	2.699	8.91	11.99
MP/°C.	649	660	1455	1552
BP/°C.	1105	2467	2920	2940
ΔH(fusion)/kcal/mole	2.13	2.51	4.1	4.2
ΔH(vap.)/kcal/mole	30.4	69.5	89.6	86.5
Electronegativity	1.2	1.5	1.8	2.2

Table VIII. Properties of Aluminum Alloys and Energy Release in Alloying Reactions[20,21].

| Alloy | Pd/Al | Ni/Al | Pd/H$_2$ |
Properties			
Weight ratios	80/20	68.5/31.5	98.5/1.5
Mole ratio	1/1	1/1	1/0.8
Density(gm/cc.)	9.6	6.04	11.1
Heat of form. (cal/gm.)	327	443	427*
Ignition temp. (°C.)	660	-	-
Melting point (°C.)	1638	1642	-

*energy due to formation of H$_2$O.

a. Pd/Al alloy. The electronegativity difference between Al and Pd is 0.7 unit. This difference is sufficiently large that polar bonding may be expected between Al and Pd. The intermetallic compound, palladium aluminide (PdAl) is obtained from this reaction. A mixture of these metals is easily ignited at the temperature of 660° C. The energy of the reaction is 327 cal./gm.

b. Ni/Al alloy. The electronegativity difference between the two elements Ni and Al is 0.3. The energy release (443 cal/gm.) is due to the heat of reaction of these two metals. Use of nickel fragments against aluminum targets did not produce an observable alloying reaction[22]. Further work is needed to obtain the ignition conditions for this alloy.

c. Pd/H$_2$ system. The absorption of hydrogen by paladium is substantial. There are two crystalline modifications[23], alpha and beta. The beta form is structurally more brittle and has a larger molar volume than the alpha phase. The energy release potential of this system(427 cal/gm), especially at high temperatures under detonation conditions, suggest its use in reactive compositions.

10. Design of High Energy Device Using Alloying Reactions.
Figure 1 presents a sketch of a design for a potential explosive device. The following considerations give a rationale for the proposed design:

a. The alloying composite(Pd/Al, Pd/H$_2$/Al or Ni/Al) provides a casing for the main reactive composition. The use of Pd/H$_2$ will provide a double boost to the reactive

composition. It will provide energy from the alloying reaction as well as supply hydrogen gas for further reaction.

b. The thick metal casing provides the inertial resistance so that sufficient time is available for the metal alloying and ignition of the reactive composition to take place.

c. The ignitant compartment may be required to "activate" the alloying composite to the temperature of the alloying reaction, or ignite the reactive composition. It need not be present, if sufficient energy is provided by the reactive composition for this purpose.

d. The reactive composition may be any high explosive, e.g., TNT or RDX. In case it is an aluminized explosive, the aluminum in the Pd/Al sandwich is not necessary. The alloying reaction will proceed with the aluminum in the reactive composition. The limiting reagent will then be the amount of palladium(or Ni) present, i.e., the amount of aluminum should be at least 20% (32% for Ni) by weight of the palladium(Ni) in the case.

e. For the case of the ammonium perchlorate/aluminum alloy reactive composition,, the proportions of AP to alloy (Al/LI, Al/Mg or Al/Mg/Li) should be 70/30 by weight. With a Pd/H2 reactive case, this system will more closely achieve the predictions of the explosion thermodynamics presented earlier.

reactive

composition

1 2   3
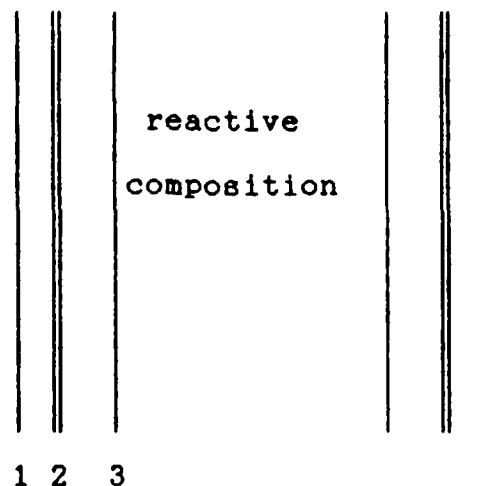
Figure 1. Device Using Reactive Alloys for Increased
Energy Release of Reactive Composition.(schematic).
(1. thick metal casing 2. alloy metal sandwich,
Pd/Al "reactive case" 3. ignitant composition(e.g.
TNT) or not present.)

1-18

IV. RECOMMENDATIONS:

1. Ignition temperatures for ammonium perchlorate and other oxidizers(e.g. fluorinated hydrocarbons) with light metal metals and light metal alloys need to be determined to ascertain precisely the nature of the oxidation process.

2. More information on the physical and chemical properties of hydrogenated metals such as Pd/H^2 is required. This information includes thermodynamic stability, e.g., the vapor pressure of hydrogen gas as a function of temperature.

3. For the lithium and magnesium alloys of aluminum and the hydrogenated metals it is important to know whether these materials may be produced in finely divided form.

4. Hydrogenation of Nickel and other metals needs to be investigated for use in " reactive case" applications

5. Electroplating of nickel and palladium at low temperatures onto aluminum metal and aluminum alloys needs investigation.

6. A small prototype of the explosive device discussed in this study needs to be tested and compared with similar devices without a "reactive case".

REFERENCES.

1. B. T. Federoff, Editor, Encyclopedia of Explosives and Related Items , Picatinny Arsenal, Dover, New Jersey, 1960, p.146.

2. Ibid., p. 149.

3. A. K. Galwey, and Jacobs, P.W.M., Proc. Roy. Soc. (London), A254 , 455, 1960.

4. L. L. Bircumshaw, and Newman, B.H., Proc. Roy. Soc., (London), A227 , 115 (1954); A227, 228(1955).

5. A. K. Galwey, and Jacobs, P.W.M., J. Chem. soc., 837(1959).

6. M. Cowperthwaite and W. H. Zwisler, Tiger Computer Program Documentation, Stanford Research Institute, Menlo Park, California, 1973.

7. W. H. Anderson and Pesante, R. E., Eighth Symposium (International) on Combustion , Williams and Wilkins, Baltimore, 1962, p. 705.

8. D. Price, Clairmont, Jr., A. R. and Jaffe, L., NOLTR-67-112, White Oak, Maryland, 1967.

9. M. A. Cook et. al., J. Phys. Chem., 61 , 189(1957).

10. Charles L. Mader, Numerical Modeling of Detonation , University of California Press, Los Angeles, 1981.

11. A. G. Gaydon and H. G. Wolfhard, Flames, 3rd. Ed., Chapman and Hall, Ltd., 1970.

12. Herbert Ellern, Modern Pyrotechnics , Chemical Publishing Company, New York, N. Y., 1961.

13. R. Friedman and Macek, A., Combustion and Flame,, 6 , 9(1962).

14. K. R. Van Horn, Editor, Aluminum, Vol. I , American Society fo Metals, Metals Park, Ohio, 1967.

15. C. A. Hampel, Editor, Rare Metals Handbook , Reinhold,Publishing Co., New York, 1955.

16. H. Ellern, Loc. Cit.., p.279.

17.R. W. Williams, Hypergolic Fragments, AFTL-TR-82-69, 1982.

18. E. Wittrock and Williams, R. E., An Investigation of Composite Hypergolic Fragments, AFATL-TR-83-76, 1983.

19. N. N. Greenwood and Earnshaw, A., Chemistry of the Elements, Pergamon Press, New York, 1984.

20. Y. S. Jouioukian, Editor, Thermochemical Properties of High Temperature Solid Materials , New York, 1967.

21. K. R. Van Horn, Loc. Cit.., p. 50.

22. R. W. Williams. Loc. Cit. , p. 2.

23. N. N Greenwood and Earnshaw, A., Loc.Cit. , p.1335.

1989 USAF-UES SUMMER FACULTY RESEARCH PROGRAM

Sponsored by the

Air Force Office of Scientific Research

Conducted by

Universal Energy Systems, Inc.

FINAL REPORT

Maneuvering Hard Target Penetrators

Prepared by: Joseph M. Brown, Ph.D.

Academic Rank: Professor

Department: Mechanical and Nuclear Engineering

University: Mississippi State University

Research Location: Air Force Armament Technology Lab

Munitions System Division

Eglin Air Force Base, FL   32542

USAF Researcher: Albert L. Weimorts, Jr.

Date: 27 September 89

Contract No.: F49620-88-C-0053

Maneuvering Hard Target Penetrators

by
Joseph M. Brown

ABSTRACT

The hard target ordinance package (HTOP) is a 500-pound class bomb designed to penetrate deeply into hardened surface emplacements. When several HTOP's are deployed simultaneously it is possible to target each one individually by incorporating propulsion and guidance and, thereby, produce a large "footprint" on the earth. Rocket motors were sized and flight performance studies were made to predict the foot print size. Typically it was determined that for 50 pounds of maneuver weight applied to a 339-pound bomb (i.e., for 15 percent weight increase) launched at 2000 feet with an 800 fps velocity, a dispersion radius of approximately 200 feet could be obtained. Weight is not a critical limit but a 3-bomb deployment pod could require a 5 or 6 inch increase in diameter to accommodate the rocket nozzles.

Some peripheral investigations were made into target penetration and into the utilization of propellants which would act as reactive fragments.

management direction and encouragement were provided by Donald Bednar. Captain Ernest Staubs provided encouragement and also produced a computer program for one of the delivery systems. David L. Lyle helped de-bug the final computer program, showed me the techniques for sweeping variables so as to obtain continuous (overnight) computer running, and showed me how to use Lotus 123 for drawing figures. His assistance was very valuable. Finally, I thank Elva Lovering and Mary Ann Crocker for typing the progress reports, briefing, and final report.

SUMMARY

The hard target ordinance package (HTOP) is a 500-pound class bomb designed to penetrate deeply into hardened surface emplacements. A package of several HTOP's can be targeted by delivery vehicle to impact only one point (small area). By incorporating simple guidance and propulsion into each HTOP it is possible to direct each bomb in the package to different spread-out target points. The addition of propulsion and guidance make an HTOP a SMART HTOP. The object of this research was to determine the extent of the area (footprint size) which can be reached by the delivery package for a given amount of additional propulsion/guidance weight. The work entailed defining the components (of solid and liquid rockets), determining realistic sizing relationships, then computing flight trajectories to determine the maximum ground dispersion. Typically it was determined that for 50 pounds of maneuver weight applied to a 339-pound bomb (i.e., for approximately 15 percent weight increase) launched at 2000 feet with an 800 fps velocity, a dispersion radius of approximately 200 feet could be obtained. Thus weight is not an extremely important limitation. An envelope of

approximately 2 inches of radius beyond the penetrator diameter probably would be required for the 2000-foot altitude, 800 fps launch velocity, 200-foot radius footprint. This would result in an increase of 5-6 inches in the diameter of the delivery vehicle payload compartment (based on 3 HTOPs).

Since weight is not extremely critical, the design should emphasize safety, ease of handling, and cost reduction instead of high performance except that higher performance items, such as propellants with high I_{sp}, should be used just to reduce the nozzle dimensions.

Maneuvering Hard Target Penetrators

INTRODUCTION

The hard target ordinance package (HTOP) is a 500-pound class bomb used to penetrate deep into hard targets such as command centers, hardened aircraft hangars, and underground ICBM sites. Acceleration type fuses are available so that detonation can be achieved after penetrating a number of different compartments.

The HTOP warhead assembly is 56.8 inches long, has a diameter of 6.65 inches, and weighs 339 pounds (which includes 49 pounds of HE).

When several HTOPs are simultaneously used against a command center the natural dispersion achieved is adequate. For smaller spaced targets, such as underground ICBM targets and hardened aircraft hangars, individual targeting can be useful. The approach being considered here is to hand-off separate target instructions to the several HTOPs in the delivery vehicle. Each HTOP then would have a

guidance and propulsion package which would execute the instructions. Clearly the target dispersion must be compatible with the propulsion (and guidance) capability of the "smart" HTOP.

The propulsion and guidance capability of the smart HTOP is measured by the ground "footprint." The footprint is the maximum forward and aft and transverse boundary which can be achieved for given launch altitude, velocity, and inclination.

In order to be used the maneuver package must be simple, light, and inexpensive. For example a rear-rocket engine with thrust-vector control and associated guidance would make HTOP an expensive guided missile and thus not a viable candidate. Wrap-around solid or liquid propellant rocket motor(s) which thrust through the center of gravity, a simple guidance/control package, and fixed aerodynamic fins to induce roll for stabilization may make up a useful system.

The guidance-control function could be provided with an inertial measurement unit (IMU) and a simple control computer. The system would be given the required trajectory, it would sense the accelerations, and it would call for impulses at particular roll locations to guide the HTOP to its target. Thrusting would always be lateral through the center of gravity. As a result of a lateral impulse, a non-zero angle of attack would be induced. However, HTOP is highly stable so that the aerodynamic forces should null out any induced angle of attack. A roll rate of a few revolutions per second would be used.

The principal problems which will be addressed here are the selection of propellants, the rocket engine design and integration, and the trade-off between high-thrust (with large nozzles and large combustion chambers if liquid propellants are used) at the beginning of

the trajectory versus smaller nozzle/smaller combustion chamber/longer thrusting engines. The optimization approach which is taken is to select a total propellant weight then determine the propellant flow rate which maximizes the footprint. In addition, sensitivity analyses are performed to determine the effect on performance of varying specific impulse, structural efficiency, and other component efficiency.

Penetration studies were made and investigations were made of the effect of using propellants which could chemically react with some targets.

PRELIMINARY VEHICLE OPTIMIZATION

In this section a simplified trajectory is used to obtain an approximation to the rocket motor characteristics, including sizing information. The results will give "ball-park" values for motor weights, nozzle dimensions, and footprint dimensions. It appears that the trade-off between high thrust/short burn time vs. low thrust/long burn time can be determined with the approximate trajectory analysis presented here.

First the general flight equations are developed. The trajectory assumptions are:

1. Initial velocity is vertical.

2. Aerodynamic drag is equal to the vehicle weight, i.e., terminal velocity has been reached).

3. Zero angle of attack is maintained at all times (i.e., stabilizing aerodynamic forces null out attack angle induced by lateral thrust).

4. Rocket thrust is initially perpendicular to the longitudinal axis and passes through the center of gravity, but the thrust remains horizontal.

5. The total vehicle weight is constant during thrusting (i.e., use the initial weight rather than the variable weight as the propellant is expended - propellant total weight is only 10 percent of the vehicle weight).

The assumptions used here result in a circular area footprint so that only the radius needs to be determined. For the thrusting phase $0 < t < t_1$

$$\Sigma F_y = my'' = T \qquad y' = Tt/m \qquad x' = 0 \qquad x = x'_0 t$$

$$y'' = T/m \qquad y = Tt^2/(2m) \qquad x' = x'_0$$

At time t_1

$$y = y_1 \qquad y_1 = Tt_1^2/(2m) \qquad x = x_1 \qquad x_1 = x'_0 t_1$$

$$y' = y'_1 \qquad y'_1 = Tt_1/m \qquad x' = x'_1$$

For the coast phase, $t_1 < t < t_2$

$$x' = x'_0 \qquad\qquad\qquad x = x'_0 t$$

$$y = y'_1 t = Tt_1 t/m$$

To compute time to stop, $x = h = x'_0 t_2$ and $y = y_2$. Now

$$t_2 = h/x'_0$$

$$y_2 = y_1 + y'_1(t_2 - t_1) = Tt_1^2/(2m) + Tt_1(t_2 - t_1)/m$$

$$= -Tt_1^2/(2m) + Tt_1 h/(mx'_0)$$

The parameter to be maximized is y_2 - which depends on T, t_1, and m.

The thrust is given by

$$T = I_{sp} w'_p$$

where I_{sp} is the specific impulse and w'_p is the propellant weight flow rate. The burning time t_1 times the weight flow rate gives the propellant weight, $w_p = w'_p t_1$. With these y_2 can be written as

$$y_2 = I_{sp} w_p h/(mx'_o) - I_{sp} w_p^2/(2mw'_p)$$

We want to fix the weight of the rocket then find the weight of propellant and propellant flow rate (which is directly proportional to the thrust) to maximize y_2.

The vehicle weight w_t is

$$w_t = w_r + w_b$$

where w_r is the rocket (motor and guidance) weight and w_b is the bomb (HTOP) weight. The rocket weight is assumed to depend upon propellant weight (propellant storage) and upon thrust (propellant flow rate). The following scaling equation is assumed

$$w_r = \gamma w_p + \epsilon T$$

where γ and ϵ are to be determined. Again using $T = I_{sp} w'_p$ gives

$$w_r = \gamma w_p + \epsilon I_{sp} w'_p$$

and

$$w_t = \gamma w_p + \epsilon I_{sp} w'_p + w_b$$

Since w_r is taken as a constant w'_p can be determined

$$w'_p = (w_r - \gamma w_p)/(\epsilon I_{sp})$$

Now we have

$$y_2 = I_{sp} w_p h/(mx'_o) - I_{sp}^2 \epsilon w_p^2/[2m(w_r - \gamma w_p)]$$

For the present time we will use m as the total vehicle weight w_t divided by g. Thus

$$y_2 = (gI_{sp}/w_t)[w_p h/x'_o - \epsilon I_{sp} w_p^2/(2wr - 2\gamma w_p)]$$

We now have y_2 as a function of constants and w_p.

The value of w_p maximizing y_2 is obtained by differentiating the bracketed factor with respect to w_p, equating to zero, and solving for w_p. This gives

$$(w_p)_{opt} = (w_r/\gamma)(1 \pm 1/(1+2\gamma\omega)^{.5})$$

where $\omega = h/(\epsilon I_{sp}x'_0)$. In order to determine which sign to use in the parentheses consider some realistic values for the input constants. Let $\gamma = 1.5$, $h = 3000$ ft, $\epsilon = .005$, $I_{sp} = 250$, and $x' = 800$ fps. Now $\omega = 3000/(.005 \times 250 \times 800) = 3$, and $w_p/w_r = (1\pm1/(1+2(1.5)(3))^{.5})/1.5 = 8.77/\text{ft}(+)$ or $.456/\text{ft}$ $(-)$. Using $w_p/w_r = 8.77$ gives $w_r = \gamma w_p + \epsilon T = 1.5(.877w_r) + \epsilon T$, or $\epsilon T = -.316w_r$, which is not possible. Using $w_p = .456w_r$ gives $\epsilon T = .316w_r$, which is possible. Thus, the negative sign must be used.

Before substituting this into y_2 to give y_{max} rearrange y_2 as

$$y_2 = \frac{gI^2_{sp}\epsilon}{2} \frac{w_r\,w_p}{w_t\,w_r} \frac{2\omega-(1+2\gamma\omega)w_p/w_r}{1 - \gamma w_p/w_r}$$

Note that for optimum w_p

$$1 - \gamma w_p/w_r = 1/\sqrt{1+2\gamma w}$$

Now using the optimum value of w_p gives

$$y_{max} = (gI^2_{sp}\epsilon/\gamma^2)(w_r/w_t)(1 + \gamma\omega - (1 + 2\gamma\omega)^{.5})$$

For example using $I_{sp} = 250$ sec, $\epsilon = .005$, $w_r = 100$ lb, $\gamma = 1.5$, $w_t = 439$ lb, $h = 3000$ ft., and $x' = 800$ fps gives $\omega = 3$ then $y_{max} = 2382$ ft. The propellant weight is $(100/1.5)(1 - 1/\sqrt{1+9}) = 45.58$. The radius above can be compared to the case where the horizontal velocity is imparted immediately and the mass varies. For the variable mass case $\Delta V = gI_{sp}\ln[w_t/(w_t - w_p)] = 883$ fps. The flight time, of course, is x'_0t_2 and $t_2 = 3000/800 = 3.75$ sec. The maximum possible horizontal range is this velocity increment times the flight time, i.e., 3311 ft.

Thus the radius achieved by minimum weight thrusting as the vehicle descends is approximately 2/3 the maximum (i.e., infinite thrust for zero time) or for an impulse thrust.

The range in the above example is appreciably more than required. However, the thrust implied by the values of these parameters and the optimal thrusting is high. The thrust is given by

$$T = (w_r - w_p)/\epsilon = w_r/[\epsilon\sqrt{1+2\gamma\omega}] = 100/[.005\sqrt{1+2(1.5)3}] = 6325 \text{ lb.}$$

This would be the thrust required of each of four nozzles. The propellant weight $w_p = (w_r/\gamma)(1-1/(1+2\gamma\omega)^{.5} = 45.6$ lb. The burn time is $TB = w_p I_{sp}/T = 45.6 \times 250/6325 = 1.80$ sec. The propellant flow rate is $w'_p = w_p/TB = 45.6/1.80 = 25.3$ lb/sec, and the nozzle/combustion chamber weight would be $\epsilon T = .005(6325) = 31.6$ lb. This is the weight of all four nozzles, or each nozzle would weigh $31.6/4 = 7.9$ pounds--which may be too small for a 6000-pound thruster. In any case, the nozzle sizes probably would be so large that they could not be integrated into the package. The thrust could be reduced almost to one half the above, i.e., to approximately 3500 pounds, by burning until almost at ground level, i.e., for 3.75 seconds instead of 1.8 seconds. Thus nozzle size (rather than weight) would drive the burning time upward for optimum design. In fact nozzle integration difficulties may be so great that the optimum design will thrust practically to the ground.

For this simplified trajectory the optimum thrust, optimum burn time, and burn time divided by flight time can be obtained in closed form. Solving for T from $w_r = \gamma w_p + \epsilon T = w_r/\epsilon - w_p\gamma/\epsilon$ and substituting the optimum w_p gives

$$T_{opt} = w_r/(\epsilon\sqrt{1+2\gamma h/(\epsilon I_{sp}x'_o)}$$

The optimum burn time $(TB)_{opt}$ is given by $I_{sp} = T/w'_p = T(TB)/w_p$ and substituting the optimum thrust and propellant weight gives

$$(TB)_{opt} = I_{sp} \epsilon(\sqrt{1+2\gamma'h/(\epsilon I_{sp}x'_0)} - 1)/\gamma$$

The flight time $TF = h/x'_0$ so that

$$(TB)_{opt}/(TF) = x'_0 I_{sp} \epsilon(\sqrt{1+2\gamma h/(\epsilon I_{sp}x'_0)} -1)/(h\gamma)$$

Since the dispersal radius was so large and since the actual maneuver package is not large, the need for high performance components is not great other than the nozzle size problem. However, high I_{sp} should be used to limit nozzle size.

The maximum footprint radius depends linearly upon the rocket weight (if propellant weight is a small portion of total package weight), and upon the parameters ϵ, γ, I_{sp}, h, and x'_0. The radius depends upon altitude h and $1/x'_0$ in the same manner, since h and x'_0 always appear in the form h/x'_0. In order to determine the sensitivity to any one of the parameters ϵ, γ, I_{sp}, h, and x'_0, it is convenient to assign values to all the other parameters. Here we will explore the sensitivity around the reference values of $\epsilon = .01$, $\gamma = 2.0$, $I_{sp} = 200$ sec, h = 2000 ft, and $x'_0 = 800$ fps. First, rewrite y_{max} in the form

$$y_{max} = (gI^2_{sp}\epsilon/\gamma^2)(w_r/w_t)[1+\gamma h/(\epsilon I_{sp}x'_0) - (1+2\gamma h/(\epsilon I_{sp}x'_0))^{.5}]$$

For determi... the sensitivity of the variables write

$$s(\epsilon) = (y_{max}/g)(w_t/w_r)(\gamma^2/I^2_{sp}) = \epsilon(1+.025/\epsilon -\sqrt{1+.05/\epsilon}) = y_{max}/k_1$$

$$s(\gamma) = (y_{max}/g)(w_t/w_r)/(\epsilon I^2_{sp}) = (1/\gamma^2)(1+1.25\gamma-\sqrt{1+2.5\gamma}) = y_{max}/k_2$$

$$s(I_{sp}) = (y_{max}/g)(w_t/w_r)(\gamma^2/\epsilon) = I^2_{sp}(1-500/I_{sp}-\sqrt{1+1000/I_{sp}}) = y_{max}/k_3$$

$$s(h) = [y_{max}/(gI^2_{sp})(w_t/w_r)(\gamma^2/\epsilon) = 1+.00125h-\sqrt{1+.002h}] = y_{max}/k_4$$

The results are

ϵ	$s(\epsilon)$	γ	$s(\gamma)$	I_{sp} sec	$s(I_{sp})$	h-FT	$s(h)$
.002	.0168	1.5	.309	100	26,800	1000	.379
.005	.0134	2.0	.263	150	35,100	2000	1.051
.01	.0105	2.5	.229	200	42,000	3000	1.834
.02	.0076	3.0	.204	250	47,700	4000	2.683
.05	.0043			300	53,000	5000	3.610

The radius varies almost hyperbolically with nozzle (ϵ) and tankage (γ) efficiencies. The radius increases with specific impulse to a power somewhere between the square root and linear. The radius varies almost linearly with deployment altitu. . (and almost linearly with the inverse of the deployment velocity). As a result of some other preliminary computations it appears that the design should use the largest nozzle (and thrust) which can be incorporated into the package. As more accurate values for γ and ω (and I_{sp}) are generated this trade-off decision should be rechecked.

PROPELLANT SELECTION

The rocket motor and propellants clearly must be inexpensive to buy and must be easy to store and maintain. These requirements immediately rule out the high-performance cryogenic propellants like liquid H_2 and O_2. Both the fuel and oxidizer must be contained in the vehicle for this application--otherwise an expensive compressor would be required to "pump" air into the motors.

The choices for liquid propellants for this application are extremely limited. The most viable choice seems to be hydrogen peroxide H_2O_2--at least for the oxidixer. H_2O_2 by itself will only produce a specific impulse of about 147 seconds (at sea level and 90 percent concentration). Approximately 42 percent by weight of

decomposed H_2O_2 is gaseous O_2 which can be used as an oxidizer for hydrocarbon fuels. The fuel RP-1 (kerosene) is especially suitable for this application. The I_{sp} of RP-1 with liquid O_2 is near 300 seconds. However, when oxidized with H_2O_2 the performance will drop sharply. A specific impulse of 230 seconds may be realistic for RP-1 and H_2O_2.

H_2O_2 and RP-1 are easy to handle, have long shelf lives, and are inexpensive. H_2O_2 does require some care in handling though. H_2O_2 reacts with almost any substance and can explode if it gets hot enough. However, much background experience is available so that handling should be safe and economical. In any case it would seem that the bomb and motor should be joined not too long before loading on the aircraft.

Consider now the selection of solid propellants. Solid propellants can be stored for years without degradation, they are easy to handle, and they are relatively inexpensive. A typical solid propellant is NH_4ClO_4-C_2H_4O, ammonium perchlorate mixed with ethelene oxide. Its density is .06 lb/in^3 and can develop a specific impulse in the 180-240 second range. A value of I_{sp} = 220 sec may be applicable for this design.

LIQUID ROCKET ENGINE DESIGN

The liquid rocket engine consists of a propellant tank, a gas pressure feed system, combustion chamber(s), and nozzles. The engine must be designed so that lateral thrusting will occur in a prescribed direction while the vehicle is rolling. Consider first the propellant feed system. Due to aerodynamic drag, the net vertical acceleration will be less than one "g"--probably much less for the non-thrusting vehicle. This level of force would keep the liquid on the bottom of the tanks. If the vehicle is thrusted in the delivery vehicle forward

direction, then there would be additional force keeping the liquid on the bottom of the tank. If thrusting is opposite the delivery vehicle forward direction, even at levels of several hundred pounds, then the liquid may not be at the tank bottom. It is thus concluded that a liquid propellant must use a positive feed system and they probably should use bladders.

At this time let us estimate the thrust levels required. HTOP flight times are of the order of 3 seconds and the delivery velocity is in the order of 1000 fps. Consider a Δv of 200 ft/s imparted in the first second of flight. This would give a footprint radius of aproximately $200(3-1) = 400$ ft for a vertically launched HTOP. Launching at an angle would change the footprint shape somewhat, but not materially change the size. For a Δv of 200 ft/s applied in 1 second, the acceleration is $200/(1) = 200$ ft/s^2 and the force required is $F = ma = 3000$ lb. A footprint radius of 40 feet (i.e., 1/10 the above radius) would require a thrust of 300 pounds (again, 1/10 the above thrust). Thrusting throughout the flight would reduce this level somewhat, but more propellant would be required. A thrust level of 500 to 1000 pounds might be anticipated for this design. The propellant weight used is the thrust force divided by the specific impulse times the time (since $I_{sp} = F/w'_p$). Thus $w_p = F t/I_{sp}$. Using 3000-pound force (400-foot radius) $t = 1$ second, and $I_{sp} = 250$ gives $w_p = 12$ lb, which is quite minimal. A 4000-foot radius footprint would only require 120 pounds of propellant. A 400-foot radius is probably more than required. Thus, propellant weight will not present a problem. Also,

flexibility, storability, and safety considerations are probably more important than propellant weight. However, higher specific impulse will result in lower nozzle size and thus will be important.

In summary now, for sizing studies we will center around the following parameters

a_o = 30°, h = 2000 ft, v_o = 800 fps, w_p = 12 lb,

γ = 4.0, ϵ = .01, I_{sp} = 220 sec, w_b = 337 lb

It appears that a footprint radius around 200 feet would result and an enveloping hole diameter of 22 inches would be required in the pod. A weight penalty of 50-100 pounds per HTOP would result.

One final item on liquid engines is to comment on the number of pulses. For flight (and thrusting) times of around 2 seconds and a roll rate of 5 cycles per second, each nozzle could thrust 10 times for a pulse time of 1/20th second. Thus, each nozzle must be "on" 1/20th second then "off" for 3/20th second for 10 pulses. For 10 pounds of propellant each pulse would expend (10/4)/10 = .25 pounds. There are 40 pulses total from the motor.

SOLID ROCKET ENGINE DESIGN

It is difficult to stop and restart solid rocket engines. As an outside possibility a controllable thrust deflector could be used along with continuous burning of a few large rockets. Our main emphasis here however is to use many small single shot solid rockets. Recall that the liquid engines required in the order of 40 pulses. Let us consider using 10 solid engines wrapped around the bomb periphery at 4 different longitudinal locations. In order for the thrust to pass through the center of gravity, two engines would fire simultaneously, and there would be only 20 pulses--which is probably satisfactory. For a

200-foot radius the maximum pulse-length induced error would be 200/20 = 10 feet. Each propellant package would be small--each would contain a fraction of a pound of propellant.

A pressurization system would not be required, as is with the liquid system. Higher chamber pressures (say 3000 psi) could easily be used. Increased chamber pressure would decrease the nozzle throat diameter (quadrupling pressure halves throat diameter). Similarly the exit diameter would change the same amount but the nozzle length would not change. The nozzle sizes for the solid engines should be about the same as for the liquid engines.

Incidentally, the guidance package for both the solid and liquid propelled ordnance packages could be placed on the aft end of the vehicles.

CONCLUSIONS

A preliminary analysis has been performed for the conceptual design of a maneuvering package to be installed in the HTOP munition. The analysis consisted of nozzle sizing, tank sizing, and flight performance analysis.

The analysis of the components was based on "textbook" types of data such as tank strengths, nozzle materials and, as such, has limited accuracy. However, scaling equations were evolved to study the effect on performance of variations in the performance components such as measured by structural efficiency, nozzle weight efficiency, and specific impulse.

Only lateral thrusting through the center of gravity was investigated. The vehicle rolled slowly, a few cycles per second, and was stabilized by aerodynamic forces. Only 40 or so pulses of thrust would be applied for maneuvering.

Liquid and solid propellants were investigated. The primary problems with liquids are pressurization and thrust modulation. The primary problem with solids is that a fixed impulse from individual rockets would be used which, to achieve the required ac' cy, might require 20 or so solid rockets. Also each solid rocket may have to have its own nozzle--so that nozzle space (and possibly weight) may be critical. It appears that solids and liquids should be investigated further.

The performance analysis showed that for about a 10% increase in weight (over the non-maneuvering HTOP) that a footprint "radius" of 200 feet could be obtained for a 2000-foot altitude launch. Thus weight does not appear to be critical. However, nozzle space requirements may be critical. For the 200-foot radius footprint an incremental vehicle radius of over 2 inches is required for each individual HTOP.

The footprint size increases markedly as launch angle in increased from the vertical. The radius is more than doubled as the angle is increased from 30° to 60°. The footprint has an almost circular shape for all launch angles.

In order to determine the trade-off between high-thrust/short-burn-time and low-thrust/long-burn-time, a rocket scaling equation was evolved that had two separate portions, one depending upon propellant weight and the other upon thrust (or, equivalently, propellant flow rate). Using this equation it was determined that minimum weight

resulted for thrusting in the order of half the flight time. The space requirement to accommodate the nozzles would appear to require thrusting for most of the flight time. (Thrusting would cease in time for the HTOP to null out the lateral thrust induced angle of attack.)

The effect on range of increasing structural weight or nozzle weight (i.e., γ or ϵ) is only reflected in the resulting increase in vehicle weight. However, if the rocket weight is held constant (and the thrust is held constant) then rocket structural weight (as measured by γ) decreases the rar · The decrease is by 0.13 for a 2.5 increase in γ. Similarly for fixed rocket weight a range decrease of 0.14 results when ϵ increases by a factor of 11. It is thus concluded that performance is not markedly affected by structural and nozzle weights.

If all vehicle and launch parameters are fixed except for varying specific impulse, then an increase in specific impulse from 140 to 220, i.e., by a factor of 1.6 the radius only increases by 0.1. This small increase results since the thrust level (and nozzle size) is fixed and the burning time is increased. The total impulse is increased by 1.6 but the added late thrusting is not as effective for increasing range.

The range increases linearly with launch altitude, as would be expected.

The range decreases with increased launch velocity. However for an increase in velocity by a factor of 3.3 the range only decreased by 0.2, which is less than expected.

RECOMMENDATIONS

The results of this investigation indicate that for a small weight penalty a maneuvering package can be applied to HTOP. Thus, further design and analysis should be performed.

A preliminary design should be evolved of a nozzle producing approximately 1000 pounds of thrust (and only 2000 lb-sec of total impulse). Primary emphasis should be given to minimize nozzle length--even at the expense of lowered efficiency. A goal of 2-inch length should be used.

The pressurization, or pumping, system needs to be defined and evaluated for the liquid system to determine its cost, reliability, maintainability, and weight. Similarly the repeated start and stop system for the liquid engines needs to be defined and evaluated.

In order to make solids feasible it may be necessary for one nozzle to serve two, or more, solid rockets each of which is fired at different times. There may be a way to utilize a one-way (flapper) valve which would prevent gas from one (firing) engine entering the exit hole of another (non-firing) engine. The use of 20 solid engines might result in 20 feet of error while 40 engines could reduce the error to 10 feet.

Theoretical aerodynamic studies need to be performed to determine the correcting aerodynamic pitching rates induced as the lateral thrusting is applied. Particular attention should be given to determine the time bet en burn-out and impact to achieve zero angle of attack.

Trajectory simulations, or at least a closed form analysis, should be performed to investigate the pulsed nature of the lateral thrust while rolling. An almost continuous integrated pulse is required for this mission.

The inertial measurement and control units need to be defined by delinearing their performance, size, weight, and other characteristics.

Finally, preliminary design drawings need to be made of the liquid and solid propellant systems.

BIBLIOGRAPHY

1. E. A. Bonney, M. J. Zucrow, and C. W. Besserer, Principles of Guided Missile Design - Aerodynamics, Propulsion, Structures and Design Practices, D. Van Nostrand Company, Inc., Princeton, NJ, 1956.

2. Howard Seifert, Space Technology, John Wiley and Sons, Inc., New York, 1959.

3. George P. Sutton, Rocket Propulsion Elements, Third Ed., John Wiley and Sons, Inc., New York, 1963.

1989 USAF-UES SUMMER FACULTY RESEARCH PROGRAM/

GRADUATE STUDENT RESEARCH PROGRAM

Sponsored by the

AIR FORCE OFFICE OF SCIENTIFIC RESEARCH

Conducted by the

Universal Energy Systems, Inc.

<u>Final Report</u>

<u>A STUDY OF IONIC POLYMER MEMBRANES FOR APPLICATION</u>

<u>AS CAPACITOR ELECTROLYTES</u>

<u>and</u>

<u>PRELIMINARY INVESTIGATIONS ON PHOTO-ACTIVATED</u>

<u>STRIPLINE SWITCHES</u>

Prepared by:	Roger K. Bunting, Ph.D.
Academic Rank:	Professor
Department and	Department of Chemistry
University:	Illinois State University
Research Location:	AFATL/MNF Eglin AFB Florida, 32542-5434
USAF Researcher:	Duane Finello, Ph.D.

Date:	27 September 1989
Contract No:	F49620-88-C-0053

A Study of Ionic Polymer Membranes for Application as Capacitor Electrolytes

and

Preliminary Investigations on Photo-activated Stripline Switches

by

Roger K. Bunting

ABSTRACT

A variety of polymeric materials and preparative procedures were investigated for electrolyte applications in high energy density capacitors. A low equivalent weight ionic polymer with high moisture content was found to give a capacitor with good voltage stability and remarkably high capacitance, but its performance was extremely temperature dependent.

Photoconducting polymers were shown to be viable materials for further development toward their application in photo-activated switching devices.

ACKNOWLEDGMENTS

I. Introduction

Earlier work in this laboratory has demonstrated that electrolytic capacitors of superior energy density can be fabricate using a solid polymer electrolyte, a perfluorinated sulfonic acid membrane (trade name Nafion) manufactured by DuPont. Low voltage capacitors with energy densities approximately 100 times the energy density of conventional capacitors were made by shock loading the polymer electrolyte between electrode surfaces at about 1 kilobar, by means of a specially made gun fixture and an explosive charge.[1]

The research described in this report was undertaken in attempt to improve upon the energy density and performance characteristics of polymer electrolyte capacitors and to seek new materials and fabrication procedures that could obviate the necessity of shock loading.

A secondary project involved preliminary research on the use of photoconducting polymers for stripline switches that could be used in fuzing devices of ordnance systems.

My invitation to participate in these projects is a consequence of my experience in a broad range of chemical systems, most specifically in polymer chemistry, and the recognition that chemical expertise combined with the engineering and materials science expertise of the laboratory personnel would result in a successful effort.

II. Objectives

The specific objectives of these projects were to a) optimize the performance characteristics of polymer electrolyte capaictors by choice of materials, b) devise a convenient and simple capacitor fabrication technique, and c) demonstrate the feasibility of photo-activated stripline switches.

III. Experimental

All capacitors were prepared using electrodes of 0.75 inch diameter titanium discs coated with ruthenium oxide (ruthenia, RuO_2) as supplied by Pinnacle Research. The ruthenia has a microporous structure that provides a huge surface area for contact with the electrolyte material. Capacitors were evaluated by charging for one minute with a constant voltage supply source; they were then disconnected and total charge was determined by discharging through a digital coulometer (Princeton Applied Research Model 379) protected by a 120 ohm resistor in series with the discharge. Equivalent series resistance (ESR) was measured on a GenRad model 1658 RLC Digibridge at a frequency of 1 kHz.

IV. Polymer Solutions

The fabrication of capacitors by the shock-loading technique no doubt owes much of its success to its ability to force the polymer electrolyte into the microscopic cavities of the ruthenia and make contact with a high proportion of this electrode surface. Solutions of polymers were investigated to determine if their deposition on the electrode surface, followed by removal of the solvent, would provide equally good contact and high capacitance.

A tetrahydrofuran (THF) solution of a phosphazene polymer, poly[bis[2-(2-methoxyethoxy)ethoxide]phosphazene] (MEEP)[2], was deposited between two electrodes. The capacitor was pressed to a polymer thickness of approximately 4 mils and placed in a vacuum chamber for 30 minutes to remove solvent. After a 2 volt charge, this capacitor was found to contain 0.16 coulombs, for a capacitance (q/v) of only .08 farads. Furthermore the capacitor was found to lose voltage rapidly. After recharging (2 volts) the potential was found to drop to 0.86 volts after only 60 seconds.

The MEEP polymer has been reported to combine readily with lithium ions.

3-5

Since the lithium ion has high electrochemical stability and would permit higher charging voltages, its effect on the electrolyte performance was investigated. The polymer solution was saturated with lithium perchlorate, and a capacitor was prepared as above using this solution. This capacitor was found to accept virtually no charge, and the system was not further studied.

It has been demonstrated[3] that Nafion can be solubilized by treatement in hot alcohols under pressure. An attempt was made to find other solvents which might dissolve Nafion under ordinary pressures so that its solutions could be investigated as were those of the MEEP. However, heating Nafion in a broad range of solvent classes (acetonitrile, tetrahydrofuran, dimethyl sulfoxide, dimethylformamide) over a period of three days produced no detectable dissolution of the polymer.

V. Other Polymer Membranes

Investigations of two new proprietary acidic polymer membranes (supplied commercially) proved to be most fruitful. A high EW (equivalent weight) and a low EW polymer were investigated. While Nafion cannot be melted without altering its constitution, the new high EW polymer was found to soften substantially above 170°C and darken only gradually as temperatures were further increased. The possibilty of preparing capacitors by pressing these membranes between electrodes at elevated temperatures was thus investigated.

A piece of high EW polymer membrane was cut to the size of the capacitor electrodes, placed between two electrodes, and the assembly was inserted in a capacitor-forming device. This device consisted of two steel blocks held together by four screws, with each inner face containing a circular cavity slightly greater in diameter than the capacitor electrodes and half the depth of the desired capacitor thickness. After assembly the device was clamped

together tightly with a C-clamp and the entire apparatus placed in an oven. The oven was turned on and heated to 182-184°C over a period of three hours. After cooling and disassembling the apparatus, the capacitor thus prepared was charged to 1 volt and found to contain 0.15 coulombs (0.15 farads). The ESR was measured as 11.5 ohms.

While this capacitor showed improvement over the MEEP capacitor, several other similar preparations gave capacitors with poor or no capacitance. It was subsequently determined that water content may play a very significant role in the performance of the membrane as a capacitor electrolyte, and the imprecise temperature control in the preparation may have substantially varied the moisture content of different capacitors. All additional capacitors were fabricated by another technique.

A press was constructed of 0.25 inch thick pieces of 6064 aluminum as shown in Figure 1. A 0.75 inch hole in the center plate was designed to contain the capacitor assembly, with the square
(4 x 4 inch) plate fixed to the
circular plate with recessed screws.
The projection in the center of the top
piece had a diameter of 0.625 inches
and was fitted with a Delrin sleeve so
that its total diameter was just
sufficiently under .75 inch that it
could fit into the cavity of the lower
circular plate. A capacitor assembly
was put into the cavity and the
apparatus placed in a Carver press with
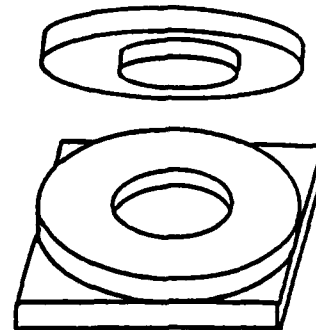
Figure 1. Apparatus for Pressing Capacitors.

heated platens. With the platens preheated to 185°C the assembly was pressed

to 5000 psi for 5 minutes. The assembly was then removed and the capacitor

retrieved by removing both top and bottom pieces from the center section.

A capacitor made from this same membrane using the apparatus of Figure 1

showed poor capacitance (.05 farads, ESR = 6.3 ohms), but after soaking in

water overnight gave excellent results of 0.43 farads and ESR = 1.6 ohms.

However, after a 1 volt charge the potential dropped to .77 volts in 60

seconds.

The low EW polymer gave the most favorable results. The low equivalent

weight molecule contains a higher concentration of mobile ions, as well as a

shorter chain length to facilitate micropore impregnation.

A capacitor prepared by pressing to a total thickness of 10 mils (two

4-mil electrodes and 2 mils of polymer electrolyte) at 185°C (5000 psi, 5

minutes) had a capacitance of 0.33 farads and ESR = 5.3 ohms. After water

treatment the capacitance was raised to 0.66 farads with ESR = 1.2 ohms.

Furthermore, this capacitor exhibited the greatest voltage stability, dropping

only from 1.00 to 0.93 volts in 60 seconds. The voltage drop is compared for

the high and low EW membrane capacitors in Figure 2.

A temperature study of the low
EW polymer capcitor was carried
out. A new capacitor was prepared
and was not subjected to water
treatment. It was heated or cooled
to desired temperature, then charged
to 1 volt and measured while
continually maintained at that
temperature.
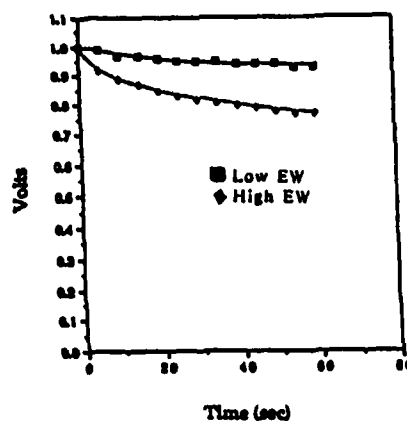
Figure 2. Voltage Stability for Capacitors
made from High and Low Equivalent Weight
Polymers.

The capacitance exhibited a marked temperature dependence. The data are shown in the table below; they provide an essentially linear relationship as shown in Figure 3.

Temperature	Capacitance	ESR (Ohms)
-20	.065	45
-10	.111	23
0	.194	8.6
10	.239	5.7
20	.296	3.4
30	.390	2.4
40	.420	1.7
50	.485	1.3
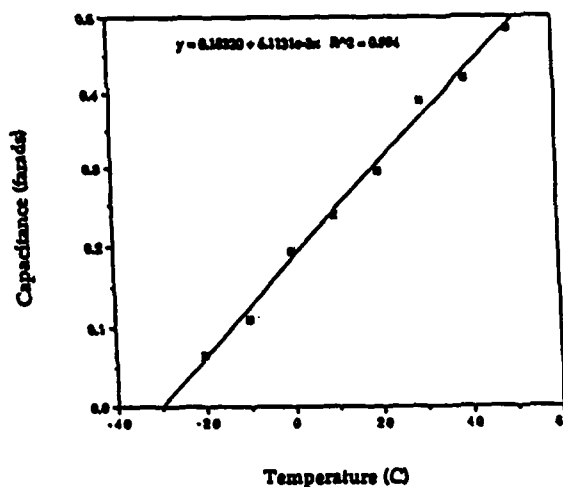
Figure 3. Capacitance as a Function of Temperature for a Low EW Polymer Capacitor.

VI. Photo-activated Switch

In recent years a wide variety of electrically conducting polymers have been synthesized and characterized.[4] Some of these exhibit photoconducting properties; that is, they are insulators unless subjected to photon excitation of electrons into a conducting band. A preliminary study was undertaken to assess the feasibility of using such a polymer as insulator between switch terminals such that visible or ultraviolet radiation could be used to cause dielectric breakdown to activate the switch.

Polyvinylcarbazole (PVK) has excellent insulating properties and is also a photoconductor.[4] A sample of this polymer was prepared by heating vinylcarbazole to its melting point (65°), then adding di-t-butyl peroxide as initiator (approximately 1% by weight). Polymerization occurred slowly; the

melted solution was stirred as it gradually thickened. When sufficient

viscosity had developed, a drop of the solution was placed in contact with two

closely spaced (0.1 - 0.5 mm) copper conductors on a printed circuit board. The

circuit board was then placed in an oven and heated to 180° for two hours to

complete the in-situ polymerization.

Connecting the two copper conductors to a high voltage source (10 kv)

verified the insulating properties of the PVK, and irradiation with a low

intensity UV source was found to initiate dielectric breakdown. Thus it appears

that development of such a photo-activated switch mechanism for fuzing circuits

is feasible.

VII. Recommendations

Further investigation of the photoconducting polymers for use in swiching

mechanisms is warranted. A systematic investigation could establish 1) the

polymer most suited to a particular application, 2) the optimum conditions for

in-situ polymerization and 3) the appropriate dopants that could be used to

extend the conducting sensitivity to desirable wavelengths.

The most promising result of this research is the establishment of ionic

polymer membranes as efficient capacitor electrolytes. The devices prepared in

this study have energy densities far superior to those of any capacitors

previously reported. Research should be continued to determine the role of

water as it affects capacitance. Other solvents with lower volatility and

greater electrochemical stability should be investigated for use in place of

water. This would provide a substantially greater applicable voltage range.

The replacement of protons of the acidic polymer membranes by various

cations should also be investigated. Electrochemically stable ions such as

lithium or quaternary ammonium ions could significantly increase the voltage

range, and a wide variety of such salts should be investigated to determine the best combination for optimum capacitor energy density and voltage stability. A significant leap in capacitor technology is near to realization.

REFERENCES

1. Finello, D., "Laminate Forming Gun Fixture," Air Force Armament Laboratory Technical Report AFATL-TR-89-63, July 1989.

2. Allcock, H.R., Austin, P.E., Neenan, T.X., Sisko, J.T., Blonsky, P.M., Shriver, D.F., "Polyphosphazenes with Etheric Side Groups: Prospective Biochemical and Solid Electrolyte Polymers," Macromolecules, 19, 1508 (1986).

3. Martin, C.W., Ezzell, B.R., Weaver, J.D., "Method for Depositing a Fluorocarbonsulfonic Acid Polymer on a Support from a Solution," U.S. Patent 4,661,411, 1987.

4. Mort, J., "Conductive Polymers," Science, 208, 819 (1980).

1989 USAF-UES SUMMER FACULTY RESEARCH PROGRAM/

GRADUATE STUDENT RESEARCH PROGRAM

Sponsored by the

AIR FORCE OFFICE OF SCIENTIFIC RESEARCH

Conducted by the

Universal Energy Systems, Inc.

<u>FINAL REPORT</u>

<u>MULTISENSOR SEEKER FOR MEDIUM RANGE AIR-TO-AIR MISSILES</u>

Prepared by: D.V. Satish Chandra

Academic Rank: Assistant Professor

Department and
  University: Kansas State University

Research Location: AFATL/AGA
                   Eglin AFB
                   Florida 32542-5434

USAF Researcher: Larry E. Lewis

Date: 28 Aug 89

Contract No: F49620-88-C-0053

Multisensor Seeker for Medium Range

Air-to-Air Missiles

by

D.V. Satish Chandra

ABSTRACT

The principal technology issues identified, and techniques proposed include a cylindrically shaped, frequency scanned, conformal radio frequency (RF) antenna array and a gimbal designed heterodyne/direct double detector infrared (IR) sensor in an array configuration. Alternative design options for both RF and IR sensors are also suggested. A comprehensive summary of advantages and disadvantages for different types of sensors is also provided. Methods of integrating information from the sensors at both pixel-level and system-level to increase the performance of the missile seekers are briefly discussed.

I. INTRODUCTION

Seekers are carried on a missile for the purpose of guiding the missile to its target. A seeker generally consists of collecting optics, detector which converts radiant energy to an electrical signal, and electronics to process the detector signal for the purpose of detecting and tracking targets. Radar and infrared are the most commonly used guidance in air-to-air missiles.

The advanced Development Section of the Air-to-Air Guidance Branch of the USAF Armament Laboratory at Eglin Air Force Base is interested in developing advanced medium range air-to-air missile seekers which would contain multiple sensors. The Advanced Development Section is particularly concerned with the development of active/passive infrared (IR) seeker, active/passive radio frequency (RF) seeker, and multimode seeker containing both IR and RF modes. The increased quantity of data and the diversity in the spectral characteristics of different sensors would aid in enhanced target detection and identification, improved track maintenance and graceful system degradation. Another advantage of using multisensor approach is to achieve near immunity to countermeasures and all weather operation.

My research interests have been in the area of signal processing, image processing, and automatic target recognition. My previous work on the development of algorithms for automatic registration and recognition of television and infrared images contributed to my assignment to the multisensor seeker feasibility study.

II. OBJECTIVES OF THE RESEARCH EFFORT:

Air-to-air missiles built to this day use either radar or infrared guidance to steer a missile on to the target. Radar guidance allows missiles to lock-on to radar returns from their targets and infrared guidance uses the heat radiation from the target to guide the missile. Studies of the air-to-air tactical mission have led to the conclusion that there exists a real need for the development of a multisensor missile seeker with improved target detection and tracking performance and at the same time capable of performing well in adverse weather conditions, and providing virtual immunity to countermeasures.

My assignment as a participant in the 1989 Summer Faculty Research Program was to study the feasibility of developing a multisensor seeker which would contain active IR and RF modes, as well as passive IR and RF modes. The application is for medium range air-to-air missiles. Specific objectives of the current research are the following:

1.   Compile a comprehensive list of advantages and disadvantages for use of each mode.

2.   Identify the technical issues to be solved in developing a multisensor seeker and propose a high level hardware configuration for such a seeker.

3.   Identify ways in which the available modes might best be used.

4.   Develop a set of first order specifications for the system which would allow potential performance to be predicted.

III. COMPARISON OF SEEKER CANDIDATES:

Radar is the commonly used sensor in air-to-air missiles. With radar excellent accuracy of range and radial velocity can be achieved with relative ease using doppler techniques. It also has good fog, cloud and smoke penetration capability. However, radar is easily susceptible to electronic countermeasures and radar imaging is impractical. Also, adequate resolution is difficult to obtain with practical apertures.

Passive infrared sensors detect IR radiation emitted by hot objects due to temperature or emissivity differences. Military targets usually have spots that are easily detected by these sensors. Infrared sensors produce high resolution images, and require small aperture and packaging. In addition, passive IR technology is mature. However, passive sensors do not provide direct range and velocity information, and have less bad weather penetration capability.

Active IR sensors or laser radars (LADARs) use reflectivity differences in the scene to create an image. Active systems provide good range and angular resolution information, have better bad weather penetration, and are insensitive to fire and sun glints. They also have good countermeasure resistance and are compatible with passive systems. Other advantages include, short pulse width, small optical window, low doppler clutter, narrow beam width for precision tracking, and capability for creating intensity, range and doppler images. Active systems provide a stable target profile while thermal edges are unstable. However, active systems produce speckled images and are sensitive to target glints. In addition, LADAR technology is not yet mature and production experience is limited.

Best imaging systems can be obtained by combining both LADAR and IR sensors for multispectral operation in both passive and active modes. The two modes can be operated independently with the capability of wide field-of-view (FOV) search for target detection and narrow FOV operation for target recognition in either active or passive mode. The combined IR/LADAR sensor has additional advantages of accurate target ranging, doppler resolution of target velocities, high image resolution and resistance to counter measures.

One of the most promising new sensor technologies is the IR focal plane array (FPA) technology. The FPA consists of elements sensitive to radiation coupled in the focal plane to a miniaturized readout circuit. They have the advantages of increased sensitivity, improved angular resolution, low cost, reliability, light weight, and capability for wide field of search. However, a few problems such as saturation effects during integration, nonuniformity, and losses in the connection area for high resolution images exist and are yet to be resolved.

IV. MULTISENSOR SEEKER:

Important factors to be considered in the design of a seeker are its reliability, light weight, and small volume. Airborne radar has proved invaluable for its ability to detect targets at long ranges, to measure range, angular position, and relative velocity precisely. Also, radar has the important advantage of performing better than the IR sensor in adverse weather conditions. However, radar is easily susceptible to electronic countermeasures and imaging by radar is impractical. The performance of air-to-air missile seekers in clutter and countermeasure environments can be improved by incorporating IR

imaging systems into the missile seeker in addition to the radar.

Because technological advances have made packages smaller and more

affordable, it is now practical to put imaging systems into missile

seekers. IR imagery can be used for target detection, tracking and

recognition of a particular shape of the target at the end of the

flight.

One possible way of incorporating IR and RF sensors into an air-to-

air missile seeker is to use a body-fixed RF conformal array and a

gimballed IR detector array. The cylindrically shaped, frequency

scanned, conformal antenna system [3] that conforms to the 7-inch

diameter airframe of the missile is shown in Figure 1. It consists of a

horizontally polarized (polarization circumferential to the missile

body) frequency scanning array, a fixed beam vertically polarized

(polarization perpendicular to the missile body) endfire array, a

switching network, a monopulse feed network, and an antenna controller.

The frequency scanning array is composed of dielectric leaky-wave line

sources located on the cylindrical surface and the endfire array

consists of four discrete slot line sources located on the same cylinder

at 90-degree intervals. The field of view (FOV) coverage of the two

interlaced arrays is shown in Figure 2. The scanning array and the

endfire array switch and fed network is shown in Figure 3. The scanning

array feed network provides two-plane monopulse sum and difference

outputs (Σ, $\Delta\theta$ and $\Delta\phi$). The endfire line sources are designed to operate

in pairs (L,R or T,B). Significant features of this system are low side

lobes, rapid scan and wide FOV about the endfire capability. The

baseline conformal array system specifications can be found in [3].

The infrared sensor consists of a dual active/passive imaging system mounted or a gimballed platform. The schematic diagram of a possible system implementation [4] with heterodyne/direct double detector array employing simultaneous imaging is shown in Figure 4. The double detector array is substituted at the focal plane of the optical system. The passive imaging system can be built to look at either 3-5 μm or 8-12 μm wavelength region and the active system uses the 10.6 μm laser transmitter. The two modes can be operated independently with each mode performing the function for which it is best suited. The baseline active/passive imaging system parameters are given in Table I. One possible way of incorporating both RF and IR sensors, and its associated hardware in the airframe of a missile seeker is shown in Figure 5.

Table I. Baseline Dual active/Passive Imaging System Parameters

Laser photon energy ($h\nu$)	1.87×10^{-20}J(10.6μm)
Transmitter power (P_T)	10 W
Transmitter/Receiver aperture (D)	10 cm
Angular resolution (α)	130 μrad
Number of detectors (N)	100 active/100 passive
Bandwidth (B)	10 kHz
Detector area (A)	10^{-4}cm^2
Detectivity (D*)	3.5×10^{10}cm $\sqrt{\text{Hz}}$/W
Heterodyne efficiency (η)	0.25
Passive optical efficiency (ϵ_p)	0.2
Active optical efficiency (ϵ_a)	0.1
Average scene reflectivity (ρ)	0.1
$\partial M/\partial T$ (at T = 300 K in 8 to 14 μm band)	0.00026/K

An alternative design for a multisensor seeker for air-to-air missiles is to use a body-fixed RF conformal array antenna such as the one described above and a relatively mature passive IR imaging sensor. Several IR staring sensors are available for missile seeker application. One such FPA is the 256 x 256 schottky barrier MOS hybrid PtSi detector

FPA developed by Hughes Aircraft [5]. The performance characteristics

of this FPA is given in Table II. The hardware block diagram is shown

in Figure 6. Another FPA architecture [8], expected to be developed in

the 1990s, uses the Z-direction or the optical radiation propagation

direction as a region for electronic circuitry and on-focal plane signal

processing. The use of Z-technology FPA to missile seeker has the

advantages of weight and power reductions in signal processing in

addition to its parallel processing capability. Another configuration

of a multisensor seeker incorporating a dipole RF antenna fixed to the

body of the missile and a passive IR focal plane sensor on a gimballed

platform as suggested by Texas Instruments [6] is shown in Figure 7.

Table II. FPA Performance Characteristics

OPERATING TEMPERATURE	77K
DETECTOR INTEGRATION TIME	16.67 milliseconds
300K BACKGROUND	9×10^4 ELECTRON/PIXEL AT FPA OUTPUT
DARK CURRENT	1.3×10^5 ELECTRON/PIXEL AT FPA OUTPUT
SIGNAL SATURATION	4.5×10^5 ELECTRON/PIXEL AT FPA OUTPUT
THERMAL RESPONSE (3.5 m LONG PASS)	3.4×10^3 ELECTRONS PER PIXEL/K
TEMPORAL NOISE	300 μV RMS AT FPA OUTPUT
D*	$1.28 \times 10^{11} \dfrac{cm - (Hz)^{1/2}}{w}$
PERCENT BLIP	39 PERCENT
NETD AT FPA	0.11°K
DYANAMIC RANGE	63dbv

V. CHOICE OF WAVE LENGTH:

Radars operating in the 3 centimeter (10 GHz) region of the X-band

provide adequate performance in smaller packages with reasonably low

atmospheric attenuation. Also, narrow bandwidths, providing high power

densities and excellent angular resolution can be achieved with antennas

small enough to fit in the small airframe of missile seekers.

Passive infrared systems use temperature or emissivity differences to produce an image, and can be built to operate in the 3-5 or 8-12 micron atmospheric windows. The 8-12 μm spectral region provides significantly better performance in low-visibility weather conditions and conditions or aerosols (fog, haze and smoke) than does the 3-5 μm region. The overall emissivity (photon flux) of tactical targets and their environmental scenes is greater in the 8-12 μm region resulting in a larger signal-to-noise ratio (SNR) between target and background signatures. However, in clear, high humidity conditions, transmissivity is better in the 3-5 μm band. If the objective is to detect isolated hot objects against a relatively cold background, the 3-5 μm band would be more suitable. For target recognition, it is important to reliably resolve small differences in temperature and emissivity throughout the imaged scene than to locate a few isolated, warm objects. Because of these fundamental advantages of 8-12 μm wavelength emissivity and transmissivity phenomena, IR sensors operating in the 8-12 μm wave band offer the best potential for imaging seekers requiring the greatest performance under the most severely demanding operating conditions.

Active systems use reflectivity differences in the scene to produce an image and usually operate in the 1.06 μm or 10.6 μm wavelength region. The 10.6 μm laser beam is known to be less attenuated by atmospheric aerosols than the 1.06 μm beam. As a result it penetrates fog and haze more easily. Also, at 10.6 μm it is possible to achieve the very large conversion gains achievable with heterodyne detection techniques and power requirements are less than 1.06 μm.

VI. MULTISENSOR FUSION:

The sensor fusion problem entails the development of methods to control and combine the data from multiple sensors for tracking and identification. The probability of sustaining a track can be improved over that of a single sensor. For example, IR detections can maintain a track that might otherwise be lost during a fade in the radar return due to cross section scintillation or jamming. Radar and IR sensors can be used synergistically with radar providing accurate angle measurements. As it is impractical for LADAR to act as a broad area search sensor, RF and FLIR sensors can be used for wide field search at long distance.

In a multiple sensor tracking system data can be fused at sensor-level or central-level or some combination of both. Central level tracking is probably the best if the system can provide adequate data transfer. However, if pure central-level tracking is used, the degraded data from one of the sensors can lead to poor central-level tracking. Excellent tracking continuity and accuracy can be obtained by combining both sensor- and central-level tracks, provided increased computational complexity and data transfer load are tolerable. The simplest approach to combining data is the heuristic method such as voting and the use of possibility theory. This method uses the experience based on large training sets. Heuristic approaches tend to throw away valuable statistical information and their region of valid application is difficult to define. However, heuristic approaches are often the best when statistical information can not be obtained with sufficient accuracy. Two alternative mathematical approaches for fusion are Bayesian and Dempster-Shafer methods.

Bayesian approach uses Baye's rule to update belief in a hypothesis based on new evidence. The application of Bayesian approach to target detection and tracking requires a complete and accurate knowledge of both the a priori probability distribution and the conditional probability matrices. Bayes theory offers a highly formalized and rigorous way to assign and propagate confidences. Also, it is unable to express itself in all sensor-specific levels of abstraction and has difficulty maintaining an accurate confidence representation. Another potential problem with Bayes theory is that it provides no formal manner in which to resolve sensor conflicts.

Dempster-Shafer evidential reasoning (DSER) combines the Bayesian notion of probabilities with Boolean notion of sets. Evidential reasoning relaxes some of the extensive information requirements of classical Bayesian probability theory, while maintaining its formal appeal, and is therefore more natural for a wide range of problems. A weakness of the Bayesian approach, the lack of a convenient representation for ignorance or uncertainty, is handled by the DSER by allowing the assignment of a probability mass value directly to uncertainty. Dempster-Shafer reasoning can accurately and efficiently manipulate information at various levels of abstraction. A major disadvantage of DSER is that the algorithm's complexity increases geometrically as the number of sensors increases, as all original sensor declarations are forever preserved. However, this may not be of great concern if only a few sensors are involved. The generalized multisensor system architecture is shown in Figure 8.

Endfire Line Source (4)

Scanning Line Source (32)
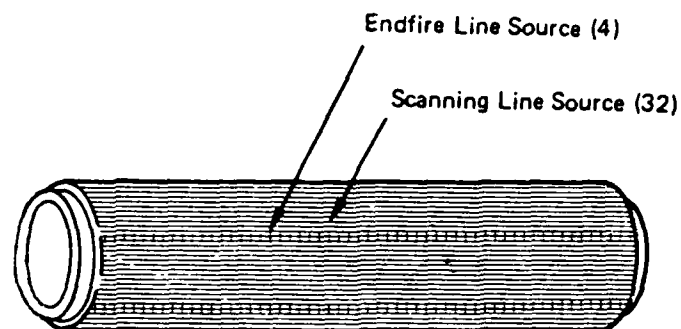
Figure 1.   Conformal RF Antenna Array

Scanning Array Coverage

Endfire Coverage

(a) Endfire and Scanning
Array Coverage

Scanning Array Beams

Forward

Aft

Squinted
Endfire
Beams

Beam 1
Beam 2
Beam 3

(b) θ and ϕ
Coordinates
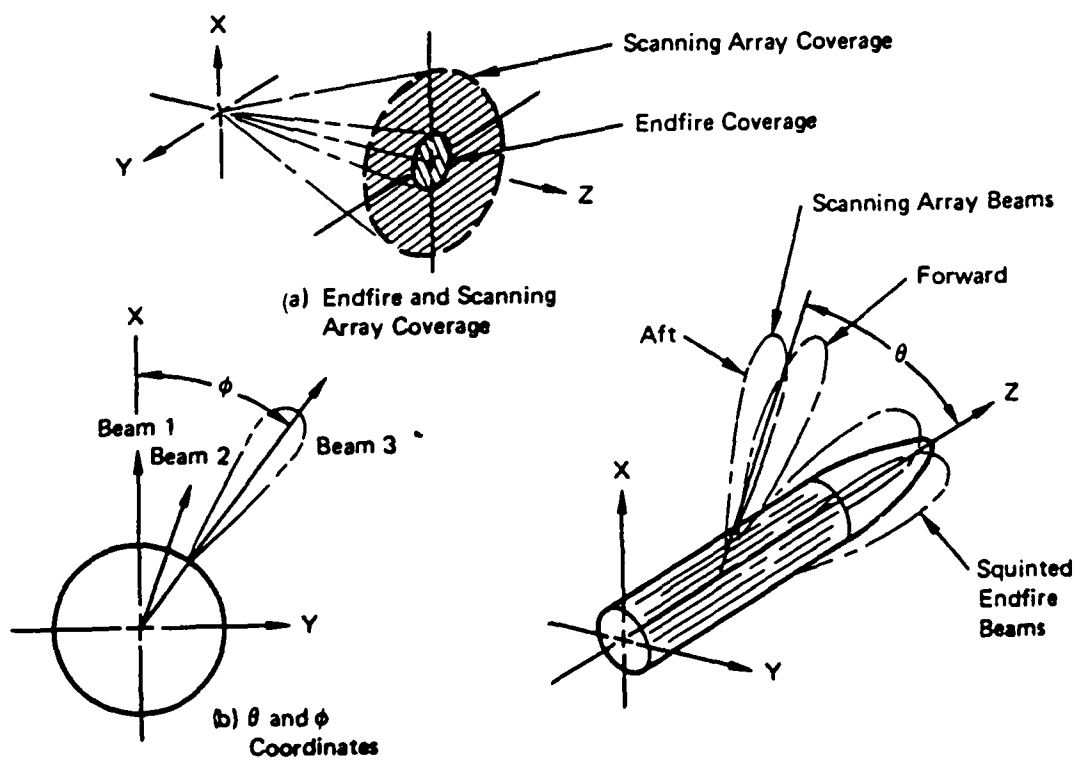
Figure 2.   Beam Coverage and Coordinates
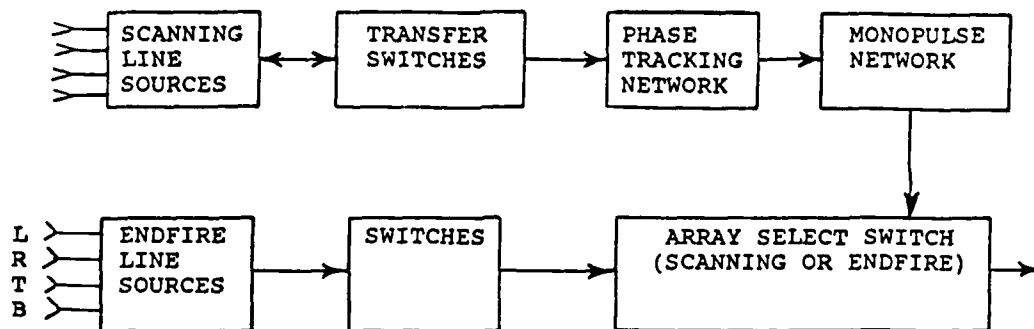
Figure 3. Switch and Feed Network for Scanning and Endfire Arrays
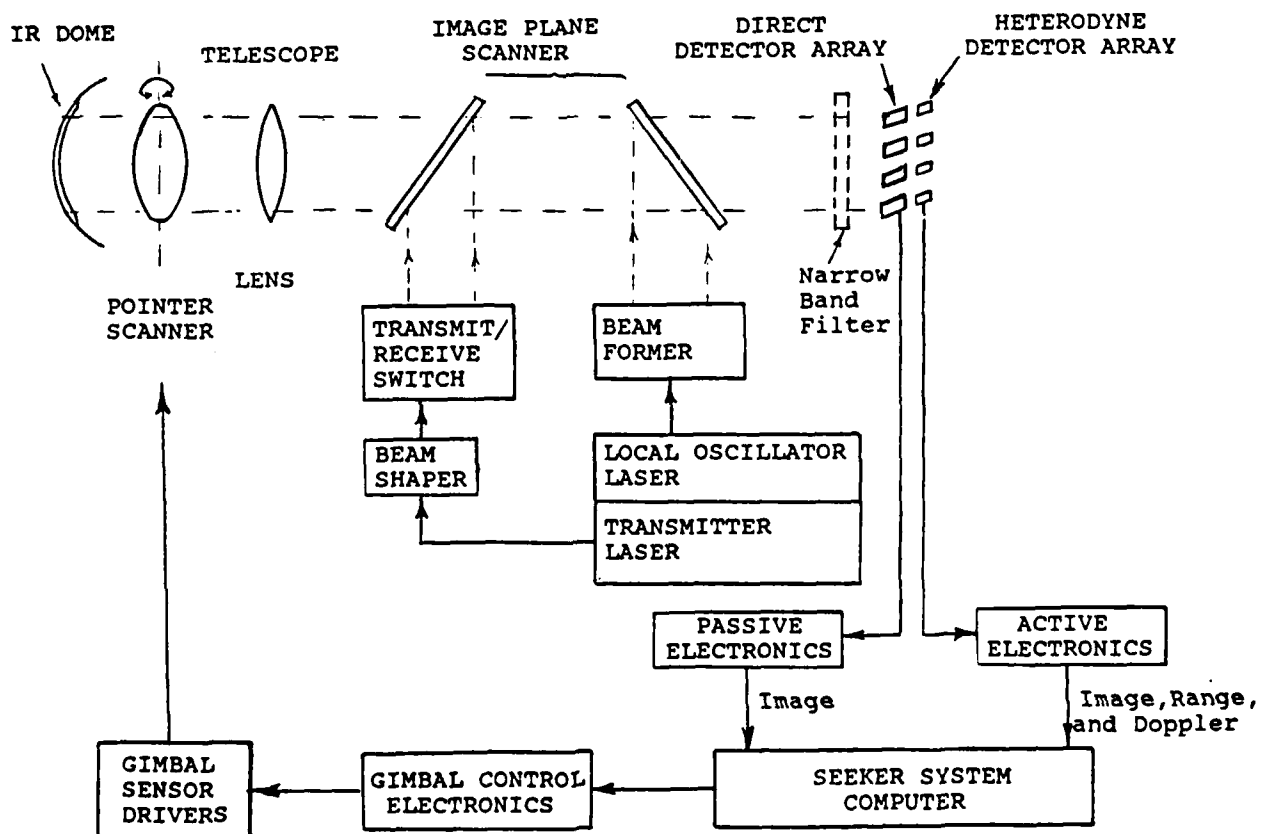
Figure 4. Functional Block Diagram of Passive/Active IR sensor
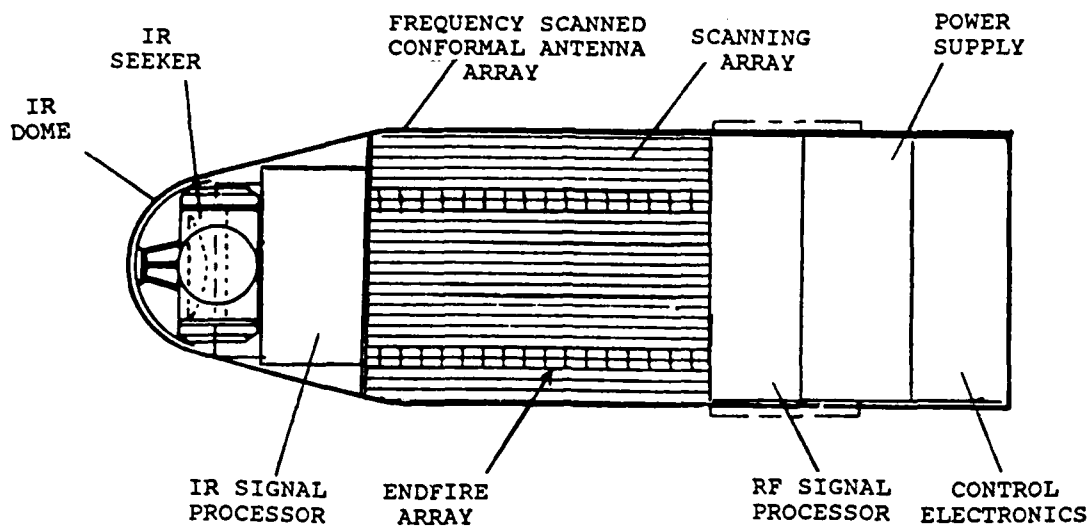
Figure 5. Multisensor Seeker with RF/IR Modes
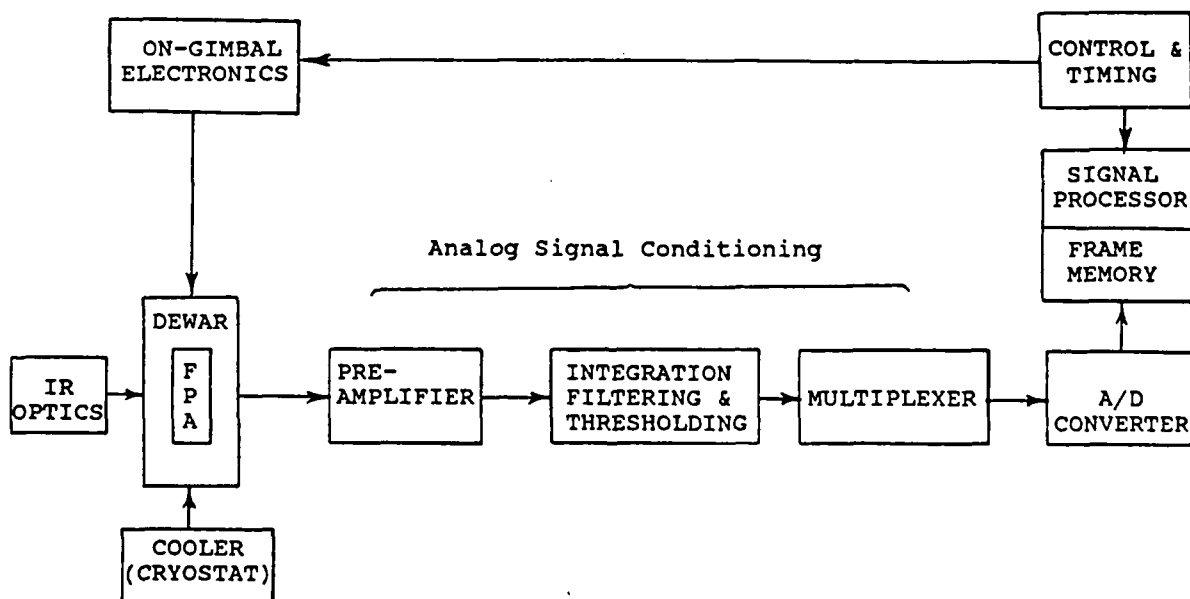
Figure 6. Functional Block Diagram of Infrared FPA
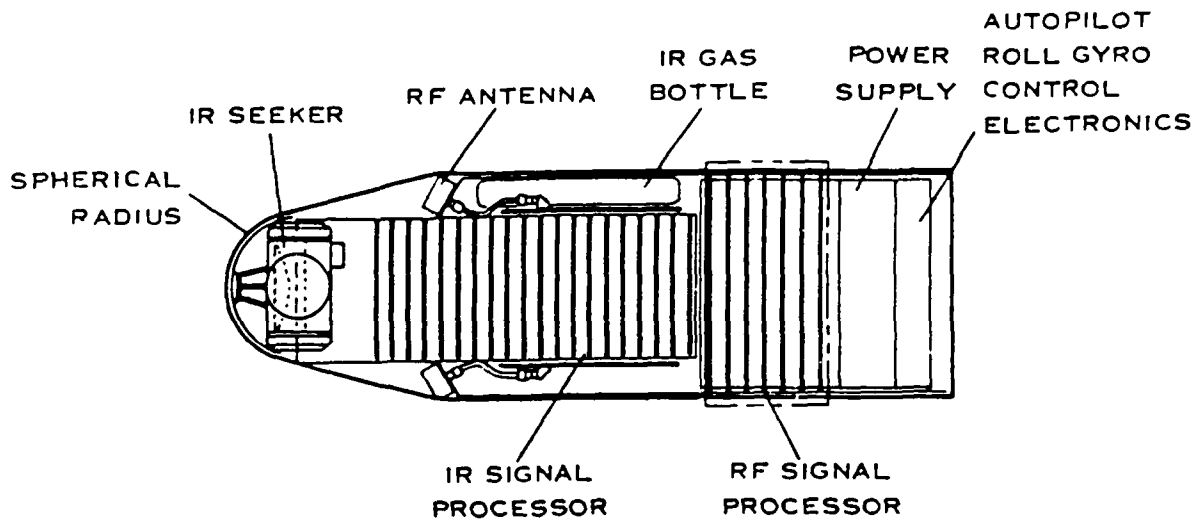
Figure 7. Dual-Mode IR/RF Missile Seeker

SP/KF - Signal Processor/Kalman Filter
FM   - Frame Memory
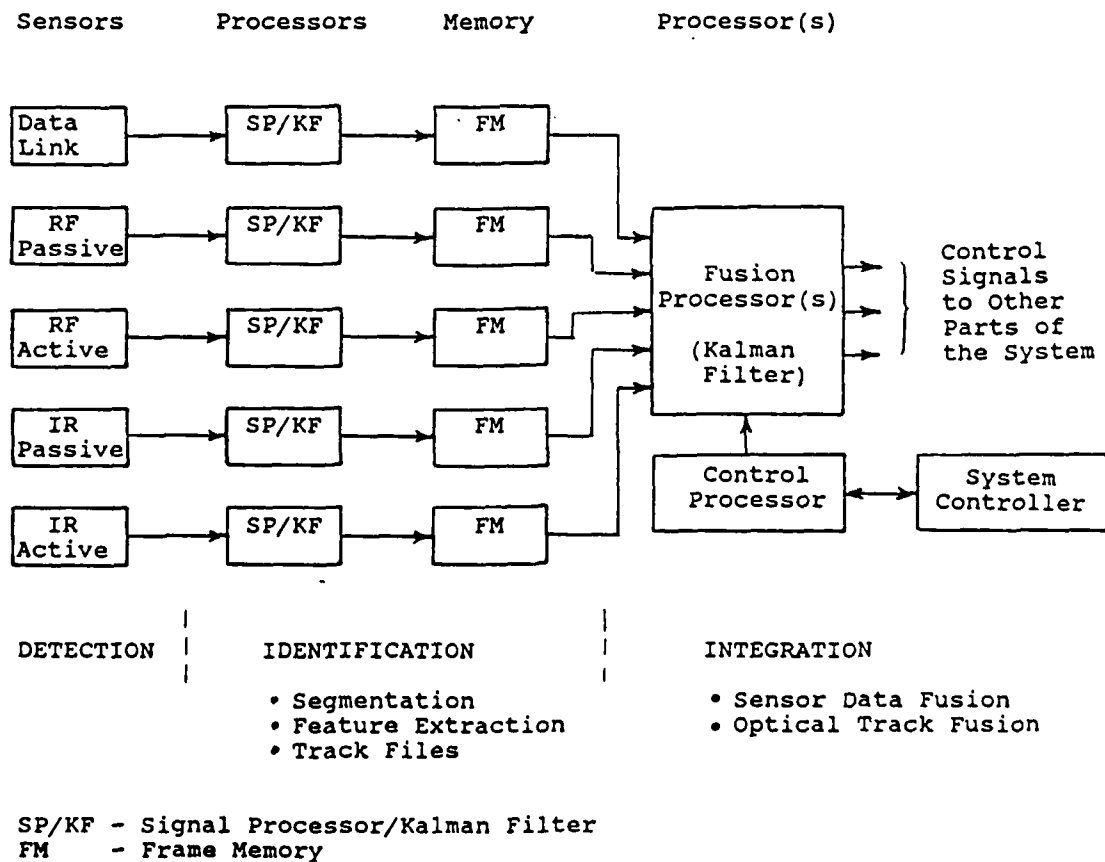
Figure 8. Multisensor System Architecture

VII. RECOMMENDATIONS:

a. Use of the latest miniaturization techniques and technological advances in the design of sensors and associated components makes feasible the development of a missile seeker employing multiple sensors requiring extreme computational requirements. Multisensor system will improve the performance of the missile seeker system and even add the capability for countermeasures. A configuration of a multisensor missile seeker with a body-fixed RF conformal antenna array and gimballed heterodyne/direct infrared imaging detector array is suggested as a promising design option for meeting accuracy, adverse weather conditions, and near immunity to countermeasures. Other possible configurations for the RF antenna include a conical microstrip antenna array mounted on the upper part of the radome and a dipole radar antenna mounted inside the missile body. These fixed configurations of the RF antenna are preferred in order to keep the inner space free for the gimbal mounted IR sensor.

b. Focal plane array provides significant advantages over the current generation IR detectors. These include a greater sensitivity in detecting and locking onto lower contrast targets, improved target information, generated by the large number of detectors which aids in reducing the potential confusion between imaged targets and clutter, and the ability to provide better terminal guidance by imaging the target. Also, FPA can be used with very simple, small-sized optics, allowing size and weight-reduction benefits for smaller diameter missile seeker designs. Hughes Aircraft has developed a 256 x 256 having the resolution, fill factor and other

characteristics needed for missile seeker sensors. The Z-technology approach, with low power, small weight, and on-focal plane processing capability provides another promising direct viewing IR imaging sensor system for air-to-air missiles.

c. In order to develop a robust system which employs multiple sensors it is necessary to integrate information from the sensors at both system level and sensor level. Heuristic approaches to multisensor fusion are often the best when sufficient statistical information is not available. Also, evidential reasoning approach, which can efficiently manipulate information at various levels of abstraction, is preferred to the statistical Bayesian approach. Another promising approach is to use neural networks for evidence combination. Neural network in addition to its learning capability, has the advantage of extremely fast implementation and graceful degradation.

d. In order to reduce the vulnerability of the launch aircraft it is desirable to provide the missile "lock-on-after-launch" capability. Now, it seems possible to achieve this due to the progress made in sensor and VHSIC technology. The follow-on research should look into efficient ways of combining information from multiple sensors at both pixel level and system level in order to enhance the target detection, identification, and tracking performance. Efficient target detection and recognition algorithms are to be developed for medium range, short range, and terminal guidance phases of the weapon delivery. Multisensor data fusion, when integrated with automatic target recognition system, can provide the intelligent seeker system the capability of a very smart weapon system.

Acknowledgements

REFERENCES

[1] George W. Stimson, Introduction to Airborne Radar, Hughes Aircraft
     Company, El Segundo, CA, 1983.

[2] Samuel S. Blackman, Multiple-Target Tracking with Radar
     Applications, Artech House, Inc., Norwood, MA, 1986.

[3] C.T. Brumbaugh, Frequency Scanned Conformal Antenna System
     Development Program, AFATL-TR-81-17, February 1981.

[4] R.C. Horney, "Dual Active/Passive Infrared Imaging Systems, Optical
     Engineering, Vol. 20, No. 6, pp. 976-980, Nov./Dec. 1981.

[5] R.A. Guilera, 256x256 Hybrid Schottky Focal Plane Arrays, SPIE Vol.
     782, Infrared Sensors and Sensor Fusion, pp. 108-113, 1987.

[6] Advanced Fire and Forget System Study, Texas Instruments, Inc.,
     Dallas Equipment Group, June 30, 1981.

[7] Focal Plane Arrays: Technology and Applications, SPIE Proc., Vol.
     865, November 1987.

[8] Infrared Detectors and Arrays, SPIE Proc., Vol 930, April 1988.

[9] P.L. Bogler, Shafer-Dempster Reasoning with Applications to
     Multisensor Target Identification Systems, IEEE Trans. Syst., Man,
     Cybern., Vol SMC-17, pp. 968-977, Nov. 1987.

[10] G. Shafer, A Mathematical Theory of Evidence, Princeton, NJ:
     Princeton Univ. Press, 1976.

1989 USAF-UES SUMMER FACULTY RESEARCH PROGRAM

GRADUATE STUDENT RESEARCH PROGRAM

Sponsored by the

AIR FORCE OFFICE OF SCIENTIFIC RESEARCH

Conducted by the

Universal Energy Systems, Inc.

FINAL REPORT

Extended Kalman Filter Tuning and Alternative Techniques

Prepared By: David A. Cicci, Ph.D.

Academic Rank: Assistant Professor

Department and Aerospace Engineering Department

University: Auburn University

Research Location: USAFATL/SAI
                   Eglin AFB, FL 32542

USAF Researcher: Craig M. Ewing

Date: August 18, 1989

Contract Number: F49620-88-C-0053

EXTENDED KALMAN FILTER TUNING AND ALTERNATIVE TECHNIQUES

by

David A. Cicci

ABSTRACT

The guidance software for a Lightweight Exoatmospheric Projectile
Simulation (LEAPSIM) was modified in order for the seeker to acquire the
target earlier in the trajectory. This required the terminal guidance
Extended Kalman Filter (EKF) to operate for a significantly longer period
of time. The EKF (as developed) was diverging and providing poor estimates
of predicted miss distances. This terminal guidance EKF was modified and
"tuned" to provide the required predicted miss distances of less than one
meter.

As an alternative to the process of tuning an EKF, a sequential estimator
based upon the theory of ridge-type estimation was developed. This
modified filter is adaptive and will not require tuning of the noise
parameters to prevent divergence. This filter was tested in the terminal
guidance phase of the LEAPSIM software.

ACKNOWLEDGMENTS

I wish to thank the Air Force Systems Command and the Air Force Office of Scientific Research for their sponsorship of this research program. I also wish to thank Universal Energy Systems, Inc. for their help in the administrative and directional aspects of this program.

In addition, I would like to thank the Air Force Armament Laboratory for providing a truly rewarding experience. In particular, I am grateful to Dr Norman Klausutis, Mr John Gagliano, Ms Sandra Lefstad, Mr Rick Wehling, Mr Craig Ewing, and Ms Anne Carstens for the assistance they've provided during this research period.

I. INTRODUCTION:

The Guided Interceptor Technology Branch of the Air Force Armament Laboratory is charged with the development of interceptor technology to be used on the kinetic energy weapon systems currently being considered for the Strategic Defense Initiative (SDI) program. The development of such technology requires the application of state-of-the-art concepts in guidance laws, control theory, estimation theory, and astrodynamics. Algorithms are currently being developed which will eventually be incorporated into onboard electronics responsible for the interceptor homing process.

My research interests are primarily in the areas of estimation theory and astrodynamics. Recent publications address estimation in ill-conditioned and unobservable orbit determination problems. Current research involves the development of sequential estimation techniques for use in problems having angles only measurements, and improvements in the methods of "quick-look" identification of foreign launch technology.

II. OBJECTIVES OF THE RESEARCH EFFORT:

The objectives set forth for this summer research program were to develop improved guidance and control algorithms for use in the kinetic energy weapon systems of the SDI program. The improved algorithms would be incorporated into interceptor simulations currently in use by the Guided Interceptor Technology Branch.

Specifically, my assignment was to evaluate the terminal guidance phase of the LEAPSIM software and determine areas in which its performance could be enhanced. The major problem was that the current filter was providing diverging results. A large amount of time was devoted to determining the proper noise parameters to be used in the EKF, i.e., tuning the filter, in order to achieve an acceptable predicted miss distance. This type of tuning effort is common in EKF applications.

In order to alleviate the problem of EKF tuning in future simulations, work was begun on the development of an adaptive-type filter to replace the EKF currently used. This adaptive filter would essentially be self-tuning and could be easily implemented into the existing software. Completion and verification of this modified sequential filter would be a major research accomplishment in the field of estimation theory.

III.

a. The original EKF provided a predicted miss distance for the given interceptor/target engagement of 9.39 meters. Plots of the position, velocity, and acceleration errors are provided in the attached Figures 1-3. The approach taken to reduce the miss distance included the following steps:

1. Review of filtering logic.

2. Derivation of the filtering equations.

3. Adjustment of the a priori covariance matrix to better match the predictions (Candy, 1986).

4. Addition of an appropriate value of process noise to the covariance propagation equations in order to establish minimum values for certain covariance terms.

b. The analysis performed in (a) yielded the following results:

1. The variable TG_RCLOSE was not being calculated within the terminal filter. This must be done since the terminal phase is now operating approximately ten times longer due to the earlier target acquisition.

2. The variance resulting from the inclusion of process noise in the solution was represented as Q t, whereas the variance should have been represented simply by Q (Maybeck, 1979). This will result in the value of Q being 100 times smaller.

3. The original values of the a priori covariance terms used in the solution were:

$$P_1 = 5929.0 \qquad P_2 = 0.0 \qquad P_3 = 135.0$$

$$P_4 = 25.0 \qquad P_5 = 0.0 \qquad P_6 = 7.0$$

Modified values which provide for more consistent error reduction are:

$$P_1 = 6.0 \times 10^5 \qquad P_2 = 1.6 \times 10^5 \qquad P_3 = 2.5 \times 10^4$$

$$P_4 = 1.0 \times 10^5 \qquad P_5 = 2.0 \times 10^4 \qquad P_6 = 6.0 \times 10^3$$

4. Since the target is not maneuvering, Q can be considered to account for process noise rather than unmodeled accelerations. This results in the elimination of the aspect angle in the determination of Q (Tapley, 1973). Also, the optimal value of Q, to be used in the acceleration components only, has been determined to be 400.0. Running the simulation with the modifications described above provides a predicted miss distance of 1.52cm as compared to the original miss distance of 9.39 meters. Plots of the position, velocity, and acceleration errors for this modified filter are provided in the attached Figures 4-6.

IV.

a. The development of an adaptive-type sequential estimator was based upon the theory of ridge-type estimation (Cicci, 1987). Ridge-type estimators have been successfully used in orbit determination problems in a batch mode (Cicci and Tapley, 1988). From this batch solution form, a sequential form of the estimator involves the use of a biasing parameter $\hat{k}$, which is calculated from the data at each observation time. From the value of $\hat{k}$, the error covariance matrix can be determined, if desired.

b. Derivation of the sequential ridge-type estimator provides a new set of filter equations as follows:

$$\hat{x} = \bar{x} + K[y - H\bar{x}]$$

$$P = [I_n - KH]/\hat{k}$$

where:

$$K = H^T[HH^T + \hat{k}\,\hat{R}]^{-1}$$

D_R = (n X n) diagonal matrix with elements D_{R_i},

$$D_{R_i} = [(H^T \hat{R}^{-1} H)_{ii}]^{-1/2}, \qquad i = 1, \ldots, n$$

$$\hat{R} = y - H\hat{x}$$

$$\hat{k} = n/\hat{x}^T D_R^{-2} \hat{x}$$

In the solution process, $\hat{k}$ is solved iteratively with $\hat{x}$. By updating the reference trajectory at each observation time, this sequential estimator can be easily implemented in an extended sequential mode.

This algorithm was incorporated into the existing LEAPSIM program. Preliminary results indicate this filter to be extremely promising, however more development is required.

V. RECOMMENDATIONS:

a. An updated version of LEAPSIM, incorporating the modifications

described in Section III of this report, has been provided to USAF

researcher Craig Ewing. In addition, these modifications have been

discussed in detail with Mr Ewing and Ms Anne Carstens of the Guided

Interceptor Technology Branch. Implementation will simply entail running

the modified version of LEAPSIM.

b. Although the performance of the adaptive filter presented in

Section IV appears quite promising, more work is required on its

development. For this reason, the algorithms are not yet ready to be

implemented. Areas in which more study are required include:

1. Convergence characteristics of the biasing parameter.

2. Divergence characteristics of the calculated error

covariance terms.

3. Covariance calculation versus propagation in the presence of

process noise.

4. Development of a multiple biasing parameter adaptive filter,

i.e., a filter which involves a different biasing parameter for each state

variable, instead of a single biasing parameter applied to all state

variables. The multiple biasing parameter batch filter has been shown

(Cicci, 1987, 1989) to provide substantially more accurate results than the

single biasing parameter case. Similar results are expected for the

sequential estimator.

Completion of the development of the alternative filter will represent a significant addition to the fields of estimation theory and guidance and control. While retaining the characteristics of an EKF, it will have the following advantages over the EKF:

1. The need to manually tune the filter will be eliminated since tuning will be done automatically within the filter itself.

2. The adaptive tuning will allow different types of engagements to be handled without the need to alter the noise parameters for each scenario.

3. Ridge-type estimators have been shown to provide more accurate estimates when the data is ill-conditioned, as is the case when angles-only measurements are used as filter inputs.

4. The adaptive filter will be better suited to handle a maneuvering target than the EKF. This characteristic may be able to provide acceptable target homing without the need to incorporate non-linear estimators in the solution process.

Completion of the development of this adaptive sequential estimator will be the subject of my proposal for the follow-on research program.

LEAPSIM – ORIGINAL CASE
POSITION ERRORS
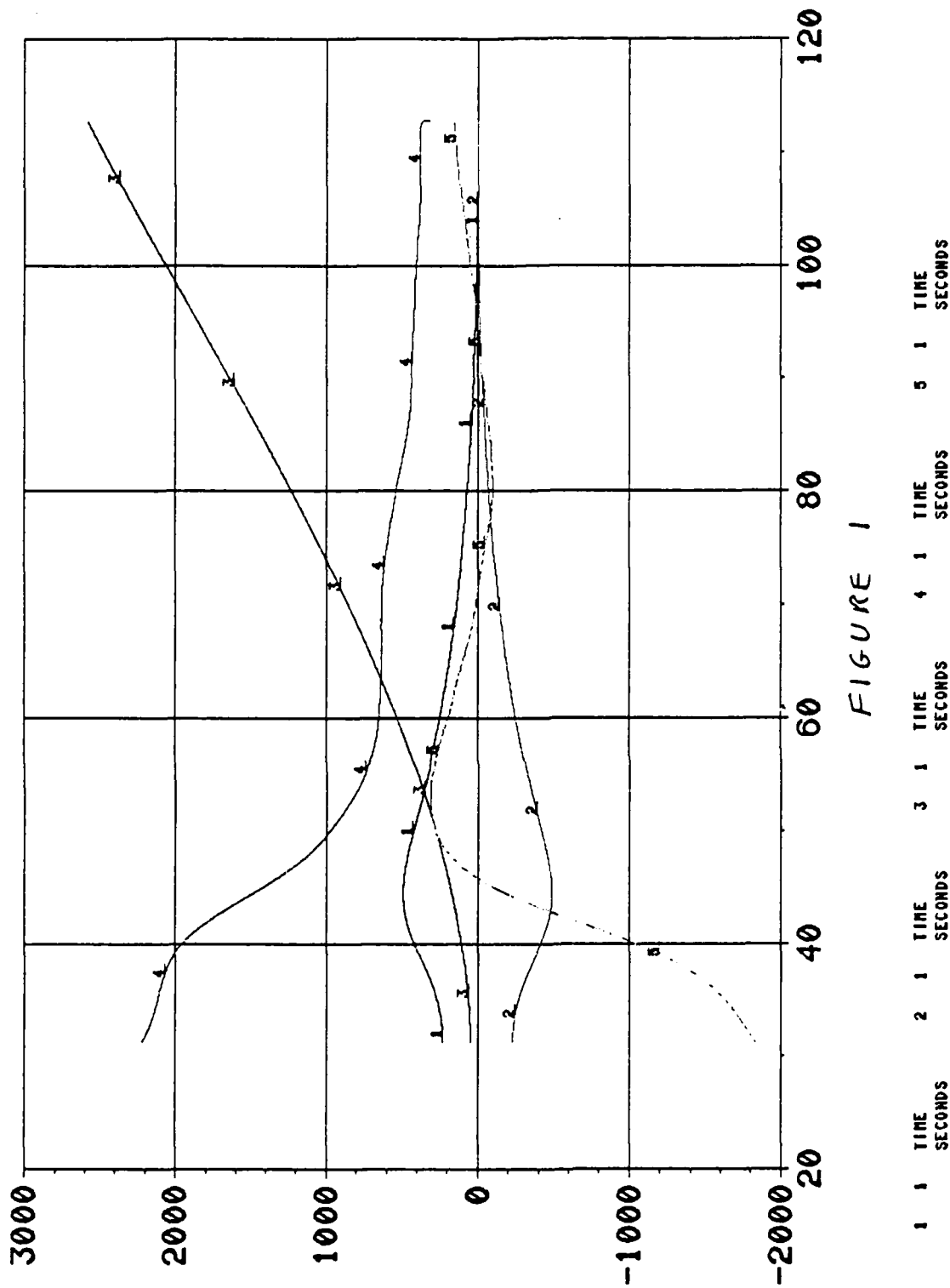
FIGURE 1

		TIME SECONDS			
1	1	TIME SECONDS			
2	1	TIME SECONDS	3	1	TIME SECONDS
4	1	TIME SECONDS	5	1	TIME SECONDS

1   1   ♦ XSDP-KLF
        METERS

2   1   - XSDP-KLF
        METERS

3   1   XPOSER-KLF
        METERS

4   1   YPOSER-KLF
        METERS

5   1   ZPOSER-KLF
        METERS

5-11

FILE 1 = LAUNCH2   05/18/89   PCS   0.37339E+07.   0.20689E+07   0.51357E+07

LEAPSIM – ORIGINAL CASE
VELOCITY ERRORS
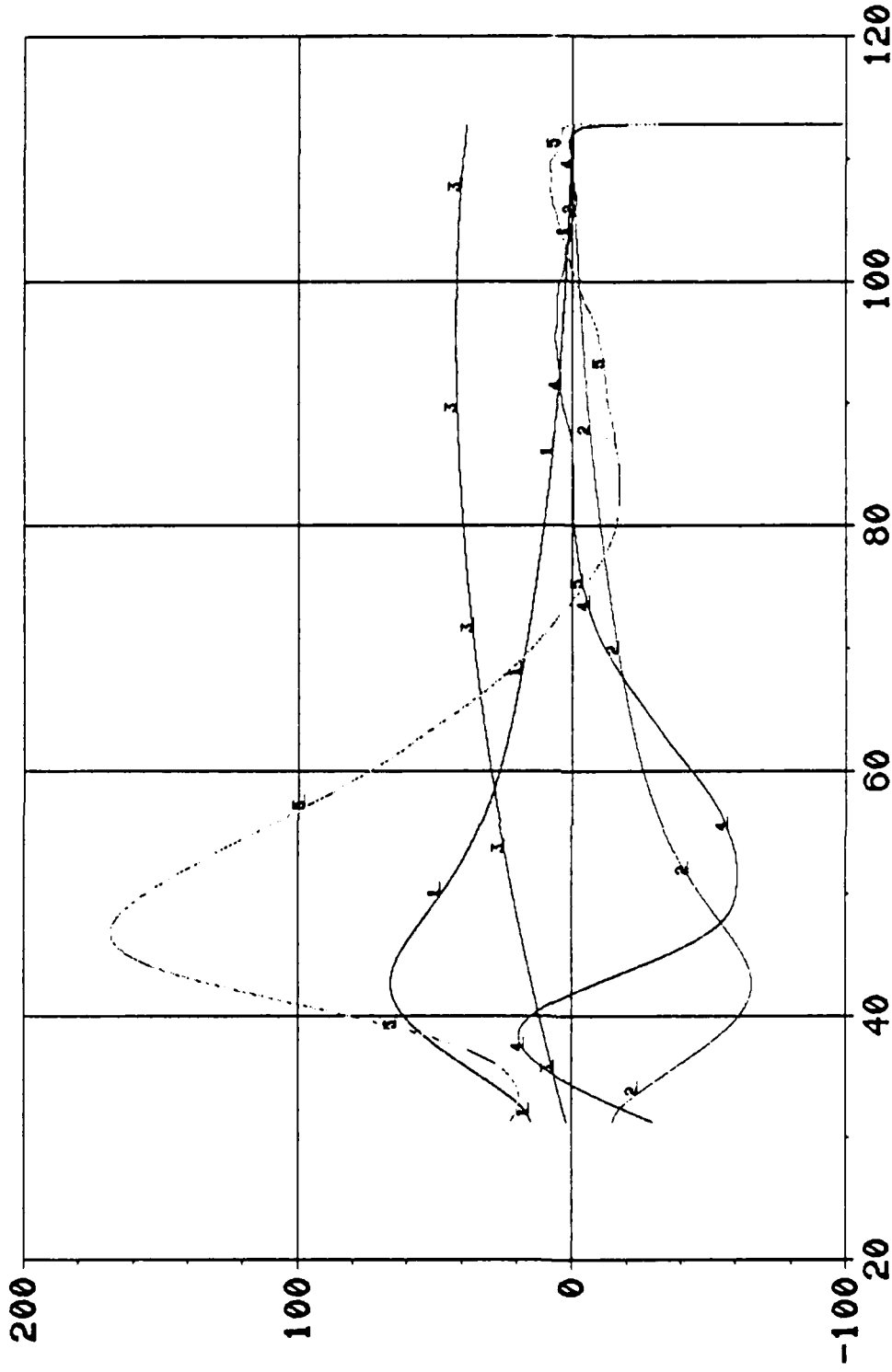
FIGURE 2

CREATED BY:
NAME:CICCI
ORG :AUBURN UNI
DATE:26-JUL-89
TIME:08:56:18

1   1   + XSDV-KLF
        M/SEC

2   1   - XSDV-KLF
        M/SEC

3   1   XVELER-KLF
        M/SEC

4   1   YVELER-KLF
        M/SEC

5   1   ZVELER-KLF
        M/SEC

5-12

1   1   TIME
        SECONDS

2   1   TIME
        SECONDS

3   1   TIME
        SECONDS

4   1   TIME
        SECONDS

5   1   TIME
        SECONDS

PCS   0.37339E+07.   0.20688E+07   0.51357E+07

05/18/89

FILE 1 = LAUNCH2

LEAPSIM — ORIGINAL CASE
ACCELERATION ERRORS
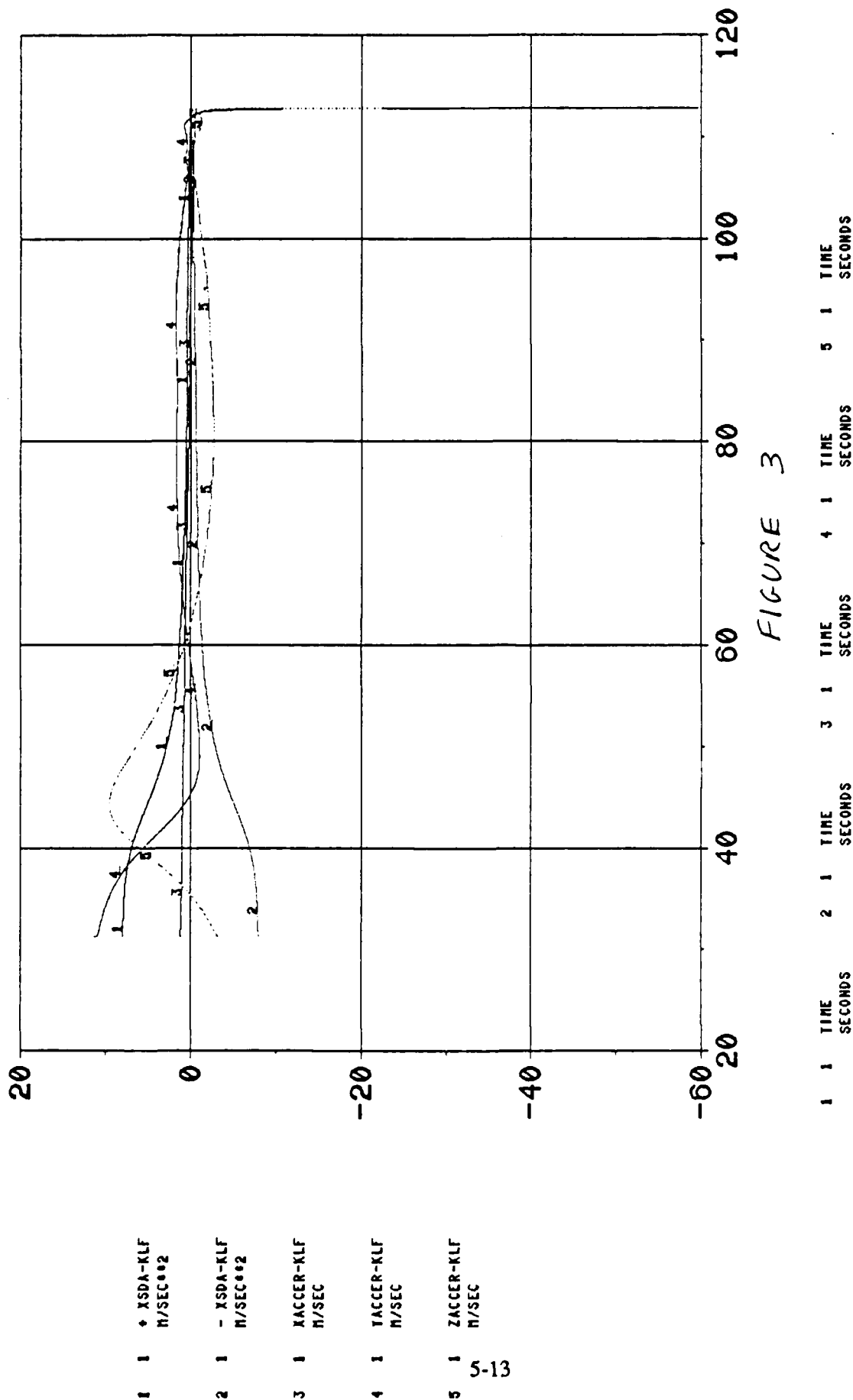
FIGURE 3

CREATED BY:
NAME:CICCI
ORG :AUBURN UNI
DATE:26-JUL-89
TIME:08:56:18

1   1   TIME
        SECONDS

2   1   TIME
        SECONDS

3   1   TIME
        SECONDS

4   1   TIME
        SECONDS

5   1   TIME
        SECONDS

1   • XSDA-KLF
       M/SEC**2

2   1 - XSDA-KLF
       M/SEC**2

3   1 XACCER-KLF
       M/SEC

4   1 TACCER-KLF
       M/SEC

5   1 ZACCER-KLF
       M/SEC

5-13

FILE 1 = LAUNCH2   05/18/89   PCS   0.37339E+07,   0.20689E+07   0.51357E+07

LEAPSIM — MODIFIED CASE
POSITION ERRORS
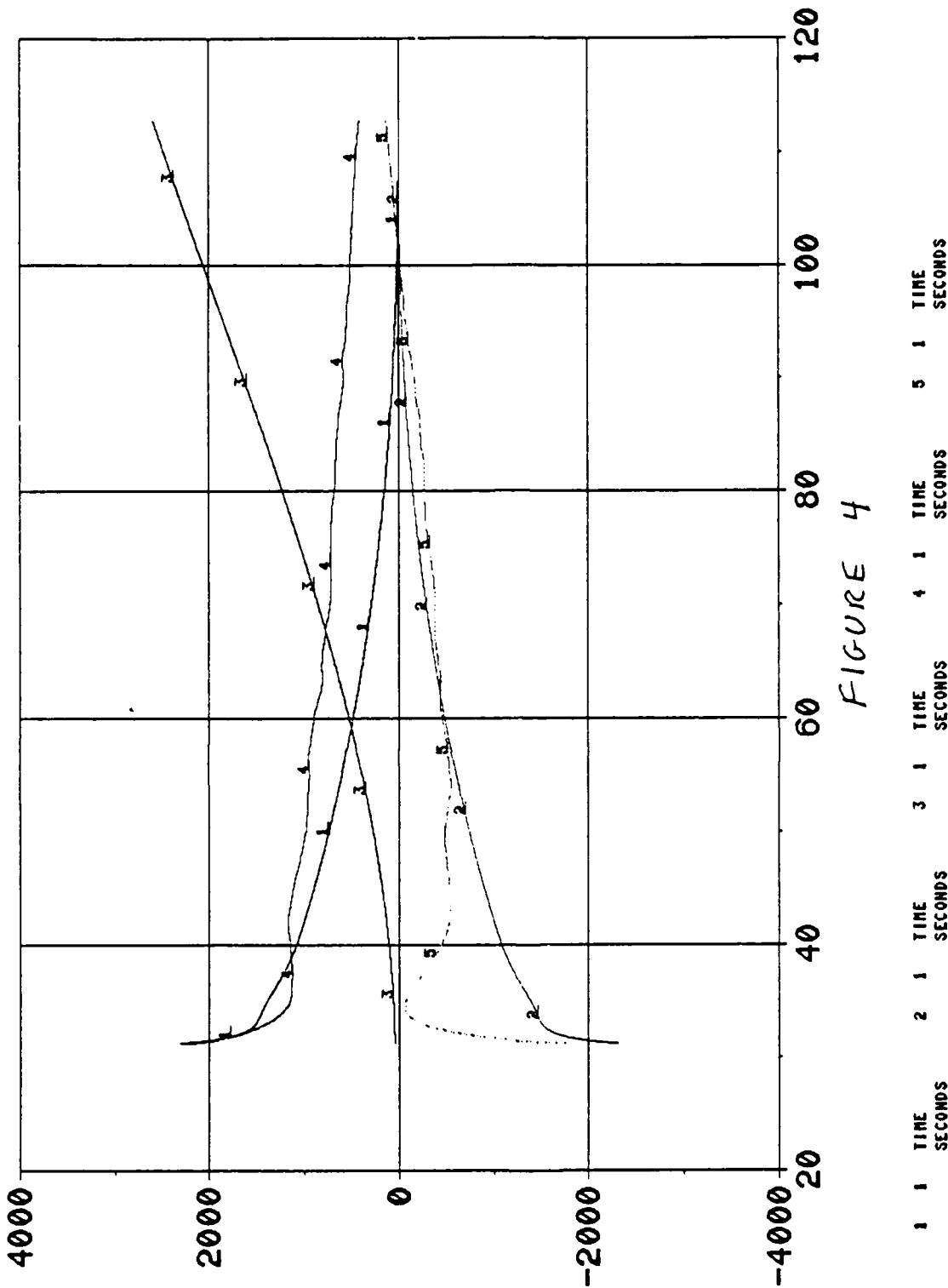
FIGURE 4

1   1   TIME
        SECONDS

2   1   TIME
        SECONDS

3   1   TIME
        SECONDS

4   1   TIME
        SECONDS

5   1   TIME
        SECONDS

PCS   0.37339E+07,   0.20689E+07   0.51357E+07

1   1   + XSDP-KLF
          METERS

2   1   - XSDP-KLF
          METERS

3   1   XPOSER-KLF
          METERS

4   1   YPOSER-KLF
          METERS

5   1   ZPOSER-KLF
          METERS

5-14

FILE 1 = LAUNCH2   05/18/89

LEAPSIM – MODIFIED CASE
VELOCITY ERRORS

FIGURE 5

5-15

LEAPSIM – MODIFIED CASE
ACCELERATION ERRORS
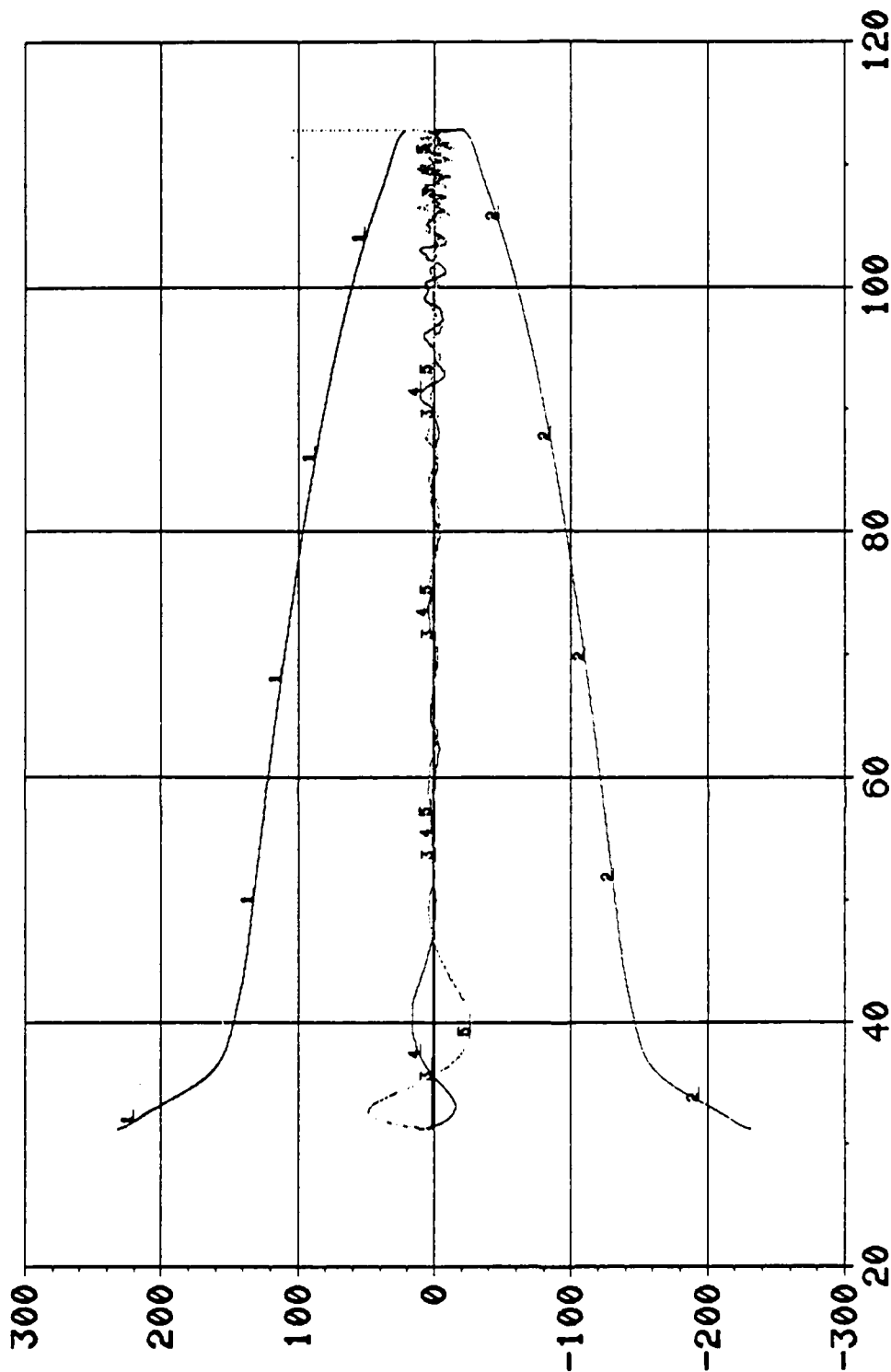
FIGURE 6

5-16

REFERENCES

Candy, J. V. Sicnal Processino: The Model-Based Arprcach, McGraw-Hill Book Company, New York, 1986.

Cicci, D. A. "Optimal A Priori Covariance Selection for the Solution of Nonlinear Inverse Problems," Doctor Dissertation, The University of Texas at Austin, Department of Aerospace Engineering and Engineering Mechanics, August 1987.

Cicci, D. A. and Tapley, B. D. "Optimal Solution of Uncbservable Orbit Determination Problems," Celestial Mechanics, 44, pp. 339-363, 1988.

Maybeck, P. S. Stcchastic Mcdels, Fstimaticn, and Control, Volume I, Academic Press, New York, 1979.

Tapley, B. D. "Statistical Orbit Determination Theory," Recent Advances in Dynamical Astrcncmy, Proceedings of the NATO Advanced Study Institute in Dynamical Astronomy, D. Reidel, Boston, MA, pp. 396-425, 1973.

1989 USAF-UES SUMMER FACULTY RESEARCH PROGRAM/
GRADUATE STUDENT RESEARCH PROGRAM

Sponsored by the

AIR FORCE OFFICE OF SCIENTIFIC RESEARCH

Conducted by the

Universal Energy Systems, Inc.

FINAL REPORT

STATISTICAL ANALYSIS OF BLAST LOADING IN CONCRETE

Prepared by: George W. Coleman Jr., M.S.

Academic Rank: Instructor

Department and   Mathematics and Computer Science

University: Elizabeth City State University

Research Location: AFATL/SAA
                         Eglin AFB FL   32542-5434

USAF Researcher: Mark Amend

Date: 14 August 1989

Contract No: F49620-88-C-0053

STATISTICAL ANALYSIS OF BLAST LOADING IN CONCRETE

by

George W. Coleman Jr., M.S.

ABSTRACT

The collected test data of the experiment of explosive loads on concrete slabs in an enclosed blast chamber was provided. The collected test data was separated into classes and sorted in databases. Statistical analysis software was used to perform regression analysis on the data. The magnitude of loads on the side of the pressure vessel and on the top face of the concrete slabs at the bottom of the vessel were analyzed by performing a regression analysis.

ACKNOWLEDGMENTS

I wish to thank the Air Force Systems Command, the Air Office of Scientific Research and the Armament Laboratory at Eglin AFB for sponsoring the Summer Faculty Research Program (SFRP), thus giving me the opportunity to become acquainted with research objectives of the Air Force. I also wish to thank Universal Energy Systems for the part they played in making the SFRP a possibility.

My experience was rewarding and enriching because of many different influences. I wish to give special thanks to George Crews (now retired) who extended the initial offer to me to work at Eglin, to John Gagliano and Dave Jerome, who provided me with a congenial and stimulating environment in which to work, to Ron Hunt and Dave Hogg, who helped me in overcoming many technical roadblocks, and lastly to Mark Amend, who freely shared with me his knowledge in every phase of this project, and who provided the catalyst for the research I conducted at Eglin.

I. INTRODUCTION:

Statistical analysis of data involves scientific methods for applying techniques such that the uncertainty of inductive inferences may be evaluated.

The Air Force Armament Laboratory has been engaged in a program to study explosive loads on concrete slabs in an enclosed blast chamber. Calculations [5] have been made of the response of the concrete, with emphasis on failure location. Of particular interest to the Laboratory is the implementation of statistical analysis of collected data.

My research interest has been in the area of statistical analysis. My specific training is in this area, my experience with teaching basic statistics and my interest in this area proved to be useful resources in enabling me to make a contribution to the implementation of statistical analysis.

II. OBJECTIVES OF THE RESEARCH EFFORT:

The explosive blast experiments [5] investigated loads on concretes varying parameters such as angle of incidence, charge weight, and standoff distance. Test data was provided which was categorized by test number. Each test number consisted of categories of test descriptions, channels, placements, stand-off, pressures (PSI) and impulses (PSI*MESC). For some tests pressure measurements were made without a concrete specimen present. Pressure transducers were mounted flush in a rigid steel plate. The stand-off is the normal distance from the charge to the plane of the specimen at the bottom of the chamber. The channel numbers corresponded to placement of blast measuring devices which measured pressures and impulses.

My assignment as a participant in the 1989 Summer Faculty Research
Program (SFRP) was to perform regression analysis on data from
measurements of loads on steel and concrete slabs in an enclosed
chamber.

III. _____:

a. The collected test data was separated into two classes. The
data was divided into side and bottom measurements. The side and bottom
measurements represent respectively, the magnitude of loads on the side
of the pressure vessel and on the top face of the concrete slabs at
bottom of the vessel. The computer software ENABLE [4] was used to
create databases to store these data and to utilize spreadsheets on a
personal computer (PC).

However once a particular data set file is extracted from the
database, that data set file could then be transferred into a directory
on the VAX computer located at Eglin Air Force Base. The reason for
doing this is because Statistical Analysis Software (SAS) [3] system for
data analysis is on the VAX computer and not on the PC. One could then
write SAS procedure files to execute regression analysis of data.
Regression analysis is fitting of an equation to a set of values. The
equation predicts a dependent variable from a function of independent
variables and parameters by adjusting the parameters such that a measure
of fit is optimized. An equation for the ith observation might be

$$Y_i = B_0 + B_1 X_i + E_i \tag{1}$$

where Y_i is the dependent variable, X_i is a independent variable, B_0 and
B_1 are unknown parameters to be estimated and E_i is an error term. The

method used to estimate the parameters is to minimize the sum of squares
of the differences between the actual dependent value and the value
predicted by the equation. The estimates are called least-squares
estimates, and the criterion value is called the error sum of squares:

$$SSE = \sum (Y_i - b_0 - b_1 X_i)^2 \tag{2}$$

where b_0 and b_1 are the values for B_0 and B_1 that minimize SSE.

The function representation of side measurements are defined by

$$P = f(W,\theta)$$

$$\text{and } I = f(W,\theta)$$

Where P = pressure (PSI), I = impulse (PSI*MSEC), W = charge weight
(lbs.) and θ = angle (radians). The angle θ is given by

$$\theta = \tan^{-1}\left(\left|\frac{R-r}{D}\right|\right) \tag{3}$$

where R is the stand-off, r is the placement and D is the uniform
distance of twenty-nine inches.

The function representation of bottom measurements are defined by:

$$P = f(R,W,\theta)$$

$$\text{and } I = f(R,W,\theta) \tag{4}$$

where P = pressure (PSI), I = impulse (PSI*MSEC), R = stand-off
(inches), W = charge weight (lbs), and θ = angle (radius). The angle θ
is given by

$$\theta = \tan^{-1}\left(\frac{r}{R}\right) \tag{5}$$

where r is the placement, and R is the stand-off.

b. The equation of free-field stresses from bombs detonating takes the form:

$$P_0 = k \left(\frac{R}{W^{1/3}} \right)^{-n} \qquad (6)$$

where P_0 is the peak pressure (PSI), R is the distance to the explosion (ft), W is the charge weight (lbs), and k = stress constant. For convenience, equation (6) is written in the form of:

$$P = KW^B \qquad (7)$$

where in terms of the above parameters we have that:

$$K = R^{-n},$$

$$B = n/3 \qquad (8)$$

We first give results for the case of side measurements. In each situation a statistical analysis was performed on pressure versus charge weight with angles of incidence held constant. It was found that there was a good correlation between pressure and charge weight for relatively small angles of incidence, refer to Table 1. The larger angles of incidence showed significantly poorer, and in some cases no, correlation between pressure and charge weight, refer to Figure 5. Therefore, as the angle of incidence increases the relative correlation between pressure and charge weight tends to decrease.

Next we give results for the case of bottom measurements. In each situation a statistical analysis was performed as pressure versus stand-off distance with charge weight held constant. It was found that there was poor correlation between pressure and stand-off distances.

Table 1 shows the SAS procedure file which executes the regression analysis. Figures 1 through 5 show SAS printouts of regression analysis of some of the results for the case of side measurements. The SAS printouts include analysis of variance, parameter estimates, observations, and plots between pressures and charge weights. In the analysis of variance Figure 1 opposite MODEL, we find df = 1. This gives the sum of squares of deviations of regression values from the means. The column headed PROB>F gives the probability that a random value of F will be greater than that observed.

IV. RECOMMENDATIONS:

a. The implementation of regression analysis of the data has been performed. The measurements of loads on concrete slabs demonstrated a linear relationship between pressure and charge weight for relatively small angles of incidence. However, the measurements of loads on steel did not demonstrate a linear relationship between pressure and stand-off distance for various charge weights.

b. Several questions arose during the course of the research. The following questions are provided as evidence of the need for future research:

1. What effects did the hemispherically capped cylinder of the chamber have on the measurements of loads on steel and concrete slabs, by a comparison between AFATL-TR-87-64 HULL Model predicting, and the actual test data, using statistical analysis?

2. What are the results of statistical analysis of the static pressure of the top and bottom cylinders?

3. Attempt to correlate peak pressure and impulse with damage to concrete specimens.

```
FILENAME DATAED '[COLEMANG.RESEA]TEST1.DAT';
TITLE 'STATISTICAL ANALYSIS OF TEST DATA';
DATA RESEARCH;
INFILE DATAED;
INPUT P W;
LABEL P ='PRESSURE (PSI)'
W ='CHARGE WEIGHT';
RUN;
PROC REG;
MODEL P = W;
RUN;
PROC PRINT;
RUN;
PROC PLOT;
PLOT P*W;
RUN;
```

Table 1 SAS procedure file program for the execution
of regression analysis of data.

STATISTICAL ANALYSIS OF DATA

PLOT OF P*W   LEGEND: A = 1 OBS, B = 2 OBS, ETC.

OBS	P	W
1	3.00646	0.00000
2	2.95277	0.00000
3	2.88332	0.00000
4	3.14090	0.39794
5	3.36510	0.39794
6	3.32029	0.39794
7	3.37060	0.39794
8	3.21171	0.39794
9	3.46003	0.39794
10	3.23233	0.39794
11	3.21232	0.39794
12	3.27509	0.39794
13	3.24167	0.39794
14	3.32106	0.39794
15	3.43947	0.39794
16	3.20256	0.39794
17	3.37500	0.39794

CHARGE WEIGHT

ANALYSIS OF VARIANCE

SOURCE	DF	SUM OF SQUARES	MEAN SQUARE	F VALUE	PROB>F
MODEL	1	0.29846629	0.29846629	35.030	0.0001
ERROR	15	0.12494938	0.008329959		
C TOTAL	16	0.42341567			

ROOT MSE	0.09126061	R-SQUARE	0.7049
DEP MEAN	3.237087	ADJ R-SQ	0.6852
C.V.	2.819468		

PARAMETER ESTIMATES

VARIABLE	DF	PARAMETER ESTIMATE	STANDARD ERROR	T FOR H0: PARAMETER=0	PROB > |T|	VARIABLE LABEL
INTERCEP	1	2.95084900	0.05269396	56.000	0.0001	INTERCEPT
W	1	0.87343354	0.14591625	5.986	0.0001	CHARGE WEIGHT

Figure 1 Regression analysis of the data where the angle of incidence is equal to .07 .

STATISTICAL ANALYSIS OF DATA

PLOT OF P*W   LEGEND: A = 1 OBS, B = 2 OBS, ETC.

DEP VARIABLE: P

```
3.45 ┤
3.40 ┤                    AAA
3.35 ┤
3.30 ┤                    AA
3.25 ┤                     B
3.20 ┤
3.15 ┤
3.10 ┤
3.05 ┤
3.00 ┤
2.95 ┤
2.90 ┤A
     └─────────────────────────────────────────
     0.00000                              0.39794
```

PRESSURE

CHARGE WEIGHT

ANALYSIS OF VARIANCE

SOURCE	DF	SUM OF SQUARES	MEAN SQUARE	F VALUE	PROB>F
MODEL	1	0.16250430	0.16250430	41.412	0.0007
ERROR	6	0.02355589	0.00392598 01		
C TOTAL	7	0.18614019			

ROOT MSE	0.06265765	R-SQUARE	0.8735
DEP MEAN	3.27125 0	ADJ R-SQ	0.8524
C.V.	1.915399		

PARAMETER ESTIMATES

VARIABLE	DF	PARAMETER ESTIMATE	STANDARD ERROR	T FOR H0: PARAMETER=0	PROB > |T|
INTERCEP	1	2.89408300	0.06265765	46.189	0.0001
W	1	1.08322252	0.16832650	6.435	0.0007

VARIABLE	VARIABLE LABEL
INTERCEP	INTERCEPT
W	CHARGE WEIGHT

OBS	P	W
1	2.89408	0.00000
2	3.25959	0.39794
3	3.30105	0.39794
4	3.30903	0.39794
5	3.25969	0.39794
6	3.37779	0.39794
7	3.26602	0.39794
8	3.40192	0.39794

Figure 2 Regression analysis of the data
where the angle of incidence is equal
to .14 .

STATISTICAL ANALYSIS OF DATA

PLOT OF P*W   LEGEND: A = 1 OBS, B = 2 OBS, ETC.

DEP VARIABLE: P

CHARGE WEIGHT

ANALYSIS OF VARIANCE

SOURCE	DF	SUM OF SQUARES	MEAN SQUARE	F VALUE	PROB>F
MODEL	1	0.38760744	0.38760744	43.000	0.0001
ERROR	19	0.16814038	0.00884949494		
C TOTAL	20	0.55574783			

ROOT MSE	0.09407175	R-SQUARE	0.6975
DEP MEAN	3.23122	ADJ R-SQ	0.6815
C.V.	2.905942		

PARAMETER ESTIMATES

VARIABLE	DF	PARAMETER ESTIMATE	STANDARD ERROR	T FOR H0: PARAMETER=0	PROB > |T|	VARIABLE LABEL
INTERCEP	1	2.8186502	0.06649730	42.394	0.0001	INTERCEPT
W	1	1.16516999	0.17605666	6.610	0.0001	CHARGE WEIGHT

Figure 3 Regression analysis of the data
where the angle of incidence is equal
to .17.

STATISTICAL ANALYSIS OF DATA

PLOT OF P*W   LEGEND: A = 1 OBS, B = 2 OBS, ETC.

P VARIABLE: P

CHARGE WEIGHT

PRESSURE

ANALYSIS OF VARIANCE

SOURCE	DF	SUM OF SQUARES	MEAN SQUARE	F VALUE	PROB>F
MODEL	1	0.31064771	0.31064771	49.057	0.0001
ERROR	10	0.06332416	0.00633242416		
C TOTAL	11	0.37397187			

			R-SQUARE	
ROOT MSE	0.07957648		0.8307	
DEP MEAN	3.162786		ADJ R-SQ	0.8137
C.V.	2.516025			

PARAMETER ESTIMATES

VARIABLE	DF	PARAMETER ESTIMATE	STANDARD ERROR	T FOR HO: PARAMETER=0	PROB > |T|
INTERCEP	1	3.00558595	0.03211602	93.585	0.0001
W	1	0.70390627	0.10049986	7.004	0.0001

	VARIABLE LABEL
	INTERCEPT
	CHARGE WEIGHT

OBS	P	W
1	3.09705	0.000000
2	3.13705	0.000000
3	3.25536	0.397940
4	3.29363	0.397940
5	3.22115	0.397940
6	3.22194	0.000000
7	2.89783	0.000000
8	2.96511	0.544068
9	3.30021	0.544068
10	3.42600	0.000000
11	2.88888	0.000000
12	3.06123	0.000000

Figure 4. Regression analysis of the data where the angle of incidence is equal to .2.

6-13

STATISTICAL ANALYSIS OF DATA

PLOT OF P*W   LEGEND: A = 1 OBS, B = 2 OBS, ETC.
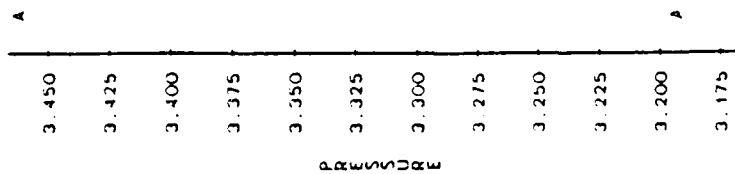
```
P
3.450     A

3.425

3.400

3.375

3.350                                              A

3.325                                                A

3.300                                                  A
                                                       A
3.275

3.250

3.225

3.200

3.175                                        A
     +----+----+----+----+----+----+----+----+----+----+----+----+----+----+----+----+
   0.395 0.405 0.415 0.425 0.435 0.445 0.455 0.465 0.475 0.485 0.495 0.505 0.515 0.525 0.535 0.545
```

CHARGE WEIGHT

DEP VARIABLE: P   PRESSURE

ANALYSIS OF VARIANCE

SOURCE	DF	SUM OF SQUARES	MEAN SQUARE	F VALUE	PROB>F
MODEL	1	0.0004443868	0.0004443868	0.048	0.8380
ERROR	4	0.03733613	0.00934032		
C TOTAL	5	0.03778052			

ROOT MSE	0.0966128	R-SQUARE	0.0118
DEP MEAN	3.317313	ADJ R-SQ	-0.2353
C.V.	2.912301		

PARAMETER ESTIMATES

VARIABLE	DF	PARAMETER ESTIMATE	STANDARD ERROR	T FOR H0: PARAMETER=0	PROB > |T|	VARIABLE LABEL
INTERCEP	1	3.37919853	0.28635199	11.801	0.0003	INTERCEPT
W	1	-0.124929	0.57235666	-0.218	0.8380	CHARGE WEIGHT

OBS	P	W
1	3.32115	0.54407
2	3.35508	0.54408
3	3.46352	0.39794
4	3.19545	0.39794
5	3.30106	0.54407
6	3.28602	0.54407

Figure 5 Regression analysis of the data
where the angle of incidence is equal
to .17 .

6-14

REFERENCES

1. Baker, W.E., Cox, P.A., Westine, P.S., Kulesz, J.J., and Strehlow, R.A., Explosion Hazards and Evaluation, Elsevier Scientific Publishing Company, Amsterdam-Oxford-New York, 1983.

2. Steel, R.G., Torrie, J.H., Principles and Procedures of Statistics, McGraw-Hill Inc. New York, 1980.

3. SAS User's Guide: Statistics Version 5 Edition, SAS Institute Inc., Cary, North Carolina,

4. Zenith Data Systems, ENABLE Version 1.15 Manual, Benton Harbor, Michigan.

5. Air Force Armament Laboratory Technical Report, AFATL-TR-87-64, "State-of-the-Art of Blast Loading and Penetration Simulation in Concrete Using the HULL Hydrocode.

6. Department of the Army Technical Manual, TM-855-1, "Fundamentals of Protective Design for Conventional Weapons, July 1984, pp 106-112.

1989 USAF-UES SUMMER FACULTY RESEARCH PROGRAM /

GRADUATE STUDENT RESEARCH PROGRAM

Sponsored by the

AIR FORCE OFFICE OF SCIENTIFIC RESEARCH

Conducted by the

Universal Energy Systems, Inc.

FINAL REPORT

A Methodology for Evaluating the Effectiveness of

Smart Submunition Systems

Prepared by:	B. D. Sivazlian
Academic Rank:	Professor
Department and	Industrial and Systems Engineering Department
University:	The University of Florida
Research Location:	USAF Armament Laboratory
	Eglin AFB, FL 32542-5000
USAF Researcher:	George C. Crews
Date:	June 23, 1989
Contract No.:	F49620-88-C-0053

A Methodology for Evaluating the Effectiveness

of Smart Submunition Systems

by

B. D. Sivazlian

ABSTRACT

A methodology is developed to assess the effectiveness of smart submunition systems. We provide a formal analysis of the aggregate problem and characterize the elements of the system. A mathematical model can be formulated which describes the temporal operation of the weapon system in a combat situation involving threats, countermeasures and uncertainty. A solution procedure is suggested and several measures of effectiveness are formalized.

ACKNOWLEDGEMENTS

I. INTRODUCTION:

Over the last decade, various DOD agencies have been involved in developing a family of weapon systems known as smart munitions (SM) which could significantly enhance the U.S. capability in the battlefield, while simultaneously improving mission survivability.

SMs have the autonomous capability to search, detect, acquire and engage targets. They can be delivered by a variety of means such as rockets, guns, dispensers, etc..., in large quantities over a large arrays of land-mobile targets. They can simultaneously engage multiple targets and be accurately delivered on selected targets without requiring an operator on the loop. The development of a methodology to assess the effectiveness of this new weapon system in a combat situation incorporating threats and countermeasures, becomes an important problem to be analyzed and studied.

My research interests have been in the area of applied probability and stochastic modeling applied to a variety of management and military problems. These have included problems in such areas as queueing, inventory, replacement, reliability, combat, aircraft sorties, convoy retardation, target tracking, etc... My consulting experience with various U.S. Army and U.S. Air Force agencies as well as with defense contractors, spanning a period of more than twenty years, has given me an excellent opportunity to be acquainted with a variety of defense missions. This experience has contributed to my assignment to the Technology Assessment Branch of the Analysis and Strategic Defense Division of the U.S. Air Force Armament Laboratory at Eglin AFB, Florida.

II. OBJECTIVES OF THE RESEARCH EFFORT:

As part of an ongoing program, the Analysis Division of the Air Force Armament Laboratory at Eglin AFB has requested its Technology Assessment Branch to provide an assessment for a Smart Submunition Technology program.

The objective of this program is to integrate advanced technologies for the next generation of smart submunitions (SM). The technologies

would be advanced technology sensors, warhead, and maneuvering, compatible with advanced aircraft and dispenser delivery systems, and capable of providing substantial increases in effectiveness over current weapons against ground mobile targets. The target set being considered for the program spans the spectrum of ground mobile targets, and includes heavy armour, softer vehicles ranging from air defense targets to light armor, and rail transport.

The technology assessment necessitated the development of an appropriate methodology for evaluating the proposed system. As a result, the following tasks had to be undertaken:

1. Study the operational characteristics of the Smart Submunition Weapon Systems;

2. Analyze the system by identifying the various components in the operation of the system as well as the targets;

3. Characterize each component and provide its advantages, disadvantages and possible countermeasures. Develop appropriate descriptive parameters which may be used as inputs in an effectiveness model;

4. Formulate a mathematical model which describes the operation of the weapon systems under combat condition by incorporating threat and by capturing the stochastic nature of the problem;

5. Develop appropriate measures of effectiveness.

These tasks constitute the outline of the present report. Due to limitations imposed on the size of the present report, the formulation of the complex mathematical model is reported only in the form of an outline.

III. THE SMART SUBMUNITION WEAPON SYSTEMS (SSWS):

The effectiveness in the use of a SSWS depends on the assumption that the ultimate engagement in the battlefield is a "many-on-many". A number of smart submunitions (SS) are delivered in the proximity of an area where several targets are located such as tanks in a tank company. Through its sensors, each submunition is capable of locating, detecting, acquiring and engaging a target of a given type. The sensors have the

capability of identifying the kind of targets (e.g. tanks or APC) that they are to engage. In general, the design of a SS is governed by the environment within which it will be deployed and the characteristics of the targets. As many factors as possible are accounted for in developing the configuration of the SS. Even then, the effectiveness of the SS may be enhanced or deterred depending upon the mode by which such weapons are delivered in the vicinity of the target. For example, a parachute-suspended SS is typically not highly maneuverable and uses a small search footprint. As such, it would not be very effective against moving targets. A better design would be a parafoil-suspended SS or an inflatable-wing SS both of which are highly maneuverable and have a larger footprint. They have the capability of guiding the SS more rapidly towards the target, thus being more effective against moving targets. In addition, a larger footprint increases the probability of acquiring a target.

For the engagement to be successful, it is necessary to deliver a large number of weapons over a given area, and to provide each weapon with the capability to search and locate a target with a high probability of success. This requires that a large number of targets be available within the footprint of the delivery weapon. The larger the footprint, the more likely the weapon will acquire a target during its search, assuming the same target density in the area. Once acquired, the discriminating sensors carried by the weapon will identify the target, select the ones to be attacked and thus pair each munition to a target of a kind. An obvious disadvantage of this system is the likelihood of more than one weapon attacking one particular target unless specific algorithms are built into the weapon system to preclude such situations. A second disadvantage is that in order to be effective, the SS must be placed in the vicinity of the target by a SS delivery system. Finally, in order to acquire and to precision guide towards the target, it becomes necessary to slow down the search and acquisition process. These disadvantages do not appear in most of the existing weapons involving one-on-one engagement in which the weapon is delivered from a much longer distance at a very high speed.

So far, of these three disadvantages, a solution has been found only to the second one in which an unmanned carrier or dispenser launched from a platform at a standoff position is used to place the weapons in the vicinity of the target. This however requires the use of a data link system which provides the platform with the necessary information about target area coordinates and target movement so that the carrier is launched and directed towards the vicinity of the target area. Additional information may have to be continuously provided to the dispenser regarding target location and the specific time at which weapons are to be released. Aerial and ground sensors are typical means to collect information on target location and movement. Aerial sensors may be in the form of remotely piloted vehicles (RPV) or unmanned air vehicles (UAV) or AWACS. A combination of aerial and ground sensors may be used. The information provided is transmitted to a C^3I post which then relays it to the launch platform. The launch platform function is to transport the dispenser and to utilize the relayed information from the C^3I post to aim and launch the dispenser from an appropriate location at a given time. The dispenser transports the SS subpacks to a given location and drops them so as to create a dispersal pattern which results in the best engagement opportunities for the SS. It must be noted that once the SS is dispensed, it depends solely on its own seekers and sensors to guide it terminally towards the target.

In detailing the effectiveness of the aggregate weapon system in the context of the mission it is supposed to be performing, one may not neglect the contribution of the intelligence gathering system used in support of the mission as well as the contribution of C^3. The reliability of the mission is as good as the reliability of its components and C^3I must be considered as an integral part of the overall system.

When developing the appropriate equations to compute the overall mission reliability as a function of time, it may be assumed that the system is made up of two subsystems. The first subsystem consists of the C^3I components providing the data link. The second subsystem consists of the smart submunition weapon system (SSWS) whose components

are the platform, the dispenser, the parafoil and the submunition.
Assuming independence of operation of these two subsystems, the overall
mission reliability is the product of the reliability of the first
subsystem and the second subsystem. Mission reliability is sometimes
used as one of the measures of effectiveness.

A very important consideration at this stage is that time becomes
an important parameter to be accounted for in the development of
appropriate measures of effectiveness. This is insignificance when
studying the mission performance of traditional weapons since they rely
on their high speed for delivery and on the element of surprise when
attacking targets. However, in the case of SSWS, weapon delivery time
is much longer. This in turn eliminates the element of surprise and
provides the enemy significant more time to react to the attacking
weapon system. Thus the enemy will have increased capability to perform
such actions as:

- maneuvering out of the range of incoming weapons;
- visually acquiring and destroying the guiding vehicle of the
  weapon;
- initiating countermeasures to minimize or eliminate the
  effectiveness of the weapon;
- securing positions by scattering or scrambling so as to decrease
  the target density in the area of attack.

Typical components of the SSWS are:
1. The air platform;
2. The dispenser;
3. The parafoil;
4. The submunition warhead;
5. The submunition sensors;

Each of these components is cha   ⁻erized next. Following some
remarks concerning the operational ei ⁻ctiveness of the weapon system,
the target element is characterized.

1. The Air Platform

In the delivery of smart submunitions, it is envisioned that an aircraft will carry a number of dispensers, each loaded with several subpacks of submunitions. From a standoff position, and following a process of target area acquisition and location, the aircraft will fire the dispensers either in salvo or in sequence so that each dispenser is capable of maneuvering towards the target area.

A typically airplatform or carriage aircraft is the F-16. This is a combat-ready fighter which can provide ground support tasks. Since it can be loaded up to 15,200 lbs of ECM pods and weapons, it could easily carry up to two 2000 lbs dispensers. The base line cost of the F-16 is $12,600,000 with an operating cost per hour of $2,400. The maximum take-off weight is 34,400 lbs with a maximum speed of 1,350 mph (mach 2.05) at 40,000 ft. Its ferry range is 2,300 miles and its radius of action is 575 miles.

Advantages

- Capability of engaging air or ground threat targets;
- Capability of reducing level of threat through ECM;
- Capability of being refueled in mid-course by refueling air tankers.

Disadvantages

- Vulnerable to forward areas enemy air defense if dispenser is to be released for rear area (2nd echelon) final engagement;
- May require the formation of an air corridor through enemy lines to reduce the level of threat from forward areas;
- High cost if aircraft is killed;
- Adverse environment or pilot error may release dispenser inadvertently over friendly areas.

Countermeasures

- Possibility of electronic or radar jamming;
- Possibility of threat from enemy SAM's or AAAs or air fighters.

Descriptive Parameters

- Range and speed;
- Average time to release dispenser from the moment aircraft enters enemy territory;

- Intensity of threat encounter;
- Probability of aircraft being killed;
- Intensity of electronic jamming encounter;
- Probability of aircraft's communication and data link being jammed and loosing its mission capability.

   2. The Dispenser

The dispenser is a container capable of self propulsion. It can either be preprogrammed to move from its launch platform towards the target area or it can be directed towards the area through a data link. Alternatively, it is conceivable that through its own sensors it has its own capability of homing towards the target area (autopliot). Once within target area vicinity, it releases the submunition subpacks either in salvo, or in sequence though an intervalometer setting. The release time of the subpacks from the time of the dispenser's release from the air platform is a variable and is constrained by the range of the dispenser. Once the subpacks are released, the dispenser being not programmed to be recovered is allowed to crash on landing and/or self-destruct.

The choice of the dispenser depends on the mission to be accomplished. This will dictate its capacity, load, speed, range and other characteristics. For example a dispenser with a longer range is desired if the weapons have to be carried from the air platform in a distant position to second echelon supply lines in an interdiction role. In addition the dispenser may have to generate a larger footprint.

   Advantages

The main advantage of using a dispenser over an aircraft is that given it is operating in the same threat environment, the dispenser if killed is significantly less valuable than the aircraft. In addition, the dispenser has a lower cross section profile than the aircraft and is substantially smaller, thus making it harder to be acquired visually or by radar and consequently less vulnerable.

Disadvantages

The following are some of the disadvantages of the dispenser:

- It lacks the sensory capability of the pilot of an aircraft and thus is incapable of judgement in critical situations;
- Its speed is lower than a conventional fighter;
- At low altitude it is vulnerable to IR homing SAMs;
- The use of any data link to direct the course, the altitude, the velocity and the release of the subpack makes it vulnerable to electronic jamming;
- If the self-destruct mechanism is not activated in the final disposition of the dispenser it may fall into enemy hands and be technologically studied for future countermeasure actions. It may thus be accessible to the enemy which can exploit its susceptibility;
- It cannot initiate countermeasures if radar acquired;
- It cannot initiate evasive actions if under threat;
- It cannot discriminate between friendly targets and enemy targets. Conceivably, a maneuvering or navigation or guidance malfunction may alter the course of the dispenser and bring it over friendly zones.

Countermeasures

- Possibility of jamming the data link system;
- Possibility of threat from enemy SAM's;
- Accessible to enemy forces following its end course.

Descriptive Parameters

- Range and speed;
- Average time from instant of dispenser release from air platform to instant of subpack releases;
- Intensity of threat encounter;
- Probability of dispenser being killed;
- Intensity of electronic jamming encounter;
- Probability of dispenser's data link being jammed and loosing its mission capability.

3. The Parafoil

The parafoil is the element used for the indirect delivery of the submunition in widely dispersed area of target elements. It is a wide-area search and control system of the targets with its own guidance. It generates the search of a target over a relatively large footprint and once the target is acquired by the submunition sensors, it controls and directs its motion towards the target so as to achieve a range from which the warhead could be fired. The payload consists of the sensor and the warhead. At the desired altitude, the subpacks in the dispenser are ejected and the submunitions released. The parafoils are then deployed and the search mode initiated. The wide area scan greatly increases the search area to compensate for large delivery errors. Once the fuze ignites the charge and an explosion is set up, the slug is formed. Simultaneously the submunition sensors and the parafoil are destroyed. The ability of a parafoil-controlled submunition to glide provides an increased search area and control to target. With an ability to change horizontal to vertical velocity ratio and to brake, the parafoil can be programmed to provide a simple terminal homing capability.

Advantages

- Large footprint area;
- Controlled delivery system and high maneuverability;
- Effective search against moving targets;
- Increase probability of acquiring a target.

Disadvantages

- Slow descent velocity 20 - 40 fps.;
- Slow horizontal velocity - 40 fps.;
- May be visually acquired;
- Must be dispensed in the vicinity of target area.

Countermeasures

- Visual acquisition makes it prone to small arms fire;
- Slow velocity may allow targets to maneuver out of the footprint area;
- Large footprint increases the time necessary to acquire a target;

- Ineffective if footprint does not contain target elements.

Descriptive Parameters

- Average time to search and acquire a target.

4. The Submunition Warhead

The objective of the warhead is to achieve mobility kill in ground mobile targets including heavy armor (tanks), softer vehicles (APCs, air defense targets, light armor) and rail transport. The means of attaining this objective is a modular Explosively Formed Penetrator (EFP). The warheads are used in shoot-to-kill sensor fuzed munitions(SFM).

In EFP warheads, the fuze ignites the explosive material (chemical energy warheads). Some of the explosive energy is used to reshape the liner and accelerate it towards the target.

The reshaping of the liner is dictated by the nature of the acquired target. Modern technology allows the design of multimode warheads. Such warheads are modular in nature and able to create either a single large slug penetrator or multislug penetrators. In the case of heavy armor, the liner is shaped into a single large slug of metal that penetrates the thick plated target at velocities of 2000 to 3000 m/s. In the case of light armor, the liner is shaped into several slugs (multislugs) of smaller size. In both instances the slug causes a hole in the armor and generates spall material. The diameter of the hole is proportional to the diameter and velocity of the penetrator. In EFP warheads, the penetrability of the slug does not depend appreciably on the distance between slug formation and targets: standoff distances may vary and are approximately 25 - 30 ft. The slug creates a hole several inches in diameter generating hundreds of spall particles.

Advantages

- EFP multimode warheads maximally effective against a spectrum of targets;
- Since slug is projected from a short distance to the target and is directed towards the most vulnerable part of the target, the probability of hit is high;

- Size, shape, material and velocity of the slug can be designed to achieve an effective probability of kill.

Disadvantages

- Because of its size, the EFP will typically achieve mobility kill rather than catastrophic kill;

- The slug achieves kill through fragments only. There is no explosive charge in the slug so there is no blast effect although blast may be induced as a secondary effect;

Countermeasures

- Armor enhancement.

5. The Subumunition Sensors

The submunition sensors perform five basic functions:

a. A search function involving target search, detection, identification, discrimination, classification and acquisition;

b. A target location function involving the location, relative speeds, coordinates and other dynamic characteristics of the target with respect to the submunition for target engagement;

c. A maneuvering function so that once target is acquired, the submunition will maneuver to an optimum lethal range and position to fire a warhead at a predetermined aimpoint;

d. Auxiliary functions such as false target rejection, false alarm elimination, warhead mode selection, etc....

Sensors perform their functions by receiving electromagnetic radiation emitted by targets and their surrounding environment. Variations in electrical pulses due to radiation changes are sent to a signal processor which perform the above functions. Sensors are characterized by their operating mode (passive, active or dual) and their operating waveband (infrared, millimeter wave, etc...).

In a passive mode, sensors receive radiation through a receiver, emitted or reflected by objects on tne battlefield. In an active mode, sensors transmit radiation through a transmitter and receive the associated reflections as well as radiation from other sources through a receiver. Sensors operating in a dual mode include typically an active

mode for target acquisition and tracking and a passive mode for the terminal phase.

We shall discuss three types of sensors: the infrared (IR) sensors, and the millimeter wave (MMW) sensors.

i. <u>IR Sensors</u>

IR sensors capture the radiant energy emitted by <u>heated</u> objects. In their simplest type, IR sensors operating in the passive mode, scan optically the target area for IR radiation in a single waveband by all bodies. A more complex design involves IR sensors that detect target signature in two different wavebands, thus allowing discrimination between a true target (e.g. tank) and a decoy (e.g. flare). Finally, for high angular resolution for target detection and tracking, imaging infrared (IIR) resulting in image like properties of the target, may be used.

<u>Advantages</u>
- Inherent day/night operating capability;
- Small size.

<u>Disadvantages</u>
- Degradation in adverse weather. IR signatures become scattered with very severe weather attenuation;
- May home on ignited targets hit by previous submunitions.

<u>Countermeasures</u>
- Paints of low emissivity;
- Shielding of hot spots;
- CAMTEX mats;
- Thermal camouflage nets;
- Multi-band screening smokes;
- Decoy flares.

ii. <u>MMW Sensors</u>

MMW sensors capture the radiant energy emitted by the reflection of <u>metal</u> objects.

<u>Advantages</u>
- Good operational capability under adverse weather conditions;

- Superior propagation characteristics through smoke, haze, dust and fog;
- More accurate angular tracking;
- High resistance to jamming.

Disadvantages
- Susceptible to rain attenuation;
- Range limited by atmospheric absorption;
- Bulky and expensive.

Countermeasures
Various types of aerosols.

Descriptive Parameters of the Submunition
- Number of submunitions;
- Average time to search and detect a target;
- Probability of acquiring a target given that it is detected;
- Probability of acquiring a false target.

7. **The Target**

Primary targets are ground mobile targets including heavy armors (tanks) as well as softer vehicles ranging from air defense targets to light armor and rail transport.

The distinguishing feature of smart munitions from other types of anti-armor weapons is that they home on their targets and/or are activated by them. They also attack targets at their most vulnerable point namely the top. Typically, a large number of smart munitions will be needed to insure defeat of a massive armored assault consisting of many targets. A barrage of thousands of these munitions would blunt armored assault and reinforcing columns.

Descriptive Parameters
- Total number of targets (true and decoys);
- Proportion of decoys to total number of targets;
- Probability of target being hit;
- Probability of target being killed given that it is hit.

IV. THE MATHEMATICAL MODEL:

The development of a mathematical model depends on several factors governing the actual conditions under which the weapon system operates. This may include for example, environment, combat scenario, operation sequence, mode of weapon delivery, weapon technology, etc...   In general, a model should be able to capture the uncertainty element present in an actual combat situation together with the evolution of the combat state at successive time epochs. Very often the objective is not on simply winning a battle, but on how quickly to win a battle. From that point of view, time becomes an important parameter to be incorporated in the model.

The stochastic aspect of the problem is characterized by $P(m,n,t)$, the probability that at time t following release from the dispenser, there are exactly m remaining live submunitions (m = 0, 1, ..., M) and n remaining live targets targets (n = 0, 1, ..., N). One can obtain $P(m,n,t)$ by developing appropriate differential - difference equations subject to a set of initial conditions, whose solution will yield expressions for $P(m,n,t)$ for all values of m, n and t. One way of obtaining the solution of these equations is through a recursive approach. Once $P(m,n,t)$ is derived, one can obtain such characteristics as the expected number of targets killed, the expected number of submunitions to kill a given number of targets, the mission reliability, as well as the measures of effectiveness.

V. MEASURES OF EFFECTIVENESS:

We develop five measures of effectiveness

1. Expected number of targets killed at time t, $\hat{n}(t)$:

$$E[\hat{n}(t)] = N - \sum_{n=0}^{N} \sum_{m=0}^{M} n\, P(m, n, t)$$

2. Expected number of submunitions to kill N-n targets at time t, $\hat{m}(t)$:

$$E[\hat{m}(t)] = M - \sum_{m=0}^{N} m\, P(m, n, t)$$

3. Probability that all targets are killed at time t:

$$\sum_{m=0}^{N} P(m, 0, t)$$

4. Expected cost to kill all targets

Let C_D = cost per dispenser

C_M = cost per submunition

Then, expected cost to kill all targets is

$$C_D + C_M \left[M - \lim_{t \to \infty} \sum_{m=0}^{M} m\, P(m, 0, t) \right]$$

5. Mission reliability

This is the probability that the dispenser successfully releases all submunitions. Let

$\hat{P}(1, 0, t)$ = probability that at time t the dispenser is operating

successfully and the submunitions are not released;

$\hat{P}(1, 1, t)$ = probability that at time t the dispenser is operating

successfully and the submunitions are released.

It is then easy to verify that

$$\frac{d\hat{P}(1, 0, t)}{dt} = - (\mu + \lambda p_1 + \nu p_2)\, \hat{P}(1, 0, t)$$

and

$$\frac{d\hat{P}(1, 1, t)}{dt} = \mu\, P(1, 0, t)$$

subject to $\hat{P}(1, 0, 0) = 1$ and $\hat{P}(1, 1, 0) = 0$

From these two equations one obtains for mission reliability

$$\hat{P}(1, 1, t) = \frac{\mu}{\mu + \lambda p_1 + \nu p_2} \left[1 - e^{-(\mu + \lambda p_1 + \nu p_2)t} \right]$$

VI. RECOMMENDATIONS:

There are three aspects of the problem that need to be considered based on the results of the present research:

1. To study the effect of countermeasures on the various probability parameters such as μ, p_A, p_H and p_K, that enter as inputs to the problem, and to assess their impact on the various measures of effectiveness;

2. To study a combat situation in which dead targets are acquired by live submunitions. This will require the development of an appropriate mathematical model much along the lines of the present methodology.

3. To derive explicit analytic solutions for each of the mathematical models considered.

REFERENCES

1. Lee, S. M. (ed), "Proceedings of the Sixth Annual KRC Symposium on Ground Vehicle Signatures", August 21-22, 1984, Keeweenaw Research Center, Houghton, MI.

2. Ogorkiewicz, R. M., "Countermeasures for Tanks, Beating Smart Munitions" International Defense Review, Vol. 22, pp. 53-57, Jan. 1989.

3. "Proceedings of the Precision Guided Weapons Symposium" GACIAC PR 88-05, IIT Research Institute, Chicago, IL, (1988).

4. Sivazlian, B. D., "Aircraft Sortie Effectiveness Model", Naval Research Logistics, Vol. 36, pp. 127-137 (1989).

5. "Smart Munitions", GACIAC SR-87-08, IIT Research Institute, Chicago, IL., (1987).

1989 USAF-UES SUMMER FACULTY RESEARCH PROGRAM/

GRADUATE STUDENT RESEARCH PROGRAM

Sponsored by the

AIR FORCE OFFICE OF SCIENTIFIC RESEARCH

Conducted by the

Universal Energy Systems, Inc.

FINAL REPORT
_____

SHOCK WAVE INITIATED DETONATION OF AN EXPLOSIVE
_____

Prepared by: Steven A. Trogdon, Ph.D.

Academic Rank: Associate Professor

Department and   Mathematics and Statistics

  University: University of Minnesota - Duluth

Research Location: AFATL/SAA
                        Eglin AFB
                        Eglin AFB, FL   32542-5434

USAF Researcher: Ronald D. Hunt

Date: 14 August 1989

Contract No: F49620-88-C-0053

SHOCK WAVE INITIATED DETONATION OF AN EXPLOSIVE

by

Steven A. Trogdon

ABSTRACT

The HULL hydrodynamics code has been modified to accommodate the shock wave detonation of an explosive. The modifications have been made relative to the physics burn module in HULL. In order to trigger a detonation a density criteria was developed which, when exceeded, would initiate the detonation. A guide is given as to how to determine this criteria. The modifications have been documented in a change file so that they can be directly incorporated in the HULL system. Comparisons have been made of an impact only scenario with an impact initiated detonation. The scenario is one that attempts to model an actual warehead under impact conditions. Significantly more damage is observed when a detonation occurs.

ACKNOWLEDGMENTS

I wish to thank the Air Force Systems Command, the Air Office of Scientific Research and the Armament Laboratory/Eglin AFB for sponsoring the Summer Faculty Research Program (SFRP), thus giving me the opportunity to become acquainted with research objectives of the Air Force. I also wish to thank Universal Energy Systems for the part they played in making the SFRP a possibility.

My stay at Eglin AFB was extremely rewarding and intellectually stimulating. I wish to give special thanks to George Crews (now retired) who extended the initial offer to me to work at Eglin, to John Gagliano and Dave Jerome who provided me with a congenial and stimulating environment in which to work, to John Collins who furnished me with indispensible computer resources and lastly to Ron Hunt who so freely shared with me his knowledge of the workings of the HULL system and who provided the catalyst for the research I conducted at Eglin.

I.   INTRODUCTION:

The equations of continuum mechanics consist of a system of coupled partial differential equations which represent basic expressions for conservation of mass, momemtum and energy. The HULL [1,2] system solves these equations in an Eulerian and/or Lagrangian framework and as such provides a useful tool for assessing, from a deterministic point of view, the potential lethality of given impact scenarios. These impact scenarios are often contemplated as occurring under conditions which preclude experimental verification. The impacting of an explosive material represents one such scenario. If sufficient energy is transferred to the explosive during he impact process then the potential exists for the initiation of a sustained detonation of the explosive.

The Air Force Armament Laboratory has for some time been engaged in a comprehensive program to study the potential lethality of kinetic energy weapons under various impact scenarios. Of particular interest to the Laboratory is the ability of certain (hypergolic) compounds to ignite spontaneously upon contact with target components. Target components may contain a wide range of fuel and/or oxidizer compounds and therefore the use of reactive (hypergolic) projectiles could increase the overall effectiveness of conventional kinetic energy weapons. The implementation, within the HULL system, of a means of modeling an impact initiated detonation would serve as a first step in understanding the effectiveness of coupling kinetic energy and hypergolic effects.

My research interests have been in the area of partial differential equations, particularly those differential equations which arise in

various branches of continuum mechanics. My most recent efforts have
been in the numerical solution of partial differential equations which
arise in fluid mechanics, namely the flow of fluids in channels and the
buoyancy induced motion of a thermally stratified fluid. My
understanding of the origin of the equations of continuum mechanics, my
familiarity with numerical algorithms used to solve these equations, my
background in programming and my understanding of several computer
operating systems proved to be invaluable resources in enabling me to
make a contribution to understanding the lethality of coupling
kinetic energy and hypergolic effects.

II.   OBJECTIVES OF THE RESEARCH EFFORT:

The HULL system is an extremely flexible system of finite
difference programs for generating and solving dynamic continuum
mechanics problems. The HULL system comes standard with two options for
modeling detonations. The first option is referred to as a physics burn
and the detonation process, when initiated, proceeds at a rate and
direction determined by the local pressure gradient and sound speed. The
second option is referred to as a programmed burn and the detonation
front proceeds at a predetermined rate at the assigned detonation
velocity. Both the point and velocity of detonation must be supplied by
the programmer. Neither one of these detonation models is self
initiating in the sense of a detonation being triggered by the
physics of what is occurring. Of the two detonation models, the physics
burn more realistically models the detonation process provided that one
knows in advance where and when a detonation will occur. It would be
desirable to incorporate within the physics burn model a mechanism for

making it self initiating, that is, to incorporate a threshold which when exceeded would trigger a detonation. Such an implementation would represent a valuable first step in studying the lethality of hypergolic munitions.

My assignment as a participant in the 1989 Summer Faculty Research Program (SFRP) was

(i)   to provide an appropriate criteria which would be used as the basi `or triggering a detonation under appropriat. .- act conditions

(ii)   to investigate how one would incorporate such a criteria in the physics burn model and to develop the necessary coding to implement such a criteria

(iii)   to compare the qualitative features of the self initiated detonation model with an impact only situation.

III.   OVERVIEW OF RESEARCH:

a.   Pertinent detonation literature was reviewed to determine an appropriate criteria for triggering a detonation. Lee and Green [3] had indicated that under certain conditions a simple density criteria led to numerical results which matched reasonably well with experiments. They provided no specifics as to how the criteria was implemented. A simple impact problem was formulated in order to understand how the physics burn model had to be modified in order to accommodate the density criteria. This simple problem will not be discussed since its

only purpose was to provide a means of generating necessary FORTRAN computer code. It was this code that was modified in order to accommodate the density criteria and the modifications were subsequently incorporated in the HULL system. The revised HULL system was checked to see if a detonation was actually occurring in a manner which was physically meaningful. A comparison was made of an impact initiated detonation in which a detonation should occur with an identical impact situation without a detonation.

b.   As a result of using density as a criteria to trigger a detonation one was able to use the physics of a simple detonation (shock) wave to compute a density threshold such that when the density exceeded the threshold a detonation occurred. Such a calculation is provided in section IV. The result of investigating how to incorporate a density criteria in the HULL system by considering first a simple problem resulted in changes which could be directly incorporated in the HULL system. These changes are given in section V. In section VI we give explicit comparisons of an impact initiated detonation with an impact only situation. The density threshold used in these comparisons was computed using the results of section IV. The input file needed to generate the detonation problem is given in section VII.

IV.   CALCULATION OF DENSITY THRESHOLD:
        _____

We outline below a simple procedure which may be utilized to establish values for a density threshold. Some of the formulas which will be used are empirical and some are analytical. A discussion of all formulas as well as any data used may be found in [4].

A quadratic curve fit to the Hugoniot of an explosive may be represented by

$$P = \rho_0 (c_0 u + s u^2) \tag{1}$$

where P is the pressure, ρ_0 and c_0 are respectively the reference density and reference sound speed of the explosive, u is the particle velocity in the explosive and s is a constant which depends upon the particular explosive. The jump condition (conservation of mass) across the detonation front (shock wave) is given by

$$\rho_0 (v - u_0) = \rho (v - u) \tag{2}$$

where v is the shock velocity, the subscripted "o" quantities are reference quantities and the nonsubscripted quantities are quantities behind the detonation front. If we linearly approximate the shock velocity as

$$v = c_0 + s u \tag{3}$$

and set $u_0 = 0$, then equation (2) with (3) may be solved for the density behind the detonation front in terms of the particle velocity as

$$\rho = \frac{\rho_0 (c_0 + s u)}{c_0 + u(s - 1)} . \tag{4}$$

We now need an expression for u. This may be found by solving (1) for u with P set equal to P^*, the set-back pressure. The set-back pressure is an experimentally determined quantity and represents that pressure

needed to initiate a detonation in an explosive. We find u to be given
by

$$u = \frac{-\dfrac{c_0}{s} \pm \sqrt{\dfrac{c_0^2}{s^2} + \dfrac{4 P^*}{\rho_0 s}}}{2} \tag{5}$$

where the positive square root is selected to yield physically
meaningful results.

For the explosive Octol we have the following data:

$P^* = 1,027,355$ kPa $\qquad\qquad \rho_0 = 1.821$ gm/cm^3

$c_0 = 3.01 \times 10^5$ cm/sec $\qquad\qquad s = 1.72$

from which we compute that $u = 1.71 \times 10^4$ cm/sec, $v = 3.30 \times 10^5$ cm/sec and
the density threshold is 1.92 gm/cm^3.

CHANGES TO HULL SYSTEM:

```
*I 50928
*KEEPTO TROGBURN BURN1
C
C       VARIABLES USED IN TROGDON-BURN1 INTITIATION KLUGE
C
        COMMON /BURN/ IBURN
C
*LABEL TROGBURN
*I 70482
*KEEPTO TROGBURN BURN1
C
        IBURN=0
C
*LABEL TROGBURN
*I 87697
*KEEPTO TROGBURN BURN1
C
        IF (IBURN.EQ.1) GO TO 110
        DENC=1.92D0
        NSTART=N
        DO 100 I=1,IMAX
          N=NSTART+(I-1)*NH
          IF (XV(N+IU).LE.EP1) GOTO 100
          DEN=XM(N+IU)/XV(N+IU)
          IF (DEN.GE.DENC) GOTO 90
          GOTO 100
90        XM(N+IB)=XM(N+IB)+XM(N+IU)
          XM(N+IU)=0.D0
          XV(N+IB)=XV(N+IB)+XV(N+IU)
          XV(N+IU)=0.D0
          IF (IBURN.EQ.1) GOTO 100
          IBURN=1
100     CONTINUE
        N=NSTART
110     CONTINUE
C
*LABEL TROGBURN
```

VI.   COMPARISONS:

We next make comparisons of an impact only scenario with an
impact initiated detonation. The impact situations are identical except
for the potential for a detonation. The density criteria discussed
earlier has been incorporated in the detonation modeling.

In Figure 1 we have, by means of a grey-scale raster plot of the density

in the respective materials, depicted the physical problem prior to impact. The problem is axially symmetric and impact occurs along this axis of symmetry. Physically, we have a cylindrical tungsten penetrator impacting a cylindrical steel shell with spherical cap at 6 kilometers/second. The spherical cap portion of the steel shell surrounds a spherical shell of explosive (octol). The region above the explosive and inside the steel shell is filled with lucite. This configuration is an attempt at modeling an actual warhead under impact conditions.

In Figures 2 and 3 we have given grey-scale raster plots of the density in the respective materials. The figures are, respectively at 7 and 14 microseconds after impact. The appearance of a shock is apparent in both of these figures. The shock is propagating at the sound speed in the explosive.

In Figures 4 and 5 we have shown raster plots when the potential for a detonation exists. The density threshold is the same as that which was determined in section IV. Figures 4 and 5 are to be directly compared with Figures 2 and 3. The propagation of the detonation front is obvious in Figures 4 and 5. The material behind the detonation front is all burned material and the front is propagating at the detonation velocity in the explosive. The damage is much more extensive when there is a detonation and the front has penetrated further into the explosive than if there had been no detonation. To illustrate the extent of the damage, we give in Figure 6 a raster plot of the detonation scenario at around 30 microseconds. Due to the detonation, the explosive material has nearly been consummed.
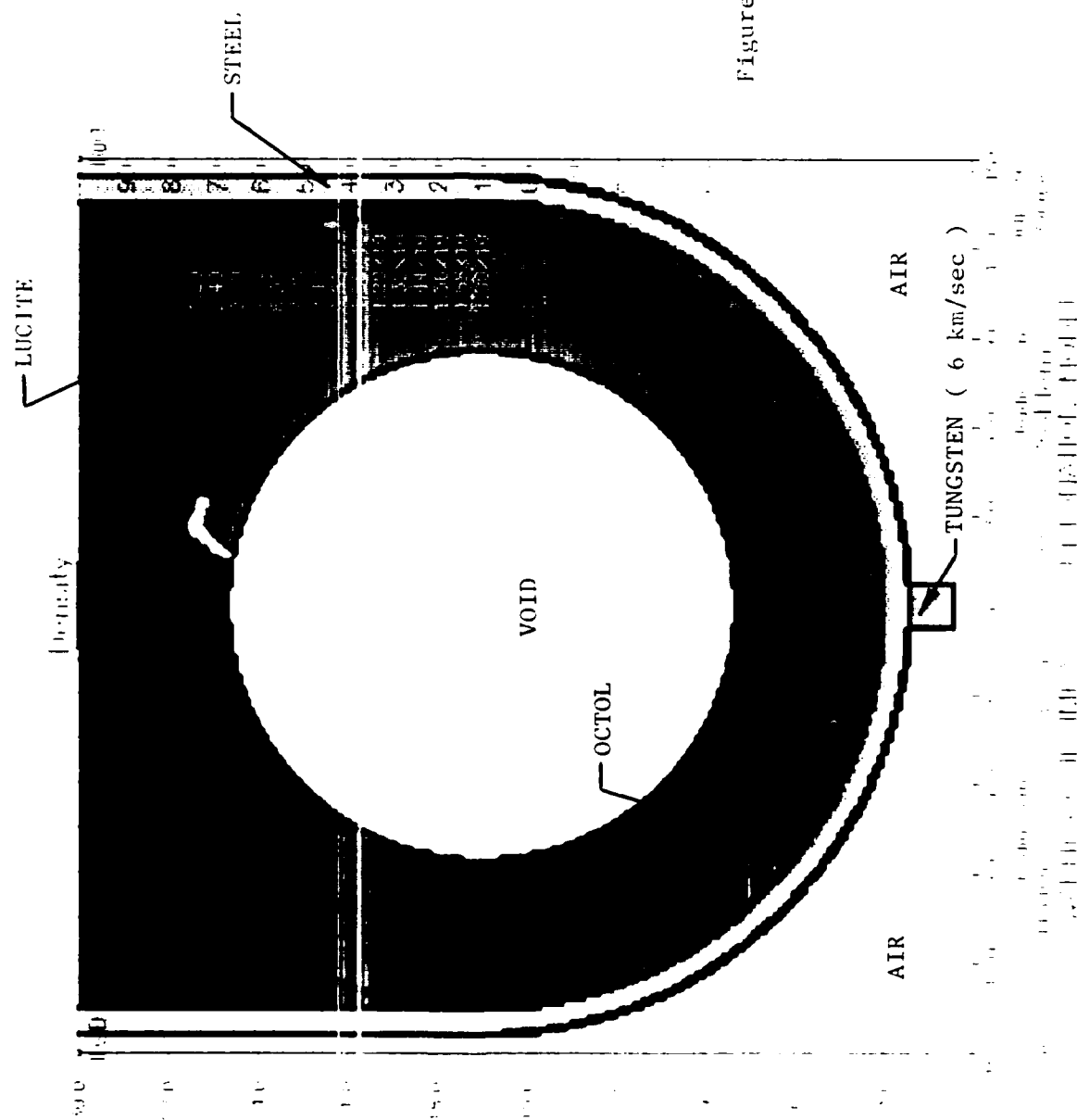
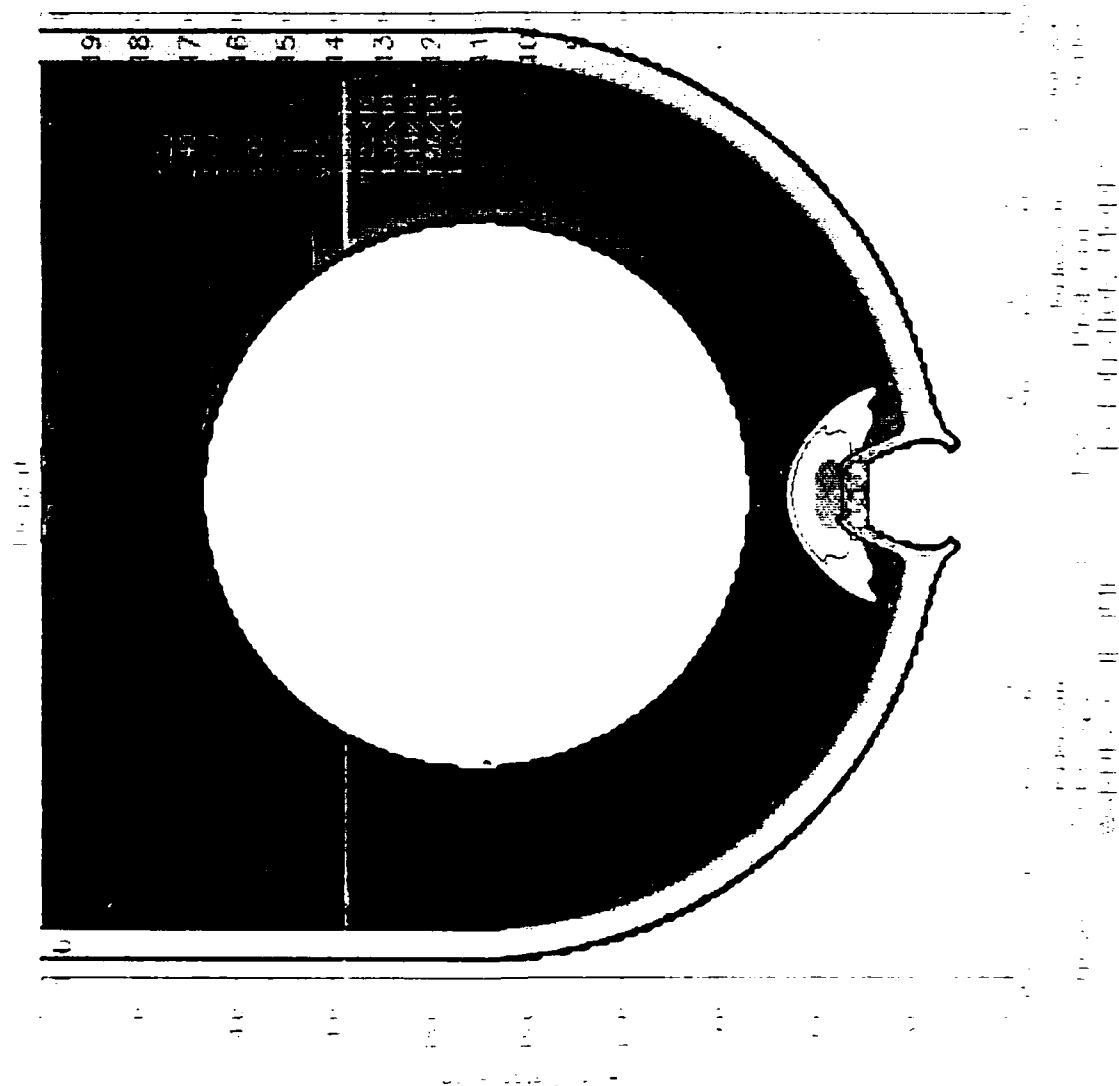Figure 1. Configuration prior to impact at 6 km/sec.

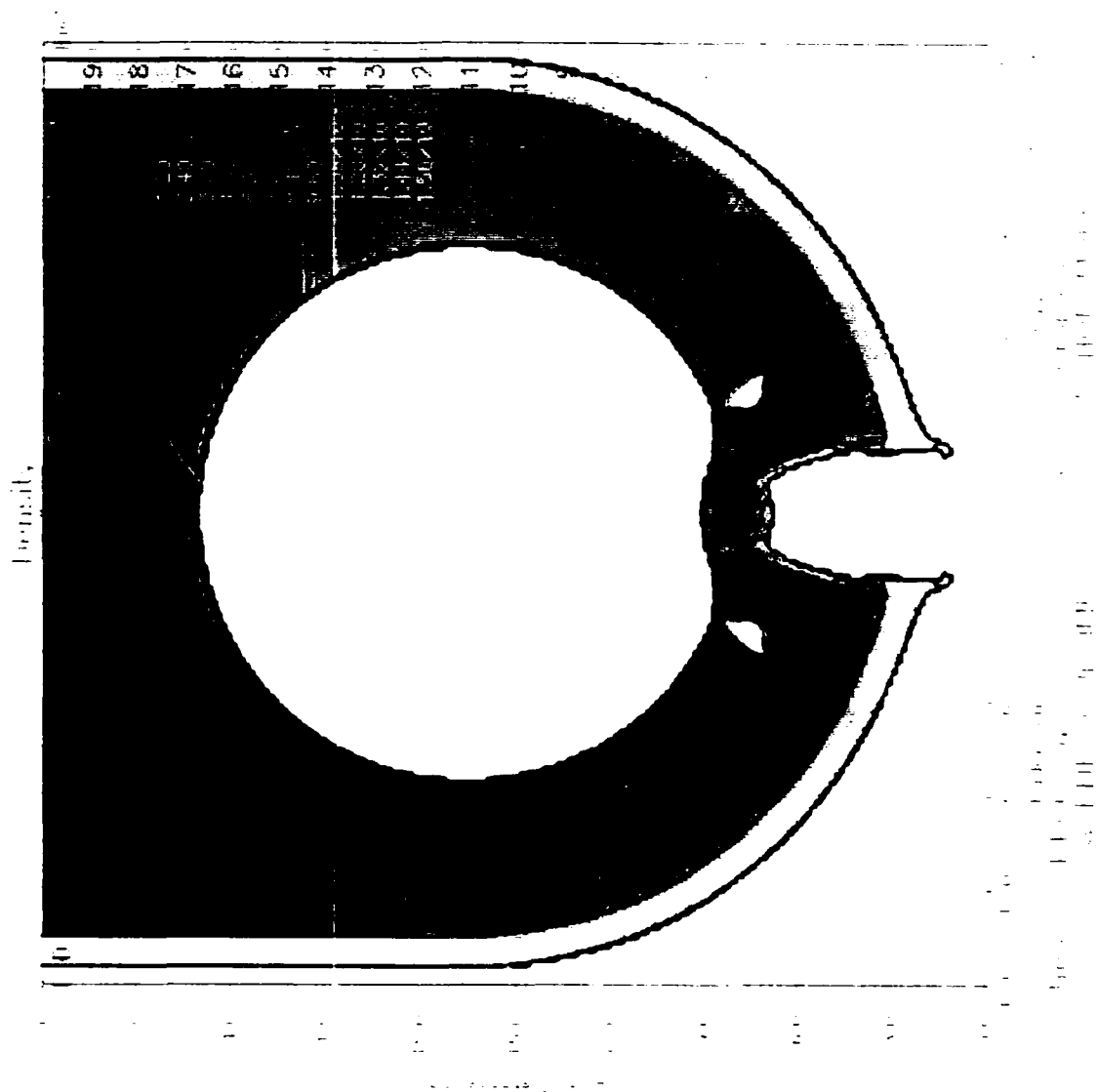Figure 2. Configuration 7 μ sec after impact without detonation.

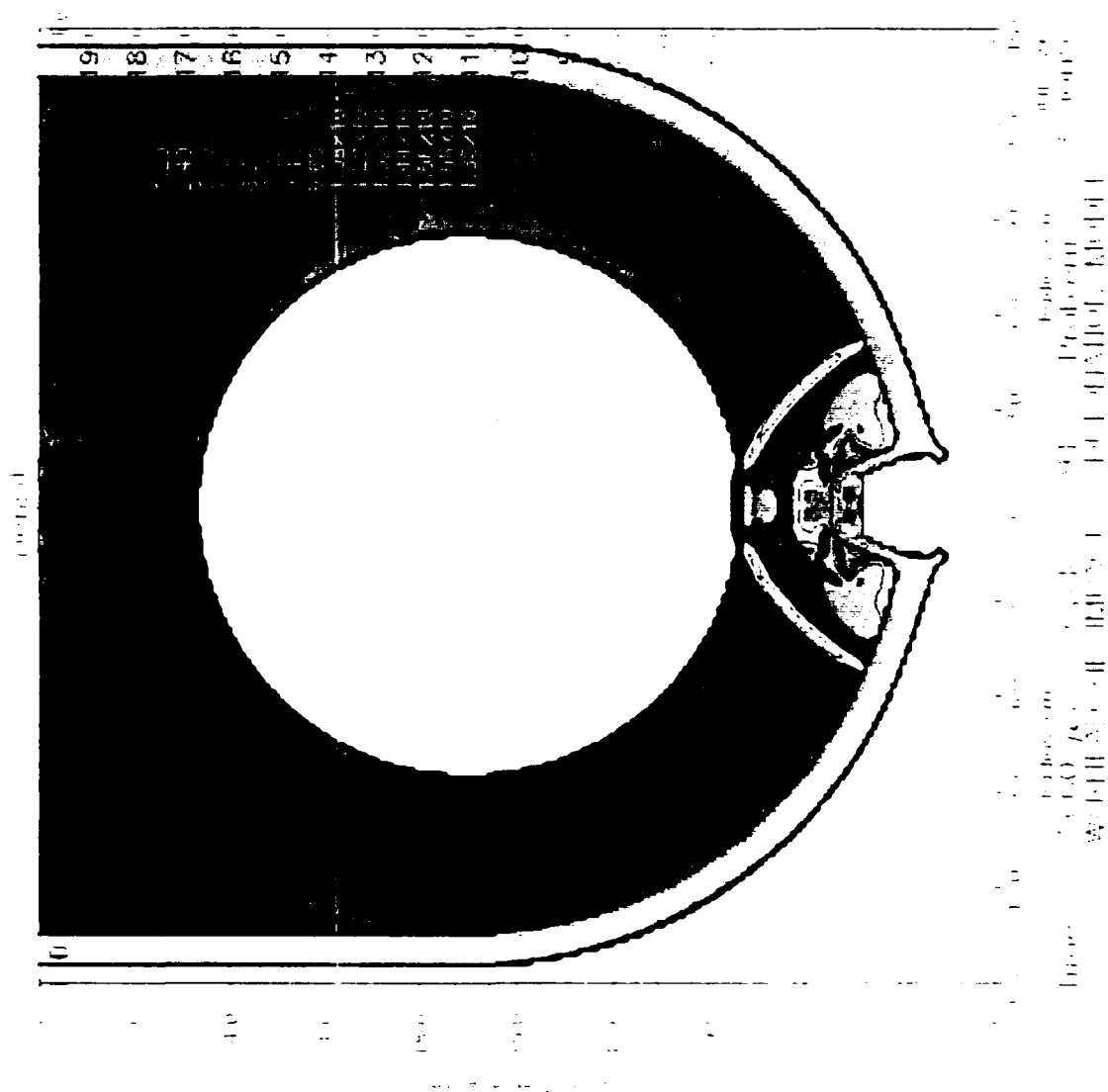Figure 3. Configuration 14 μ sec after impact without detonation.

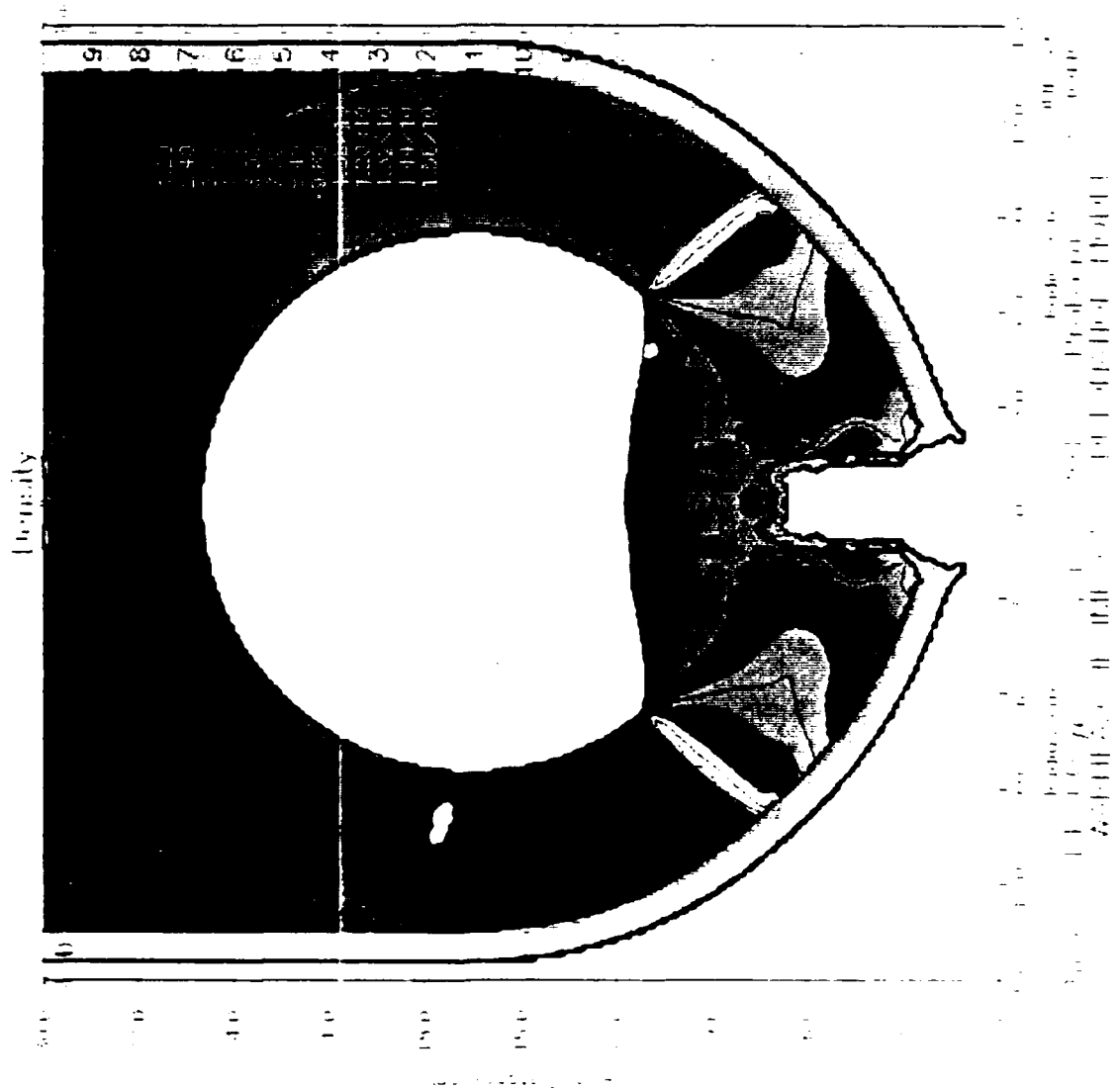Figure 4. Configuration 7 μsec after impact with detonation.

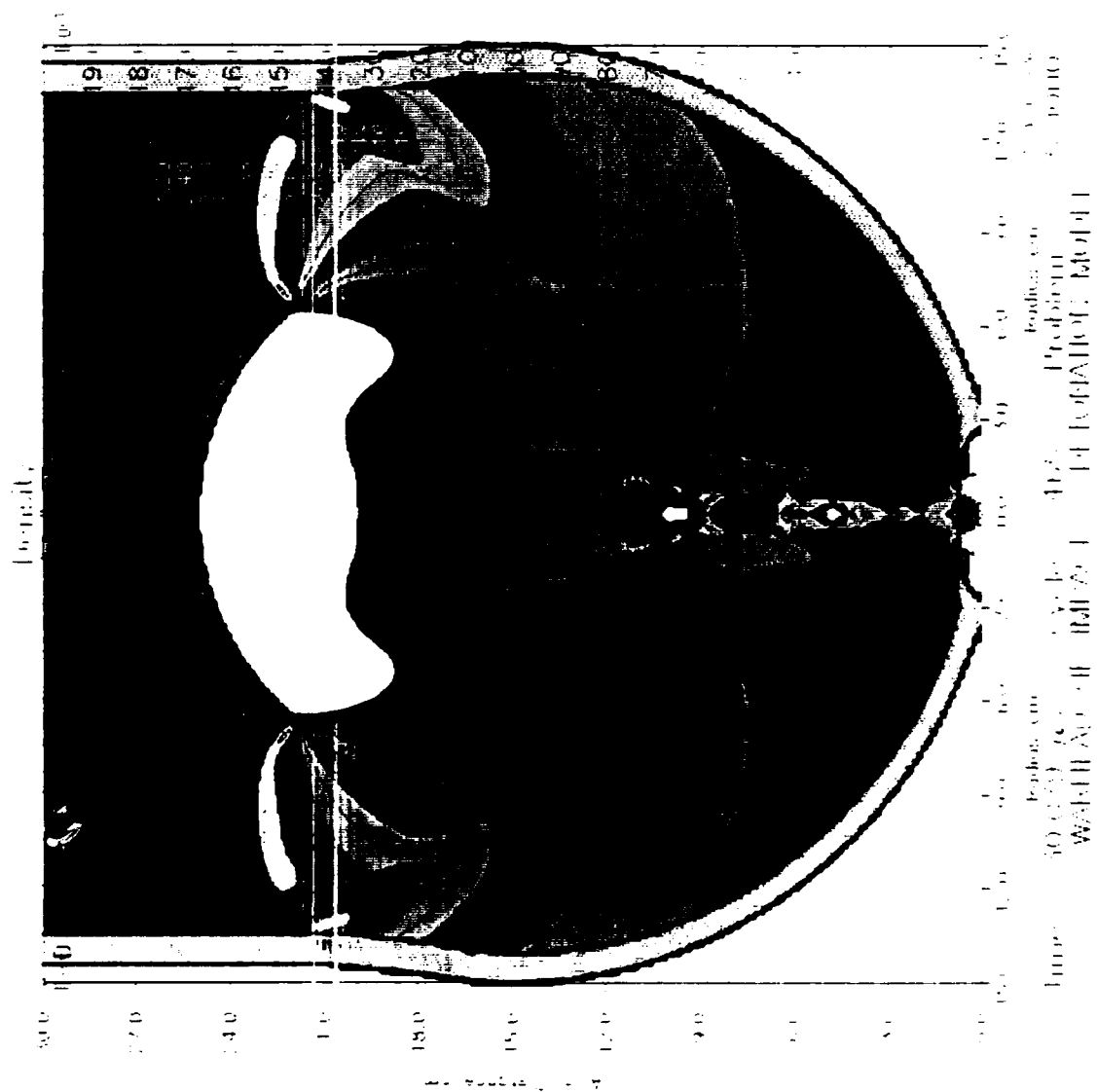Figure 5. Configuration 14 μ sec after impact with detonation.

Figure 6. Configuration 30 μ sec after impact with detonation.

VII. INPUT FILE TO GENERATE DETONATION PROBLEM:

```
KEEL PROBLEM=5.0000
STRESS=0 STRAIN=1 FAIL=1
VISC=1 DVISC=2
IMAX=193 JMAX=225
IQ=7 JQ=17
UREZ=0 VREZ=0
HEADER
 WARHEAD HE IMPACT - DETONATION MODEL
NM=6 AIR=1 FE=2 MOCTOL=3 OCTBRN=4 LUCITE=5 W=6
BURN=1
MESH
X0=0 XMAX=28.95 NX=193
Y0=0 YMAX=33.75 NY=225
GENERATE
 PACKAGE FE RECTANGLE X1=13.5 Y1=16.5 X2=14.4
 PACKAGE FE CIRCLE XC=0 YC=16.5 RAD=14.4
 DELETE CIRCLE XC=0 YC=16.5 RAD=13.5
 DELETE RECTANGLE X1=0 Y1=16.5 X2=14.4
 PACKAGE LUCITE RECTANGLE X1=0 Y1=16.5 X2=13.5
 DELETE CIRCLE XC=0 YC=16.5 RAD=13.5
 PACKAGE MOCTOL CIRCLE XC=0 YC=16.5 RAD=13.5
 DELETE CIRCLE XC=0 YC=16.5 RAD=8.55
 PACKAGE AIR CIRCLE XC=0 YC=16.5 RAD=8.55
 PACKAGE W V=6.0E5 RECTANGLE X1=0 Y1=.6 X2=.75 Y2=2.1
 PACKAGE AIR RECTANGLE
 DELETE RECTANGLE X1=0 Y1=16.5 X2=14.4
 DELETE CIRCLE XC=0 YC=16.5 RAD=14.4
 DELETE RECTANGLE X1=0 Y1=.6 X2=.75 Y2=2.1
```

VIII. RECOMMENDATIONS:

a.   Modeling a shock initiated detonation of an explosive has been implemented using to the physics burn model of HULL. A change file has been provided in section V of this report which will allow these changes to be implemented with any running of the HULL system. The research presented herein represents a first step in studying the more complex problem of the lethality of hypergolic munitions. The present modeling possesses several limitations:

(i)   It can only model detonations. There are other types of reactive responses, namely; retonation and deflagration which are of importance and deserve to be analyzed.

(ii)   It cannot model situations in which the penetrator outruns the detonation front. There are situations where this could be important.

b.   Several questions arose during the course of the research. These questions are provided as evidence of the need for future research:

(i)   Does the shock initiated detonation model that has been incorporated in the physics burn model actually model reality? Perhaps a way to answer this question is to perform a series of experiments to see how closely results can be matched with reality.

(ii)   Can the reactive responses of retonation and deflagration be handled within HULL through modifications or do new modules have to be built which handle these phenomena?

(iii)   What is the effect of considering the shock-to-detonation transition? The modification to the physics burn model of HULL assumed that this transition was instantaneous.

(iv)   Can the detonation front be overdriven, that is can the physics of an impact scenario spawn a detonation front that moves at a speed that is faster than the detonation velocity in the explosive?

REFERENCES

1. HULL Documentation, Vol. I, Technical Discussion,
   Orlando Technology, Incorporated, Shalimar,
   FL., 1987.

2. HULL Documentation, Vol. II, Users Manual, Orlando
   Technology, Incorporated, Shalimar, FL., 1987.

3. Lee, E.L. and L.G. Green, "Detonation of Explosives in
   Accidents," Energy and Technology Review, Lawrence
   Livermore National Laboratory, Livermore, CAL.,
   Jan. - Feb. 1988, pp. 29 - 36.

4. Department of the Army Technical Manual TM 9-1300-214,
   Military Explosives, Chapter 4, Sept. 1984,
   pp. 4-1 - 4-17.

1989 USAF-UES SUMMER FACULTY RESEARCH PROGRAM

GRADUATE STUDENT RESEARCH PROGRAM

Sponsored by the

AIR FORCE OFFICE OF SCIENTIFIC RESEARCH

Conducted by the

Universal Energy Systems, Inc.

<u>FINAL REPORT</u>

<u>Distributed Filter Architecture</u>

<u>Implementation with VLSI</u>

<u>And</u>

<u>Expert Systems</u>

Prepared by:	Asad Yousuf
Academic Rank:	Assistant Professor
Department and	Engineering Technology Department
University:	Savannah State College
Research Location:	AFATL/AGI Eglin AFB Eglin, FL 32542
USAF Researcher:	Mr. Michael Wallace
Date:	August 21,1989
Contract No:	F49620-88-C-0053

Distributed Filter Architecture

Implementation with VLSI

And

Expert Systems

by

Asad Yousuf

<u>ABSTRACT</u>

This research project aims at obtaining an architecture
for a distributed filter. Much of the existing literature
was reviewed and the suggested architecture is shown to
have both, memory, speed and complexity advantages over the
conventional filter. Simplified software procedures were
developed to compute table look up contents on the VAX 11/785
and the Numerix MARS 432 series array processors in the
RSPL/IPL laboratories at the Air Force Armament Laboratory.

The proposed architecture was implemented with the VLSI
technology and final die size was estimated to demonstrate
its effectiveness. Software for design/development of
integrated circuits is also suggested.

Finally, expert system techniques applicable to the pattern
recognition environment is suggested to enhance the existing
capabilities of the RSPL/IPL laboratories at Eglin Air
Force Base.

ACKNOWLEDGMENTS

I would like to thank the Air Force Systems Command and
Air Force Office of Scientific Research for sponsorship
of this research. Special acknowledgement goes to
Universal Energy Systems for providing me the opportunity
to work at the US Air Force Armament laboratories for the
summer of 1989.

I am immensly thankful to Mr. Michael Wallace (Chief, Radar
and Image Simulation Section) for his support,
encourgement, a truly delightful and productive working
atmosphere.

Additional appreciation goes to Mr. Michael Deiler (Program
Manager RSPL/IPL laboratories), Mr.Steve Halprin (System
Manager) and Mr. Lee Presswood (Program Manager of IPL) for
their assistance in my study of this project.

Last but not least, I acknowledge with great appreciation
the support of my home institution and especially that of
Dr. M. C. Robinson (Dean) and Dr. Lester B. Johnson
(Department Head of Engineering Technology) at Savannah
State College, Savannah Ga.

INTRODUCTION:

As a result of VLSI fabrication technology, all forms of information processing are dramatically reducing in cost. One area in which VLSI is most pronounced is in the field of real-time signal processing. Through VLSI technology, implementation of powerful real time signal processing is possible.

The AGI division of the Armament Laboratory at the Eglin Air Force Base is moving toward improving signal processing techniques. My research this summer is a step toward that goal.

The availibility of low cost, high performance memory chips have promoted the study of memory intensive architectures by replacing time consuming conventional arithmetic operations with high speed table look up calls producing high data throughputs.

This paper discusses implementation of a Chebyshev filter based on distributed arithmetic concepts. First, the architecture of the filter is designed/developed and then the individual devices of the architecture are implemented with the VLSI technology concepts.

Knowledge-based or expert systems are being applied in a variety of domains; solving problems of control, monitor and diagnostics. Providing automation in pattern recognition environment is a dynamic area for the application of Artificial Intelligence in the AGI division of the Armament Laboratory at Eglin Air Force Base.

II. OBJECTIVES OF THE RESEARCH EFFORT:

The RSPL/IPL laboratories at Eglin AFB are a full functional computing facilities incorporating high resolution image processing, algorithm development and validation, seeker performance validation, statistical analysis of data and other functions.

Currently, there are no tools for design/development of integrated circuits in the area of Digital Signal Processing. The RSPL/IPL laboratories at present do not have any Expert System environment applicable to pattern recognition.

The principle objectives of my research as a participant in the 1989 Summer Faculty Research Program (SFRP) were to:

1. Design/Implement an architecture of a distributed filter.
2. Suggest some software for design/development of integrated circuits.
3. Investigate the MARS 432 series array processor.
4. Suggest some Expert System techniques applicable to pattern recognition environment.

Specifically, the research effort aims at introducing an architecture for a distributed filter that is shown to have both memory, speed and complexity advantages over the conventional filter. Long term objectives of the research are to investigate expert system techniques.

It was decided by my focal point that an investigation
into the development/implementation of a more specific
Expert System techniques applicable to the RSPL/IPL
laboratories , can be undertaken during the summer of 1990
and can be continued at my home institution with the funding
from a mini-grant.

III.

a. Numerous methods for classical linear shift invariant
filters now exist. Low cost high performance memory chips
have promoted the study of memory intensive architecture.
A 4th order Chebyshev filter, having a transfer function
is expressed as :

$$H(z) = \frac{.00183 \; (1 + z \char`^ -1)}{(1-1.49 \; z\char`^-1 +.84 \; z\char`^-2)(1-1.15 \; z\char`^-1 +.64 \; z\char`^-2)}$$

In time domain one can express the above as:

$$Y(n) = Ai \; x(n-i) + Bi \; y(n-i)$$

Since there are 9 binary valued variables on the right hand
side of the filter model. A $2\char`^9$ x n bit memory unit is
needed.

The architecture of the system is illustrated in Figure 1.
A Fortran program is developed to compute table look up
contents on the VAX 11/785 and MARS 432 series array
processor. Programmable Logic Array (PLA) based table look up
is also generated.

The effectiveness of developed architecture can be evaluated by implementing it on a chip. The three main blocks on the chip are: Shift registers, PLA and Adder. These blocks are placed next to each other in the center of the chip, between the two ports.

Decoupling design from frabication allows IC designers total freedom from process technology. Estimating the final die size of semicustom d   gn is important for the ASIC design engineers. The MOSIS accepts design files using standard design rules and standard mask languages (CIF or GDS) via computer networks (ARPANET,TELENET or CSNET). The link of such a design process is shown in Figure 2.

The final die is estimated by computing the cell area of the individual cells invoked from the cell library and calculating the complexity for the architecture under discussion.

COMPLEXITY	CELL AREA	CELL NAME	FUNCTION
8	269 X 881	74LS393	4-Bit Shift register.
16	89 x 139	FA.MAG	2-Bit Full Adder
2	190 x 380	PLA.MAG	15 Inputs 48 p-terms 4 outputs

A1 = 8 x 269 x 881 = 1895912 Sq micron

A2 = 16 x 89 x 139 = 1979936 Sq micron

A3 = 2 x 190 x 380 =144400 Sq micron

Total Cell Area = A1 + A2 + A3 = 4020248 Sq micron

Total routing area = (60%) * (Total area)

$$= (.6) * (4020248) = 2412148.8 \text{ Sq micron}$$

Total area = Total cell area + Total routing area

$$= 4020248 + 2412148.8 = 6432397$$

Die size = 2.536 x 2.536 mm.

The standard frame used is 28p46x34, with 7 pads on each side and a total number of pads equals 28.

Artificial Intelligence is a field of Computer science that can take many forms. One form of AI, Expert or Knowledge-Based system can identify optimal attack scenerios to hit enemy airfield, selects friendly airbases, aircraft type and munitions capable of making the attack, and then calculates the effects of attack.

The process of knowledge acquisition is recogonized as one of the most difficult and time consuming activities in constructing an Expert System. The model based technique can be used to simplify the process of knowledge acquisition.

Knowledge representation based on frames can be used to represent generic information. Frames are composed of complex data structure and procedures. Frames are often built in terms of hiearchy, so that frames at lower levels of the hiearchy can inherit properties from the frames at higher levels. Frames can also inherit properties from more than one parent. Thus frame representation approach can be used to construct a model for pattern recognition.

Pattern matching is the process of comparing symbolic expression to determine if one is similar to another. The pattern matching procedure is a key element of a rule-based expert system program. Although LISP itself has no pattern matching built in, it is easy to write pattern-matching procedures in LISP. Pattern matching procedures can easily be developed on the VAX 11/785 in the RSPL/IPL laboratories.

Evidently, much of the expert's knowledge can be represented as a collection of rules, all of which have the following forms:

```
(Rule <name>
        (IF <antecedent assertion 1>
            <antecedent assertion 2>
            . . .
            <antecedent assertion n>
        (THEN <consequent assertion 1>
              <consequent assertion 2>
            . . .
              <consequent assertion n>
```

These rules are called if-then rules, situation rules, or production rules. Systems based on such rules are being applied in variety of domains; solving problems of control, monitor and diagnostic.

Frames can be used to represent the facts known about an object, previously stored as a set of property values on the property list of the object.

b. The design of the distributed filter architecture was sucessfully completed and implemented. The standard frame with the pin numbers is shown in Figure 3. Pin numbers and their description are as follows:

PIN #	Description	I/O
1	(SD) Serial data input	I
2	(CP) Clock pluse input	I
3	(CL) Clear input	I
4	(+/-) 2's complement	I
5-20	D0 - D15 (Data output)	O
21	(VCC) Power	I
22	(GND) Ground	I

Simplified software procedures for table look computation is shown on pages 12 - 15. The software procedures were developed on a VAX 11/785 and MARS 432 series array processor.

The procedures were implemented in Numerix Fortran to demonstrate the efficiency of Numerix Fortran.

IV. RECOMMENDATIONS:

a. The distributed filter architecture that was designed and developed can be implemented using standard design rules and standard mask languages (CIF or GDS) via computer networks (ARPANET, TELENET or CSNET). To enhance the process of minimization, timing verification and layout generation, software tools such as ESPRESSO (Boolean expression minimization), MPLA (PLA generator), MAGIC (Graphical tool) and CRYSTAL (Timingverifications) are recommended.

The Numerix NMX 432 is a modern array processor that can improve the computational speed of the host computer. A typical application program will run 20 - 100 times faster when the NMX-432 is included as part of the system. Interfacing the Array Processor to the external world can be attained by the NMX-432 high speed A/D converter line which consist of 5 high speed data acquisition packages.

b. Expert or Knowledge-Based systems are transforming computers into truly intelligent assistants. Unlike traditional computers, which perform computational tasks based on programmed procedure and data, these new generation computers are able to draw human reservoirs of knowledge, emulating many patterns of human thought.

Expert system design methodology applicable to the RSPL/IPL laboratories is illustrated in Figure 4. Domain expert in an area such as radar analysis and modeling systems, describes facts, concepts, goals and rules in knowledge representation language and the inference engine manages the reasoning process ie, the application of knowledge at run time. By using the mouse and keyboard, the user can change the data base causing the system to perform screen updates reflecting new representations.

To implement Expert System techniques in the RSPL/IPL laboratories, it is suggested to acquire Automated Reasoning Tool designed by the Inference Corporation for developing Knowledge-Based Systems.

```
0001            PROGRAM MSIA1
0002            REAL *4 ARRAY1(9),ARRAY2(512),SUM
0003            INTEGER*2 IERR(6),ISTAT(4)
0004            INTEGER*4 STRADR,ARRAY1ADR,ARRAY2ADR,SUMADR
0005            INTEGER*4 ARID,ARLUN,ABNLUN
0006            DATA ABNLUN,ARLUN/2,0/
0007            WRITE (6,*)'ENTER THE ID OF THE DESIRED MARS UNIT'
0008            READ (5,*)ARID
0009            CALL ARATT(ARLUN,ARID,IERR)
0010            CALL ARABN(ARLUN,ABNLUN,'MSIA1.ABN',1,-1,IERR)
0011            CALL ARRUA('MSIA1',STRADR,IERR)
0012            CALL ARVRA('MSIA1','ARRAY1',ARRAY1ADR,IERR)
0013            CALL ARVRA('MSIA1','ARRAY2',ARRAY2ADR,IERR)
0014            CALL ARVRA('MSIA1','SUM',SUMADR,IERR)
0015            READ (*,103) (ARRAY1(I),I=1,9)
0016     103    FORMAT (F20.12)
0017            CALL ARPUT(ARLUN,9,ARRAY1,3,-1,ARRAY1ADR,1,0,IERR)
0018            CALL ARRUN(ARLUN,STRADR,IERR)
0019            CALL ARHWT(ARLUN,ISTAT,-1,IERR)
0020            CALL ARGET(ARLUN,512,ARRAY2,3,-1,ARRAY2ADR,1,0,IERR)
0021            WRITE(6,100)ARRAY2
0022     100    format(1x,3e27.13)
0023            STOP
0024            END
```

PROGRAM SECTIONS

	Name	Bytes	Attributes						
	0 $CODE	231	PIC CON REL LCL	SHR	EXE	R
D	NOWRT LONG					
	1 $PDATA	107	PIC CON REL LCL	SHR NOEXE	R
D	NOWRT LONG					
	2 $LOCAL	2432	PIC CON REL LCL NOSHR NOEXE	R
D	WRT LONG					

        Total Space Allocated   2770

ENTRY POINTS

      Address   Type   Name

    0-00000000   MSIA1

VARIABLES

      Address Type Name   Address Type Name   Address T
ype Name   Address Type Name

    2-00000850 I*4 ABNLUN   2-00000848 I*4 ARID   2-0000084C
I*4 ARLUN   2-0000083C I*4 ARRAY1ADR
    2-00000840 I*4 ARRAY2ADR   **   I*4 I   2-00000838
I*4 STRADR   **   R*4 SUM
    2-00000844 I*4 SUMADR

ARRAYS

    Address   Type   Name   Bytes Dimensions

    2-00000000 R*4   ARRAY1   36 (9)
    2-00000024 R*4   ARRAY2   2048 (512)
    2-00000824 I*2   IERR   12 (6)
    2-00000830 I*2   ISTAT   8 (4)

LABELS

    Address   Label   Address   Label

    1-00000063 100'   1-0000005F 103'

FUNCTIONS AND SUBROUTINES REFERENCED

  Type Name   Type Name   Type Name   Type Name
          Type Name   Type Name

        ARABN   ARATT   ARGET   ARHWT
              ARPUT   ARRUA
        ARRUN   ARVRA

0001

COMMAND QUALIFIERS

  FOR/LIST=MSIA1.LST MSIA1

  /CHECK=(NOBOUNDS,OVERFLOW,NOUNDERFLOW)
  /DEBUG=(NOSYMBOLS,TRACEBACK)
  /STANDARD=(NOSYNTAX,NOSOURCE_FORM)
  /SHOW=(NOPREPROCESSOR,NOINCLUDE,MAP,NODICTIONARY,SINGLE)
  /WARNINGS=(GENERAL,NODECLARATIONS,NOULTRIX)
  /CONTINUATIONS=19 /NOCROSS_REFERENCE /NOD_LINES /NOEXTEND_SOURCE /F77
  /NOG_FLOATING /I4 /NOMACHINE_CODE /OPTIMIZE /NOANALYSIS

COMPILATION STATISTICS

  Run Time: 0.94 seconds
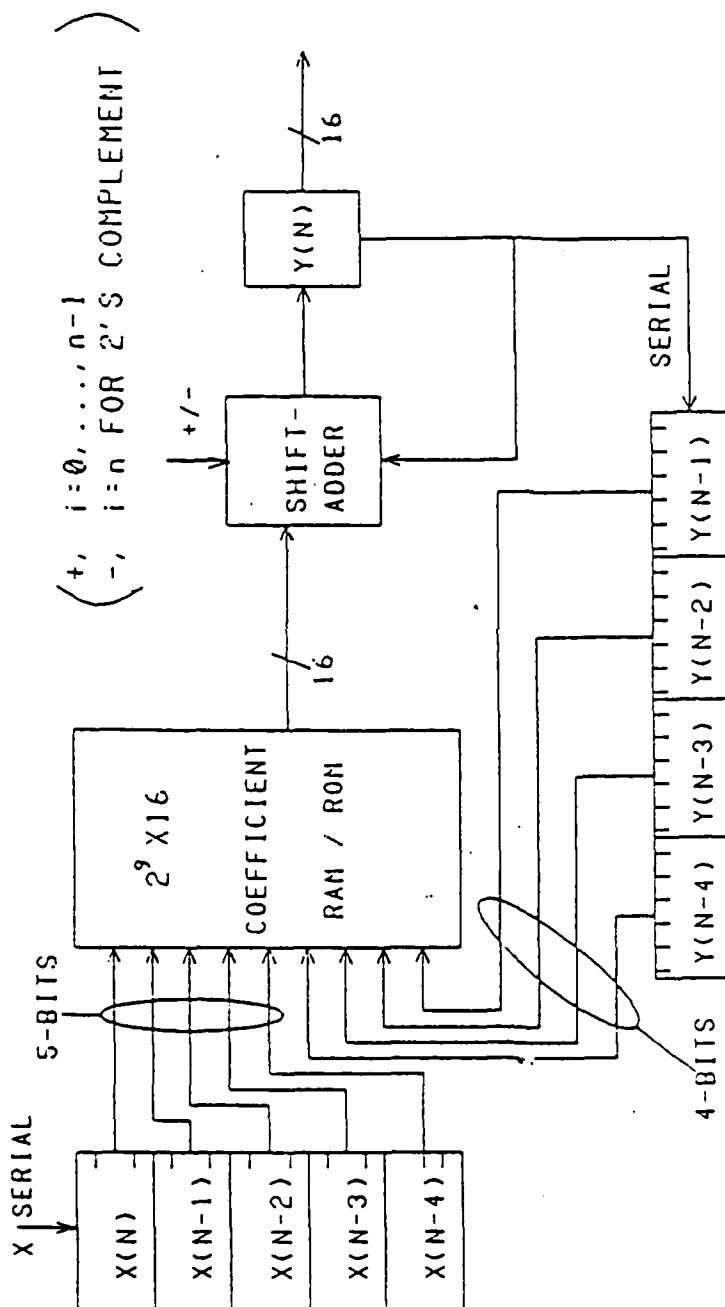 Elapsed Time: 1.38 seconds
  Page Faults: 549
  Dynamic Memory: 335 pages

```fortran
      PROGRAM MSIA1
      DIMENSION ARRAY1(9),ARRAY2(512)
      INTEGER J,NUM
      REAL*4 ARRAY1,ARRAY2,SUM,ITEMP
      DO 163 L=1,512
      SUM=0.0
      NUM=L-1
      DO 157 I=1,9
          ITEMP=NUM/2
          J=NINT((NUM)-(2*ITEMP))
          NUM=ITEMP
      IF (J.EQ.0) GOTO 157
      SUM =SUM + ARRAY1(I)
157   ENDDO
      ARRAY2(L)=SUM
163   ENDDO
      STOP
      END
```

$$\left(\begin{array}{l} +, \quad i=0,\ldots,n-1 \\ -, \quad i=n \text{ FOR 2'S COMPLEMENT} \end{array}\right)$$

X SERIAL

X(N)
X(N-1)
X(N-2)
X(N-3)
X(N-4)

5-BITS

2^9 X16 COEFFICIENT RAM / ROM

16

SHIFT-ADDER   +/-

Y(N)   16

SERIAL

Y(N-4) Y(N-3) Y(N-2) Y(N-1)

4-BITS

DISTRIBUTED FILTER ARCHITECTURE

ARCHITECTURE	DATA RATE KHZ	IC COUNT	PERCENT $ MEMORY	PERCENT $ S/R	PERCENT $ ALU	KHZ/$
CONVENTIONAL:250ns multi.	54.4	77	15.58	41.56	42.85	680.9
CONVENTIONAL:85ns multi.	117.5	137	8.76	23.36	67.88	857.5
CONVENTIONAL: VLSI ALU	86.8	49	9.92	26.41	63.60	690.5

FIGURE 1

FIGURE 2

STANDARD CELL LIBRARY

STANDARD DESIGN RULES

STANDARD FRAMES

STANDARD PACKAGE

RSPL/IPL DESIGN HOUSE

MOSIS SILICON FOUNDRY

PACKAGED

CHIP

CIF OR GDS

VIA CSNET

FIGURE 3

DSP

SD 1
CP 2
CL 3
+/ 4
D0 5
D1 6
D2 7

D3 8
D4 9
D5 10
D6 11
D7 12
D8 13
D9 14

D10 15
D11 16
D12 17
D13 18
D14 19
D15 20
VCC 21

NC 28
NC 27
NC 26
NC 25
NC 24
NC 23
GND 22

EXPERT SYSTEM DESIGN METHODOLOGY

USERS

SYSTEM CONCEPT

IDEAS

IDEAS

USER ENGINEERING
USER CHANGES
DATA BASE USING
KEYBOARD AND MOUSE

SYSTEM UPDATES
SCREEN TO REFLECT
NEW REPRESENTATION

INFERENCE ENGINE
PROBLEM SOLVING
STRATEGIES
OPPORTUNISTIC
RULE APPLICATIONS
HYPOTHETICAL REASONING
CONSISTENCY
MAINTENANCE
SEARCH
TEST
AND
RELEASE

DESIGN ENGINEERING
DOMAIN EXPERT
(RADAR ANALYSIS AND
MODELING SYSTEMS)

KNOWLEDGE BASE
1. FACTS
2. CONCEPTS
3. GOALS
4. RULES

KNOWLEDGE REPRESENTATION
LANGUAGE

FEEDBACK

FEEDBACK

SYSTEM DEFINITION

FIGURE 4

REFERENCES

1. C.S. Burrus, "Digital Filter Structures described by distributed arithmetic filters," _IEEE Transaction on circuits and systems_. Dec 1977, pp. 674-680.

2. Weste, _Principles of CMOS VLSI Design_.

3. John Newkrik and Robert Mathews, _The VLSI Designer's Library_.

4. Henry C. Mishkoff, _Understanding Artificial Intelligence_

5. Edwin New "Knowledge Based Control and Redundancy Techniques used in NASA's Kate project." _AI Applications Office NASA, Kennedy Space Center_.

6. Duke P. Briscoe, "Expert systems in Government Symposium", _Computer Society Press_.

7. Dr. H. Kobayashi, _Custom VLSI Design_, Department of Electrical and Computer Engineering, University of South Carolina.

8. Guy Rabbat, _Hardware and Software Concepts in VLSI_.

9. Tim Hartnell, _Exploring Artificial Intelligence on your IBM PC_, Bantam Books.

10. John R. Jamieson, "A mandate for autonomous control and monitor systems." _AI Applications Office KSC_.

11. CMOS Cell Library, _Center for Machine Intelligence_ Department of Electrical and Computer Engineering University of South Carolina.

12. Guner S. Robinson, "Knowledge-based Engineering and Expert Systems," _Computer Society Press_.

1989 USAF-UES SUMMER FACULTY RESEARCH PROGRAM/ GRADUATE STUDENT RESEARCH PROGRAM

Sponsored by the

AIR FORCE OFFICE OF SCIENTIFIC RESEARCH

Conducted by the

Universal Energy Systems, Inc.

FINAL REPORT

RESPONSE OF INFRARED DETECTORS TO PULSED RADIATION

Prepared by:	Brian P. Beecken
Academic Rank:	Assistant Professor
Department and	Physics Department
University:	Bethel College
Research Location:	AEDC Arnold AFB Tullahoma, TN
USAF Researcher:	P. David Elrod
Date:	11 Aug 89
Contract No:	F49620-88-C-0053

RESPONSE OF INFRARED DETECTORS TO PULSED RADIATION

by

Brian P. Beecken

ABSTRACT

The ability of an infrared detector to respond quickly to pulsed radiation is of great importance to a new generation of test systems that sequentially irradiate the individual pixel elements of a focal plane array. An investigation of the response times of IR detectors has revealed a fundamental limit, applicable to all types of detectors, which is close to the pulse lengths (on the order of microseconds) of a current test system. Factors that lengthen the response time of a particular type of detector beyond the fundamental minimum have been examined. The response time constant of an extrinsic photoconductor may be altered by changing such conditions as the applied bias and the background photon flux.

I. INTRODUCTION

An important task performed at Arnold Engineering Development Center (AEDC) is the testing of infrared focal plane arrays. Infrared (IR) detectors of this type are designed for a variety of tactical and strategic missions. In the future, IR detectors will probably serve crucial roles in a space-based defense system where they will be used for surveillance, discrimination, and tracking.

The high cost of putting equipment in space necessitates extensive ground-based testing. For many years now, the use of blackbodies for the measurement of responsivity, dynamic range, detectivity, and other figures-of-merit for IR detectors has been standard practice. Nevertheless, testing a detector's ability to discriminate and track objects in space requires the generation of complex moving scenes -- a task that is both difficult and expensive with conventional blackbodies.

AEDC has approached this problem by developing a revolutionary method for testing IR detectors called the Direct-Write Scene Generation (DWSG) system. In this system, a laser beam is deflected in such a manner that each individual detector element of the focal plane array is exposed to a brief pulse of radiation. The laser beam is deflected by an acousto-optic device. The dynamic scene content is input to a computer which electronically controls the acousto-optic device. Thus, the laser beam is scanned across the focal plane array and "paints" the scene one pixel at a time in a method analogous to that of the electron beam in a television set.

Prior to the Summer Faculty Research Program at AEDC, I had spent two years working in the area of IR detection at Texas Instruments in Dallas. Part of my time was spent in a laboratory testing the linearity of response of

a detector element at various levels of background radiation. Another major responsibility was the development of a test station for a focal plane array with over four thousand pixels. During this time I became interested in the principles of semiconductor physics that determine the operating characteristics of IR detectors.

My experience in testing IR detectors, combined with my interest in the basic physics behind their operation, made the assignment to the DWSG project a natural one and, I believe, a productive one.

II. OBJECTIVES OF THE RESEARCH EFFORT

The primary objective of my summer research effort was to support the development of the DWSG system. I was asked to review the overall DWSG concept and the assumptions and technologies that underpin it. The purpose of this evaluation was to identify any weaknesses and false assumptions inherent in the DWSG system.

A significant amount of effort was devoted to developing the proper framework from which to proceed on this analysis task. I started by attending a Scene Generation Workshop which provided a good background for the nature of the testing problem and the approaches various groups were taking to solve it. Time was spent studying the present blackbody-based test chamber at AEDC which is used to calibrate the DWSG for each test. Of course, much effort was expended on understanding how the DWSG system itself worked. I also had the privilege of reviewing data as it was obtained from tests performed on both the blackbody-based test chamber and the DWSG.

Throughout the familiarization process I developed many questions and doubts about various aspects of the system. This time of searching and questioning was the check that the laboratory desired, and fortunately, most of the issues raised were easily dismissed. There was, however, one potential problem area that refused to go away: how long are the response times of the detectors and are these response times consistent?

The DWSG is designed to operate at real-time speeds. The focal plane arrays consist of thousands of pixels, and the picture content of an entire array (i.e., a "frame") is usually read out to the sensor electronics as frequently as every millisecond or tenth millisecond. Therefore, if each pixel is to be irradiated during one frame, the beam's visitation time at each detector element must be on the order of microseconds.

The issue here is twofold. When irradiated by a short pulse, will the detector element respond quickly enough to give the same output signal that it would give when irradiated by the continuous photon flux from a real scene? And secondly, will the output signal from the detector persist for several frames after the pulse is over? These questions cut quickly to the essential core: how well will the DWSG system be able to simulate real life scenes?

The issue of detector response time is what absorbed the majority of my efforts at AEDC. In order to answer the above questions, I established two goals. First, I attempted to determine what fundamental limitation existed on the speed at which an IR detector could respond to incident photons. Second, I decided to examine a popular type of detector to see if it had a minimum response time that was longer than the fundamental limit.

III. FUNDAMENTAL LIMITATION ON DETECTOR RESPONSE TIME

A. Approach:

Before starting any research project, it is standard procedure to determine what, if any, work has been done in the field previously. Infrared detectors have been the focus of research and development efforts for over three decades. Consequently, I expected a quick search of the literature to yield some references to the response time limitations of IR detectors.

B. Results:

Workers in the field have long considered a detector's response time to be an important characteristic of its performance. A common detection technique is to modulate the incoming signal flux with a mechanical chopper. This technique is used to eliminate baseline drifts and discriminate against electrical noise, but it requires a reasonably fast detector response. Similarly, the electrical frequency at which detectors are run may also put demands on a detector's ability to respond quickly to the incident photons.

For these reasons, standard references such as the <u>Infrared Handbook</u> [1] discuss the frequency response of IR detectors. The variation of a detector's output signal current I as a function of frequency f can usually be written as

$$I(f) = \frac{I(0)}{\sqrt{1 + (2\pi f \tau_{tc})^2}}. \tag{1}$$

When a detector's output follows this form, it will exhibit the classic 3 dB per octave rolloff illustrated in Fig. 1. The response time constant is $\tau_{tc} =$

$1/(2\pi f_{3dB})$. Obviously, a good measure of the response time of the detector is simply the time constant. The crucial question here is what physical significance does τ_{tc} have? Once this question is answered, then the conditions that alter the time constant can be determined.

Many authors (e.g., ref. 2) take the time constant τ_{tc} to be simply the free carrier lifetime. There is a good reason for making this identification. In the common photon detector (the only type of IR detector considered in this report), incident photons produce electron-hole pairs in the interior of the semiconductor material. If n is the number of these excess free carriers and τ is their lifetime, then the continuity equation can be written as

$$\frac{dn}{dt} = g - \frac{n}{\tau}. \tag{2}$$

Here we have represented the carrier generation rate by g and have assumed the influx and efflux of carriers cancels out.

Equation (2) is easily solved. If the photons start to strike the detector at t = 0, then

$$n = \tau g(1 - e^{-t/\tau}). \tag{3}$$

Because a detector's output signal is proportional to the number of carriers, this solution clearly shows that the signal's rise time will be exponential. Similarly, the detector's response to the end of a pulse of photons will be an exponential decay. In both cases the time constant is τ which is also the carrier lifetime. Furthermore, the Fourier transform of the detector's

response to a photon pulse gives the frequency response of Eq. (1). Thus, the time constant of Eq. (1) may simply be the carrier lifetime.

Knowing that a meaningful characterization of a detector requires some explanation of its response time limitations, Borrello [3] sought a fundamental relationship between detectivity D* and response frequency. Using very general arguments, Borrello derived an expression which gives the maximum detectivity possible as a function of carrier lifetime τ:

$$\text{max } D^* = \frac{\tau}{2} \left(\frac{\sigma}{\varepsilon h}\right)^{1/2} \tag{4}$$

where ε = photon energy

and σ = photon capture cross section.

Equation (4) implies that as the frequency of operation of a particular detector is increased, the detectivity will remain constant until an upper limit (determined by the carrier lifetime) is reached. Borrello named this frequency f*. If the time constant of Eq. (1) is indeed the carrier lifetime, then f* is the same as the 3 dB point discussed above. Thus,

$$f^* \approx f_{3dB} = 1/(2\pi\tau). \tag{5}$$

Equation (4) can now be recast in a convenient form:

$$\text{max } D^* f^* = \frac{1}{4\pi} \left(\frac{\sigma}{\varepsilon h}\right)^{1/2}. \tag{6}$$

This expression explicitly shows that speed and detectivity are mutually limiting in a fundamental way. If a detector is forced to run at frequencies higher than f*, then the maximum detectivity possible will be limited. However, increasing speed will not always cause a decrease in detectivity; that only will happen when the detector is already operating at maximum D*f*. Likewise, decreasing the operating frequency will not necessarily increase detector performance but only allow for that possibility.

Borrello compiled a number of experimental results and found that D*f* has a value of about 10^{18} cm $Hz^{3/2}$/watt. For HgCdTe detectors, f* ~ 1 MHz, which corresponds to τ ~ 0.2 μsec. Fortunately, this fundamental limit on response time is less than the pulse widths used in the DWSG system. Caution must be exercised, however, because the difference is only one order of magnitude or less. If there is any factor that forces a detector's response time to be longer than the fundamental limit, then the performance of the DWSG testing will be affected. Most likely the decrease in detectivity will appear as a lowered response to the incident radiation.

IV. RESPONSE TIMES OF EXTRINSIC PHOTOCONDUCTORS

A. Approach:

Having found in the literature a fundamental limit to the response time of IR photon detectors, it seemed appropriate to search further and see if work had been done on factors which might slow a detector's response. I knew that the response time constant could be a complicated function of such things as background flux, signal flux, temperature, and detector bias. The

goal is to determine how these conditions may effect the testing of IR detectors in the DWSG system.

Due to the complexity inherent in this problem, I decided to narrow my focus to one specific type of IR detector. AEDC had previously observed delays in response during the testing of focal plane arrays made of extrinsic photoconductors. Also, we were already aware of some papers dealing with this subject [4, 5]. Consequently, the logical approach was to investigate research that had already been performed on extrinsic photoconductors.

B. Results:

The issue of response times in extrinsic photoconductors was studied at length by Williams [6, 7, 8]. He demonstrated experimentally that the response time constant is often longer than the carrier lifetime. This additional delay was dependent on the applied bias and the background flux. Such results have a good theoretical explanation.

Before discussing Williams' work more thoroughly, a brief explanation of how an extrinsic photoconductor works will help fix our thoughts. A photoconductor is essentially a slab of semiconductor material sandwiched between two electrodes (Fig. 2). A bias voltage is supplied across the electrodes and the current is monitored. When photons of sufficient energy strike the surface, they break up electron-hole pairs. If impurities have been added to the semiconductor, it is called an extrinsic photoconductor, and it will respond to lower energy photons. In this case, incident photons excite electrons (for an n-type semiconductor) into the conduction band. The resulting increase in conductivity changes the current flow through the device. Such current changes constitute the output signal of the detector.

When a short pulse of photons creates extra charge carriers in the conduction band, they are rapidly swept out of the material by the applied bias, leaving the ionized atoms in the lattice behind. These fixed ions create an electric field which is superimposed on the electric field caused by the applied bias voltage. As time goes on, the ions are neutralized as new carriers move into the region. The amount of fixed charge decays exponentially with a time constant given by

$$\tau_\rho = \epsilon \rho , \qquad (7)$$

where ϵ = permittivity of photoconductor ($C^2 / N\, m^2$)

and ρ = resistivity of photoconductor ($\Omega\, m$).

Often, τ_ρ is called the "dielectric relaxation" time constant. Obviously this time constant is proportional to the resistivity of the photoconductor. Such a relationship makes intuitive sense because a lower resistivity will allow carriers to flow into the charged region and neutralize it more readily. Because the charged region is absorbing carriers that would ordinarily contribute to the current flow, the detector's output signal current will be delayed. The length of this delay will be discussed later in this section.

The response time phenomena has been studied in a variety of ways. Williams [8] was actually able to measure a two time constant response on oscilloscope traces of the detector's output. Figure 3 is a representation of what was observed. The steep part of the response is probably the normal detector response limited by the carrier lifetime as discussed in the previous section. The more gradual slope is attributed to the filling of the charged

region or the "dielectric relaxation." Good agreement was found between the values of τ_ρ calculated by Eq. (7) and those determined experimentally.

Williams discovered that the amplitude of the slower response was a function of the applied electric field. The initial width W of the charged region is simply the distance the carriers are transported in the applied field. Therefore,

$$W = \mu \tau E, \tag{8}$$

where $\quad\quad\quad\quad \mu$ = carrier mobility (velocity/E)

and $\quad\quad\quad\quad E$ = electric field due to applied bias.

It stands to reason that the larger the charged region is compared to the photoconductor's thickness, the larger the current absorbed in this region. Consequently, the amplitude of the response delay (as shown in Fig. 3) increases as the applied field E is increased. The field can be increased by raising the bias or shortening the distance between the photoconductor electrodes. Williams showed both methods had a similar effect.

The amplitude of the slow response was observed to be comparable to the fast response amplitude when W is on the order of the electrode spacing L. This result is significant because the photoconductive gain G is normally defined as

$$G = \frac{\mu \tau E}{L} = \frac{W}{L}. \tag{9}$$

Consequently, when an extrinsic photoconductor has a photoconductive gain that approaches or exceeds unity, the slow "dielectric relaxation" will dominate the detectors response.

The question now arises as to the length of the detector's response time. Williams [7] asserts that the total response time constant τ_{tc} is simply the sum of the fast and slow components:

$$\tau_{tc} = \tau + \tau_\rho . \tag{10}$$

It is well-known that the resistivity ρ of a photoconductor is given by

$$\rho = L / (\eta\mu q\phi_b\tau), \tag{11}$$

where η = quantum efficiency,

          q = charge of electron,

and ϕ_b = background photon flux.

Substituting Eqs. (7) and (11) into Eq. (10) yields

$$\tau_{tc} = \tau + \frac{\varepsilon L}{\eta\mu q\phi_b\tau} . \tag{12}$$

As expected, Eq. (12) shows τ_{tc} increasing with carrier lifetime τ, but after reaching some minimum value the detector's response time constant will actually begin to increase with decreasing τ. Because the second term of

Eq. (12) depends on ϕ_b, the point at which this happens will be determined by the background flux (c.f., Fig. 4). The minimum value of the time constant is easily determined:

$$\text{min } \tau_{tc} = 2\left(\frac{\epsilon L}{\eta \mu q \phi_b}\right)^{1/2}. \qquad (13)$$

The implications for testing extrinsic photoconductors with the DWSG system are important. If the detector is operating near the minimum illustrated in Fig. 4, then a decrease in the background flux will increase the response time. Since the response time will be approaching the pulse lengths, it will probably be necessary to increase the pulse intensity in order to maintain the desired output signal. Similarly, if the background flux is increased the detector may appear more sensitive. Thus, any change in background must be accompanied by a recalibration of the DWSG system with data obtained from the blackbody-based test chamber.

Another potential problem is the persistence from one frame to the next of the detector's response to the incident pulse. Data taken on the DWSG so far indicate that this is not a problem. However, plans are in the works to reduce the background flux which may increase the signal's persistence. Such action will require the retaking of these data.

Because the amplitude of the slow response depends on the field applied to the photoconductor, caution must be used when testing. A change in bias or a switch to a detector with greater electrode spacing will change the magnitude of the "dielectric relaxation" effect. Such a change, although not necessarily effecting the response time, could significantly alter the detector's output signal.

V. RECOMMENDATIONS

A. Implications of this Research:

A fundamental limit on response time has been found. This minimum is only approximately one order of magnitude smaller than the laser pulse lengths currently used in the DWSG system. Apparently, because of the limitations of IR detectors, the DWSG system can not be run much faster than is being done at the present. Also, if for some reason a particular type of detector has a response time somewhat slower than the fundamental limit, then the responsivity of that detector will appear to be reduced in DWSG tests. Under some circumstances, it may not be possible to sufficiently irradiate such a detector with pulsed radiation to simulate the desired real-life scene.

The second part of this research effort took a careful look at a specific type of IR detector. For the extrinsic photoconductor, the response time is often longer than the fundamental limit. How much longer depends strongly on the background photon flux. The amplitude of this slow response is dependent on such factors as the applied bias and the photoconductor's electrode spacing. The implications are clear. Changes to the DWSG testing environment must be accompanied by a careful examination of the detector's response. It is very likely, especially if the background flux is lowered significantly, that in some cases the detector's responsivity will be reduced. It is also possible that persistence effects may become a problem.

B. Follow-on Research:

Much work remains to be done. The computer models developed by McGuigan [4] and Peters [5] should be studied in light of the response time

dependences of extrinsic photoconductors discussed in this report. A cursory examination of their work appears to indicate that such ideas were not fully incorporated. By utilizing the principles of response times and using DWSG data as it becomes available, it may prove possible to build a more adequate model. Such a model could have significant predictive value, both for testing with the DWSG and for the design and application of IR detectors.

The work started this summer should be extended to include intrinsic photoconductors. Because an intrinsic semiconductor typically has a resistivity that is four orders of magnitude less than an extrinsic semiconductor, it is unlikely that response time constants will have the same form as discussed in Section V. The limitations that do exist should be determined.

Response times longer than the fundamental limit most likely occur in other types of detectors besides photoconductors. Photovoltaic and metal-insulator-semiconductor devices are important types of detectors that need to be investigated. Efforts should be devoted primarily to a careful search of the literature. Undoubtedly work has been done in this area. The task is to locate, understand, and apply it.

One more area of concern is the issue of signal persistence from frame-to-frame. Whereas a reduced response may be compensated to some extent by increased pulse intensity, the persistence of a signal could conceivably render the dynamic feature of the DWSG system useless. The reset of the detector that occurs between the frames may prevent the signal's persistence. It would, however, seem prudent to understand the physical mechanism involved for each of the detector types.

The goal of the follow-on research recommended here is to obtain an adequate theoretical understanding of the response time limitations of IR

detectors. Such knowledge can be used profitably to determine beforehand where the potential troublespots are in testing with the DWSG system.

ACKNOWLEDGEMENTS

REFERENCES

1. Wolfe, W. L. and G. J. Zissis, eds., The Infrared Handbook, Environmental Research Institute of Michigan, Ann Arbor, Michigan, 1985, p. 11-51.

2. Dereniak, E. L. and D. G. Crowe, Optical Radiation Detectors, Wiley, New York, 1984, p. 99.

3. Borrello, S. R., "Detection Uncertainty," Infrared Physics, 1972, Vol. 12, pp. 267-270.

4. McGuigan, D., "Computer Modeling of Non-Uniformly Illuminated Extrinsic Photoconductors," Hughes ENB Book 1, Seq. 63, Rev. A, 21 November 1980.

5. Peters, R. D., "Understanding DRE and its Consequences Using a Computer Model," LTV Aerospace and Defense, Design Information Release, Dir. No. 3-57000/5DIR-02, 17 April 1985.

6. Williams, R. L., "Relaxation Phenomena in High-Resistivity Ge:Hg," J. Appl. Phys., 1967, Vol. 38, pp. 4802-6.

7. _____, "Speed and Sensitivity Limitations of Extrinsic Photoconductors," Infrared Physics, 1969, Vol. 9, pp. 37-40.

8. _____, "Response Characteristics of Extrinsic Photoconductors," J. Appl. Phys., 1969, Vol. 40, pp. 184-192.

$$\tau_{tc} = \frac{1}{2 \pi f_{3dB}}$$
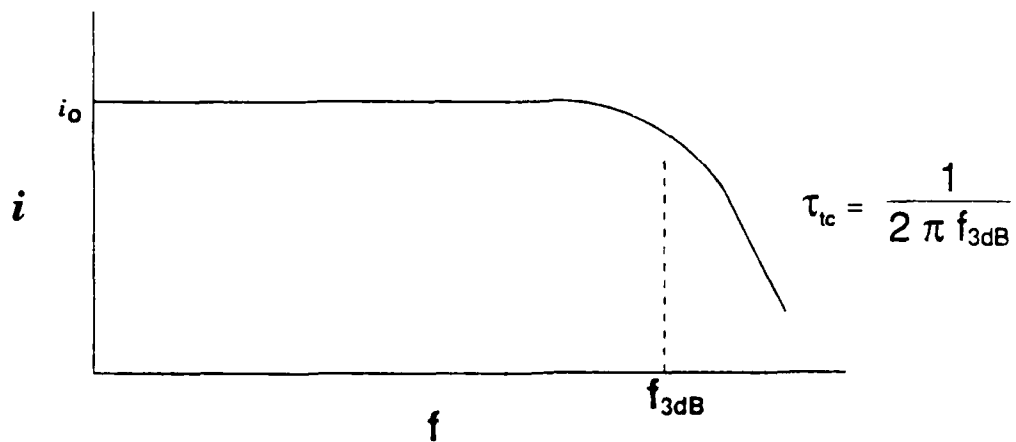
Fig. 1 - Representation of a typical detector's output signal as a function of frequency.

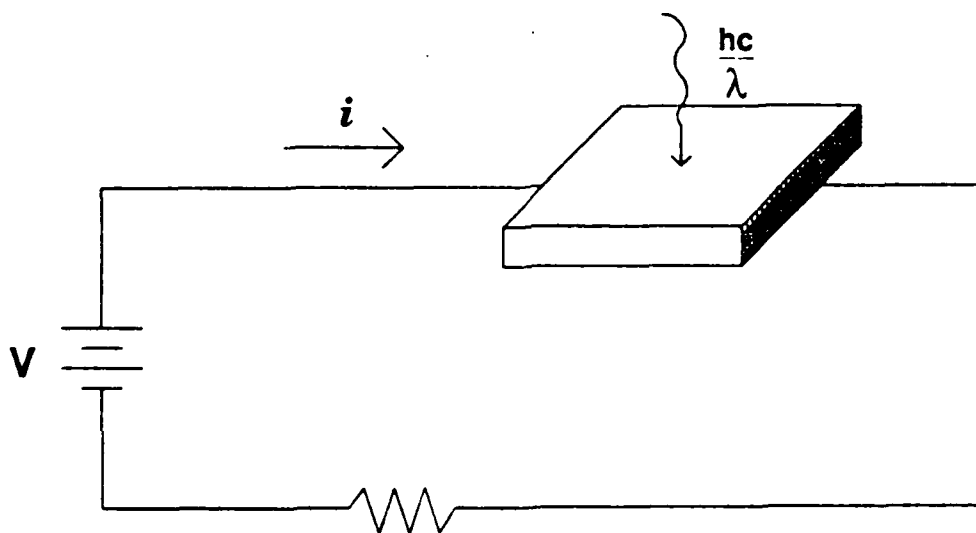**Fig. 2 - Schematic of a photoconductor.**

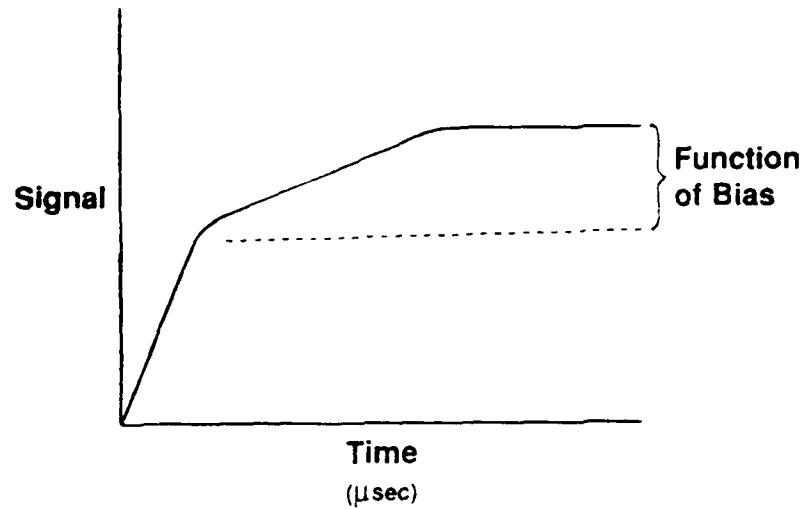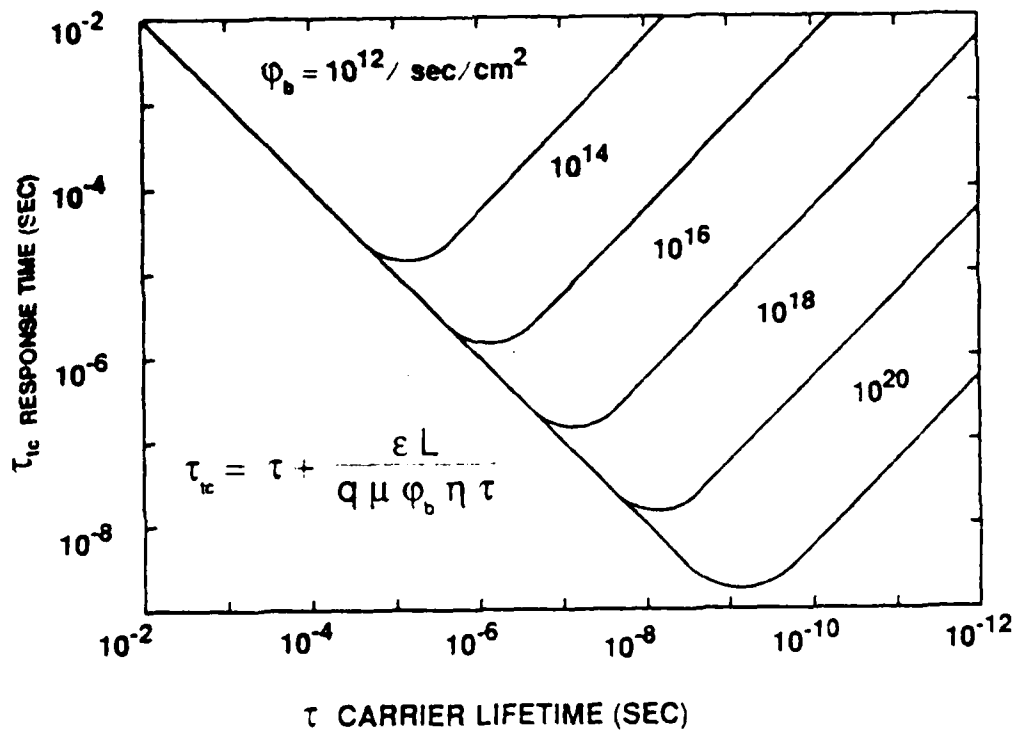Fig. 3 - Illustration of the two time constant response observed by Williams [8].

$$\tau_{tc} = \tau + \frac{\varepsilon L}{q \mu \varphi_b \eta \tau}$$

Fig. 4 - Detector response time as a function of background flux and carrier lifetime (from ref. 7).

1989 USAF-UES SUMMER FACULTY RESEARCH PROGRAM

GRADUATE STUDENT SUMMER SUPPORT PROGRAM

Sponsored by the
AIR FORCE OFFICE OF SCIENTIFIC RESEARCH

Conducted by the
Universal Energy Systems, Inc.

FINAL REPORT

AN ANALYSIS OF FOCAL PLANE IRRADIANCE EFFECTS ON IR DETECTORS

Prepared by:	Lee I. Britt, M.S.
Academic Rank:	Instructor
Department and	Physics
University:	Grambling State University
Research Location:	ASF Space Systems Branch
	Arnold Air Force Base
	Tennessee 37389-5000
USAF Research:	Mr. Don Williams
Date:	14 August 1989
Contract No.	F49620 88-C-0053

An Analysis of Focal Plane Irradiance Effects on IR Detectors

by

Lee I. Britt

ABSTRACT

An analysis of focal plane irradiance effects due to CO_2 laser radiation is presented. Specific detail is given to vibrational analysis of a germanium acousto-optic cell, induced polarization effects in selected detector media, and laser induced thermal stress phenomena. A model is given that describes laser induced damage for three distinct exposure time periods.

ACKNOWLEDGEMENTS

I would like to thank the Air Force Systems Command and the Air Force Office of Scientific Research for sponsorship of this research. I am very grateful to Universal Energy Systems for selecting me as a participant in the 1989 Summer Faculty Research Program. I wish to also thank Mr. Carlos Tirres for directions and materials.

There are a number of people in the Calspan group that helped make my experience at AEDC both rewarding and enriching. I would like to thank Mr. Don Williams for help with the research problem and the location of key technical personnel.

Many thanks are due to Dr. Heard Lowry, Mr. David Elrod, Mr. Sid Steely, and Mr. Jim Sisco for both reference material and many enlightening technical discussions.

I wish to also express my appreciation to Ms. Serbrinne Mosley for her care and diligence in typing. Special appreciation is due to my wife, Alma, and our children, Tayanna, Jamal, and LeShundra for patiently enduring my absence this summer.

I. INTRODUCTION:

The Direct Write Scene Generator (DWSG) offers a new and very promising method for the simulation of real world IR scene content. One DWSG source can produce a multiple beam rake that can sweep across an entire focal plane with a single scan in a fashion analogous to pulling a rake across a yard. The multiple beams are produced by laser light that is Bragg diffracted as it passes through a vibrating acousto-optic (AO) cell

Future technology trends indicate that in an effort to more accurately simulate the total scene that an IR detector will be exposed to, smaller spot sizes will be incident on detectors in the focal plane. Since this will result in higher power densities on the detectors, a predictive analysis of the resulting irradiance effects is needed

My past research efforts have been in the areas of Electronic Warfare and Electro-Optical Systems Analysis and Evaluation. I have been involved in spectrophotomic and spectroradiometric evaluation and testing of IR sources. I have performed laser induced damage studies on selected target materials I have also taught courses in Atomic and Experimental Physics as well as physics for the Life Sciences.

My knowledge and familiarity with IR systems and radiometry resulted in my assignment to develop an analysis of focal plane irradiance effects on IR detectors.

II. OBJECTIVE OF THE RESEARCH EFFORT

One of the experimental designs for the DWSG at AEDC uses radiation emitted by a CO_2 laser as a source of scanning radiation. The CO_2 laser produces radiation with a wavelength of 10.6 μm and it's very powerful. The radiation is directed through an AO cell and ultimately to IR detectors in the focal plane.

Many accomplishments have been made with the DWSG, however very few investigations have been performed on irradiance effects on IR detectors

The general objective here then will be to present an analysis that will give some insight into laser induced polarization effects and the damage mechanism in IR detectors.

III. SCANNING METHODOLOGY

We begin with a discussion of the AO cell since it is the source of the scanning laser beams.

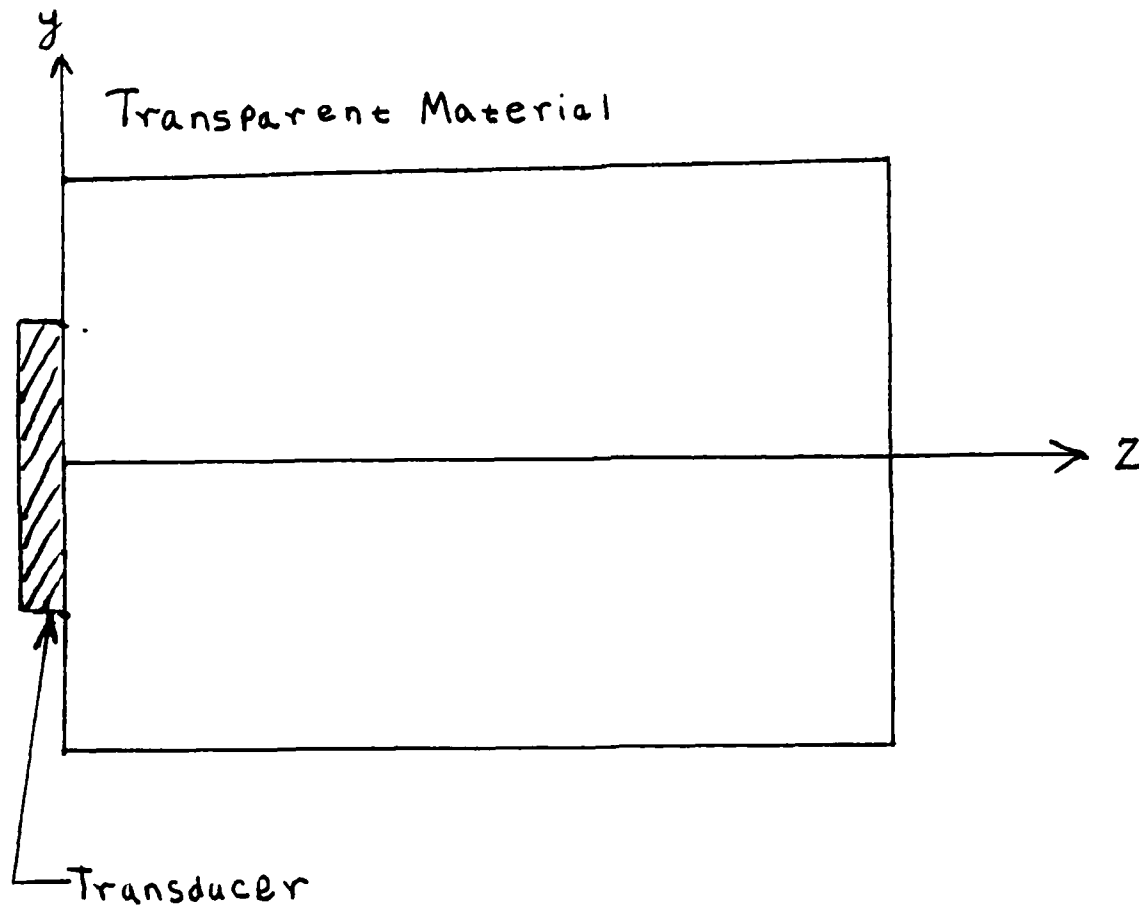An illustration of an AO cell is shown in Figure 1.

Figure 1. Basic Acousto-Optic Device

The AO cell consists of a rectangular block of germanium with a piezoelectric transducer attached to its base. When the transducer is connected to a source of alternating voltage, periodic mechanical stress forms in the piezoelectric material. This stress is then transferred to the block of germanium and gives rise to alternating regions of compression and rarefaction in the AO cell that are separated by a distance of one sound wavelength.

If the germanium has an orientation such that its long axis is parallel to the z-axis as shown in Figure 1, the equation for the longitudinal oscillations in the material is given by

$$\frac{\partial^2 U}{\partial z^2} = \frac{1}{V^2} \frac{\partial^2 U}{\partial t^2}$$

(1)

where V is the velocity of sound in a solid given by

$$V = \frac{E}{\rho}$$

(2)

E is young's modulus, ρ is the density, U is the displacement of the cross-section of the material with abscissa z at time t (i.e., U(z,t)).

The solution to Eq. (1) is obtained by using separation of variables or Laplace transforms. If the transducer applies a forcing function given by Eq. (3)

$$F = F_0 \sin(\omega t + \Theta).$$

(3)

then forced oscillations of the material are given by Lebedev, Skalskaya, and Uflyand (1965) as

$$U(z,t) = \frac{F_0 V}{ES\omega} \frac{\sin \frac{\omega z}{V}}{\cos \frac{\omega \ell}{V}} \sin(\omega t + \Theta)$$

(4)

where S is the cross-sectional area of the material and ℓ is its length

11-6

The solution to the wave equation can be standing waves or traveling waves. Standing waves are undesirable because they would tend to make the reflective planes stationary; when the laser radiation strikes these non-moving planes, excessive heating can result. Heating can also result from the transducer.

The heating could lead to degradation of the optical properties of the material and ultimately to the destruction of the AO cell. Therefore, efforts should be made to avoid standing wave configurations (standing waves exist only when the acoustic frequency and medium dimensions allow an integral number of half wavelengths of the acoustic wave to fit precisely within the boundaries of the medium. The sound absorber at the end of the sample assures that only traveling waves will propagate in the medium. The periodic compressions and rarefactions in the media also produce periodic variations in the materials' density and refractive index. This makes the regularly spaced reflective fronts act like a moving diffration grating.

A useful parameter of this grating given by Yariv (1971) is the diffraction efficiency given by

$$D = \sin^2 \left| \frac{\Pi \ell}{\sqrt{2} \lambda} \left(\frac{n^6 p^2}{\rho v_s^3} I_{ac} \right)^{\frac{1}{2}} \right|$$

(5)

Where n is the index of refraction, p is the photoelastic constant of the medium, ρ is the density, v_s is the velocity of sound, I_{ac} is the acoustic intensity, ℓ is the interaction length, and λ is the incident light wavelength in the material. As in normal diffraction of light, the grating gives rise to various diffraction orders. When the beam passes through the AO cell, it is directed to the detector elements in the focal plane of the DWSG as a multibeam rake. To increase the range of deflection, a two-axis system is incorporated that gives two-dimensional deflections.

One possible replacement material for germanium is TlAsSe as suggested by Skurnick, Davidian, and Greenebaum (1979). This material displays significant improvement over germanium and could be an attractive alternative.

IV. POLARIZATION EFFECTS

Polarization effects seem to be most strongly demonstrated in pyroelectric detectors. These detectors are very attractive because of their unique ability to carry out sensitive detection of infrared radiation at room temperature. Fundamentally, the principle of operation of these detectors is based on the fact that the pyroelectric material possesses a permanent polarization Ps, prior to the application of an electric field.

This polarization depends on the material temperature as well as the crystal symmetry and bonding. Since all known pyroelectric materials are dielectrics, the change in polarization results in a proportional change in dielectric constant. If the pyroelectric material is connected to an external circuit, the temperature dependent permanent polarization causes charge to flow.

When radiation on the detector causes heating (i.e., irradiation by CO_2 laser) there is a resulting expansion of the crystal lattice spacing and a change in electrical polarization occurs.

Dereniak and Crowe (1984) point out that a good indicator of change in polarization of this type of detector is the pyroelectric coefficient expressed by

$$ p = \frac{\partial P_s}{\partial T} $$

(6)

Where p is the pyroelectric coefficient, P_s is the permanent polarization, and T is the temperature change.

This coefficient is a measure of the rate of change of electric polarization with respect to temperature change. They further point out that from the equivalent circuit of the pyroelectric detector the effects of a change in polarization in the material can be determined. Consider the pyroelectric equivalent circuit shown in Figure 2.
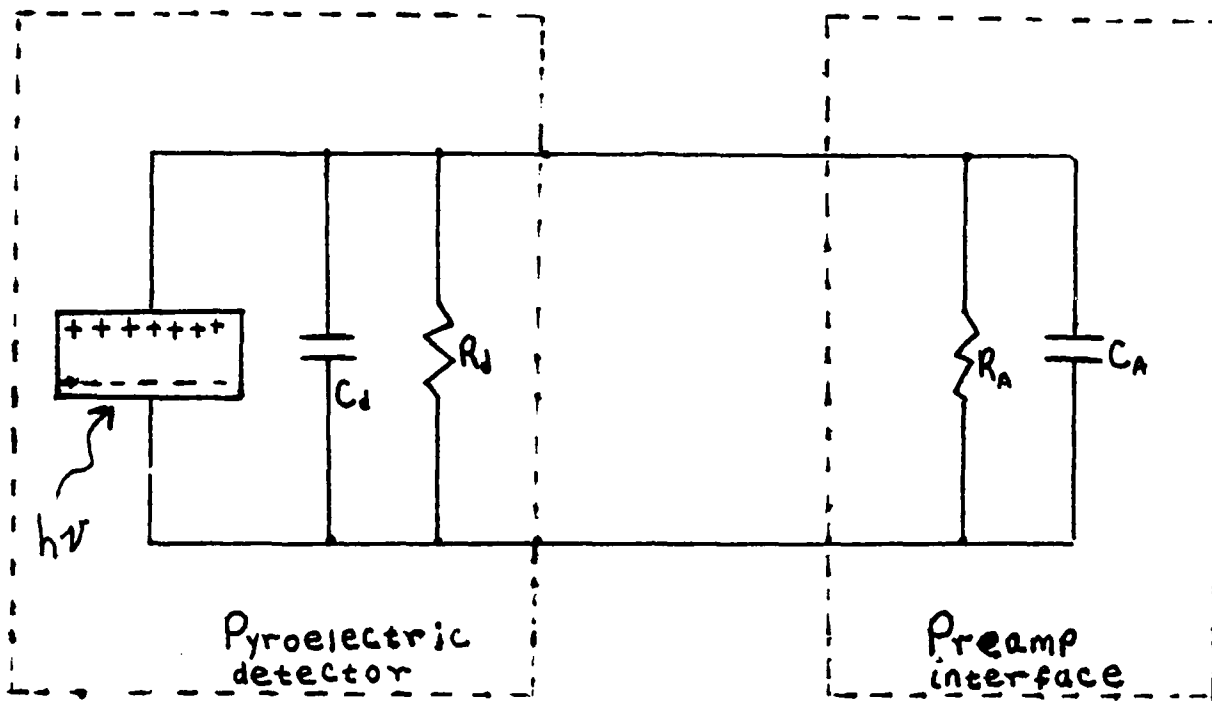
Figure 2. Pyroelectric Equivalent Circuit

A temperature change in the material produces a polarization charge that causes a current that is a function of frequency

$$i_d = \omega p A_d \Delta T$$

(7)

where ω is the radian frequency, A_d is the detector area, and $\_T$ is the temperature change.

Since the voltage responsivity is the current (i_d), multiplied by the impedance, we have

$$V_o = \frac{i_d R_d}{1 + \omega^2 R_d^2 C_d^2}$$

(8)

$$V_o = \frac{\omega p A_d R_d \Delta T}{1 + \omega^2 R_d^2 C_d^2}$$

(9)

Because the polarization change manifests itself in the form of the easily measurable electrical parameters of current and voltage, it is possible to determine the effects of laser induced polarization in the material.

V.   LASER HEATING EFFECTS

One of the future technology directions for the DWSG is to go to smaller spot sizes on the focal plane. This will be done in an effort to completely simulate the scene that an IR detector will be exposed to When this is attempted with the CO_2 laser, a greater power density will be incident upon the detector's front face. This will produce excessive heating in the detector material, that will lead to a degradation in the detector's performance and ultimately to irreversible detector damage.

These considerations are important because they may be used to help predict the effects of intense laser radiation on space based surveillance or optical tracking systems.

In these devices the first thing that occurs in the chain of information flow is to focus light from the scene onto an appropriate detector. This typically results in an optical gain in the radiation in going from the imaging optics to the focal plane and a corresponding increase in the power density. In the case of a CO_2 laser, this could damage the detector. Bartoli, et al, (1975) suggests a thermal model for laser induced damage that is valid for both photoconductive and photovoltaic detectors. For short irradiation times ($\tau < 10^{-6}s$), the energy per unit area that produces permanent damage in the material is constant and is given by

$$E_o = \frac{\Delta T_{th}\, \rho c}{(1-R)\alpha}$$

(10)

Where E_o is the energy per unit area of the radiation incident on the crystal, ΔT_{th} is the critical temperature increment on the detector surface, ρ is the density of the material, C is the specific heat, R is the reflectivity of the surface and α is the absorption coefficient. In this case, the power P_o is inversely proportional to τ.

For intermediate times ($10^{-6}s < \tau < 10^{-2}s$) the energy per unit area is

$$E_0 = \frac{\Delta T_{th} \, \rho c}{(1-R)\alpha} \left(\frac{t}{\tau_0}\right)^{\frac{1}{2}}$$

(11)

and P_0 is inversely proportional to the square root of τ. Finally, for long times ($\tau > 10^{-2}s$) the energy per unit area is given by

$$E_0 = E_{\Delta T} \left[1 + \frac{kta(m)^{\frac{1}{2}}}{a \tan^{-1}\left(\frac{4kt}{a^2}\right)^{\frac{1}{2}}} \right]$$

(12)

Where

$$E_{\Delta T} = \frac{\Delta T_{th} \, \rho c}{(1-R)\alpha}$$

(13)

Here P_0 asymptotically approaches a constant. For the DWSG, the time spent on each pixel element (dwell time) is

$$t_d = \left(\frac{t_i N_b}{N_r N_c}\right) - 2\mu s$$

(14)

Where τ_d is the dwell time, τ_i is the integration time, N_b is the number of beams, N_r is the number of rows, and N_c is the number of columns.

The models for all three regions of irradiance time behavior show good agreement with experiments.

VI.   CONCLUSIONS AND RECOMMENDATIONS

While germanium is currently commonly used as the bulk material for infrared AO cells, TlAsSe has been pointed out as one material that has shown significant improvement over germanium and it could be used as an alternative choice.

Polarization effects in IR detectors are most evident in pyroelectric detectors These effects may be determined by measuring changes in current and voltage in the pyroelectric detector circuit.

Reducing the laser beam to smaller spot sizes on the focal plane could induce higher power densities on the detectors. This can result in heating and irreversible damage to the detector material that can be described for three distinct temporal regions of irradiance.

Since smaller spot sizes have associated with them very high electric fields strengths, there is a need for an analysis that models these effects as well as the effects of self focusing.

REFERENCES

1. Bartoli, F., L. Esterowitz, M. Kruer, and R. Allen, "Thermal Modelling of Laser Damage in 8-14 μm HgCdTe photoconductive and PbSnTe Photovoltaic Detectors", *Journal of Applied Physics*, October 1975, pp. 4519-4525.

2. Lebedev, N. N., Skalskaya, I. P., and Uflyand, Y. S., *Worked Problems in Applied Mathematics*, New York, New York, Dover Publications, Inc., 1965.

3. Skurnick, E. W., W. Davidian, and M. Greenebaum, "Acousto-Optic Deflector Performance at 10.6 μm ', *Active Optical Devices*, 1979, Vol. 202, pp 56-62.

4. Yariv, A., *Optical Electronics*, Holt, Rinehard, and Winston, 1971.

1989 USAF-UES Summer Faculty Research Program

Sponsored by the
AIR FORCE OFFICE OF SCIENTIFIC RESEARCH
Conducted by the
Universal Energy Systems, Inc.

FINAL REPORT

Code Development For Design Of A High Temperature
Hypersonic Facility Mixer

Prepared by:	Dr. Brian R. Circelli
Academic Rank:	Assistant Professor/Ch.E.
Department and:	Chemical Engineering Department
University	University Of Mississippi
	University, MS 38677
Research Location:	Arnold Engineering Development Center
	Computational Fluid Dynamics Section
	Technology And Analysis Branch
	Arnold Air Force Base, TN 37389
USAF Researcher:	Frederick L. Shope
Date:	September 1, 1989
Contract No.:	F49620-88-C-0053

Code Development For Design Of A High Temperature Hypersonic Facility Mixer

by

Brian R. Circelli

ABSTRACT

Preliminary calculations have been performed that suggest that PARC-3D may be a suitable CFD code that can be used as a starting point in developing a code that can be used in the design of a high temperature hypersonic facility mixer. The results indicate that the code can handle large regions of subsonic flow and massive regions of flow separation. The turbulence model that is presently being used in the PARC-3D code appears adequate for the test case presented. There is great uncertainty however, due to the turbulence model, of the results that will be generated for the numerical simulations currently being planned which include surface injection of multiple sonic or supersonic jets within the mixer.

ACKNOWLEDGEMENTS

I. INTRODUCTION

New hypersonic test facilities are currently being planned for construction at AEDC to support the development of aeropropulsion, aerothermal, and aerodynamic testing. One particular test facility being proposed is the Hypersonic Facilities Complex (HYFAC), which must be capable of handling very high temperatures and pressures, and delivering high quality flow at large Reynolds numbers. HYFAC will consist of various state-of-the-art components which include: an arc-heater, a mixer, a nozzle, and a test section. This research project focuses on the development of a computer code for the design of a high temperature hypersonic facility mixer.

The primary purpose of a mixer in hypersonic flow generation is to break up the hot core of fluid exiting from the heating source by injecting cold flow uniformly into the hot flow and mixing thoroughly the hot/cold flows such that uniform profiles exit the mixer and enter the test section. The mixer will also be used to decrease the pressure and enthalpy and increase the air flow rates to provide multiple Mach number capabilities of the facility.

The computer code to be modified/developed must be able to accurately predict surface heat transfer rates, velocities, and stagnation enthalpy. The code must allow for, the surface injection of multiple sonic or supersonic jets, large regions of subsonic flow, massive flow separation, accurate modelling of the turbulent mixing process, and be three-dimensional in nature.

My particular interests in this project lie in the development and validation of a 3-D computer code that would accurately simulate the complex flow process within the mixer, and the study of the fundamental physics of the turbulence that is generated. My specific area of expertise is, the direct numerical simulation of turbulent flows using spectral methods.

II. OBJECTIVES OF THE RESEARCH EFFORT

The primary objective of this research project was to
develop a computer code that could be used as a tool to
assist in the design of a high temperature hypersonic
facility mixer. This goal included the selection/
modification of an already existing CFD code as well as
the selection/modification of an appropriate turbulence
model to be incorporated into the code. Preliminary calcu-
lations for the design of the mixer were to be performed.

While substantial progress was made throughout this
effort, the accomplishment of the initial objective will
require much longer than a ten week period. Since the
development of HYFAC is essential for the design of the
next generation of flight vehicles, continued funding on
this project is recommended.

III. WORK PERFORMED

The work that was performed at AEDC was broken down
into three phases. Phase I consisted of the selection of an
existing CFD code and an appropriate turbulence model as a
starting point for the project. Phase II of the project
consisted of gathering data that could be used as a bench
mark in validating the code. Phase III consisted of
modifying/executing the computer code and comparing the
generated results with experiments.

A. Phase I

The PARC-3D code was selected as the starting point of
the work to be performed. PARC-3D is a modified version of
the Pulliam ARC-3D code (1). The code was chosen on the
basis of its ability to accurately simulate basic fluid
dynamic phenomena in a variety of test flow cases (see
Ref.(2)). The code is a 3-D time dependent Navier-Stokes
solver and uses the Beam-Warming approximate factorization

algorithm (3). Currently, PARC-3D uses the Baldwin-Lomax turbulence model (4) which provides algebriac first order closure.

B. Phase II

A literature search was performed to obtain experimental data that could be used to validate the results generated by PARC-3D. It was decided that the 7 Inch High Temperature Tunnel experiments (7" HTT) that were performed at NASA Langley Research Center (5,6,7) would be an excellent choice to validate the CFD code. The 7" HTT utilizes a mixer in the exact same manner that is currently being proposed in HYFAC. Invitational orders were cut at AEDC to allow the author the opportunity to visit NASA Langley and obtain further information about the experiments performed. The original blueprints of the 7" HTT mixer were brought back to AEDC along with data that was generated from experiments performed at the mixer design conditions. Additional data concerning measurements taken inside the mixer during the experiments has been promised (8).

C. Phase III

Appropriate length scales were extracted off the original blueprints of the NASA Langley 7" HTT mixer and a grid was constructed to represent the mixer. An axisymmetric 3-D flow assumption was made to reduce the storage requirements necessary and to decrease the CPU time for the numerical simulations. Figure 1 represents a 2-D view of the generated 3-D grid which consists of a full Chebyshev mesh in the streamwise direction, a half Chebyshev mesh in the radial direction, and a uniform mesh in the circumferential direction. The mesh is rather unique in that it automatically clusters grid points in regions where flow resolution problems are anticipated, ie., near the two throats and near the mixer wall. the number of grid points used in generating the mesh for the simulations performed was 83x25x11. The reference temperature,

reference pressure, Reynolds number, Prandtl number, and turbulent Prandtl number were set equal to 3600 °R, 2.88E+06 lb/ft^2, 3.20875e+07, 0.72, and 0.90, respectively, and were used as input parameters into the PARC-3D code.

IV. RESULTS

The numerical simulations to be performed were broken down into three phases. The first phase involved performing simulations with no mass injection at the mixer walls to see if the PARC-3D code could predict a reasonable solution to the somewhat intracate flow geometry of the mixer. In the second phase, simulations would be performed with mass injection at the surface of the mixer, with the initial conditions and the injection flow rates being specified as those used in the NASA Langley 7" HTT experiments at the design condition. If the results generated by the PARC-3D code were consistent with the NASA Langley experimental data, then work would be continued to phase III, which would consist of two separate parts.

The first part would involve improving the turbulence model which is currently used in PARC-3D. Work would begin in modifying PARC-3D such that a two-equation turbulence model such as the k-ε model, or an algebraic stress transport turbulence model would be incorporated into the code. While this work was being carried out, if the results generated by the PARC-3D code using the Baldwin-Lomax turbulence model were adequate, then alternate configurations for the HYFAC mixer would be investigated for their ability to meet the demands placed on HYFAC. Because of the time constraint of ten weeks and the complexity of the project, phase II and III could not be performed. Follow-up funding for this work is currently being pursued.

A. Phase I.

The preliminary results of the flow dynamics within the generated mixer grid, with no mass injection at the wall, appear to have been reasonably simulated. Although there is no experimental data to compare with the generated data, qualitatively the general trends of the flow fields appear to have been successfully predicted.

Figures 2-6 represent contour plots of the generated steady state solution of the static pressure, density, static temperature, velocity, and Mach number field in the flow at the z=1 plane of the grid. The contours of the pressure and density field suggest that within the center portion of the mixer, there is a region of relatively constant pressure and density. In this region, the pressure is a maximum and the fluid behaves locally as if it were incompressible. The contours of the temperature field indicate the undesired presence of a core of hot fluid near the center of the mixer. It is exactly this hot core region that must be adequately broken up if a high quality flow is desired at the test section of HYFAC. The contours of the total velocity/Mach number show the presence of a region of relatively slow moving flow near the rapid diffuser section. Qualitatively, strong normal mass injection in this region has the best chance of being felt at the centerline and breaking up the hot core flow. The Mach number contours also indicate that the flow in the center of the mixer is subsonic and in the incompressible flow regime.

V. CONCLUSIONS

The PARC-3D code appears to be a reasonable choice as a starting point in developing a CFD code that can be used in the design of possible geometric configurations for the HYFAC mixer. The results that have been presented show that

the code can qualitatively predict the correct flow dynamics. Although the turbulence model currently used in the PARC-3D code appears acceptable for the test case presented, the incorporation of alternate turbulence models into the CFD code should be considered when surface injection is applied to the mixer.

VI. RECOMMENDATIONS

The following points should be considered when viewing the results presented in this report:

1. At the point where steady state was achieved, the residuals in the code were of the order of 1.0E-06. This is not an acceptable order of magnitude for convergence on a CRAY-XMP/12 mainframe. However, there was insufficient time to investigate the cause of such a low convergence rate.

2. In order to address the point raised above, increased grid resolution in the axial flow direction is highly recommended. The data generated from PARC-3D indicate that the largest values of the residuals occur near the center of the mixer, where the grid cluster is very low. Intuitively, the addition of more grid points in that region should lower the order of magnitude of the residuals.

3. The work described in phase II and phase III of the results section should be performed in conjunction with a parallel experimental program to design the HYFAC mixer.

VII. REFERENCES

1. Pulliam, T.H., "Euler And Thin Layer Navier-Stokes Codes: ARC-2D, ARC-3D," CFD Users Workshop, UTSI, Tullahoma, TN, March 12-16, 1984.

2. Cooper, G.K., G.D. Garrand, and W.J. Phares, "PARC Code Validation For Propulsion Flows," AEDC-TR-32, January 1989.

3. Beam, R. and R.F. Warming, "An Implicit Finite Difference Algorithm For Hyperbolic Systems In Conservation Law Form," J. Comp. Phys., Vol. 22, September 1976, pp. 87-110.

4. Baldwin, B.S. and H. Lomax, "Thin Layer Approximation And Algebraic Model For Separated Turbulent Flows," Paper No. 78-257, AIAA 16th Aerospace Sciences Meeting, Huntsville, AL, January 1978.

5. Kelly, H.N. and A.R. Wieting, "Modification Of NASA Langley 8-Foot High Temperature Tunnel To Provide A Unique National Resource Facility For Hypersonic Air Breathing Propulsion Systems," NASA-TM-85783, Langley Research Center, Hampton, VA, May 1984.

6. Reubush, D.E., R.L. Puster, and H.N. Kelly, "Modification To The Langley 8-Foot High Temperature Tunnel For Hypersonic Propulsion Testing," AIAA-87-1887, AIAA/SAE/ASME/ASEE 23rd Joint Propulsion Conference, San Deigo, CA, June 29 - July 2, 1987.

7. Puster, R.L. and D.E. Reubush, "Development And Modification Of The Langley 8-Foot High Temperature Tunnel For Propulsion Testing And Improved Test Capability," 68th Semi-Annual Meeting Of The Supersonic Tunnel Association, OSU, Columbus, OH, October 22-23, 1987.

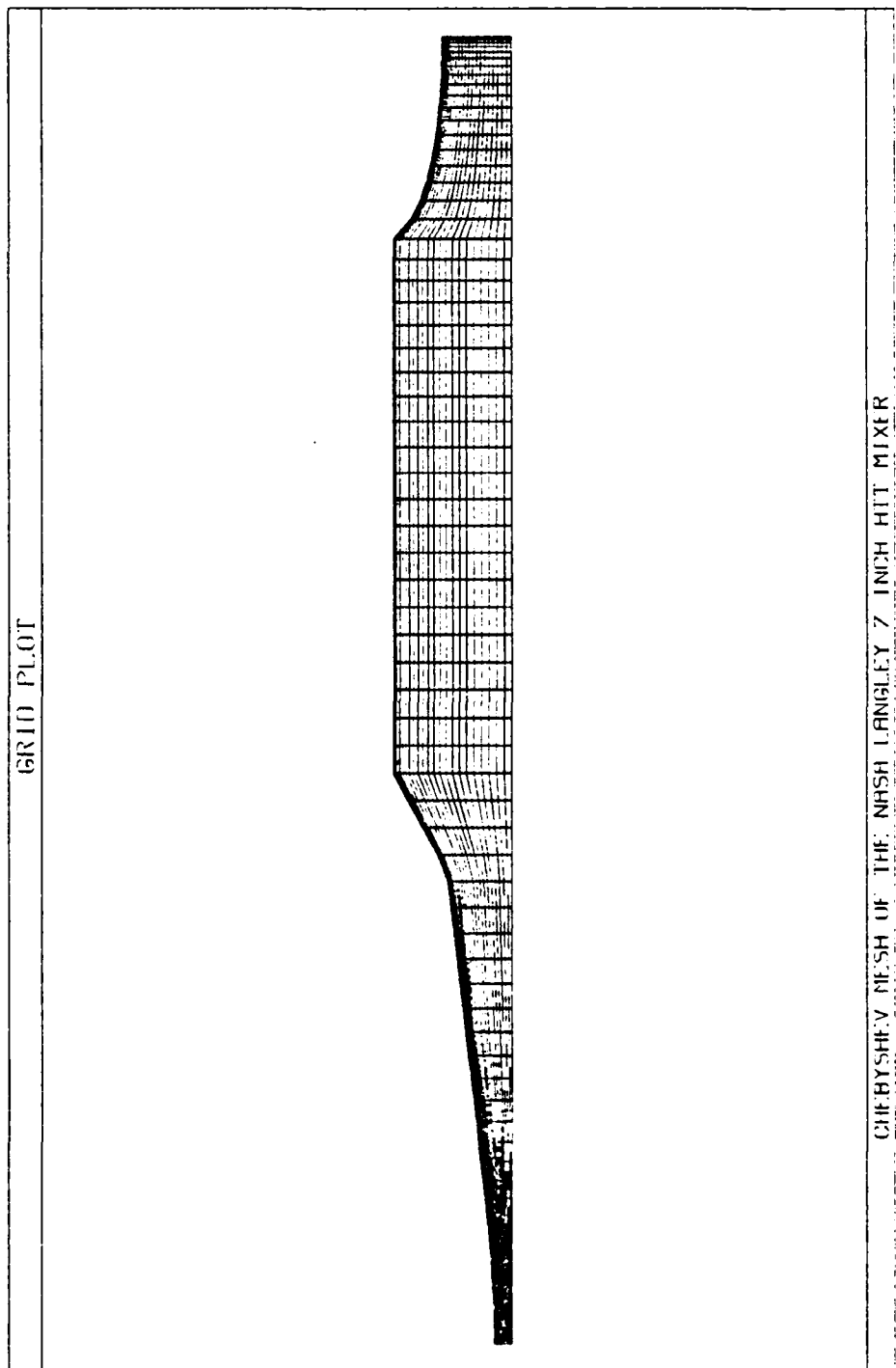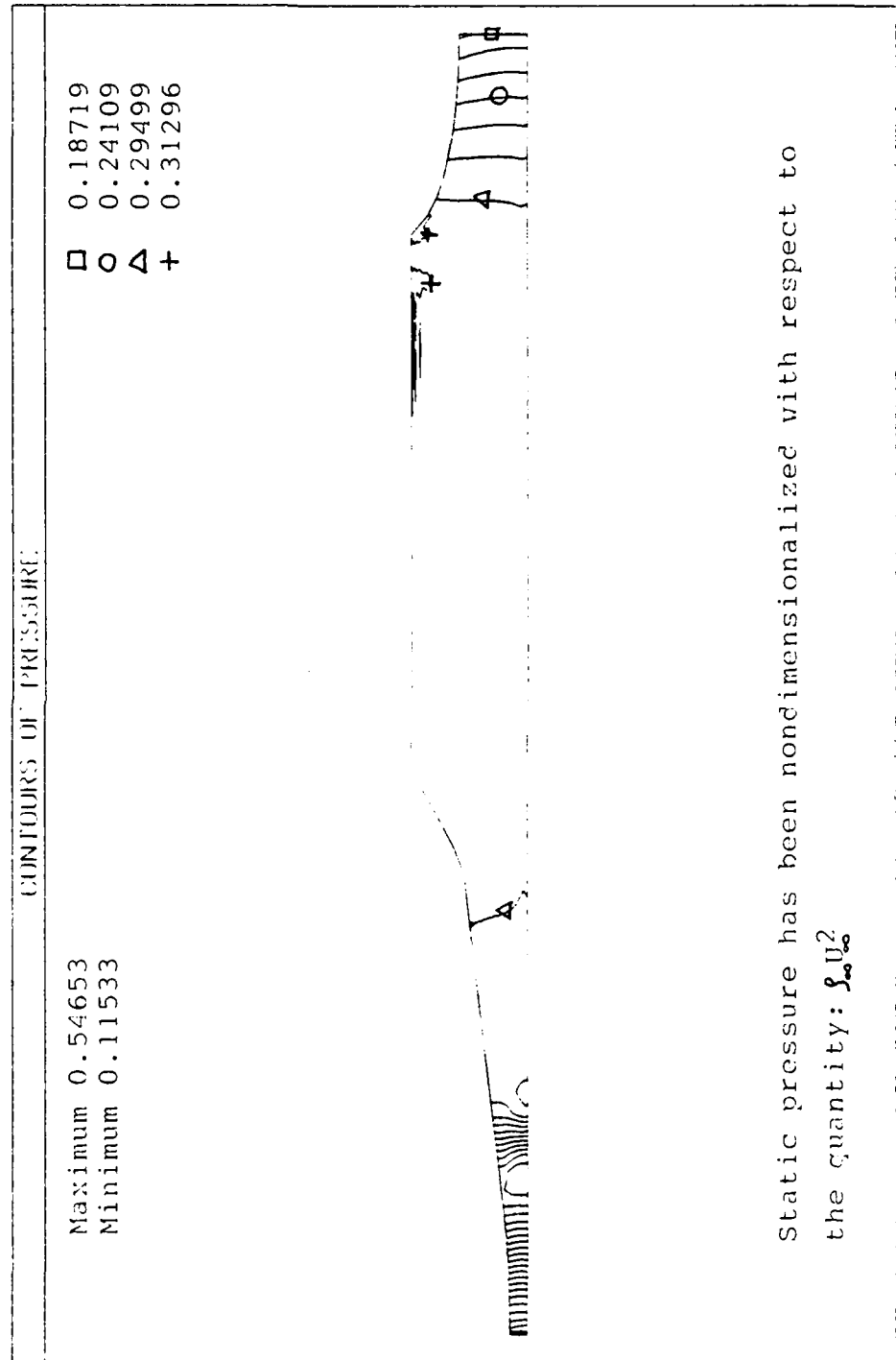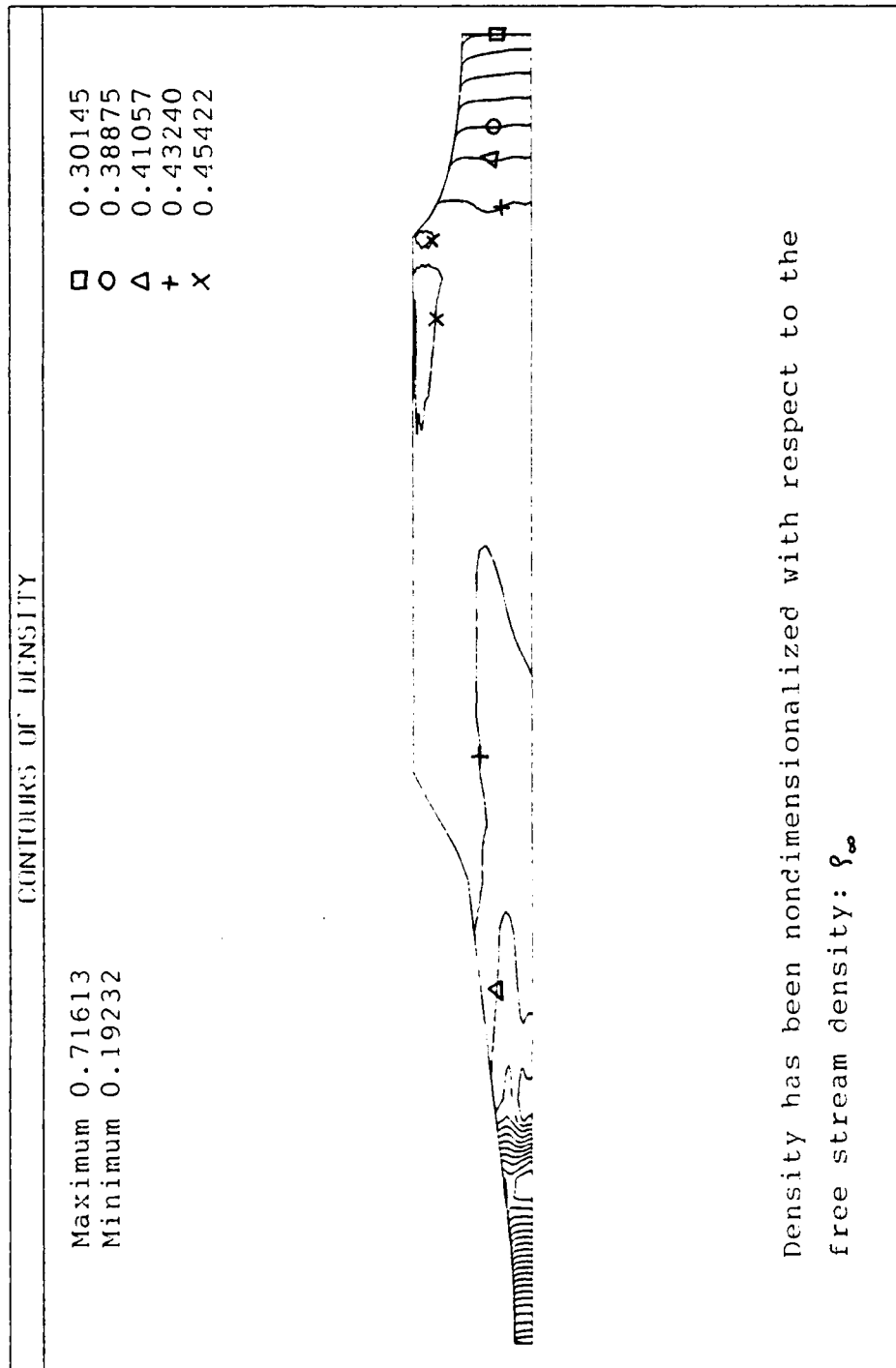8. Puster, R.L., NASA Langley Research Center, Hampton, VA, private communication.

Figure 1.

GRID PLOT

CHEBYSHEV MESH OF THE NASA LANGLEY 7 INCH HTT MIXER

Figure 2.

CONTOURS OF PRESSURE

Maximum 0.54653
Minimum 0.11533

□ 0.18719
○ 0.24109
△ 0.29499
+ 0.31296

Static pressure has been nondimensionalized with respect to the quantity: $\rho_\infty U_\infty^2$

12-12

Figure 3.

CONTOURS OF DENSITY

□	0.30145
○	0.38875
◁	0.41057
+	0.43240
×	0.45422

Maximum 0.71613
Minimum 0.19232

Density has been nondimensionalized with respect to the free stream density: ρ_∞

Figure 4.

CONTOURS OF TEMPERATURE

Maximum 0.07762
Minimum 0.05764

□   0.07179
○   0.07096
◁   0.07013
+   0.06846
×   0.06596
▷   0.06430

Static temperature has been nondimensionalized with respect to the stagnation free stream temperature: $T_{0\infty}$

Figure 5.

CONTOURS OF TOTAL VELOCITY

□   0.06351
○   0.12702
◁   0.190ᴇ3
+   0.31755
×   0.50807
▷   0.76211

Maximum 1.58773
Minimum 0.06351

Velocity has been nondimensionalized with respect to the
free stream velocity: U_∞

Figure 6.

CONTOURS OF MACH NUMBER

Maximum 1.90914
Minimum .07637

□	0.07637
○	0.15273
◁	0.22910
+	0.38183
×	0.61093
▷	0.91639

1989 USAF-UES SUMMER FACULTY RESEARCH PROGRAM/
GRADUATE STUDENT RESEARCH PROGRAM

Sponsored by the

AIR FORCE OFFICE OF SCIENTIFIC RESEARCH

Conducted by the

Universal Energy Systems, Inc.

<u>FINAL REPORT</u>

<u>Laser-Induced Fluorescence of Iodine and Sodium for Application
in Resonant Doppler Velocimetry of Hypersonic Flows</u>

Prepared by:	Dr. Stephen H. Cobb
Academic Rank:	Assistant Professor
Department and	Department of Physics
University:	Murray State University
Research Location:	AF/DOTR
	Arnold Engineering Development Center
	Arnold AFS, Tennessee
USAF Researcher:	Carl Brasier
Date:	August 21, 1989
Contract No.:	F49620-88-C-0053

Laser-Induced Fluorescence of Iodine and Sodium for Application in Resonant Doppler Velocimetry of Hypersonic Flows

by

Stephen H. Cobb

ABSTRACT

Laser-induced fluorescence in iodine and sodium has been monitored under a variety of conditions in an effort to evaluate these species as potential candidates for use in a hypersonic resonant Doppler velocimeter system. Iodine fluorescence was recorded near 611 nm as a function of temperature, perturber gas pressure, and laser intensity with particular interest in detecting changes in linewidth and location. Absorption of laser radiation by sodium vapor was recorded as a function of temperature in order to determine the absorption line shape which might be observed in the test cell environment.

ACKNOWLEDGEMENTS

I wish to thank the Air Force Systems Command and the Air Force Office of Scientific Research for sponsorship of this research. I also thank those at Arnold Engineering Development Center (AEDC) for allowing me to participate in this effort, and Universal Energy Systems for administration of this program.

I am particularly grateful to several individuals for their support and direction. Carlos Tirres is to be commended for organizing the SFRP program at AEDC. Ron Kohl and W. K. McGregor helped to explain and define the desired research goals. I am indebted to Bill Phillips for making me aware of the research opportunities at AEDC. Ron Porter's ring dye laser expertise was essential to the success of this project. I was fortunate to work most closely with Carl Brasier. I appreciate his support, advice, experience and easygoing manner. He helped to make this research project rewarding and enjoyable.

I. INTRODUCTION:

The Resonant Doppler Velocimeter (RDV) is a non-intrusive diagnostic technique which uses laser-induced fluorescence (LIF) from atoms or molecules in a flowing gas to measure the velocity, temperature, and pressure of the gas. (1, 2) The flow field is probed by an intersecting tunable dye laser which is directed so that it has a component in the direction of the flow. Since the atoms are moving, they exhibit a Doppler shifted peak absorption frequency. The fluorescence resulting from this shifted absorption may be compared to that of a stationary system, allowing the determination of the velocity component in the direction of the probe beam.

Sodium atoms and iodine molecules are often chosen as the fluorescing species in RDV experiments. (3, 4). Both are well-studied and are known to exhibit strong visible fluorescence. Sodium is naturally occurring in some high temperature exhaust systems, thus eliminating the need to seed the flow via external means. Iodine has a high room temperature vapor pressure, and thus can be seeded easily into lower temperature flow fields. As part of an effort to assess the feasibility of implementing the RDV technique in a hypersonic test cell at AEDC, there is interest in conducting preliminary experiments monitoring sodium and iodine absorption and fluorescence under a variety of stationary test conditions. These results may then be used as a reference for data obtained under flowing gas conditions.

My research interests have included the creation and characterization of metal clusters using laser induced fluorescence spectroscopy and the identification and development of novel chemical laser processes. Previous experience in working with sodium cluster generation and associated fluorescence detection systems was helpful in this research effort.

II. OBJECTIVES OF THE RESEARCH EFFORT:

The desired objectives of my appointment in the Summer Faculty Research Program (SFRP) at AEDC were:

A. To continue the extensive literature search already in progress concerning atomic and molecular fluorescence (particularly in iodine and sodium), fluorescence line broadening mechanisms, and the RDV technique.

B. To assist in establishing and testing a laser-induced fluorescence system in the laboratory, using equipment presently on hand.

C. To conduct basic fluorescence and absorption measurements in iodine and sodium vapor as a function of temperature, perturber gas pressure, and incident laser intensity. These data would be used in determining resolution limits, detection sensitivity, and laser intensity requirements necessary for future RDV experiments. Also, the absorption/fluorescence lineshape and position were to be monitored for use as a reference when conducting RDV experiments.

D. To provide recommendations concerning implementation of the RDV technique in a hypersonic test cell.

III. RESULTS OF THE RESEARCH EFFORT:

Relevant information on iodine and sodium fluorescence was compiled in an extensive literature search. This information was reviewed and those papers were selected which described work most applicable to our proposed experiment. A bibliography of this literature was prepared for future reference.
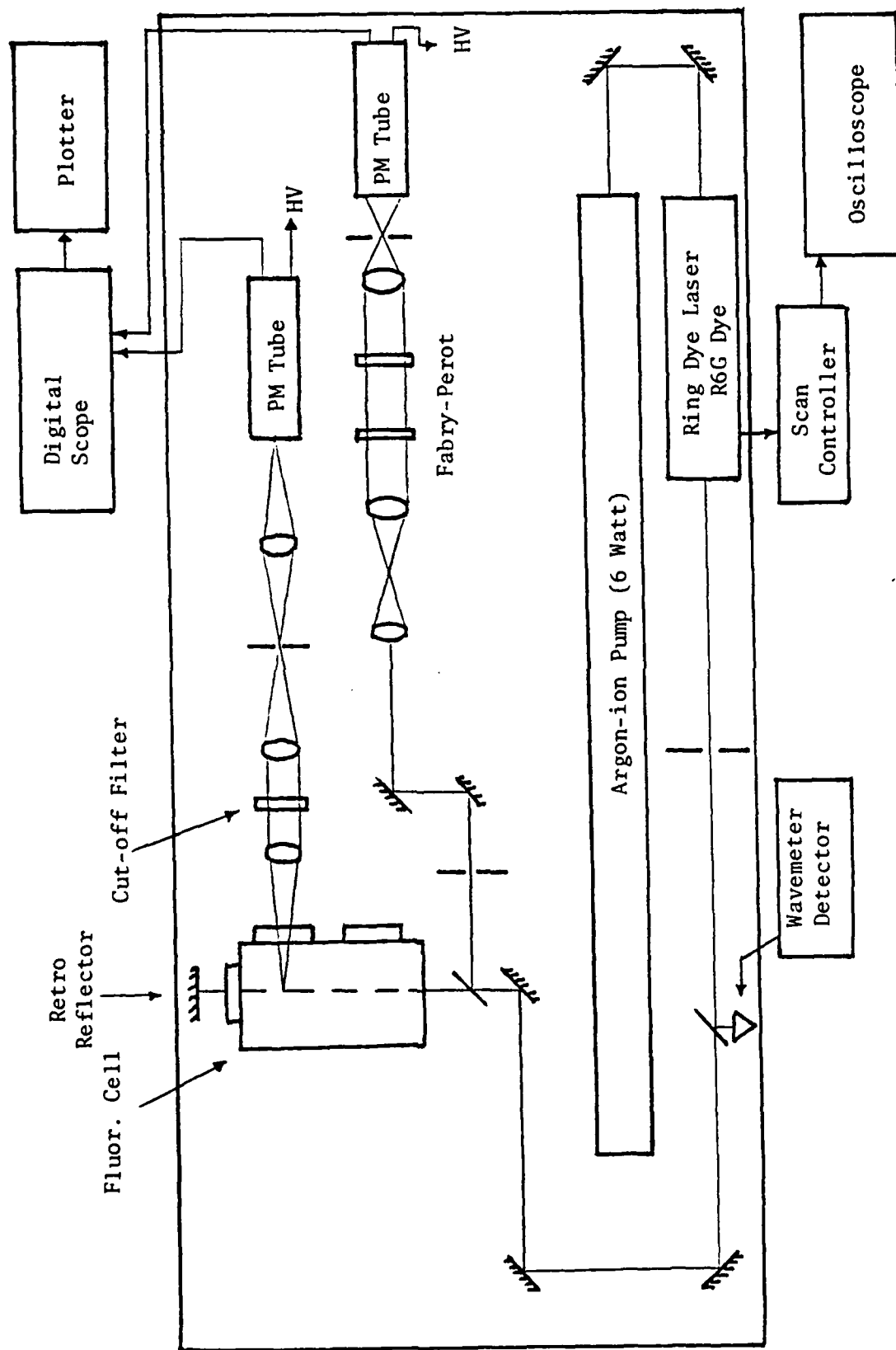
Figure 1. Schematic of Experimental Equipment.
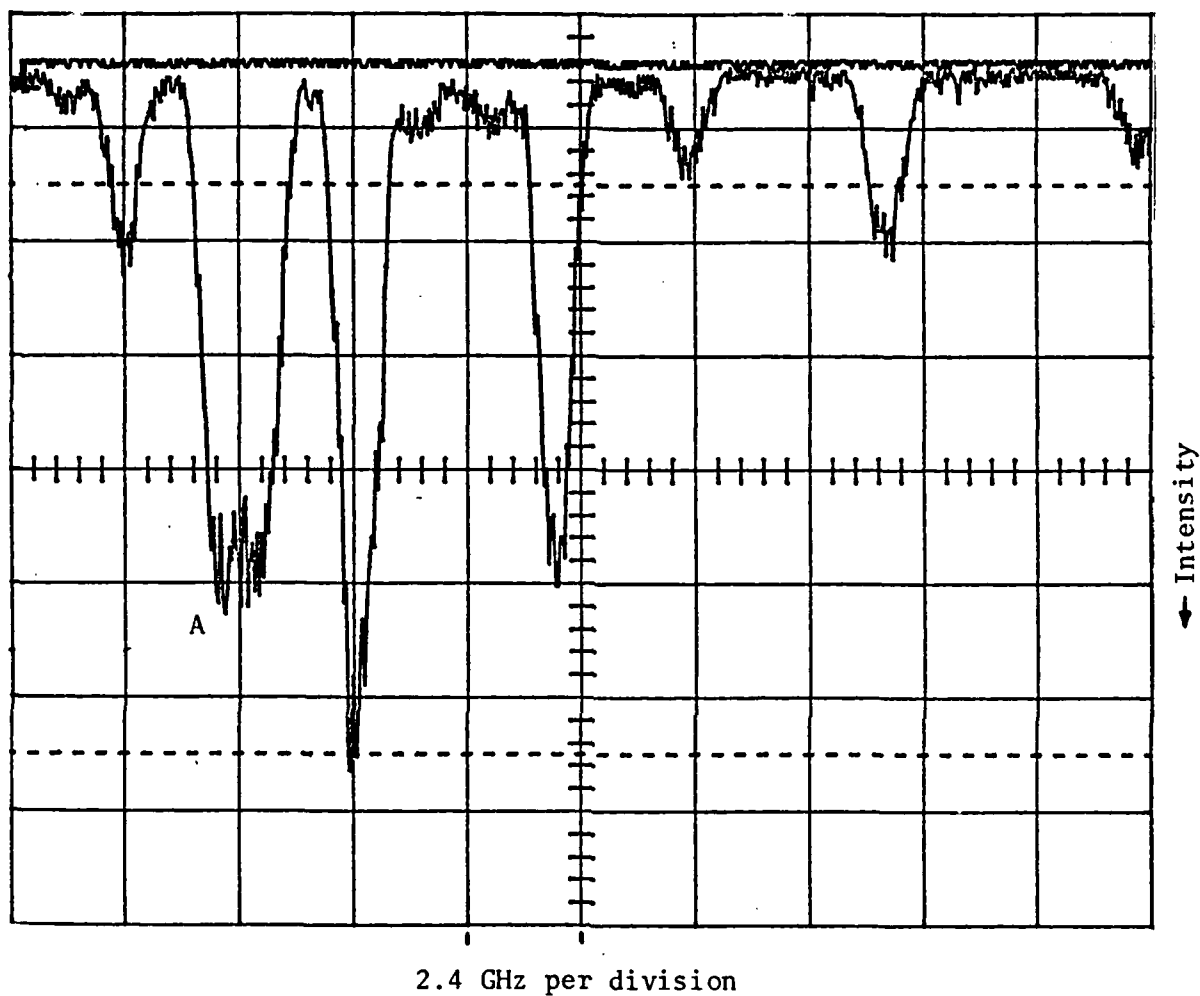
2.4 GHz per division

Figure 2.   Typical Iodine Fluorescence Spectrum near 611 nm.
Excitation wavelength 590.6nm; Total width of trace
is 24 GHz; Temperature 300K; Pressure 5 Torr.   Downward
peaks are fluorescence features.   "A" marks the region
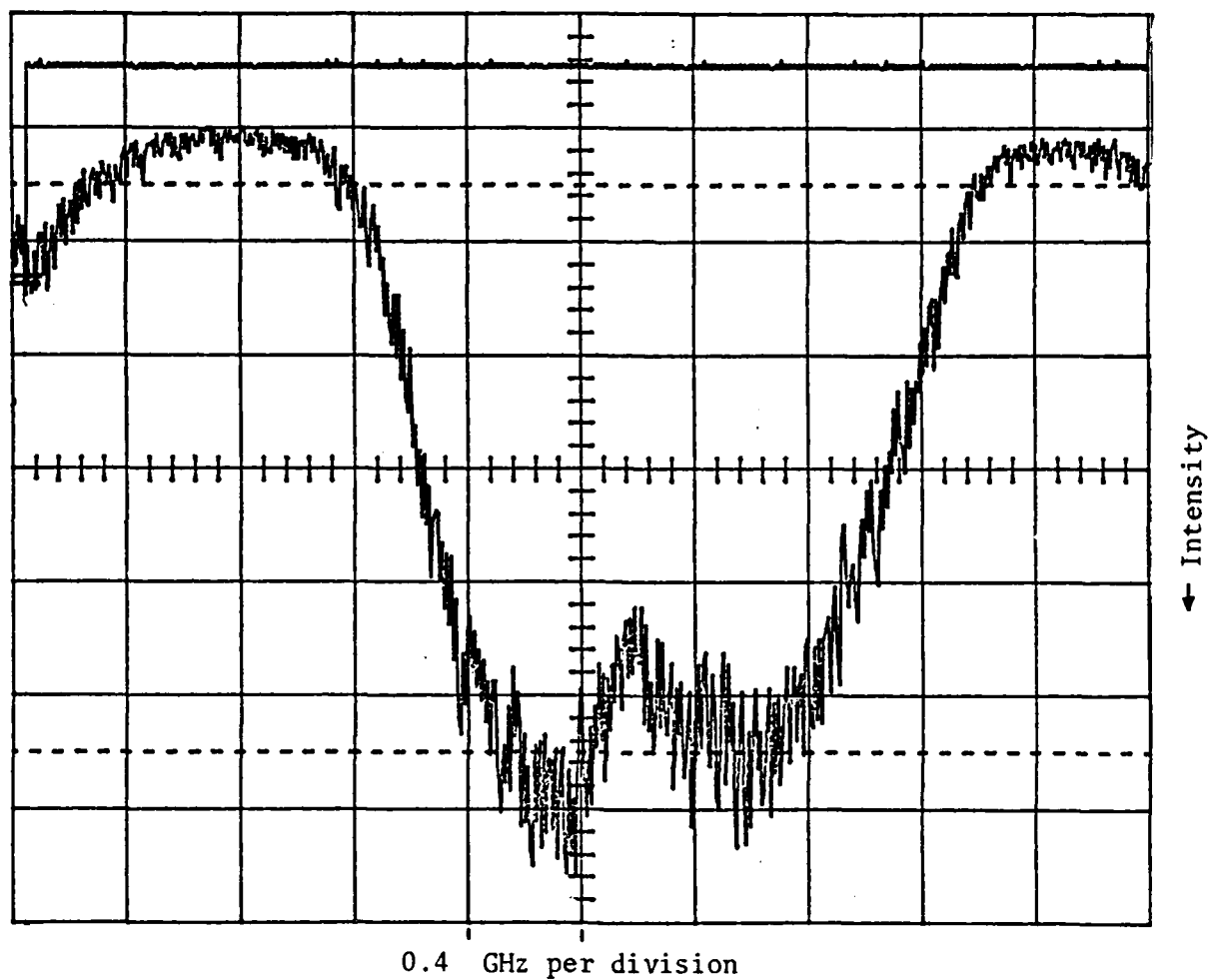shown in an expanded view in Figure 3.

0.4 GHz per division

Figure 3. Iodine Fluorescence Feature A from Figure 2, showing overlap of two peaks. Peak separation is 640 MHz.

A. Iodine

Initial experimental efforts concentrated on designing an excitation and detection system for observing iodine fluorescence. Figure 1 shows the arrangement of the equipment assembled for this purpose. A Spectra-Physics Model 171 Argon-ion laser was used to pump a Coherent 699-21 ring dye laser. Using Rhodamine 6G dye, the ring laser was capable of delivering ~ 1W of single frequency radiation peaking at ~ 590 nm. The ring dye laser was able to scan a frequency of 30 GHz in 0.25 sec. A Fabry-Perot interferometer monitored the laser line to check single mode frequency stability. The laser was directed into a fluorescence cell which was evacuated to the millitorr range. Fluorescence was detected at 90° to the beam direction through a cut-off filter which served to block scattered laser light while transmitting the fluorescence. The output of an RCA 8644 PMT with an S-20 response was passed to a LeCroy 9400 digital oscilloscope. Fluorescence plots were recorded on screen and dumped to an HP7475A plotter.

A ring dye laser wavelength near 590.6 nm yielded fluorescence in iodine vapor peaking at 611 nm. A portion of a typical 30 GHz scan at room temperature resulted in the fluorescence plot shown in Figure 2. Iodine fluorescence peaks are numerous and often are spaced closely or overlap. Figure 3 shows two iodine peaks separated by 640 MHz. No single fluorescence feature was found with FWHM less than ~ 800 MHz. This observation is in agreement with the reported limit of the hyperfine structure contribution to linewidth being 0.025 - 0.030 cm^{-1}, or ~ 780 - 940 MHz (5).

As nitrogen was allowed to backfill into the system, the FWHM of a single fluorescence peak was recorded, along with the amplitude of the fluorescence signal and the shift in location of maximum fluorescence. These results are summarized in Table 1.

At nitrogen pressures above 200 Torr, all fluorescence structure broadens and overlaps to a degree which makes linewidth measurements difficult. This is

Table 1. Iodine Fluorescence Data. Excitation λ = 590.6 nm, Fluorescence
$\lambda \sim 611$ nm, T = 300 K.

N_2 Pressure Torr (atm)	Fluor. Feature FWHM GHz	Frequency Shift of Fluor. Peak, MHz
11 (0.014)	0.8	0
70 (0.09)	1.0	--
110 (0.14)	1.2	+64
150 (0.20)	1.5	--
200 (0.26)	--.--	+200

Table 2. Iodine Fluorescence Data. Excitation λ = 590.6 m, Fluorescence
$\lambda \sim 611$ nm, N_2 pressure $\sim$ 11 Torr.

Cell Temp (K)	Relative Maximum Fluor. Intensity, (mV)
300	500
311	760
320	1140
331	880

consistent with observations by Westblom and Alden (6). Figure 4 depicts the broadening and line shift observed as nitrogen perturber gas pressure is increased. At 110 Torr, the pressure broadening was 400 MHz. Thus the ratio of pressure shift to pressure broadening is about 0.16, in good agreement with Hiller and Hanson (7). Also, it was noted that as expected, increasing pressure in the cell led to a marked decrease in fluorescent intensity due to collision induced quenching effects.

Fluorescence was also monitored over a moderate range of cell temperatures. These results are listed in Table 2. There was no apparent change in linewidth of the fluorescence as laser power was varied from 25 mW down to 2 mW. For a 3 mm diameter beam, this corresponds to a range of 350 mW/cm^2 to 28 mW/cm^2. Attempts to improve detection resolution using an OMA or a Fε y-Perot interferometer provided no advantage over the system described above.

B. Sodium

Sodium is found in some high temperature exhaust flows in parts per billion concentrations. Based on this information, calculations have been performed which indicate a typical sodium number density in the range ~ 10^9 atoms/cm^3. Following the treatment of Fairbank, Hansch, and Schawlow (8), the optimum sodium number density for observing fluorescence in a typical test cell whose dimensions have been defined by AEDC personnel has been calculated as approximately 5 x 10^9 atoms/cm^3. This fortuitous agreement in optimum and expected Na densities has prompted interest in using sodium as a flow velocity tracer atom. This number density can be obtained from a Na source held at approximately 100°C. (8). The limited range of temperatures achievable in the fluorescence cell made its use impractical for studying sodium fluorescence. An optical heat pipe was selected as the best source of reaching adequate Na number densities, even though its geometry was not well-suited for fluorescence measurements. Initial attempts to observe forward-directed fluorescence near the
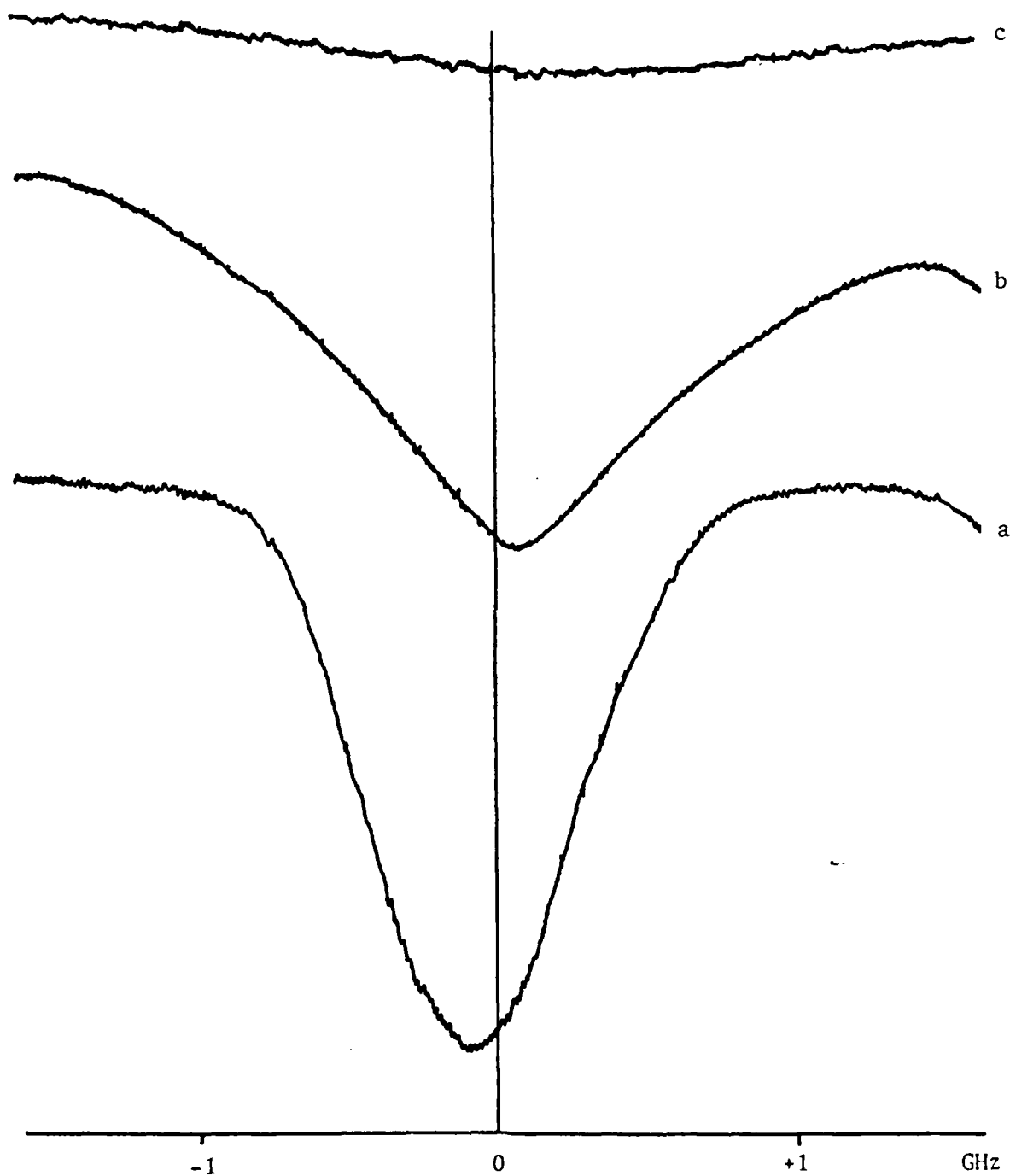
Figure 4. Fluorescence line broadening and shift observed
in iodine vapor, temperature 300K. a) Nitrogen
pressure 11 Torr; b) Nitrogen pressure 110 Torr;
c) Nitrogen pressure 200 Torr.

excitation laser beam met with limited success, and it was decided that laser absorption measurements would be more fruitful.

Using a geometry similar to that depicted in Figure 1, the fluorescence cell was replaced by a Comstock optical heat pipe, and the transmitted beam detected by a silicon photodiode. At 200°C, total extinction of the transmitted beam was observed at 589.0 and 589.6 nm, corresponding to the D lines of atomic sodium.As the cell was cooled, the absorption peak was observed to narrow to a FWHM corresponding to the 1.5 GHz Doppler width of the transition (9) (Figure 5). Table 3 summarizes the results of this investigation. At 195°C, the Na vapor pressure is ~ 6 x 10^{-7} atm, which corresponds to a number density of ~ 10^{13} atom/cm^3. The absorption feature became very difficult to pick out at temperatures below 160°C. In future experiments it may be necessary to heat the pipe to approximately 200°C to locate the resonant frequency, then allow the pipe to cool to the desired temperature while maintaining the laser settings. In Figure 5, the same absorption peak is observed in each case.

Walkup et. al. (9) has reported that for products of laser intensity and pressure exceeding 0.1 mW Torr, the familiar hyperfine doublet feature (4) distorts to a single, structureless line. For pressures of interest to AEDC, any reasonable beam intensity will place the experiment in this "optically-pumped" regime. However, at laser intensities on the order of 12 mW/cm^2, laser saturation occurs (9). Saturation effects can alter energy level populations and thus disturb the transition lineshape in a non-uniform manner. If possible, it seems best to avoid operating the laser at saturation intensity.

Table 3. Sodium Absorption Data. λ = 589.6 nm, Pressure = 6 Torr

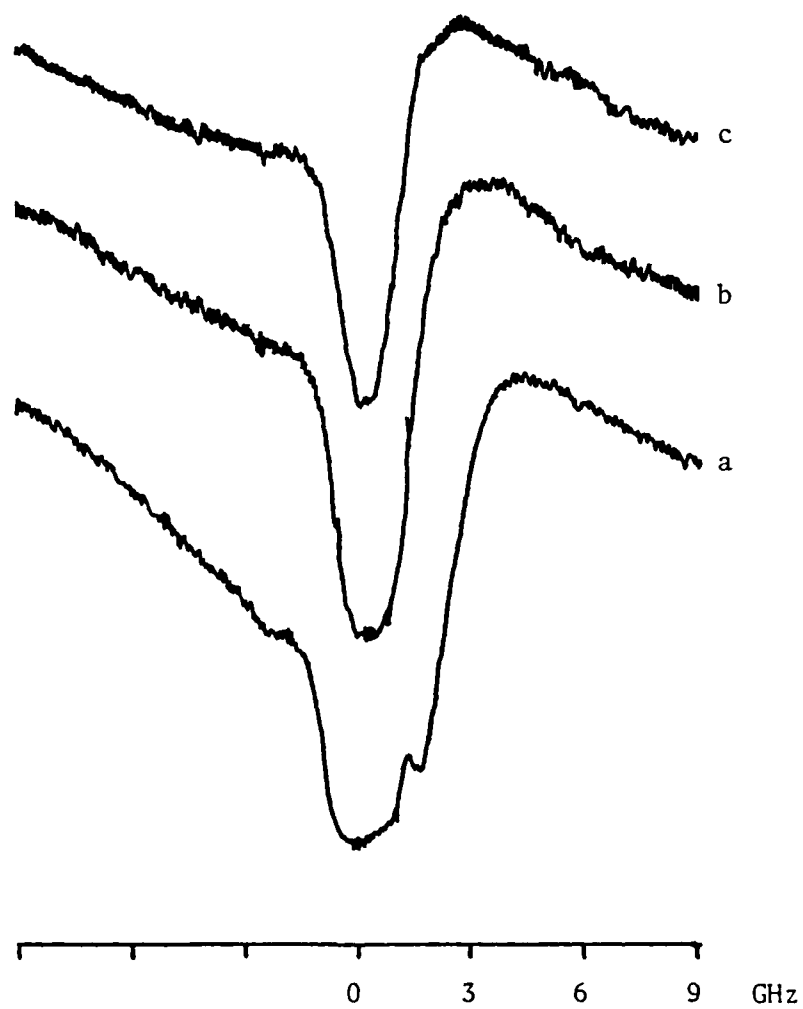| Temperature (C)	Intensity of Abs. Feature (mV)	FWHM of Abs. Feature (GHz)
195	20.5	5.5
185	19.5	2.5
175	16	2.1
165	10	1.5

Figure 5. Narrowing of sodium absorption line at 589.6 nm
as a function of temperature. a) 195C, b) 185C,
c) 175C.

It has also been reported (1) that using nitrogen as the perturber gas causes a shift of the resonance line to the red as pressure is increased. A frequency shift of 6.76 GHz P(atm) SQRT(300K/T) has been predicted. This is a relatively large shift, and should be observed in experiments using a perturbing gas in the heat pipe.

IV. RECOMMENDATIONS:

Effort should be made to locate researchers experienced in techniques associated with RDV. Exchanging information with these individuals improves the efficiency of setting up a reliable experiment. Visiting a laboratory with a working RDV system would be beneficial in accelerating the learning process. Through conversation with R. B. Miles, it is suggested we adopt a laser bounce-back technique so as to accurately measure the Doppler shift without having to rely on reference cells. By reflecting the laser back on itself, one obtains an upshifted and downshifted resonance line. The Doppler shift is then half the separation of these peaks. R. K. Hanson (3) has had experience in RDV using iodine as the tracer molecule, and also in incorporating a modification into the scanning laser to provide faster repetition rates. He has invited AEDC personnel to visit his laboratory, and this opportunity should not be overlooked.

The results of the iodine fluorescence experiments indicate that iodine as a tracer molecules is not well-suited for the conditions present in the ASTF C-1 inlet system. At perturber gas pressures above approximately 150 Torr (0.2 atm), the iodine fluorescence lines are greatly pressure broadened and their intensity decreases markedly. A search for other fluorescence candidates for use under room temperature conditions would be advised.

Much more experimental work remains in order to reliably monitor sodium fluorescence. Optical heat pipes and Na vapor cells are available with side-view ports for measuring fluorescence. Often, these cells have reservoirs which may be held at a separate temperature from the rest of the cell, giving greater versatility in

their operating parameters. Line broadening and shifts need to be examined in perturber gases other than nitrogen, preferably in gas mixtures like those anticipated in the test cell, and over a range of temperatures and pressures.

There should be future effort in designing a small scale flowing gas system in the laboratory so that the RDV technique could be assessed outside of the test cell environment. This could be an effort as simple as painting a salt water solution over the nozzle of a flame burner and exciting Na fluorescence in this flow, or it could extend to a more elaborate vacuum-chamber system with iodine or sodium seeded into a flowing gas.

For sodium concentrations in the range of interest, detection of fluorescence by bare PMT may not be sensitive enough. A photon counting/pulse discriminating detection system or an image intensified camera may be required to achieve the desired signal to noise ratios. This option will be easier to assess after reviewing the results of the aforementioned Na fluorescence experiments.

REFERENCES

1. Miles, R. B., "Resonant Doppler Velocimeter", Phys. Fluids 18(6), pg. 751, June 1975.

2. Zimmermann, M., and Miles, R. B., "Hypersonic-Helium-Flow-Field Measurements with the Resonant Doppler Velocimeter", Appl. Phys. Lett. 37(10), pg. 885, 15 Nov. 1980.

3. McDaniel, J.C., Hiller B., and Hanson, R. K., "Simultaneous Multiple-Point Velocity Measurements Using Laser-Induced Iodine Fluorescence", Optics Letters 8(1), pg. 51, Jan. 1983.

4. Cheng, S., "Resonant Doppler Velocimetry in Supersonic Nitrogen Flow", Ph.D. Thesis, Princeton University, Princeton, New Jersey, 1982.

5. Gerstenkorn, S. and Luc, P., "Assignments of Several Groups of Iodine Lines in the B-X System", J. Mol. Spect. 77, pg. 310, 1979.

6. Westblom, U. and Alden, M., "Spatially Resolved Flow Velocity Measurements Using Laser-Induced Fluorescence from a Pulsed Laser", Optics Letters 14(1), pg. 9, Jan. 1, 1989.

7. Hiller, B. and Hanson, R. K., "Simultaneous Planar Measurements of Velocity and Pressure Fields in Gas Flows Using Laser-Induced Fluorescence", Appl. Optics 27(1), pg. 33, 1 Jan. 1988.

8. Fairbank, W. M., Hansch, T. W., and Schalow, A. L., "Absolute Measurement of Very Low Sodium-Vapor Densities User Laser Resonance Fluorescence", J. Opt. Soc. Am. 65(2), pg. 199, Feb. 1975.

9. Walkup, R., Spielfiedel, A., Phillips, W. D., and Pritchard, D. E., "Line-shape Changes Due to Optical Pumping of Na in Buffer Gas", Phys. Rev. A 23(4), pg. 1869, Apr. 1981.

FINAL REPORT

Thermal Analysis of Bodies Subjected to Aerodynamic Heating

Prepared by: John E. Francis

Academic Rank: Professor

Department: School of Aerospace & Mechanical Engineering

University: University of Oklahoma

Research Location: USAF/AEDC
                       Arnold AFB
                       Tullahoma, Tenn.

USAF Researcher: R.K. Matthews
                     B. Feather
                     Calspan

THERMAL ANALYSIS OF BODIES SUBJECTED TO AERODYNAMIC HEATING

by

John E. Francis

ABSTRACT

The work undertaken on this project was comprised of two completely different problems. One problem was to predict the thermal response of a bomb in an extremely cold environment when subjected to a typical flight mission profile. Of particular interest was to determine if the MIL standards were reasonable. A finite element analysis of the bomb using axisymmetric geometry and 148 elements indicated that based on the assumed flight scenarios and conditions, the MIL standards were reasonable; however, we feel the limiting initial (storage) temperature was extreme. The second project undertaken was to determine the thermal response of EM Windows under a re-entry environment. The windows are diathermanous and a combined conductive and radiative analysis was necessary. For the purposes of this study a planar model was utilized with specularly reflecting boundaries following Fresnel's law. The windows were assumed to emit and absorb but scattering was ignored. The model studied was grey and results were compared to the optically dense and pure conduction solutions.

ACKNOWLEDGEMENTS

I wish to thank the Air Force systems command and the Air Force Office of Scientific Research for the support provided to me for this summer program and for making their laboratories accessible to me. I am very appreciative to Universal Energy Systems for their timely and helpful administration of the program.

I particularly want to thank Richard K. Matthews and Brian Feather for providing the research problems and for their invaluable assistance and support. Their encouragement and concern made the program very rewarding for me. My Effort Focal Point, Mr. Carlos Tirres was most helpful and supportive to me. Finally, I want to thank our Section Head, Mr. Greg Wannenwetch for his support of my project.

I. INTRODUCTION:

The environmental extremes from extremely low temperatures to the aerodynamic heating of re-entry vehicles have caused and continue to require the Air Force to focus a substantial effort on thermal analysis. The Calspan Aerothermodynamics section at the Arnold Engineering and Development Center was interested in determining the temperatures achieved in the fuzes of bombs under extreme environmental conditions. Their interest was to see if the MIL Standards used in bomb fuze design were ever likely to be reached under specific flight scenarios.

There is also a very active interest in the heat transfer in electromagnetic windows. These windows used in guidance of weapons are diathermanous and any thermal analysis should include the effect of both conduction and radiation heat transfer.

I was assigned to work on these problems since my research is in the area of heat transfer. My earlier work in combined conductive and radiative heat transfer was particularly appropriate to address the electromagnetic windows problem.

II. OBJECTIVES OF THE RESEARCH EFFORT

The objectives of the summer effort were separate for the two distinct and different problems addressed.

The objective for the thermal analysis of the bomb fuze was to predict temperatures achieved at different locations in the bomb fuze under a number of flight scenarios consistent with the environmental extremes given by the customer (Eglin AFB). We were then to determine if the MIL Standards used as a design criteria were too restrictive.

The objective in the electromagnetic window problem was to determine

the effect including radiation heat transfer had on the temperature distribution in the window.

The pure conduction and optically dense radiation solutions were being used and our goal was to improve on these solutions in order to more accurately predict the temperature distribution.

III. THERMAL ANALYSIS OF THE BOMB FUZE

The approach taken to analyze the bomb was to use an axial symmetric model for the system and determine the time varying temperature for the two dimensional model thus generated. A finite element code was used to determine the conductive heat transfer in the bomb. The model consisted of 148 elements with the bomb made of four different materials. A steel outer shell, a soft-seal, an explosive and the fuze. Flight scenarios of various cruise speeds, cruise times, dash speeds and dash times were modeled at varying ambient conditions. Also included in the model were various magazine storage conditions as reported in the literature. Material property data was taken from government reports. The results of the finite element program were compared to similar devices which had undergone wind tunnel testing. These results indicated the model was very reasonable. The bomb was modeled to be at an initial temperature determined by storage conditions. The bomb was suddenly exposed to an environment dictated by the altitude ambient condition and aircraft speed. The recovery temperature was utilized with convective heat transfer coefficients taken from experimental data available at AEDC. The details of the results and configurations studied were reported in an AEDC report and will not be reported here, however, the study indicated that for the extreme environment & storage conditions provided the MIL standards

used for the fuze design were reasonable. However, our survey of previous studies of magazine storage temperatures and discussions with Air Force and Navy Pilots make us believe the initial temperature restrictions we were requested to impose are not realistic.

IV. COMBINED CONDUCTIVE & RADIATIVE ANALYSIS OF ELECTROMAGNETIC WINDOWS

The specific problem addressed was that of an electromagnetic window exposed to very high temperature air in an arc tunnel facility. The air was reported to be dry and particulate free. The convective heat transfer coefficient was known or could be determined. The duration of the run in the arc facility was to be of the order of two seconds and the window was made of fused silica however the results of the study should be applicable to other materials where combined conduction and radiation occur.

Experimental measurements had indicated that the temperature penetration depth in the 2 seconds was of the order of one eight inch. For the purposes of this study the window was modeled as a one dimensional slab with specularly reflecting surfaces. For the fused silica scattering can be neglected so an absorbing and emitting media was used as the model. Clearly spectral distribution should be considered but because of the short time available a grey model was assumed. Figure 1 is a sketch of the model used. Many investigators have analyzed combined conductive and radiative heat transfer in a one dimensional media [1-6] but not with the boundary conditions of this study.

The governing differential equation is given by:
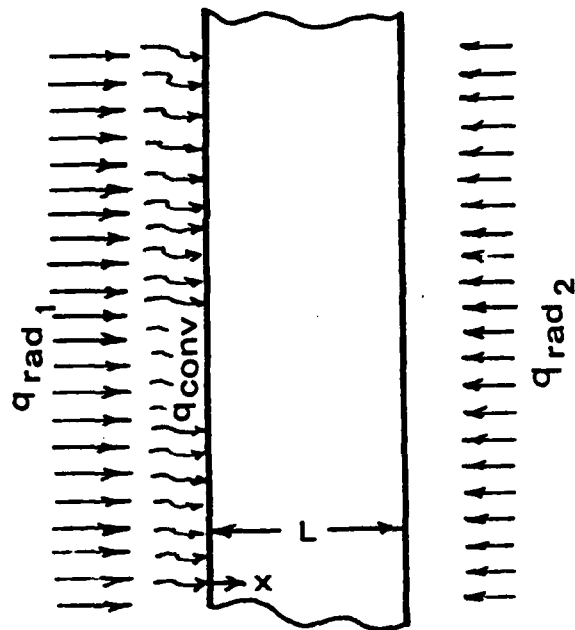
Geometry of Window Model

FIGURE 1

$$\rho c \frac{\partial T}{\partial t} + \frac{\partial}{\partial x} \left[-k \frac{\partial T}{\partial x} + \text{qrad} \right] = 0 \tag{1}$$

where k is thermal conductivity

ρ is density

c is specific heat

T is temperature

qrad is the radiative flux

x is the position

The boundary conditions are

1) @ x = 0 $\quad h(T_{aw} - T) + \text{qrad}_{1 \text{ incident}} = -k \frac{\partial T}{\partial x}\bigg|_{x=0} + \text{qrad}_{x=0}$ $\tag{2}$

2) @ x = L $\quad -k \frac{\partial T}{\partial x}\bigg|_{x=L} + \text{qrad}_{x=L} = -\text{qrad}_{2 \text{ incident}}$ $\tag{3}$

and the initial condition is

@t = 0 $\quad T = T_{initial} = T_{ref}$ $\tag{4}$

The radiative flux is given by:

$$\text{qrad }(\vec{r}) = 2\pi \int_0^1 I(\vec{r},\mu)\mu d\mu \tag{5}$$

where $\mu = \cos O$ and O is the polar angle.

Writing the intensity in the positive x direction as $I^+(\tau,\mu)$ and the intensity in the negative x direction as $I^-(\tau,\mu)$. The absorption coefficient "κ" is used to define optical depth such that $\kappa dx = d\tau$.

The transport equation for an absorbing and emitting medium can then be written as

$$\mu \frac{dI^+(\tau,\mu)}{d\tau} = -I^+(\tau,\mu) + n^2 \frac{\sigma T}{\pi}^4(\tau) \tag{6}$$

$$-\mu \frac{dI^-(\tau,\mu)}{d\tau} = -I^-(\tau,\mu) + n^2 \frac{\sigma T^4}{\pi}(\tau) \tag{7}$$

where n is refractive index & σ is the Stefan Boltzmann constant. Using integrating factors we obtain

$$I^+(\tau,\mu) = C_1(\mu)e^{-\tau/\mu} + \frac{n^2}{\mu} \int_0^\tau \exp\left(\frac{t-\tau}{\mu}\right) \sigma \frac{T(t)}{\pi}^4 dt \tag{8}$$

and

$$I^-(\tau,\mu) = C_2(\mu)e^{\frac{\tau-\tau_0}{\mu_\tau}} + \frac{n^2}{\mu} \int_\tau^{\tau_0} \exp\frac{-(t-\tau)}{\mu} \frac{\sigma T(t)^4}{\pi} dt \tag{9}$$

τ_0 is the optical thickness given by $\tau_0 = \int_0^L \kappa dx = \kappa L$

The radiative flux is given by

$$q(\tau) = 2\pi \int_0^1 [I^+(\tau,\mu) - I^-(\tau,\mu)] \mu d\mu \tag{10}$$

The radiative boundary conditions are given by

1) @ $\tau=0$ $I^+(0,\mu) = \rho(\mu) I^-(0,\mu) + \alpha(\mu) I_1(\mu)$ incident

2) @ $\tau=\tau_0$ $I^-(\tau_0,\mu) = \rho(\mu) I^+(\tau_0,\mu) + \alpha(\mu) I_2(\mu)$ incident

$\rho(\mu)$ is the directional specular reflectance given by Fresnel's Relations

$\alpha(\mu) = 1-\rho(\mu)$ is the directional absorptance

When the equations are non-dimensionalized with the variables

$$\theta = \frac{T}{T_{ref}} \qquad t^{*} = \frac{\kappa^{2}Kt}{\rho c} = \alpha\kappa^{2}t \tag{11}$$

$$h^{*}= \frac{h}{\kappa K} \qquad N = \frac{\kappa K}{4n^{2}\sigma T_{ref}^{3}} \quad \text{Conduction/Radiation Number} \tag{12}$$

$$\frac{\partial\theta}{\partial t^{*}} - \frac{\partial^{2}\theta}{\partial\tau^{2}} + \frac{\partial q^{*}}{\partial\tau} = 0 \tag{13}$$

with

$$q^{*}(\tau) = \frac{1}{2N} \int_{0}^{1}[C_{1}^{*}(\mu) \exp(-\tau/\mu)- C_{2}^{*}(\mu)\exp(\frac{\tau-\tau o}{\mu})]\mu d\mu \tag{14}$$

$$+ \int_{0}^{\tau} \theta^{4}E_{2}(\tau-t)dt - \int_{\tau}^{\tau o} \theta^{4}E_{2}(t-\tau)dt \tag{15}$$

where

$$C_{1}^{*}(\mu) = \left[B+ \rho(\mu)\exp(-\tau_{o}/\mu) \int_{0}^{\tau o}\exp(\frac{t-\tau_{o}}{\mu}) \frac{\theta^{4}dt}{\mu} + \right.$$

$$\left. \rho(\mu) \int_{0}^{\tau o}\exp(\frac{-t}{\mu}) \frac{\theta^{4}dt}{\mu} \right] / \left[1-\rho(\mu)^{2}\exp(-2\tau_{o}/\mu) \right] \tag{16}$$

$$B = \frac{\alpha(\mu)\epsilon_1\Theta_{s_1}^4 + \rho(\mu)\alpha(\mu)\epsilon_2\Theta_{S_2}^4 e^{-\tau_0/\mu}}{1-\rho(\mu)^2 e^{-2\tau_0/\mu}} \qquad (17)$$

$$C_2^*(\mu) = A + \alpha(\mu)\epsilon_2\Theta_{s_2}^4 + B\,\rho(\mu)e^{-\tau_0/\mu} \qquad (18)$$

$$A = \rho(\mu)\, C_1^*(\mu)\exp(-\tau_0/\mu) + \rho(\mu)\int_0^{\tau_0} \exp\left(\frac{t-\tau_0}{\mu}\right)\frac{\Theta^4}{\mu}\,dt \qquad (19)$$

The reflectance $\rho(\mu)$ is determined from the Fresnel Reflectance equation.

These equations are subject to the initial condition

$$\text{at}^* = 0 \qquad \Theta = 1$$

In order to include the possibility of a radiation load on the boundary, the boundary conditions were modified to be:

$$1)\ @\ \tau = 0 \quad -\frac{\partial\Theta}{\partial\tau} + q_{rad} = h^*(\Theta_{a\omega} - \Theta) + \frac{\alpha\epsilon_1\Theta_{s_1}^4}{4n^2 N} \qquad (20)$$

$$2)\ @\ \tau = \tau_0 \quad -\frac{\partial\Theta}{\partial\tau} + q_{rad} + \frac{\alpha\epsilon_2\Theta_{s_2}^4}{4n^2 N} = 0 \qquad (21)$$

14-11

FIGURE 2

Coupled Conduction/Convection Results

After 2 Seconds
$L = 0.05643$ ft.
$h = 0.237$ Btu/S.ft^2.R

Optically Thick Limit

Absorption Coefficient $\kappa = 177.2$ ft^{-1}, $N = 100$

Pure Conduction Limit

Optical Depth Ratio τ/τ_o

Temperature Ratio, θ

14-12
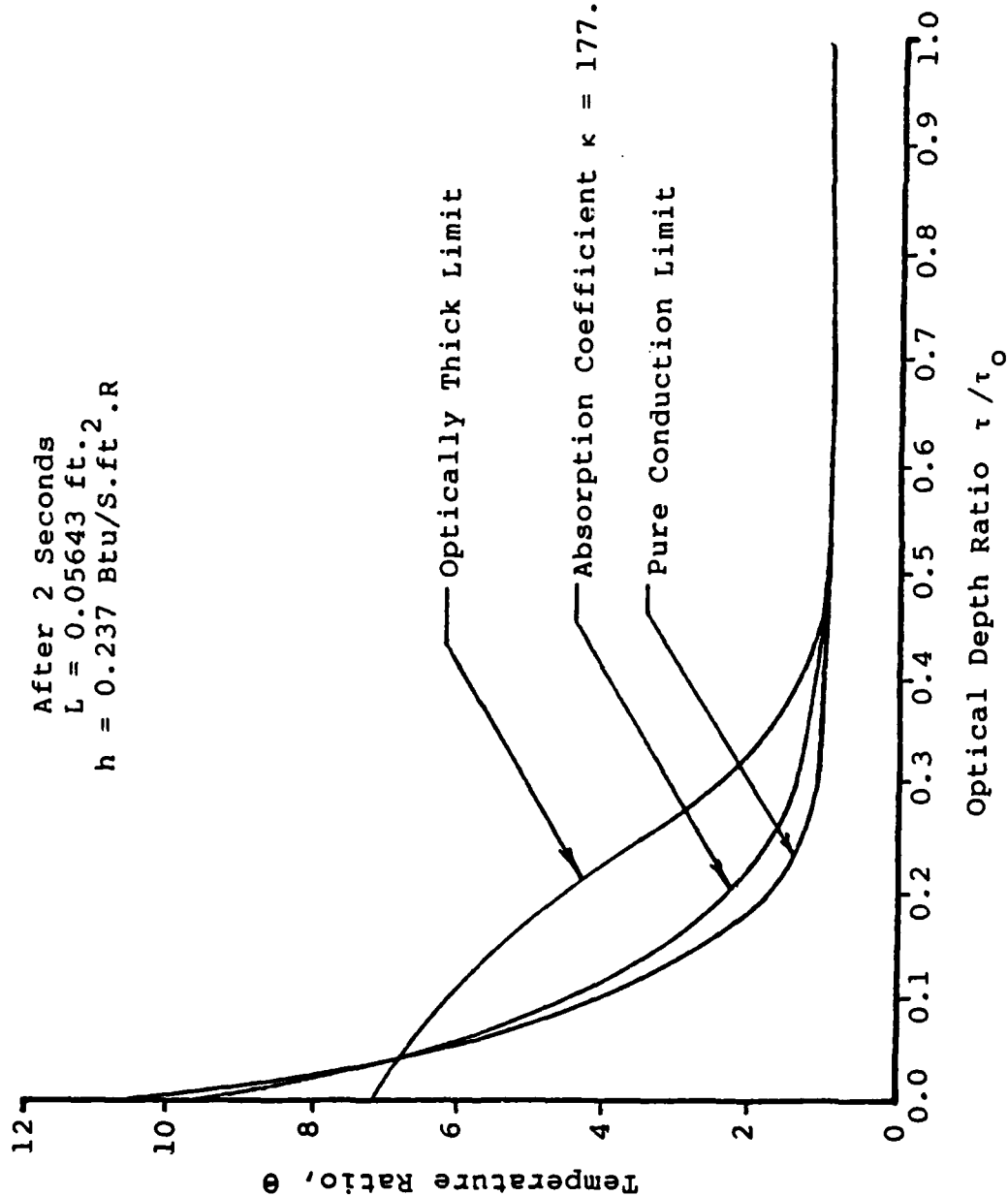
FIGURE 3

Coupled Radiation/Conduction Results

$\kappa = 177.2$ ft.$^{-1}$
$N = 100$
$L = 0.05643$ ft.
$h = 0.237$ Btu/S ft.^{2}R

$\tau/\tau_o = 0.0$

$\tau/\tau_o = 0.1$

$\tau/\tau_o = 0.2$

$\tau/\tau_o = 0.3$

TEMPERATURE RATIO, θ

TIME, S
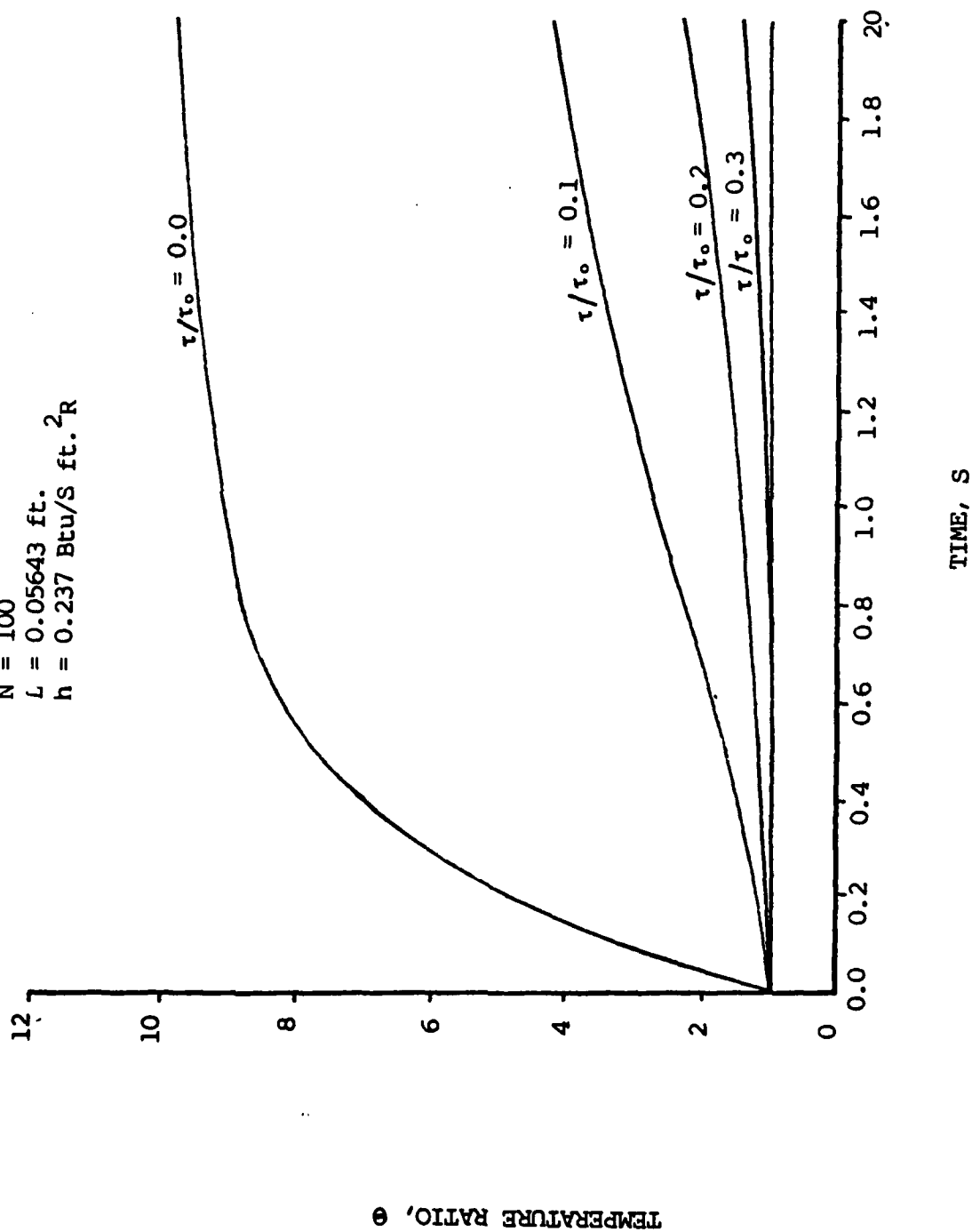
where ϵ_1, ϵ_2, Θ_{s_1}, Θ_{s_1} are used to account for the radiative flux incident on the boundaries given in equations 2 & 3. The equations must be solved numerically and since we are interested in a solution for very short time ($t \leq 2s$) the explicit finite difference formulation was chosen. The program with ten nodes and a 0.01s time step had errors less than 1% in the pure conduction limit; however, the optically thick limit encountered difficulties. As the optical thickness τ_o increases the integrals are over a larger range and the quadratures become less accurate. We overcome this by making the grid smaller. As we increase the number of nodes the solution approaches the optically thick limit. Figure 2 is a typical result from the program after 2 seconds time and figure 3 is a typical temperature versus time result. The numerical solution was run for a variety of material property values. A detailed description of the finite difference equations utilized and the program listing were provided to the AEDC.

IV. RECOMMENDATIONS

The result of this work can be used to predict the temperature distribution in electromagnetic windows with better accuracy than the pure conduction or optically thick limits. The results are limited because of the assumptions made; however, a substantial improvement is made over the models previously used.

The model can be greatly improved by accounting for the wavelength dependent properties. This would necessitate an implicit formulation of the problem and an iterative solution to the system of nonlinear equations. Currently, windows are being studied which have scattering centers within. These can be modeled analytically. The temperatures achieved are so extreme that the surface windows may change phase at the surface. Additional studies should be undertaken to include the

14-14

phase change at the surface and to look at the multidimensional model
for the window.

REFERENCES

1. Viskanta, R., "Heat Transfer by Conduction and Radiation in Absorbing and Scattering Materials" Journal of Heat Transfer, Trans. ASME, Series C, Vol. 87, No. 1, Feb. 1965 pp. 143-150.

2. Viskanta, R., and Grosh, R.J., "Heat Transfer by Simultaneous Conduction and Radiation" International Journal of Heat and Mass Transfer, Vol. 5, 1962 pp 729-734.

3. Fernandes, R., Francis, J. and Reddy, J.N., "A Finite Element Approach to Combined Conductive and Radiative Heat Transfer in a Planar Medium" Heat Transfer and Thermal Control, AIAA Thermophysics Progress in Aeronautics and Astronautics, Vol. 78, 1981 pp 92-109.

4. Fernandes, R. and Francis, J., "Combined Radiative and Conductive Heat Transfer in a Planar Medium with a Flux Boundary Condition using Finite Elements" Spacecraft Thermal Control, Design and Operation, AIAA Thermophysics Progress in Aeronautics and Astronautics, Vol. 86, 1983, pp 328-344.

5. Gardon, Robert, "A Review of Radiant Heat Transfer in Glass" Journal of American Ceramic Society Vol 44, No. 7, 1961 pp 305-312.

6. Goldstein, Marvin E. and Howell, John R., "Boundary Conditions for Diffusion Solution of Coupled Conduction and Radiation Problems, NASA TN D-4618, 1968.

1989 USAF-UES SUMMER FACULTY RESEARCH PROGRAM

GRADUATE STUDENT RESEARCH PROGRAM

Sponsored by the

AIR FORCE OFFICE OF SCIENTIFIC RESEARCH

Conducted by the

Universal Energy Systems, Inc.

<u>FINAL REPORT</u>

Diagnostics for Determination of Arc Plasma Parameters of the AEDC HEAT H1 Arc Heater

Prepared by: Orlando E. Hankins, Ph.D.

Academic Rank: Assistant Professor

Department and   Department of Nuclear Engineering
University: North Carolina State University

Research Location: Technology and Analysis Branch
                      Hypersonics Section
                      Arnold Engineering Development
                      Center
                      Arnold Air Force Base, TN 37355

USAF Researcher: E. J. Felderman

Date: 9 August 1989

Contract No: F49620-88-C-0053

Diagnostics for Determination of Arc Plasma Parameters of the AEDC HEAT H1 Arc Heater

by

Orlando E. Hankins

Abstract

Arc sources have been used to produce high enthalpy and high velocity gas flows for many years. In particular, vortex-stabilized arc heatershave been used to generate high enthalpy, supersonic flow fields necessaryfor aerospace materials testing. To improve the operation of the present-day devices and to scale to larger arc heaters, the parameters of the gas flows in the heater and the parameters of the arc itself must be monitored or determined. Current and future techniques for the measurement of arc plasma parameters are examined for the HEAT H1 Arc Heater. In particular, the use of visible and UV spectroscopy for the measurement of arc parameters is discussed.

Acknowledgements

I wish to thank the Air Force Systems Command and the Air Force Office of Scientific Research for sponsorship of this research. Universal Energy Systems must be mentioned for their concern and help to me in all administrative and directional aspects of this program. In particular, I would like to thank Mr. Carlos Tirres for his help.

A number of people contributed to making my experience rewarding and enjoyable. My technical focal point, John Felderman, was instrumental in getting me started in the right direction and providing support. Charlie Fisher introduced me to the available diagnostic facilities and provided the background information on past diagnostic techniques. Dennis Horn answered my questions on basic arc heater design and filled me in on the local sites. I also have special thanks for Joe Milillo for his help and support, particularly in planning follow-on research. Overall, everyone was of great help and encouragement and their friendliness was greatly appreciated.

I. Introduction

In the natural progression of technology, there is currently an intense interest by the military in developing vehicles capable of hypersonic velocities. Such aircraft require ground level exposure of materials in high enthalpy flows to test for damage as well as high velocity wind tunnel testing of aerodynamic stability and structural integrity. Arc heaters are potential drivers for such facilities. However, the current arc heaters must be scaled up to larger sizes.

At Arnold Engineering Development Center, unique arc heater facilities are used for material testing under high enthalpy conditions. There are also plans to scale the current facilities up in size to provide a high enthalpy driver to a hypersonic wind tunnel. Scaling an arc heater up in size requires an understanding of the basic physics driving the arc and its interaction with the vortex gases and the wall. The effort thus far has been theoretical. However, in order to benchmark predictive codes, a few key parameters of the arc must be experimentally measured.

My research interests have been in the area of plasma diagnostic development for dense plasmas and plasma-material interactions between low-temperature plasmas and surfaces. I've worked on monitoring the x-ray emission from hot electron plasmas in the ELMO Bumpy Torus Device at Oak Ridge National Laboratory and the monitoring of visible emission and other parameters from an electro-thermal gun. My knowledge of dense arc plasmas and my knowledge of diagnostic techniques for such plasmas contributed to my assignment to the Hypersonics Section of the Technology and Analysis Branch of the Calspan Corporation at Arnold Engineering Development Center.

II. Objectives

Currently, major theoretical and computational efforts are being made to understand the physics in the H1 Arc Heater at AEDC. The H1 Arc Heater is a segmented, vortex-stabilized arc heater used for material testing under high enthalpy and pressure regimes. Diagnostics have been and are being designed and tested to measure the parameters of the plasma flow exiting the nozzle on the downstream side. Thus far, the only direct measurements of the arc itself within the arc heater have been with high speed cameras that view the arc through a quartz window upstream from the arc. The cameras are used to measure the arc rotation speed. Since the parameters of the arc and the surrounding vortex gas are important benchmarks for any predictive code for scaling of the H1 Arc Heater design to a larger device, the Hypersonics Section is interested in what diagnostics could be developed to better monitor the inside of the arc heater.

My assignment was: 1) to review past experimental data (raw and processed) and make suggestions for improving the analysis of the data and for modifying the present setup; 2) to design new diagnostics for the current H1 Arc Heater; and 3) to do some laboratory simulations or participate in taking data during technology tests on the arc heater. Due to the slipping of the technology testing, the third objective could not be done during my ten week period. Instead, I worked on a code that would predict the parameters of the arc based on experimental measurements. This code would supplement current predictive arc codes.

In the following sections, I will address the progress that was made on each objective. In section III, the present diagnostic techniques for the arc will be summarized. In section IV, the possible additional diagnostic techniques that can be applied to the arc will be reviewed. In section V, a summary of the preliminary computer coding will be presented along with some results. Finally, section VI will summarize my recommendations and my suggestions for follow-on research.

III. Current Arc Diagnostics

During typical operation of the H1 Arc Heater, several bulk parameters are specifically set: the current, the chamber pressure, and the mass flow rate of the gas (air). Once these items are set, the applied potential is measured, the exit gas enthalpy and temperature leaving the nozzle is measured, and the total heat flux to the wall is deduced from the temperature change in the cooling water to the wall. During technology tests, the heat flux per segment can be obtained by measuring cooling water delta-T's at each module, therefore providing some information on axial distribution. The potential difference between the modules can also be measured, which provides a radially averaged electric field strength vs. axial location.

The heat flux measurements have been used to predict segment burnout and to compare to the overall power balance of the device. The axial measurements can be compared to predictive codes that calculate wall heat flux. Along with the measurements of exit gas enthalpy, the heat flux data can also be used to deduce bulk gas temperatures. Due to the unknown heat transfer characteristics of the cooling water next to the channel walls in the modules (laminar flow, nucleate boiling, or film boiling), the temperature of the module walls facing the arc can not be easily determined.

The applied potential (V) is related to the plasma current by

$$V = i \left(R + dL/dt \right) + L \, di/dt \tag{1}$$

where i is current (amperes), R is resistance (ohms), L is inductance (henries), and d/dt is the derivative with respect to time. In

general, di/dt is equal to zero. If dL/dt can be ignored, the the
average plasma resistance can be determined from the measured current
and potential. The plasma resistance can then be used to deduce plasma
temperature. Axial potential drop data can then be used to calculate
volume-averaged temperature along the axial extent of the chamber,
provided the arc radius can be deduced. The change in inductance with
time, dL/dt, is related to the arc geometry, while changes in arc
resistance is more closely related to temperature changes in the arc
due to fluctuations. It may be possible to look at the frequency
dependence of voltage fluctuations and deduce information concerning
arc geometry fluctuations and turbulence. However, no calculations
have been done on that subject in this report.

By using all of the bulk and axial measurements, zero- and one-
dimensional arc parameters can be deduced that can be used to benchmark
analytical codes. An example of how this can be done is demonstated in
Program Calctemp in section V.

IV. Additional Diagnostic Techniques

The main measuring techniques used in thermal plasmas have been
divided into three catagories by Fauchais, et al. (1989): a) intrusive
methods which employ material probes (water cooled and/or used in a
transient mode); b) passive radiation techniques which utilize
radiation emitted by the plasma or plasma carried particles; and c)
active radiation techniques which use an external source of radiation
(incoherent or coherent) to probe the system by transmission,
absorption, scattering, or reflection. While all three catagories have
been used at the nozzle exit of the H1 Arc Heater, only the passive
radiation techniques (in particular, visible and UV spectroscopy) can
be used to monitor the arc without major modifications in the heater.
However, there are several problems related to the specific
characteristic of thermal plasmas that make them difficult to diagnose.
First, the plasma is very bright, sometimes requiring special filtering

equipment. This light intensity can change by six orders of magnitude during a radial scan from the axis to the wall due to gradients in temperature from the plasma core through the surrounding gases. The steep gradients require that the measured volume be small and may require that the data be inverted. The steep gradients may also lead to demixing problems that can change the chemical composition of the plasma at a given location from the initial gas composition. The high heat fluxes will require that any window used to monitor the arc be cooled. Also, there will be natural arc fluctuations even during steady-state operation. In addition, the high degree of swirl in the heater gas flow coupled with the magnetically driven arc rotation at the electrodes forces the arc into the shape of a flexible helix with variable pitch and radius. Since the arc is not stationary, it is very difficult to stay focussed onto a specific location in the arc.

With these difficulties in mind, it is still possible to obtain meaningful information about the arc from passive measurements of visible and ultra-violet light from the plasma. Currently, the H1 Arc Heater has a quartz end-window upstream of the anode through which the arc rotation is observed with a high speed camera. Also, a quartz side-window has been built that can replace a segment on any module. The side-window has not been tested under operation conditions, but the end-window in now a regular feature. These ports can be used for observing the arc.

In observing the arc, there is a question as what form the emission spectrum will take, what features will be specifically monitored, and what arc parameters can be measured. There are three possible types of spectra that can be expected: a) black-body; b) continuum radiation with atomic, ionic, and/or molecular lines; or c) continuum radiation with atomic and/or molecular absorption lines. It is not unreasonable to expect black-body radiation from a high pressure arc heater plasma. The intensity per unit wavelength from a black-body

is represented by

$$I(\lambda) = \{1 - \exp[-K(\lambda)\ d\ ]\}\ B(\lambda) \qquad (2)$$

where I is intensity, K is the absorption coefficient, and d is the thickness. B is the Planck function represented by

$$B(\lambda) = \frac{1.19 * 10^{-20}}{\lambda^5} [\exp(1.439/\lambda T) - 1]^{-1}\ \text{w}/(\text{cm}^2*\text{ster}*\text{A}) \qquad (3)$$

where T is temperature in K, and λ is wavelength in angstroms. From the shape of the spectrum, the temperature can be obtained.

However, calculations made by Wilson and Grief (1968) for plasmas at pressures above 10 atmospheres and temperatures less than 18,000 K predict that the radiation flux would be less than black body and that >50% of the emission would be in the visible and infrared continuum. Therefore, black-body emission is probably not likely except in the infrared portion of the spectrum.

If the spectrum consists of a continuum plus emission lines, several methods are available to obtain the arc parameters. According to Morris, Krey, and Bach (1966), the emission from an optically thin line is given by

$$I = \frac{hc\ g\ A\ N(T)/U(T)}{\pi\lambda}\ \exp(-E/kT) \int_{o}^{\infty} L(\lambda)\ d\lambda\ \ W/(\text{cm}^3*\text{ster}) \qquad (4)$$

where h is planck's constant, c the speed of light, g the statistical
weight of the upper level, A the transition probability per unit time,
N the species number density, U the species partition function, E the
energy of the upper excited state, and L the line shape parameter. If
the plasma is in Local Thermodynamic Equilibrium (LTE), then an
absolute measurement of the intensity of a line can be used to obtain
plasma temperature and the species density. Absolute intensity
calibrations can be difficult to do, but by measuring the relative
intensities of two or more neutral or ion lines from a single species,
a Boltzmann's plot can be done from which temperature can be
calculated. However, if the arc is not in LTE, the temperature
measured will be indicative of the excitation temperature, not the
electron temperature (Fauchais, et. al.), According to Taylor and Ali
(1986), who calculated collisional radiative recombination and
ionization coefficients for nitrogen and oxygen plasmas, LIE. may not be
reached in such plasmas until the electron density is greater than 1 *
10^{18} cm-3. Present estimates for the H1. Arc. Heater place the electron
density at more than an order of magnitude less.

However, the electron density is expected to be high enough within
the arc to measure Stark Broadening of neutral and ionic emission
lines, which does not depend on LTE. The Stark Broadening effect gives
lines a Lorentzian profile with a half-width given by Griem (1964,1974)
as

$$\Delta\lambda = 2 * 10^{-6} w\, n_e \left[1 + 1.75 * 10^{-4}\, n_e^{1/4}\, \alpha \left(1 - \frac{0.068^{1/6})}{T_e}\right)\right]$$

(5)

where w and α are tabulated by Griem for various atomic and ionic
lines. A knowledge of the electron density allows one to deduce arc
temperature from other considerations, even when the arc is not in LTE.

Molecular emission bands may be present away from the center of the arc. The molecular bands can also be used to measure vibrational and rotational temperatures, which can be related to the electron temperature. Blackwell, et al. (1989) determined vibrational and rotational temperatures in a nonequilibrium air plasma by comparing experimental measurements with a code developed by C. Park (1985) that generates an air emission spectrum from inputted temperature values and number densities.

The biggest problem with observing emission from the arc is the optical thickness of the surrounding gases. Calculations by Wilson and Nicolet (1967), Churchill et al. (1967), and Taylor and Ali (1987) indicate that the mean free path for visible light in an air plasma at temperatures greater than 1 ev and high pressure would be less than 1 cm. Therefore, when the arc radius is approximately 1 cm or greater, light from the plasma center will be greatly attenuated. Fortunately, near the arc attachment location where the end-window is located, the arc radius should be less than 1 cm. As the temperature of the gases drops away from the arc, the mean free path of the light greatly increases. Near the wall, where gas molecular and neutral densities are high, the temperature may be about 1000 K and the mean free path is greater 100 cm. Near the arc, where temperatures may be about 8000 K, the optical thickness is about 10 cm. Again, at the end-window, the thickness of the gas with the higher temperatures should be much less that 10 cm, so optical thickness (which would result in absorption lines instead of emission lines) should not be a problem. This is qualitatively verified by the fact that the arc can be easily seen during high pressure operation with the high speed camera. However, for the side window, the average gas temperature is much higher, and absorption may be a problem. In that case, absorption line measurements may have to be done. It is also possible to use the continuum between the absorption lines and bands as a temperature and density diagnostic. For a single species, the continuum emission is

given by Morris, et al. (1966) as

$$I = 5.443 * 10^{-46} Z^2 g \frac{N_e N_i}{T^{\frac{1}{2}}} e^{-C2/\Lambda T} + 40.03 * 10^{-24} \frac{e^{-C2/\Lambda T}}{\Lambda^3} \sum_{n\ell J} \sigma_{n\ell J} N_{n\ell J}$$

(6)

where Z^2 is effective nuclear charge, g is the gaunt factor, C_2 is the 2nd radiation constant, N_i is the number density of a given species, N_{n1J} is the number density of the species in the level n,l,j, and σ_{n1J} is the cross-section corresponding to the n,l,J level which can be found in Griem (1964). Typically, the continuum is optically thinner than the lines. However, the determinations of densities and temperatures for multi-species plasmas are very difficult and will call for extensive coding.

VI. Computer Coding

Some calculations were made using a zero-dimensional code that is a modification of the ZEUS code used at North Carolina State University. The code is still incomplete at this time. ZEUS is a 0-D, time-dependent code that calculates plasma parameters for an electrothermal accelerator. The modified code, called CALCTEMP, is a steady-state, 0-D code that calculates arc parameters using the known current, applied potential, and pressure. CALCTEMP calculates the volume-averaged resistivity of the arc and uses that to calculate temperature. The electron-ion collisions are treated by a modified Spitzer resistivity and the electron-neutral collision cross-sections are obtained from Dresvin (1977). The code treats the arc as a single fluid composed only of nitrogen and oxygen and with an isothermal temperature distribution. A comparison of CALCTEMP volume-average temperatures with SWIRL ARC peak temperatures for a particular set of conditions is shown in figure 1. SWIRL ARC (Shaeffer, 1978) is a

steady-state, 2-D code that treats vortex-stabilized arcs. In figure 1, temperature is plotted versus the arc radius as it increases in size between the electrodes. There is good agreement over the length of the arc heater. A more detailed code would include radial conduction and axial convection of enthalpy out of the arc. However, there was not enough time to make additions to the program. The program is used to demonstrate a way that measured experimental parameters can be fed back into analytical codes in order to obtain a better physical understanding of the processes in the arc heater.

VII. Conclusions and Recommendations

Based on the studies mentioned in the prior sections, it is recommended that a series of spectroscopic measurements be undertaken through the quartz end-window upstream of the arc during technology tests. The measurements should be made using an optical multichannel analyser system in order to take advantage of the technology of photodiode arrays. The work should be done in three phases. In the first phase of experiments, a narrow dispersion grating be used (ex. 300 grooves per inch for a 1024 diode array) to allow the widest spectral range. These runs will be for spectral identification (black-body, emission lines, or absorption lines). The measurements need not be time-resolved, thereby providing a combination of arc and background gas emission. However, since the arc should have a much higher temperature than the background, most of the emission will be from the arc. Quartz fiber optics (1 mm or less diameter) should be used to bring the light to the spectrometer. The fiber optics are small enough not the restrict the view of the high speed camera and will limit the amount of light seen preventing saturation of the photodiodes. Also, the fiber optics can help with the spatial resolution in the later phases. It is suggested that the wavelength range be 300 to 600 nm. This is so that the following lines (bands) may be seen if they are present: CuI (510.5, 515.3, 521,8), NI (492.8, 520.1), NII (510.4), OI (533.1), N_2 (2+) and (1+), and N_2^+ (1-). The wavelength interval

between 490 and 530 nm will have the least interference with molecular emission and absorption.

In the second phase, a wider dispersion grating can be used. Based on phase I measurements, if atomic lines are present, relative intensities can be used for temperature measurements, and line widths can be used for density measurements. If the bands are present, similar methods can be used for temperature and density determinations. In this phase, time-resolution will be important, since the arc will be rotating in and out of the line of sight. Neutral filters may have to be used so that an intensifier can be used with the photodiode array. During this phase, the end-window should be tested with a high-speed camera in order to observe arc motion in a turbulent gas flow.

In phase III, it is suggested the radial measurements be performed on both the end window and the side window. This can be done by either by using a motorized drive for the fiber optics, scanning a mirror, or using a SIT. which is a intensified photodiode array target in rectangular matrix which allows for the measurement of spatial and spectral simultaneously. With time-resolution added, the parameters of the arc and surrounding gases can be measured.

Follow-on research on the above recommendations will involve three aspects: theoretical preparation for the phase I technology test; analysis of phase I experimental data and recommendations for phase II technology tests; and detailed analysis of phase II experimental data. Research dealing with phase III would depend on the timetable for technology testing on the H1 Arc Heater. Further follow-on research that will be pursued in a mini-grant include theoretical/computation calculations of voltage fluctuations with arc geometry and temperature, and calculations of the physics of collisional sheaths between high-pressure plasmas and surfaces. The sheath physics is important to the understanding of the arc attachment process upstream of the nozzle in arc heaters.

References

H. E. Blackwell, Eric Yuen, Sivaram Arepalli, Carl Scott, "Nonequilibrium Shock Layer Temperature Profiles from Arc Jet Radiation Measurements," AIAA-89-1679, June 1989.

H. E. Blackwell, F. A. Wierum, S. Arepalli, and C. D. Scott, "Vibrational Measurements of N_2 and N_2^2 Shock Layer Radiation," AIAA-89-0248, January 1989.

D. R. Churchill, B. H. Armstrong, R. R. Johnson and K. G. Muller, "Absorption Coefficients of Heated Air: A Tabulation to 24000 K," JQSRT 6.371 (1966).

Physics and Technology of Low-Temperature Plasmas, S. V. Dresvin (Ed.),

The Iowa State University Press, 1977.

P. Fauchais, J. F. Coudert, and M. Vardelle, "Diagnostics in Thermal Plasma Processing," in Plasma Diagnostics, Vol. 1, Edited by Orlando Auciello and Daniel L. Flamm, Academic Press, Inc. 1989.

Hans R. Griem, Plasma Spectroscopy, McGraw-Hill, Inc., 1964.

Hans R. Griem, Spectral Line Broadening by Plasmas, Academic Press, 1974.

J. C. Morris, R. U. Krey and G. R. Bach, "The Continuum Radiation of Oxygen and Nitrogen for Use in Plasma Temperature Determination," JQSRT 6, 727 (1966).

Chul Park, "Nonequilibrium Air Radiation (NEQAIR) Program: Users Manual," NASA TM-86707, 1985.

J. F. Shaeffer, "Swirl Arc: A Model for Swirling, Turbulent, Radiative Arc Heater Flowfields," AIAA Journal, Vol. 16, No. 10, October 1978.

Ronald D. Taylor and A. W. Ali, JQSRT 38, 29 (1987).

Ronald D. Taylor and A. W. Ali, JQSRT 35, 373 (1986).

Ronald D. Taylor and A. W. Ali, JQSRT 35. 213 (1986).

K. H. Wilson and R. Grief, "Radiation Transport in Atomic Plasmas,"

JQSRT 8, 1061 (1968).

K. H. Wilson and W. E. Nicolet, "Spectral Absorption Coefficients of Carbon, Nitrogen and Oxygen Atoms," JQSRT $\underline{7}$, 891 (1967).
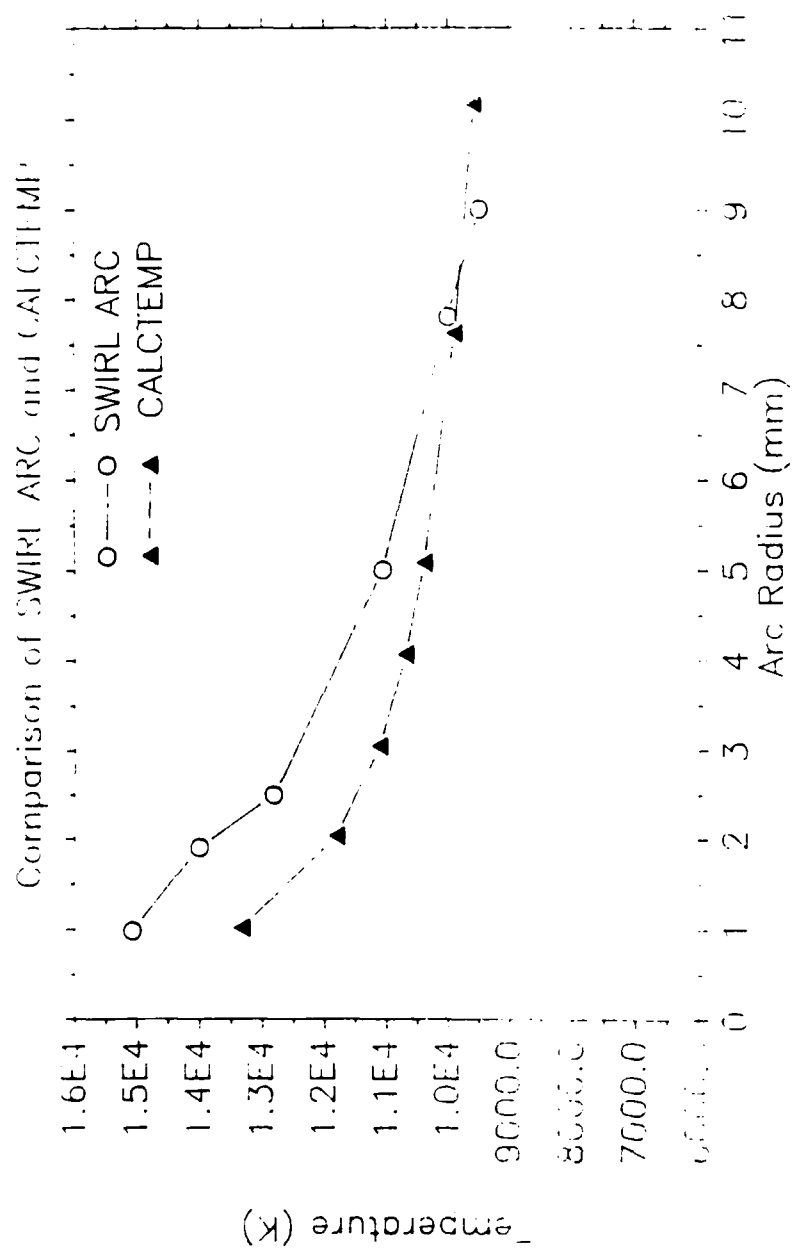
Figure 1. Comparison of SWIRL ARC peak temperatures versus CALCTEMP volume-averaged temperatures as the radius of the arc is increased.

1989 USAF-UES SUMMER FACULTY RESEARCH PROGRAM/

GRADUATE STUDENT RESEARCH PROGRAM

Sponsored by the

AIR FORCE OFFICE OF SCIENTIFIC RESEARCH

Conducted by the

Universal Energy Systems, Inc.

<u>FINAL REPORT</u>

<u>THE DESIGN OF JET MIXERS FOR AN ARC HEATER: AN EXPERIMENTAL APPROACH</u>

Prepared by: Lang Wah Lee

Academic Rank: Professor

Department and   Mechanical Engineering

  University: University of Wisconsin - Platteville

Research Location: AEDC
                   Arnold AFB
                   Tullahoma, TN   37389

USAF Researcher: Frederick L. Shope

Date: August 7, 1989

Contract No: F49620-88-C-0053

THE DESIGN OF JET MIXERS FOR AN ARC HEATER - AN EXPERIMENTAL APPROACH

by Lang Wah Lee

ABSTRACT

The modeling requirements for the mixing process inside a jet mixer where a stream of high temperature air from an arc heater mixes with another stream of injected air at ambient temperature are studied. Two mixing mechanisms are identified in the mixer and this fact necessitates the use of two sets of governing equations. Normalizing these equations yields six dimensionless parameters which provide the most general conditions for similitude studies. However, two of the parameters, the Grashof number and the Froude number, are found to pose conflicting requirements on the scaling laws and cannot be satisfied simultaneously. Experiments are proposed to find out which one of the two parameters is of lesser importance. If one of these two parameters can be excluded from consideration, then water can be used in pilot mixer testing to yield both qualitative and quantitative information relevant to the design of a prototype mixer. An experimental scheme using mass transfer to simulate the heat transfer process is also proposed.

ACKNOWLEDGEMENTS

I. INTRODUCTION

Arc heaters were developed at the Arnold Engineering Development Center more than twenty years ago to provide a high temperature and high speed air streams to simulate the conditions encountered by high-performance aircrafts and space vehicles. To keep pace with the development in the space program, attempts were made over the years to enlarge the performance envelope of the arc heaters and to develop a better means to control their operation. Such attempts were not always successful because it was found that the arc heaters would not perform satisfactorily at high mass flow rate. One promising way to solve this problem is to attach a mixer to the arc heater such that the heated air from the heater would mix with injected air (at ambient temperature) in the mixer, and the mixture would then be ejected through a nozzle to the test section. With this approach the control of temperature and mass flow rate can easily be achieved by changing the injection ratio while the operating conditions in the arc heater would not undergo substantial changes. Moreover, this method is also expected to bring about a more uniform mean temperature profile and a reduction in temperature fluctuation at the test section because of the process in the mixer.

The development of the mixer was envisioned by Shope (1989) to include four phases. They are 1) the selection of mixer configuration, 2) the analysis, 3) the computer simulation, and 4) the testing. Three mixer configurations, of which two are crossflow jet mixers and the third a coflow jet mixer, were proposed for consideration. Because of the complexity of the mixing process, the development of the mixer was believed to be primarily an experimental task, and a pilot mixer project was conceived for such purpose. Prior to the development of the pilot mixer, the scale-up laws, the test fluid, the instrumentation and measurement techniques must be determined.

My research interests have been in the area of turbulent flow and, in particular, the application of turbulence theory to various engineering problems in thermo-fluid systems. Such problems include the flow in stirred tanks, heat and mass transfer for particles suspended in turbulent fluids, transport phenomena in canopy flows, and the experimental study of wake flow behind three-dimensional blunt objects.

II. OBJECTIVES OF THE RESEARCH EFFORT

Model testing would be useful to the design of a mixer only when the scale-up laws are known. At present, such scale-up laws for jet mixers cannot be found in the literature and it is the responsibility of the designer to solve this issue. My preliminary objective is to determine the similarity parameters for a jet mixer and use them to obtain the scale-up laws. The similarity parameters would also be used to check whether an on-hand water tunnel facility can be used to simulate the mixing process in the envisioned prototype mixer.

During the course of my study, my goal was broadened and the task came out to be a preliminary study in preparation for the development of the pilot mixer. The preliminary study involves with the following three aspects:

1)   the deviation of similarity parameters,
2)   the selection of test fluids,
3)   the design of experimental setup and measurement techniques.

The central issue of the project is the derivation of similarity parameters because they determine the scale-up laws and provide a criterion for selection of test fluids. Based on the selection of test fluids, the experimental setup and the measurement technique can subsequently be decided.

III. PROJECT DEVELOPMENT AND RESULTS

a. According to Kline (1986), there are three methods to derive similarity parameters, namely, the Buckingham π theory, the force ratio method, and the method of normalizing the governing equations. Of these three methods, the third one is most direct and reliable and is thus the method used in this research. However, some of the equations involved are too lengthy to be included in this short report. To overcome this difficulty this report will present an approach involving the use of both the second and third method. In other words, the third method will be used where the equations are not too lengthy. If this is not the case, the force ratio method will be used in the presentation instead. Since all the forces were identified from the governing equations, the results so obtained are identical to those obtained from normalization of the equations.

The use of any of the above methods requires a clear understanding of physical process in the mixer. A study of the physical process revealed the presence of two distinct mixing mechanisms in a jet mixer, one occurs in the neighborhood of the injected jets and the other occurs downstream of a point where the injected jets penetrate into the cross-stream and meet each other at the central axis of the mixer. Since these two mechanisms occur at different regions of the mixer, the mixer is then divided into two fields to be studied separately. The front part of the mixer is called the near field where the flow consists of two streams, i.e., the jet stream and the cross-stream. The mixing is accomplished by entrainment in which the fluid of the cross-stream is sucked into the jet stream. The rear part of the mixer is called the far field where the jets have lost their identity after colliding with each other. Mixing in the far field is accomplished mainly by turbulent diffusion. Corresponding to these two mixing mechanisms, there are two sets of governing equations and two sets of similarity parameters.

The motions of the two streams in the near field are in turn governed by two different subsets of equations, one for the jet stream and the other for the cross-stream. The similarity parameters for the cross-stream will be derived from governing equations, but those for the jet stream will be derived from force ratio method because the equations for the jet are too lengthy. It must be noted that the solutions to the two streams are coupled because the two streams have a common interface where continuity in stresses and velocities must be maintained.

The governing equations for the cross-stream are the Navier-Stokes equations which can be written in the following form:

$$\rho_o \frac{D \vec{U}_o}{Dt} = - \nabla p + \mu \nabla^2 \vec{U}_o + \vec{X} \tag{1}$$

The pressure field in the cross-stream causes the bending of the jet stream and the pressure gradient would act along the radial direction of the bent jet, i.e.

$$|\nabla p| = \frac{\partial p}{\partial r} \approx \rho_j \frac{U_j^2}{r} \tag{2}$$

where r is the radius of curvature of the bent jet and ρ_j is the density of the jet fluid. After substituting (2) into (1), normalization of the resultant equation yields the following parameters (the process is the same as that of Moussa, et al., 1977, except the body force term):

$$\frac{fL}{U_o}, \frac{\rho_j}{\rho_o} \frac{L}{r} \left(\frac{U_j}{U_o} \right)^2 \cos\theta, \frac{\nu}{U_o L}, \frac{Lg}{U_o^2} \tag{3}$$

16-7

where   Uo - velocity of the cross stream

L - characteristic length scale

θ - angle between the direction of the jet stream and the cross-stream

f - vortex shedding frequency

The first term in (3) is the Strouhal number, the third and fourth term are respectively the reciprocal of the Reynolds number and the Frounde number. The second term consists of the product of two elements, i.e., the momentum flux ratio $\rho_j U_j^2/\rho_0 U_0^2$ and the geometry factor $L/r \cos \theta$. The latter element represents the bending geometry of the jet and must be determined from the trajectory of the jet itself. The computation of jet trajectories is very involved, as demonstrated in the works of Patankar, et al. (1977) and Makihata, et al. (1979). Since our task is to find similarity parameters, we will use the force ratio method to avoid the need of presenting complicated equations.

The motion (and thus the trajectory) of a jet is governed by the following five forces:

i.   the drag force

$$F_D \sim \frac{1}{2} C_D \rho_{o'} |\overrightarrow{U}_j - \overrightarrow{U}_o|^2 L^2$$

ii. the inertial force of the jet fluid

$$F_i \sim \frac{1}{2} \rho_j U_j^2 D_j^2$$

iii. the viscous force of the jet fluid

$$F_j \sim \mu_j U_j D_j$$

iv. the inertia force of the entrained fluid

$$F_I \sim \frac{1}{2} \rho_o a \cdot \overrightarrow{U_j} - \overrightarrow{U_o} U_o L^2$$

v. the buoyancy force

$$F_b \sim (\rho_o - \rho_j) g L^3$$

where C_D is the drag coefficient and a is the entrainment coefficient. These five forces will yield four force ratios, i.e.

$$\frac{F_D}{F_I}, \frac{F_I}{F_I}, \frac{F_b}{F_I}, \frac{F_I}{F_o} \tag{4}$$

These four force ratios would ensure similar bending geometry of the jets represented by $L/r \cos \theta$ as shown in (3). Thus (4) and (3) are coupled and the combination yields the similarity parameters for the near field.

Similarity parameters for the far field are obtained from the normalization of governing equations illustrating the process of turbulent mixing. Turbulent mixing is described by two parameters: the scale of segregation L_S (which is a measure of the size of the unmixed clumps of one ingredient) and the intensity of segregation (which represents the difference between the ingredients being mixed). When two streams of fluids at different temperatures are mixed, the intensity of segregation is defined as

$$I_S = \frac{\Delta T^2}{\Delta T_o^2} \tag{5}$$

where ΔT - the rms value of the fluctuating temperature

ΔT_0 - the initial rms value of the fluctuating temperature

The scale of segregation L_S is defined as

$$L_S \approx \int_o^\infty g(r)dr$$

where

$$g(r) = \frac{\overline{\Delta T(x)\,\Delta T(x+r)}}{\Delta T^2} , - \text{ the spatial correlation function of the fluctuating temperature}$$

According to Broakey (1967), I_S gives a better description of the degree of mixing than L_S does. In other words, it would be sufficient to use I_S to describe the result of mixing.

In the far field, the turbulence is approximately isotropic because the collision of jets causes not only the destruction of the jets, but also the cancellation of vortices in the wake as well as in the jet. The assumption of isotropy was used in previous works (Lee, et al., 1964; McKelvey, et al., 1975) to predict mixing in pipeline mixers and coflow mixers. The predicted results agree reasonably well with experimental observations. In this work isotropic turbulence will also be assumed for the flow in the far field.

Corsin (1964) found that mixing in isotropic turbulence follows the exponential law, i.e.

$$I_S = e^{-t/t_c} \qquad (6)$$

where t - time

tc - time constant of mixing

The value of t_C can be evaluated from the following equations:

i) for gas $(Pr \leq 1)$

$$t_c = \left(\frac{5}{\pi}\right)^{2/3} \frac{2}{3 - Pr^2} \left(\frac{L_S^2}{\varepsilon}\right)^{1/3}$$

ii) for liquid $(Pr \gg 1)$

$$t_c = \frac{1}{2} \left[3\left(\frac{5}{\pi}\right)^{2/3} \left(\frac{L_S^2}{\varepsilon}\right)^{1/3} + \left(\frac{\nu}{\varepsilon}\right)^{1/2} \ell n \, Pr \right]$$

where Pr - Prandtl number

ε - rate of dissipation

ν - kinematic viscosity.

Normalization of Equation (6) yields the following time ratio:

$$t_R/t_c \qquad (7)$$

where t_R is the residence time of the fluids in the mixer

$$\left(t_R = \frac{length \; of \; mixer}{U_o} \right)$$

b. The similarity parameters for the near field are obtained by grouping the parameters in (3) and (4). After substituting L (characteristic length of the jet) with D_o (the inner diameter of the mixer) and rearranging, we have nine dimensionless parameters. They are: the Strouhal number, the Fronde number, two Reynolds numbers (one for the jet stream and the other for the cross stream), the Grashof number, the momentum ratio $(\rho_j U_j^2/\rho_o U_o^2)$, the diameter ratio D_j/D_o, the entrainment coefficient α, and the drag coefficient C_D.

The above results are more general than those of Moussa, et al. (1977) whose study is confined to non-buoyant flow. Comparison with

the experimental finding of Kamotani, et al. (1972) indicates that the dimensionless parameters recommended by Kamotani, et al. is only a subset of the parameters derived in the present work. In Kamotane's work, attention was confined to the trajectory of the jet and the experimental variables were often confined to limit ranges. Thus the conclusions reached in that experimental work cannot be regarded as general. Nevertheless, the fact that the experimental finding is admissable to the present findings should reinforce confidence in the method used in this research.

The nine similarity parameters mentioned above are for a single jet in cross flow. In a mixer there are a number of jets arranged in rows. In that case there will be neighboring effect between jets and such phenomenon was studied by Holderman, et al. (1977). Holderman, et al. pointed out that the neighboring effect is dependent on the ratio of distance (between injection ports) to diameter (of the ports). Such a ratio is called the pitch-to-diameter ratio S/Dj where S is the distance between injection points.

Adding the pitch-to-diameter ratio and the time ratio to the dimensionless group results in a total of eleven similarity parameters for a jet mixer. Of the eleven parameters, three of them (the Strouhal number, the drag coefficient, and the entrainment coefficient) can probably be omitted because their values remain basically unchanged under most situations; and two of them (the diameter ratio and the pitch-to-diameter ratio) would automatically be satisfied if geometrical similarity is ensured. After dropping these five parameters, the remaining six parameters are: the two Reynolds numbers, the Froude number, the Grashof number, the momentum flux ratio, and the time ratio. These six parameters are the general conditions for dynamic similarity.

IV. RECOMMENDATIONS

a. The six similarity parameters mentioned above are now used to guide the design of the experiment. It was found that no common fluids (air or water) at ambient temperature can satisfy all six similarity parameters. Three of the parameters, namely the Reynolds number (for the cross stream), the Grashof number, and the Froude number, would impose conflicting requirements. To satisfy all the requirements, the fluids used in the mixer must have approximately the same density ratio as that in the prototype (in the prototype mixer, the density ratio can reach as high as 20; instead of: this high density ratio can be achieved by either mixing CO_2 with H_2 or CO_2 with He). This difficulty would not occur if either the Froude number or the Grashof number is unimportant. If this is indeed the case, then both air and water at ambient temperature can be used as the test fluids and the mixing process can be simulated by mixing either liquids (fresh water and salt water) or gases (air and CO_2).

If Froude number is unimportant, then the liquid system is a more suitable test medium. Under this condition the diameter of the pilot mixer can be one-sixth of that of the prototype mixer to guarantee similarity in the near field, while the length of the former should double the length of the latter for similarity in the far field. If the gas system (air and CO_2) is used, the diameter of the pilot mixer would be half of that of the prototype, and the length of the two mixers would be roughly the same. On the other hand, if the Grashof number is unimportant, then the gas system is more advantageous than the liquid system.

The selection of that fluid is thus heavily dependent on the type of similarity criteria being considered in the study.

b. According to the discussion of previous sections, there are at least three problems that require further attention. The first problem

16-13

concerns with determination of similarity criteria. Since common fluids at ambient temperature cannot satisfy all six similarity parameters, the relative importance of these parameters must be weighed to see whether it is possible to drop either the Froude number or the Grasof number form consideration. Answer to this problem can be obtained only by experimental means. For example, in an experiment two setups are to match all but the Froude number. If there is no difference in the mixing result, then the Froude number can probably be excluded from consideration and the liquid system mentioned in previous sections should then be used as the test medium.

The second problem concerns with the correlation relation between heat and mass transfer. If data obtained from mass transfer are used to simulate those from heat transfer, the scale ratio between these two transfers must be known. This scale ratio can probably be derived analytically but an experimental verification of the analytical results would also be desirable.

The third problem concerns the development of a mathematical model to correlate the turbulence characteristics in the far field to the flow in the near field. In other words, it is desirable to be able to predict LS and ε from the injection scheme which includes the momentum ratio and the arrangement of injection ports. Once this is established, a mathematical model for the mixing process can readily be developed and this would greatly facilitate the design process.

c. The geometrical parameters, represented by both the diameter ratio D_j/D_o and pitch-to-diameter ratio S/D_j, will have significant effects on the performance of a mixer, and a proper selection of them is important. For example, large D_j/D_o usually ensures good penetration of the jets and is thus beneficial to the mixing in the near field, but this may also enlarge the scale of segregation which would impair mixing in the far field. A proper balance of these two effects must be considered by the designer. The proper selection of S/D_j is

also very important. If S/Dj is too small, then the jets will feed on
each other, resulting in poor mixing with the cross-stream fluid in the
near field. If S/Dj is too large, then a large portion of the cross
stream will bypass the jets and impair mixing in the far field. Proper
selection of these parameters must be relied on experiment which is
critical to the design of mixers.

REFERENCES

Brodkey, R. S., The Phenomena of Fluid Motions, Addison-Wesley
      Publishing Company, 1967.

Corsin, S., The Isotropic Turbulent Mixer: Part II. Arbitrary
      Schmidt Number, AIchE Journal, Vol. 10, 1964, pp. 870-877.

Holderman, J. D., et al., Mixing of a Row of Jets with a Confined
      Crossflow, AIAA Journal, Vol. 15, 1977, pp. 243-249.

Kamotani, Y., et al., Experiments on a Turbulent Jet in a Cross Flow,
      AIAA Journal, Vol. 10, 1972, pp. 1425-1429.

Kline, S. J., Similitude and Approximation Theory, Springer-Verlag
      Publishing Company, 1986.

Lee, J. and R. S. Brodkey, Turbulent Motion and Mixing in a Pipe, AIchE
      Journal, Vol 10, 1964, pp. 187-193.

Makihata, T. and Y. Mijai, Trajectories of Single and Double Jets
      Injected into a Crossflow of Arbitrary Velocity Distribution,
      Journal of Fluid Engineering, Vol. 101, 1979, pp. 217-223.

McKelvey, K. N., et al., Turbulent Motion, Mixing, and Kinetics in a
Chemical Reactor Configuration, AIchE Journal, Vol. 21, 1975, pp. 1165-
1176.

Moussa, Z. M., et al., The Near Field in Mixing of a Round Jet with a
    Cross-Stream, Journal of Fluid Mechanics, Vol. 80, 1977, pp. 49-
    80.

Patankar, S. V., et al., Prediction of the Three-Dimensional Velocity
    Field of a Deflected Turbulent Jet, Journal of Fluid Engineering,
    December 1977, pp. 758-762.

Shope, F. L., Private communication, 1989.

1989 USAF-UES SUMMER FACULTY RESEARCH PROGRAM

GRADUATE STUDENT RESEARCH PROGRAM

Sponsored by the

AIR FORCE OFFICE OF SCIENTIFIC RESEARCH

Conducted by the

Universal Energy Systems, Inc.

FINAL REPORT

Prepared by: Chun Fu Su, Ph.D.

Academic Rank: Assistant Professor

Department and   Physics Department

University: Mississippi State University

Research Location: AEDC
                    Tullahoma TN   37389

USAF Researcher: W.D. Williams

Date: 16 August 89

Contract Number: F49620-88-C-0053

<u>Laser-Induced Fluorescence (LIF) of</u>

<u>Nitric Oxide (NO)</u>

by

Chun Fu Su

<u>ABSTRACT</u>

Some lifetimes of various electronic states of the NO molecule were collected. A digital computer program (DNOLIF.FOR) was established to calculate and plot the LIF spectrum by a single-photon process. Several options of the code are explained. An LIF spectrum of the vibrational transitions of NO was recorded in the wavelength region between 200 nm and 340nm.

Acknowledgements

I. INTRODUCTION

The NO molecule is a stable diatomic molecular radical. The molecule is a key molecule in the chemistry of the upper atmosphere and an important but dangerous pollutant. It has also been detected in an interstellar molecular cloud. Moreover, this molecule is important to combustion chemistry and turbulent flows. Accurate measurements of temperature and species concentration provide the fundamental diagnostic input to characterize combustion system and turbulent flows. It is obvious that this molecule can provide many interesting insights to various fundamental processes.

The electron beam fluorescence technique (EBF) (1-3) and laser-based techniques, such as Raman scattering (CARS), have been used to detect the rarefied gas flows at the AEDC (4-6). Both could measure the densities of N_2 and CO_2 over the range of 10^{12} to $10^{16} cm^{-3}$. Recently, laser-induced fluorescence (LIF) techniques have been developed to probe the density down to 10^{12}cm-3. The LIF techniques may be the most useful for the AEDC needs.

For most monatomic or diatomic gas species present in the flow fields, the required excitation wavelengths are in the ultraviolet (UV) region, and the resulting fluorescence is also in the same region but on the high wavelength side. These species can be excited by single photon or multiphoton processes. Two photon laser-induced fluorescence technique has been developed at the AEDC and used to observe flow field satisfactorily (7). In order to obtain more information about the technical advantages of this diagnostic process, it is worthwhile to develop single photon LIF techniques.

II. OBJECTIVES OF THE RESEARCH EFFORT

The main work of this project is to collect the important spectroscopic parameters of NO and to establish a mathematical model to predict the LIF rotational spectrum. The experimental spectrum is also needed to provide data for comparison with the analytical model.

III. Analytical Model

A. The electronic structure, vibrational, and rotational states of this molecule have been well studied. It is not difficult to find the needed molecular parameters in the literature. No previous experimental data will be presented here; however, some lifetimes of various electronic states for this molecule (8) are shown in Table I. This information may be important for future AEDC studies.

B. In order to establish a mathematical model, the equations for the rotational energy levels and the transition probabilities were needed. Only two electronic states were considered in this project: the $^2\Sigma$ state and the $^2\Pi$ state. The $^2\Sigma$ state belongs to Hund's case(b), and the $^2\Pi$ state belongs to either case(a), or case (b), or to cases intermediate between (a) and (b). For a vibrational state of the $^2\Pi$ state, there are two sublevels, F_1 ($J = k+\frac{1}{2}$) and F_2 ($J = k-\frac{1}{2}$). K is the pure rotational quantum number and J is the coupled quantum number. The $^2\Sigma$ state is similar. The calculation process for the rotational energy levels used in the McKenzie and Gross' digital computer program (9) was used here.

The transition probabilities in two and three photon spectra are different from those of one photon sspectrum. Several groups

(10-12) have derived the formulas for the former. For the latter, the transition probability formulas were expressed explicitly in the coupled quantum number published by Earls (13) from those obtained by Hill and Van Vleck (14). Dieke and Crosswhite (15) used those formulas for OH. There are 12 branches: six are main branches and the other six are satellite branches. The transition probability formulas are:

$$\begin{matrix} R_2 \\ S_{21} \end{matrix} \quad \frac{2J+1}{2J+2} \quad ((2J+1) \pm U((2J+1)^2 - 2a))$$

$$\begin{matrix} R_1 \\ Q_{12} \end{matrix} \quad \frac{2J+1}{2J+2} \quad ((2J+1) \pm U((2J+1)^2 + 2(a-4)))$$

$$\begin{matrix} Q_2 \\ R_{21} \end{matrix} \quad \frac{2J+1}{2J+2} \quad \left(\frac{(2J+1)^2 - 2 \pm U((2J+1)^3 - 8J - 2a)}{J} \right)$$

$$\begin{matrix} Q_1 \\ P_{12} \end{matrix} \quad \frac{2J+1}{2J+2} \quad \left(\frac{(2J+1)^2 - 2 \pm U((2J+1)^3 - 8J + 2(a-4))}{J} \right)$$

$$\begin{matrix} P_1 \\ O_{12} \end{matrix} \quad \frac{2J+1}{2J} \quad ((2J+1) \pm U((2J+1)^2 - 2a))$$

$$\begin{matrix} P_2 \\ Q_{21} \end{matrix} \quad \frac{2J+1}{2J} \quad ((2J+1) \pm U((2J+1)^2 + 2(a-4)))$$

branches, the upper symbols R_2, R_1, etc., while the - sign
    is for the satellite branches, the lower symbols S_{21}, Q_{12},
    etc.; a is a coupling constant.

Some of the major steps in this calculation are summarized
    below:

1. The upper electronic state here is either the $^2\Sigma$ state or the
   $^2\Pi$ state, while the lower one is the $^2\Pi$ state. The rotational
   energy levels were calculated in wave number (cm^{-1}) then

converted to wavelength (nm).

2. The definition of the selection rules used in Ref. 15 and their transition probability equation defined above were used in the calculation. The partition function $(2K+1)\exp\left(-\dfrac{BK(K+1)}{kT}\right)$ of the upper rotational energy level was multiplied by the transition probability to determine the transition intensity factor. Here B,K,k, and T are the rotational constant (cm^{-1}), rotational quantum number, Boltzmann constant (cm/K), and temperature (K), respectively.

3. The computed wavelength with transition intensity factors were sorted in descending order of wavelength. The intensity factor of a transition that is separated from the previous one by less than 0.0015 nm will be added to the previous transition. After this process a stick type rotational spectrum can be plotted.

4. The Gaussian line shape was used for the convolved spectrum. At a particular wavelength w, the intensity contribution due to a certain line of wavelength w_i is

$$I_i(w) = P_i\, e^{-\ln 2 \left(\frac{w-w_i}{W}\right)^2},$$

where P_i is the transition intensity factory of this line and W is its half width at the half maximum point. The total contribution is

$$I(w) = \sum_i P_i\, e^{-\ln 2 \left(\frac{w-w_i}{W}\right)^2},$$

where the units of w, w_i and W are in cm^{-1}. After this process, the convolvedspectrum can be plotted.

Several options may be selected for calculation of convolved spectra. In particular,

1. delta: separation of two adjacent delta points; a small value (0.5 cm^{-1} or less) will be required for a smooth curve.

2. hwhm: half width half maximum (cm^{-1}) can be adjusted to match the observed spectrum.

3. itest: 0 for stick spectrum and 1 for convolved spectrum.

4. tem: temperature (K).

5. fh and fl: used to select a particular wavelength (nm) region.

6. jq: rotational quantum number (may be changed to a particular number).

7. au: represents coupling constant; it affects the spectral intensities.

It is necessary to point out the relations between two different notations.

Dieke and Crosswhite's

symbols used here	Example	Other Authors(16)
Q_{12}	7 7½ ---- 7 6½	$^{Q}R_{12}$
O_{12}	6 6½ ---- 8 7½	$^{O}P_{12}$
Q_{21}	7 6½ ---- 7 7½	$^{Q}P_{21}$
R_{21}	7 6½ ---- 6 6½	$^{R}Q_{21}$
S_{21}	7 6½ ---- 5 5½	$^{S}R_{21}$
P_{12}	6 6½ ---- 7 6½	$^{P}Q_{12}$

In order to be sure of the reliability of the program, two checks were made. The predicted wavelengths from the code (DNOLIP.FOR) agreed with those from McKenzie and Gross' program. The convolved spectrum agreed fairly well with the observed one (16).

IV. EXPERIMENTAL WORK

The fluorescence spectrum of vibrational transitions and excitation fluorescence spectrum of rotational transitions were, respectively, run by an Excimer Laser EMG 150. The laser wavelength was fixed at 193 nm and the grating of 2365 lines/mm was slowly rotated in the wavelength region between 200 nm and 340 nm to record a fluorescence spectrum of vibrational transitions. The observed spectra for two pressures of NO are shown in Figures 1 and 2. It is apparent that pressure does affect the spectral shape. Therefore, molecular density, which is directly related to pressure, can be adequately estimated by the spectral shape. The wavelength shown on the horizontal axis was calibrated by a mercury lamp. Calculated spectra shown in Table II indicated that the observed spectrum contains at least two sets of vibrational transitions, one is $A^2\Sigma - X^2\Pi$ and the other is $D^2\Sigma - X^2\Pi$. The fluorescence occurred after the excitation of v' = 6 of the $B^2\Pi$ state, which has an energy difference of 194 nm with respect to the ground vibrational state of the $X^2\Pi$. An excitation fluorescence spectrum of the rotational transitions is shown in Figure 3. The observed spectrum agrees with the fact that not many observable transitions were expected in the wavelength range of 193 nm and 194 nm. No further analysis will be made due to a lack of observed information.

V. RECOMMENDATION

The program length of ten weeks was not long enough to collect a sufficient amount of data to make positive recommendations. However, according to the observed spectra and theories, positive statements can still be made for this project. The single photon LIF technique can be used to observe the spectra of various pressures. Consequently, molecular densities can be determined from LIF spectra. If one can provide the observed spectra of different temperatures, then one can estimate the temperatures. It is worthwhile to develop a new method for the diagnostic process of the ground test facilities.

Table I. Measured Lifetimes of Nitric Oxide.

Electronic State	Vibrational State	Lifetime (nsec)
$A^2\Sigma$	v=0	187
	v=1	187
	v=2	177
	v=3	165
$D^2\Sigma$	v=0	16.1
	v=1	15.0
	v=2	11.9
	v=3	10.4
$C^2\Pi$	v=0	2.7

Table II. Calculated Vibrational Transition Wavelengths

Transition		Wavelength(nm)
$D^2\Sigma$	$-X^2\Pi$	
v'	v''	
0	2	202.2
0	3	210.0
0	4	218.0
0	5	226.9
0	6	236.2
0	7	246.1
0	8	256.7
0	9	268.1
$A^2\Sigma$	$-X^2\Pi$	
0	0	226.9
0	1	236.9
0	2	247.8
0	3	259.5
0	4	272.1
0	5	285.8
0	6	300.8
0	7	317.0
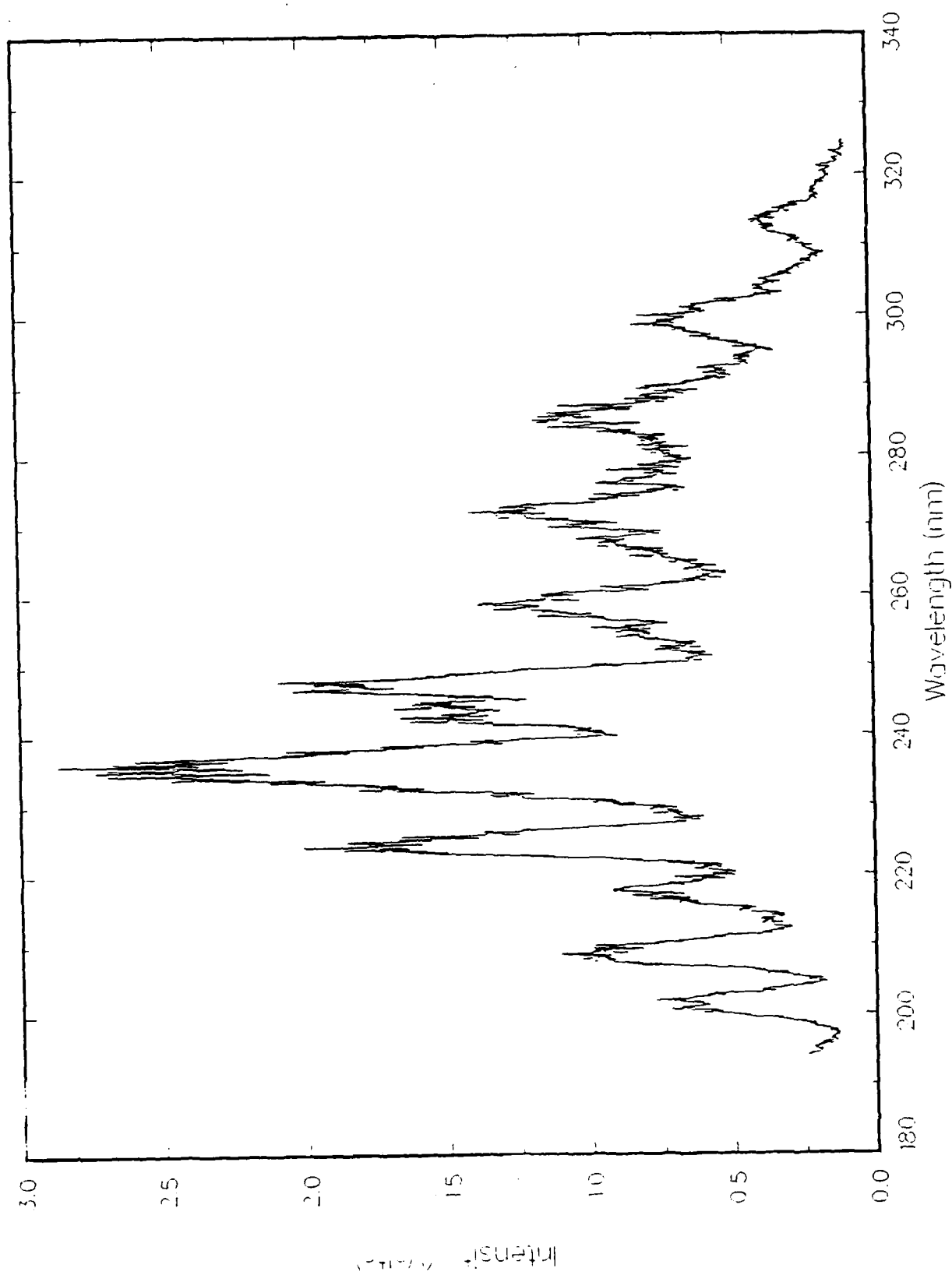
Figure I.   IIO Fluorescence Spectrum, P = 100 Torr, Laser Energy = 70 mJ.
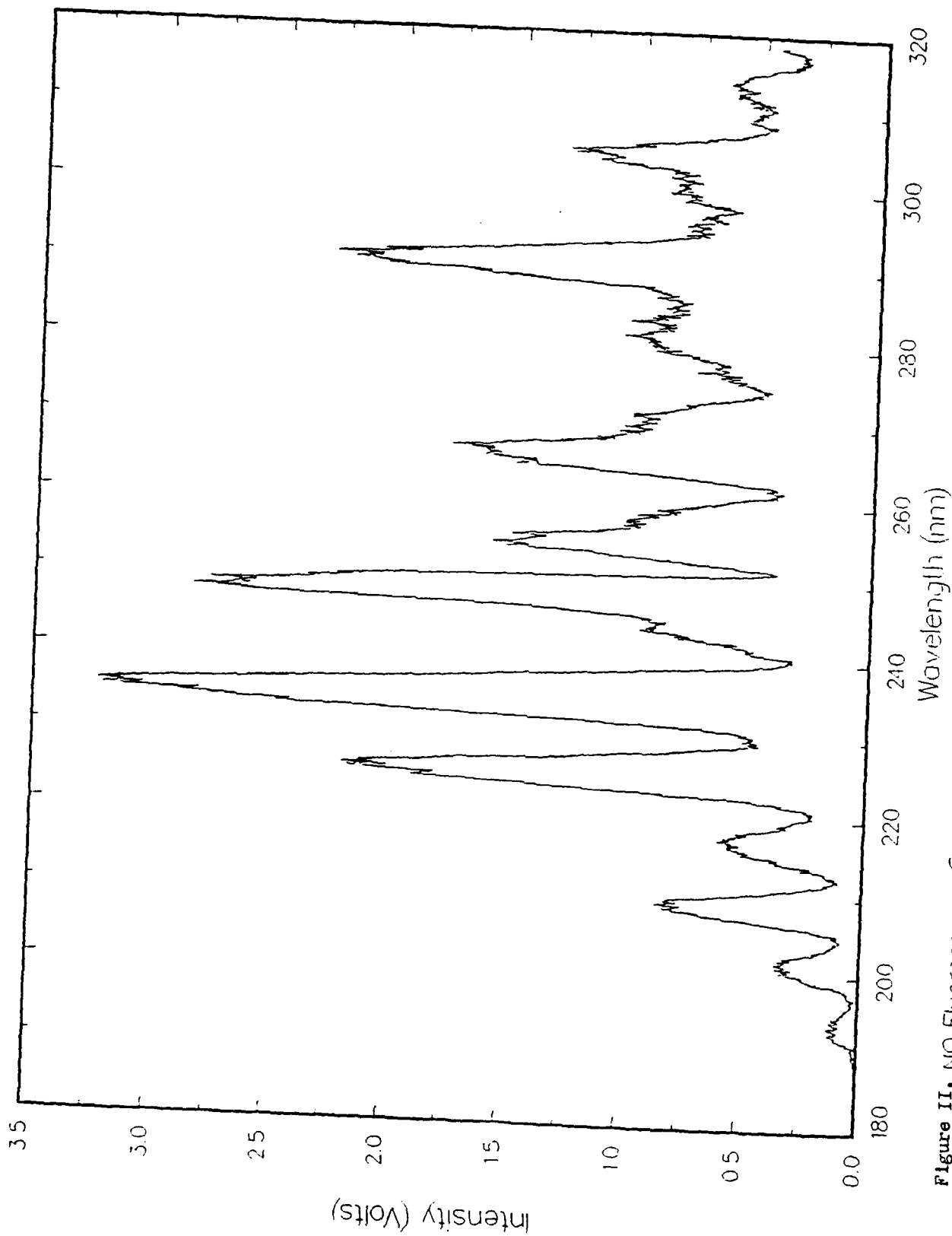
Figure II. NO Fluorescence Spectrum, P = 10 Torr, Laser Energy = 75 mJ, PMT HV = 1700 V.
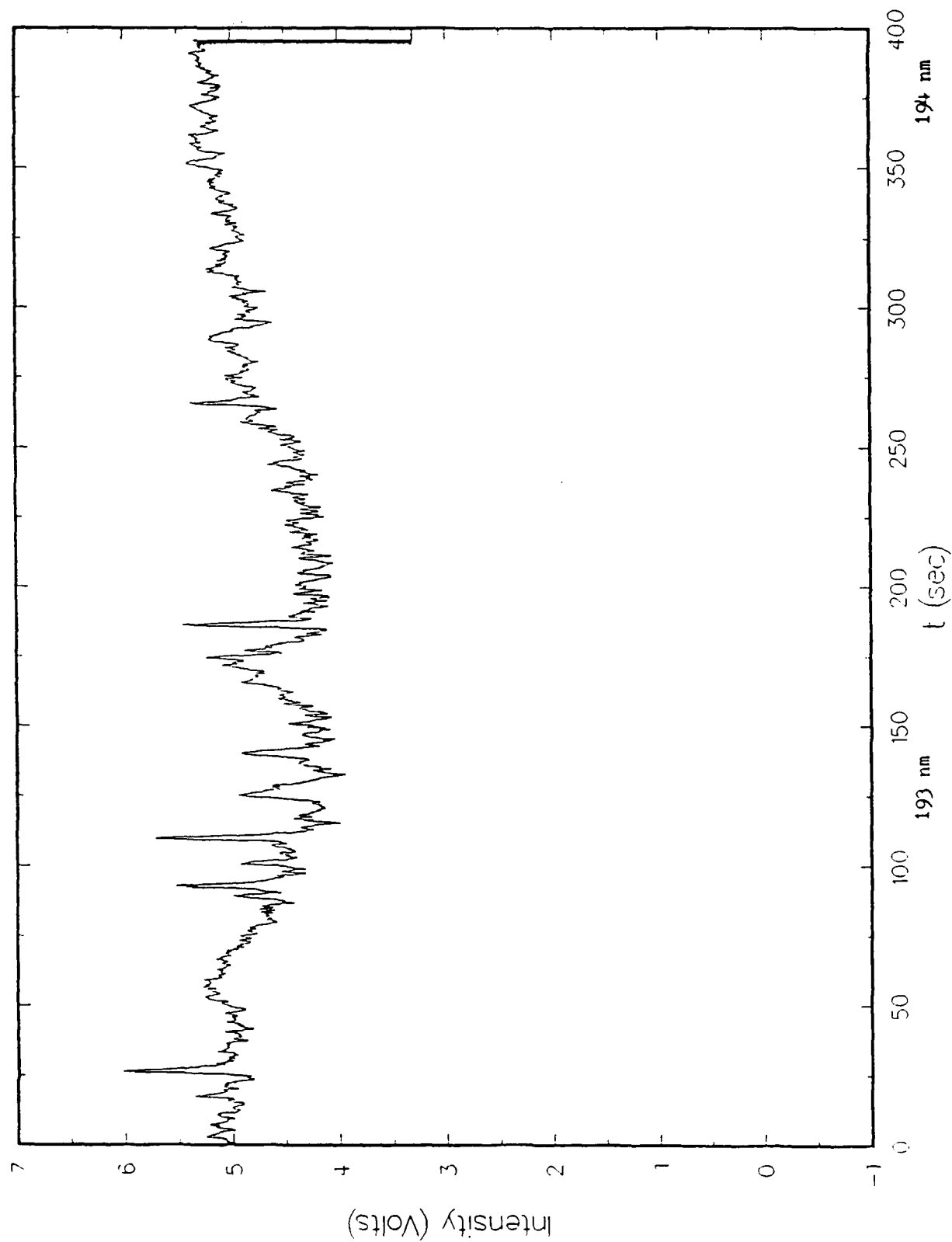
Figure III. NO Excitation Spectrum.

REFERENCES

1. Williams, W.D., et al. "Electron Beam Probe for a Low Density Hypersonic Wide Tunnel." AEDC-TR-76-61 (AD-727004), July 1971.

2. Powell H.H. et al. "Bipropellant Engine Plume Contamination Problem. Vo 1. II, Chamber Measurements-Phase 2." AEDC-TR-79-28 (AD-A078412), November 1979.

3. Bailey, A.B. et at. "Measurements of Flow Field Properties in the Forward and Backflow Region of a Nozzle Plume." JANNAF 14th Plume Technology Meeting, November 1983.

4. Williams, W.D. et al. "Laser-Raman Flow Filled Diagnostics of Two Large Hypersonic Test Facilities." AEDC-TR-79-88 (AD-A078289), December 1979.

5. Williams, W.D. et al. "Laser-Raman Measurements in a Ducted, Two-Stream, Subsonic H_2/Air Combustion Flow." AEDC-TR-79-74 (AD-A078112), December 1979.

6. Williams, W.D. et al. "Raman Scattering Diagnostic Development Using an Excimer/Dual Dye Laser System, I." AEDC-TR-83-15 (AD-B075604), July 1983.

7. Price, L.L. et al. "Development of Two-Photon Laser-Induced Fluorescence Diagnostics and an Application to a Pulsed Flow." AEDC-TR-85-60, December, 1985.

8. Smith, A,J. et al. "Measured Lifetimes of the $A^2\Sigma^+, D^2\Sigma^+$ and $C^2\Pi$ States of NO." Phys B: Atom, Molec. Phys. 1978 Vol II, No 18, PP 3263-3272.

9. This program used in Ref. 7 to calculate and plot the fluorescence spectrum of NO by two photon process.

10. Chen, K.M. and Yeung, E.S. "Rovibronic Two-Photon Transition of Symmetric Top Molecules." J. Chem. Phys. $\underline{69}$, 43 (1978).

11. Brag, R.G. and Hochstrasser, R.M. "Two-Photon Absorption by Rotating Diatomic Molecules." Mole. Phys. $\underline{31}$, 412 (1976).

12. Halpern, L.B. et al. "Rotational Line Strengths in Two-and Three-Photon Transitions in Diatomic Molecules." J. Mol. Spectrosc. $\underline{79}$, 1 (1980).

13. Earls, L.T. "Intensities in $^2\Pi$ -$^2\Sigma$ Transitions in Diatomic Molecules." Phys. Rev. $\underline{48}$, 423 (1935).

14. Hill, E. and Van Vlech, J.H. "On the Quantum Mechanics of the Rotation Distortion of Multiplets in Molecular Spectra." Phys. Rev. $\underline{32}$, 250 (1928).

15. Dieke, G.H. and Crosswhite, H.M. "The Ultraviolet Bands of OH Fundamental Data." J. Quant. Spectrosc. Radiation Transfer. $\underline{2}$, 97 (1962).

16. Scheingraber, H. and Vidal, C.R. "Fluorescence Spectroscopy and Franck-Condon-Factor Measurements of Low-Lying NO Rydberg States." J. (Opt. Soc. Am. B $\underline{2}$, 343 (1985).

1989 USAF-UES SUMMER FACULTY RESEARCH PROGRAM/

GRADUATE STUDENT RESEARCH PROGRAM

Sponsored by the

AIR FORCE OFFICE OF SCIENTIFIC RESEARCH

Conducted by the

Universal Energy Systems, Inc.

<u>FINAL</u> <u>REPORT</u>

<u>SPECTROSCOPIC</u> <u>MONITORING</u> <u>OF</u> <u>EXHAUST</u> <u>GASES</u>

Prepared by: R. H. Tipping

Academic Rank: Professor

Department and   Physics

  University: University of Alabama

Research Location: Arnold Engineering and Development Center
                    Arnold Air Force Base
                    Tullahoma, TN 37389

USAF Researcher: William Phillips

Date: 20 September, 1989

Contract No: F49620-88-C-0053

Spectroscopic Monitoring of Exhaust Gases

by

R. H. Tipping

ABSTRACT

Anaylses of existing laboratory spectroscopic data for two molecules, CO and O_2, which are important constituents in both engine and rocket exhausts, have been made in order to compile a database that can be used with existing computer codes to infer temperature and concentration profiles from spectroscopic monitoring of exhaust gases. In addition, a software program was developed that will enable one to ascertain optimal spectral regions for future monitoring of other important molecules, e.g. CO_2 or H_2O.

Acknowledgments

I wish to thank my summer colleagues, Bill Phillips and Chad Limbaugh, for many useful discussions throughout the summer. I would also like to acknowledge Carlos Tirres and the Universal Energy Systems for their efficient management of the summer program, and the Air Force Office of Scientific Research and the Arnold Air Force Base for their sponsorship of this enriching project.

I. INTRODUCTION

The measurement of the physical characteristics of exhaust gases from conventional jet engines and rockets is important both from the testing and the developmental standpoints. These characteristics include the concentration and temperature profiles for the more important combustion products. One of the most useful methods for the determination of these data is through spectroscopic monitoring. However, in order to obtain quantitative results, laboratory spectroscopic data must first be obtained and analyzed in order to compile a necessary database.

While existing compilations such as the HITRAN database (Rothman et al., 1986) are available, they are designed primarily for atmospheric applications and are valid only for temperatures around 300 K. Because many spectroscopic transitions that are important at the higher ambient temperatures found in exhaust gases (typically 1000 K or higher) arise from "hot bands", they are not included in these compilations. Thus, for quantitative applications to hot gases, these databases must be expanded to include a very large number of additional transitions originating from thermally excited levels.

II. OBJECTIVES OF THE RESEARCH EFFORT:

The objectives of the research effort were the following. First, to analyse existing spectroscopic data for two diatomic molecules, CO and O_2, important in rocket and engine exhausts, and to compile a database that could be used with existing computer codes in order to infer needed engineering data, e.g. concentration and temperature profiles. Results for other relevant diatomic molecules, e.g. NO, OH, etc., could be obtained using similar methods.

The second objective was to study the 0.9 micron region of water vapor. In particular, to investigate the strengths of the spectral lines in this region to determine optimal wavelength windows for monitoring this species. However, because of the complexity of the spectrum and the absence of high temperature laboratory data, a compilation similar to that for CO or O_2 is not possible at present. Nevertheless, using existing data, a software program was developed in order to display the evolution of the measured (low temperature) spectral lines with temperature. This is a necessary first step in order to select spectral regions for future monitoring. If a high temperature compilation of H_2O lines becomes available, more accurate predictions and calculations can be made.

III.

Carbon monoxide (CO) is a common combustion product that has strong infrared (vibration-rotational) transitions which can be used spectroscopically to monitor exhaust gases. The database for these transitions was compiled in the following way. First the laboratory frequency and intensity data was analyzed in order to determine the standard Dunham energy-level coefficients and dipole-moment coefficients, respectively. The former were used as input in order to generate a potential energy that could be used in a program to solve the Schrodinger equation (Chackerian and Tipping, 1983). This allows one to calculate the frequencies of the desired transitions even though many of those originating from higher energy levels have not been measured spectroscopically. It also allows one to calculate the strengths of the lines using the experimentally determined dipole-moment function. These results were then incorporated with other relevant data (for instance, initial-state energy, half width, temperature dependence of the half width, etc.) and arranged in the HITRAN format.

The explicit vibration-rotational transitions included were the following: $v = 0$ to 10, where $\Delta v = 0$ to 4, and $J = 0$ to 150, where v and J are the vibrational and rotational quantum numbers, respectively. In total, some 13,500 transitions are included in the compilation and these should be sufficient to characterize the spectrum of CO up to a

temperature of several thousand degrees. Because of their potential use to other reseachers, e.g. astronomers, this data is being incorporated with similar data from other molecules in a "hot gas tape" (Selby, 1989). Also, results of the calculation were made available on 4 floppy disks.

The Schumann-Runge electronic bands of O_2 (B(v') $^3\Sigma_u$ <-- X(v) $^3\Sigma_g$), whose wavelengths lie in the visible spectral region between 195 and 225 nm, are not only useful for monitoring exhaust gases, but they are also important in the absorption of sunlight in the Earth's atmosphere (Yoshino et al., 1983). Because of this latter application, a compilation of strengths and frequencies was available from the Air Force Geophysics Laboratory (AFGL). However, on close inspection of the existing compilation, discrepancies in initial-state energy levels and line strengths were apparent for some of the transitions, and it was decided to generate a new compilation using the results available in the scientific literature.

The existence of two unpaired electons in O_2 ("triplet state") leads to more complicated expressions for allowed energies than in the more typical $^1\Sigma$ ("singlet state") molecules. Because of spin-spin and spin-rotation interactions, the energie are split into three distinct components whose term values are denoted by F_1, F_2, and F_3

Herzberg, 1950). The $F_2(J)$ term values (corresponding to $J = N$, where J is the total and N is the rotational angular momentum quantum numbers, respectively) can be written as

$$F_2(J) = T + B_V x - D_V x^2 + 2\lambda_V/3 - \gamma_V + 2\lambda_D x/3 - \gamma_D x \qquad (1)$$

where $x = J(J + 1)$, T_V is the electronic energy, B_V and D_V are the usual rotational and centrifugal stretching parameters for the vibrational level v, λ_V and λ_D the corresponding spin-spin parameters, and γ_V and γ_D the corresponding spin-rotation parameters. The values of $F_1(J)$ and $F_3(J)$, for which $J = N + 1$ and $N - 1$, respectively, must be obtained by diagonalizing the 2x2 matrix (Cheung et al., 1986):

$$\begin{vmatrix} T_V + B_V(x + 2) - D_V(x^2 + 8x + 4) & -2x^{1/2}[B_V - 2D_V(x + 1) \\ \quad -4\lambda_V/3 - 2\gamma_V - 4\lambda_D(x + 2)/3 & \quad - \gamma_V/2 - 2\lambda_D/3 \\ \quad - 4\gamma_D(x + 1) & \quad - \gamma_D(x + 4)/2] \\ \\ -2x^{1/2}[B_V - 2D_V(x + 1) - \gamma_V/2 & T_V + B_V x - D_V(x^2 + 4x) \\ \quad -2\lambda_D/3 - \gamma_D(x + 4)/2] & \quad + 2\lambda_V/3 - \gamma_V \\ & \quad + 2\lambda_D x/3 - 3\gamma_D x \end{vmatrix}$$

The values of the molecular parameters for the ground electronic state (Johns and Lepard, 1975) include $T_0 = -1.3315925$ cm^{-1} such that $F_2(0) \equiv 0$; this convention is also followed in the definition of T_V, for the B(v') state. Results obtained for v = 0 in the ground electronic state gave better agreement with experimental measurements than

previous calculations (Veseth and Lofthus, 1974); similar results obtain for other vibrational levels and for the excited electronic vibrational levels. Once the energy levels are known, the frequencies for the six strongest branches ($\Delta J = \Delta N = \pm 1$, $R_i(N)$ and $P_i(N)$ where $i = 1, 2, 3$) or the six much weaker satellite branches ($\Delta J \neq \Delta N$) can easily be calculated. The results in the form of a line atlas were made available on a floppy disk.

The strength of spectroscopic transitions can be given in a number of equivalent ways (Smith, 1985). For the Schumann-Runge transitions, most workers report the dimensionless band oscillator strengths defined by

$$f(v',v'') = \frac{mc^2}{\pi e^2 \, N(v'')} \int \sigma(\nu) \, d\nu \qquad (2)$$

where the factor $mc^2/\pi e^2 = 1.13 \times 10^{12}$ cm^{-1}, $N(v'')$ is the fractional Boltzmann population in the initial level v'', and the integral of the cross-section $\sigma(\nu)$ is carried out over all rotational lines having frequencies ν (in cm^{-1}) that contribute to the band. Individual oscillator strengths can be calculated from the band oscillator strengths using appropriate Boltzmann factors and Honl-London factors (Herzberg, 1950). Other information such as half widths could be added to this database, as in the case of CO, but this was not done because of lack of time.

18-9

In addition to the work described above on CO and O_2, some initial progress was made on the problem of selecting optimal spectral regions in the 0.9 micron water vapor bands. Because of the complexity of this spectral region and the absence of sufficiently accurate laboratory spectra of hot H_2O, no database comparable to that for diatomic molecules exists. Some transitions that are strong at room temperature have been analyzed and catalogued (Rothman et al., 1986); their strength at a higher temperature can easily be calculated. We have written a computer program which does this calculation and displays the results as a function of temperature. From such plots, one can easily see within a given spectral region which transitions increase in strength as the temperature increases, and which decrease noticeably. Thus, by investigating various spectral regions, one can identify optimal regions which contain transitions of both types. These regions are suitable for spectroscopic monitoring because from the intensities of the transitions, one can determine the ambient temperature. It must be emphasized, however, that the output of such plots is only as good as the input; as mentioned previously, the currently existing input database is woefully incomplete because of the absence of most hot transitions whose strengths at room temperature are low, but whose strengths will increase dramatically as the temperature increases. This is especially true in the higher frequency spectral regimes (e.g. the visible).

IV. RECOMMENDATIONS

a.   The database for CO is a vast improvement over previous compilations; this should allow one to calculate accurately CO absorption or emission at temperatures up to several thousand degrees.   This database should supplant those in current use.

b. The database for the Schumann-Runge bands of O_2 should be completed by the addition of experimentally measured half widths and the results verified against other compilations (viz. that of AFGL when the discrepancies noted above have been resolved), and against laboratory data.   Much of this latter validation has already been performed (Phillips, 1989).

c. The database for water vapor should be extended to incorporate many more hot bands.   This task is, however, a major effort, and will require a large amount of both experimental and theoretical work.

d. Work similar to that accomplished for CO should be undertaken for other diatomic species of interest; for instance, boron containing compounds such as BO or BH, or other less exotic species such as NH, OH or NO.   This work can be completed within a reasonable time using existing experimental data and ab initio calculations.

REFERENCES

Chackerian, C. and R. H. Tipping, "Vibration-Rotational and Rotational Intensities for CO Isotopes," _J. Mol. Spectrosc._, 1983, Vol. 99, pp. 431-449.

Cheung, A.S.C., K. Yoshino, W. H. Parkinson, and D. E. Freeman, "Molecular Spectroscopic Constants of $O_2(B^3\Sigma_u)$: The Upper State of the Schumann-Runge Bands," _J. Mol. Spectrosc._, 1986, Vol. 119, pp. 1-10.

Herzberg, G., _Spectra of Diatomic Molecules_, Princeton, New Jersey, Van Nostrand, 1950.

Johns, J.W.C. and D.W. Lepard, "Calculation of Rotation-Electronic Energies and Relative Transition Intensities in Diatomic Molecules", _J. Mol. Spectrosc._, 1975, Vol. 55, pp. 374-406.

Phillips, W. 1989, (private communication).

Rothman, L.S. et al., "The HITRAN Database: 1986 Edition," _Appl. Opt._, 1986, Vol. 26, pp. 4058-4097.

Selby, J. 1989, (private communication).

Smith, M.A.H., et al., "Intensities and Collision Broadening Parameters from Infrared Spectra", in _Molecular Spectroscopy: Modern Research_, ed. K. Narahari Rao, Orlando, Florida, Academic Press, 1985.

Veseth, L. and A. Lofthus, "Fine Structure and Centrifugal Distortion in the Electronic and Microwave Spectra of O_2 and SO," Mol. Phys., 1974, Vol. 27, pp. 511-519.

Yoshino, K., et al., "High Resolution Absorption Cross Section Measurements and Band Oscillator Strengths of the (1,0)-(12,0) Schumann-Runge Bands of O_2," Planet. Space Sci., 1983, Vol. 31, pp. 339-353.

1989 USAF-UES SUMMER FACULTY RESEARCH PROGRAM

GRADUATE STUDENT RESEARCH PROGRAM

Sponsored by the

AIR FORCE OFFICE OF SCIENTIFIC RESEARCH

Conducted by the

Universal Energy Systems, Inc.

<u>FINAL REPORT</u>

<u>DISTRIBUTED AND PARALLEL IMAGE AND SIGNAL PROCESSING</u>

Prepared by: D. Mitchell Wilkes, Ph.D.
                      Ben A. Abbott
                      Lester E. Lynd, Jr.
                      Richard S. Souder

Academic Rank: Professor and Graduate Students

Department and   Electrical Engineering Department

   University: Vanderbilt University

Research Location: AEDC
                      Arnold AFB, TN   37389

USAF Researcher: Capt. Ted Bapty

Date: 16 Aug 89

Contract No: F49620-88-C-0053

DISTRIBUTED AND PARALLEL IMAGE AND SIGNAL PROCESSING

by

D. Mitchell Wilkes, Phd.

Ben A. Abbott

Lester E. Lynd, Jr.

Richard S. Souder

ABSTRACT

Automatic programming is used to develop parallel and real-time processing structures under the Multigraph Programming and Execution Environment (MPEE). The MPEE is a high level software development environment that uses AI techniques and graphic editors to model the signal flow within a signal processing system. This work forms the basis of this final report, and is already showing the feasibility of such tools to ease the generation of large-scale signal processing and image processing systems.

Acknowledgements

We wish to thank the Air Force Systems Command and the Air Force Office of Scientific Research for sponsorship of this research. Universal Energy Systems must also be commended for their concern and help to us in all administrative and directional aspects of this program.

Our experience was rewarding and enriching because of many different influences. Capt Ted Bapty provided us with support, encouragement, and a truly enjoyable working atmosphere. The help of Jim Nichols, Mike Stokes, and Tom Tibbals was invaluable in overcoming many technical roadblocks.

Finally, we would like to thank Carlos Tirres for all his help in insuring that our experiences at AEDC would be memorable.

I. INTRODUCTION:

Current technology for implementing signal processing systems able to operate in fluctuating environments merely allows adaptive systems to adjust parameters within a fixed processing structure. In the Vanderbilt University Department of Electrical Engineering, a programming and execution environment has been developed which enables the adaptive system to change its own processing structure while it is running. Signal processing systems able to modify their own processing structure during run-time are known as structurally adaptive signal processing systems. The system used to build and implement these processing structures is the Multigraph Programming and Execution Environment (MPEE). The MPEE is a high level software environment that uses AI techniques and graphic editors to model and implement the signal flow within a signal processing system.

Although structurally adaptive systems can be designed and implemented by using existing programming languages, the MPEE handles the tedious task of determining which processing tasks must be performed and in what order. This task is crucial for systems in which the processing

structure is allowed to change dynamically. The MPEE creates an execution environment that resembles the signal flow graph of the processing system. This feature allows the execution environment to determine the proper scheduling of the processing tasks during system reconfiguration. This ability would be quite difficult to implement using existing programming languages, and the programmer would have to generate a new dynamic scheduling system for each new application program.

The MPEE graphic editor eases the transition from small signal processing algorithms to large-scale systems. The programming environment of the MPEE allows the user to create iconic (ICON) pictures of the signal processing task. These processing tasks may then be connected together so that the user can graphically observe the signal flow of the processing system being created.

II. OBJECTIVES OF THE RESEARCH EFFORT:

The goals of the Vanderbilt research group were threefold. First, the Kyoto Common Lisp (KCL),

Multigraph (MGK), and Hierarchal Design Language (HDL)

were ported over to the 386 based INTERACTIVE (c) UNIX

(c). This goal allowed the systems generated by HDL to

be distributed to the onboard transputers where

benchmarks on system performance could be performed.

Second, a large-scale image processing system was

designed to demonstrate the feasibility of performing

image processing under the MPEE, as well as to

demonstrate the feasibility of using transputers for

image processing. Also, a method for remotely calling

DOS-based PC image processing resources from a central

workstation was developed. The third, and final goal,

was to simulate a small Computer Aided Dynamic Data

Monitoring and Acquisition System (CADDMAS) in software

on a distributed PC/transputer computing system.

During the 1989 SFRP these three goals were

accomplished and benchmark tests provided the necessary

results to assess the feasibility of using transputers

with the MPEE.

III. INSTALLATION OF MGK, HDL, AND KCL ON THE 386 PC:

a. Before the summer began, the objective to place the MPEE on Arnold equipment proved to be a sizeable problem. One fifth of the man hours for the summer term were used to accomplish this goal. The main difficulty arose as a result of the immature nature of the INTERACTIVE (c) UNIX (c). Since such a large portion of the summer period was spent on this problem the specific details are covered by the following section.

During the SRP 1988 the MGK was ported to a single T414. Subsequently, under a mini-grant, the Lisp version of the MGK was ported to the 386 under Microport (c) UNIX (c) and set up to communicate with the Transputers.

b. Problems running under INTERACTIVE (c) began during installation. It seems there is a bug in the INTERACTIVE (c) installation program that does not take care of known bad sectors of the hard disk during its format operation. After many crashes and reinstallations, a method of installing contrary to the instructions proved to work correctly. That is, format the disk using DOS (c) utilities and tell the UNIX (c) installation to merely look at the disk but not to write to it during disk format and check. After this modification to the installation

procedure, the UNIX (c) quit crashing (it had been crashing about once a week).

Compiling KCL (c) required the system parameter ULIMIT to be set to the maximum, 12088. The Transputer device driver installation was different from Microport (c) but correctly documented.

The documentation on the SELECT mechanism for reading the keyboard was weak and forced us to use that of the Silicon Graphics machine to get it to work.

Innumerable system parameters were modified to allow processes large enough to run KCL and MGK under X11. As well, these big programs would crash in strange ways when the Everex only had four megabytes of RAM. These problems went away after three more megabytes were added. However, a new problem suspected of being a bus speed incompatibility arose (but far less often). Faslink did not work and was modified to be static (this will be changed to use faslink for future systems).

The GNU-C compiler was ported during this effort due to the inefficient code produced by INTERACTIVE (c) CC. NFS had many bugs (or a few verified and several more suspected). It was finally removed since it was not required.

Finally, with just two weeks left in the program, everything was taped together and the system was ⌐le. The most interesting thing learned from this portion of the work is that System V UNIX (c) is not always portable.

IV. IMAGE PROCESSING UNDER THE MPEE:

a. To study the feasibility of performing image processing under the MPEE, a simple, but rather extensive collection of image processing tools was built up using HDL. Also, several data structures were designed to allow the image information to be handled more easily by the processing tools.

The image processing system contains many algorithms and techniques currently being utilized in the field. These include convolution (spatial domain filtering), histogram equalization, unsharp masking, and homomorphic filtering. Morphological operations including median filtering were implemented as well. Also, a form of adaptive histogram equalization was added to the system. All of these functions were implemented in primitives and compounds under HDL.

Since image processing requires handling enormous amounts of data, two data structures were developed to ease the burden of passing information. The image data structure contained every pixel value in the image, the number of rows and columns in the image, and the original x and y values of the upper left corner of the image. The original x and y values indicate the origin of the image relative to a parent image. For large full size images, the original x . d y are zero. For subimages extracted from the larger images, these values indicate the pixel location where the subimage came from in the "parent" image. A similar data structure was utilized for the filter masks used in convolution operations.

b. The image processing system running under the MPEE proved to work very well. All of the scripts ran flawlessly and the data structures allowed for simple passing of information. Although computation times were just adequate, the speed with which different processing schemes could be implemented by relatively unskilled programmers was impressive. The iconic editor provided for rapid prototyping of many different scenarios.

V. DISTRIBUTED IMAGE PROCESSING:

a. After the image processing system had been developed
and MGK/HDL had been ported to the 386/Transputer
platform, the final step necessary for processing images
on transputers involved slight modifications to the image
processing tools already developed.

The first step was to choose which processing tools
would best lend themselves to parallel processing.
Convolution and adaptive histogram equalization were
chosen because they are compute-intensive and portions
of the image may be processed in parallel.

The method chosen for implementing the processing was
the so called "farming" technique. The image was split
into several pieces with each transputer performing the
desired operation on that portion of the image. After
all pieces were processed, the image was merged back
together. Two different tacks were taken to farm the
image to the transputers. In one scenario, a control-
router primitive splits the image into pieces, sends the
pieces to transputer, receives the processed pieces back,
and merges the processed image together. An input to the
control-router specifies how large each piece should be.

Therefore, each transputer could be called upon many times. In the other scenario, a router primitive splits the image into four pieces and sends them to the processors. A separate primitive receives the processed pieces and merges them. Each transputer is used only one time in this approach.

b.   The parallel image processing system worked very well. The farming technique seemed to be very appropriate for the problem. Both scenarios for parcelling the images to the transputers worked well. Convolution was performed using the first and more complicated farming scenario while adaptive histogram equalization used the latter farming scenario. The farming scenarios were assigned as such because adaptive histogram equalization requires that the portions of the image overlap to some degree. Although the more complicated scenario uses a "smarter" control-router, if the pieces of the image were too small, it seemed that too much time was wasted on parcelling and routing the image. However, if the size of the pieces was fairly large, the technique worked well. Both techniques demonstrated a computational speedup greater than 3.0

over running on a single transputer (benchmarks are provided at the end of this paper). The maximum speedup achievable would be a performance ration of 4.0. and is dependent on the parallelism present in the processing algorithm. Our most highly parallel algorithm yielded a speedup of 3.95, thus indicating that the processing overhead of the MPEE is negligible in this application. Also impressive was the speedup of about 5 that the one transputer had over the 386 machine alone.

VI.   REMOTELY CONTROLLED IMAGE PROCESSING RESOURCES:

a.   Although the application of transputers to the image processing problem showed a tremendous advantage, there exist already many PC/DOS-based hardware and software image processing systems. To fully utilize all facilities, a system was needed to allow use of these facilities from one location. An MGK/HDL system was developed as a controller for the various PC-based resources.

This system was implemented using FTP (c) (File Transfer Protocol) software. The FTP is used to send batch files and necessary data files to the PC. The PC

waits for the files to be passed from the workstation and then executes the batch file. The batch file contains the necessary instructions for the image processing resources on the PC. These resources may include display capabilities, array processors, or other image processing-specific hardware or software. Once the batch file executes, the PC sends the results back to the workstation via the network using FTP.

b. The MGK/HDL remote control system has shown promise. Display devices and array processing boards linked to the PC have been successively used within the image processing system already developed. This greatly enhances the capabilities of the original image processing system and could lead to using existing PC resources for many compute-intensive operations.

VII. COMPUTER AIDED DYNAMIC DATA MONITORING AND ACQUISITION SYSTEM (CADDMAS):

a. The first task in the simulation of a small CADDMAS system was the writing of the necessary C scripts for the

primitive computational blocks. These included double_to_complex_script (for converting real data to complex data for the FFT), fft_script (for performing a frequency analysis of the data), mag_phase_script (for converting the complex output of the FFT to magnitude and phase format), auto_correlation_script (for estimating the autocorrelation function of the raw data), the simulator_script (for synthesizing data), and the plot_data_script (for displaying results graphically in an X11 window). These C scripts were then incorporated into the HDL as primitives, and the primitives were used to develop higher-level compounds.

b. The higher-level compounds included one_channel (a simple simulation of a single CADDMAS channel that performs an FFT, autocorrelation, and displays these along with the raw data) and three_channels (three one_channel compounds running together on a single transputer). Timing tests were run on the one_channel compound and it was discovered that 25 data packets (each containing 1024 points) could be processed in 13.8 seconds (with the display scripts removed) (see benchmark table at the end of this document). This

results in one packet processed every 555 msec, which is
an encouraging result for a software simulation. With
FFT and autocorrelation performed on a DSP chip, we
expect these times to drop by an order of magnitude or
more. It was observed that the overhead of the MGK was
negligible in this application.

VIII. RECOMMENDATIONS:

a. Distributed Image Processing System:

   1. There should be exploration of structural
adaptivity within the existing image processing
structure.

   2. Further investigation of "smarter" approaches to
using distributed processing in the image processing
system is warranted. A better approach would be to have
the MGK builder take into consideration the hardware
architecture available. Thus, the end user need not
concern himself with the methods of efficiently
distributing the problem across the architecture.

   3. More research needs to be conducted toward the

remote control function for image processing and other applications. Many of the current obstacles could be overcome by having a smaller version of MGK running under DOS on the various machines.

b.   Computer Aided Dynamic Data Monitoring and
     Acquisition System (CADDMAS):

1.   The PC/transputer communications link is too slow for effective real-time display, thus we recommend a video board driven directly by the transputer.

2.   The CADDMAS simulation systems were quickly and easily developed for transputer using the MPEE. This illustrates the rapid prototyping and ease of development available through the MPEE. These techniques should be applied at AEDC to reduce the development time and ease programming of new test scenarios.

3.   Future work on CADDMAS should investigate the issues of dynamic reconfiguration of the processing system during runtime. This capability of the MPEE was not adequately addressed during this summer research period.

4.   Alternatives to the graphic editing interface

should be investigated, e.g., some problems at AEDC are already specified in a "spreadsheet-like" format. This should be studied along with an investigation of the scheduling and task distribution associated with these problems.

BENCHMARK RESULTS

Image Processing:

Filtering:

image size	filter size	no. of subimages(size)	architecture	execution time
128x128	9x9	4 (32x128)	80386/20	56.19 sec.
128x128	9x9	4 (32x128)	1 - T800/20	21.44 sec.
128x128	9x9	4 (32x128)	4 - T800/20	5.75 sec.

Performance ratio = 21.44 / 5.75 = 3.73

Adaptive Histogram Equalization:

image size	block size	no. of subimages	architecture	execution time
128x128	30x30	4	80386/20	598.29 sec.
128x128	30x30	4	1 - T800/20	86.92 sec.
128x128	30x30	4	4 - T800/20	28.03 sec.

Performance ratio = 86.92 / 28.03 = 3.1

image size	block size	no. of subimages	architecture	execution time
200x200	3x3	4	80386/20	1967.70 sec.
200x200	3x3	4	1 - T800/20	329.71 sec.
200x200	3x3	4	4 - T800/20	83.56 sec.

Performance ratio = 329.71 / 83.56 = 3.95

CADDMAS: Single channel software simulation processing
25 1024pt. data packets.

Processing performed:	execution time
FFT	4.042 sec.
FFT, log-magnitude, autocorrelation	13.888 sec.

COMPARISON OF T800/20 TO VAX 11/780 FPA: Results of using the
LINPACK benchmark, May 1988.

T800/20	.37 MFLOPS
VAX 11/780 FPA - running VMS 4.5	.14 MFLOPS

BIBLIOGRAPHY

1. Lynd, Jr., L. E., "Structurally Adaptive Signal Processing," M.S. thesis, Vanderbilt University, 1989.

2. Sztipanovitis, J. and Wilkes, D. M., "Structurally Adaptive Signal Processing Systems," presented at the 1988 Digital Signal Processing Workshop, South Lake Tahoe, CA, September, 1988.

3. Biegl, C., Karsai, G., Sztipanovitis, J., Bourne, J., Mushlin, R., and Harrison, C., "Execution Environment for Intelligent Real-Time Systems," Proc. of the 8th Annual IEEE/EMBS Conference, Dallas, TX, pp. 807-811, 1986.

4. Sztipanovitis, J., Biegl, C., Karsai, G., "Graph Model-Based Approach to Representation, Interpretation and Execution of Real-Time Signal Processing Systems," International Journal of Intelligent Systems, 1988 (in press).

5. Sztipanovitis, J., and Purves, R. B., "Coupling Symbolic and Numeric Computations in Distributed Environment," Proc. of the Workshop on Coupling Symbolic and Numeric Computations, Seattle, WA, pp. 13/0-13/13, 1987 (will be published by North-Holland Publishing House in 1988).

1989 USAF-UES SUMMER FACULTY RESEARCH PROGRAM

Sponsored by the

AIR FORCE OFFICE OF SCIENTIFIC RESEARCH

Conducted by the

Universal Energy Systems, Inc.

<u>FINAL REPORT</u>

<u>MAGNETIC PERTURBATIONS OF THE STRUCTURAL CHARACTERISTICS, PHOTOPHYSICAL PROPERTIES, AND PHOTOCHEMICAL BEHAVIOR OF CRYOGENIC NOBLE GAS-ALKALI METAL MATRICES</u>

Prepared by:	John W. Kenney, III
Academic Rank:	Assistant Professor of Chemistry
Department and	Department of Physical Sciences--Chemistry
University:	Eastern New Mexico University
Research Location:	Astronautics Laboratory, ARIES group, Edwards Air Force Base, California
USAF Researcher:	Dr. Mario Fajardo and Dr. Stephen L. Rodgers
Date:	9 August 1989
Contract No:	F49620-88-C-0053

MAGNETIC PERTURBATIONS OF THE STRUCTURAL CHARACTERISTICS, PHOTOPHYSICAL PROPERTIES, AND PHOTOCHEMICAL BEHAVIOR OF CRYOGENIC NOBLE GAS-ALKALI METAL MATRICES

by

John W. Kenney, III

ABSTRACT

There is considerable interest in preparing cryogenic cooled rocket fuels containing high concentrations of reactive low atomic mass metals isolated as individual atoms. These metal atoms can increase the specific impulse of the rocket fuel substantially by combining with the oxidizer to generate large amounts of energy. The technique of laser ablation of lithium metal has been shown to be highly effective in producing significantly increased atomic concentrations in cryogenic matrices of the light noble gases. Comparisons with Knudsen oven generated lithium/noble gas matrices indicate that the higher kinetic energy of the ablated lithium atoms enables them to access tighter trapping sites that are unavailable to thermal lithium beams. Ablation experiments are reviewed and compared with details of Knudsen oven experiments. The technique of magnetic circular dichroism spectroscopy as a probe of these high energy sites is discussed and initial approaches to magnetic circular dichroism experiments are discussed.

ACKNOWLEDGMENTS

I would like to thank the Air Force Systems Command and the Air Force Office of Scientific Research for their sponsorship of this research project. It is a pleasure to acknowledge Universal Energy Systems for supporting me through the Summer Faculty Research Program. The ARIES Research Group at the Astronautics Laboratory provided a stimulating atmosphere in which to carry out this research.

I take particular pleasure in acknowledging the many contributions and the scientific creativity of my collaborator, Dr. Mario Fajardo. Finally, I would like to acknowledge the support and enthusiasm of my technical focal point, Dr. Stephen L. Rodgers.

I. INTRODUCTION:

It is well known that significant increases in the specific impulse (I_{sp}) of a rocket propellant may be achieved by injecting powders of reactive, low atomic mass metals (e.g., lithium (Li) or aluminum (Al)) into the combustion chamber (1). The I_{sp} increase may be attributed to the enthalpy boost derived from the large exothermic heat of formation of the metal oxide (e.g., $\Delta H_f(Al_2O_3) = -1675.7$ kJ mol^{-1} at 298 K and 1 atm). Aside from the inherent technical complexities associated with storing and delivering a precisely metered flow of each component of a tripropellant system (metal powder + fuel + oxidizer), one must pay a fundamental thermodynamic penalty for using a metal powder as a reactant: the endothermic heat of sublimation of the metal. Since the heat of sublimation of the metal is implicitly accounted for in the heat of formation of the metal oxide, any strategy that effectively delivers isolated metal atoms (2) to the combustion chamber stands to add the heat of sublimation of the metal to the enthalpy boost: i.e.,

Reaction with metal powder $xM(s) + yO_2(g) \rightarrow M_xO_{2y}(s)$ $\Delta H_f << 0$

Sublimation of metal $-[M(s) \rightarrow M(g)$ $\Delta H_{sub} >> 0]$

Reaction with metal vapor $xM(g) + yO_2(g) \rightarrow M_xO_{2y}(s)$ $\Delta H = \Delta H_f - x\Delta H_{sub}$
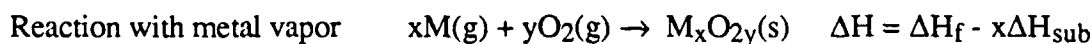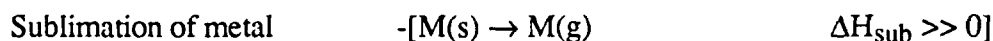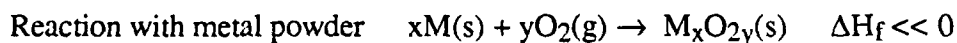
where $|\Delta H| >> |\Delta H_f|$. To place some quantitative values on these processes, let us consider Al metal with $\Delta H_{sub} = 301.3$ kJ mol^{-1}. The formation of $Al_2O_3(s)$ from $Al(g)$ rather than $Al(s)$ imparts an additional $-2\Delta H_{sub} = -602.6$ kJ mol^{-1} to the reaction; boosting the enthalpy production from -1675.7 kJ mol^{-1} to -2278.3 kJ mol^{-1}, an increase of 36 %. In the case of Li metal, the formation of $Li_2O(s)$ from $Li(g)$ rather than $Li(s)$ gives an additional $-2\Delta H_{sub} = -302$ kJ mol^{-1}.

To recover this sublimation enthalpy for propulsion, the reactive metal must be delivered to the rocket in atomized form prior to launch; i.e., the chemical or physical processes that separate the reactive metal atoms must be carried out on the ground using ground-based sources of energy. Practical considerations dictate that the metal atoms be dispersed into a medium or a matrix. From a thermodynamics perspective, we will allow

the loss of some of the enthalpy of sublimation by the formation of weak, metastable metal-matrix bonds:

Reaction with metal powder $\quad xM(s) + yO_2(g) \rightarrow M_xO_{2y}(s) \quad \Delta H_f \ll 0$

Sublimation of metal $\quad -[M(s) \rightarrow M(g) \quad\quad\quad\quad \Delta H_{sub} \gg 0]$

Disperse atoms in matrix $\quad -[M(g) \rightarrow M(ma) \quad\quad\quad\quad \Delta H_{mat} < 0, \text{ small}]$

Reaction with matrix metal $\quad xM(ma) + yO_2(g) \rightarrow M_xO_{2y}(s) \quad \Delta H = \Delta H_f - x\Delta H_{sub}$
$$+ x\Delta H_{mat}$$
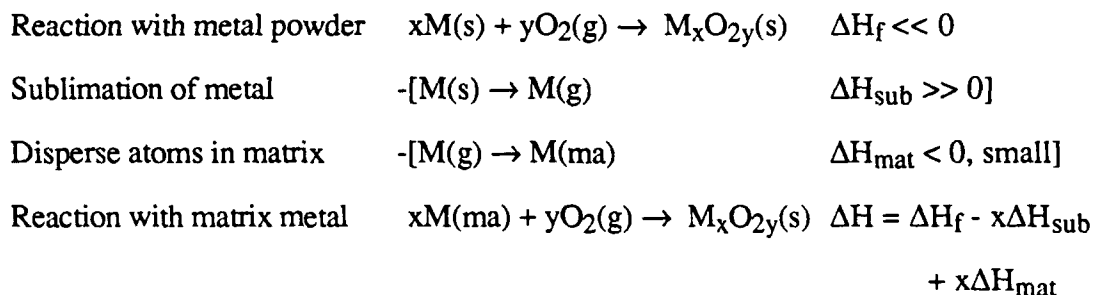
If reactive metal atoms can be dispersed in a matrix of cryogenically cooled rocket fuel, then one stands to recover a significant portion of the sublimation enthalpy of the metal (i.e., $-x(\Delta H_{sub} - \Delta H_{mat})$ vs. $-x\Delta H_{sub}$) with the added benefit of combining metal + fuel into a single matrix. Much recent work in high energy density materials (HEDM) research has, therefore, focused on ways to disperse high concentrations of metals into cryogenic matrices with the ultimate objective of dispersing the metal in a cryogenically cooled rocket fuel (e.g., H_2, N_2H_4, N_2H_3R). The technique of laser ablation of the solid metal followed by trapping of the ejected metal vapor in a cryogenically cooled matrix shows great promise. Of particular interest and significance from the standpoint of rocket propulsion is new spectroscopic evidence that the laser ablation technique produces trapped metal atoms in unusual, high energy matrix sites that heretofore have not been observed in metal matrices prepared from thermally generated metal vapor beams from Knudsen cells (3).

II. OBJECTIVES OF THE RESEARCH EFFORT:

Promising laser ablation experiments on Li metal at the Astronautics Laboratory had been initiated only recently at the beginning of the research period. Experimental refinements had not yet progressed to the point where direct comparisons, crucial to the evaluation and interpretation of the new laser ablation results, could be made between metal-containing matrices generated from metal vapors produced by the laser ablation and Knudsen oven methods. The primary objective was, therefore, to develop the Knudsen oven matrix isolation capability to the point where previously reported spectra (4-6) of

matrix isolated Li, as generated by the Knudsen oven technique, could be reproduced. Secondary objectives were to implement spectroscopic probes of the matrix isolated Li atoms that would yield insights into the nature of the metal atom--matrix host atom interactions, with special emphasis on magneto circular dichroism (MCD) measurements. The MCD technique is particularly powerful in elucidating the nature of the matrix-induced perturbations (e.g., matrix site effects, spin orbit coupling, vibronic coupling, Jahn-Teller effects) of matrix isolated metal atoms (7-16).

III.   KNUDSEN OVEN EXPERIMENTS:

A cryogenic noble gas matrix doped with a small quantity of Li exhibits characteristic multiplet absorptions that can be identified as the matrix-perturbed $^2S \rightarrow {}^2P$ transition of atomic Li. These multiplet absorptions appear near the gas phase transition of 670.8 nm. The nature of these multiplet absorptions depends upon the noble gas substrate, the substrate temperature and annealing history, and the Li concentration in the substrate. The interpretation of these spectra is typically related to the type or types of matrix trapping sites into which the Li atoms are weakly bound. Also of interest and significance are vibronic, Jahn Teller, and spin orbit coupling effects associated with these trapping sites. At higher Li concentrations and at higher matrix temperatures, absorptions in the visible and near infrared attributed to Li_2 begin to appear (4). Initial Li matrix isolation experiments based upon Knudsen oven generated Li at the Astronautics Laboratory failed to give characteristic Li multiplets. Absorption spectra of these matrices revealed bands in the visible and near infrared similar to those reported to be Li_2 bands by earlier researchers (4-6). These matrices were prepared using noble gas deposition rates that were roughly one order of magnitude lower than those reported in the literature (4-6).

The Knudsen oven design initially used in the Astronautics Laboratory experiments featured a vertically mounted stainless steel oven radiatively heated by a glowing filament. A thermocouple well was welded into the center of the oven. This oven design was similar to that reported by Andrews and Pimentel (17). It was thought that the use of ceramic

20-6

spacers and Varian Torr-Seal epoxy in crucial high temperature regions of the oven could be responsible for the anomalous Li matrix isolation data; i.e., the Li could be reacting with outgassing materials. Also of concern in the original Knudsen oven design was the weld in the thermocouple well. The placement of the thermocouple well was not optimum for accurately monitoring the temperature of the Li in the oven and the weld itself was thought to be a source of contamination, particularly since is was exposed directly to molten Li. Problems were also encountered with the radiative heater, a possible source of outgassing contaminants and a hot surface accessible to vaporized Li.

A new oven heater based upon an Omega clad heating element (stainless steel coated wire with internal magnesium oxide insulation) was wound around a cylindrical stainless steel oven unit. This heating element, similar in principle to the heating elements used in electric stoves, allowed the oven to be heated to 500 °C while maintaining a heating element temperature close to the oven temperature. The stainless steel cladding, directed through Swagelock fittings to the outside, simultaneously provided support for the oven and served as an inert barrier to the heater filament so that vaporized Li only had access to clean stainless steel surfaces, minimizing chances for contamination reactions. The oven itself, machined out of a piece of 0.5" stainless steel stock, featured a 45° spark-plug type compression seat for sealing the oven chamber after loading with Li. The oven was mounted horizontally and aligned so that a 0.050" orifice at the end of the oven pointed toward the cryogenically cooled window upon which the noble gas matrix was deposited. The junction of a type E thermocouple fabricated out of the same Omega clad wire used for the heater was attached to the oven near the orifice by means of a set screw. The thermocouple was directed through a Swagelock fitting to the outside. Fine adjustments of oven position could be made by changing the contact point between the anchored thermocouple and the Swagelock ferrule. The entire oven was surrounded by a tantalum heat shield. It was placed in a stainless steel vacuum fitting that mated to the cryostat. These modifications gave a clean stainless steel/tantalum oven assembly that functioned

without a hot filament. The rigid mounting of the thermocouple junction near the oven orifice assured accurate temperature readings.

It was found that Li/argon matrices prepared using the new oven were almost identical to the matrices prepared with the earlier oven design. Contamination, outgassing, and hot filament reactions were ruled out; the spectra were assumed to be those of Li_2. A change to Li/krypton matrices also gave predominantly Li_2 spectra. It was found, however, that the characteristic triplet of matrix isolated atomic Li could be produced if the Knudsen oven temperature was dropped from the usual deposition temperature of 400 °C (4) to approximately 350-365 °C. Long deposition times, 12-24 hr, were required. Under these conditions, only a small fraction of the deposited Li ended up as atomic Li. In all of these experiments, the noble gas flow rate was kept roughly one order of magnitude below that reported by Andrews and Pimentel (4) under the assumption that slow deposition would give optically clear matrices of high quality. By increasing the krypton flow rate to a value close to the Andrews/Pimentel value and maintaining an intermediate oven temperature of 375 °C, atomic Li could be trapped as the major component. Matrices prepared under these conditions exhibited spectra virtually identical to literature spectra (4-6). These matrices were not as optically transparent as the matrices prepared under slow deposition conditions. At higher concentrations of Li, surface recombination reactions predominate giving matrix isolated dimers as the primary product. With lower concentrations of Li (higher concentrations of krypton), atomic Li can be isolated in the matrix.

IV.   LASER ABLATION EXPERIMENTS:

The production of matrix isolated atomic Li by laser ablation gives rise to absorption triplets that are blue shifted relative to the atomic triplets observed in matrix isolation experiments based upon thermally generated Li from Knudsen cells (3). Moreover, the ablation technique allows very high concentrations of atomic Li to be matrix isolated in very short periods of time. Noble gas flow rates one order of magnitude lower

than those used in Knudsen cell experiments give highly satisfactory results. As the noble gas flow rate is increased, a red shoulder grows in on the edge of the blue shifted triplet. This red shoulder is centered over the spectral region where the Knudsen triplet occurs. Careful examination of Knudsen generated atomic matrices in Kr reveals a very small blue triplet absorption. In xenon, the laser ablation and Knudsen techniques give essentially identical spectra. These data can be explained if it is assumed that the highly energetic Li atoms generated by laser ablation have sufficient kinetic energy to burrow into the matrix to access tighter binding sites that give blue shifted spectra. High noble gas flow rates tend to make the matrix more plastic facilitating thermalization of the Li atoms, hence the grow in of the red shoulder. The weak blue triplet signal derived from matrices prepared from thermally generated Li, indicates that only a very small fraction of the Li atoms have enough kinetic energy to enter the tighter trapping sites. The larger size of the xenon atom makes site access less dependent upon Li atom kinetic energy. Ablation experiments with Ar show the greatest difference from Knudsen experiments. Ablation into Kr matrices gives mixtures of red and blue triplets with the blue triplet strongly predominating. In both Ar and Kr the site or sites that give rise to the blue triplet tend to be thermally stable but photochemically unstable as tested by dye laser excitation experiments and matrix heating experiments. The red triplets are photochemically stable but thermally unstable.

V.   MAGNETO CIRCULAR DICHROISM (MCD) EXPERIMENTS:

An MCD experiment was set up to test for the magnetic field induced circular dichroism of matrix isolated Li as generated by the laser ablation technique. The MCD is a potentially valuable probe of the site(s) giving rise to the blue shifted triplet. An Xe substrate was chosen as the test case since this noble gas choice gave the largest MCD effect in Knudsen oven generated Li matrices (13-14). After the laser ablated Li/Xe matrix was prepared, it was sandwiched between permanent magnets that gave a field of ~0.2 T (2000 Gauss) in the window/matrix region. The field was measured by a calibrated Hall probe. The sample window and magnets were aligned at 45° to the direction of

20-9

propagation of the circularly polarized light beam. The effective magnetic field along the direction of propagation was (2000 Gauss)/$\sqrt{2}$ = 1414 Gauss = 0.14 T. Circular polarization was achieved by passing the light from a quartz halogen lamp through a quartz Glan-Thompson linear polarizing prism and directing the output into a Fresnel rhomb. The Glan-Thompson polarizer was oriented respectively at +45° and -45° with respect to the Fresnel rhomb to give left circularly polarized (lcp) and right circularly polarized (rcp) light. When the Glan-Thompson polarizer and the Fresnel rhomb were oriented ±45° with respect to one another, the resulting output is only slightly modulated by turning the polarization direction of a second linear polarizer through a full 360°. This behavior is indicative of almost complete circular polarization. Absorption spectra of the matrix in the magnetic field were taken with lcp and rcp, and the difference $\Delta A' = A_L' - A_R' = \Delta\varepsilon'Cl = (\varepsilon_L' - \varepsilon_R')Cl$ (Note: primes are used to denote field on condition) was divided by the magnetic field strength and plotted as a function of wavelength or wavenumber to generate the MCD spectrum. The y axis units are, therefore, absorbance/Tesla. The sensitivity of the apparatus was estimated to be 0.01 absorbance unit with 1000 or 2000 scan signal averaging of both the lcp and rcp absorption spectra. Detection was accomplished through a monochromator equipped with an optical multi-channel analyzer (OMA). Unfortunately, the $\Delta A'$ was too small, given the weak magnetic field employed, to give a measurable MCD spectrum. Matrix stability over time posed another significant problem in this experimental design. The close proximity of magnet pole pieces at room temperature to the matrix at ~10 K resulted in slow degradation of the matrix from thermal radiation effects. Matrix degradation between the lcp and rcp runs effectively overwhelmed any magnetically induced distinctions.

VI.   RECOMMENDATIONS:

a.   Implementation: The laser ablation technique has the potential to rapidly produce high concentrations of atomic metal in thermally stable high energy sites in substrates of the smaller noble gases. These results suggest that studies of laser ablated Li be extended to

include actual rocket fuels as the cryogenic substrates (e.g., $H_2(s)$, $N_2H_4(s)$). Also to be tried are cryogenic "sandwiches", for example a layer of solid hydrogen covered with a layer of solid neon. The neon layer thickness could, in principle, be adjusted so that it would absorb almost all of the kinetic energy of the laser ablated Li atoms, which would then glide to a stop in a solid hydrogen matrix. Changes in the ablating laser wavelength could be used as another control of Li kinetic energy. Laser ablation followed by velocity selection of ejected Li atoms (e.g., by including a rotating sector device between the Li target and the substrate) should be tried to achieve quantitative control of the Li beam. Pulsed substrate deposition experiments, timed to be either in phase or out of phase with the ablating laser pulses, should be performed to investigate the effects of local annealing induced by matrix gas flow. These experiments will offer an insightful contrast to the continuous flow substrate deposition experiments with laser ablation (experimental approach to date). Tools are now at hand to measure how much Li can be doped into a cryogenic matrix at a given temperature. Experiments should be carried out to determine optimum conditions for maximizing atomic Li concentrations in matrices by laser ablation.

b.   Follow-on Research: Apart from the applied research questions addressed above, an effort should be made to understand in detail the nature of the high energy trapping sites that can be accessed by laser ablation. The characterization of these sites by careful experimentation and by theoretical modeling is needed to provide insight into how to produce sites of this type in a wide variety of cryogenic matrices, in particular, rocket fuels. MCD spectroscopy of these Li trapping sites is therefore needed. Spectroscopic techniques based upon strong magnetic fields (0.5-5.0 T), cryogenic temperatures (10-1.8 K), and state-of-the-art phase sensitive detection of the MCD signal *via* high frequency photoelastic polarization modulation technology should be implemented. The luminescence spectra of laser ablated Li matrices should be investigated for magnetic perturbations: in this case, magnetic perturbation of luminescence lifetimes and magneto circularly polarized luminescence (MCPL).

REFERENCES

1. Gordon, L.J.; Lee, J.B. *J. Am. Rocket Soc.* **1962**, *32*, 600.

2. A distinction must be made between the enthalpy of sublimation of a metal, ΔH_{sub}, the enthalpy required to convert the metal in its standard state (solid) to a vapor (which may consist of a mixture metal atoms, dimers, trimers etc.) and the enthalpy of atomization, ΔH_{atom}, the enthalpy required to convert the solid metal into a vapor of isolated atoms. The difference between ΔH_{atom} and ΔH_{sub} can be related to the dissociation enthalpies of species $M_y(g)$ into atoms (y M(g)) weighted by the appropriate mol fractions of these species in the vapor. For Li, $\Delta H_{sub} = 151$ kJ mol^{-1} and $\Delta H_{atom} = 162$ kJ mol^{-1}, indicating that only a small fraction of the vapor consists of polyatomic species, even under standard conditions. From the standpoint of rocket propulsion, the atomic metal vapor is more desirable than a standard vapor, although the difference is small. Thermodynamic arguments developed on the basis of ΔH_{sub} and ΔH_{atom} of the metal will give "essentially" the same numbers, so the more familiar ΔH_{sub} is employed in the text.

3. Fajardo, M.E. "Matrix Isolation Spectroscopy of Metal Atoms Generated by Laser Ablation", High Energy Density Materials Contractors Conference, March 12-15, 1989, New Orleans, LA.

4. Andrews, L.; Pimentel, G.C. J. Chem. Phys. **1967**, *47*, 2905-2910.

5. Belyaeva, A.A.; Predtechenskii, Y.B.; Shcherba, L.D. *Opt. Spectrosc.* **1973**, *34*, 21-24.

6. Wright, J.J.; Balling, L.C. *J. Chem. Phys.* **1980**, *73*, 3103-3106.

7. Douglas, I.N.; Grinter, R.; Thompson, A.J. *Mol. Phys.* **1974**, *28*, 1377-1388.

8. Krausz, E.R.; Mowery, R.L.; Schatz, P.N. *Ber. Bunsenges. Phys. Chem.* **1978**, *82*, 134-136.

9. Mowery, R.L.; Miller, J.C.; Krausz, E.R.; Schatz, P.N.; Jacobs, S.M.; Andrews, L. *J. Chem. Phys.* **1979**, *70*, 3920-3926.

10. Brittain, R.; Powell, D.; Voigtman, E.; Vala, M. *Rev. Sci. Instrum.* **1980**, *51*, 905-910.

11. Miller, J.C.; Mowery, R.L.; Krausz, E.R.; Jacobs, S.M.; Kim, H.W.; Schatz, P.N.; Andrews, L. *J. Chem. Phys.* **1981**, *74*, 6349-6361.

12. Grinter, R.; Stern, D.R. *J. Mol. Structure* **1982**, *80*, 147-150.

13. Lund, P.A.; Smith, D.; Jacobs, S.M.; Schatz, P.N. *J. Phys. Chem.* **1984**, *88*, 31-42.

14. Rose, J.; Smith, D.; Williamson, B ¯ Schatz, P.N.; O'Brien, M.C.M. *J. Phys. Chem.* **1986**, *90*, 2608-2615.

15. Samet, C.; Rose, J.L.; Williamson, B.E.; Schatz, P.N. *Chem. Phys. Lett.* **1987**, *142*, 557-561.

16. Grinter, R.; Singer, R.J. *Chem. Phys.* **1987**, *113*, 87-97.

17. Andrews, W.L.S.; Pimentel, G.C. *J. Chem. Phys.* **1966**, *44*, 2361.

1989 USAF-UES SUMMER FACULTY RESEARCH PROGRAM

Sponsored by the

AIR FORCE OFFICE OF SCIENTIFIC RESEARCH

Conducted by the

Universal Energy Systems, Inc.

<u>FINAL REPORT</u>

I_{sp} ENHANCEMENT VIA ADSORPTION/ABSORPTION OF SMALL ENERGETIC MOLECULES ON SOLID PROPELLANTS

Prepared by:	M. Inga S. Kenney
Academic Rank:	Instructor of Chemistry
Department and	Department of Physical Sciences--Chemistry
University:	Eastern New Mexico University
Research Location:	Astronautics Laboratory, ARIES group, Edwards Air Force Base, California
USAF Researcher:	Dr. Stephen L. Rodgers
Date:	9 August 1989
Contract No:	F49620-88-C-0053

I_{sp} ENHANCEMENT VIA ADSORPTION/ABSORPTION OF SMALL ENERGETIC MOLECULES ON SOLID PROPELLANTS

by

M. Inga S. Kenney

ABSTRACT

The total payload that a rocket can carry can only be as large as the energy available to lift it into space. That energy comes directly from the rocket fuel. To increase the carrying capacity of a rocket, the energy content of the rocket fuel must be increased without drastically increasing the mass of the fuel itself. One way to amplify the energy of the fuel is to add high energy density materials (i.e., small, very energetic molecules) to the fuel. Azide molecules are one class of high energy density materials.

Studies show that these azide molecules can be added to alkali halides possessing a combination of cation to anion size ratio and a crystal packing structure. The azide--alkali halide adducts exhibit stability over time, yet release significant amounts of energy when heated. Quantitative measurements show azide inclusion in alkali halides between 5-15 percent. These studies indicate that it may be possible to tune the energy content of a rocket fuel by the addition of a high energy content azide which forms a weak bond to the fuel.

ACKNOWLEDGMENTS

I would like to thank the Air Force Systems Command and the Air Force Office of Scientific Research for their sponsorship of this research project. It is a pleasure to acknowledge Universal Energy Systems for supporting me through the Summer Faculty Research Program. Thanks are due to the ARIES research group at the Astronautics Laboratory at Edwards Air Force Base for making this research stimulating and fun to work on the project itself and with the people.

I would also like to thank Dr. Pat Carrick for creative discussions and for helping with the IR instrumentation and spectra, and Dr. Stephen L. Rodgers for encouragement and excitement in this project. Especially, I would like to thank my husband, Dr. John W. Kenney, III, for all his help and support in this project. Finally I would like to acknowledge the support and encouragement of Dr. Patrice Caldwell, Dean of the College of Liberal Arts and Sciences at Eastern New Mexico University.

I.   INTRODUCTION:

The change in enthalpy of a reaction can be related to the kinetic energy of the reaction through the equation: $\frac{1}{2}m_{av}(\Delta V)^2$ = kinetic energy = ΔH_{rxn}. Specific impulse, I_{sp}, a change in the speed of the product molecules of a reaction, is then shown to be $I_{sp} = \Delta V = \left(\frac{2\,|\Delta H|}{m_{prod}}\right)^{1/2}$. To increase the specific impulse of any substance, rocket fuel, an increase in the absolute value of ΔH with only a negligible increase in the mass of the products is necessary. One way to increase the enthalpy of a system is to add energy to that system in the form of light or heat. Another way is to add highly energetic, small molecular mass molecules.

One class of such highly energetic molecules is the azides, with the general structure RN_3, where R = H, halide, alkyl, metal. The azides possess three nitrogen atoms bonded together with single, double, and triple bonds in a resonance type of structure (1).

$$N\equiv N-N \Leftrightarrow N=N=N \Leftrightarrow N-N\equiv N$$

The true azide ion, N_3^-, takes the center, double bonded structure and is relatively stable. It has N=N bond lengths equal at 116 pm (2). The stability of the azide molecules move from ionically bonded (true azide ion) to covalently bonded--very unstable; NaN_3 more stable than $HN_3 > CH_3N_3 > FN_3$ with FN_3 having almost a completely covalent bond between the fluorine and the nitrogen.

The stability problem becomes clearer as the bonds between the nitrogens in the azide are investigated. In the true azide ion, each end nitrogen is double bonded to the center nitrogen with exactly the same bond strength. When another atom, hydrogen for example, attaches itself to one of these end nitrogens in a more covalent manner, the nitrogen to which it is attached must necessarily change its bonding slightly to the center nitrogen. In the pure covalent azide, the resonance form R-N-N≡N predominates (R-N-N bond angle approximately 112°), with bond lengths N-N ~140 pm and N≡N ~109 pm. As the triple bond becomes shorter, and the single bond longer, the molecule becomes less

stable. This instability is reflected in the tendency of the azide to split into N_2 gaseous molecules and RN reactive fragments which may further decompose or react (3-5).

II. OBJECTIVES OF THE RESEARCH EFFORT:

The explosiveness of azide molecules has been known for almost a century. They are a class of highly energetic, low molecular mass molecules. Studies by Haller during the early 1940's indicated that these energetic azides absorbed or adsorbed onto alkali halides, in particular potassium fluoride (3). The objective of this research was to investigate the azide's cohesiveness with potassium fluoride, and to discover other substrates that showed this same tendency. Once the azide was attached to the substrate, the resulting substance would be studied using differential scanning calorimetry (DSC) to determine the energy content.

III. HYDROGEN AZIDE PREPARATION:

Hydrogen azide, HN_3, was prepared in a manner similar to the method reported by Benard and Cohn (6). Stearic acid and sodium azide were mixed in a ratio of ~20 to 1 and melted with gentle heat using a heating mantle. A slow flow of argon gas was introduced into this mixture to help force the $HN_3(g)$ through the substrate of choice (see figure 1).
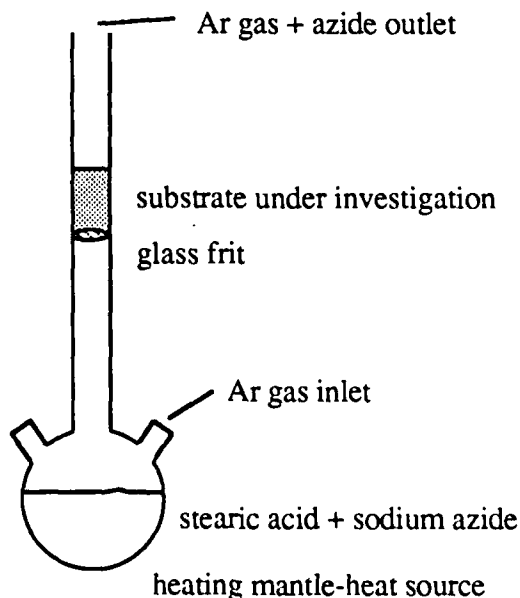
Figure 1. Hydrogen azide introduction to substrate.

IV.   METHYL AZIDE PREPARATION:

Methyl Azide was prepared following the method of Rice and Grelecki (7) by reacting dimethyl sulfate with sodium azide in an alkaline solution. The methyl azide produced is in the gaseous form. Argon gas was used to direct the flow of methyl azide gas through the substrate of choice as in the production of hydrogen azide gas.

V.   DIFFERENTIAL SCANNING CALORIMETRY:

A differential scanning calorimeter (DSC) operates on the principle of power compensation, the objective being to keep the temperature of the sample the same as the temperature of the reference. The energy evolved or absorbed by the sample is compensated for by adding or subtracting an equivalent amount of electrical energy to the resistance heater (see Figure 2). In this manner, ΔH is measured directly.

sample   reference

platinum sensors
individual heaters
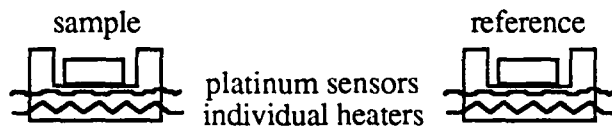
Figure 2. Differential Scanning Calorimeter sample and reference cells

VI.   REACTIONS WITH SUBSTRATES:

Hydrogen azide gas was passed over dried and ground (particle size not monitored) potassium fluoride, KF. Figure 3 shows the DSC thermogram of this substance with interesting exothermic properties, illustrating the ab/adsorption of HN_3. (Normal dry, halide salts show no endotherms, or exotherms in the temperature region under study.) The solid line is the regular DSC trace of KF with HN_3 and the dashed line is a DSC trace taken immediately afterward, on the same sample, by cooling the sample to the lower limit (50 °C) and then running another DSC trace.

The same experimental procedure was used with ammonium perchlorate, AP, a well known rocket fuel. The DSC trace of this sample substance showed only a normal AP thermogram. Ammonium nitrate, AN, a high explosive and cyclotrimethylene trinitramine,
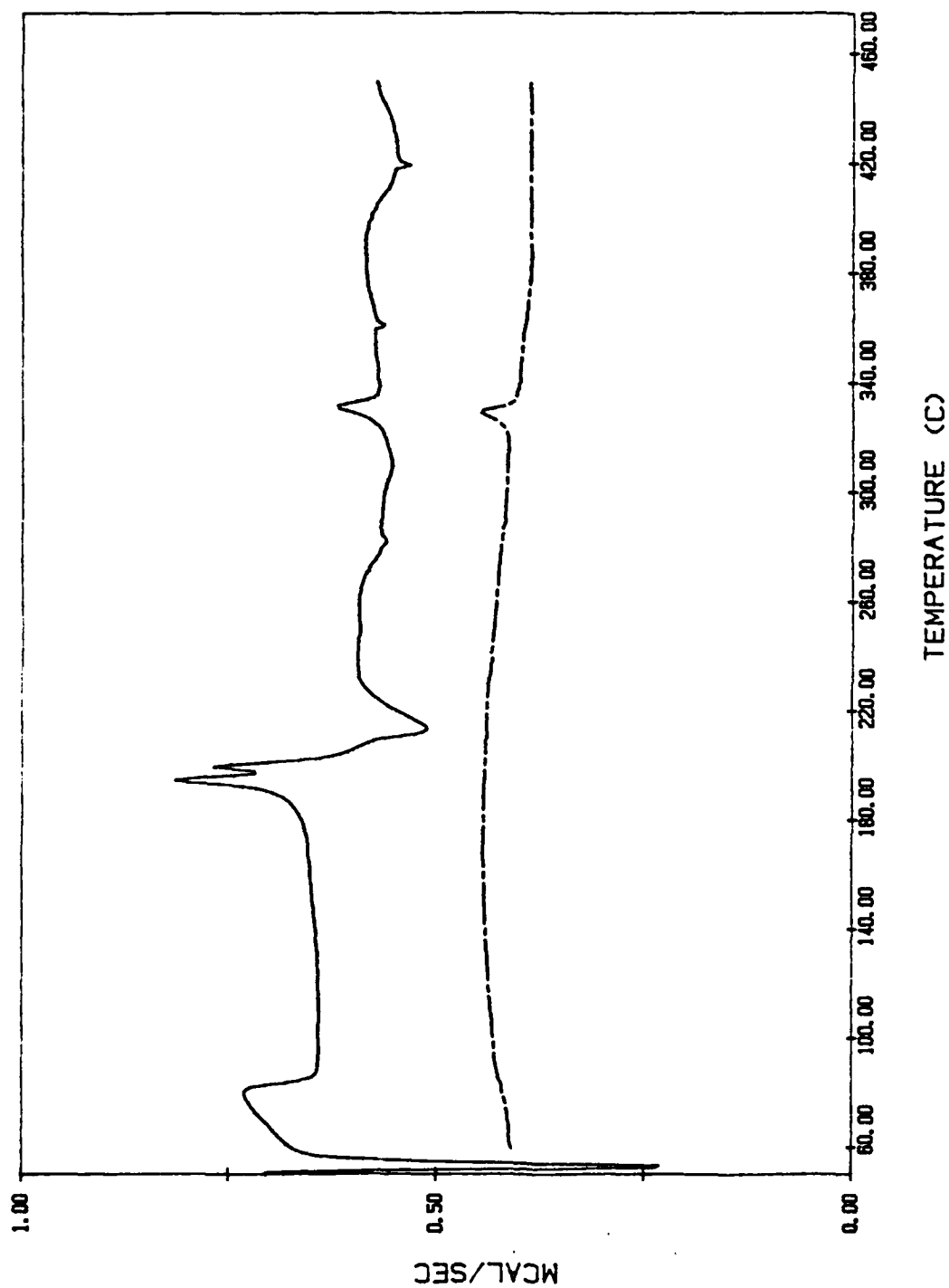
Figure 3. Differential Scanning Calorimetric thermograms of KF with HN_3 ——— , and a second trace of KF + HN_3 immediately following the first run — - - -.

TEMPERATURE (C)

MCAL/SEC

hexogen, RDX, a rocket fuel were also tried without showing positive results for HN3 inclusion.

Another alkali halide, sodium fluoride, NaF, was tried but did not pick up any HN3.

Activated charcoal was used as the substrate. The activated charcoal did pick up some HN3 as shown in the DSC trace given in figure 4.

Rubidium fluoride, RbF, was tried as a substrate. A sample of RbF straight from the bottle picked up a small amount of HN3 as evidenced by a thermogram, so the RbF was vacuum heated to 182 °C to try to dry the RbF. RbF is deliquescent and as such picks up water rapidly. The vacuum-dried and heated RbF was subjected to a flow of HN3(g). This experiment formed two layers: a loose, powdery layer on the top of the reaction set-up and a hard, conglomerated layer on the lower part of the reaction set-up. Both of these layers were subjected to differential scanning calorimeter (DSC) measurements. The loose powder showed no prominent reaction, with the DSC returning an almost identical thermogram to that of the vacuum-dried RbF before reaction. The hard conglomerated sample had to be broken and scraped out of the tube. This hard layer gave a very prominent reaction--a very energetic exothermic peak on the DSC thermogram. Figure 5 shows both the loose fraction, solid line, and the hard fraction, dashed line of representative RbF DSC thermograms. In two separate calculations, both mass difference and thermodynamic data, the RbF was calculated to have picked up 5 - 15% HN3. A sample of the hardened RbF + HN3 was placed into the vacuum oven at room temperature and vacuum-dried for approximately 4 days. The vacuum-drying seemed to have no or only a very small effect on the behavior of the DSC thermogram.

LiNO3 was tried but this substrate failed to pick up any HN3.

Tetramethylammonium fluoride, (CH3)4NF, TMAF, was tried. The reaction between TMAF and HN3 produced a "gooy" and wet looking product, though tests on the product showed that the substance contained no water. A sample was checked on the DSC

TEMPERATURE (C)
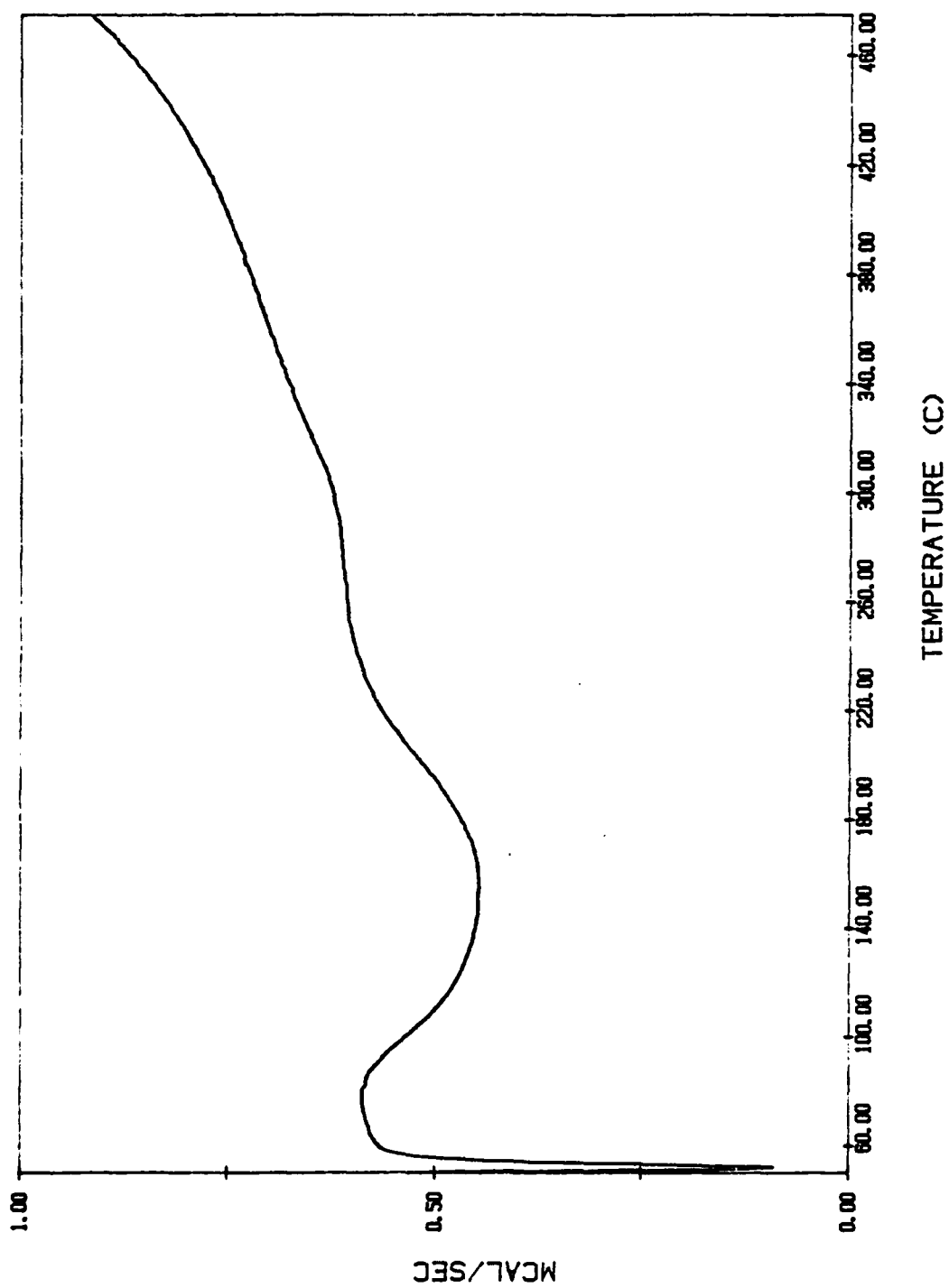
Figure 4. Differential Scanning Calorimetric thermogram of activated charcoal + HN_3.
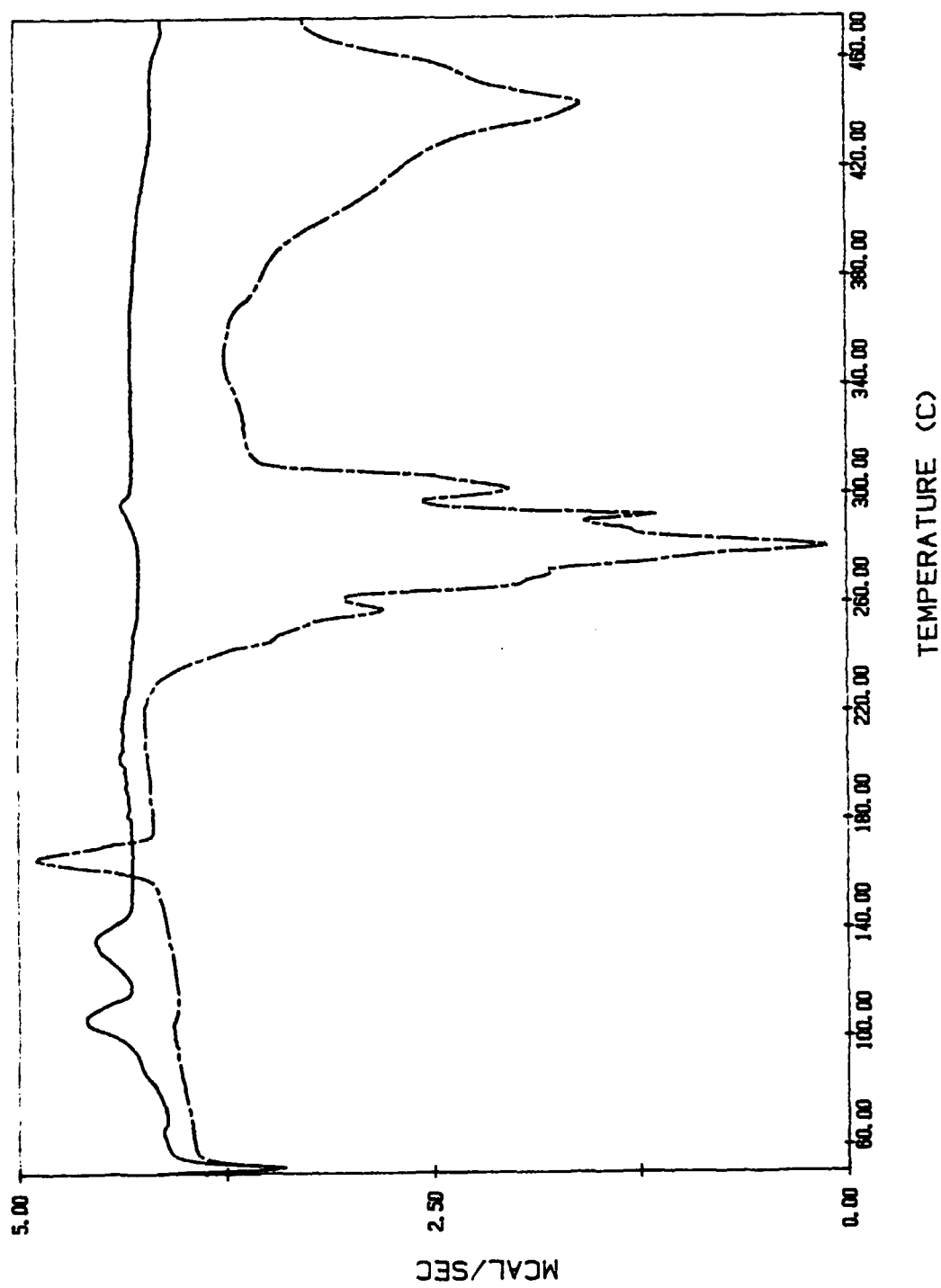
Figure 5. Differential Scanning Calorimetric thermograms of the loose fraction of RbF + HN₃ ——— , and the hard fraction of RbF + HN₃ — · — · .

after being taken directly from the reaction tube; this gave very inconclusive results. A second sample was purged with dry Ar(g) in the reaction tube after all reaction had taken place. This second sample showed that there was a reaction of some sort between the TMAF and the HN_3, but that the reaction changed the nature of both of the reactants, not just attaching the HN_3 to the TMAF in an ab/adsorption manner.

RbCl was tried but this solid substrate failed to ab/adsorb $HN_3(g)$.

CsF was subjected to a flow of HN_3 gas in an Ar carrier gas, and this substrate, similar to the RbF, showed two distinct fractions, a loose powdery fraction and a harder, more crusty fraction. The loose fraction gave a distinctive DSC thermogram revealing only small amounts of HN_3 gas had been picked up by the CsF. The harder fraction picked up much larger amounts of HN_3, as evidenced by the relatively larger exotherms produced by a DSC scan. Figure 6 shows an overlay of the CsF loose fraction (solid line) with the harder fraction (dashed line).

Drierite, a chemical drying agent containing mostly $CaSO_4$ with some $CaCl_2$ (a deliquescent agent) and $[CoCl_4]^{2-}$ (a color indicating compound), was exposed to HN_3. This substance failed to pick up any HN_3.

Two compounds were exposed to methyl azide, CH_3N_3, gas. Unfortunately, both KF and RDX (a rocket propellent) failed to ab/adsorb the CH_3N_3 under the conditions in which they were exposed. More experimentation is needed in this area.

Samples of KF and RbF that had been previously exposed to HN_3 (3 to 6 weeks earlier) were again checked for azide content using the DSC. Both gave similar thermograms to ones taken before with only some small changes.

VII.   <u>INFRARED SPECTRA</u>:

Infrared spectra (IR) were taken of samples exposed to HN_3. These spectra confirmed the DSC results showing distinct HN_3 bands in compounds that had ab/adsorbed the HN_3, and no such bands in compounds that gave negative DSC results (8-9). Samples of KF, RbF, and CsF, exposed to HN_3 gave almost identical IR spectra as
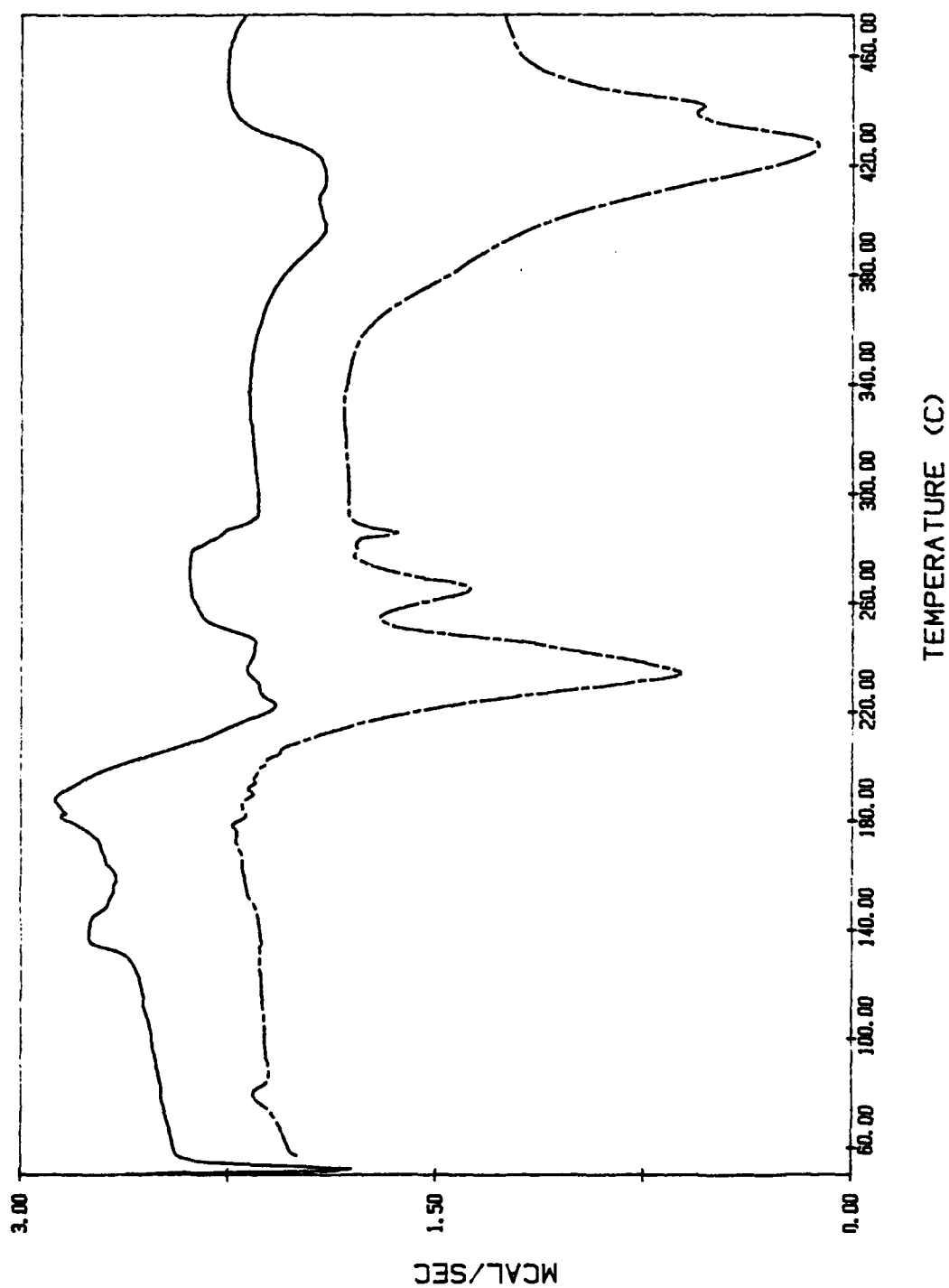
Figure 6. Differential Scanning Calorimetric thermograms of the loose fraction of CsF + HN₃ ——— , and the hard fraction of CsF + HN₃ — · — · —.

shown in figure 7 from top to bottom, respectively. Table 1 lists the wavenumbers of the prominent peaks. These materials were then subjected to a DSC run, and IR spectra were taken. The decomposition of the KF + HN$_3$ gave only a single IR peak, but both RbF + HN$_3$ and CsF + HN$_3$ gave complicated IR spectra. Shown in figure 8, top to bottom, are the IR spectra of, respectively, KF, RbF, and CsF reactions with HN$_3$ followed by DSC runs. It was noted that both RbF + HN$_3$ and CsF + HN$_3$ reacted with the aluminum sample pans used in the DSC (the KF + HN$_3$ did not react with the pans used). These compounds were then run in gold DSC sample pans, and the IR spectra obtained more closely resembled that of the KF + HN$_3$ with only a single distinct peak around 2035 cm^{-1}. The thermograms from the runs in the Au DSC pans showed different behavior from that of the materials run in Al, giving evidence of catalysis by the Al pans.

Table 1.   Infrared spectra of HN$_3$ on KF, RbF, and CsF in cm^{-1}.

KF + HN$_3$	RbF + HN$_3$	CsF + HN$_3$
2099 sh	2099 sh	2094 sh
2035	2032	2033
1524	1526	1523
1254	1256	1255
1236 sh		1234
649	648	649
642	642	642

VIII. DISCUSSION:

HN$_3$ gas reacted with KF, RbF, CsF, and charcoal in a cohesive manner. The three alkali halides, KF, RbF, and CsF all possess an NaCl crystal lattice and are deliquescent. NaF also has these properties. The only difference between the NaF and the others seems to be the size of the cation to anion, where in NaF the cation is smaller than the anion and in the others, KF, RbF, and CsF, the cation is larger than the anion. Other
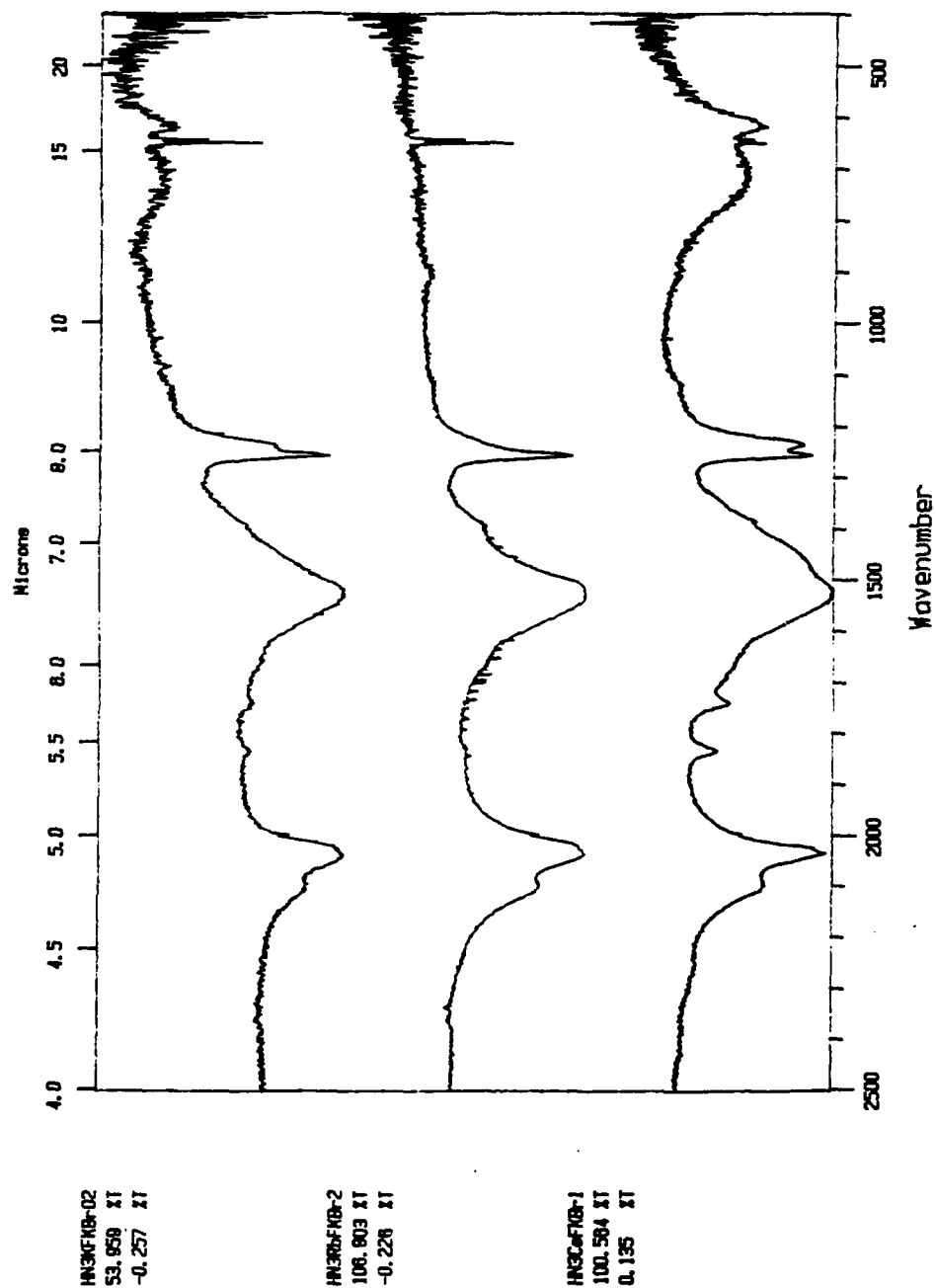
Figure 7. Infrared Spectra of (top to bottom) KF + HN$_3$, RbF + HN$_3$, and CsF + HN$_3$.
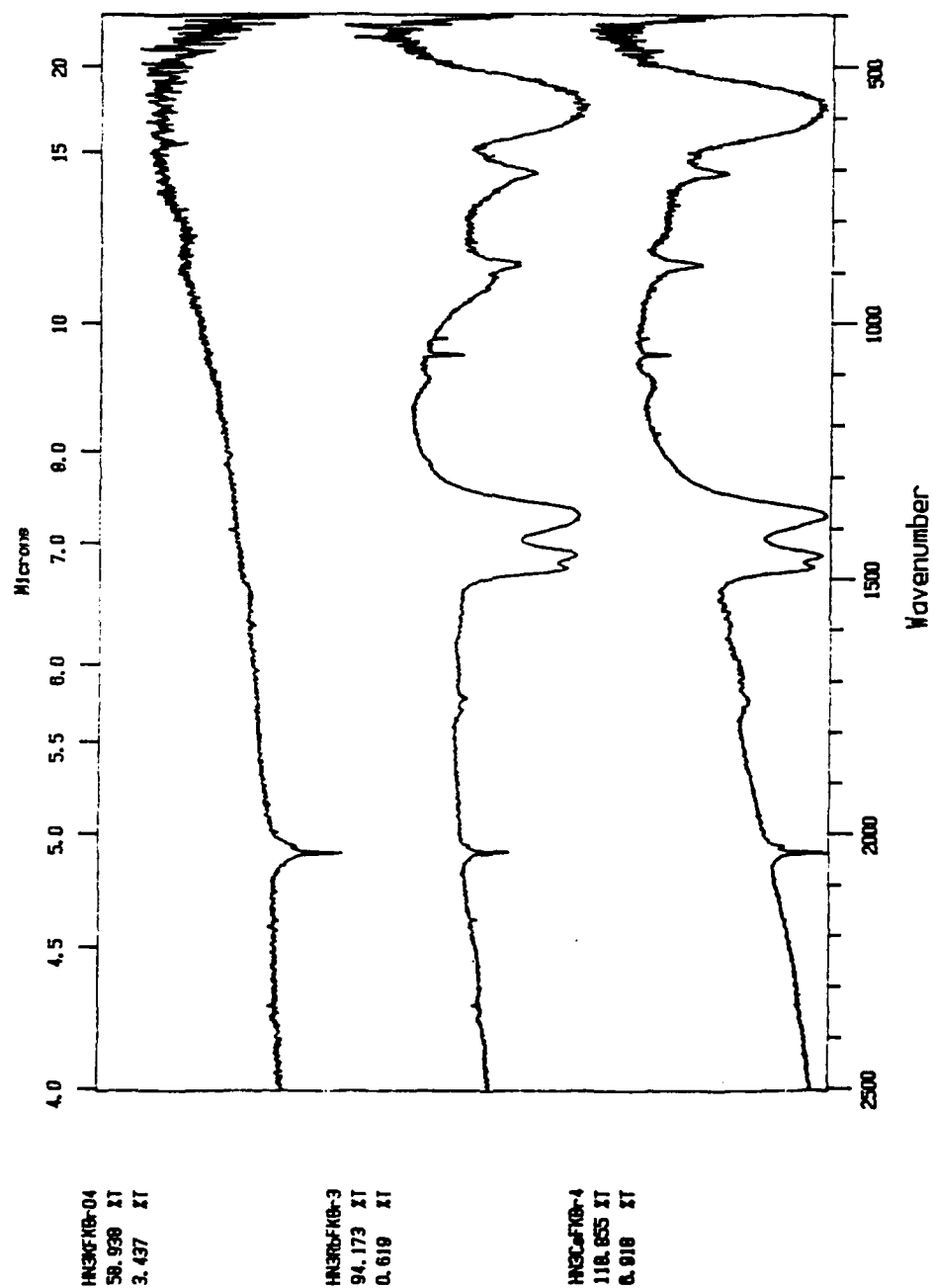
Figure 8. Infrared Spectra of (top to bottom) KF + HN₃, RbF + HN₃, and CsF + HN₃ after differential scanning calorimetry in Al pans.

substrates with the NaCl lattice type did not pick up any HN_3 molecules. Other substrates that were deliquescent also did not pick up HN_3. This seems to point to both a necessary size and a type of hole for the HN_3 to be included.

The infrared spectra of the KF, RbF, and CsF reactions with HN_3 show distinct HN_3 bands, with only one band misplaced. The 1524 cm^{-1} band is absent in HN_3 spectra while a band at 1150 cm^{-1}, the H-N-N bend, is present. A formal charge analysis of HN_3 indicates a build up of negative charge on the nitrogen that is bound to hydrogen. It is postulated that the electrostatic interaction between this nitrogen and the metal cation of the alkali halide, makes it more difficult for the H-N-N bend to occur, thus resulting in an increase in the bending frequency over that observed in the gas phase spectra of HN_3 (see figure 9). In this same scheme, a compound with a small cation and a large anion may not be able to bind to the nitrogen as well because of the relative size of that small cation.

$$-(1+\delta) \qquad +1$$
$$N \text{------} N \equiv N$$
$$+\delta \diagup \quad \vert$$
$$H \qquad \vert$$
$$\vert$$
$$M^+$$
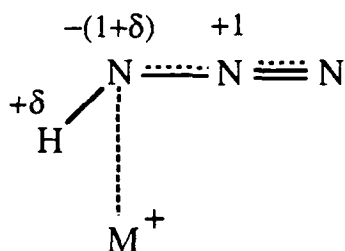
Figure 9. Azide resonance with alkali metal cation.

IX. RECOMMENDATIONS:

a. Implementation: It is now known that azides bind to several alkali halides, activated charcoal, and react with ammonium salts. This suggests that azides can be attached to a solid rocket fuel whose chemical and physical properties mimic in some significant way those properties necessary for binding in these test systems. The successful enhancement of I_{sp} of a solid propellant *via* azide attachment rests upon careful elucidation of the binding in the test systems coupled with the design of propellants that have the potential to bind azides in a similar manner.

b.   Follow-on Research: Hydrogen azide was introduced to the chosen substrates in a very gentle reaction. The azide was just allowed to flow over the substrate with a carrier gas. More rigid conditions--condensation, increased azide production, etc.--may produce a greater content of the azide included on the substrate, and may create azide-substrate interactions where none existed before. Experimental conditions that maximize the uptake of an azide on a solid substrate, particle size, purity, dryness, contact time, photochemical conditions, temperature, and pressure, need to be further investigated.

Exactly how the azide is attached to the substrate is of great interest. Work with X-ray diffraction/powder patterns could give more insight into the mode and placement of the azide on the substrate; hole size needed, cation/anion interaction. Rocket fuels could then be crystallographically grown to the necessary size or with the proper electronic characteristics.

Other techniques that will give information about the bonding and interactions of the azide with a substrate include: (a) scanning electron microscopy (SEM)--to see the surface and investigate the porosity of a substrate. (b) color centers--by introducing lattice defects, charged holes, to help monitor the rate of the azide addition by color changes, or to increase/decrease the amount of azide included in the substrate. (c) raman studies--to monitor the molecular vibrations of the absorbing molecules as the azide attaches. (d) luminescence--to access the excited states of the molecules, particularly powerful when coupled with the color center studies. (e) gas chromatography-mass spectra--investigation of the products of the azide-substrate adduct decomposition as a function of sample temperature (sample to be placed on solid sample inlet probe and heated).

REFERENCES

1. Greenwood, N.N.; Earnshaw, A. *Chemistry of the Elements*; Pergamon: Oxford, England, 1986; p 496.

2. 116 pm = 1.16 Å = 2.19 bohr

3. Haller, J.F. Ph.D. Dissertation, Cornell University, 1942.

4. Sneed, M.C.; Brasted, R.C. *Comprehensive Inorganic Chemistry*; D. Van Nostrand: New York, 1956; Vol. 5, p 48. Sneed, M.C.; Maynard, J.L.; Brasted, R.C. *Comprehensive Inorganic Chemistry*; D.Van Nostrand: New York, 1954; Vol. 3, p 232.

5. Jolly, W.L. *The Inorganic Chemistry of Nitrogen*; W.A. Benjamin: New York, 1964; p 62.

6. Benard, D.J.; Cohn, R.H. *Model Studies of Chemically Bound Excited States*, interim report submitted by Rockwell International's Science Center in Thousand Oaks, CA.

7. Rice, F.O.; Grelecki, C.J. *J. Phys. Chem.*, **1957**, *61*, 830.

8. McDonald, J.R.; Rabalais, J.W.; McGlynn, S.P. *J. Chem. Phys.*, **1970**, *52*, 1332.

9. Dows, D.A.; Pimentel, G.C. *J. Chem. Phys.*, **1955**, *23*, 1258.

1989 USAF-UES SUMMER FACULTY RESEARCH PROGRAM/
GRADUATE STUDENT RESEARCH PROGRAM

Sponsored by the
AIR FORCE OFFICE OF SCIENTIFIC RESEARCH
Conducted by the
Universal Energy Systems, Inc.
<u>FINAL REPORT</u>

<u>STUDIES TOWARD THE SYNTHESIS OF PENTANITROBISHOMOCUBANE</u>

Prepared by: Lynn Maruyama Kirms, Ph.D.

Academic Rank: Assistant Professor

Department and   Chemistry Department, Southern Oregon State College
University:

Research Location: Astronautics Laboratory, (LSX), Edwards AFB

USAF Researcher: Jeffrey W. Gilman, Ph.D.

Date: August 31, 1989

Contract No: F49620-88-C-0053

STUDIES TOWARD THE SYNTHESIS OF PENTANITROBISHOMOCUBANE

by

Lynn Maruyama Kirms

ABSTRACT

Polycyclicpolynitro cage compounds represent a potential source of new fuel additives. An attractive feature of caged molecules is their compactness and accompanying high strain energy. Addition of energetic groups such as nitro groups to the cage system enhances the explosive properties of these compounds. Two approaches to the synthesis of one polycyclicpolynitro compound, pentanitrobishomocubane, were explored. A key intermediate for the first route required the synthesis of the Favorskii ring contraction product, 10,10-dimethoxy-2-carbomethoxy$(5.2.1.0^{2,6})$deca-3,8-diene-5-one. Synthesis of this precursor was investigated. Synthetic studies on the second route focused on determination of conditions for the allylic oxidation of 9-carbomethoxy-10-hydroxytricyclo$(5.2.1.0^{2,6})$deca-4,8-diene, a difficult transformation to effect. The desired allylic alcohol could be obtained in reasonable yield by use of SeO_2 in dioxane/water. Access to this important precursor will provide entry not only to the pentanitrobishomocubane system, but possibly to the tetranitrohomocubane system as well.

ACKNOWLEDGEMENTS

I. INTRODUCTION:

Polycyclicpolynitro cage molecules are of interest as a new class of energetic materials with potential military applications as additives to fuels and propellants. The compact carbon cages of these compounds provide highly strained systems; a feature which may contribute to explosive performance. These molecules also possess high densities, an advantage in volume-limited applications. The addition of nitro groups to these cage molecules results in even higher densities and increased explosive power. Performance criteria for these molecules include detonation pressure and detonation velocity which vary with cage systems and the number of nitro substitutions.[1,2] Polycyclicpolynitro cage compounds may be useful as a replacement for aluminum in minimum smoke missiles. HMX is currently used, however, it is more sensitive to detonation in comparison to some of the caged nitro compounds.

Some of the polycyclicpolynitro compounds that have been synthesized are depicted in Scheme 1.[1] Construction of these highly strained carbon skeletons are themselves synthetically challenging; additionally, strategies for elaboration of the nitro substitutions must be incorporated into the overall synthesis. Direct nitration of preformed cage systems is not a generalized method.

The Aries group of the Astronautics Laboratory at Edwards AFB recently started work on the synthesis of polycyclicpolynitro cage molecules under the direction of Dr. Suresh Suri, who has previous experience in this area. As a 1989 Summer Faculty Research Program (SFRP) participant, I was given a choice of several synthetic projects to work on, one of which was the caged nitro compounds. My past experience in natural products synthesis provided me with the synthetic background necessary to conduct research in the field of polycyclicpolynitro cage molecules.

II. OBJECTIVES OF THE RESEARCH EFFORT:

The synthesis of three nitro and four nitro analogs of bishomocubane were reported by Marchand's group in 1984.[3,4] Pentanitrobishomocubane has never been synthesized. Synthesis of the five nitro bishomocubane was desired to study the effect of an additional nitro group on the density and explosive properties of these molecules. While some of

SCHEME 1
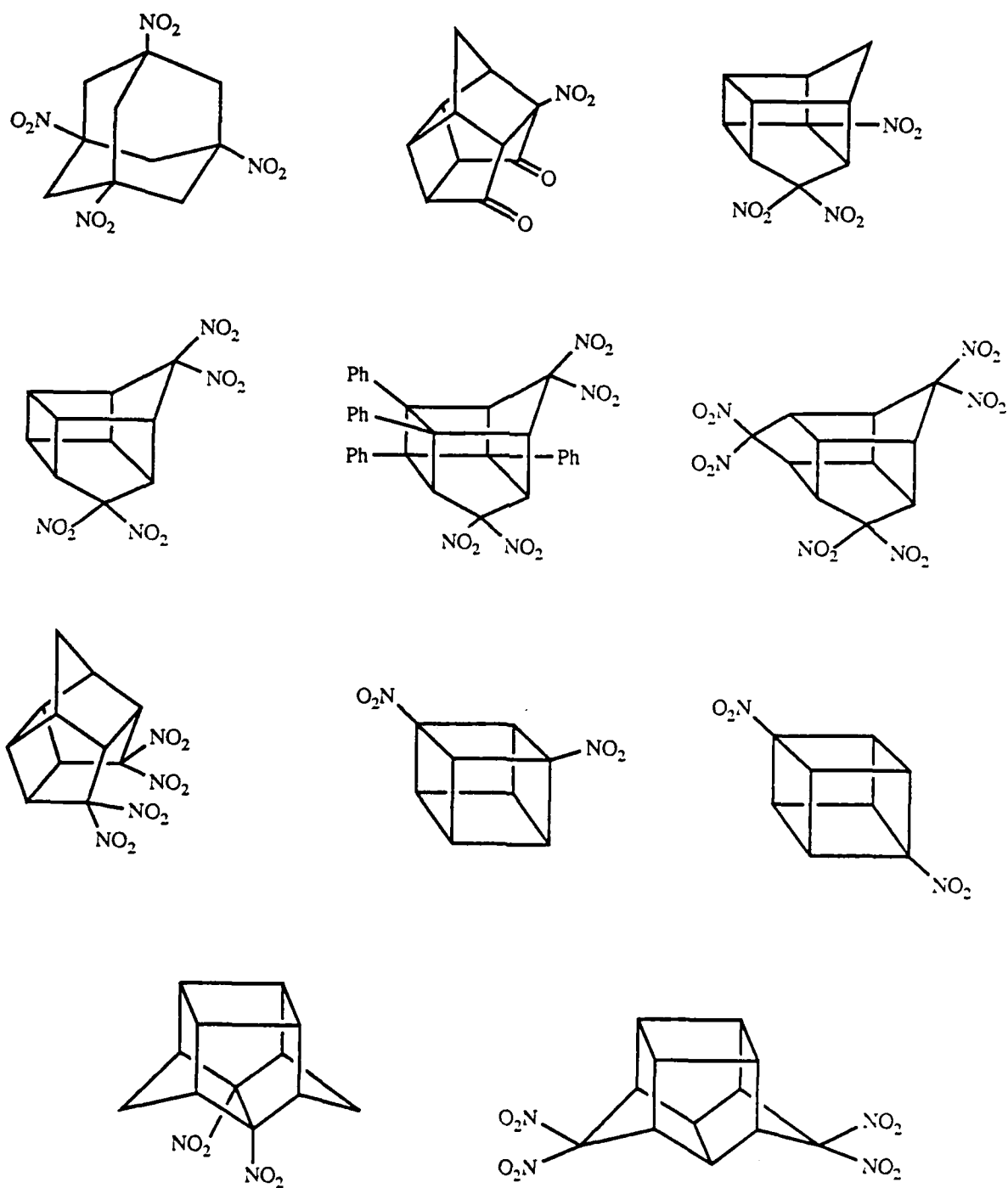
the chemical methodology established in the chemical literature for polycyclicpolynitro cage molecules could be utilized in the synthesis of pentanitrobishomocubane, the synthetic complexity of adding nitro groups to the bishomocubane system demanded a new approach for the five nitro system.

A retrosynthetic analysis for the synthesis of pentanitrobishomocubane is given in Scheme 2. It has been established[3] that a ketone could be elaborated into a geminal di-nitro species, while a carbomethoxy group could serve as a precursor to a single nitro group.

SCHEME 2
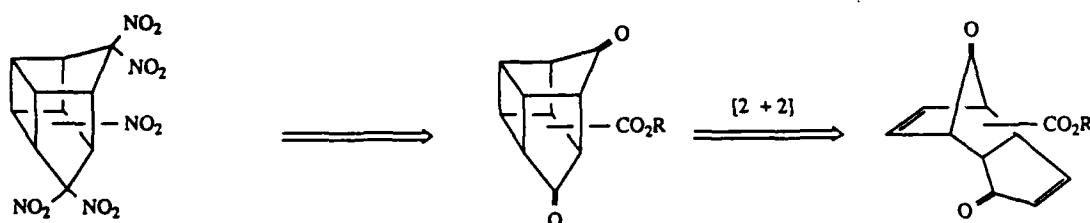
Two possible routes (A and B), to pentanitrobishomocubane are given in Schemes 3 and 4 respectively. Route A begins with the Diels Alder reaction of p-benzoquinone and tetrachlorocyclopentadiene dimethyl acetal.[5] Dechlorination of the adduct 3, by the method of Prinzbach[6] is expected to give the dechlorinated species 4. Selective epoxidation with hydrogen peroxide and sodium carbonate (H_2O_2, Na_2CO_3) yields the epoxide, 5. Favorskii ring contraction of 5 mediated by sodium hydroxide/methanol (NaOH, MeOH) affords the enone 6. Photocycloaddition of 6 produces the caged compound 7 which can be deprotected and further elaborated to the pentanitrobishomocubane system.

The other proposed approach, Route B, involves the Diels Alder adduct 9, of cyclopentadiene and p-benzoquinone. Treatment of 9 with H_2O_2 and Na_2CO_3 is envisioned to afford the epoxide 10. Subsequent reaction of 10 with NaOH, MeOH yields the Favorskii ring contraction product 11. Use of a novel sodium borohydride, cerium III ($NaBH_4$, Ce III) mediated [3,3] sigmatropic rearrangement observed by Suri and Rodgers[7] gives 13 from 11. Allylic oxidation of 13, an unestablished conversion, yields the allylic alcohol 14. Pyridinium chlorochromate (PCC) oxidation of 14 produces the enone 15, followed by [2+2] photocycloaddition to give the caged product 16. The pentanitrobishomocubane molecule 17 made by Route B is a positional isomer of caged nitro compound 8, the final product of Route A.

SCHEME 3, ROUTE A

73%

SCHEME 4, ROUTE B

22-7
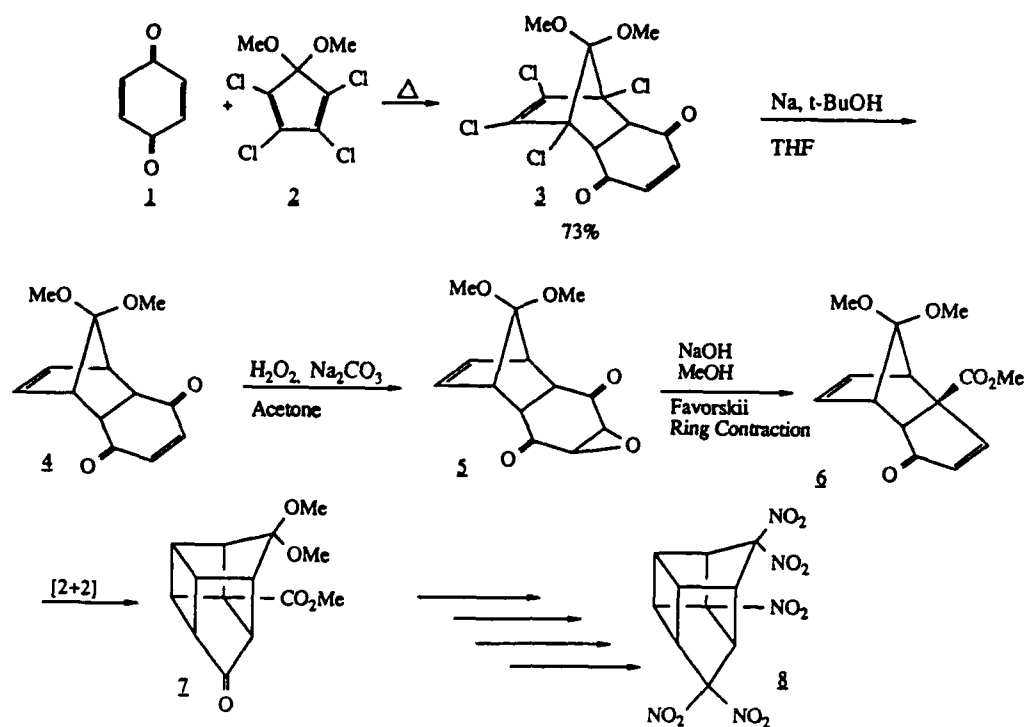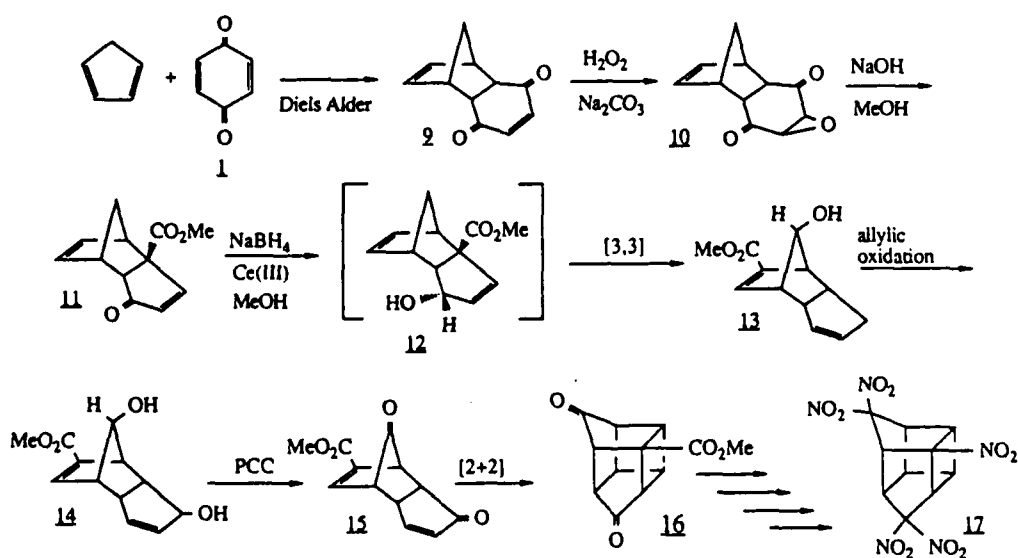
III. ROUTE A , SYNTHETIC INVESTIGATIONS:

Attention was first directed toward obtaining the dechlorination product 4. It was found that Prinzbach's conditions afforded only the aromatized dihydroquinone 18 when 3 was refluxed with sodium, t-butanol in tetrahydrofuran (Na, t-BuOH, THF) see Scheme 5. The aromatic product could be obtained in 34% yield after an hour at ambient temperature with apparently no dechlorination occurring. Formation of the dihydroquinone species could be observed by TLC at temperatures as low as -35°C. Although the dihydroquinone species could conceivably be converted back to the quinone oxidation state, this molecule would no longer be of use as it would have an additional double bond.

SCHEME 5
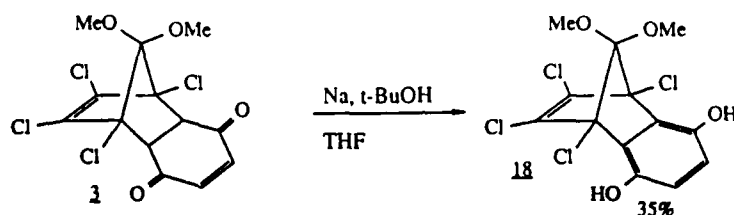
It was thought that aromatization could be precluded by attempting a dechlorination on a protected quinone moiety, such as 20, formed by a Diels Alder reaction between tetrachlorocyclopentadiene dimethyl acetal and 1,4-benzoquinone dimethyl diketal (Scheme 6). The dimethyl diketal could then be selectively deprotected and the synthesis carried out as previously outlined. Protected bridge ketones have been shown to be more resilient to deprotection than their quinone counterparts and require stronger acidic conditions for removal of the protecting group.[4]

SCHEME 6

22-8
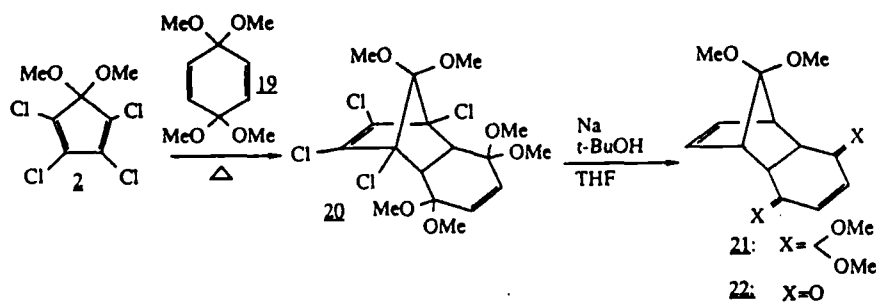
Unfortunately, reaction of 2 and the protected quinone 19, when refluxed for 24 hours in toluene, afforded a large quantity of what appeared spectroscopically to be a dimer of benzoquinone dimethyl diketal. NMR and IR data also indicated that the quinone system had again aromatized. This result was further investigated by refluxing 19 alone in toluene over a 24 hour period, however, no reaction was observed. An impurity in the tetrachlorocyclopentadienone dimethyl acetal must catalyze the reaction or the molecule itself is involved in mediating the dimerization.

The tendency for quinone monoketals to undergo reduction to the hydroquinone oxidation state is documented. The dimethyl monoketal is particularly prone to aromatization while the mono ethylene ketal of quinone is stable at 180°C for 24 hours.[8] It was decided to use the bisethylene ketal in the initial Diels Alder reaction on the assumption that the aromatization trends for the monoketals also applied to the corresponding bisketals. The Diels Alder reaction conditions (refluxing toluene) were well within the described temperature boundary.

The bisethylene ketal was prepared by transketalization[8] of benzoquinone dimethyl diketal 19 in 58% yield and was subsequently reacted with tetrachlorocyclopentadienone dimethyl acetal. No product formation occurred. Reaction of these same reagents in a sealed ampule heated at 140 - 170 °C for 24 hours produced a black polymer-like material. A white solid was isolated from the reaction mixture, the structure of which remains unidentified.

An alternative to use of a protected quinone to preclude aromatization in the dechlorination step was to selectively hydrogenate the double bond on the quinone, thereby eliminating a handle by which aromatization could take place. The double bond could then be re-inserted after dechlorination had taken place by use of reagents such as benzene selenic anhydride. Keinan's group had used zinc chloride ($ZnCl_2$) with diphenylsilane (Ph_2SiH_2) and a palladium (0) catalyst to reduce conjugated carbonyls.[9] Attempts to reduce compound 3 under these conditions once again resulted in formation of the dihydroquinone 18 in 40% crude yield! While other methods for selectively reducing enones were available, it was decided that the tendency for the quinone system to aromatize was too much to contend with and work was begun on Route B.

IV. SYNTHETIC STUDIES, ROUTE B:

The chemistry for Route B (Scheme 4) had been worked out by Dr. Suri up to the allylic oxidation of 13. Scheme 7 depicts the one step allylic oxidations that were attempted on the rearrangement product 13. Endocyclic allylic oxidations of small ring systems with selenium dioxide (SeO_2) and t-butylhydroperoxide (t-BuOOH) to afford allylic alcohols are notoriously difficult [10] and it was found that our system was no exception. An attempted chromium hexacarbonyl ($Cr(CO)_6$)[12] oxidation of 13 directly to the diketone proceeded in extremely low yield.

SCHEME 7
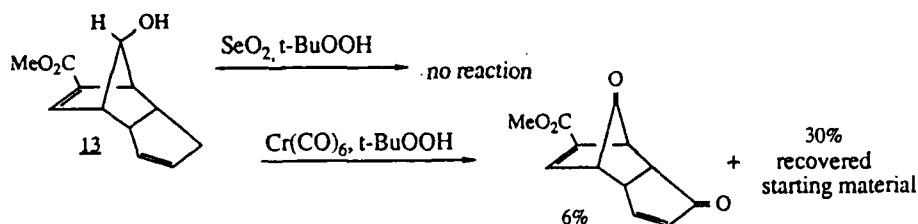
Other approaches to the diketone were considered at this time. These proposed conversions are shown in Schemes 8 and 9. Scheme 8 shows a possible three step transformation of 13 to the diketone 15 via allylic bromination. Bromination of 13 with N-bromosuccinimide (NBS) gives the allylic bromide 23 which is hydrolyzed under acidic conditions to afford the corresponding alcohol 14 and possibly its allylic isomer. The very mild acidic conditions necessary for this transformation should not affect the carbomethoxy ester. Oxidation of the allylic alcohol 14 yields the desired diketone. Another potential route to the diketone 15 is depicted in Scheme 9 and begins with epoxidation of 13 with m-chloroperbenzoic acid (MCPBA). Allylic alcohol 25 is expected to be the product of treatment of epoxide 24 with lithium diisopropylamine (LDA). Diketone 26 formed by PCC oxidation of compound 25, is an isomer of the diketone formed by the conversion shown in Scheme 8. The pentanitrobishomocubane ultimately formed by this route is a positional isomer of that formed by the allylic bromination route.

SCHEME 8
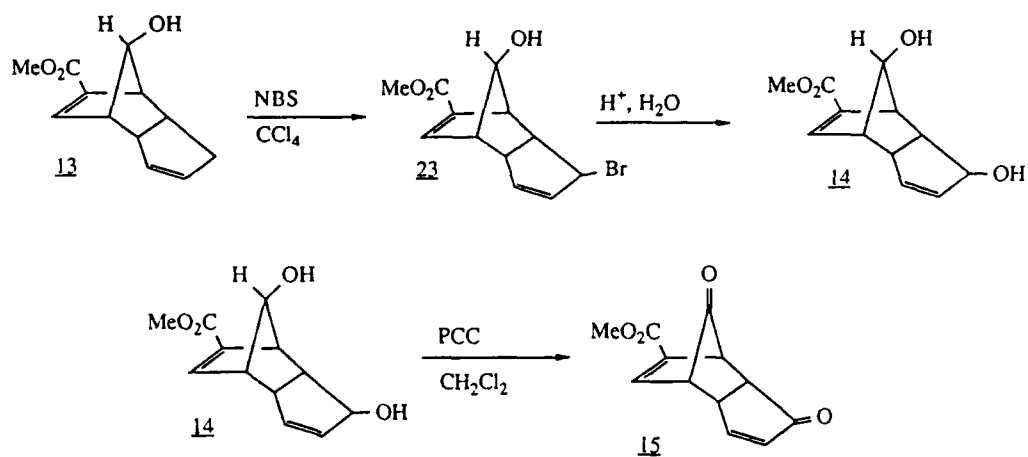
SCHEME 9
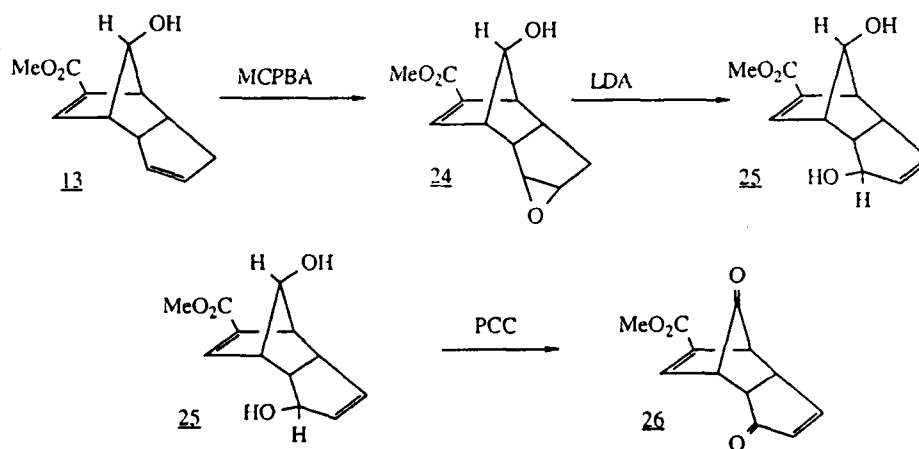
Allylic bromination of compound 13 using NBS was attempted. An IR spectrum of the main product showed no OH stretch, indicating that the hydroxy group on the bridge had probably been replaced by a bromine. If this route were pursued, the hydroxy group must be oxidized first to prevent bromination of the bridge.

Fortunately, at this juncture, a reference noting the use of SeO_2 in refluxing dioxane/water for allylic oxidation on a system strikingly similar to ours was discovered.[11] When compound 13 was subjected to these conditions, the coveted allylic alcohol was obtained in 48% yield! The yield can be improved with modification of the reaction conditions and method of purification. Access to the allylic alcohol 14 is crucial to the success of the synthesis of pentanitrobishomocubane shown by Route B (Scheme 4). All of the other steps of the synthesis are considered to be straightforward or have precedence from the synthesis of other analogs of bishomocubane.

V. RECOMMENDATIONS:

A preliminary photocycloaddition reaction was attempted on alcohol 14 prior to oxidizing it to the ketone. The NMR and IR data obtained for one of the isolated products looks promising for a cage compound but more work is required to confirm this. A small scale PCC oxidation of the diol 14 appeared to result in the oxidation of only one of the hydroxy groups. The bridge hydroxy group is likely the more resistant to oxidation of the two alcohols as incorporation of an sp^2 center on the bridge would be more difficult than on the five membered ring. It still must be determined whether the [2+2] cycloaddition will work better on the diketone precursor 15 or on the diol 14. Plans call for Dr. Suri to work out the photocycloaddition step and then to complete the synthesis of pentanitrobishomocubane by elaboration of the ketone and carbomethoxy functionalities to five nitro groups using established methodology.[3] Scheme 10 details this synthesis using the diketone as the precursor for cycloaddition.

Further plans for research with the receipt of a mini-grant would center on using the key precursor, diol 14, in the synthesis of a tetranitrohomocubane system. No polynitrohomocubane molecules are known.[1] Such a system is interesting because its carbon skeleton is probably more strained than that of the bishomocubane molecule as it lacks one of the methylene groups. Scheme 11 shows the proposed synthesis. Selective epoxidation of the five membered ring on 15 with MCPBA provides the epoxide 27. A

Favorskii ring contraction on <u>27</u> to extrude one carbon of the skeleton occurs next. The molecule now has <u>two</u> carbomethoxy groups that can be fashioned into nitro groups. Photocycloaddition of <u>28</u> affords the homocubane cage molecule. The carbomethoxy moieties and the ketone can now be transformed into nitro and geminal di-nitro species respectively by use of the same methodology shown in Scheme 10 for pentanitrobishomocubane. It is also possible to make a different positional isomer of tetranitrobishomocubane using a different diketone as the precursor, such as compound <u>26</u> generated in the synthesis outlined in Scheme 9. The use of these tetranitrohomocubane molecules as fuel additives could be studied and compared to similar findings for other polycyclicpolynitro cage compounds.

SCHEME 10

SCHEME 11

MeO$_2$C ... $\xrightarrow{\text{MCPBA}}$ ... $\underline{27}$ $\xrightarrow[\text{Favorskii Ring Contraction}]{\text{NaOH, MeOH}}$ ... $\underline{28}$

$\underline{15}$

$\underline{28}$ $\xrightarrow{[2+2]}$

Tetranitrohomocubane

$\underline{26}$
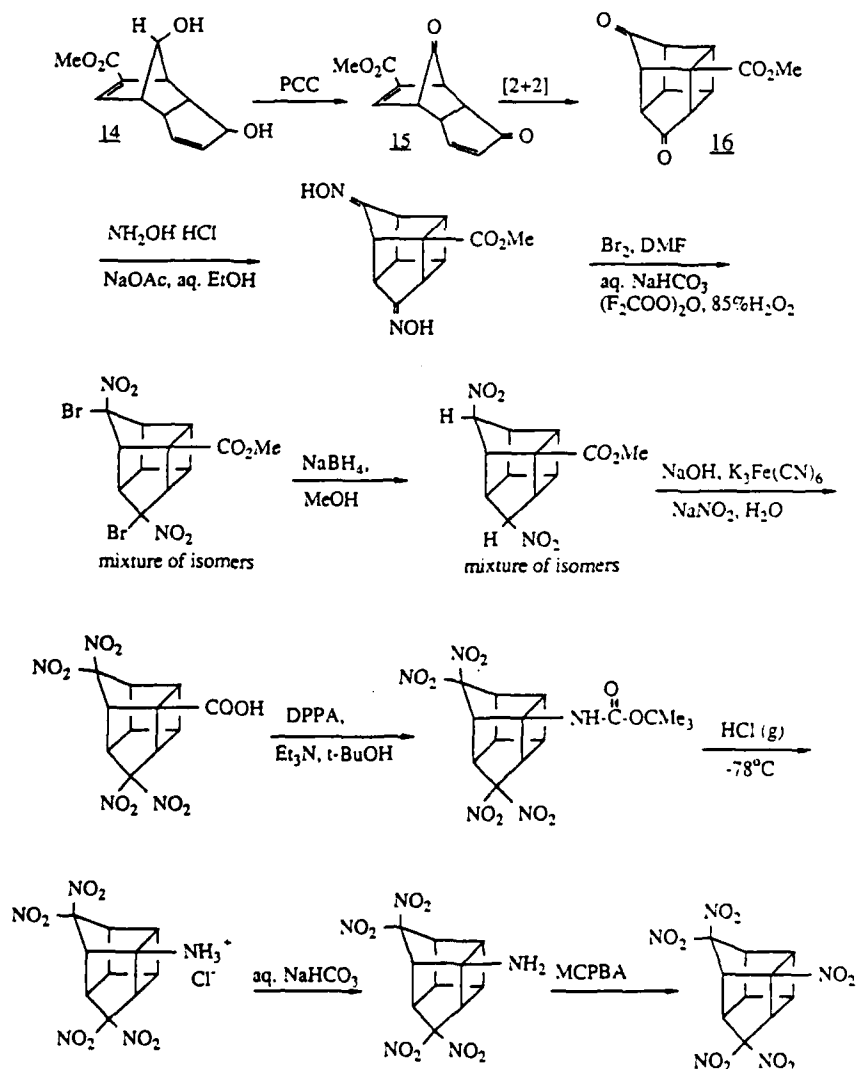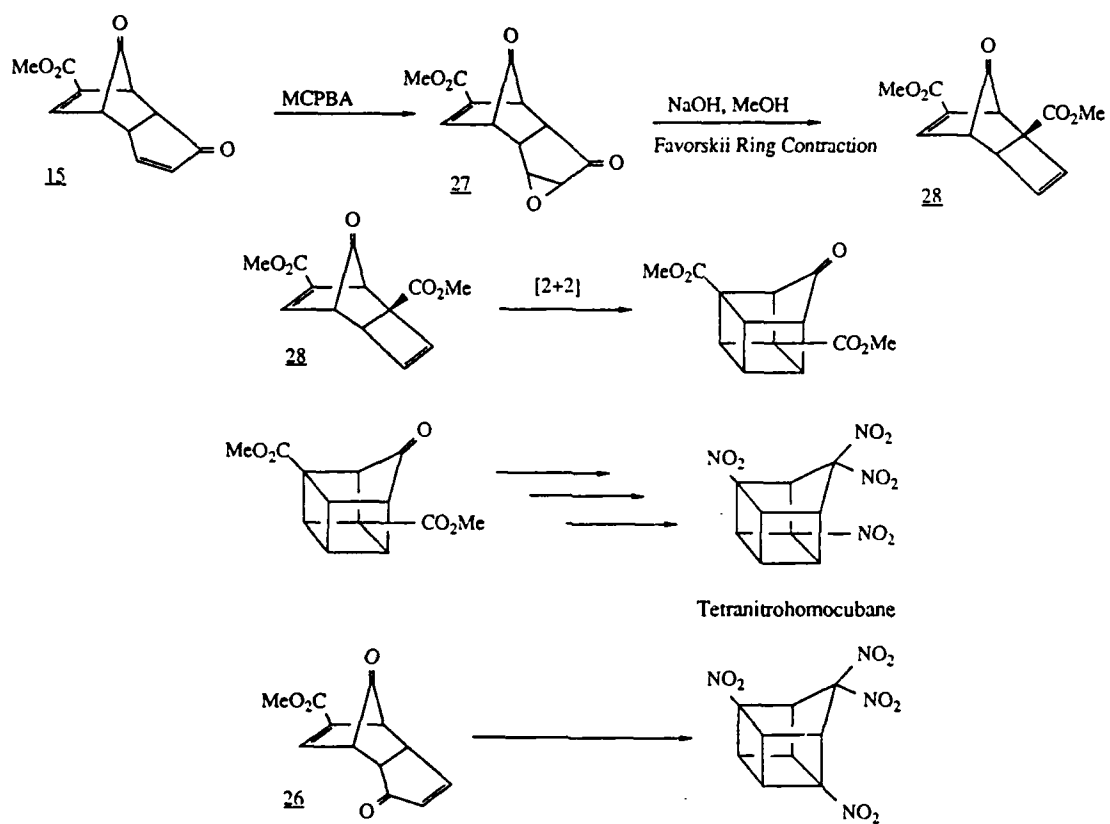
REFERENCES

1.   Marchand, A.P.; Tetrahedron, 1988, 44, 2397-2395.

2.   Marchand, A.P., Arney, B.E., Dave, P.R., and Rajapaksa, D., "New Polynitropolycylic Energetic Materials", Seventh Annual Working Group Meeting on Synthesis of High Energy Density Materials, Parsippany, New Jersey, June, 1988, pp. 365-405.

3.   Marchand, A.P., Suri, S.C.; J. Org. Chem., 1984, 49, 2041-2043.

4.   Marchand, A.P., Reddy, D.S.; J. Org. Chem., 1984, 49, 4078-4080.

5.   Marchand, A.P., Chou, T.; J. Chem. Soc. Perkin I, 1973, 1948-1951.

6.   Fessner, W.D., Sedelmeier, G., Spurr, P.R., Rihs, G., Prinzbach, H.; J. Am. Chem. Soc., 1987, 109, 4626-4642.

7.   Suri, S.C., Rodgers, S.; Tett. Lett., 1988, 29, 4031-4034.

8.   Capparelli, M.P., Swenton, J.S.; J. Org. Chem., 1987, 52, 5360-5364.

9.   Keinan, E., Greenspoon, N.; Tett. Lett., 1985, 26, 1353-1356.

10. Sharpless, K.B., Verhoeven, T.R.; Aldrichimica Acta, 1979, 12, 63-74.

11. Takano, S., Inomata, K., Ogasawara, K.; J. Chem. Soc. Chem. Comm., 1989, 271-272. See also: Rosenblum, M.; J. Am. Chem. Soc., 1957, 79, 3179.

12. Pearson, A.J., Chen, Y.-S., Han, G.R., Hsu, S.-Y., Ray, T.; J. Chem. Soc. Perkin Trans. I., 1985, 267-273.

1989 USAF-UES SUMMER FACULTY RESEARCH PROGRAM

Sponsored by the

AIR FORCE OFFICE OF SCIENTIFIC RESEARCH

Conducted by the

Universal Energy Systems, Inc.

FINAL REPORT

THE PREPARATION OF POLY(IMIDE SILOXANE) POLYMERS:

OXYGEN RESISTANT SPACE POLYMERS

Prepared by: Mark A. Kirms

Academic Rank: Assistant Professor

Department and University: Chemistry Department, Southern Oregon State College

Research Location: Astronautics Laboratory, Edwards AFB

USAF Researcher: Dr. Jeff Gilman

Date: August 27, 1989

Contract No: F49620-88-C-0053

THE PREPARATION OF POLY(IMIDE SILOXANE) POLYMERS:

OXYGEN RESISTANT SPACE POLYMERS

by

Mark A. Kirms

ABSTRACT

Benzophenonetetracarboxylic dianhydride (BTDA) was condensed with several aniline systems possessing siloxane moieties in the 3-position of the aromatic amine. The aniline derivatives were prepared in a series of steps sarting with 3-bromoaniline. The poly(imide siloxane) copolymers produced from these condensation reactions have been shown to be high performance polymeric materials which are resistant to oxygen degredation. Degradation of materials by oxygen is a concern for spacecraft flying in Low Earth Orbit (LEO). It was discovered that two independent routes could be used to obtain the desired poly(imide siloxane) copolymers. Self-condensation of silanol diimide monomers, as well as imidization of diamines with BTDA, gave desirable copolymeric material. In addition to the poly(imide siloxane) copolymers, routes were explored for the preparation of siloxane- graft poly(imide siloxane) copolymers.

Acknowledgments

It is with much gratitude that I acknowledge the sponsorship of the Air Force Systems Command, the Air Force Office of Scientific Research, Universal Energy Systems, Inc., and the Astronautics Laboratory, Edwards AFB. It was a pleasure to have the opportunity to work in a rapidly expanding area of chemical research. The environment at the Astronautics Laboratory was enjoyable to work in, and the personnel was very helpful and easy to get along with.

I particularly wish to thank Dr. Jeff Gilman for his help and enlightenment with the Space Polymer project, and Dr. Suresh Suri for his input and overall interest in organic chemistry. Both these men saw to it that the stay at Edwards was as smooth as possible.

I. Introduction:

The project described in these pages deals with the preparation of polymeric materials which are resistant to oxygen atom degradation. The United States Air Force is interested in such materials since it has been shown that materials on aircraft flying in Low Earth Orbit (LEO) have experienced a considerable amount of degradation due to bombardment by atomic oxygen.[1] This degradation will affect such systems as the Space Shuttle and Space Station.

Edwards AFB is one of the few installations within the Air Force which is equipped to conduct research in the field of organic chemistry. The oxygen resistant polymeric materials envisioned to meet the needs of the Air Force are organic molecules consisting of interwoven siloxane and imide monomers, and, as such, Edwards is the most likely place from which to carry out such syntheses.

My background as a synthetic organic chemist has spanned several areas of expertise. I have been involved with the synthesis and study of the physical properties of bridged annulenes, high temperature rearrangements of aromatic compounds, the synthesis of strained, small ring molecules and the utilization of these compounds in organic synthesis, and the development of methodology for the asymmetric synthesis of medium to large ring ether systems.

II. Objectives of the Research Effort:

The goal of this project was to prepare polymers which would be resistant to oxygen atom degradation as well as possess the properties associated with high performance materials. The materials chosen for preparation were copolymers consisting of a polyimide backbone with polysiloxane chains. Polyimides are high performance materials with good thermal and mechanical properties, yet, they can be insoluble in many common organic solvents. Siloxanes have the ability of rendering the polyimide soluble in organic solvents while also possessing the ability to be oxygen atom resistant.[2] The materials sought after were to have the basic structure (1) shown below:
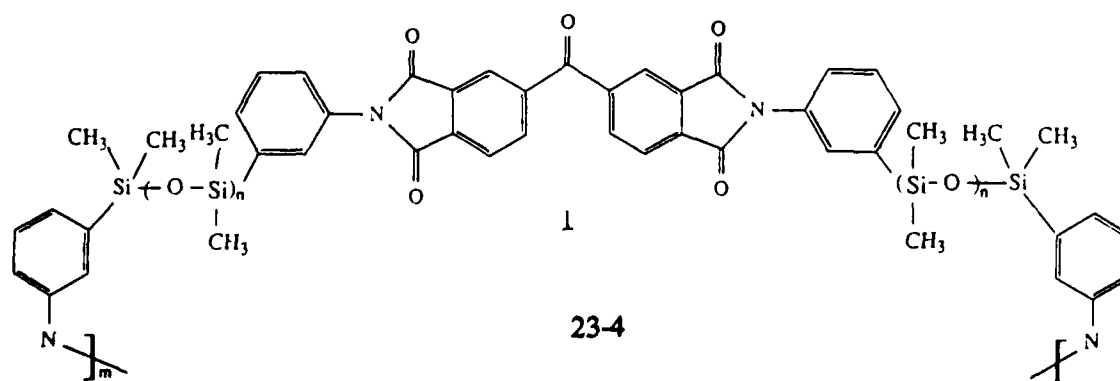
The copolymer 1 was envisioned to arise from the imidization of diamino monomer 2 with 3,3',4,4'-benzophenonetetracarboxylic dianhydride (BTDA):

2

BTDA

1
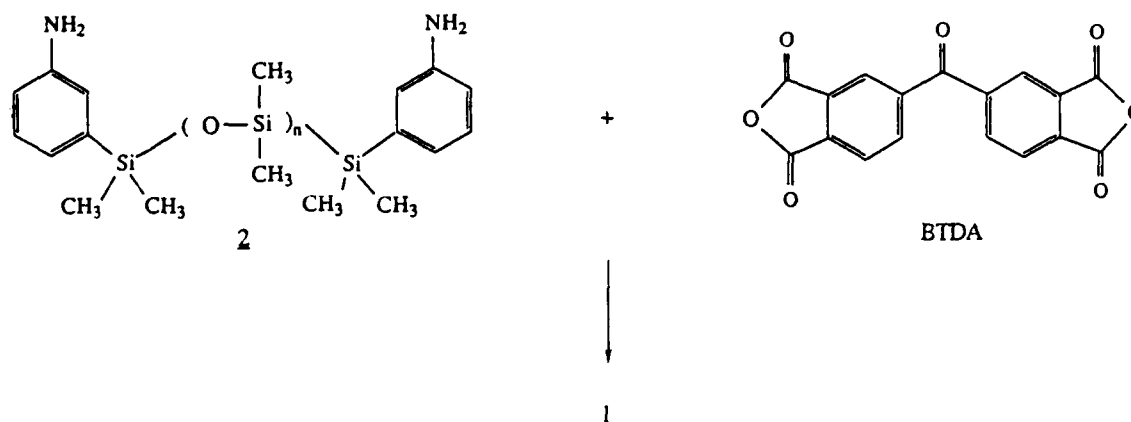
The dianhydride BTDA is commercially available. Several poly(imide siloxane) systems with a structure such as 1 could be prepared by simply varying the siloxane chain length in the diamino monomer 2. McGrath and co-workers have successfully extended siloxane chains in polymeric materials through the reaction of siloxanes with octamethylcyclotetrasiloxane (D_4):[3]

D_4
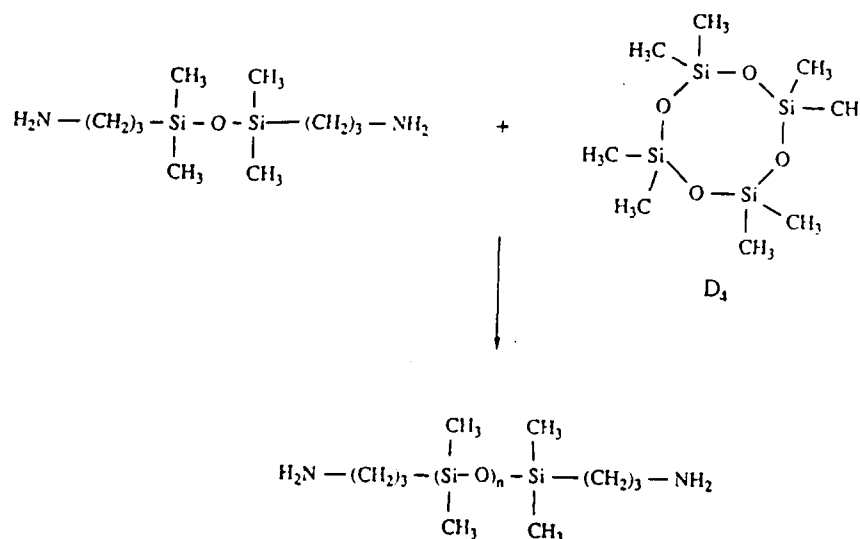
Based upon this methodology it should be possible to prepare several poly(imide siloxane) systems starting with the diamino siloxane monomer 4. Monomer 4 was envisioned to arise from (3-aminophenyl)dimethylsilanol 5, although it was not clear at the

onset of the project exactly how this transformation would be effected, which should be readily available from the commercial 3-bromoaniline:

4

5
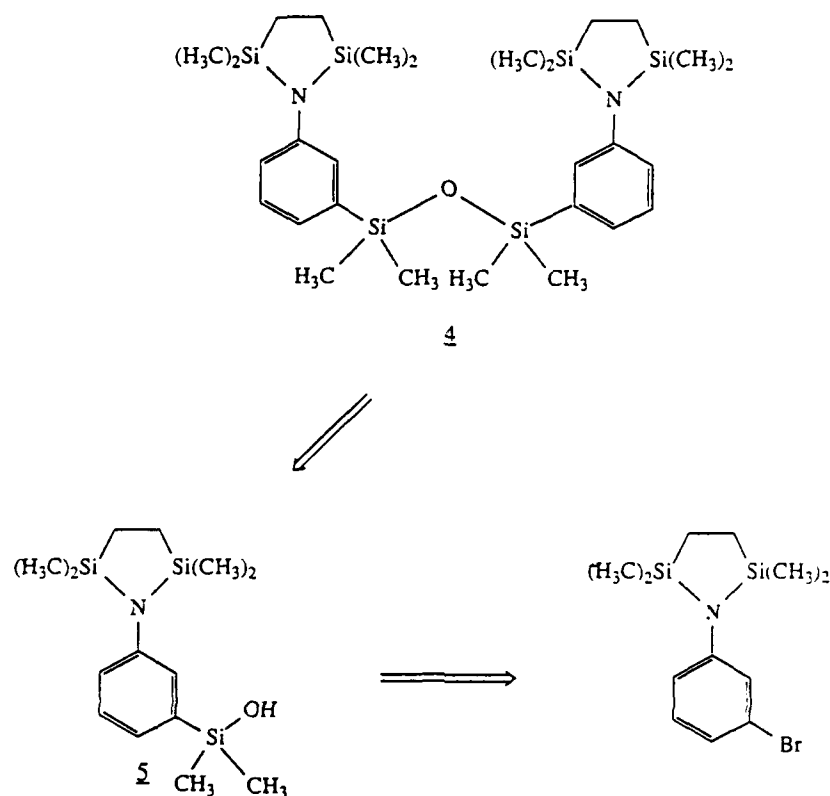
In addition to copolymers of the type **1**, grafted copolymers (**6**) were another target of investigation. These systems would provide an additional site from which siloxane chains could be extended. It was desirable to determine at what point additional siloxane would cause an overall detriment to the poly(imide siloxane) material. It has been shown that such a "saturation point" can be reached even though additional siloxane will necessarily lend better oxygen atom resistance to such materials.[4] In order to achieve the desired grafting, conversion of the ketocarbonyl of BTDA into a siloxane would be the most appropriate method for introducing such siloxane grafts. However, such an approach might be plagued by the inability to reduce the ketone in the presence of the two anhydrides. Consequently, the route shown below was envisioned for the preparation of these graft copolymers.
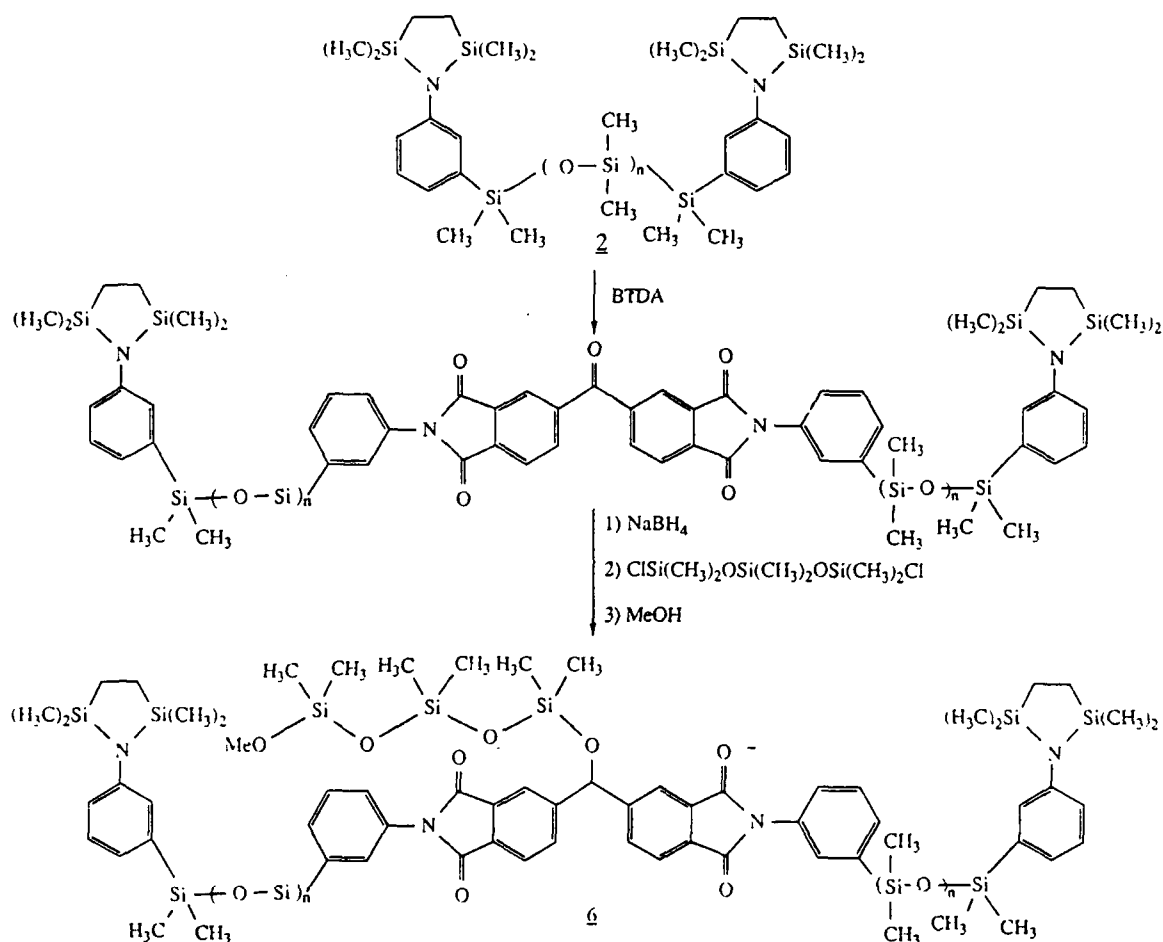
III. Approaches

3-Bromoaniline was the precursor used for most of the syntheses. In order to carry out the desired halogen/lithium exchange reaction on this molecule, it was necessary to protect the amine. Thus, 3-bromoaniline was heated with an equivalent amount of 1,1,4,4-tetramethyl-1,4-bis(N,N-dimethylamino)disilethylene to give the protected amine 7 in greater than 90% yield.[5] Compound 7 was now ready to be treated with BuLi followed by quenching of the resulting anion with chloro dimethylsilane. Depending upon the conditions employed, several products could be obtained from the reaction. The desired, and primary, product obtained from the reaction was the silane 8 as shown below:
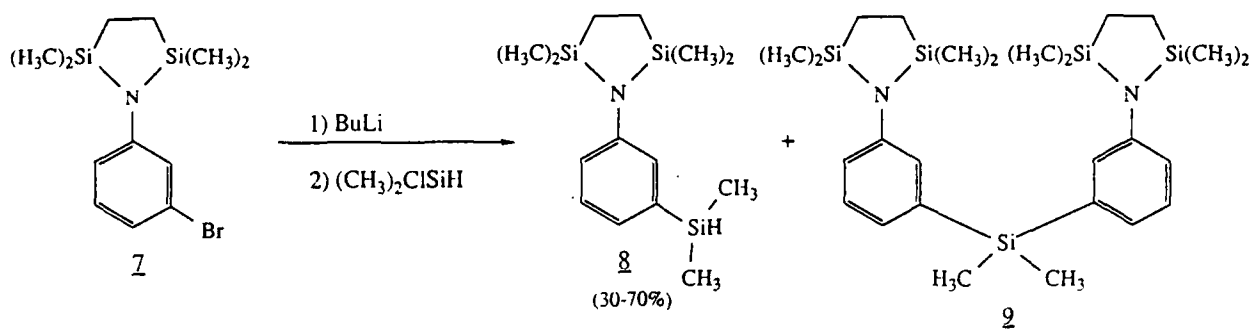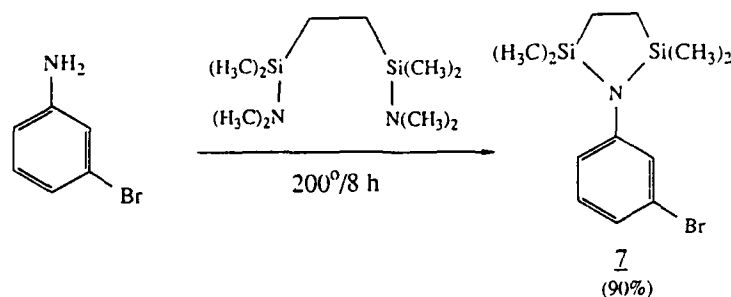
A by-product of this reaction was the dimeric silane $\underline{9}$, presumably obtained from the nucleophilic attack of the lithium anion of $\underline{7}$ upon the silane $\underline{8}$. Inverse addition of the lithium anion of $\underline{7}$ to a solution of the chloro dimethylsilane would undoubtedly result in a decreased formation of $\underline{9}$ during this reaction. Nonetheless, $\underline{8}$ could be obtained in a 70% yield. In addition to these two products, the unprotected form of $\underline{8}$, that is (3-aminophenyl)dimethylsilane ($\underline{10}$), could be obtained directly by pouring the crude reaction mixture into a saturated $NaHCO_3$ solution followed by a standard work-up. The amine protecting group, while being inert to alkyllithium reagents, appears to be quite sensitive to aqueous base and acid conditions.[6] Consequently, care must be taken during the reaction and the work-up procedure to ensure that it is not lost.
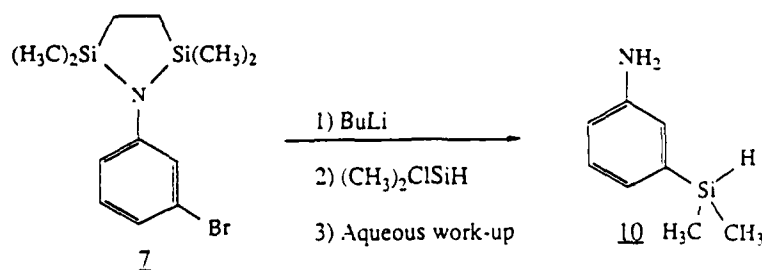
Silane $\underline{8}$ was now in a position to be converted to the corresponding silanol derivative. It was naively assumed that this transformation could be obtained by simply

heating 8 in aqueous tetrahydrofuran (THF). After carrying out a reflux overnight, the only product isolated was the partially deprotected compound 11:
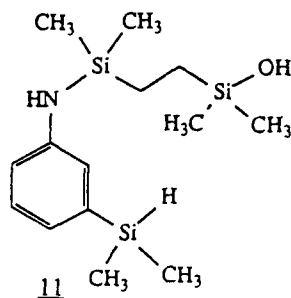
It was quite apparent from this reaction that the Si-N bond was considerably more labile than the Si-H bond, confirming once again the sensitivity of the amine protecting group to aqueous conditions. The desired transformation was effected in a less than obvious fashion using 5% Pd/C in THF.[7] It is presumed that the standard hydrogenation conditions employed will first cause dehydrogenation to occur at the silicon atom in 8 by exchange of hydride from silicon to the catalyst surface. Silanes themselves are known to be hydrogenation reagents,[8] so this is a logical assumption to make. At this point the hydride is exchanged at silicon for a hydroxy group which is present in the reaction mixture. Silanol 12 was obtained in excellent yield (98%), however, it could only be obtained once. The reaction just described was performed six times. Only once (the very first time) was 12 obtained. The other five times the desired silane to silanol transformation occurred, but the amine protecting group was also lost to give the deprotected form of the molecule 13. Amine 13 was obtained in an equally good yield. All the reagents employed to carry out the reaction were freshly prepared, however, no change in the outcome of the reaction occurred. No explanation can be given at this time why the desired protected molecule 12 was obtained only once.

(H₃C)₂Si — Si(CH₃)₂
N

8 H₃C CH₃ Si H

Pd/C
THF/ph=7

NH₂

13 H₃C CH₃ Si OH

Pd/C,
THF/ph=7

(H₃C)₂Si Si(CH₃)₂
N

12 H₃C CH₃ Si OH
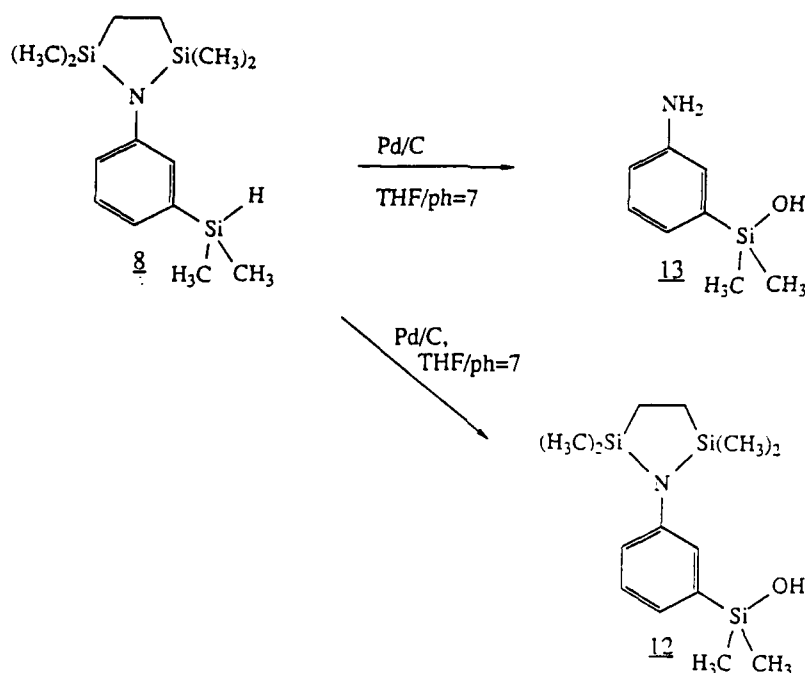
At the time that silanol 12 was prepared it was not known how to condense it to give the desired diamino monomer 4. As an alternative way of achieving the envisioned goal, 12 was reacted with 1,3-dichlorotetramethyldisiloxane to afford the diamino monomer 14 in a somewhat disappointing yield of 13%. As noted in Scheme I, the protecting group was lost, however, it is believed that it was lost during the work-up and not during the reaction. Diamine 14 was in a position to be reacted in several ways. The siloxane chain could be extended by reaction with D₄ as previously mentioned. Considering the amount of material obtained, it was decided to simply carry out the polymerization of 14 with BTDA. Initially one equivalent of BTDA was reacted with 14. This formulation was chosen so that the polymer obtained would have amine groups located at the termuni of the polymer allowing for further polymerization if desired. The reaction was followed by TLC which showed the presence of a new compound below the starting diamine monomer. After refluxing in chlorobenzene for several hours there appeared to be a 1:1 mixture of this new material and the starting diamine 14. Consequently, another equivalent of BTDA was added to the reaction mixture. This caused an immediate disappearance of the new material that had been developing in the reaction mixture as well as a disappearance of the remaining starting material. What remained according to TLC was a new compound which was quite reluctant to move off the base-spot of the TLC slide. The material isolated was a bright yellow, plastic-like film. From the spectral data so far obtained (IR and ^{1}H NMR) it appears the structure of the polymer (15)

is that shown in Scheme I. It is assumed that this poly(imide siloxane) is end capped with anhydride groups according to the formulation used in the preparation of the material.

Scheme I.
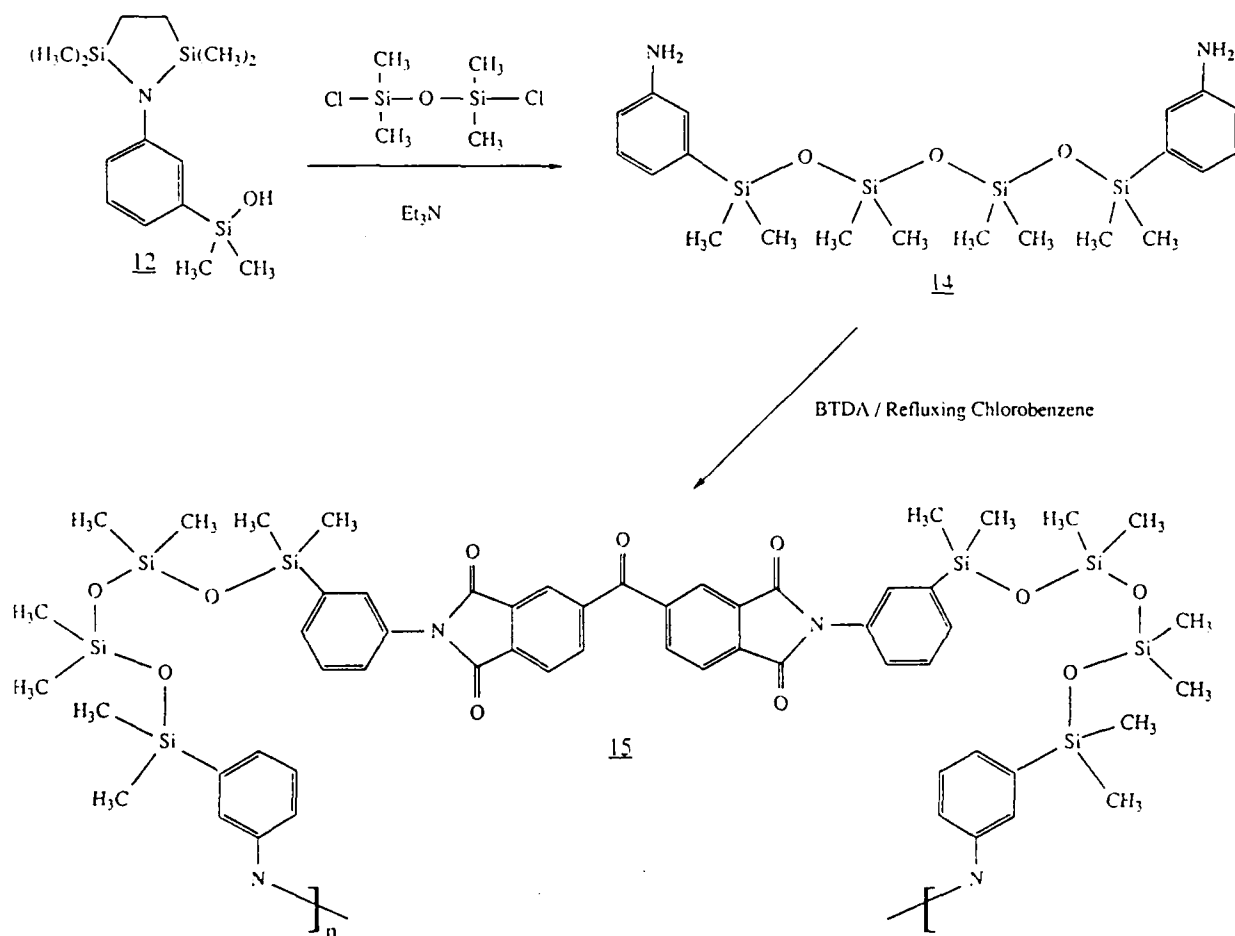
The conditions for the imidization (i.e. refluxing chlorobenzene) were arrived at during preparation of model compounds for studies on graft polymers. It was decided that the reaction of protected amine 7 with BTDA would yield a diimide from which studies could be conducted on the conversion of the ketone carbonyl to a siloxane chain. This would enable the prepartion of graft copolymers. An initial attempt to carry-out the imidization in refluxing toluene[7] met with no success owing to the insolubility of BTDA in toluene. Attention was turned to the solvent 1,2-dichloroethane since it was found to dissolve BTDA when warm. The result of refluxing 7 with BTDA in 1,2-dichloroethane was the amic acid 16 and not the diimide 17. Diimide 17 was obtained by refluxing 16 in chlorobenzene. It was reasoned that full imidization did not occur in 1,2-dichloroethane

because the temperature was not high enough. Consequently, refluxing chlorobenzene provided enough energy to achieve imidization(the difference in boiling points between 1,2-dichloroethane and chlorobenzene is 83° and 132°). The conversion of 7 to 17 is shown in Scheme II.

Scheme II.
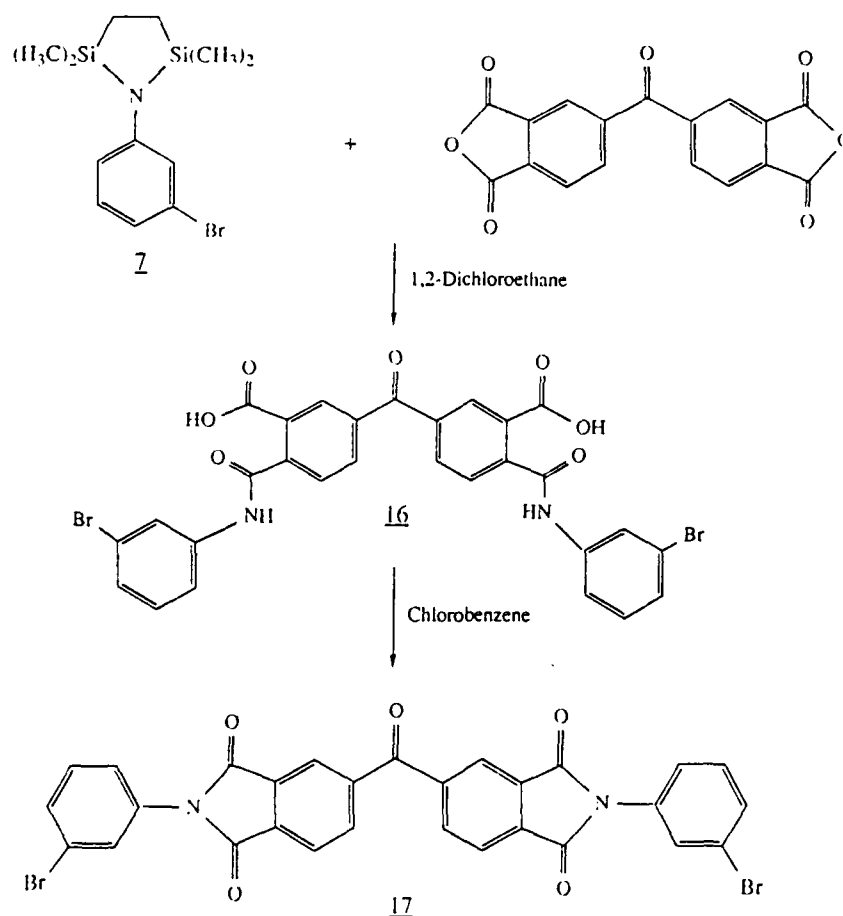
An attempt was made to convert the ketone of 17 to a siloxane group by the reaction of 17 with NaBH4 followed by the addition of 1,3-dichlorotetramethyldisiloxane to the resulting anion and finally the addition of methanol as shown below. The envisioned product, 18, could not be positively identified from the soluble products which were isolated. The majority of material recovered from the reaction was the starting material 17. Diimide 17 is unfortunately not particularly soluble in most organic solvents, and as a result the reaction was for the most part heterogeneous.
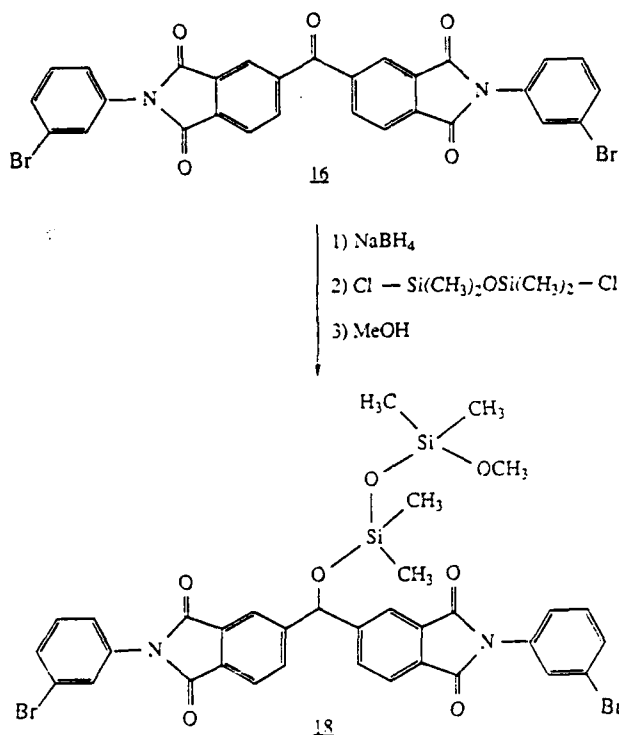
Although the goal of preparing a poly(imide siloxane) copolymer had been realized in the preparation of 15, the likelihood of making more of the material was remote. Copolymer 15 was prepared from the reaction of BTDA and diamino monomer 14. Unfortunately, repeated attempts to obtain 12, the precursor to 14, had failed to yield anything but the unprotected form of the molecule (13). It was necessary at this juncture to convert 13 into a profitable monomer for polymerization. The possibility existed to reprotect the amine group of 13, however, there was little chance that this would be a clean reaction since 13 possesses two nucleophilic sites which may react with the required 1,1,4,4-tetramethyl-1,4-bis(N,N-dimethylamino)disilethylene. In fact, this is the problem with 13. Any electrophilic reagent added to the molecule may reacti at oxygen or nitrogen. It was felt that under mild basic conditions electrophiles could be added to the silanol preferentially. Thus, two equivalents of 13 were reacted with one equivalent of 1,3-dichlorotetramethyldisiloxane in THF in the presence of Na_2CO_3. At first glance it appeared that no reaction had taken place according to TLC and the ^{1}H NMR taken of the crude reaction mixture recovered after work-up. The reaction was repeated using BuLi as the base and performing the reaction at -25°C with no apparent change in the outcome. Closer scrutiny of the data showed that a new compound had been made and was assigned

23-13

the structure 19 resulting from attack of the electrophile at the nitrogen atom of 13 as shown below:
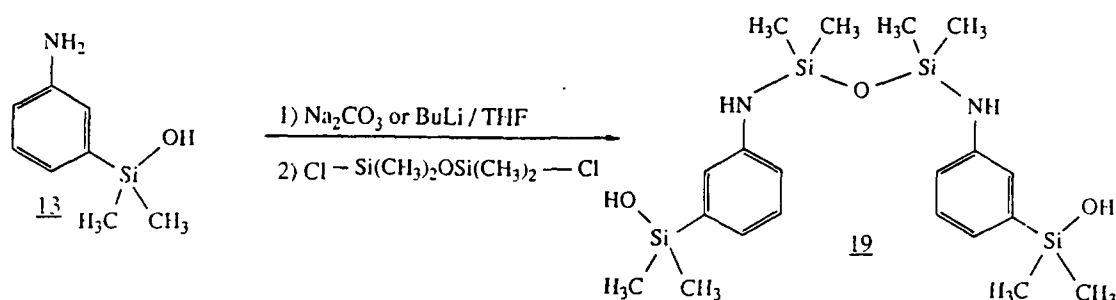
Compound 19 is not useful for the purposes of making the desired polymers. Fortunately, 19 was not the structure of the molecule isolated from the above described reactions. It was later discovered that the product obtained was the diamine 4. Apparently treatment of 13 with base will cause the self-condensation to occur. In fact, it was discovered that this self-condensation occurred by simply heating 13 in refluxing chlorobenzene or by even by allowing 13 to stand neat for several days:
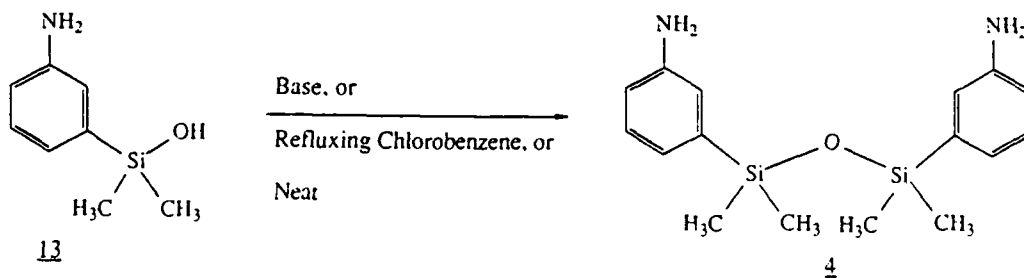
The data obtained on the product from the reaction of 13 with BTDA prompted a closer examination of the above reactions. The expected product 20 was to be used as a

monomeric species from which the desired poly(imide siloxane) copolymers could be prepared in a slightly different fashion as seen in Scheme III:

Scheme III.
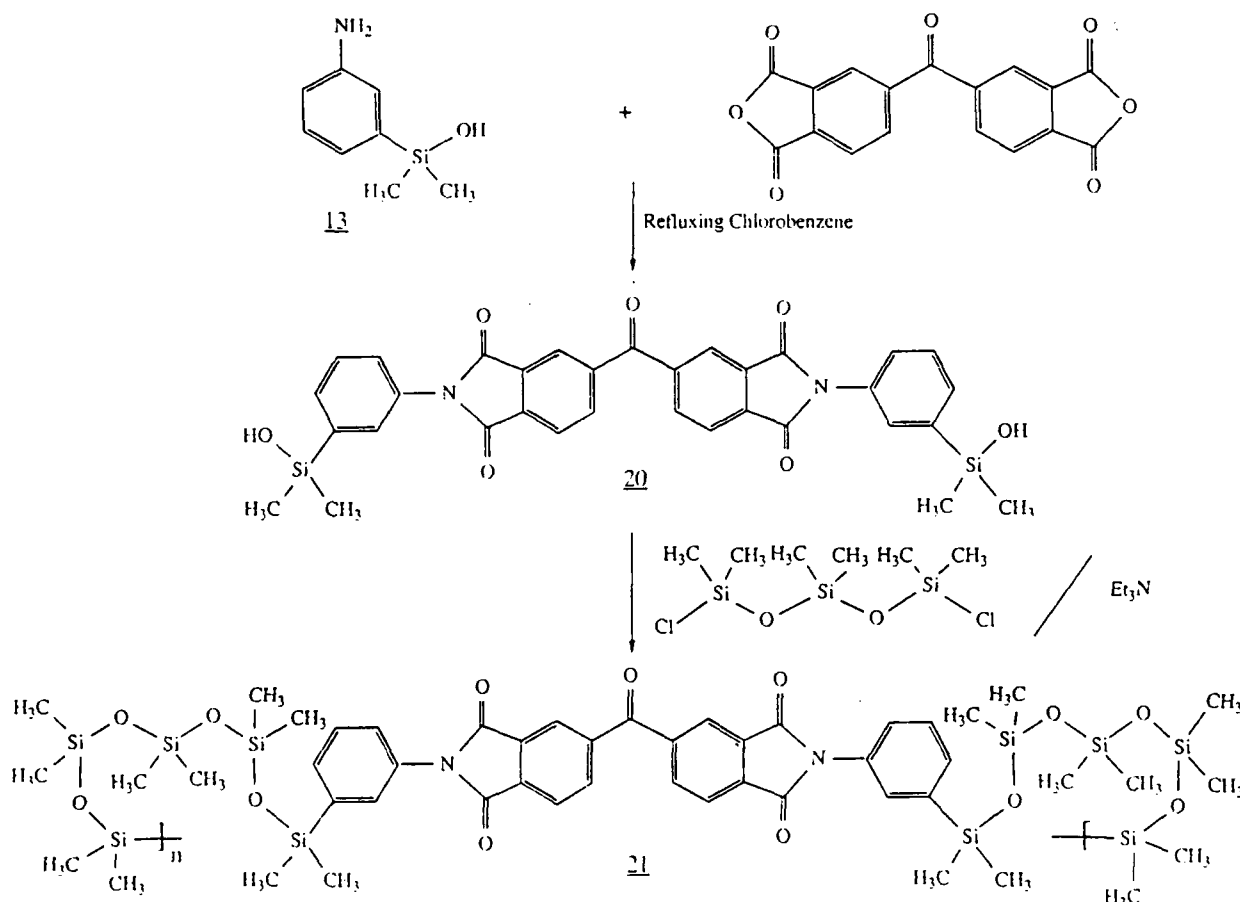
Initially it was presumed that 20 was indeed the product obtained from the reaction of 13 with BTDA, and, as a result, 20 was reacted as shown in Scheme III to obtain poly(imide siloxane) 21. The first hint that something was awry was the recovery of starting material from the reaction. Upon taking the IR spectrum of the starting material it was found that no hydroxy group was present. The ^1H NMR spectrum of the molecule indicated an imide structure with siloxane groups. It was concluded that diimide 20 had formed but had undergone self polymerization under the reaction conditions to give 22:
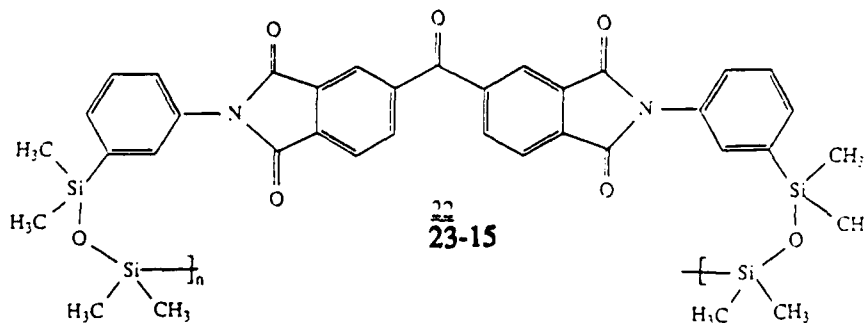
These results prompted the self-condensation reaction of <u>13</u> to give <u>14</u> and substantiate that the silanol could yield the siloxane, as well as confirming that <u>4</u> was the product obtained from the reaction of <u>13</u> in base.

IV. **Recommendations**:

The project now stands at a very convenient place. The synthesis of various poly(imide siloxane) materials can be prepared quickly from diamine <u>4</u> using McGrath's methodology for extending siloxane chains using D$_4$. The most immediate thing to do will be to vary the siloxane chain in <u>4</u> and carry out the accompanying polymerization with BTDA under refluxing chlorobenzene conditions. The materials prepared will have varying degrees of siloxanes depending upon how much D4 was reacted with <u>4</u> as shown below:
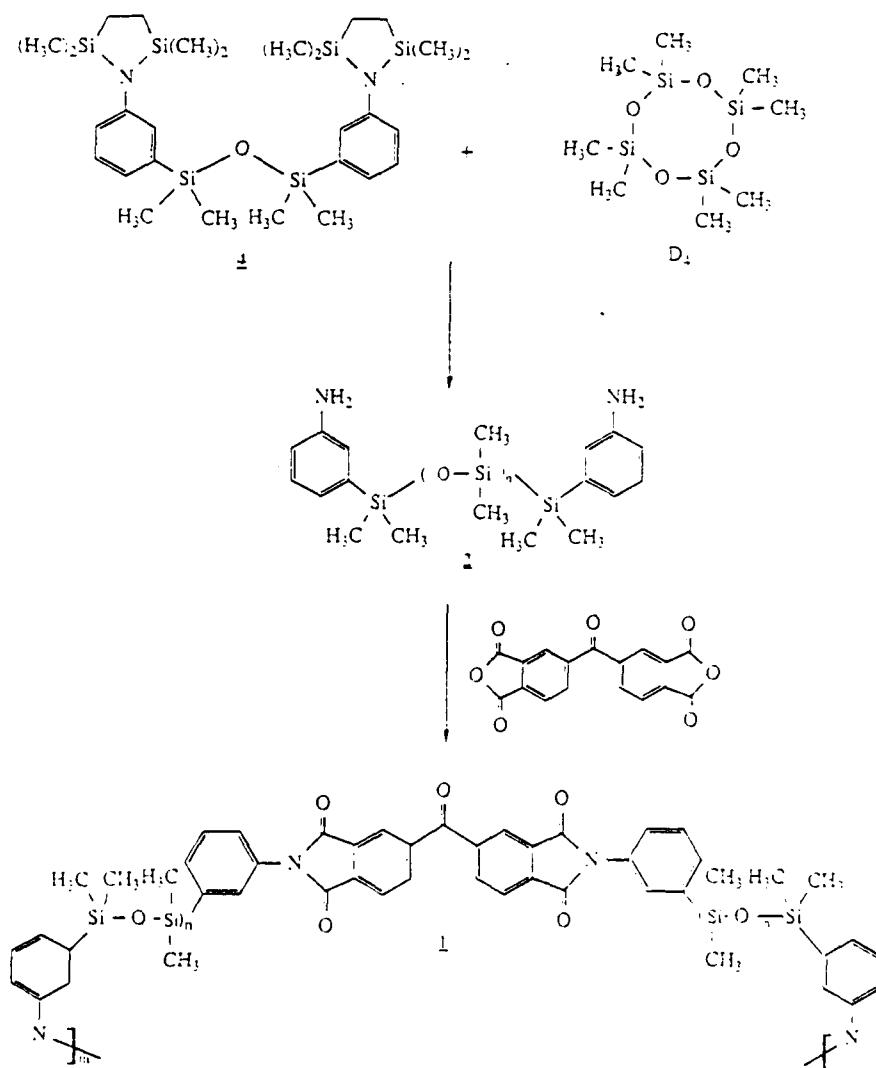
The materials prepared, along with the two polymers 15 and 22 which have already been prepared, will be submitted for testing to determine their resistance to oxygen atom degradation.

In conjunction with the above study, efforts will be directed at obtaining the graft polymers previously mentioned. This problem will be approached on two fronts. The first will be to prepare a diimide compound which is more soluble than diimide 17. Initial efforts have already been undertaken in this area. Silanol 10 has been reacted with BTDA to give tentatively the diimide silane 23 shown below:
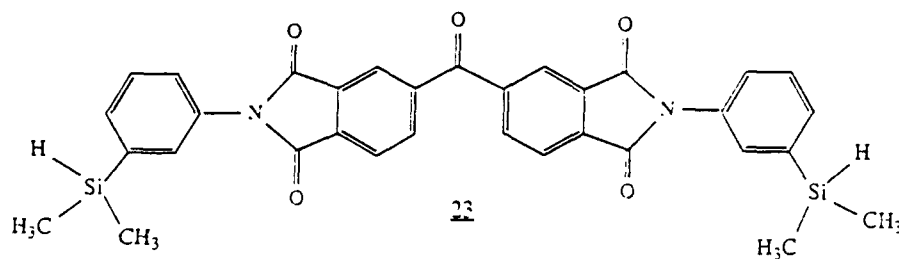
Diimide 23 is soluble in some organic solvents and should be more amenable to NaBH4 reduction than was 17. Scheme IV depicts the route envisioned for the preparation of graft poly(imide siloxane) copolymers employing diimide 23. This synthesis will allow the siloxane chains in the grafted and backbone portion of the polymer to be independently extended employing the D4 technology.

Another approach to the problem is to attempt a selective reduction of the ketone in BTDA employing reagents such as thexylborane or diisobutylaluminum hydride which have been shown to reduce ketones in the presence of other reactive carbonyls.[9] Again, this approach will allow for the two different siloxane chains within the polymer to be independently extended as shown in Scheme V.

Scheme IV.
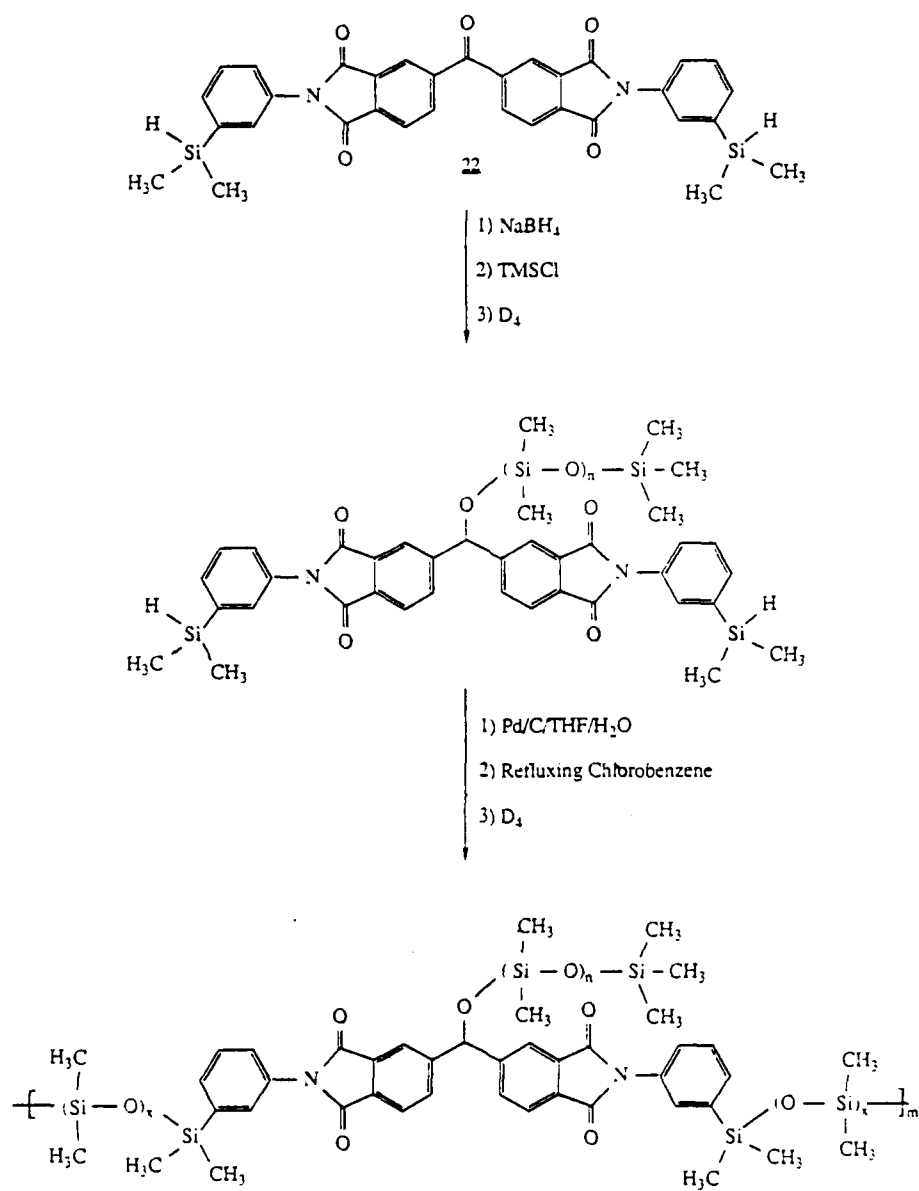
Scheme V.
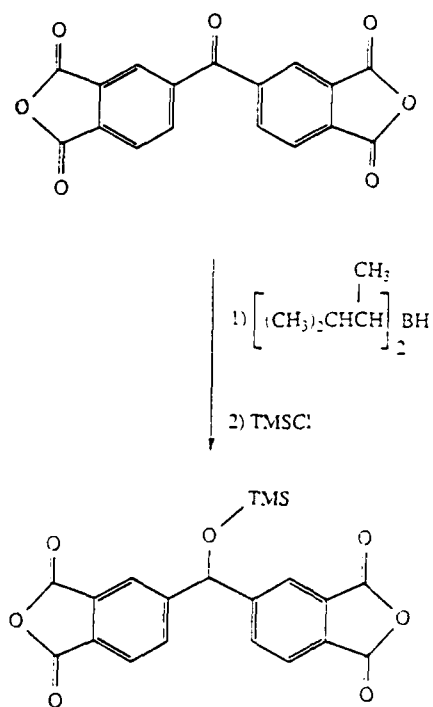
V. References

1) Leger, L. J.; Visentinet, J. T. J. Spacecraft, **1986**, 23, 505 and rteferences cited therein.

2) Arnold, C. A.; Summers, J. D.; Bott, R. H.; Taylor, L. T.; Ward, T. C.; McGrath, J. E. SAMPE Symposium No. 32, **1987**, pg. 586.

3) McGrath, J. E.; Sormani, P. M.; Elsbernd, C. S.; Kilic, S. Makromol. Chem., Macromol. Symp. 6, **1986**, 67.

4) Arnold, C. A.; Summers, J. D.; Chen, Y. P.; Bott, R. H.; Chen, D.; McGrath, J. E. Polymer, **1989**, 30, 986.

5) Gugenheim, T. L. Tetrahedron Letters, **1984**, 25, 1253.

6) Djuric, S.; Venit, J.; Magnus, P. Tetrahedron Letters, **1981**, 22, 1787.

7) Dougherty, T. K. personal communication.

8) Colvin, E. W. "Silicon in Organic Synthesis", Butterworths Monographs in Chemistry and Chemical Engineering, London, **1981**.

9) a) Brown, H. C.; Bigley, D. B.; Arora, S. K.; Yoon, N. M. J. Am.Chem.Soc., **1970**, 92, 7161. b) Masamune, S.; Seider, R. T.; Wilson, K. E. J. Chem. Soc.,Chem. Commun. **1970**, 213.

1989 USAF-UES SUMMER FACULTY RESEARCH PROGRAM

GRADUATE STUDENT RESEARCH PROGRAM

Sponsored by the

AIR FORCE OFFICE OF SCIENTIFIC RESEARCH

Conducted by the

Universal Energy Systems, Inc.

FINAL REPORT

NUMERICAL PRESENTATION OF STRESS ANALYSIS, DESIGN AND FRACTURE MECHANICS FOR COMPOSITE MATERIALS AND STRUCTURES

Prepared by:	Faysal A. Kolkailah, Ph.D., P.E.
Academic Rank:	Professor
Department and	Aeronautical Engineering
University:	Cal Poly, San Luis Obispo
Research Location:	Astronautics Laboratories Edwards AFB Edwards, CA 93523
USAF Researcher:	Jim A. Koury
Date:	28 September, 1989
Contract No:	F49620-88-C-0053

NUMERICAL PRESENTATION OF STRESS ANALYSIS, DESIGN AND FRACTURE MECHANICS FOR COMPOSITE MATERIALS AND STRUCTURES

by

Faysal A. Kolkailah, Ph.D., P.E.

ABSTRACT

With an ultimate goal of identifying areas for development of mutual interest for the government, industry and the University for better understanding the finite element approach to analyze and to design composite structures, a research and a survey of the finite element codes was carried out. Also, different fracture mechanics methods coupled with a finite element code were employed to study the stress intensity factor for crack propagation. The results obtained are in a general agreement with the analytical solutions.

ACKNOWLEDGEMENTS

I would like to thank the Edwards Air Force Astronautic Laboratory for sponsorship of this research. Also, I wish to express my thanks to Universal Energy Systems for their directional and administrative help and support.

I would like to take this opportunity to express my deep gratitude to both Mr. Jim Wanchek and Mr. Jim Koury for their technical support and help during the course of this research effort. I enjoyed very much working with such a fine group in an excellent environment of teamwork. Special thanks are due to everyone at the Composite Lab for their patience and support during this summer.

I. INTRODUCTION

1.   Finite Element Methods

The Finite Element Method (FEM) is one wherein the difficulty of mathematically solving large complex geometric problems, such as the stress analysis of jet transport aircraft, is transformed from a differential equation approach to an algebraic problem, wherein the building blocks or finite elements have all the complex equations solved for their simple shape (say a triangle, rod, beam, etc.). In their formulation, the behavior of each element is represented by an element to the nodal displacements. The representation of the relationships of these important variables for the little, but not infinitesimal, elements is determined through a Rayleigh-Ritz approach just for each element. In contrast to the conventional matrix analysis, in which the relations between forces and displacement are derived exactly, the solution for the elements utilizes only approximately displacement functions within each element. Once this is done, a matrix, which represents the element, of size equal to the number of unknowns for the element can be produced. This is now a linear algebraic relation and not a differential equation. The entire problem can thus be cast as a larger algebraic equation by assembling the element matrices within the computer in much the same way that the real problem is built with many simple pieces of material.

The finite element method is, then, a technique of using local, approximate solutions to build up a solution for an entire domain. The key here is the simplicity and elegance of the approach.

The basic premise of the finite element method is that the solution region can be analytically modeled or approximated by replacing it with an assemblage of discrete elements. Since these elements can be put together in a variety of ways, they can be used to represent exceedingly complex shapes. This allows the finite element method unlimited scope and applicability in terms of geometry, parameter, or type of problem. The finite element model gives a better approximat   to the region and requires fewer

nodes as compared to the finite difference method. Also, a better approximation to the boundary shape results because the curved boundary is represented by a series of straight lines. Huebner [1] makes the statement that "The finite element method is particularly well suited for problems with complex geometries.

2.   Fracture Mechanics

The strength of any material is inherently related to flaws which are always present. Specifically, the strength of composites are governed by their flaw-initiated characteristics. From that, one can see that the mechanics of fracture including crack propagation are of extreme importance in the design analysis of composite structures. Fatigue and fracture mechanics criteria are now a part of every airplane design.

Consider a structure in which a crack develops. Due to the application of repeated loads or even a monotonic loading combined with the effects of environment and time, this crack will grow in time. The longer the crack, the higher the stress concentration induced by it. This implies that the rate of crack propagation will increase with time. Due to the presence of the crack the strength of the structure is decreased. The residual strength of the structure decreases progressively with increasing crack size. After a certain time, the residual strength will have become so low that the structure cannot withstand accidental high loads that may occur in service. From this moment on, the structure is liable to fail. If accidental high loads do not occur, the crack will continue to grow until the residual strength has become so low that fracture occurs under normal service loading. Many structures are designed to carry service loads that are high enough to initiate cracks, particularly when pre-existing flaws or stress concentrations are present. The designer has to anticipate this possibility of cracking and consequently he has to accept a certain risk that the structure will fail. This implies that the structure can have only a limited lifetime. Of course, the probability of failure should be at an acceptable low level during the whole service life. In order to ensure this safety, we have to predict how fast cracks will grow and how fast the residual

strength will decrease. Making these predictions and developing prediction methods are the ultimate objects of fracture mechanics.

Broek [2] states these following questions as the important points to be addressed by any fracture mechanics analysis method:

a. What is the residual strength as a function of crack size?

b. What size of crack can be tolerated at the expected service load; i.e. what is the critical crack size?

c. How long does it take for a crack to grow from a certain initial size to the critical size?

d. What size of pre-existing flaw can be permitted at the moment the structure starts its service life?

e. How often should the structure be inspected for cracks?

Fracture mechanics methods provide satisfactory answers to some of these questions and useful answers to the others. Several disciplines are involved in the development of fracture mechanics design procedures. One of the important factors is the engineering load-and-stress analysis for an actual structural design with design loads. Applied mechanics provide the crack tips stress fields as well as the elastic and plastic deformations of the material in the vicinity of the crack. The predictions made about fracture strength can be checked experimentally. Material science concerns itself with the fracture processes on the scale of atoms and dislocations to that of impurities and grains. From a comprehension of these processes the criteria which govern growth and fracture should be obtainable. These criteria have to be used to predict the behavior of a crack in a stress-strain field. An understanding of the fracture processes can also provide the material parameters of importance to crack resistance; these have to be known if materials with better crack resistance are to be developed.

3.   Finite Element Methods in Fracture Mechanics

Over the last decade or so, the finite element method has become firmly established as a standard procedure for the solution of practical fracture problems. One of the primary and direct applications of the finite element analysis (FEA) is involved with evaluation of the stress intensity factor because of its importance in the field. A number of techniques has been suggested for evaluating this parameter from finite element results but adequate representation of the crack tip singularity is a problem common to most of these methods.

As a general guideline, the tendency among numerical analysts currently is to use a finite element code with conventional elements and to evaluate the crack driving force through a path-independent contour such as J. This technique allows the crack-tip region to be modeled with much less mesh refinement than is necessary to model the singular behavior directly and eliminates the need for a library of special elements. However, the applicability of crack tip elements and singularity elements remains quite viable because of the ambiguity of the interpretation of results at this current stage in the employment of FEM in the fields of LEFM and EPFM. With the high growth rate of the theory and mathematical understanding of these phenomena, and the presence of the variety of complex subjects such as crack propagation, stress corrosion, fatigue, or creep failure, there is considerable room for a variety of techniques. In fact, for the value of comparison, it is beneficial to entertain various methods of approach. Finally, though, when the concepts are understood and the research is resolved and organized into a set standard of methodology for damage tolerance in practical engineering structures, choices based on the accuracy, performance, range of applicability, complexity, and computational requirements of the alternative approaches will have to be made.

II. OBJECTIVES OF THE RESEARCH EFFORT

The main task of this study was to conduct a survey of the existing finite element codes needed at the Astronautics Laboratory (AL) for the analysis and design of composite structures. Also, to study and evaluate the existing codes at the AL.

These objectives, have an ultimate goal of identifying areas needed to support and enhance the analysis and the design of composite structures using the finite element techniques. The finite element technique will also be used in determining the performance losses due to damage.

During my SFRP, a literature review was conducted and several finite elements codes were investigated. Also, an effort to identify an interface of bridge building between the dynamic and control group and the composite structural group was carried out. The areas of mutual interest for enhancing the design and fabrication of composite structures to support the control group were discussed with both groups.

Finally, a finite element code was employed for different fracture mechanics methods to evaluate the stress intensity factor for crack propagation.

III. FINITE ELEMENT CODES EVALUATION AND CLASSIFICATION

1. Finite Element Codes Evaluation

The evaluation of commercial finite element systems has received much attention recently. John Robinson in the U.K. has had a continuing series of simple element verification tests to assess pathological behavior and aspect ratio problems (e.g. temperature load, skewed plate, two-bar truss, etc.) in "Finite Element News", where he invites the submittal of solutions using different analysis codes. Noor published in 1981 a detailed tabular survey of 35 nonlinear

general and special-purpose programs [3]. Fredricksson and Mackerle in Sweden specialize in the periodic comparative cataloging of hundreds of finite element codes from many countries [4]. In 1982, this author presented an evaluation of eight U.S. general-purpose codes [5], and commented on their strengths and weaknesses, documentation quality, user support and availability, element library, material library, and procedures library. The worldwide response to this article has been overwhelming and positive, with an estimated readership of around five thousand. Requests to reproduce it for circulation have come from many service bureaus, computer manufacturers, engineering firms, consultants, and professors. This tremendous response merely points out the perennial thirst in the community for meaningful code evaluation information, as finite element codes proliferate and grow more complicated all the time.

One thoughtful set of code evaluations was sponsored by the U.S. Government Inter-agency Software Evaluation Group (ISEG) in the period 1978-1982 [6]. This effort produced detailed evaluation studies of four commercial finite element codes: ADINA--1977 Version [7]; COSMIC/NASTRAN--Level 17.5 [8]; STAGSC-1 [9]; and ABAQUS--Version 3 [10]. For the first time ever, these third-party evaluation studies examined program capabilities, documentation quality, program architecture (or data base management), element library, and procedures library. Advanced verification problems were selected to test accuracy, convergence, and efficiency characteristics against other codes and published solutions. It should be noted, however, that these studies were tinged with controversy before, during, and after each evaluation effort. Questions were raised such as: Why was the COSMIC version of NASTRAN selected, rather than the more popular and capable MSC version? Why was this evaluation performed by Swanson Service Corporation, an affiliate of Swanson Analysis Systems, Inc., the developer of ANSYS and a competitor to NASTRAN? Why did the ADINA and ABAQUS evaluations not utilize the latest versions of the code to their full range of capabilities, nor consider their heat transfer capabilities, field problems, and other special capabilities, etc.? The point here is that although these supposedly impartial evaluations by knowledgeable experts were planned with the noblest of objectives, the end results were

controversial, and in the case of ADINA and ABAQUS, there were strong objections to the conclusions by both code developers who felt they were treated unfairly. Software evaluation is thus extremely difficult and is often likened to shooting at a moving target--not an easy exercise even for an expert marksman.

2. Finite Element Codes Classification

One reasonable code classification scheme is to divide codes according to varying degrees of nonlinearity, for instance:

> Linear--STARDYNE, SAP, SPAR-EAL, EASE2, SUPERB, STRUDL, ASAS, etc.
>
> Linear to moderately nonlinear--ANSYS, MSC/NASTRAN, SAAS, etc.
>
> Nonlinear--ABAQUS, ADINA, MARC, ASAS-NL, FENRIS, ASKA, WECAN, DIAL, PLANS, STAGSC, DYNA3D, PAFEC, etc.

The choice of a proper code depends on the user's day-to-day needs. All of the codes named have their own fans and many companies use two or more codes to suit their analysis needs. To select a code for the first time, one should consider such factors as:

- Program analysis capabilities, including assumptions and limitations;
- User support (especially crucial for nonlinear analysis);
- Documentation quality;
- Developer reputation, reliability, and responsiveness;
- User convenience and protection (model generation, input checking, error message quality);
- Code efficiency in the class of problems of interest;
- Performance in "standard" benchmark tests;
- Code availability, portability, and maintainability on different computers (in particular, the quality of the version on your computer;
- Interactive pre- and post-processing capabilities (built-in or separate package);
- Educational services (training courses, user conferences, assistance by data centers and consulting organizations).

3. General Versus Special Purpose Codes

For a large company, one predicament is whether to maintain an in-house general-purpose finite element code or to lease one which is commercially available. For a medium-sized or small company, the question is whether to access a commercial code, develop and maintain its own special-purpose codes, or both. There are pros and cons of each option and the decision depends on user sophistication, his needs, and resources.

In the American aerospace industry, MSC/NASTRAN is thus seen to be the most popular general-purpose code. Virtually all these companies have also developed their own special-purpose codes. If we were to examine a cross-section of the nuclear and power-generation industries, the leading codes are probably ANSYS, ABAQUS, MARC, ADINA, etc. Codes like NISA and SUPERB enjoy popularity in manufacturing firms with automotive products, mostly around Detroit and in the Midwest. And STRUDL has a sizable following among civil engineers, with a strong emphasis on beam elements.

One perennial question is whether commercial, general-purpose codes can ever be made efficient and cost-effective enough to compete with special-purpose codes in selected areas. Some such areas where analyses have been traditionally done (at least in the U.S.) using special-purpose software include: 2D and 3D composite structures, computational aerodynamics (long dominated by finite difference codes), solids and shells of revolution, visco-elasticity, solid propellants and their containment structures, fluid-structure interaction (again dominated by finite difference codes like PISCES, STEALTH 2D and 3D, etc.), and soil-structure interaction. My own guess is probably not, at least for quite a while. The FEA marketplace is large enough, with enough diverse applications, that there will always be plenty of room for good general-purpose and special-purpose software.

IV. NUMERICAL PRESENTATION FOR STRESS INTENSITY FACTOR

In order to better illustrate the concepts of finite elements analysis in fracture mechanics, a problem of given geometry, material, and load conditions has been chosen. For simplicity, it was decided to restrict the study to the linear elastic analysis. The dumb-bell fatigue specimen used in this study is shown in figure 1. It is made of erosion resisting material with ultimate stress S_u of 50 Kg/mm², yield stress, S_y of 35Kg/mm² and elongation % of 33.5%. The mesh utilized for this analysis is shown in figure 2. For the program algorithm, subroutines, and documentation, reference [11] should be consulted. There have been some changes made with the program for reasons of output format reference.

As to the analytical equation for evaluation stress intensity factors for the crack extending from an elliptical hole in the center of a thin plate under tension, an approximation was made using a circular hole corrected for the factor between the stress concentration factors of the ellipse and the circle. Using the equation developed by Inglis as shown in reference [11]

$$K_t = (S_y)_{max}/S = (1+2A/B)$$

where

A=semi-major axis
B=semi-minor axis

For the ellipse, a K_t of 3.57 was found. For a circle, the K_t is 3.0. Therefore a factor of 1.19 must be applied to the circle to obtain the elliptical concentration factor. For a circular hole with cracks emanating from both sides, the following equation gives the stress intensity factor [2]

$$K = s(pa)^{\frac{1}{2}}((D/2a)+1)$$

where

a=crack length

Assuming an average diameter of the ellipse to be the same as the diameter of the circle and applying the correction factor shown above, the following equation is achieved:

$$K = 1.19s(pa)^{\frac{1}{2}}(((A+B)/4a)+1)$$

Using the stress near the crack tip and the crack length of 2, K is analytically predicted to be

Kn = 600.0 with s~155

1.   Evaluation of the Stress Intensity Factor

The methods for stress intensity factor evaluation considered in this paper are strain energy release rate (including the virtual crack extension approach) and the J-integral technique along with the crack tip elements extrapolation.

2.   Crack Tip Elements Extrapolation

For crack tip elements, the K value can be directly evaluated by displacement variation at points along a radial line emanating from the crack tip. Using nodes 15, 14, 13 and an angle theta = 180 deg., the K is given to 553.3 which is a more agreeable number. The error between this and the theoretical is around 7.8%. Since the leaning of the analytical answer itself was towards the lower side, this answer seems acceptable by the engineering standards

3.   Virtual Crack Extension Approach

In this method the crack is advanced by perturbing the nodal points in the crack tip zone in the direction of the crack advance. Figure 4 shows a representation of the principle. In particular nodes 13, 15, 17, 50, 52, 54 are perturbed first by 0.500 units, by 0.05 units, and by 0.005 units. The answers for stress intensity factors are given as 607.2, 595.9, and 594.4. These give errors of 1.2%, 0.8%, and 1.0% respectively. These give good results.

4.   Strain Energy Release Rate

For this method, the crack is advanced in the present code by nodal release. The stress-strain calculation are performed twice and an average crack length is figured out for this step. Using the nodes 15, 16, 17, 18 to be releases the K is found to 640.1.

Releasing nodes 15, 16 only gives a K of 623.4. These values are then extrapolated back to the original crack tip length. This gives a final K value of 606.6 with an error of 1.1%. This shows good agreement with this method and the theoretical analysis as well. Also, it gives more trust in the analytical value since two methods have agreed well with it so far.

5. J-Integral Method

In this approach, the J-integral, a path-independent line integral is evaluated along a contour path surrounding the crack tip. The path employed in solution passes through the gaussian points in the elements used. A picture of this concept is shown in figure 5. The stress intensity factor for a path going through elements 8, 14, 13, 4, 5, the most reliable in terms of the stress fields developed around the elliptical cutout, gives a value of 591.3 for gauss point = 3 and 591.2 for gauss point = 2. This is an error of 1.4% which can be considered a good agreement.

Conclusions

Having seen that the methods are generally in agreement with the analytical solution, and have errors on both sides of the mark, the analytical first-hand approximation seems to have been correct. If a mean of all the K values is to be taken, we get a stress intensity value of 591.4 with an uncertainty of 6.1%. This says that all the methods utilized are in general agreement with each other when engineering accuracy is considered. It is felt from the numbers presented and with a subjective view of the process, the results are very good.

For the future work the numerical analysis of composite structure failures will be considered. The predicted results will be compared with the experimental data.

V. CONCLUSION AND RECOMMENDATIONS

In conclusion, my participation in the 1989 Summer Faculty Research Program (SFRP) was very fruitful and enjoyable. I enjoyed very much working a fine group in an excellent environment of teamwork.

My recommendations are based on the results of the summer's effort in identifying certain areas of common interest to enhance the design and analysis of composite structures.

1. I was impressed with the way that the research efforts at the AL combining learning by doing and hands on techniques especially in the areas of fabrication, testing and measurement. I would like to commend Mr. Koury for his effort in the area of thermoplastic composite, and I will be interested in knowing about the final results.

2. As to the interface of bridge building between the dynamic and control group with the composite structural group,

    a. for better accuracy of the experimental data (material properties) provided to the dynamic group by the composite group, an experimental program coupled with analytical technician is needed.

    b. independent of the Finite Element Code employed in the analysis, a basic study for the assumption of each code is recommended, especially the assumption of handling the composite material as a homogeneous material.

3. Many finite element codes (general- and/or special-purpose) are available at AL and they can be employed as fine tools for the numerical analysis task.

In fulfilling the ultimate goal of this research effort of identifying areas for development of mutual interest for the government, industry, and the University for better understanding of composite stress analysis design and fracture mechanics I will be submitting a proposal for "Finite Element Analysis for Complex Structure." This structure will be built at the Astronautics Laboratory. I did discuss the outline of the proposal with Mr. J. Koury and we are in a full agreement on the need for this task.

REFERENCES

1.   Huebner, K. H., and Thornton, E. A., <u>The Finite Element Method for Engineers</u>, 2nd Ed., John Wiley and Sons, New York, 1982.

2.   Broek, D., <u>Elementary Engineering Fracture Mechanics</u>, Nordhoff International Publishing, Leyden, 1974.

3.   Noor, A. K., "Survey of Computer Programs for Solution of Nonlinear Structural and Solid Mechanics Problems," Computers and Structures, Vol. 13, 1981, pp. 425-465.

4.   Fredriksson, B. and J. Mackerle, "Partial List of Major Finite Element Programs and Descriptions of Some of Their Capabilities," Chapter 12 in State-of-the-Art Surveys on Finite Element Technology (Eds. A. K. Noor and W. D. Pilkey), ASME Publication H00290, 1983, pp. 363-404.

5.   Fong, H. H., "An Evaluation of Eight U.S. General Purpose Finite-Element Computer Programs," Proceedings of the 23rd AIAA/ASME/ASCE/AHS Structures, Structural Dynamics and Materials Conference, New Orleans, Louisiana, May 10-12, 1982, Part 1, pp. 145-160. AIAA Paper No. 82-0699-CP.

6.   Nickell, R. E., "The Interagency Software Evaluation Group: A Critical Evaluation of the ADINA, NASTRAN, and STAGS Structural Mechanics Computer Programs," Report to the Office of Naval Research, Arlington, Virginia, Contract N00014-79-C-0620, December 1981.

7.   Padovan, J. and T. Y. Chang, "Evaluation of ADINA: Part 1 (Theory and Programming Descriptions), Part II (Operating Characteristics)," University of Akron, Akron, Ohio, Final Reports No. AUE-801 and -802 to the Office of Naval Research, Contract N00014-78-C-0691, June 8, 1980.

8. Jones, J. W., H. H. Fong, and D. A. Blehm, "Evaluation of the NASTRAN General Purpose Computer Program," Swanson Service Corporation, Huntington Beach, California, Report No. 81980 to the Office of Naval Research, August 1980. [Also: Fong, H. H. and J. W. Jones, "An Evaluation of COSMIC/NASTRAN," Third World Congress and Exhibition on Finite Element Methods, October 12-16, 1981, Beverly Hills, California (Proceedings published as New and Future Developments in Commercial Finite Element Methods, ed. J. Robinson, Robinson and Associates, Dorset, England, 1981, pp. 324-338); and Jones, J. W. and H. H. Fong, "Evaluation of NASTRAN," Structural Mechanics Software Series - IV (ed. N. Perrone and W. D. Pilkey), University Press of Virginia, Charlottesville, 1982, pp. 147-237.]

9. Thomas, K. and L. H. Sobel, "Evaluation of the STAGSC-1 Shell Analysis Computer Program," Westinghouse Electric Corporation - Advanced Reactor Division, Madison, Pennsylvania, Report WARD-10881 to the Office of Naval Research, Contract N00014-79-C-0825, August 1981. [Also: Thomas, K., "Evaluation of STAGSC-1: A Nonlinear Shell Analysis Program," Structural Mechanics Software Series - V (ed. W. D. Pilkey), University Press of Virginia, Charlottesville, 1984.]

10. Chang, T. Y. and S. M. Wang, "Evaluation of A Nonlinear Finite Element Program - ABAQUS," University of Akron, Akron, Ohio, Final Report No. AUE-821 to the Office of Naval Research, Contract N00014-78-C-0691, March 15, 1983.

11. Owen, D. R. J. and Fawkes, A. J., Engineering Fracture Mechanics: Numerical Methods and Applications, Pineridge Press Ltd., Swansea, U.K., 1983.

FIGURE CAPTIONS

Figure 1   Dumb-bell shaped fatigue specimen containing an ellipticle hole in the center and in the rolling plane

DOGBONE SPECIMEN

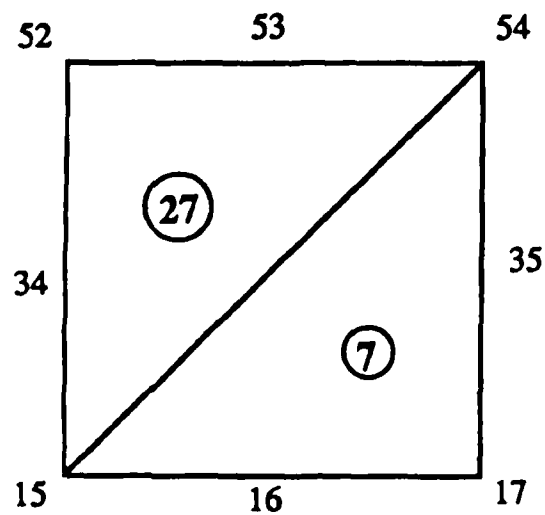**Figure 1**

MATERIAL GEOMETRY

Figure 2

Finite Element Mesh

Figure 3

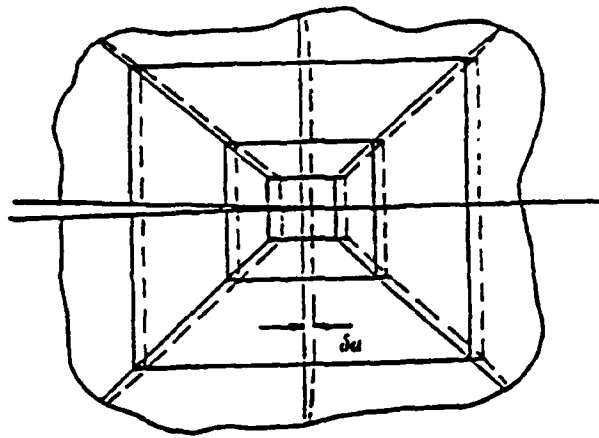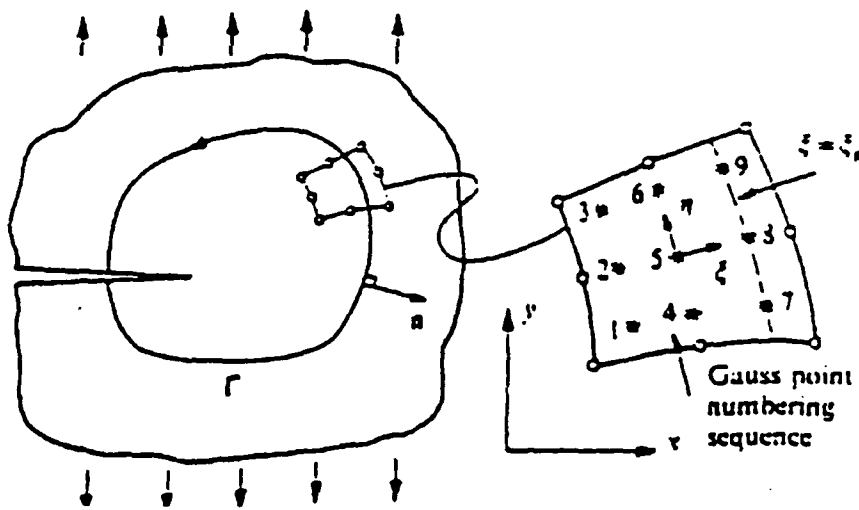**TRIANGULAR CRACK TIP ELEMENT**

Figure 4

Figure 5

Figure 6

1989 USAF-UES SUMMER FACULTY RESEARCH PROGRAM/

GRADUATE STUDENT RESEARCH PROGRAM

Sponsored by the

AIR FORCE OFFICE OF SCIENTIFIC RESEARCH

Conducted by the

Universal Energy Systems, Inc.

FINAL REPORT

Fracture behavior of a composite solid rocket propellant

Prepared by: Dr. Bipin K. Pai

Academic Rank: Associate Professor

Department and   Department of Engineering

  University: Purdue University Calumet

Research Location: AL/RKPL, Astronautics Laboratory

                      Edwards Air Force Base

                      California 93523-5000

USAF Researcher: Dr. Jimmy Liu

Date: September 9, 1989

Contract No: F49620-88-C-0053

Fracture behavior of a composite solid rocket propellant

by

Bipin K. Pai

ABSTRACT

The fracture behavior of a composite solid propellant
was investigated by mechanically loading a pre-cracked
biaxial strip specimen in an Instron Testing machine. The
effect of different center crack lengths and different
strain rates of loading were studied by calculating the
energies of deformation for each case. In each case, the
biaxial strip specimen was loaded at a constant strain rate
until the center crack started to initiate. At this point
the specimen was unloaded, allowed to relax and then
reloaded at the same strain rate to failure. The fracture
surface when the material failed was observed to have a
"zig-zag" shape. Several specimens were tested to failure
and in every case the characteristic "zig-zag" fracture
surface was obtained.

ACKNOWLEDGEMENTS

I wish to thank the Air Force Systems Command and the Air Force Office of Scientific Research for sponsoring this research project. I also wish to thank Universal Energy Systems for their help in the administration of the program and for their quick responses to all my queries.

I had a very rewarding summer research experience at the Astronautics Laboratory. In particular I would like to thank Dr. Jimmy Liu who helped me ..n every aspect of the research project by having several useful discussions. Thanks are also due to Dr. Paul Blatz whose experience and knowledge in the area of viscoelasticity proved very helpful. The classes conducted by Dr. Blatz also stimulated my thinking. The technical expertise of Jim King in helping me conduct the experiment is very much appreciated. I wish to also thank Verne Labeaux for making sure that the camera and video tape equipment were available when needed and Kelley Palmer for rushing the machining of the strip biaxial specimens. Timely discussions with John O'Drobinak and Dr. Shirl Breitling also proved helpful in the various stages of the project. I also wish to thank Dave Ferguson, Berge Goshgarian and Cpt. Mark Husband for their support and encouragement.

I INTRODUCTION:

Cracks occurring in solid rocket propellants can change the burn performance and in many cases lead to catastrophic failures. For this reason it is important to study the mechanical behavior of solid rocket propellants. In particular, fracture behavior of solid rocket propellants have to be analyzed by mechanical testing of solid propellant samples.

The Rocket Propulsion Division of the Astronautics Laboratory at Edwards Air Force Base is particularly interested in solid rocket propellant development and besides other aspects of propellant development, is also concerned with the mechanical testing of composite soliu propellants. Of late, the concern is to understand the process of crack initiation and propagation in a solid propellant, because it has far-reaching implications in being able to prevent possible catastrophic disasters. To this end, Dr. Jimmy Liu has been devoting much of his time in trying to understand the fracture behavior of solid propellants.

My research interests have been in the area of mechanical behavior of materials and in particular, mechanical testing of materials. My work on the finite element analysis of crack initiation and growth in circumferentially notched austenitic stainless steel specimens led to my assignment to the Mechanical Testing Section of the Solid Propellant Development Division of the Astronautics Laboratory at Edwards Air Force Base.

II OBJECTIVES OF THE RESEARCH EFFORT:

The objectives of the present summer research project were to characterize the material response and fracture behavior of a composite solid rocket propellant. The fracture behavior of the solid propellant was investigated by using a pre-cracked strip biaxial specimen. In order to study the effect of varying loading conditions such as strain rates and the effect of different crack lengths, three different strain rates of loading and three different crack lengths were used. The total and elastic energies of deformation for the above conditions were calculated from the strip chart curves of load versus deformation.

In addition to determining the energies of deformation, the strip biaxial specimens were loaded to failure and the fracture surface was observed.

III   DESCRIPTION OF THE BIAXIAL TEST

Unlike uniaxial tests, where the test fixtures in the mechanical testing machine are relatively simple, in the case of the strip biaxial test, there are several stages in getting the specimen ready for testing. First, the strip biaxial specimens have to be machined with great care because the high elongation solid propellant is also highly viscoelastic. Also the specimens have to be bonded to the aluminum end tabs as shown in Figure 1. This is to insure that the center of the specimen experiences biaxiality in the stresses when a uniaxial load is applied to the end tabs. (See Appendix I). The specimens were bonded to the aluminum end tabs with a Kalex Urethane adhesive using a bonding jig to ensure perfect alignment of the pin holes. They were then allowed to cure for about 24 hours.

A center crack was then made using a pre-cut blade of proper length; care was taken to ensure that the cut was made perpendicular to the specimen surface. Also grid lines 0.05" by 0.05" were drawn with a fine pen on the surface of the specimen.

The experimental setup of the Instron testing machine, along with the strip chart recorder, is shown in Figures 2 and 3. The strip biaxial specimen is attached to the two crossheads of the machine by pins. The upper crosshead is stationary and is attached to the load cell, while the lower crosshead is movable. The testing begins when the lower crosshead is allowed to move down thereby causing the specimen to be in tension. The test was conducted at a constant strain rate. As the load on the specimen increases the crack begins to grow. We made the assumption that the crack initiates when it grows a length of 0.05". At this point the loading direction is reversed i.e. the lower crosshead is allowed to move up. The specimen is unloaded until there is no load on the specimen. This can be determined from the strip chart recorder. The specimen is allowed to relax until there are no residual stresses. The load is then applied again at the same strain rate until the specimen fractures.

IV RESULTS

From the strip chart one can determine the total energy of deformation, which is the area under the load curve, and also the elastic energy, which is the area under the unload curve. Numerical integration, using Simpson's one-third

rule and three-eighths rule, was used in evaluating the areas under the load-deformation curves. The test described above was performed on several specimens, for center crack lengths of 0.5", 1.0" and 2" and at strain rates of 0.1 in./min., 0.5 in./min. and 2 in./min. At least two or three samples were tested for each combination of crack length and strain rate. The total and elastic energies of deformation were calculated for all cases. Tables 1 and show respectively the total and elastic energies as a function of cross-head speeds and crack lengths. Figure 4 shows a plot of the total energy and figure 5 shows a plot of the elastic energy for various crack lengths with the strain rate of loading as a parameter. From the plots one can see that the total energies and the elastic energies are reasonably constant for the three crack lengths for any one particular strain rate of loading. However more specimens with various crack lengths have to be tested at different strain rates of loading, and the results analyzed before one can conclude that the energies are indeed independent of crack length.

One single observation that stood out in all the tests was that when the specimens were loaded to failure, the fracture surface had a "zig-zag" shape. The "zig-zag" fracture surface seems to suggest that the failure is by shear mode. The twelve photographs shown in figures 6a

through 61 depict the progressive growth of a two inch long center crack of Specimen # 23, which was loaded at a strain rate of 0.5 in./min. The characteristic "zig-zag" shape of the fracture surface is very prominent especially towards the end of the test.

V RECOMMENDATIONS

(a) The results of the work done indicate that the number of experiments done are not enough to conclusively predict the dependence of the elastic or total energies of deformation on either the crack length or the strain rate of loading. More experimental tests need to be performed before one can conclusively make any statement about the dependence of the energies on the crack length or strain rate of loading.

However, since all the experiments were recorded on video tape, it is possible in the future to determine the displacement field around the crack tip by measuring the displacement of the grid lines. Also to determine the displacement field for future experiments a more sophisticated method of drawing the grid lines on the su⌐ace of the specimen is recommended.

(b) The time spent on the above project, ten weeks in all, although very productive, was not nearly enough to implement several experimental strategies to improve data collection and reduction. As indicated above, future experiments on the strip biaxial specimens should focus on obtaining more accurate data of the displacement field near the crack tip. This can be done by (1) coming up with a method of accurately marking the grid lines on the specimen surface and (2) digitizing the photographed grid lines so that a computer data reduction is possible. A method similar to the one adopted by Post, Smith and Czarnek of Virginia Polytechnic Institute & State University may be employed. A detailed research proposal for a mini-grant will soon be submitted to the Air Force Office of Scientific Research (AFOSR).

REFERENCES

Burnside, C. H., Knauss, W. G., Leeming, H., Svob, G. J., and Landel, R. F., "The Strip Biaxial Test" , JANNAF Solid Propellant Mechanical Behavior Manual, Sec. 4.5.2, July 1983.

Post, D., Smith, C. W., and Czarnek, R., "Crack Opening and Extension in Inert Solid Propellant - An Experimental Study" Air Force Astronautics Laboratory Report TR-87-043, September 1987.

Willard, D., "Propellant Training Manual" Air Force Rocket Propulsion Laboratory Report TM-84-034, November 1984.

Oberth, A. E., "Principles of Solid Propellant Development", Chemical Propulsion Information Agency (CPIA) Publication 469, September 1987.

Timoshenko, S. P., and Goodier, J. N., Theory of Elasticity, 3rd. Ed., McGraw-Hill Book Co., Inc., New York, 1970.

Byars, E. F., Snyder, R. D., and Plants, H. L., Engineering Mechanics of Deformable Bodies, 4th Ed., Harper & Row Publishers, New York, 1983.

Table 1

Total energies as a function of cross-head

speeds and crack lengths

XHD Speed -->	0.1 in/m	0.5 in/m	2.0 in/m
Crack Lengths			
0.5 in.	13.70 in-#	17.47 in-#	17.44 in-#
1.0 in.	12.49 in-#	16.89 in-#	16.71 in-#
2.0 in.	11.96 in-#	14.12 in-#	13.97 in-#

Table 2

Elastic energies as a function of cross-head

speeds and crack lengths

XHD Speed -->	0.1 in/m	0.5 in/m	2.0 in/m
Crack Lengths			
0.5 in.	4.90 in-#	6.59 in-#	7.98 in-#
1.0 in.	5.18 in-#	6.18 in-#	6.33 in-#
2.0 in.	4.70 in-#	5.36 in-#	5.89 in-#
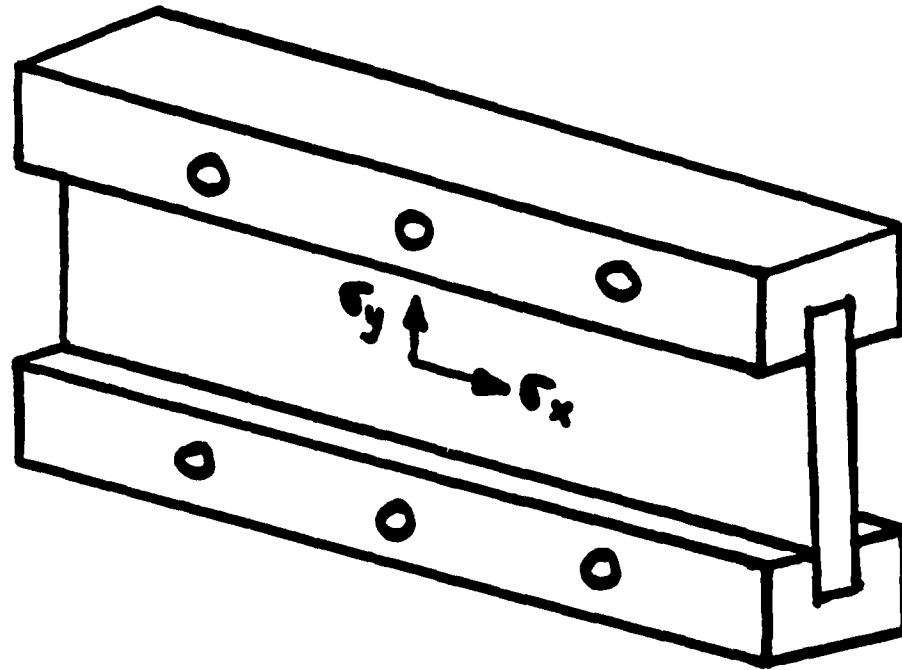
Fig. 1 End-bonded strip biaxial specimen
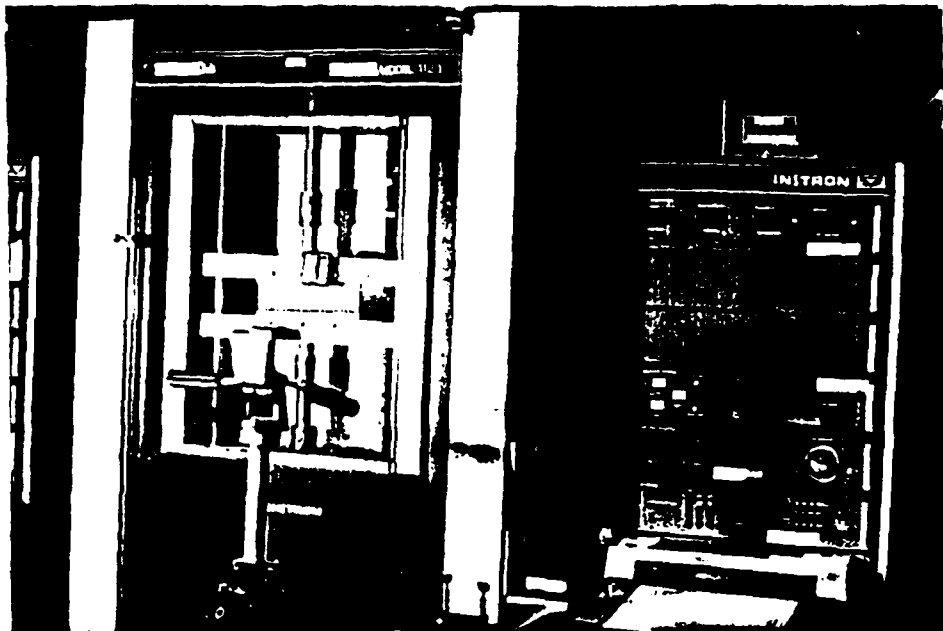
Fig. 2 Instron testing machine
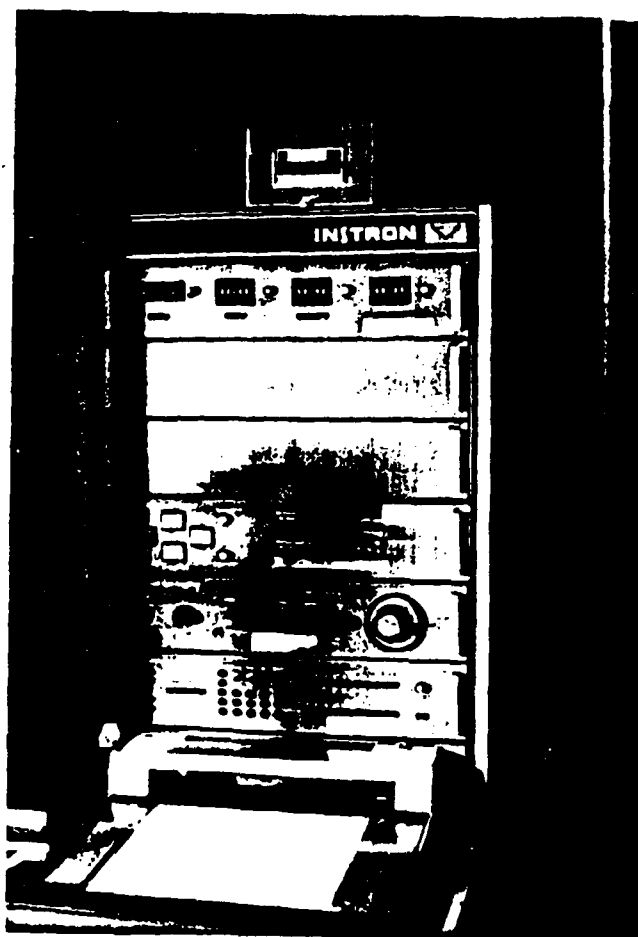
Fig. 3 Instron control stack and strip chart recorder

Fig. 4 Total energy versus crack length at various strain rates

- 0.1 in./min.   + 0.5 in./min.   * 2.0 in./min.
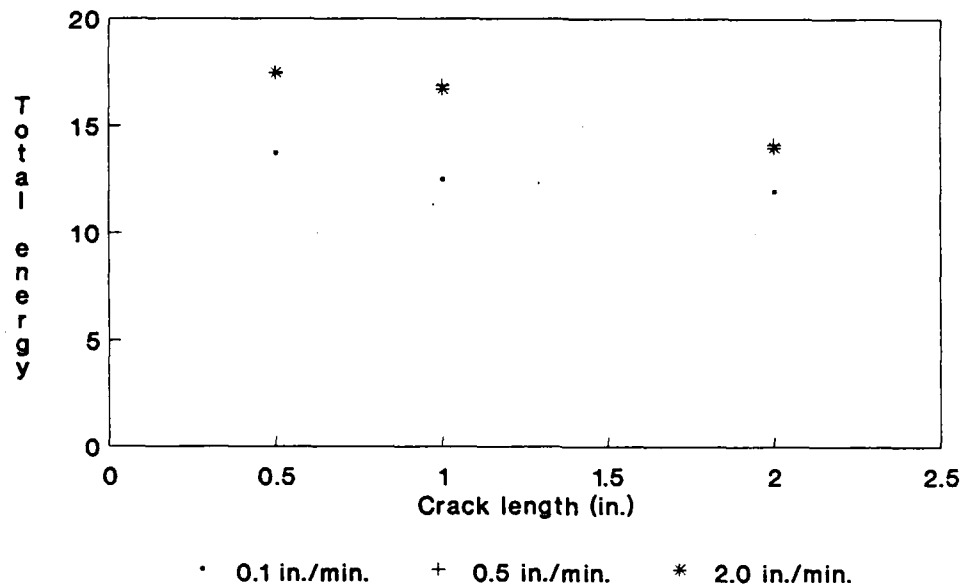
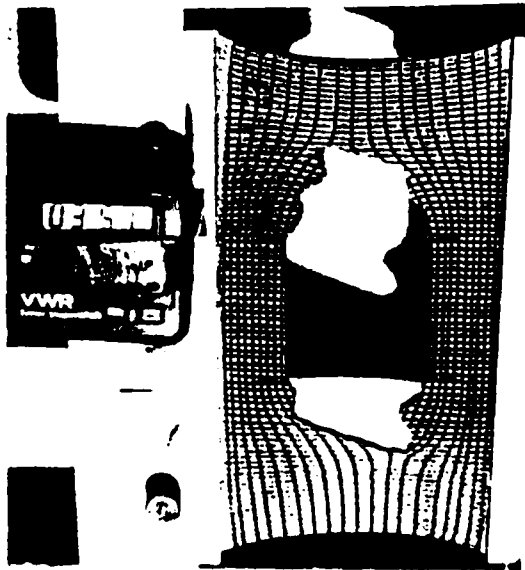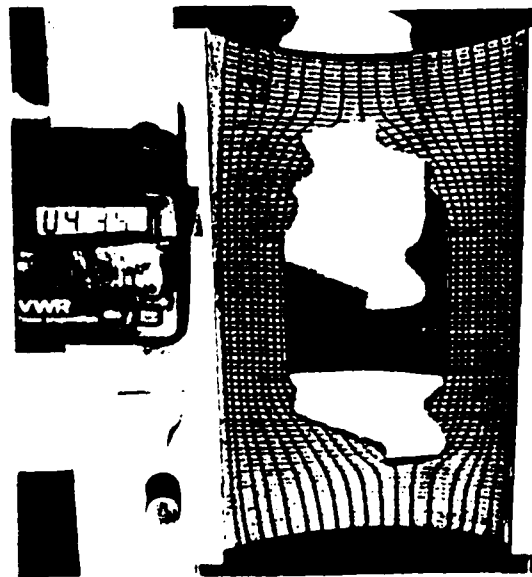# Fig. 5 Elastic energy versus crack length at various strain rates

□ 0.1 in./min.   × 0.5 in./min.   ◇ 2.0 in./min.
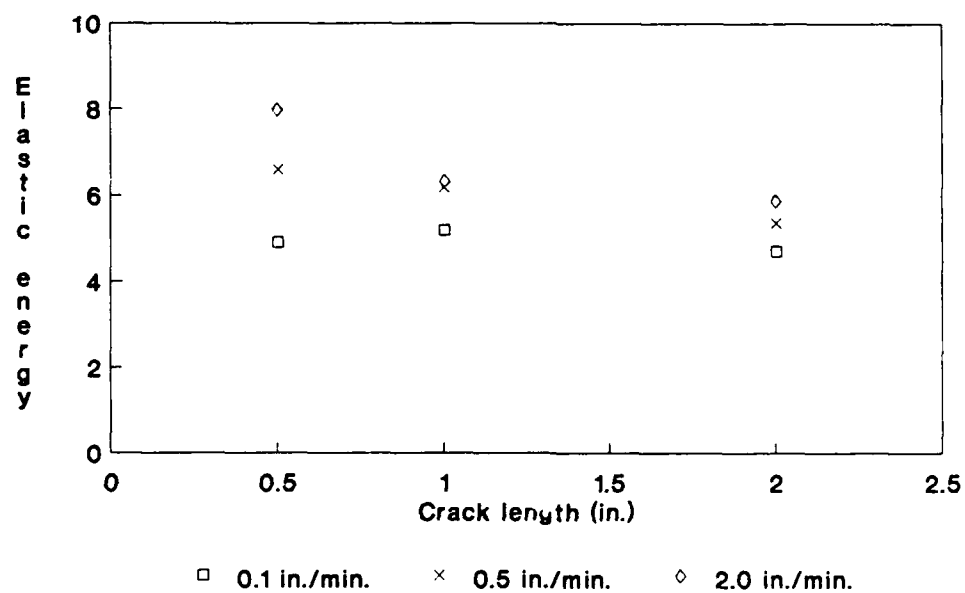
Fig. 6a

Fig. 6b
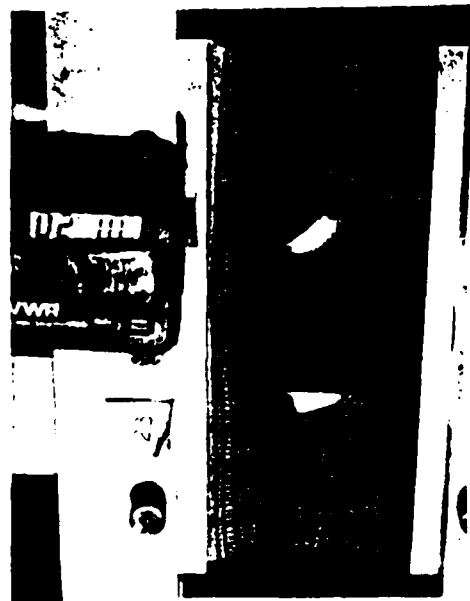
Fig. 6c
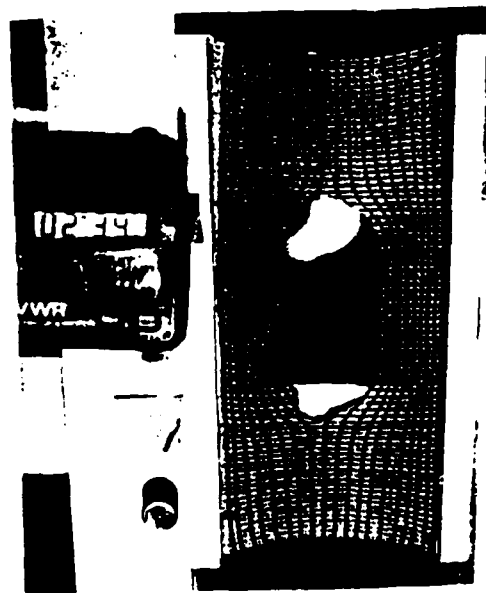
Fig. 6d

Fig. 6a - 6l Series of twelve photographs showing the growth of a 2" long center
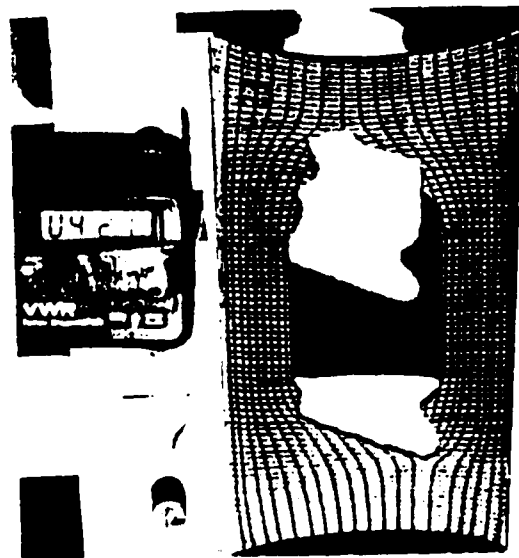crack of Specimen # 23 at a crosshead speed of 0.5 in./min.

Fig. 6f

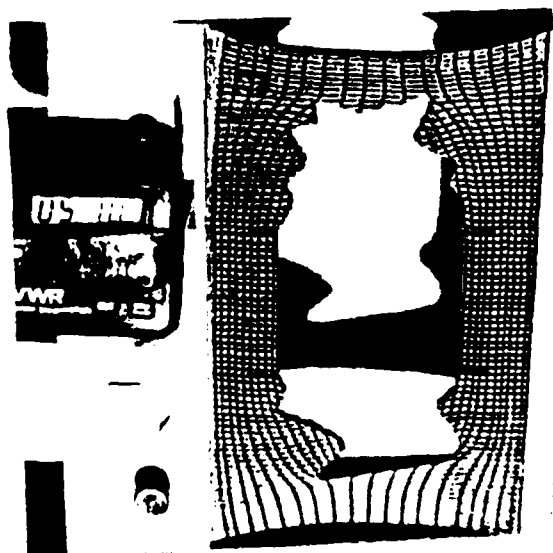Fig. 6h
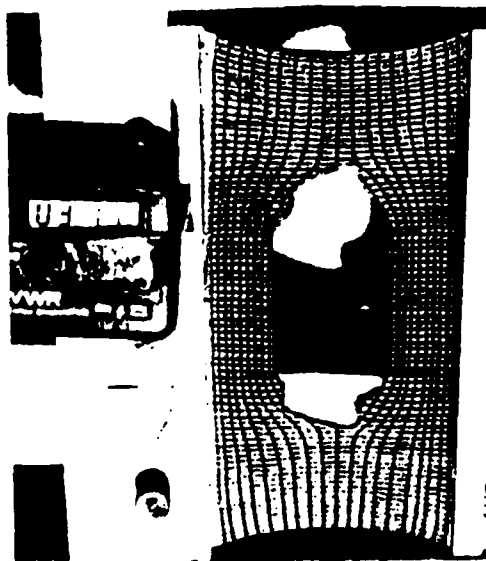
Fig. 6e
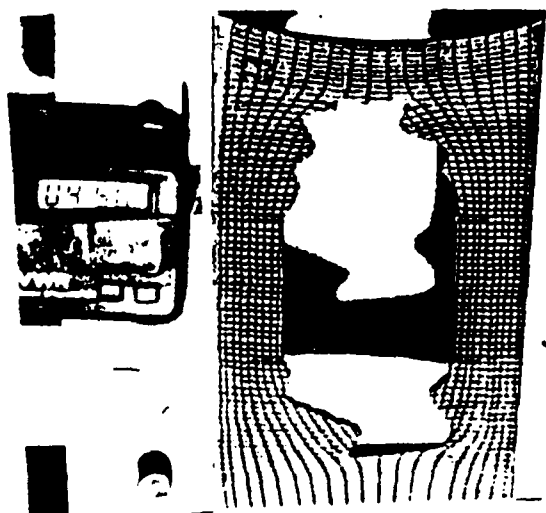
Fig. 6g

Fig. 6j

Fig. 6l

Fig. 6i

Fig. 6k

APPENDIX I

Using a linearly elastic stress analysis, it can be shown that an infinite biaxial strip specimen bonded to end tabs and loaded uniaxially will experience stress biaxiality at the center of the specimen.

We shall assume that the displacements are

$$u_y = \mathcal{E}_o \cdot y$$

$$u_x = 0$$

and that $\sigma_z = 0$. Therefore the strains are $\mathcal{E}_y = \mathcal{E}_o$, $\mathcal{E}_x = 0$ and from Hooke's Law:

$$\mathcal{E}_2 = \mathcal{E}_x = (1/E) \cdot (\sigma_2 - \mu \cdot \sigma_1) = 0$$

$$\mathcal{E}_1 = \mathcal{E}_y = (1/E) \cdot (\sigma_1 - \mu \cdot \sigma_2) = \mathcal{E}_o$$

Therefore the stresses are:

$$\sigma_1 = [E / (1- \mu^2)] \cdot \mathcal{E}_o$$

$$\sigma_2 = [\mu \cdot E / (1- \mu^2)] \cdot \mathcal{E}_o$$

The ratio of the two stresses σ_2 and σ_1 is:

$$\sigma_2 / \sigma_1 = \mu$$

If the value of μ is approximately 1/2, this is the value of the biaxiality ratio of the stresses.

1989 USAF-UES SUMMER FACULTY RESEARCH PROGRAM

Sponsored by the

AIR FORCE OFFICE OF SCIENTIFIC RESEARCH

Conducted by the

Universal Energy Systems, Inc.

FINAL REPORT

ROBUST CONTROL OF A L EXPERIMENTAL GRID USING

REDUCED ORDER MODELS

Prepared by:	VITTAL S. RAO Ph.D.
Academic Rank:	Professor
Department and University:	Department of Electrical Engineering University of Missouri - Rolla
Research Location:	Astronautics Laboratory Edwards Air Force Base Edwards, CA 93523
USAF Researcher:	Alok Das, Ph.D.
Date:	September 18, 1989
Contract No:	F49620-88-C-0053

ROBUST CONTROL OF A L EXPERIMENTAL GRID
USING REDUCED ORDER MODELS

by

Vittal S. Rao

ABSTRACT

The design of control strategies for large space structures presents challenging problems. One is the presence of a large number of closely-spaced, lightly damped, coupled modes. Another difficulty in controller design arises from the presence of unmodelled dynamics as well as incorrect knowledge of the structural parameters. a robust controller design methodology based on linear quadratic Gaussian with loop transfer recovery (LQG/LTR) is particularly suitable for the control of large flexible structure. A procedure is developed to reduce the computational and implementation requirements by designing LQG/LTR controllers based on reduced order models of the structures. The balance-truncation model reduction method is used to derive a control synthesis model. These reduced order models are used to design linear quadratic regulators with observers and LQG/LTR controllers for A L experimental grid structure.

ACKNOWLEDGEMENTS

I wish to thank the Air Force systems command and the Air Force office of Scientific Research for sponsorship of this research. Thanks are also due to Universal Energy System for excellent administration of the program.

My research experience at Astronautics Laboratory was very fruitful and rewarding. The author wish to thank Dr. Alok Das for providing support, encouragement and an excellent atmosphere for conduction research. Many thanks are due to Mr Wade Schlaegel for providing excellent computer facilities. The author also wishes to thank Mr. Joel Berg. and Prof. Ji C. Wang for fruitful discussions. The encouragement of Mr. L. Kevin Slimak, Branch chief, is greatly appreciated.

I INTRODUCTION:

In recent years, an increased amount of research effort has been directed toward the design of controllers for large space structures. The control objectives are vibration damping, mode shape requirements and attitude control. The design of control strategies for large space structures presents challenging problems. One is the presence of a large number of closely-spaced, lightly-damped coupled modes. Another difficulty in controller design arises from the presence of unmodelled dynamics as well as incorrect knowledge of the structural parameters, which can cause instability. A control strategy which can guarantee stability and provide satisfactory performance in the presence of model uncertainties, is called a robust controller. These uncertainties may include modelling error between the control synthesis model and the actual system, parameter variations and the effects of various disturbances on system performance. Among the various design methods for robust controllers, the linear quadratic Gaussian with loop transfer recovery (LQG/LTR) design procedure has many advantages. This methodology will result in control systems with excellent stability robustness, command following, disturbance rejection and sensor noise suppression properties.

The LQG/LTR design methodology is particularly suitable for the control of large flexible structures due to the considerable modelling inaccuracy that inherently exist in the mathematical models. Sundararajan, et al (1987), Joshi and Armstrong (1987), Yadavalli (1987), have successfully applied LQG/LTR methodology for the design of robust controllers for flexible structures. The computational requirements of the method are excessively high for large flexible structures. In this paper a procedure is developed to reduce the computational and implementation requirements by designing LQG/LTR controllers based on reduced order models of the structures.

The balance-truncation model reduction method has many advantages (Moore 1981). This representation is based on controllability and observability (location of actuators and sensors) considerations of the structural system. The frequency response characteristics of this reduced model are such that the spectral norm of the model reduction error is large at low frequencies and small at high frequencies. Prakash and Rao (1989), have developed a modified

reduced order model which has a good frequency response match at low frequencies. These reduced order models preserve stability, controllability and observability. An expression for error due to model reduction is also developed. These reduced order models are used to design linear quadratic regulators (LQR) and LQG/LTR controllers for the Astronautics Laboratory, Air Force Systems command (AL) experimental grid structure.

My research areas of interest are large scale control systems, stabilization and control of space structures robust control of multivariable systems. My work on the control of large space structures using reduced order models contributed to my assignment to the robust control of AL experimental grid using reduced order models.

II OBJECTIVES OF THE RESEARCH EFFORT:

An experimental grid structure is built at the Astronautics Laboratory, Air Force System Command (AL) to develop a simple ground test bed for future large flexible structures. The principal objective of this research facility has been to achieve satisfactory agreement between theoretical results and experimental measurements. (Das et al 1987)

The two-dimensional experimental structure shown in Fig. 1 consists of a 5' x 5' grid made up of 2" wide, 1/8" thick aluminum strips. At every point where the vertical and horizontal strips cross each other, they are connected by four rivets, thus effectively removing any play at the joints. The grid hangs vertically down, being cantilevered at the top to a large I-beam anchored to a cinder block wall.

The structural vibrations are monitored using high sensitivity, low mass piezoelectric accelerometers. Permanent magnet DC motor torquers are used as actuators for the grid. The grid can be exited by an electrodynamic shaker or a quartz impulse hammer.
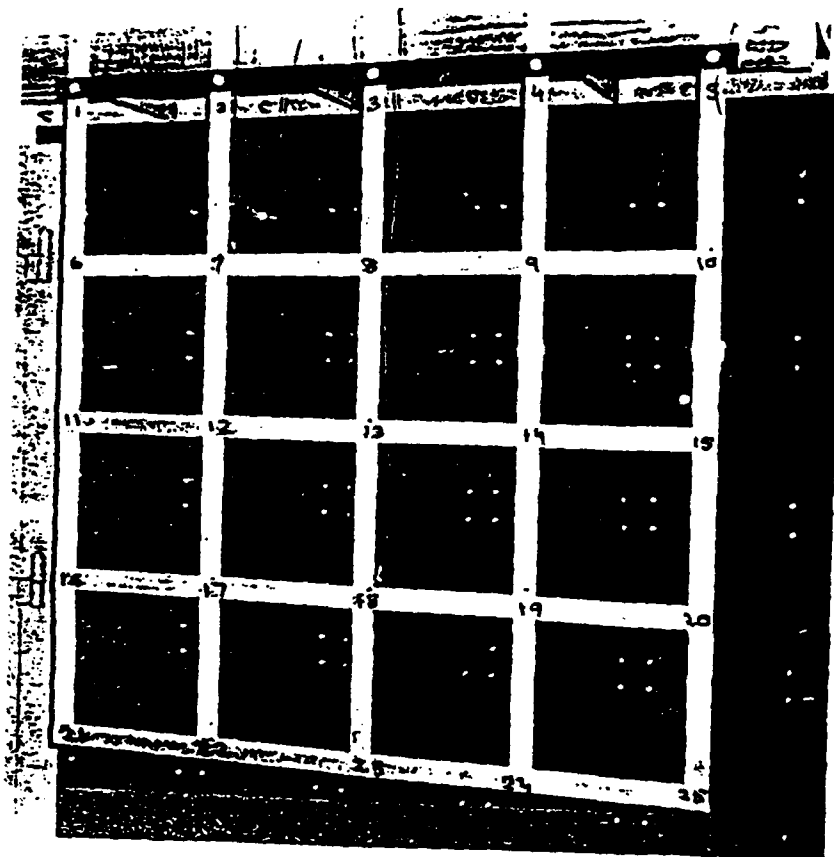
Fig. 1.   A L Experimental Grid

My research objectives are

(1)   Determination of linear state variable model of the structure using
       NASTRAN package

(2)   Incorporation of models of actuators, sensor, amplifier gains with grid
       structure.

(3)   Obtaining a reduced order model of the structure.

(4)   Design of robust controllers to experimental grid structure using reduced
       order models.

(5)   Simulation studies of closed loop system.

III STATE VARIABLE MODEL OF THE GRID STRUCTURE:

A model of the structure which relates inputs and outputs is needed for control design purposes. A theoretical mathematical model of the structure is developed using finite element methods. The natural frequencies of the Nastran finite element model are compared with the experimentally obtained natural frequencies of the grid.

In order to design robust controllers for structure we need a state variable representation of the grid. A procedure for realization of a state variable model for finite element model is given below.

The experimental grid structure is represented by 75 degrees of freedom (DOF) finite element-model. Each grid mode has three DOFS: translation in Z direction and rotations about horizontal and vertical axes. Equation of motion of the grid are given by

$$[m]\ddot{q} + [c]\dot{q} + [k]q = F(t) \qquad \qquad ...(1)$$

The vector q(t) represents the physical coordinates of the structure.
A 10-mode model representation of the grid is evaluated by using a linear transformation and truncation

$$q = \Phi\eta \qquad \qquad ...(2)$$

where η = Model coordinates of the structure
Φ = eigenvectors

Modal representation of the grid structure is given by

$$\ddot{\eta} + \text{diag}(2\zeta\omega_1,...2\zeta\omega_{10})\dot{\eta} + \text{diag}(\omega_1^2,...\omega_{10}^2)\eta = \Phi^T\mathcal{A}\,u(t) \qquad ...(3)$$

where F(t) = u(t)
$\mathcal{A}$= A matrix contains information about
location and type (x - torquer / y - torquer)
of actuators
ζ = A uniform damping of 0.005 is assumed
for every mode.

A state variable model corresponding to Eq. (3) is given by

$$\dot{x} = \begin{bmatrix} 0 & I \\ -Lambda & -Zetamat \end{bmatrix} x + \begin{bmatrix} 0 \\ \Phi^T A \end{bmatrix} u \qquad \text{...(4)}$$

$$\dot{x} = Ax + Bu$$
$$y = Cx + Du \qquad \text{...(5)}$$

where
$$\dot{x} = \begin{bmatrix} \eta \\ \dot{\eta} \end{bmatrix}$$

$$Lambda = diag(\omega_1^2, \omega_2^2, ... \omega_{10}^2)$$
$$Zetamat = diag(2\zeta\omega_1, ... 2\zeta\omega_{10})$$

Transfer function matrix $G(s) = C(SI - A)^{-1}B + D$ ..(6)

The effects of gravity on the accelerometer measurements are incorporated in the output equation.

The first ten-natural frequencies of the grid determined by using NASTRAN finite element model and experimental set up are given in Table 1.

TABLE 1 Comparison of Natural Frequencies

Mode #	NASTRAN (Hz)	Experiment (Hz)
1	0.7784	0.762
2	1.9093	1.810
3	4.1641	4.110
4	4.9618	5.150
5	6.3587	6.220
6	10.7318	10.750
7	10.8196	11.05
8	11.3227	11.50
9	13.8646	13.80
10	16.092	16.6

IV MODELS OF ACTUATORS AND SENSORS

In this phase of study, the dynamics of sensors and actuators are not considered. The gains of various components in the input/output channel are identified. A block diagram representation of a single channel is given below:
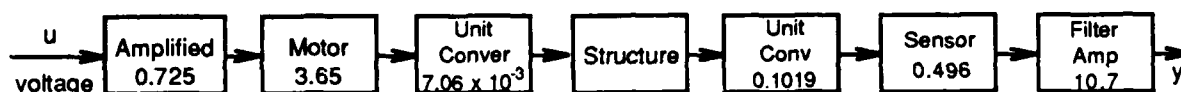
V REDUCED ORDER MODEL OF THE STRUCTURE:

A large number of procedures are available in the literature for deriving reduced order models (Jamshidi, 1983). Moore (1981) has introduced a balanced-truncation model reduction method based on controllability/observability consideration. This reduced order modelling technique is appropriate for large space structure problems. However the frequency response characteristics of their reduced model are such that the spectral norm of the model reduction error is large at low frequencies and small at high frequencies. In order to design LQG/LTR controllers based on reduced order modes, it is desirable to obtain a reduced order model which offers a good match at low frequencies. Prakash and Rao (1989) have introduced modifications to balanced-truncation procedure and these models are used to design LQR, LQG/LTR controllers in this report.

The state variable model of the structure represented by Eqs. (4 and 5) is transformed to an internally balanced realization using a linear transformation

$$x = T\vartheta \qquad \qquad ...(7)$$

The internally balanced system in partitioned form is given by

$$\dot{\vartheta}_1 = A_{11b}\vartheta_1 + A_{12b}\vartheta_2 + B_{1b}u$$
$$\dot{\vartheta}_2 = A_{12b}\vartheta_1 + A_{22b}\vartheta_2 + B_{2b}u \qquad \qquad ...(8)$$
$$y = c_{1b}\vartheta_1 + c_{2b}\vartheta_2 + Du$$

A reduced order model which contains dominant Hankel Singular values and low frequency matching is given by

$$\dot{\vartheta}_r = A_r \vartheta_r + B_r u$$
$$y = C_r \vartheta_r + D_r u \qquad \qquad \text{...(9)}$$

where

$$A_r = A_{11b} - A_{12b} A_{22b}^{-1} A_{21b}$$
$$B_r = B_{1b} - A_{12b} A_{22b}^{-1} B_{2b}$$
$$C_r = C_{1b} - C_{2b} A_{22b}^{-1} A_{21b} \qquad \qquad \text{...(10)}$$
$$D_r = D - C_{2b} A_{22b}^{-1} B_{2b}$$

The transfer function of the reduced order is given by

$$G_r(s) = C_r(sI - A_r)^{-1} B_r + D_r \qquad \qquad \text{...(11)}$$

various properties of the reduced order model are presented by Prakash and Rao (1989).

The steady state values for (8) and (11) are the same. A typical spectral norm of the model reduction error is given below:
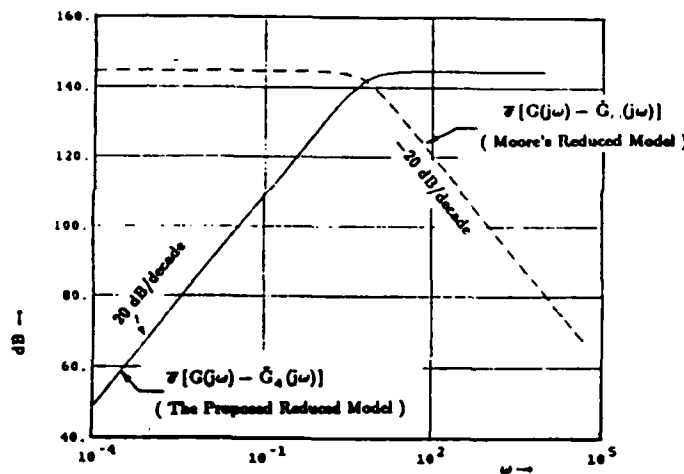
Using the internally balanced representation of the system, for a given actuator and sensor locations, it was found that the dominant modes are 9, 7, 3, 5, 8 and 2. Hence 6-mode (12-th order) reduced order model is obtained by using balancing truncation method. The eigenvalues and zeros of the system are given in Table 2.

TABLE - 2

Mode #	Eigenvalues of 10-Mode Model	Eigenvalues of 6-Mode Model	Zeros of 10-Mode Model
9	-0.43557±j87.113	-0.43507±j87.12	13.344±j61.584*
7	-0.33991±j67.981	-0.3289±j67.86	-13.898±j61.397
3	-0.13082±j26.164	-0.1311±j26.16	1.5685±j65.708*
5	-0.19976±j39.952	-0.1996±j39.95	0.69084±j3.993*
8	-0.3557±j71.141	-0.329±j70.927	-0.69223±j3.994
2	-0.05998±j11.997	-0.0601±j11.997	-0.05069±j15.316
6	-0.3371±j67.423		-2.2017±j65.708
1	-0.02445±j4.8907		-0.00309±j3.3845
10	-0.50555±j101.109		-0.53093±j104.38
4	-0.15588±j31.175		-0.15541±31.097

*Right half zeros

VI DESIGN OF ROBUST CONTROLLERS FOR EXPERIMENTAL GRID:

A schematic diagram of the AL experimental grid is shown in Fig. 1. The x-torquers (actuators), are located at node numbers 22 and 24 and a y-torquer is placed at node number 18. The accelerometers are placed at node numbers 14, 21 and 25.

A brief introduction to robust controller design methodology is given below:

Among the various design methods for robust controllers, the linear quadratic Gaussian with loop transfer recovery (LQG/LTR) design procedure has many advantages. This methodology is particularly suitable for the vibration damping of large flexible structures. The LQG/LTR design procedure (Doyle and Stein, 1981) can be summarized as follows:

(1) Define a nominal model of the structure. Augment pure integrators to the plan for zero steady-state tracking error. Define the performance and stability barriers in the frequency domain.

(2) For the loop broken at output, design a Kalman filter by adjusting the weighting matrices to meet the robustness specifications at high and low frequencies.

(3) Design a linear quadratic regulator for recovering the stability margins of the closed loop system.

(4) Verify the closed loop performance of the system.

The computational requirements of this methodology are excessively high for large flexible structures. Hence a procedure is developed to reduce the computational and implementation requirements by designing LQG/LTR controllers based on reduced order models of the structure.

A dynamic compensator for vibration suppression, is designed using a standard linear quadratic regulator with observer and robust controller methodologies. The results are given below:

(1) <u>Linear quadratic regulator with observer</u>

For the original 20th-order state variable model

$$\dot{x} = Ax + Bu \qquad \qquad \qquad ...(12)$$
$$y = Cx + Du \qquad \qquad \qquad ...(13)$$

The performance index is chosen as

$$J = \int_0^\infty (x^T Q x + u^T R u)\, dt \qquad \qquad ...(14)$$

where R = unity matrix
$\quad\quad\quad\;$ Q = $\text{diag}(1,1...1,\omega_1^2,...\omega_{10}^2)$
$\quad\quad\quad\;$ ω_i = natural frequencies in radians / sec.

A 12-th order reduced order model is derived by using balanced realization method:

$$\dot{x}_r = A_r x_r + B_r u \qquad \qquad \qquad ...(15)$$
$$y = C_r x_r + D_r u \qquad \qquad \qquad ...(16)$$

with performance index

$$J_m = \int_0^\infty (x_r^T Q_m x_r + u^T R u)\, dt \qquad \text{...(17)}$$

where

$$Q_m = [I_r \;\; 0] T_b^T Q T_b \begin{bmatrix} I_r \\ \cdots \\ 0 \end{bmatrix} \qquad \text{...(18)}$$

T_b = Linear transformation matrix for balanced realization

The singular value plots of original and reduced order models are given in Fig. 2.
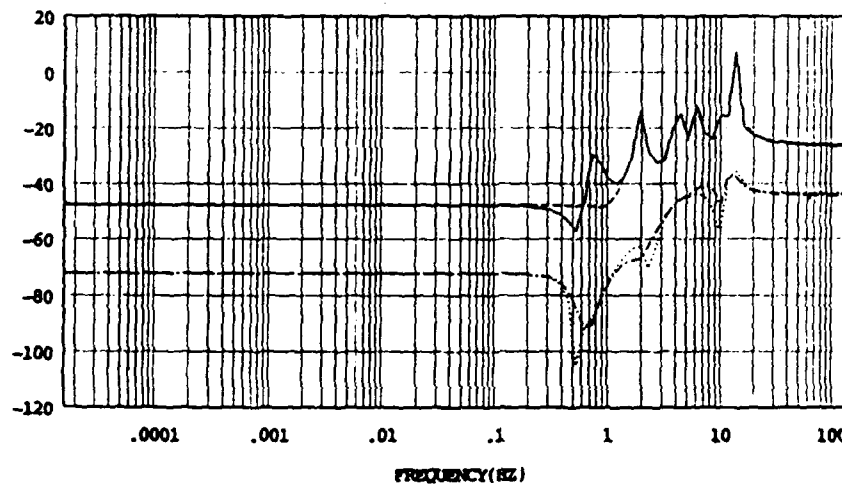

Fig 2.   Singular Value Plots of Original and Reduced Order Models

By using standard results, a regulator and asymptotic observer are derived. The closed loop implementation of the compensator is shown in Fig. 3.
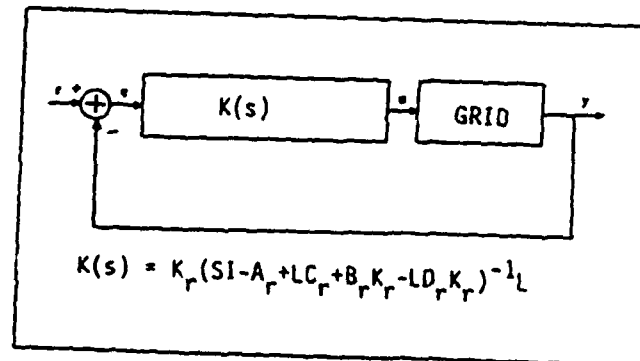

$$K(s) = K_r(SI - A_r + LC_r + B_r K_r - LD_r K_r)^{-1} L$$

Fig 3. LQR/Observer Implementation

A comparison of 20th order open loop system and 12th order closed loop system initial condition responses for mode #9 excitation is given in Fig. 4. It can be noticed from the figure that the closed loop system is well damped.
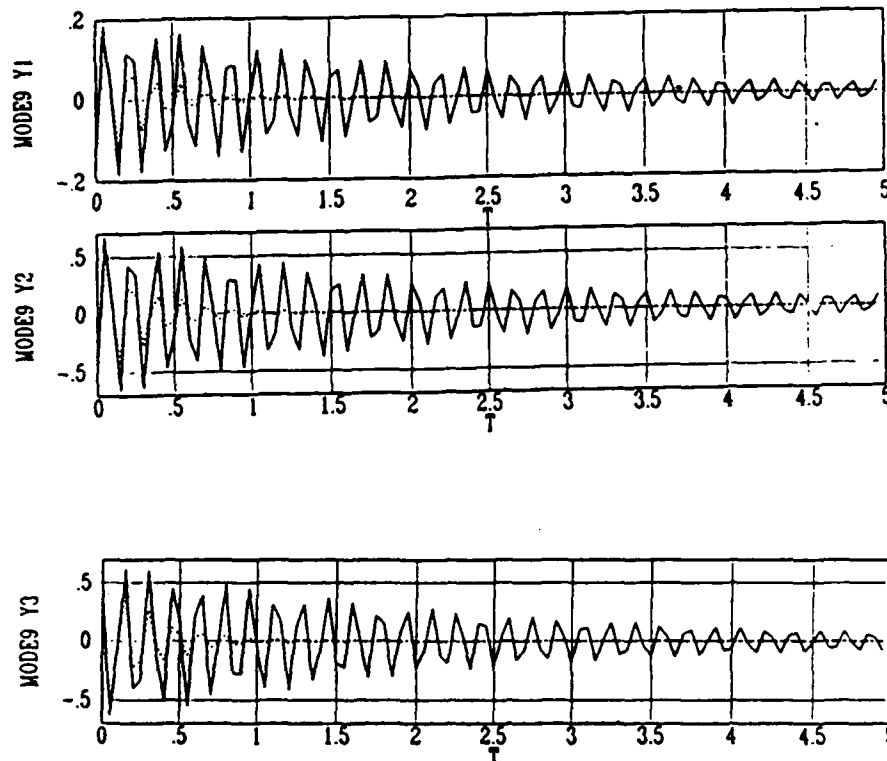

Fig. 4. Open and Closed Loop Responses for Mode #9 Excitation

(2)   LQG/LTR Controller

A linear quadratic Gaussian with loop transfer recovery procedure is used to design a robust controller to the grid structure. The reduced order model represented by Eqs. 15 and 16 is used as the design plant model. To achieve zero steady state error in the system, a bank of three integrators are augmented with a reduced order model. The augmented system is given by

$$\begin{bmatrix} \dot{\vartheta}_r \\ \dot{\vartheta}_a \end{bmatrix} = \begin{bmatrix} A_r & B_r \\ 0 & 0 \end{bmatrix} \begin{bmatrix} \vartheta_r \\ \vartheta_a \end{bmatrix} + \begin{bmatrix} 0 \\ I_a \end{bmatrix}^e \qquad \qquad \text{...(19)}$$

$$y = \begin{bmatrix} C_r & D_r \end{bmatrix} \begin{bmatrix} \vartheta_r \\ \vartheta_a \end{bmatrix} \qquad \qquad \text{...(20)}$$

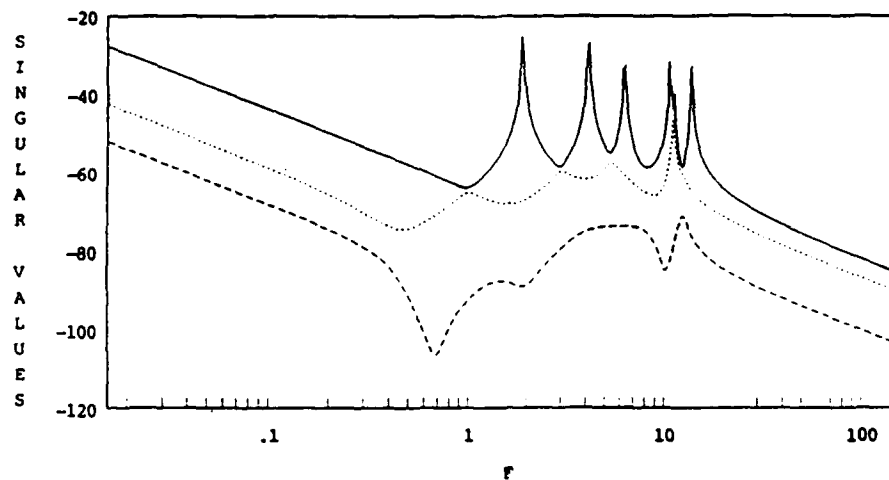The maximum and minimum singular value plots of the augmented system are shown in Fig. 5.

Fig. 5   Singular Value Plot of the Augmented System

By using the procedure described in the paper a robust controller is evaluated for augmented system.

Kalman Filter Design:

Since we are interested in the time response of the closed loop system we select the tuning parameters Γ and μ of Kalman filter to attain high loop gain and desired target feedback loop. The parameters $\Gamma = [0 \quad I_a]'$ and $\mu = 10^{-7}$ were chosen. The singular value plot of the target feedback loop shows a characteristic of -20dB/decade rolloff at high frequency and this is the desired loop shape [Fig. 6].
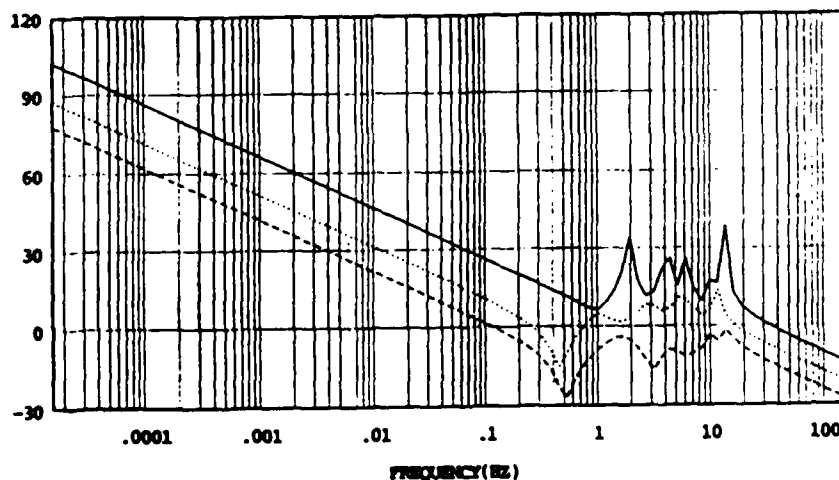

Fig. 6.   Singular Value Plot of Target Feedback Loop

Linear Quadratic Design:

The loop transfer is recovered by designing a linear quadratic regulator with tuning parameters $q^2 = 10^8$ and Rho = 1. Figure 7 shows the maximum and minimum singular values of actual loop G(s)K(s) and target feedback loop. There is a reasonable match between the plots. The recovery parameters are selected as a compromise between performance and stability.
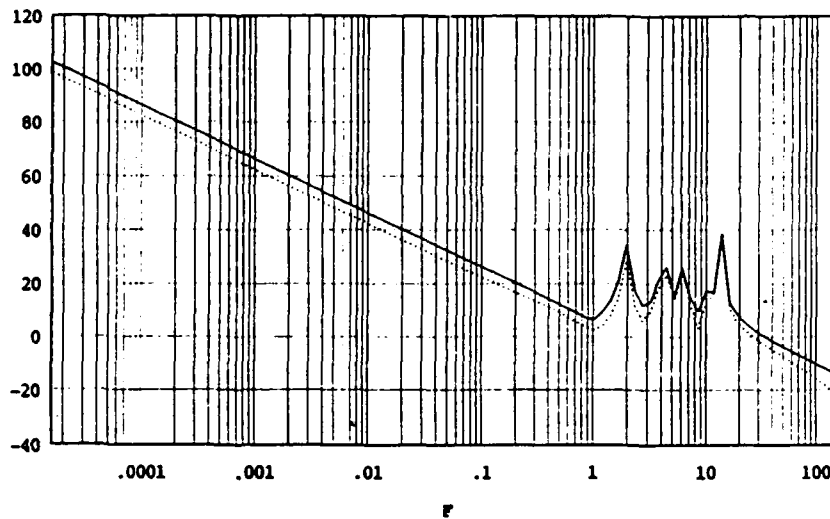

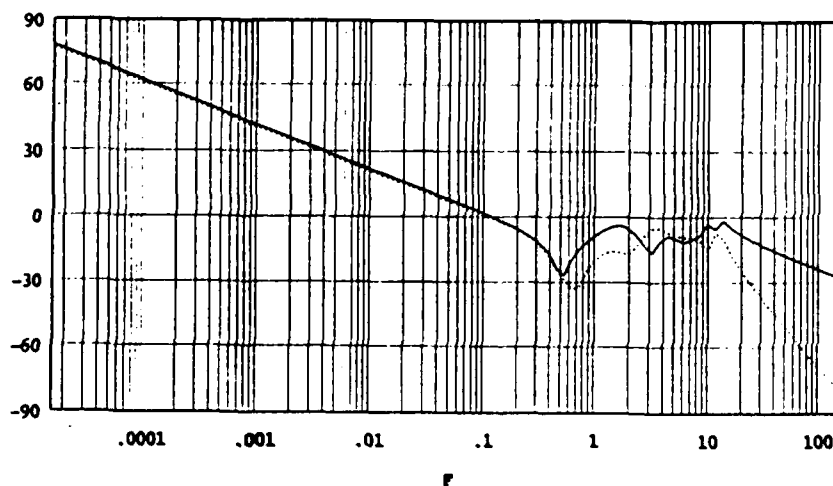Fig. 7a.   Maximum Singular Value Plot of TFL and G(s)K(s)

Fig. 7b.   Minimum Singular Value Plot of TFL and G(s)K(s)

It may be noted that the bank of integrators at the input of the plant introduced as a design requirement is now considered as part of the compensator for implementation.

The performance of the reduced order compensator implemented on the original, 10-mode, (20th order) truth model is tested. The closed loop system is stable and the performance is acceptable.

VII RECOMMENDATIONS:

a.   A procedure for active control of large space structures using reduced order models is presented i this research report. A modified balancing-truncation algorithm is used for deriving reduced order models. It is recommended that these reduced order models be compared with models derived bu using comparent cost analysis, optimal projection/Maximum Entropy (OP/ME) methods.

b.   The mathematical model of the experimental grid structure is non-minimal phase. The direct application of robust controller methodologies to non minimal phase models presents some problems. It is desirable to modify robust controller techniques for accommodating non minimal phase models.

c.   It is also recommended to evaluate the error bound on the reduced order modeling process and utilize this error in the design of robust controllers using reduced order models.

d.   The practical implementation of robust controllers on the experimental grid is an interesting and challenging job. It is recommended that the robust controllers be implemented and compare the response of the open loop and closed loop system for the effects of parameter variations, unmodelled dynamics, sensor and system noises.

REFERENCES

Das, A., T.J. Strange, W.T. Schlaegel and J.M. Ward (1987). "Experiment in Modelling and Parameter Estimation of Flexible Structures." Proceedings of Second NASA/DOD CSI Technology Conference, Nov 1987.

Doyle, J.C. and G. Stein (1981). "Multivariable feedback design: Concepts for a Classical/Modern Synthesis." IEEE Trans. on Automatic Control, Vol. AC-26, No. 1, pp. 4-16.

Jamshidi, M. (1983) "Modeling andControl" Elsevier Science publishing.

Joshi, S.M. and E.S. Armstrong (1987). "Design of Robust Line-of-Sight Pointing Control System for the Scole Configuration." Proceedings of American Control Conference, pp 1125-1127.

Moore, B.C. (1981). "Principal Component Analysis in Linear System: Controllability, Observability and Model Reduction." IEEE Trans on Automatic Control Vol AC-26, No. 1 pp 17-32.

Norris, M.A., R.C. Thomson and A-Das (1988). "Low-Frequency Response of Accelerometer for Observer Design in a Gravity Environment."

Prakash R. and S.VittalRao (1989). "Model Reduction by Low-Frequency Approximation of Internally Balanced Representaion." To be presented at 28th Control and Decision Conference.

Sundararajan, N., S.M. Joshi and E. M. Armstrong (1987). "Robust Controller Synthesis for a Large Flexible Space Antenna." AIAA J. of Guidance, Control andDynamics Vol. 10, no. 2, pp 201-208.

Yadavalli, R.K. (1987). "Robust Stabilization Under Mode Truncation and Parameter Variations." Proceedings of American Control Conference, pp 490-495.

1989 USAF-UES SUMMER FACULTY RESEARCH PROGRAM

Sponsored by the

AIR FORCE OFFICE OF SCIENTIFIC RESEARCH

Conducted by the

Universal Energy Systems, Inc.

<u>FINAL REPORT</u>

A Neural Network Approach to the Adaptive Control of

Large Space Structures

Prepared by: Richard A. Robertson

Academic Rank: Professor

Department and   Mathematics Deparment
University: California State Polytechnic University, Pomona

Research Location: USAFAL/VSSS
                      Edwards AFB
                      Edwards AFB, CA 93523

USAF Researcher: Dr. Alok Das

Date: 18 Aug 89

Contract No: F49620-88-C-0053

Acknowledgements

ABSTRACT

A Neural Network Approach to the Adaptive Control of Large Space Structure
Richard Robertson

This paper presents an attempt to synthesize, explain, and extend the research of Dr. Andrew G. Barto and his colleagues on networks of neuron-like adaptive computing elements for solving complex control problems. Unlike most other adaptive learning systems studied in the past, this approach requires no "teacher" that instructs each individual adaptive element on how it should respond to its inputs. Instead it utilizes a "critic" that is only able to assess certain gross consequences of the collective activity of all the network elements. The key idea is to endow each adaptive element with learning capabilities that are sophisticated enough to enable it to increase its own performance in the face of uncertainty, using any information that is locally available.

This approach is applied to a hypothetical, overly-simplified problem in the adaptive control of a large space structure (LSS). The main purpose here is to illustrate the potential power of these methods in the context of a distributed network of sensors, actuators, and microprocessors. These computing elements are assumed to be connected in parallel for rapid-response adaptive control of a complex, poorly understood LSS dynamical system on-orbit, with noisy, low-quality environmental feedback.

I. Introduction

Since they contain obvious parameters capable of being adjusted through experience, the so-called "connection weights", networks of neuron-like adaptive elements seem to offer a natural mechanism for solving difficult control problems, such as those faced by proposed large space structures (LSS) [3]. The anticipated combination of very large size and relatively low mass yields systems which possess little structural rigidity [4]. This flexibility causes severe technical problems when combined with the very precise pointing and shape control requirements of future LSS missions such as Space Based Laser (SBL) and Space Based Radar (SBR).

One approach to the control of LSS is to try to adapt the control law in near-real time to achieve precise and robust control of the actual structure, based on real-time estimation of the closed-loop response in a reference model. An evaluation of the state-of-the-art in adaptive control indicates that as poorly known and complex as many LSS are expected to be, achieving stable, high precision control will require the inclusion of system identification techniques. Blindly assuming a structural model derived, say, from a finite element code such as NASTRAN, is unwarranted and dangerous for a new generation of extremely flexible LSS which make use of innovative materials, joint mechanisms, and erection/deployment techniques.

Instead of using a model to predict how the system will respond to given inputs, system identification uses the observed response of the system to known inputs to deduce a predictive model. In practice, system identification techniques involve statistical estimation; system properties are derived from samples of noisy data. As stated in

[5], "It is evident that the state-of-the-practice in system identification is far from being adequate to meet the enormous challenges posed by the deployment or erection of large space structures." "Methods of parameterization which lead to the definition of a relatively few distributed parameters should be sought." "Research should also be directed toward the development of non-parametric methods that recover an input-output map of critical structural loadpaths." "We should be looking for algorithms that are more appropriate for parallel computation."

The approach taken is this paper is largely based on the work of Dr. Andrew G. Barto and his colleagues at the University of Massachusetts, Amherst. Supported by the AFOSR and the Air Force Wright Avionics Laboratory (Contract F33615) for more than a decade, Dr. Barto [3,6,7,8] has proposed, modified, extended, and simulated a modern theory of adaptive neural networks capable of solving difficult control problems. His research has been motivated by A.H. Klopf's concept of the "hedonistic neuron" [9,10] as an opportunistic network agent capable of improving performance in a wide range of conditions and under considerable uncertainty. Apparently growing out of work done for the Air Force Cambridge Research Laboratories, Klopf's hypothesis is that a neuron "learns" how to attain certain types of rewarding stimuli and avoid punishing stimuli by electrochemically adjusting the transmission efficacy of its synapses. This neuronal adjustment (depolarization/hyperpolarization) occurs according to the consequences of its discharges as fed back through pathways both internal to the nervous system and external to the organism.

Most of the adaptive network elements studied in the past, including the infamous *Perceptron*[11] and the *ADALINE*[12], can learn within

a network only if they are instructed by a knowledgeable "teacher" that can explicitly tell them how to respond to their inputs. Although the environment of an adaptive network may be able to assess consequences of the collective activity of all the network components, it usually does not know the desired responses of individual elements and cannot even evaluate their individual behavior. Barto and his colleagues endow their adaptive elements with more complex learning algorithms capable of improving performance with low-level environmental reinforcement, under conditions of considerable uncertainty.

They assume that the design of a controller for a complex, poorly understood system need be based on very little knowledge of the controlled system's dynamics. Moreover, the evaluative feedback provided to the controller may be of much lower quality than is required by standard adaptive control methods and previously studied networks of neuronlike adaptive elements such as those mentioned above.

In this paper an attempt will be made to explain the salient features of the theory of "associative search networks". This theory has been applied to difficult learning control problems by Barto and his colleagues, involving learning by "statistical cooperation" of neuronlike adaptive network components [13]. In addition, modifications, extensions, and synthesis of these concepts and methods will be suggested for possible application to the control of LSS, perhaps as a complement to more traditional adaptive control/system identification techniques. Recommendations for further research, computer simulations, and preliminary experimentation will also be made.

II. Objectives of the Research Effort

My assignment as a participant in the 1989 Summer Faculty Research Program (SFRP) has been to study the feasibility of using a neural network approach for the active control of proposed large space structures (LSS). A major obstacle to achieving accurate and robust control of such large, flexible structures is the extreme difficulty in adequately modeling and testing their on-orbit structural dynamics.

My approach has included a careful search through the recent literature for innovative attempts to achieve adaptive control of complex, poorly understood dynamical systems. I have chosen to follow the lead of Dr. Andrew G. Barto and his colleagues who have focused on adaptive reinforcement learning systems composed of networks of neuron-like computing elements. Connected in parallel for enhanced real-time response, the required microprocessing chips would individually possess relatively powerful problem-solving capabilities, while demanding very simple I/O and receiving only low-quality environmental feedback.

I have tried to synthesisize and explain Barto's concepts and methodology as refined over the years. I have also extended and modified his results, applying them to a hypothetical pointing-accuracy control problem in the domain of LSS. Limitations on space in this report have caused me to include some of the disscussion of concepts, previous simulation results, and specific suggestions for future research in my soon-to-follow Research Initiation Program (RIP) proposal. Concrete recommendations will be made for steps to be taken to refine, simulate, and test these ideas and techniques in order to pursue their potential real-world applicability.

III. Associative Search Network

As it is customarily known in the control community, a *control surface* is a mapping or function that associates with each possible input situation the "best" (optimal) action for that situation. Many methods exist for representing a control surface, ranging from pure computational schemes (with the function specified by equations to be evaluated) to pure table-lookup schemes (with values of the function precomputed for many arguments and stored in a table).

An *associative memory system* (AMS) is a mechanism for storing control information that combines properties of both computational and table-lookup methods. Consisting of a large number of neuronlike processing elements that compute in parallel, an AMS enables the coding of information in terms of distributed patterns of activity rather than via specific storage locations.

Barto and his colleagues have been studying a type of AMS, called an *associative search network* (ASN), in which the network need not be told by some external process what (optimal) pattern to associate with each key. Instead, the ASN utilizes a kind of *reinforcement learning* which helps direct the network in searching for that pattern which maximizes an external "payoff" or reinforcement signal. This reinforcement may be of very low quality and/or infrequently supplied, as might be expected in a complex, poorly understood dynamical system. As this type of learning with a "critic" proceeds, each key causes the retrieval of increasingly better choices for the associated pattern.

The ASN combines two types of learning usually considered separately: pattern recognition and search. It solves a pattern recognition problem

by learning to respond to each key with the appropriate output pattern; then it performs a stochastic search to maximize a "payoff" function.

The ASN mechanism addresses one of the hardest and most important problems for both brains and artificial learning systems to solve: the so-called "credit assignment" problem. A fundamental problem in any learning system is to determine what parts of a complex, interacting set of components, decisions, or actions deserve credit (blame) for improvement (degradation) in the overall performance of the system. This problem is aggravated when evaluative feedback to the system is not very informative, is corrupted by noise, or occurs infrequently.

IV. Associative Search Element

Associative search elements (ASEs) constitute the main neuron-like components in the postulated adaptive network. Since an important assumption here is that the environment is unable to provide individual ASE "neurons" with desired responses for specific input "stimuli", each one must discover for itself what responses lead to performance improvements. Initially, in the absence of any better control surface information, an ASE generates random actions on receipt of input signals. Based on feedback, possibly low-level, that evaluates the problem-solving consequences of its actions, an ASE "tunes in" input signals to bias the action generation process, contingent on the input "key". The random component of this "generate-and-test" or trial-and-error search process introduces the variety that is necessary for subsequent selection by evaluative feedback.

Each ASE in a network is assumed to have "n" time-varying input

("context") pathways with input signals $x_i(t)$, one (scalar) output pathway with ("efferent") signal $y(t)$, and a pathway for the evaluative feedback, $z(t)$. Associated with each input pathway x_i is a real-valued "connection weight" $w_i(t)$; let $W(t)$ denote the corresponding weight vector. Let $s(t)$ denote the weighted sum at time t of the context inputs:

$s(t) = \sum w_i(t)x_i(t) = W(t) \cdot X(t)$, the "dot product" of the weight vector with the input vector. The ASE's output $y(t)$ is determined from the input vector $X(t)$ as follows: $y(t) = f\{s(t) + \text{noise}(t)\}$, where noise(t) is a real-valued random variable with given probability density function, and f might be the sort of threshold output function ($f(x) = +1/-1$) utilized in Barto's simulations [3,8,14,21].

According to the output function, f, described above and its dependence on "noise(t)", actions are generated even in the absence of nonzero input signals. Thus the input weights only determine the probability of an action rather than the action itself; the learning process itself updates the action probabilities. The weights w_i change over (discrete) time as follows: $w_i(t+1) = w_i(t) + \alpha z(t)e_i(t)$, where α is a positive "learning constant" determining the rate of change of w_i. $z(t)$ is either the performance evaluation (reinforcement) provided directly by the environment or a prediction of the eventual reinforcement as generated by an *adaptive critic element* (described below). $e_i(t)$ represents the "eligibility" of input pathway i at time t, as proposed by Klopf [9]. In general terms, the eligibility of a pathway reflects the extent to which input activity on that pathway was paired in the past with element output activity. It is therefore a time-decaying trace of the products $y(\tau)x_i(\tau)$ for times τ preceding t.

The basic idea is that when activity takes place on a given input pathway that pathway becomes (more) eligible to have its weight modified, and that it retains (decreasing) eligibility for some time after that activity. If the reinforcement indicates improved performance, then the weights of the eligible pathways are changed so as to make the corresponding ASE more likely to respond the same way it did. If the reinforcement shows degraded performance, the weights are changed to increase the likelihood of the ASE responding differently. Instead of explicitly remembering what action was chosen, this mechanism contributes a different amount to the trace depending on what action, $y(t)$, was taken. In other words, the eligibility trace of an input pathway to an ASE contains information not only about how long ago there was activity on that pathway but also about what action was taken then.

V. Adaptive Critic Element

The *adaptive critic element*, or ACE, receives an externally supplied scalar reinforcement signal from the environment which is of low quality and, perhaps, infrequent. Its job is to assess the significance of this reinforcement in the context of its knowledge of the current state of the network. The ACE then computes a prediction of the eventual reinforcement to be obtained from the environment, depending on the possible patterns of actions to be taken by the ASEs corresponding to the context inputs. The central idea behind the ACE's "learning algorithm" is that predictions are formed that predict not only reinforcement but also future predictions of reinforcement.

Let $z(t)$ represent the actual reinforcement (or performance evaluation) signal transmitted by the "environment" to the ACE, with $z(t)$ the

corresponding signal pre-processed by the ACE for each of the ASEs. In order to transform z(t) (possibly noisy, infrequent, and of low-quality) into a more informative $\mathbf{z}$(t), the ACE must determine <u>a prediction</u>, p(t), <u>of eventual reinforcement</u> that depends on the input vector X(t).

Roughly speaking, an eligible pathway to the ACE changes connection weight whenever the actual reinforcement, z(t), plus the current prediction, p(t), differs from the value p(t-1) that was predicted for this sum. This rule provides a means for iteratively determining weight values such that p(t-1) approximates z(t) + p(t). <u>By attempting to anticipate its own prediction, this learning rule yields predictions that tend to be the earliest indications of eventual reinforcement.</u> The ACE's output $\mathbf{z}$(t), the impi ved or internal reinforcement signal, is computed from these predictions by: $\mathbf{z}$(t) = z(t) + p(t) - p(t-1).

VI. Neural Network Control of LSS

In order to illustrate some of the concepts introduced above, consider the following "toy" example from the adaptive control domain of LSS. No attempt has been made to realistically model any current or proposed actual structure. The picture to be conveyed is that of a hypothetical pedestal for, say, a space-based laser or radar dish which rests on top of a flimsy, on-orbit space platform with many possible displacement nodes and modes of vibration.

The primary control task under consideration is to maintain, within an acceptable tolerance range, the pointing direction of the pedestal relative to some fixed inertial direction, with a secondary task of maintaining some measure of control over the shape of the platform. It is assumed that passive control mechanisms are in place in addition to appropriate sensors, including gyroscopes, accelerometers, and various optical devices, perhaps embedded in composite material.

More specifically, the principal control problem is to maintain the pointing angle of the dish's vertical support (direction PQ in Figure 1) within some tolerance cone about the nominal direction. It is assumed that the capability exists for, say, gyroscopically sensing when the support crosses first into a warning buffer angle and then into an alarm region, at which times some control actions are called for to keep the pointing angle near-nominal. Moreover, it is supposed that appropriate sensing devices are located at platform "nodes" A, B, C, and D which can detect distances between nodal pairs, giving a measure of flatness or bend (or in-plane deformation). A line-of-sight optical device is presumed to be at pedestal basepoint P which is able to detect whether each anchor position E, F, G, and H is "above/level-with" or "below" P
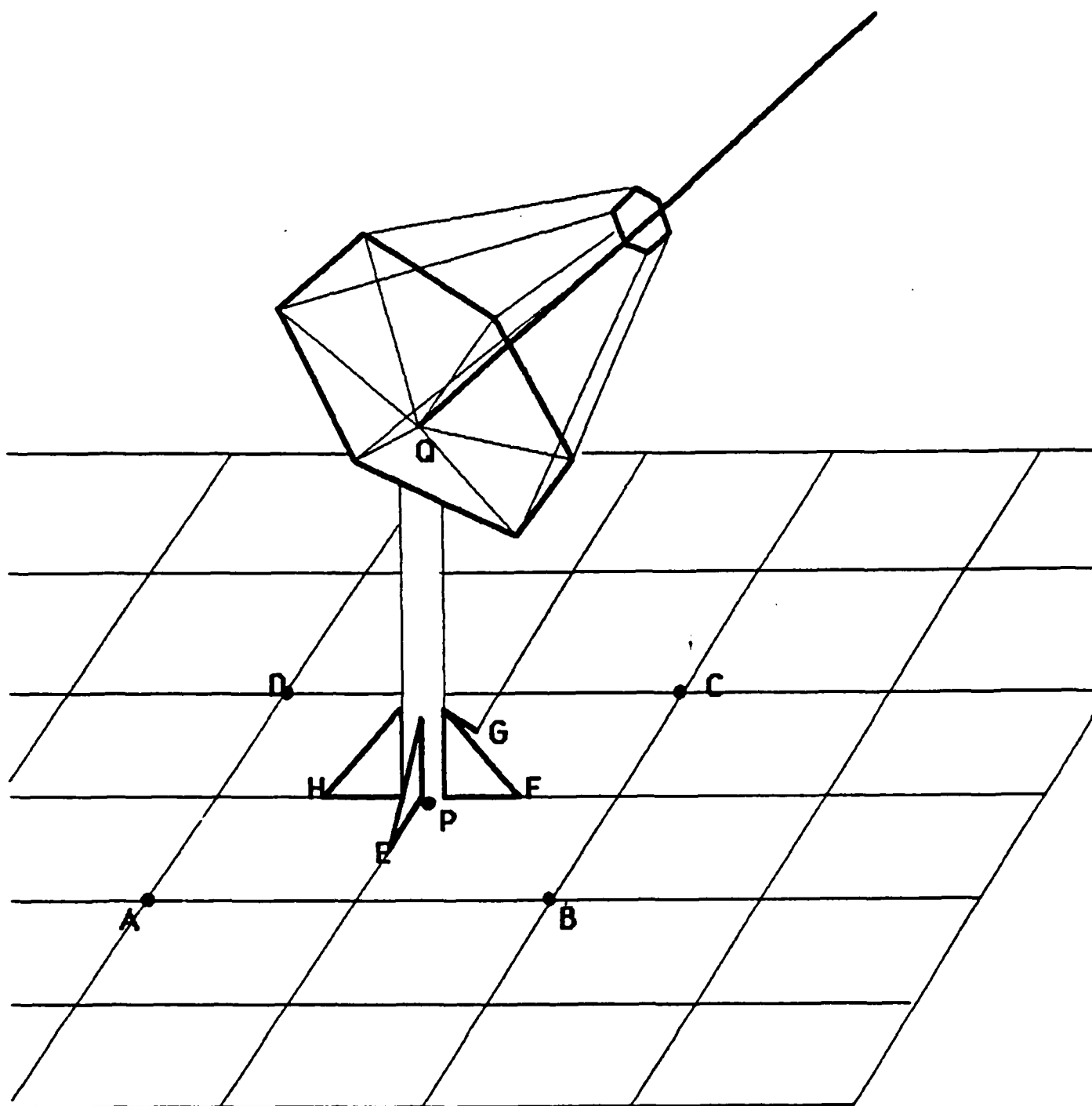
Figure 1

Adaptive Control of Pointing Direction $\overline{PQ}$

(say, $E_p(t) = +1$ or -1). Actuators (such as thrustors capable of firing "up/down" and/or "right/left") are assumed to be in place at anchor locations E, F, G, and H, along with passive control devices at various platform positions.

Following the lead of Barto and his colleagues, it is assumed that adaptive computing elements of the associative search element type (or ASEs, described in detail above) are located at anchor positions E through H. An adaptive "critic" element (or ACE) is taken to be in place at P, receiving the infrequent warning signal, $z(t)$, that the support has left the nominal pointing cone, $z=0$, and entered into the warning cone buffer, $z=-1$, or entered into the alarm region, $z=-2$, from the warning buffer. The ACE regularly predicts the expected environmental "reinforcement", $\mathbf{z}(t)$, based on the current nodal separations, and supplies this pre-processed "internal reinforcement" to each of the ASEs.

The problem of acquiring a control surface for this situation exhibits some of the features of Barto's pole-balancing scenario [3], as well as some found in his treatment of "landmark learning" [14]. The impressive successes demonstrated by his computer simulations under similar circumstances [3,7,17,21] lend credence to his methodology as modified and applied here.

In this setting the four ASEs at locations E, F, G, and H as well as the ACE at P receive "neutral" scalar input in the form of the six nodal separation distances $d_{AB}(t)$ through $d_{CD}(t)$, in addition to $E_p(t)$ through $H_p(t)$. Perhaps randomly driven or "tuned" at first, each adaptive output control device, say the "up/down" ASE at E, has a ("up/neutral/down") unit-pulse response capability ($y_E(t) = +1, 0, -1$, respectively). The

correct response at location E would be dependent on whether E is currently above or below P ($E_P(t) = +1$ or -1). This might be handled by a pair of ASEs "splitting" as in [8] to adaptively form features for storing the appropriate context responses.

The possibility of additional "right/neutral/left" response capability (say, $x_E(t) = +1,0,-1$) could be dealt with by "doubling-up" on the ASEs at locations E through H. The hardware for this "splitting" and/or "doubling-up" might simply require the use of individual but slightly more complex microprocessors at E through H.

VII. Expected Neural Network Behavior

This postulated neural network is capable of being driven at first by random inputs to the, say, "up/down" ASEs at anchor positions E through H; this may be complemented or even replaced by a pre-determined sequence of input scenarios. Operating in discrete time steps, the neural net learns to optimize its responses via low-quality environmental feedback, as improved upon by the ACE, or "critic", at P. It learns to associate patterns of input activity afferent to E through H with more or less successful pedestal pointing.

The network is "tuned-in" in the spirit of system identification, by a succession of input patterns and the corresponding pointing angle responses (near-nominal/in-danger/in-alarm). Continued presentation of input scenarios, even with patterns dissimilar to those already encountered should, via the network's generalization capabilities, rather quickly bring the pointing angle back to (or maintain it at) near-nominal,

despite forces, collisions, etc., not yet experienced or even foreseen.

The adaptive "critic" element at P receives the same nodal separation inputs, as well as the crude evaluative feedback of pointing accuracy, $z(t_i)$, provided by the environment ($z=0$, near-nominal; $z=-1$, in-danger; $z=-2$, in-alarm). Using a learning algorithm which takes into account (time-decaying) information about prior input activity on specific afferent pathways and resulting output accuracy, the ACE's connection weights v_j are updated, and a prediction of eventual environmental response, $z(t_i)$, is provided to each of the ASEs.

Through its own rather complex learning algorithm each ASE synthesizes the internally-modified (by the ACE) evaluation of pointing angle accuracy, z, with the pattern of "neutral" input activity. Its connection weights w_{ij} are updated in such a way as to make it more likely to respond the same way to this same pattern of inputs if the pointing angle has improved, but less likely to do so if a less desirable pointing position has resulted.

As demonstrated by Barto's simulations as reported in [3,7,17,21], the ACE quickly learns to accurately predict the environmental responses, even when stochastically driven initially. The ASEs simultaneously learn to form input pattern/output response associations which converge toward optimality, even for input patterns never before experienced, after sufficient learning experience [8,14,21].

VIII. Recommendations

a) At first glance, the neural network research presented in this Report seems too immature to seriously consider its immediate implementation. However, it is hoped that enough of the "flavor" and promise of this approach has been presented to stimulate interest and suggest some possibilities for eventual incorporation into LSS control system design.

During the latter part of this summer I became aware of an Air Force contract recently awarded to the Martin Marietta company to apply very similar methodology. The $800,000+, three-year contract was given to Martin Marietta to utilize a classical conditioning neural network computer model developed by the Air Force at Wright Avionics Laboratory to control a six-jointed robot arm. The computer model, called *Drive-Reinforcement Learning System*, or DRLS, is based on the Technical Report AFWAL-TR-87-1139, "A Neuronal Model of Classical Conditioning," by Harry Klopf. It should be remembered that Klopf's previous research and theories of the "hedonistic neuron" formed the basis for Dr. Barto's subsequent work at the University of Massachusetts.

b) There are several fruitful avenues for follow-on research to this work. An obvious and significant direction is that of settling on a preliminary LSS control scenario which is neither too trivial nor too ambitious, perhaps a variant on the hypothetical pointing-accuracy "application" in the report, for computer simulation/testing. Barto's simulation results alluded to in the Report and available in detail in several of the cited references (and my Appendix) are impressive and encouraging. However, it is true that modifications and extensions of his concepts/methods have been proposed, and further changes will no doubt also be required. It remains to be seen how well the reported successes

carry over to this new and more demanding setting.

It is my intention to find out as much as I can about the Martin Marietta and AFWAL efforts, trying to ferret out the similarities to and contrasts with Barto's work as presented here. The AFAL's significant commitment to the adaptive control of large space structures and the development and possible utilization of intelligent sensors and actuators seems a natural setting for this methodology. If possible, I will try to obtain copies of the computer models to be used by the groups mentioned above as well as the underlying documentation.

It seems to me that the best interests of the Air Force would be served by a cooperative, parallel effort at applying the DRLS, or a modification of it, to another problem domain of interest. As a mathematician with background in artificial intelligence research I feel that I could add a unique perspective on the whole issue of adaptive machine learning.

If, as is hoped, my obtained simulation results are promising enough, it seems reasonable to "breadboard" the kind of adaptive computing elements discussed in the Report, connect a small number of them in parallel, and design/implement a logical sequence of simple adaptive control tasks.

Another recommended path for research effort is to pursue the most recent work of Barto and his associates on the so-called *associative reward-penalty* , or A_{R-P}, element [13,15,16,17,18]. This adaptive computing element with its more theoretically-justified learning algorithm is a generalization of the work reported on here, and it represents an effort to provide a more formal basis for the results previously obtained by computer simulation.

BIBLIOGRAPHY

[1] V.R. Lesser and D.D. Corkill, "Functionally accurate, cooperative distributed systems", *IEEE Transactions on Systems, Man, and Cybernetics*, SMC-11 (1981)

[2] A.G. Barto, "An approach to learning control surfaces by connectionist systems", in *Vision, Brain, and Cooperative Computation* (Arbib and Hanson eds.), MIT Press (1987)

[3] A.G. Barto, R.S. Sutton, and C.W. Anderson, "Neuronlike adaptive elements that can solve difficult learning control problems", *IEEE Transactions on Systems, Man, and Cybernetics*, SMC-13 (1983)

[4] G.A. Norris, 1Lt, USAF, "Initial Operational Capability of the ASTREX Large Space Structures Testbed", AFAL report

[5] E. Denman et al., "Identification of Large Space Structures on Orbit", AFRPL TR-86-054

[6] R.S. Sutton and A.G. Barto, "Toward a modern theory of adaptive networks: Expectation and prediction", *Psychological Review* 88, no.2 (1981)

[7] A.G. Barto, R.S. Sutton, and P.S. Brouwer, "Associative search network: A reinforcement learning associative memory", *Biological Cybernetics*, 40 (1981)

[8] A.G. Barto, C.W. Anderson, and R.S. Sutton, "Synthesis of nonlinear control surfaces by a layered associative search network", *Biological Cybernetics*, 43 (1982)

[9] A.H. Klopf, "Brain function and adaptive systems - a heterostatic theory", AFCRL Research Report 72-0164 (1972)

[10] A.H. Klopf, *The Hedonistic Neuron: A Theory of Memory, Learning, and Intelligence*, Hemisphere (1982)

[11] F. Rosenblatt, *Principles of Neurodynamics*, Spartan (1962)

[12] B. Widrow and M.E. Hoff, "Adaptive switching circuits", WESCON Convention Record, IV (1960)

[13] A.G. Barto, "Learning by statistical cooperation of self-interested neuron-like computing elements", *Human Neurobiology*, 4 (1985)

[14] A.G. Barto, "Landmark learning: An illustration of associative search", *Biological Cybernetics*, 42 (1981)

[15] A.G. Barto and P. Anandan, "Pattern-recognizing stochastic learning automata", *IEEE Transactions on Systems, Man, and Cybernetics*, SMC-15 (1985)

[16] A.G. Barto, "Game-theoretic cooperativity in networks of self-interested units", in *Neural Networks for Computing*, AIP Conference Proceedings 151 (1986)

[17] A.G. Barto and R.S. Sutton, "Simulation of anticipatory responses in classical conditioning by a neuron-like adaptive element", *Behavioral Brain Research*, 4 (1982)

[18] A.G. Barto and M.I. Jordan, "Gradient following without back-propagation in layered networks", *IEEE First International Conference on Neural Networks*, II (1987)

[19] A.G. Barto, P. Anandan, and C.W. Anderson, "Cooperativity in networks of pattern recognizing stochastic learning automata", in *Adaptive and Learning Systems: Theory and Applications* (K.S. Narendra ed.), Plenum (1986)

[20] O.G. Selfridge, R.S. Sutton, and A.G. Barto, "Training and tracking in robotics", *Proceedings of the Ninth Annual IJCAI*, II (1985)

[21] A.G. Barto, ed., "Simulation experiments with goal-seeking adaptive elements", Technical Report AFWAL-TR-84-1022, Avionics Laboratory, Wright-Patterson AFB (1984)

[22] *Neurocomputing* (Anderson and Rosenfeld eds.), MIT Press (1988)

[23] *Neural Networks and Natural Intelligence* (Grossberg ed.), MIT Press (1988)

[24] *Neural and Massively Parallel Computers/The Sixth Generation*, B. Soucek and M. Soucek, Wiley-Interscience (1988)

[25] *Parallel Distributed Processing: Explorations in the Microstructure of Cognition* (Rumelhart and McClelland eds.), MIT Press (1986)

1989 USAF-UES SUMMER FACULTY RESEARCH PROGRAM/

GRADUATE STUDENT RESEARCH PROGRAM

Sponsored by the

AIR FORCE OFFICE OF SCIENTIFIC RESEARCH

Conducted by the

Universal Energy Systems, Inc.

<u>FINAL REPORT</u>

<u>CRYOGENIC HEAT PIPES</u>

Prepared by:	Larry W. Swanson
Academic Rank:	Assistant Professor
Department and	Department of Engineering
University:	University of Denver
Research Location:	AL/VSSP Edwards Air Force Base, CA 93523
USAF Researcher:	Michael Powell
Date:	5 September 1989
Contract No.:	F49620-88-C-0053

CRYOGENIC HEAT PIPES

by

Larry W. Swanson

ABSTRACT

Research topics important to the development of cryogenic heat pipe systems were reviewed and studied including heat pipe diode and thermal switch configurations, the thermophysical properties of cryogenic fluids, heat pipe computer codes, and the evaporating/condensing meniscus in a capillary tube. A gas gap thermal switch with a solenoid valve or an adsorption block as an evacuation mechanism was found to be the best choice for a monodirectional cryogenic heat pipe system. A preliminary assessment of cryogenic fluids indicated that Ne, O_2, and CH_4 were the most favorable fluids at temperatures of 30 K, 60 K, and 120 K, respectively. Cryogenic mixtures or cryogenic fluids with surfactant additives were found to be potential research areas for improving working fluid heat transport capability. The formulation of a mathematical model describing the evaporating/condensing meniscus in a capillary tube has produced five coupled nonlinear ordinary differential equations. A qualitative assessment of the equation set has shown that both evaporation at the interface and the London-Van der Waals forces increased the meniscus pressure driving force whereas condensation at the interface decreased the meniscus pressure driving force.

ACKNOWLEDGMENTS

I. INTRODUCTION

Cryogenic heat pipes have many potential applications aboard spacecraft such as coupling detectors to cold plates or radiators, maintaining detectors and other devices at constant temperature, and acting as switching devices for hybrid cooler systems. Cryogenic heat pipes pose a number of problems that differ from ambient or high temperature heat pipes: 1) large property variation over a small temperature range, 2) very low heat transport capability due to the low surface tension of cryogenic working fluids, 3) low thermal conductivity working fluids, 4) extensive insulation problems in an ambient environment, 5) scarcity of working fluids over certain temperature ranges, and 6) storage problems in an ambient environment due to high internal pressure. The Astronautics Laboratory at Edwards Air Force Base is interested in developing cyrogenic heat pipe systems with the following specifications:

1) heat pipe temperatures - 30 K, 60 K, 120 K
2) monodirectional heat transfer
3) storage temperature - 350 K
4) ambient temperature during operation - 275 K

Over recent years, my primary research interests have been based on improving heat pipe technology. Some of these research topics have included heat pipe heat exchanger design, transient dry-out in heat pipes, multi-form heat pipe radiators, wick microstructural design, and meniscus phase change phenomena. These interests, coupled with the cryogenics expertise at the Astronautics Laboratory, provided a research team well suited to the study and development of cryogenic heat pipe systems.

II. OBJECTIVES OF THE RESEARCH EFFORT

The focus of my research effort at the Astronautics Laboratory was to study various aspects of cryogenic heat pipes and their use in cooling cryogenic devices. The primary objectives of the research included identifying heat pipe diode and thermal switch configurations, acquiring and evaluating thermophysical property data for cryogenic fluids, obtaining heat pipe computer codes, and formulating a mathematical model of the evaporating/condensing meniscus in a capillary tube.

A literature search was performed to identify various heat pipe diodes and thermal switches, with the goal of specifying configurations which satisfy known system specifications. The search will also be used to define other system specifications important to the design of monodirectional cryogenic heat pipes.

Thermophysical property data for cryogenic fluids have been compiled with the

objective of discerning their effectiveness as heat pipe working fluids. The use of cryogenic fluid mixtures and surfactant additives in heat pipes has also been investigated.

A number of Governmental agencies, Universities, and Companies have been contacted to obtain heat pipe computer codes which determine heat pipe transport limitations as well as simulate both steady-state and transient operation. The objective of this effort was to determine which computer codes were best suited for use in both fundamental research and system evaluation at the AstroLab. The codes selected will then be adapted to the AstroLab computer systems.

A mathematical model of the evaporating/condensing meniscus in a capillary tube was also formulated to gain a more thorough understanding of the heat transport pumping mechanism in heat pipes. Current heat pipe models assume that the adverse capillary pressure in the condensing meniscus is negligible and the capillary pressure in the evaporator is maximum. These assumptions may be invalid during normal heat pipe operation yielding unrealistically high heat transport values. The development and results of this model will enhance our understanding of how wick microstructure influences the heat pipe energy transport capability, a critical factor in the development of advanced heat pipe wicks for cryogenic applications.

III. HEAT PIPE DIODE AND THERMAL SWITCH CONFIGURATIONS

A literature review of heat pipe diode and thermal switch configurations has been performed to determine which configurations have potential application to the AstroLab cryogenic heat pipe study. Important system specifications include: 1) monodirectional heat transfer, 2) reproducible shut-off time which may be slow or fast depending on the particular application, 3) high switching ratio, and 4) a sufficiently large "off" thermal resistance. The shut-off time is the time a system takes to effectively prevent heat from leaking into the protected device. The switching ratio is the ratio of the "off" thermal resistance to the "on" thermal resistance. The required "off" thermal resistance can be evaluated once the maximum allowable heat leak to the protected device is defined. Specific values of the shut-off time and maximum heat leak for the AstroLab cyrogenic heat pipes have not been specified to date. The literature search has shown that the operational characteristics, such as those defined above, and transport mechanisms vary considerably for each diode or switch configuration.

The heat pipe diode shown in Figure 1 has a wicked reservoir or trap block attached to evaporator end of the heat pipe. During normal operation, the reservoir is maintained at a temperature high enough to prevent the working fluid vapor from condensing in the

reservoir wick. When the condenser temperature exceeds the evaporator temperature causing the heat pipe to operate in a reverse heat transport mode, the reservoir is cooled sufficiently to force working fluid vapor to condense in the reservoir wick. The condensation process in the reservoir depletes the heat pipe of working fluid, causes dry-out in the evaporator, and effectively turns off the heat pipe. The heat pipe is restarted by heating up the reservoir, drying out the reservoir wick, and replenishing the heat pipe with it's working fluid.
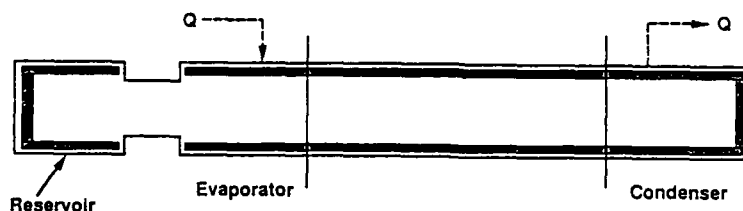

Figure 1.   Heat Pipe Diode Configurations.

Heat pipe diodes studied in the past [1-3] have shown a fairly wide range of shut-off times ranging from 10 minutes to 2 hours. The specific value of the shut-off time is dependent on the heat transfer rate as well as the heat pipe size and configuration. Values for the switching ratio were not available in any of the papers found in the literature and have to be calculated to make reasonable comparisons with thermal switches.

Thermal switches offer an alternative way of forcing monodirectional energy transfer in heat pipes. The switch operates in either an "on" or "off" mode which couples or decouples, respectively, the heat pipe to the heat source. The types of thermal switch configurations which have been studied in the past include: 1) gas gap switch with a valve or valves [4-6], 2) gas gap switch with a gas adsorption block [7,8], and 3) thermal expansion switch [9].

The gas gap configuration has received considerable attention in the literature and is shown in Figure 2. This type of thermal switch is composed of concentric cylinders with conductive fingers separated by a small gap which is filled with a conductive gas. The switch "on" mode is accomplished by filling the gap with enough gas to ensure that a gas continuum exists in the gap. The switch "off" mode occurs after the gas is evacuated generating a nonconductive free molecular transport regime. The shut-off time for this

type of thermal switch varies from less than 1 minute to 10 minutes. In most cases, the switching ratios for these devices are very high ranging from 1000 to 10,000.
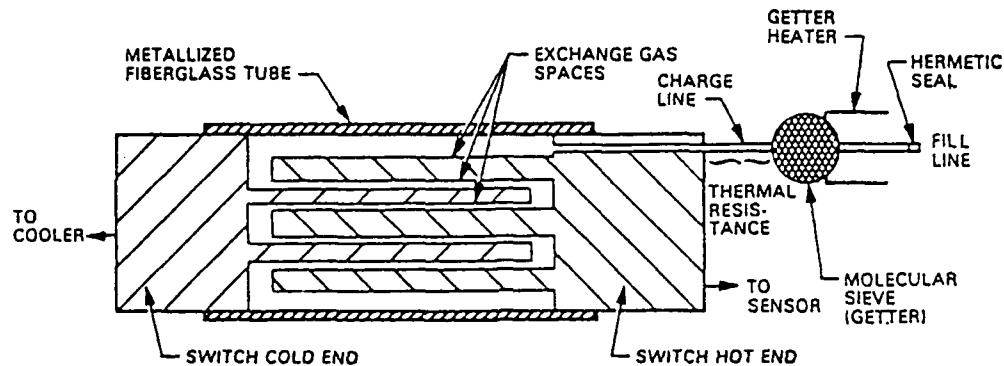

<u>Figure 2.</u>   Gas Gap Thermal Switch with a Gas Adsorption Block
(Taken from [7]).

Unlike the gas gap thermal switch, the thermal expansion switch relies on the difference in the thermal expansion coefficient between two dissimilar metals. This creates a shrink-fit situation depending on the temperature. At higher temperatures a gap is created between the two metals producing a high thermal resistance. As the switch is cooled the high expansion metal contracts onto the low expansion metal and opens the switch. The switching ratio for this device ranges from 100 to 500. Values for the shut-off time were not reported in the literature.

IV. <u>POTENTIAL WORKING FLUIDS FOR CRYOGENIC HEAT PIPES</u>

The selection of a working fluid is a critical aspect of heat pipe system design. The working fluid plays an important role in defining the operational limitations of the heat pipe which serve as primary heat pipe design criteria. Evaluating a working fluid also requires a thorough examination of it's thermophysical and thermochemical properties. Important fluid properties include: 1) material/fluid compatibility, 2) good thermal stability, 3) wettability (zero isothermal contact angle), 4) large figure of merit (FOM),

and 5) large priming factor (PF). Figure 3 shows the operational temperature range for standard cryogenic working fluids.
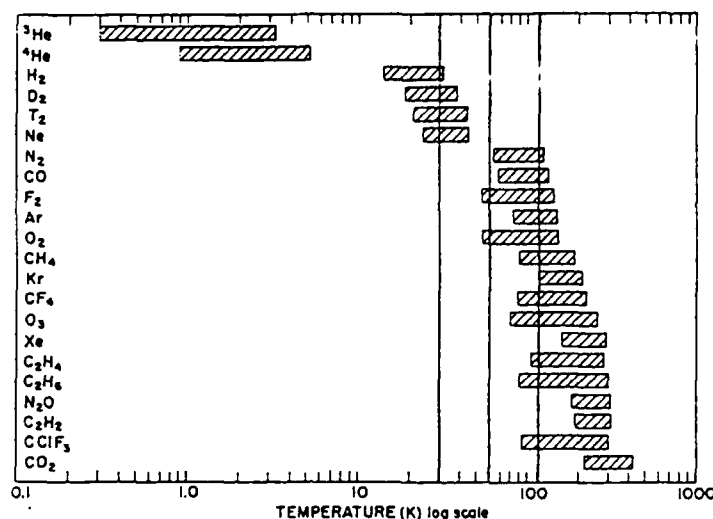

Figure 3.   Cryogenic Liquid Temperature Range [13].

Potential working fluids for the temperature specifications given earlier include:

        30 K - H_2, D_2, T_2, Ne

        60 K - O_2, F_2, OF_2

        120 K - O_2, F_2, Ar, CH_4, C_2H_6, and many others.

The figure of merit, priming factor, and other thermophysical property data for some cryogenic working fluids have been compiled in Table 1. Although this compilation is not complete, there are some notable trends in the data which influence the selection of an appropriate working fluid.

The data for H_2 and Ne, which are both potential 30 K fluids, show that both species have nearly equal priming factors which are fairly high for cryogenic liquids. Ne, however, has a figure of merit which is over five times as large as that for H_2. Ne is also a less hazardous gas to work with than H_2. Thus, Ne appears to be the favorable working fluid based on the available data.

At a temperature of 60 K, O_2 appears to be a more favorable working fluid than F_2 because both it's priming factor and figure of merit are slight larger than those for F_2. O_2 is also less corrosive than F_2.

Table 1.   Properties of Select Cryogenic Fluids.

Temperature	Fluid	T_3 (K)	T_c (K)	P_c (atm)	ρ (g/cm²)	σ (dynes/cm)	h_{fg} (J/g)	μ (centipose)	P.F. (cm/sec)	FOM (J/sec·cm²)
at 30K	H_2	14	33	12.8	.054	0.414	298	.0091	45.6	734
	Ne	25	44	26.9	1.151	4.16	80.8	.0974	42.71	3,972
at 60K	F_2	54	144	51.5	1.669	20.6	187	.637	32.3	10,093
	O_2	54	155	50.4	1.282	21.1	238	.580	36.4	11,099
at 120K	F_2	54	144	51.5	1.218	3.51	118	.124	28.3	4,068
	Ar	84	151	48.0	1.16	4.75	126	.116	40.9	5,985
	O_2	54	155	50.4	0.974	6.16	174	.113	54.5	9,236
	CH_4	91	190	45.4	0.412	12.2	495	.101	120.9	24,639

At 120 K, CH_4 is obviously the best choice because it's priming factor and figure of merit are at least twice as large as those for the other fluids. CH_4 is also preferred because it is less likely to contaminate the heat pipe wick and container.

Fluid wettability is also an important factor in selecting a working fluid and is characterized by the isothermal contact angle between the working fluid and the wicking material. A small isothermal contact angle, approximately equal to zero, is desired for most heat pipe designs. The magnitude of the contact angle is determined by the intermolecular forces near the vapor-liquid-solid contact line (interline). Wayner [10] has developed a model of the interline region which has shown good agreement with published data on the apparent contact angles of the n-alkane PTFE system. This model can be used to estimate the apparent contact angle for various material/working fluid combinations.

Even though choices among standard cryogenic fluids can be made, the fluids selected may still lack the pumping capability required by the system specifications. An

alternative approach may be the use of cryogenic fluid mixtures or surfactant additives. Semiempirical relationships for fluid mixture properties can be found in Reid et al. [11]. The simplest mixture viscosity for nonpolar liquids is given as

$$\ln \mu_m = \sum_{i=1}^{n} x_i \ln \mu_i, \tag{1}$$

where μ is the viscosity and x is the liquid volume, weight, or mole fraction. This expression assumes that mixture viscosity is a monotonic function of composition. An estimate of the mixture surface tension for two nonpolar liquids is

$$\sigma_m = x_1 \sigma_1 + x_2 \sigma_2 - \frac{\gamma}{2RT} (\sigma_1 - \sigma_2)^2 x_1 x_2 \tag{2}$$

where μ_1, μ_2 are the component surface tensions and x_1, x_2 are the bulk mole fractions. γ is an average surface area for the molecules constituting the system (see [11] for details). This expression shows that the mixture surface tension is always less than the mole fraction average surface tension. It should be noted that vapor-liquid equilibrium data are also required to determine the vapor mixture composition and operational temperature range for different liquid mixture compositions. Research concerning cryogenic liquid mixtures is currently underway at the Jet Propulsion Laboratory and the National Bureau of Standards [12].

The addition of surfactants also appears to be a possible way of improving the pumping capability of cryogenic working fluids. Low concentrations of surfactants are known to increase the surface tension of liquids without significantly altering their vapor-liquid equilibrium properties. Unfortunately, due to time constraints, this area of research was not pursued to any degree this summer.

V. HEAT PIPE COMPUTER CODES

A number of organizations have heat pipe computer codes which may be of some use to the AstroLab. Most of the codes address heat pipe transport limitations, steady-state operation, and transient operation. Table 2 shows the current status in acquiring computer codes for the AstroLab. Code evaluation and adaptation will take place once the codes have been received.

Table 2.   Current Status in Heat Pipe Computer Code Acquisition (August 1989).

ORGANIZATIONS	COMMENTS	CONTACTS	
LANL	CONTACTED - send PC code	M. Merrigan	(505) 667-6466
AFWRDC	CONTACTED - code not available (NUF)	J. Beam	(513) 255-6241
NASA LeRC	CONTACTED - code not available (NUF)	A. Uhasz	(216) 433-6165
JPL	CONTACTED - further correspondence required	R. Richter	(213) 354-3253
GTECH	CONTACTED - further correspondence required	G. Colwell	(404) 894-3246
WSU	CONTACTED - further correspondence required	A. Fagri	(513) 873-2501
UCLA	CONTACTED - further correspondence required	I. Catton	(213) 825-5320
Aerospace	CONTACTED - further correspondence required	A. Johnson	(213) 336-7271
Battelle	CONTACTED - code not available		
Thermacore	NOT CONTACTED		
TRW	NOT CONTACTED	D. Antonius	
Hughes	NOT CONTACTED		
OAO	NOT CONTACTED		

VI. MATHEMATICAL MODEL OF THE EVAPORATING/CONDENSING MENISCUS IN A CAPILLARY TUBE `

The capillary forces occurring in the evaporator and the condenser sections of a heat pipe constitute the basic driving force for internal fluid circulation. Under normal operating conditions, the rate at which fluid is circulated determines the energy pumping capacity of the heat pipe. The net capillary force is generated by the integral effect of the evaporating and condensing menisci. Despite the complicated nature of these capillary forces, the heat transport capability of a heat pipe is usually determined by equating the capillary pressure to the liquid pressure drop in the wick, assuming that the adverse capillary pressure in the condenser is negligible and the capillary pressure in the evaporator is maximum. This is commonly known as the capillary limitation and presumably represents the point at which dry-out begins in the evaporator. Unfortunately, the maximum capillary pressure (used to evaluate the wicking limitation) can not be used as the capillary pressure for mathematical simulations of both steady and transient heat pipe operation. This is due to the fact that the actual capillary pressure is dramatically affected by the interfacial phenomena characterizing the menisci during evaporation and condensation.

Although the heat pipe has been studied extensively in the past, very little effort has

28-11

been put forth to understand the basic mechanism describing the evaporating and condensing menisci. Past studies which address the vapor-liquid interface in heat pipes [14-16] treat the interface as a macroscopic phenomenon and are semiempirical in nature since they require mass transfer data. A mathematical model derived from first principles should actually generate values for the mass transfer rate since the mass transfer rate is not a true parameter of the system. A second drawback of the past macroscopic models describing the vapor-liquid interface is that they neglect both microscopic interfacial phenomena and molecular interactions taking place near the vapor-liquid-solid contact line, known as the interline. The inclusion of these phenomena into an integral formulation of the macroscopic interface similar to that derived in [15] will yield a solution that does not require the use of mass transfer data. This type of integral formulation will also be amenable to formal optimization techniques which can be used to determine the optimal radial and axial pore size distributions. These distributions represent fabrication parameters which are essential to the design of advance heat pipe wicks. The foundation of this design technique, however, begins with a fundamental understanding of the evaporating/condensing meniscus, preferably for a simple wick geometry.

The forthcoming mathematical model describes the fluid mechanics, heat transfer, and interfacial phenomena characteristic of the evaporating/condensing meniscus in a capillary tube. The formulation includes the full three-dimensional Young-Laplace equation, Marangoni convection, London-Van der Waals forces, and nonequilibrium interface conditions. The model is based on the pioneering work of Wayner [17-21] and is similar to the model of Mirzamoghadam and Catton [22].

Figure 4 shows the various flow regions and coordinate system used to describe the evaporating/condensing meniscus in a capillary tube. The origin of the axial coordinate (x) is at the interline while the origin of the radial coordinate (r) is at the tube center. r_i is the distance from the axial centerline to the meniscus interface. Each region is briefly described as follows:

1) Interline region - the London-Van der Waals forces (intermolecular forces) are important and significantly affect the apparent contact angle and interfacial curvature.
2) Meniscus region - London-Van der Waals forces are small and the interfacial curvature dominates the capillary pressure creating an attenuated Hagen-Poiseuille flow field.
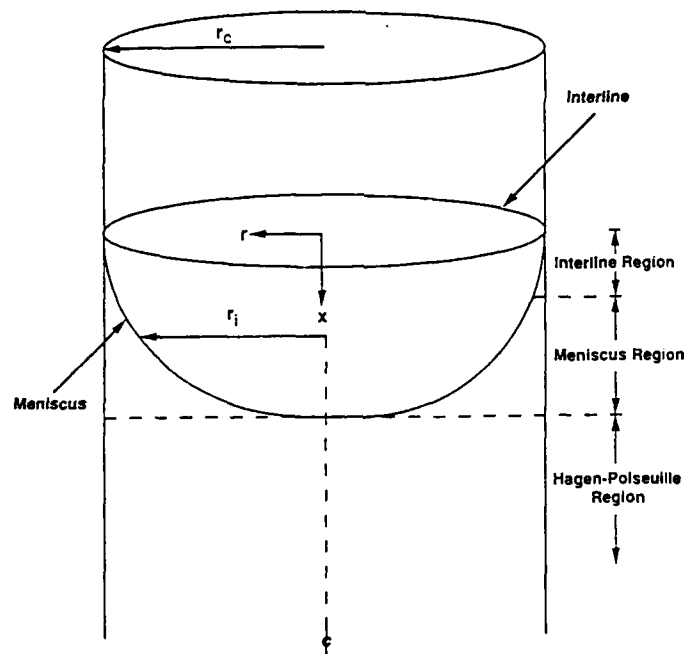3) Hagen-Poiseuille region - Hagen-Poiseuille flow.

Figure 4. Flow Regions for the Evaporating/Condensing Menis-
cus in a Capillary Tube.

A mathematical model of the evaporating/condensing meniscus in a capillary tube
can be formulated under the following assumptions:

1) Steady-state two-dimensional laminar flow.
2) Incompressible flow.
3) The advective and convective terms are negligible.
4) The radial pressure gradient is negligible.
5) The temperature in the bulk vapor is equal to the interfacial vapor temperature.
6) The pressure in the bulk vapor is constant.
7) No slip at the wall.

Under these conditions, the momentum equation describing flow in the meniscus and
interline regions is (radial coordinates)

$$-\frac{dP_{l,i}}{dx} + \frac{\mu_l}{r}\frac{\partial}{\partial r}\left(r\frac{\partial u}{\partial r}\right) = 0, \tag{3}$$

with boundary conditions of

$$r = r_i \;, \quad \mu_L \frac{\partial u}{\partial r} = \frac{\partial \sigma}{\partial x} \;,$$

$$r = r_c \;, \quad u = 0 \;.$$

The first boundary condition equates the interfacial shear stress to the change in surface tension with respect to position, thus accounting for Marangoni effects at the interface. The solution to this differential equation is straightforward yielding

$$u = \frac{1}{4\mu_L} \frac{dP_{Li}}{dx}(r^2 - r_c^2) + \left(\frac{r_i}{\mu_L} \frac{d\sigma}{dx} - \frac{r_i^2}{2\mu_L} \frac{dP_{Li}}{dx} \right) \ln \frac{r}{r_c} \;. \tag{4}$$

Note that this profile correctly reduces to the Hagen-Poiseuille velocity profile when the interface is at the axial center of the tube ($r = r_i = 0$). The liquid pressure in the velocity profile can be evaluated using a modified form of the Young-Laplace equation given by

$$P_{Li} = P_{vi} - \sigma K - \frac{\bar{A}}{(r_c - r_i)^3} \;. \tag{5}$$

The second term on the right side of the equation is the capillary pressure (due to interfacial curvature) and the third term is the disjoining pressure for nonpolar liquids (Deryagin et al. [23]) due to the London-Van der Waals forces near the interline. Note that when the meniscus is near the wall ($r_c \approx r_i$), the disjoining pressure dominates the capillary pressure; the disjoining pressure also decreases rapidly as the interface gets further away from the tube wall. An expression for the interfacial curvature in a capillary tube has been derived by Philip [24] and is given as

$$K = \frac{1}{r_i [1 + (dr_i/dx)^2]^{1/2}} - \frac{d^2 r_i/dx}{[1 + (dr_i/dx)^2]^{3/2}} \;. \tag{6}$$

The local mass transfer rate at any axial position in the liquid can be derived by integrating the velocity profile over the flow cross-sectional area between the tube wall and meniscus interface. This produces

$$\dot{m} = \frac{1}{F_i} \frac{dP_{Li}}{dx} - \frac{F_2}{F_i} \frac{d\sigma}{dT_i} \frac{dT_i}{dx} \;, \tag{7}$$

where the chain rule has been used in the second term to exemplify the Marangoni effect ($d\sigma/dT_i$). The functions F_1 and F_2 are cumbersome functions of r_c and r_i. The integrated mass continuity equation in the liquid is (radial coordinates)

$$W_{li} = \frac{\cos \theta}{2\pi \rho_l \, r_i} \, \frac{d\dot{m}}{dx} \, ,$$

(8)

where θ is the local contact angle given by $\tan^{-1}(-dr_i/dx)$ and W_{li} is the liquid velocity normal to the interface. The interfacial pressure in the vapor phase can be determined by combining equation (8) with the Schrage expression [25] for the interfacial mass flux assuming the interfacial temperature is approximately equal to the temperature in the vapor phase,

$$P_{v_i} = P_v + \left(\frac{2-c}{2c}\right)\left(\frac{RT_i}{2\pi}\right)^{1/2} \frac{\cos \theta}{r_i} \, \frac{d\dot{m}}{dx} \, .$$

(9)

Conservation of energy at the interface requires setting the heat flux normal to the interface equal to the latent heat due to evaporation. This gives

$$\frac{dT_i}{dx} \, \frac{dr_i}{dx} - \left.\frac{\partial T}{\partial r}\right|_{r_i} = \frac{h_{fg}}{2\pi \rho_l \, r_i} \, \frac{d\dot{m}}{dx} \, .$$

(10)

Conservation of energy in the liquid can be expressed as

$$u \, \frac{\partial T}{\partial x} = \frac{\alpha}{r} \, \frac{\partial}{\partial r} \left(r \, \frac{\partial T}{\partial r}\right) \, ,$$

(11)

with boundary conditions of

$$r = r_i \, , \quad T = T_i (x)$$

$$r = r_c \, , \quad T = T_w = const.$$

The solution to this partial differential equation can be approximated using the von Kármán integral method assuming a linear temperature profile of

$$T = T_i + \frac{T_w - T_i}{r_c - r_i} (r - r_i).$$

(12)

The resulting expression is given as

$$\left(\frac{F_3}{4\mu_\ell}\frac{dT_i}{dx}\right)\frac{dP_{\ell i}}{dx} + \frac{r_i F_5}{\mu_\ell}\frac{d\sigma}{dT_i}\left(\frac{dT_i}{dx}\right)^2 - \left(\frac{r_i^2 F_5}{2\mu_\ell}\frac{dT_i}{dx}\right)\frac{dP_{\ell i}}{dx} + \left(\frac{F_4}{4\mu_\ell}\frac{dr_i}{dx}\right)\frac{dP_{\ell i}}{dx}$$

$$+ \frac{r_i F_6}{\mu_\ell}\frac{d\sigma}{dT_i}\frac{dT_i}{dx}\frac{dr_i}{dx} - \left(\frac{r_i^2 F_6}{2\mu_\ell}\frac{dr_i}{dx}\right)\frac{dP_{\ell i}}{dx} = \alpha\left(T_w - T_i\right), \quad (13)$$

where F_3, F_4, F_5, and F_6 are cumbersome functions of r_c, r_i, T_c, and T_i. Combining and rearranging equations (4-13) produces the following set of coupled nonlinear ordinary differential equations

$$\frac{dr_i}{dx} = D_1 \,, \tag{14}$$

$$\frac{dT_i}{dx} = \frac{\frac{dP_{\ell i}}{dx} - F_1\dot{m}}{F_2\frac{d\sigma}{dT_i}} \,, \tag{15}$$

$$\frac{d\dot{m}}{dx} = \frac{2\pi r_i k_\ell}{h_{fg}} D_1 \frac{dT_i}{dx} - \frac{2\pi r_i k_\ell}{h_{fg}}\frac{T_w - T_i}{r_c - r_i} \,, \tag{16}$$

$$\frac{dD_1}{dx} = (1+D_1^2)^{1/2}\left\{-\frac{P_v - P_{\ell i}}{\sigma} - \left(\frac{2-C}{2C}\right)\left(\frac{RT_i}{2\pi}\right)^{1/2}\frac{\cos\theta}{\sigma\,r_i}\frac{d\dot{m}}{dx} + \frac{\bar{A}}{\sigma(r_c-r_i)^3}\right\} + \frac{1+D_1^2}{r_i} \,, \tag{17}$$

$$\frac{dP_{\ell i}}{dx} = \frac{\alpha(T_w - T_i) - \frac{r_i F_5}{\mu_\ell}\frac{d\sigma}{dT_i}\left(\frac{dT_i}{dx}\right)^2 - \frac{r_i F_6}{\mu_\ell}D_1\frac{d\sigma}{dT_i}\frac{dT_i}{dx}}{\frac{F_3}{4\mu_\ell}\frac{dT_i}{dx} - \frac{r_i^2 F_5}{2\mu_\ell}\frac{dT_i}{dx} + \frac{F_4}{4\mu_\ell}D_1 - \frac{r_i^2 F_6}{2\mu_\ell}D_1} \,. \tag{18}$$

It appears that a Runge-Kutta fourth order algorithm can be used to solve this equation set. However, if difficulties arise an implicit method, such as the Adams-Moulton algorithm, can be implemented. Qualitative aspects of how evaporation, condensation, and the London-Van der Waals forces influence the pumping capability of a capillary tube can be discussed by simply rearranging equation (17) noting that K is the interfacial curvature given by equation (6),

$$P_v - P_{\ell i} = \sigma K - \left(\frac{2-C}{2C}\right)\left(\frac{RT_i}{2\pi}\right)^{1/2}\frac{\cos\theta}{r_i}\frac{d\dot{m}}{dx} + \frac{\bar{A}}{(r_c-r_i)^3} \,. \tag{19}$$

For an evaporating meniscus, the local mass transfer rate decreases with x because less evaporation occurs as the interface gets further away from the hot wall. Thus, $d\dot{m}/dx$ is negative and the second term in equation (19) is positive. Evaporation, therefore, increases the pressure difference between the vapor and liquid and intensifies the capillary pumping driving force. The third term, which represents the London-Van der Waals force, is also positive and similarly causes an increase in capillary pumping capability near the interline. Thus, both evaporation and intermolecular forces improve the heat transport capability of the meniscus in a capillary tube.

On the other hand, when condensation occurs $d\dot{m}/dx$ is positive and the second term in equation (19) is negative. Condensation, unlike evaporation, decreases the capillary pumping driving force. This may destabilize the meniscus because the London-Van der Waals term and the condensation term are opposite in sign.

The actual quantitative results of this study will likely show that current heat pipe transient and steady-state simulations require a more thorough treatment of the evaporating and condensing menisci. The model will also help define more realistic heat pipe capillary pumping capability with the ultimate goal of improving wick microstructure design.

VII. RECOMMENDATIONS

The forthcoming recommendations apply to the topical areas discussed in Sections III - VI of this report and are categorized accordingly.

Heat Pipe and Thermal Switch Configurations - The information given in Section III suggests that a gas gap thermal switch is the best device for the AstroLab heat pipe system. However, further study is required to determine whether a solenoid valve or an adsorption block evacuation mechanism should be used. This study will require determining and comparing the shut-off times and transient heat transfer characteristics of gas gap switches which use both evacuation devices.

Potential Working Fluids for Cryogenic Heat Pipes - The first task is to obtain a complete set of thermophysical property data for standard cryogenic fluids which are potential heat pipe working fluids at 30 K, 60 K, and 120 K. A comparison similar to that discussed in Section IV should then be made to determine the most viable working fluids. A decision between these fluids can then be based on a calculation of the maximum heat transport limitations. If the heat transport characteristics of these working fluids are not sufficient, both cryogenic mixtures and surfactant additives should be considered.

Heat Pipe Computer Codes - The acquisition and adaptation of heat pipe computer codes

are critical in evaluating various heat pipe designs. Thus, a continued effort in this area is essential.

Mathematical Model of the Evaporating/Condensing Meniscus in a Capillary Tube - The groundwork for a theoretical study of the evaporating/condensing meniscus in a capillary tube has been set in Section VI of this report. Follow-on research will be proposed for the OSR mini-grant including: 1) obtaining the solution to equations (14)-(18) and reporting the results, and 2) formulating a model which couples the evaporating meniscus to the condensing meniscus, each located at opposite ends of a capillary tube. Task 2 is the first step in simulating a process similar to that found in an actual heat pipe and will provide valuable insight into how an evaporating mensicus and condensing meniscus interact. Future research topics include: 1) experimental studies of the evaporating/condensing meniscus, 2) meniscus stability (theoretical/experimental), 3) meniscus studies of more complex wick structures (i.e. screen-groove configurations), and 4) wick structure optimization.

REFERENCES

1. Williams, R.J., "Investigation of a Cryogenic Thermal Diode," AIAA Paper Number 78-416, 1978.

2. Sun, T.H, and Praeger, R.C., "Development of a Switchable Cryogenic Heat Pipe for Infrared Detector Cooling," AIAA Paper Number 74-751, 1974.

3. Basiulis, A., "Unidirectional Heat Pipes to Control TWT Temperature in Synchronous Orbit," Symposium on Thermophysics and Thermophysics of Space Flight, Palo Alto, CA, 1970.

4. Schember, H., personal communication, Jet Propulsion Laboratory, August 1989.

5. Nast, T., Bell, G., and Barnes, C., "Development of Gas Gap Cryogenic Thermal Switch," Advances in Cryogenic Engineering, V27, 1981, pp. 1117-1124.

6. Hustvedt, D.C., "Systems Considerations for Cryogenic Thermal Switch Development," Advances in Cryogenic Engineering, V31, 1985, pp. 915-923.

7. Frank, D.J., and Nast, T.C., "Getter-Activated Cryogenic Thermal Switch," Advances in Cryogenic Engineering, V31, 1985, pp. 933-940.

8. Chan, C.K., "Gas Adsorption/Adsorption Heat Switch," Jet Propulsion Laboratory Publication 87-7, Final Report of Phase I, 1987. Phase II is under study at TRW.

9. Naes, L, and Nast, T., "A Self-Actuated Thermal Switch for Operation with Redundant Mechanical Refrigerators," Advances in Cryogenic Engineering, V31, 1985, pp. 925-932.

10. Wayner, P.C. Jr., "Interfacial Profile in the Contact Line Region of a Finite Contact Angle System," Journal of Colloid and Interface Science, Volume 77, Number 2, 1980, pp. 495-500.

11. Reid, R.C., Prausnitz, J.M, and Sherwood, T.K., The Properties of Gases and Liquids, Third edition, McGraw-Hill Book Company, 1977.

12. Jones, J., personal communication, Jet Propulsion Laboratory, August 1987.

13. Williams, J.D., and Edeskuty, F.J., "Liquid Cryogens," CRC Volume II, Properties and Applications, 1983.

14. Ambrose, J.H., Chow, L.C., and Beam, J.E., "Transient Heat Pipe Response and Rewetting Behavior," Journal of Thermophysics and Heat Transfer, V1, No.3, 1987, pp. 222-227.

15. Beam, J.E., "Unsteady Heat Transfer in Heat Pipes," Ph.D. Dissertation, School of Engineering, University of Dayton, 1985.

16. Beam, J.E., "Transient Heat Pipe Analysis," AIAA Paper 85-0936, 1985.

17. Wayner, P.C. Jr., Kao, Y.K., and LaCroix, L.V., "The Interline Heat-Transfer Coefficient of an Evaporating Wetting Film," <u>International Journal of Heat and Mass Transfer</u>, V19, 1976, pp. 487-492.

18. Preiss, G., and Wayner, P.C. Jr., "Evaporation from a Capillary Tube," <u>Journal of Heat Transfer</u>, V98, No. 2, 1976, pp. 178-181.

19. Wayner, P.C. Jr., "The Effect of the London-Vander Waals Dispersion Force on Interline Heat Transfer," <u>Journal of Heat Transfer</u>, V100, No. 1, 1978, pp. 155-159.

20. Wayner, P.C. Jr., "The Use of Interfacial Phenomena in Change-Of-Phase Heat Transfer," Heat Transfer in Thermal Systems Seminar-Phase II, National Cheng Kung University, Tainan, January 1986.

21. Parks, C.J., and Wayner, P.C. Jr., "Surface Shear Near the Contact Line of a Binary Evaporating Curved Thin Film," <u>AIChE Journal</u>, V33, No. 1, 1987, pp. 1-10.

22. Mirzamoghadam, A., and Catton, I., "A Physical Model of the Evaporating Meniscus," <u>Journal of Heat Transfer</u>, V110, No. 1, 1988, pp. 201-207.

23. Deryagin, B.V., Newpin, S.V., and Churayev, N.V., "Effect of Film Transfer Upon Evaporation of Liquids from Capillaries," <u>Bull. R.I.L.E.M.</u>, V29, 1965, pp. 93-98.

24. Philip, J.R., "Unitary Approach to Capillary Condensation and Adsorption," <u>Journal of Chemical Physics</u>, V66, No. 11, 1977, pp. 5069-5075.

25. Schrage, R.W., <u>A Theoretical Study of Interphase Mass Transfer</u>, Columbia University Press, New York, 1953.

1989 USAF-UES SUMMER FACULTY RESEARCH PROGRAM/

GRADUATE STUDENT RESEARCH PROGRAM

Sponsored by the

AIR FORCE OFFICE OF SCIENTIFIC RESEARCH

Conducted by the

Universal Energy Systems, Inc.

FINAL REPORT

DESIGN AND DEVELOPMENT OF A FLEXIBLE

MULTI-BODY DYNAMICS EXPERIMENT

Prepared by: Roger C. Thompson, Ph.D.

Academic Rank: Assistant Professor

Department and   Aerospace Engineering

   University: The Pennsylvania State University

Research Location: Astronautics Laboratory/VSSS
                          Edwards AFB
                          Edwards, CA 93523

USAF Researcher: Alok Das, Ph.D.

Date: 18 September 1989

Contract No: F49620-88-C-0053

DESIGN AND DEVELOPMENT OF A FLEXIBLE

MULTI-BODY DYNAMICS EXPERIMENT

by

Roger C. Thompson

ABSTRACT

The ground-based testing of flexible spacecraft and robotic space manipulators is highly dependent upon the construction of the experimental apparatus. An experimental facility is under development for the study of the behavior of multi-body systems with regard to dynamic interactions, modeling techniques, and control methodologies. A preliminary design was developed for an air film "flotation system" that will minimize the frictional loads on the structure (about a single axis) and simulate, as much as possible, the free motion experienced in an orbital environment. Experimental tests were performed to determine the design criteria of the experiment as a whole, the flotation system in particular, and the degradation of the motion due to the implementation of the air film supports. Other aspects of the multi-body experiment that were examined were the specifications of an optical, real-time position sensing system and the design of the joints of a two-link, flexible test article.

Acknowledgements

I wish to thank the Air Force Office of Scientific Research/Air Force Systems Command for sponsoring the Summer Faculty Research Program under which this research was performed. The summer program is extraordinarily beneficial to faculty because it promotes technical exchange with Air Force researchers and provides exceptional facilities for conducting ground-based experiments. In addition, I wish to thank Universal Energy Systems for managing this program and for their direction and assistance.

I wish to acknowledge the guidance and support provided by Dr. Alok Das who served as my Technical Focal Point. His confidence and assistance are greatly appreciated. I also wish to thank Capt. John Ward who is the Project Manager of the Multi-body Dynamics Experiment for providing information and assistance throughout the summer. I must also acknowledge the tireless support provided by Mr. Waid Schleagel in helping me to understand the computational facilities and by Mr. Angel Cruz in fabricating hardware for the experiments.

I. INTRODUCTION:

The motion of complex vehicles composed of multiple modules con-
nected by flexible components (multi-body dynamics) is a topic of in-
tense interest for developers of the next generation of large-scale
spacecraft. Because of the complexity of large space structures, math-
ematical modeling techniques must rely upon equally complex numerical
codes to predict the behavior of the structure. Consequently, the
accuracy of the individual codes will depend upon the degrees-of-freedom
permitted in the model and any simplifying assumptions about the motion
and controls that will be encountered. The accuracy of the mathematical
models constructed by each algorithm is usually estimated through com-
puter generated simulations. Although some experimental facilities are
in place, there has not been a consistent, large-scale, ground-based
test-bed available for independent laboratory testing of multi-body
dynamics and control technology.

Facilities for testing spacecraft dynamics are usually highly
specialized. Because the environment of space cannot be duplicated on
the Earth's surface, experiments are designed to examine very specific
subsystems or simplified motions. Initial test articles typically
consisted of simple structures: a rigid central body with flexible
elements attached (not multi-body structures). Examples include the
Draper/RPL experiment and the JPL Antenna experiment, both of which were
supported by the Astronautics Lab. Other recent experiments (Refs. 1-3)
in flexible manipulators differ in that they are true multi-body struc-
tures, but the purpose of the experiments is to control the flexibility
of manipulators alone. The Astronautics Lab proposes to build a facil-

ity for the purpose of fundamental research in the behavior of multi-body spacecraft.

One of the principal missions of the Astronautics Laboratory is to investigate and verify concepts that will be employed in future satellite systems. Therefore, the Vehicle Systems branch of the Astronautics Laboratory is acutely aware of the need for a thorough analysis of the behavior, modeling, and control methodologies as applied to multi-body spacecraft. Consequently, a project to design and construct a suitable experiment has been initiated. In addition to my interest in structural dynamics and controls, my industrial experience in machine design and project coordination were contributing factors in my assignment to this project.

II. OBJECTIVES

The objective of the Astronautics Lab is to produce a "generic" vehicle for various studies in multi-body dynamics. As related to other operational facilities, the Multi-Body Dynamics Experiment will be designed to be highly adaptable such that many different experiments (with different goals) can be executed on the same apparatus. In addition, the test-bed is to be designed to allow other vehicles to replace the original should the need arise. The immediate requirement for the Astronautics Lab is to test modeling software either commercially available or sponsored through other government agencies. However, the long-term goal for the project is to test all aspects of multi-body behavior. Individual topics to be examined will include, but not be limited to,

coupled motions, sensor/actuator dynamics, control/structure interac-
tion, and optimal control technology.

The objective of the 1989 Summer Faculty Research Program (SFRP)
is to determine suitable designs for the initial experiments. Beyond
simply designing the structure, consideration must be given to the kind
of data that must be observed, methods of data acquisition, and com-
patibility of subsystems with the global objective of the Lab. My
assignment for the SFRP is to participate in the detailed design of the
apparatus and the data collection systems.

The estimated date for the experiment to go into operation is just
prior to the summer of 1990. Although this is not a large-scale pro-
ject, the design phase will certainly extend beyond the time frame of
the 1989 SFRP. Therefore, I plan to participate (possibly with funding
from the Research Initiation Program) throughout the coordination,
assembly, testing, and initial experimental phases of the project.

III. PRELIMINARY DESIGN

The design of an experimental apparatus is wholly dependent upon
the phenomenon that is to be investigated. Consequently, a careful
preliminary review of the requirement and goals of a proposed experiment
must precede the detailed design phase. The Astronautics Lab commis-
sioned the Jet Propulsion Laboratory to define the requirements and
produce a preliminary design of the facility. The final report by
Scheid and Schliesmann (Ref. 4) was delivered at the beginning of the
1989 SFRP.

The proposed experiment is a two-link flexible manipulator moving in a horizontal plane to eliminate gravitational loading from affecting the motion (Fig. 1). To simulate, as close as possible, the free motion in space, the structure will be supported by air bearings over a highly polished, extremely flat and level granite table. The JPL report then proceeds to define the baseline requirements for the two-link structure, the control computer, and the sensors.

More detailed specifications for the granite table and the scale of the structure were included as appendices. The justification for choosing the table material was given and manufacturing tolerances on surface finish, local flatness, and overall flatness were defined. The nominal dimensions for the structural components, drive requirements (motor and bearing loads), and shoulder joint design were then tabulated for three principal frequencies.

IV. Detailed Design

The task for the 1989 SFRP was to proceed with the detailed design of the experiment, using the work by Scheid and Schliesmann as a guide. The immediate items to be addressed were the optical tracking system, air flotation system, and elbow joint design.

A. Optical Tracking System

Although the two-link structure will be fully instrumented with different sensors (accelerometers, angle encoders, and strain gages) an optical tracking system would serve as an independent, non-contact

source for verification of the other sensor data and as a backup system for overall control of the experiment. Control experiments will require continuous, "real-time" information; therefore, we concluded that a real-time optical tracking system would be preferred if such a system could be made available.

The heart of the optical system is one or more charge-coupled device (CCD) cameras operating at 60 Hz. A one-camera system has advantages in simplicity; however, in order to cover the area of the table in a single frame with 1 mm resolution, an image plane of 4000 x 4000 pixels would be required. Commercially available cameras rarely exceed 1024 x 1024 pixels. Unfortunately, multi-camera arrangements add complexity to the system because they must be synchronized with respect to time, and overlapping images must be processed to compensate for the inter-image distortion. In addition, the data transfer requirements for either single or multi-camera systems would require 960 million bits of data to be stored each second.

After we determined these constraints, we discussed alternative systems with the representatives from JPL. It was immediately clear that another technique for optical tracking must be found, and that this would require a longer time frame than the summer program allowed. Because JPL has personnel experienced in optical systems, they will continue the detailed design of the tracking system.

B.   Air Flotation System

The majority of the research effort during the 1989 SFRP was devoted to the air-bearing flotation system. The design of the flotation

system would determine the constraints on the design for the remainder of the experiment. The questions to be addressed were: what design would achieve the best results, how much mass could a given design lift, how stable will the system be during rapid (high speed) motions, what are the air supply requirements (flow rate and pressure), and what sources can produce the air needed for the system.

An initial design of a flotation pad (Fig. 2) was fabricated at the Astronautics Lab. Removable acrylic plates were used to distribute the air and provided a means of easily and inexpensively testing different patterns and sizes of vent holes. The supply of air was provided from a compressed gas cylinder; line pressure and air gap were measured vs. mass "lifted" by the device.

Two designs were examined first: a 3-hole plate with 1/8 in. diameter holes and a 36-hole plate with 1/32 in. diameter holes (the 36-hole pattern is indicated in Fig. 2). The tests were conducted on a granite table similar in flatness and surface finish to the table specified for the Multi-Body Dynamics Experiment. Calibrated masses were loaded onto the pad (as equally distributed as possible) and the gas flow was gradually increased until the pad was free-floating.

The initial tests were quite surprising; the 3-hole plate did not perform well although the total vent area is 34% larger than the other plate. In fact, we could not take data for this test because the pad was "grounded" by the smallest mass (100 g) that we had available. However, the 36-hole design performed far better than we had anticipated, and because of the results of these tests, the 36-hole pattern was duplicated with larger (3/64 in. diameter) holes. The lifting capacity vs. line pressure is given in Table 1 for both 36-hole designs.

In each case, we found that the air gap required for free motion was 0.004 in. and the line pressure was substantially reduced for the plate with larger holes (the vent area is 2.25 times larger). By repeating the load tests with dynamic pressure and flow rates measured at the compressed gas cylinder, we determined that a flow rate of 16 L/min would be necessary to lift 3 kg. It should be noted that the volume flow rate was the same for both 36-hole designs, as we might expect, because the air gap, the mass lifted, and the exit pressure were the same. Qualitatively, the 36-hole pattern is quite stable; we detected no degradation of the performance when speeds were increased.

Table 1. Lifting Capacity of 36-Hole Plates

| | Line Pressure (psi) | |
Lifting Capacity (g)	1/32 dia. Holes	3/64 dia. Holes
836.8	0.0*	0.0*
1081.0	0.0*	0.0*
1324.5	0.5	0.0*
1567.2	1.0	0.0*
1809.2	1.5	0.0*
2009.2	2.0	0.0*
2209.2	2.5	1.0
2479.9	4.5	1.3
2749.6	6.0	1.5
3082.0	10.0	1.7
3581.2	----	1.9

* indicates no measurable gauge motion

The line pressure is a significant factor in defining a suitable source of air. The air must be supplied at a given pressure and volume flow rate; it is the relative magnitude of these two quantities that will determine the operational characteristics of the air source. We have verified that the volume flow rate varies principally with the mass that must be lifted, and the line pressure is a function of the design

of the plate. With a lower line pressure, more options are available for selecting an air source. For example, with light loads to be lifted, a high volume, low pressure fan may prove acceptable for the 3/64 in. dia. design but not for the 1/32 in. dia. hole configuration.

Attempts to mathematically model the performance of the flotation system were not successful. The fluid dynamics is so dominated by viscous effects, on a microscopic level, that predictions based upon a simple model were in-correct by two orders of magnitude; the flow regime more closely resembles a "lubricating" flow. We will attempt to develop a usable model, in a project at the Pennsylvania State University (PSU), for estimating the line pressure and flow rate as a function of lifting capacity and hole size.

The second 36-hole plate design was accepted as a baseline configuration for the flotation system, and we then began examining potential sources that could supply the correct air flow. Several options for delivering the air were considered: on-board compressors or fans, on-board gas cylinders, and a central compressor or cylinder with flexible tubing as a conduit to the flotation pads. The systems carried on the structure are attractive because the effect on the dynamic behavior of the structure is easy to predict; the entire source is self-contained with well known mass and moment of inertia properties.

Miniature compressors develop sufficient pressures (up to 6 psi), but the flow rates are extremely low: rarely exceeding 2 L/min. Similarly small axial fans, such as cooling fans for electronic equipment, have an acceptable flow rate, but the pressures are not high enough to lift more than 1 kg. Commercially available compressors and fans with adequate performance characteristics invariably exceed 3 kg and are

physically too large for the Experiment. On-board gas cylinders can produce the correct pressures and flow rates, but they are also very heavy. A laboratory-sized cylinder 4 inches long with a 3 inch diameter has a mass of 2 kg, not including the regulator required to reduce the pressure. However, operating at an internal pressure of 1800 psi, the cylinder can supply air to one flotation pad for only 30 sec when lifting a 3 kg load. Consequently, this approach is also unacceptable, and we conclude that the Experiment must use a centralized compressor or cylinder as the source for the air flotation system.

Our next task, given the necessity of using tubing to distribute the air, was to estimate the effect of the plumbing on the dynamic behavior of the flexible links. A simple test was set up in the lab to measure the change in the natural frequency and damping of a similar flexible component. A thin, uniform aluminum beam of approximately the same size as a link in the Multi-Body Dynamics Experiment was vertically cantilevered to a rigid base. An accelerometer, mounted at the free end, was used to measure the response of the beam. An initial deflection is imparted to the beam, and the tip accelerations are recorded for later analysis. The experiment is conducted on the aluminum beam alone, and is then repeated with 3/8 in. diameter Tygon® tubing secured to an edge of the beam.

The measurements indicated a mode 1 frequency shift from 1.52 Hz (with no tubing) to 1.47 Hz with the tube in place. An analytical model based solely upon the added mass of the tubing (the increase in stiffness is ignored) was used to predict a frequency shift from 1.48 Hz to 1.42 Hz respectively. Note that including the stiffness of the tube would cause the predicted value of the frequency to more closely ap-

proach the measured response. We attempted to determine the damping

factors from the accelerometer output by isolating the principal fre-

quency (i.e. removing any electronically induced drift) and calculating

the logarithmic decrement. However, the results were inconsistent with

the known behavior; the analysis indicated that the damping factors were

reduced from 0.022 for the beam alone to 0.012 for the beam and tube. A

data analysis software package was used in this procedure, and the

errors are probably due to the inability of the program to fully isolate

the very low-frequency drift observed in the data (see Fig. 3). Never-

theless, from the measured response, and supported by the analytical

predictions, we can conclude that the presence of the tubing for air

distribution will only marginally affect the motion of the flexible

links. The degradation will be measurable, but it will not be suffi-

cient to alter the predominant behavior of the structure.

C.   Articulated Joint Design

The most important part of the design of the actual vehicle is the

two hinged joints: the "shoulder" is fixed to the granite table, and the

"elbow," which connects the two flexible links, floats on one of the air

bearings. The shoulder can rotate in a full circle, but the elbow has a

limited, but large-angle, motion. Because Scheid and Schliesmann had

considered the shoulder joint design in their final report (a sketch

and some specifications on the power, control, and data acquisition

circuitry), they should continue to develop this component of the struc-

ture. However, because the elbow design is dependent upon the capacity

of the flotation system, that portion of the project was included in the SFRP.

Unfortunately, the detailed specifications of the elbow were not completed during my appointment at the Astronautics Lab; the flotation system fabrication and experiments consumed more time than we anticipated. Because I will continue to be involved in this project during the remaining stages, I will complete the elbow development at PSU. The Astronautics Lab plans to begin acquiring the individual components in late 1989, and the complete structural design should be completed before then.

V. RECOMMENDATIONS

The design of the Multi-Body Dynamics Experiment and the timetable for completing the project are proceeding along a logical path. We have addressed, over the Summer, a number of factors that would greatly affect the performance of the facility, and many of these problems have been resolved. However, there remains some areas that must be considered in much more detail.

The optical tracking system is perhaps the most obvious single element that is, at present, undefined. For many experiments, a real-time, precision optical tracking device will not be required because the data will be collected and batch processed after the completion of each test. Nevertheless, incorporating a real-time tracking system into the initial phase of the program is highly recommended. The growth potential of the Experiment will be maximized from the beginning; the facil-

ity will have a unique, advanced, and flexible sensor technology avail-
able for all experiments.

The air bearing tests during the SFRP revealed a stable, practical
design for the flotation system. The configuration of the test article
was certainly not an optimal design, but we observed no deficiencies in
the performance of the air flotation pads with regard to the objectives
of the Experiment. The present concept provides an inexpensive, easily
modified, and easily manufactured flotation system. Because the mass
flow rate of the gas is the governing factor in determining the lifting
capacity, attempts to optimize the design will probably yield minimal
results for the time spent in examining this issue. Instead, the proto-
type should be accepted in its current form, and the final dimensions
and specifications will be determined such that the mass of the pads
will be minimized.

Because the researchers at JPL who will continue to be involved in
this project have a prototype design for the shoulder joint, it is rec-
ommended that they proceed with the detailed design for that component.
The elbow design, which was briefly examined during the SFRP, can be
completed at the Pennsylvania State University. Close correspondence
between the Astronautics Lab, JPL, and PSU will insure that compatibil-
ity between components, standardization of the hardware, and coordina-
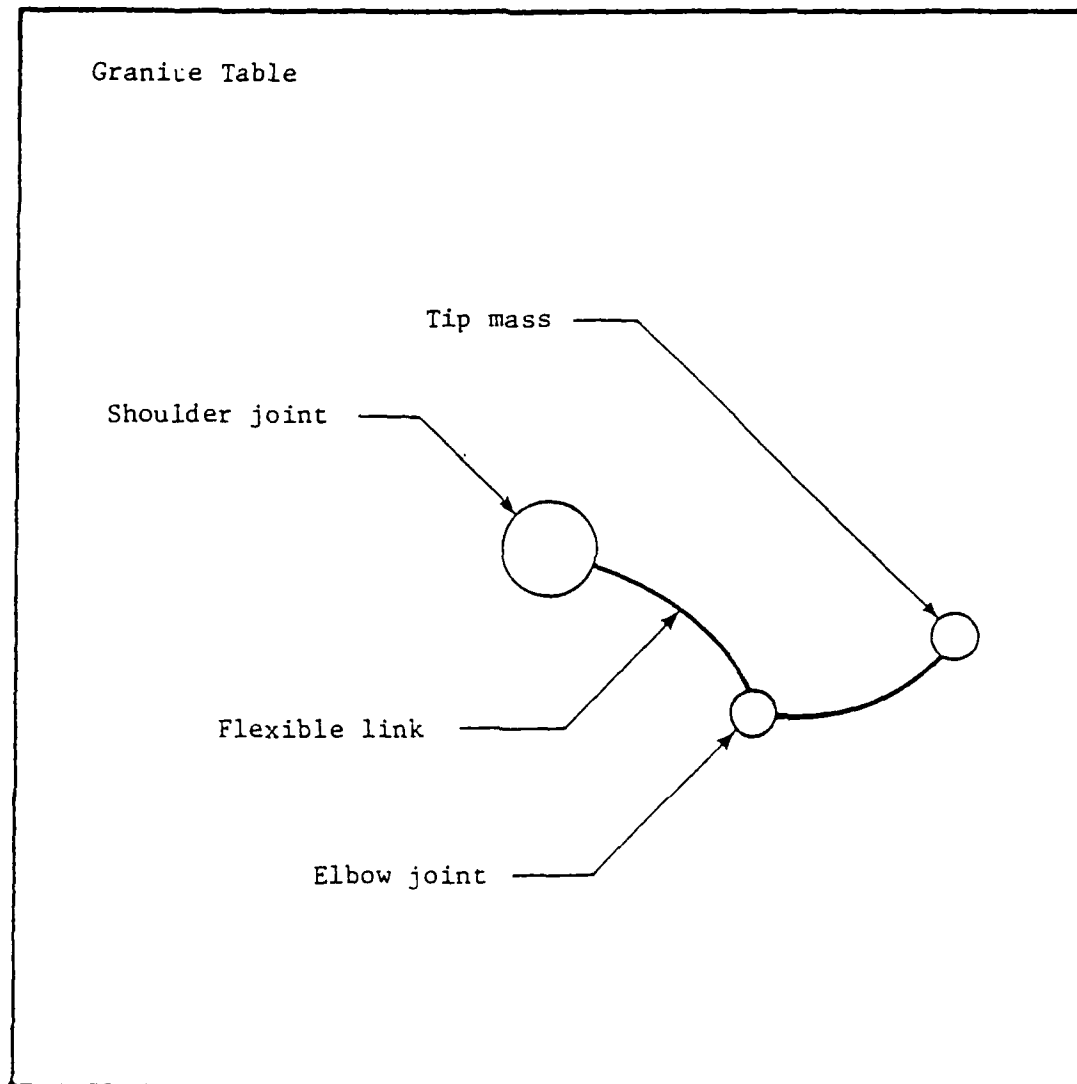tion with the Astronautics Lab is maintained.
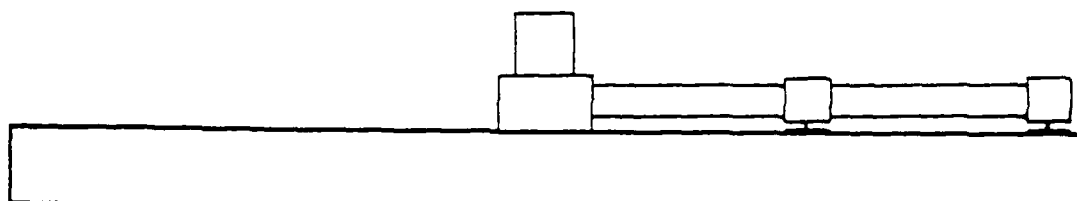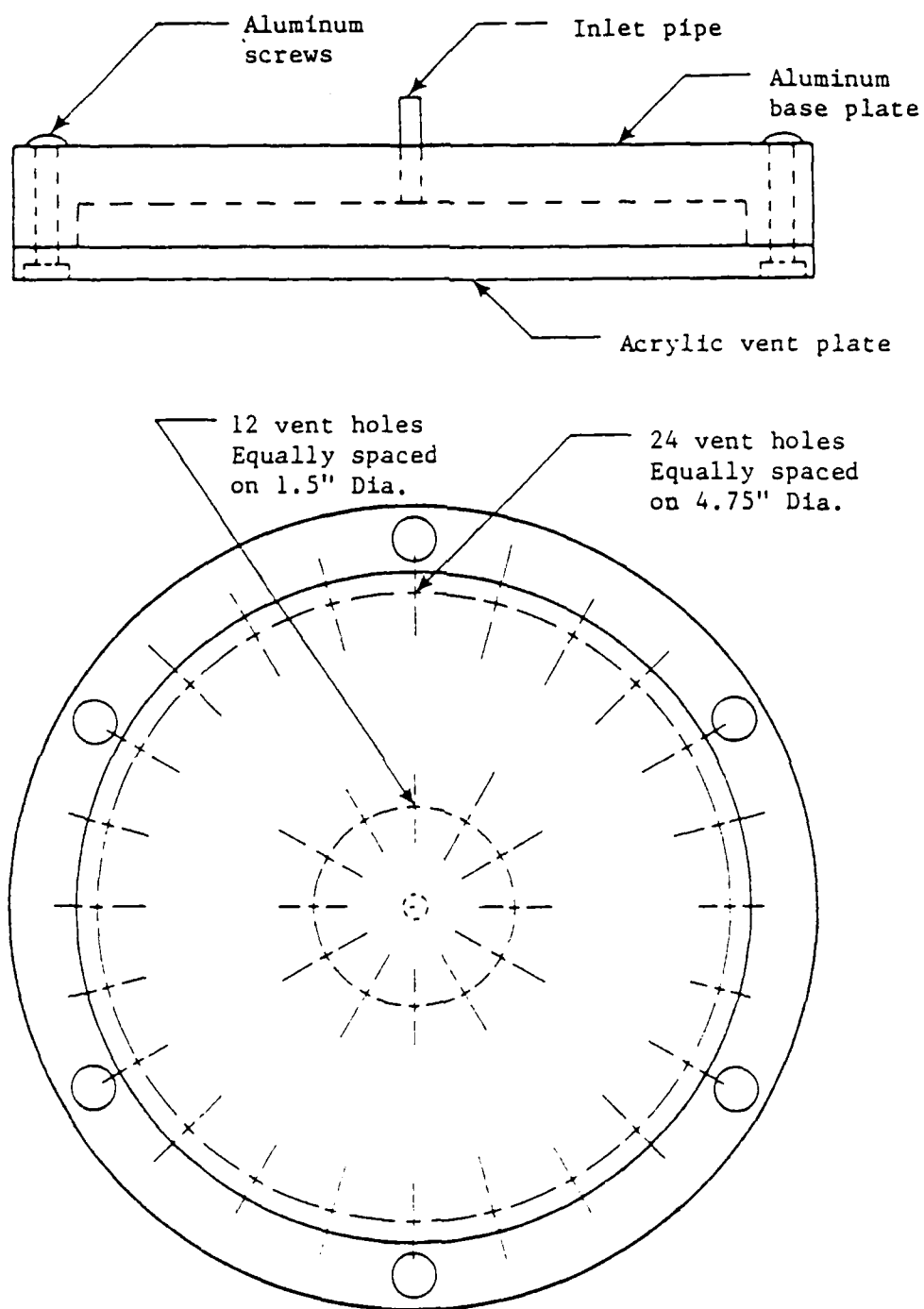
Figure 1   Multi-Body Dynamics Experiment
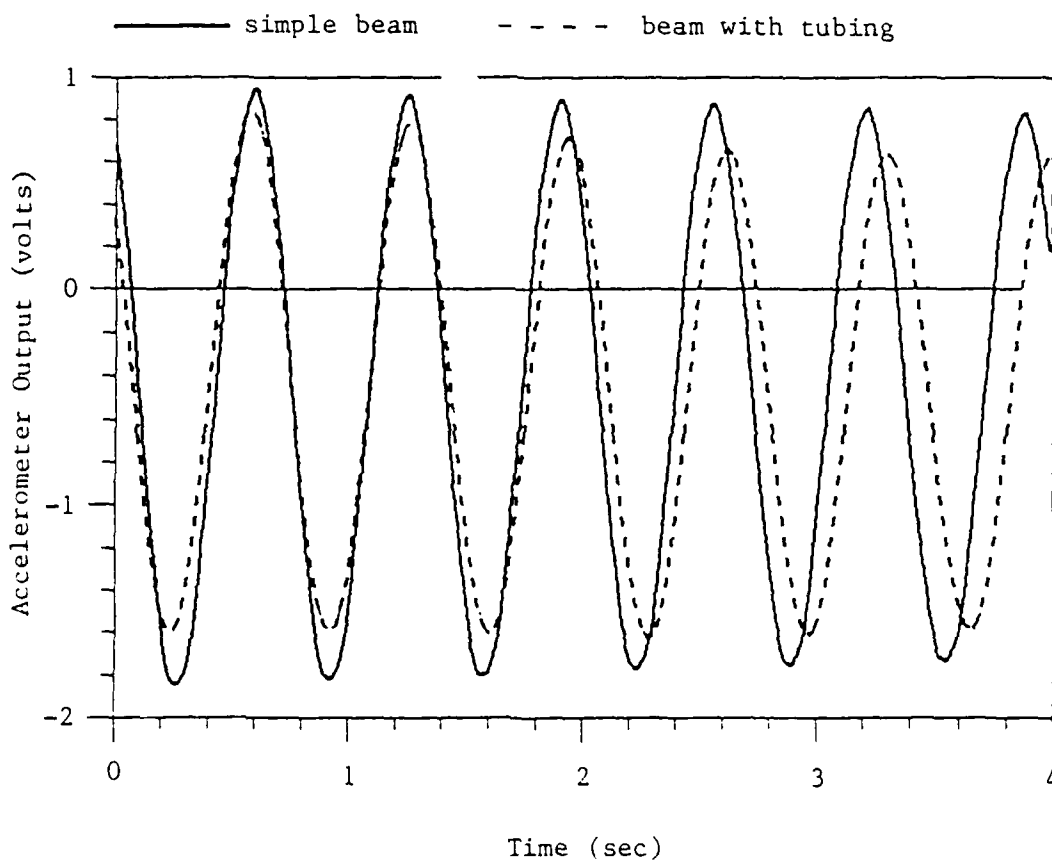
Figure 2   Experimental Flotation Pad

Figure 3   Effects of Flexible Tubing on the
           Response of a Cantilevered Beam

REFERENCES

1.   Oakley, C. M. and Cannon, R. H., "Initial Experiments on the Control of a Two-Link Manipulator with a Very Flexible Forearm," Proceedings of the 1988 IEEE Robotics and Automation Conference, pp. 996-1002.

2.   Buchan, K. S., Carusone, J., and D'Eleuterio, G. M. T., "RADIUS - A Laboratory Facility for the Study of the Dynamics and Control of Elastic Manipulators," Presented at the Seventh VPI&SU/AIAA Symposium on Dynamics and Control of Large Structures, Blacksburg, VA, May 8-10, 1989.

3.   Schmitz, E. and Ramey, M., "A Simplified Dynam. Model for an Experimental Planar Manipulator with an Elastic Forearm," Presented at the American Control Conference, Pittsburgh, PA, June 21-23, 1989.

4.   Scheid, R. E. and Schliesmann, R. G., "Multibody Dynamics Experiment: Requirements Definition and Preliminary Design," JPL Report No. JPL D-6472, May 30, 1989.

1989 USAF-UES SUMMER FACULTY RESEARCH PROGRAM

GRADUATE STUDENT RESEARCH PROGRAM

Sponsored by the

AIR FORCE OFFICE OF SCIENTIFIC RESEARCH

Conducted by the

Universal Energy Systems, Inc.

Final Report

SYNTHESIS OF ACTIVE SPACE STRUCTURE VIBRATION
CONTROL SYSTEMS FOR AN ASTREX TEST ARTICLE

Prepared by :   Ji C. Wang, PhD, PE

Academic Rank :   Professor

Department and   Mechanical Engineering

 University   :   San Jose State University

Research Location :   USAF/AL/VSSS
                        Astronautics Laboratory
                        Edwards AFB, CA 93523

USAF Researcher :   Dr. Alok Das

Date :   15 Sep 89

Contract No :   F49620-88-C-0053

Synthesis of Active Space Structure Vibration Control Systems for an ASTREX Test Article

by

Ji C. Wang

ABSTRACT

Two active vibration control systems and a fine-pointing servo-control system for an ASTREX test article are designed. The independent modal space vibration control system controls the first 20 elastic modes of the structure with 20 point actuators. The control law design for this system is simple, but the control energy level required is too high for a practical space application. The linear quadratic regulator vibration control system which controls the 20 elastic modes with 15 point actuators works well. Its control energy is much realistic than that of the first control system. Unique design problems related to disturbuted parameter control systems are addressed, these are placement of a finite quantity of point actuators/sensors on the structure, determination of a critical subset of structural modes for control, and data processing for observation spillover reduction and the modal states estimation. In addition, a multi-loop PID control system for a fine-pointing of the test article is studied.

I   INTRODUCTION

The US Air Force Astronautics Laboratory (AFAL) at Edwards
AFB is currently developing the Advanced Space Structures
Technology Research Experiments (ASTREX) facility. This large
space generic structure testbed is designed to provide the
structural control research and space development communities with
a versatitle facility for demonstrating advanced structures and
control technologies on realistic models of high performance
spacecraft. The ASTREX ground test facility enables both large
angle slewing and subsequent vibration/pointing/shape control of
a variety of flexible bodies [1]. The initial test article will
be a 5-m diameter dynamically scaled model of a space based laser
beam expander. This ASTREX test article will be mounted on a
three-axis spherical air bearing table which is supported by a
pedestal fixed on the gound. An innovative set of
sensors/actuators will be installed on the test article, and a
real time control and data acquisition computer will monitor and
control the motion of the structure for structural dynamic study,
structure system identification methodology development, and
modern control algorithms evaluation.

This report summarizes the work performed during the 10 weeks
at the Edwards AFB (June-August, 1989). The principle goals of
the Summer project are 1) to investigate modern control systems
and the associated hardwares (types of sensors / actuators, and
their placement on the structure) for active vibration suppresion

of the test article, 2) to investigate a fine-pointing
servo-controlled system for small angle attitude control.
The results of this Summer study will serve as the preliminary
design information to conduct the planned research objectives at
the Laboratory.

Study of future large space structures is a challenge
research area. There is a limited number of research
laboratories in this country where it is equiped with a modern
realistic space structure testbed. Designing of a future space
structure control system requires a good understanding of
structure dynamic, modern control theory , and on modern
instrumentation and digital computer system. My research
interests for last 20 years have been in the application of
modern control theory to mechanical, electro-mechanical, and
aeronautic systems. I have worked for two years at industry
for attitude control of a communication satellite . I have
been a senior researcher, for last eight years, at NASA Ames
research center for helicopter dynamic system identification
and vibration control. I have been teaching these subjects for
last 20 years at the San Jose State University, and I am the
director of the Instrumentation and Control Laboratory. My
technical background will enable me to contribute in the
control system design for the ASTREX test article.

II.   OBJECTIVES OF THE RESEARCH EFFORT

The active vibration suppression is an important control
problem of large space structure (LSS) system. For some space

applications,the amplitude of the vibration, which may be induced

from external distrubances or from commanded maneuvers like large

angle slewing, must be controlled to an acceptable level within a

finite time. Active vibration control system employes the use of a

feedback system which incorporates a sensing of structure

vibration and calculation of the control input signals for

actuators to dump the vibration present. Large structures are

continum strucutres requiring large dimensional models to

accurately predict their dynamic behavior. However, since on-board

computer capacity 's limited, so active control of LSS systems

must be accomplished with a controller of substantially smaller

dimension than that of the dynamic structure model . In designing

an active structure control system, one must first identify a

critical subset of structure modes to form a reduced-order

model. Once a reduced model is obtained a variety of modern

control system design methods can be applied for active control

of those modes which are modeled in the reduced model.

Another critical design problems for control of large

dimensional sytem with a reduced order controller are the control

and observation spillover . The observation spillover problem is

particularly critical, because an ill-designed system may cause

the unmodelled residual modes to be unstable. If the observation

spillover can be eliminated or reduced, then controll spillover

along cannot casue pole-shifting of the residual modes.

My summer projects are to design active control systems which

not only dump vibration, but simulatneously accomplishe small

angle pointing and trucking of the ASTREX test article . The

control system studied is depicted in Fig. 1   . In the
control system shown   , the active vibration control system
controls the first 20 elastic modes. The rigid body modes of
the test article are estimated from the encorder outputs
installed on the air bearing system. The rigid body part of motion
in the vibration sensor outputs is substracted out, and the
remaining sensor outputs which contain only elastic motion of the
structure are processed with bandlimited filters to reduce
observation spillover effect. A modal state observer is used to
estimate the 20 modal states from the filtered sensor outputs
mentioned above. The first vibration control system designed is
an ideal independent modal space control system. The 20 elastic
modes are independently controlled by 20 actuators and 20
co-located sensors. The second vibration control system is
designed based on the linear quadratic regulator method.
The number of actuators and sensors used for this system are 15
each. A fine-pointing small angle attitude control system is
designed for the test article. This system is a multi-loop
proportional+integral+derivative (PID) control system, the
controller gain matrices are designed based on the linear
quadratic regulator method.
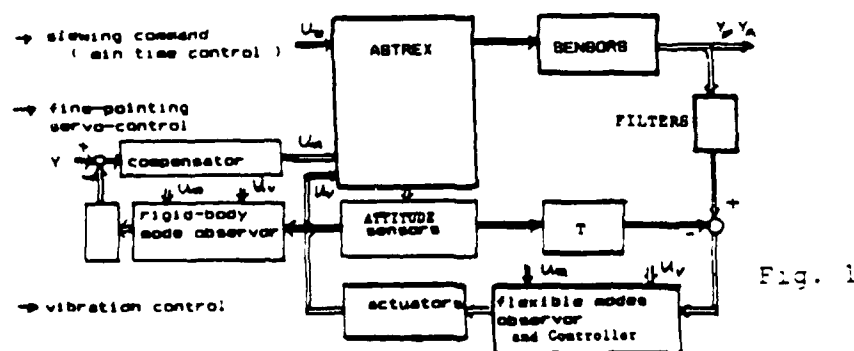
Fig. 1

III.   STRUCTURAL DYNAMIC MODEL

A NASTRAN finite element method is used to obtain a mathematical description of the ASTREX test article. The standard second order matrix differential equation which governs the flexural vibration of the structure can be expressed as

$$M \ddot{q}(t) + C \dot{q}(t) + K q(t) = F(t) \tag{1}$$

Here, mass M , damping C , and stiffness K matrices are each a $n' \times n'$ matrix. The vector $q(t)$ is a $n' \times 1$ vector representing the physical displacements of the structure at all node-points. $F(t)$ is a $n' \times 1$ control input vector acting at each node point of the structure, and n' is the degree-of freedom modeled in the finite element analysis.

A NASTRAN finite element model of the test article provided by Boeing Aerospace was used in this study for control system synthesis. The model provides the eigen-values and the associated mass normalized eigen-vectors (mode shapes) for the case with the damping term $C = 0$ in Eq.1 . The modal domain structural dynamic model is then

$$\ddot{\eta}(t) + D_0 \dot{\eta}(t) + \Lambda_0 \eta(t) = \phi^T F(t) \tag{2}$$

here η is the $n \times 1$ modal displacement vector , which is related to the physical displacement $q(t)$ by the transformation matrix ϕ ; $q(t) = \phi \eta(t)$. The transformation matrix ϕ is a collection of n eigen-vectors such that

$$\phi^T M \phi = I_n \quad, \quad \phi^T K \phi = \Lambda_0 = \left[\omega_\lambda^2 \right] \quad, \quad D_0 = \left[2 \zeta_\lambda \omega_\lambda \right]$$

here, I_n , Λ_0 and D_0 are diagnal matrices and ω_i are ζ_i the natural frquency and the damping of the i-th mode .

(ζ_i = 0.005 is assumed in this study for all i)

For a practical application , since the number of actuators r for vibration control will be much less than n', so only a subset of F(t); U(t) , will be used for active control of the structure. The forcing term in Eq. 2 is now replaced by

$$\phi^T F(t) = \phi^T A \, U(t) = \phi^*(p) \, U(t) \qquad . \quad (3)$$

here $\phi^*(p) = \phi^T A$, p represents the r point actuator locations on the structure, and the matrix A (n'x r) selects the corresponding actuator commands U(t) which is a subset of F(t).

The sensor outputs can be described as

$$y_d(t) = S(p_d) \, q(t) = S(p_d) \, \phi \, n = \phi^*(p_d) \, n \qquad (4)$$

$$y_r(t) = \phi^*(p_r) \, \dot{n} \qquad , \qquad y_a(t) = \phi^*(p_a) \, \ddot{n}$$

here $\phi^* = S \phi$ (m x n') , and p is the m point sensor locations, and the subscript d,r and a indicate the types of sensors ; displacement, rate and acceleration senors, repectively. S (p) is the sensor selection matrix .

To obtain the linear time invariant state dynamic equation for control system design, we define the modal state vector (N x 1, with N = 2 n) as $X = [n , \dot{n}]^T$, then the standard state space representation of the structure is

$$\dot{X} = A \, X + B \, U$$
$$Y = C \, X + D \, U \qquad (5)$$

where

$$A = \begin{bmatrix} 0 & I_n \\ -\Lambda_0 & -D_0 \end{bmatrix} \qquad B = \begin{bmatrix} O_n \\ \phi^T(p) \end{bmatrix}$$

The C and D matrices will depend on the types of sensors
installed on the structure.

The Boeing finite elements model consists of 380 nodes (253
for the test article, and 127 for the pedestal). The total
degrees-of-freedom (DOF) of the model is 2283 (3 rotational
DOF for rigid motion of the test article, 1518 DOF for elastic
motion of the test articel, and 762 DOF for the pedestal). For
the active vibration control systems study, the first 48 elastic
modes of the test article are retained in Eq. 2 ; $n = 48$ ($N=96$).
This 96-order model of Eq.5 is considered to be the true
representation of the structure in the simultion study.   The
eingen-values of the first 20 modes are tabulated in Table 1 .
*The natural frequencies of the structure range from 12.297 Hz to
118.222 Hz.*

IV.   ACTUATORS AND SENSORS LOCATIONS

The actuator locations influence the ultimate physical
realization of the control laws, therefore their locations must be
carefully chosen to assure not only the controllability of the
system but the actuator commands are within the physical limits.
The sensor locations must be also be carefully chosed to assure
the observability of the system for estimation of the strucutre
modes and to minimize the impacts of measurement noises and model
errors upon the control performance.

Two methods are studied for determination of the best actuator/ sensor locations; A) Modal-Shape Method, and B) Controllability (Observability) Method. These two methods can complement each other in determining the final hardware locations [2].

It is commonly understood that to minimize input control energy for structural control the actuators must be placed at the most flexible locations of the structure. The most flexible locations can be determined from the mode shapes (eigen-vectors) of the structure. The Modal-Shape method is used to select a candidate set of actuators (types and locations). Table 2 summarizes the the selected actuator locations (node points) and types of the actuators (T_1 , T_2 , T_3 are force actuators in x- , y- and z- direction, and R_1, R_2 and R_3 are torque actuators about x- , y-, and z-axis). The Controllability Method determines actuator energy level for control of each mode.

The complexity of the controller depends on the types of sensor installed on the structure. In this study we assumed the sensors are co-located with the actuators.

1.0D+02 *

OPEN-LOOP	CLOSED-LOOP POSITION AND VELOCITY FEEDBACK	CLOSED-LOOP VELOCITY FEEDBACK
-0.0039 + 0.77271	-0.0255 + 0.77231	-0.0254 + 0.77341
-0.0039 + 0.77781	-0.0224 + 0.77751	-0.0224 + 0.77871
-0.0046 + 0.91511	-0.0448 + 0.91401	-0.0450 + 0.91401
-0.0052 + 1.04751	-0.0085 + 1.04751	-0.0085 + 1.04771
-0.0059 + 1.18541	-0.0063 + 1.18551	-0.0062 + 1.18561
-0.0061 + 1.21251	-0.0261 + 1.21121	-0.0263 + 1.21171
-0.0069 + 1.38061	-0.0338 + 1.38021	-0.0338 + 1.37931
-0.0090 + 1.80411	-0.0381 + 1.80391	-0.0383 + 1.80461
-0.0098 + 1.96861	-0.0457 + 1.97701	-0.0613 + 1.97981
-0.0099 + 1.98341	-0.0457 + 1.98151	-0.0613 + 1.98641
-0.0100 + 2.00491	-0.0595 + 1.99631	-0.0216 + 1.99261
-0.0101 + 2.02161	-0.0273 + 2.02071	-0.0518 + 2.02101
-0.0105 + 2.10711	-0.0517 + 2.10691	-0.0179 + 2.10631
-0.0112 + 2.24661	-0.0181 + 2.25401	-0.0280 + 2.25451
-0.0114 + 2.27451	-0.0310 + 2.26561	-0.0574 + 2.26311
-0.0122 + 2.43291	-0.0215 + 2.43281	-0.0211 + 2.43151
-0.0134 + 2.67371	-0.0151 + 2.67371	-0.0151 + 2.67381
-0.0135 + 2.7092	-0.0289 + 2.70921	-0.0138 + 2.70921
-0.0140 + 2.79131	-0.0311 + 2.79121	-0.0310 + 2.78991
-0.0150 + 3.01201	-0.0164 + 3.01251	-0.0163 + 3.01231

Node Location	type
4	R_1
31	R_1
206	R_1
208	R_1, R_3
215	T_1, R_1, R_2
218	T_1, T_2, R_3
226	T_1, T_2, R_1, R_2
227	T_1, T_2, R_3
241	R_3
256	R_3

Table 2 actuator location and type

Table 1 eigen-values of the structure

V. STATES OBSERVER DESIGN

For modal domain vibration control system design a state observer is needed to estimate modal states from sensor outputs. The performance of control system depends on the accuracy of the estimated states. The convergence of the estimated states to the true states depends on the math model of the system and also the types of sensors installed on the structure.

A accelerometer is a common sensor in vibration measurement, and a displacement sensor can be designed with a strain gage assembly, but a rate sensor for space application may be difficult to built. Three observers are studied. In the first case we assumed only displacement sensors are used to generate feedback signals. Each output of the sensors is filtered with a first-order filter to attenuate high frequcency part of the signal above the natural frequency of the 20-th mode of the structure (the cut-off frequency of each filter is 130 Hz), and an observer is designed based on the filtered displacement signals. The objective of using a filter in the loop is to minimize observation spillover of those modes which were not included in the observer math model. In the second design case, we assumed displacement sensors and accelerometers are used to measure vibration of the structure. Each sensor output is pass through the filter mentioned above. These filtered sensor signals are input to a kinematic observer for estimation of the rate signals. The displacement signals and the estimated rate signals are then used by the observer for estimation of the modal states (see Fig. 2 and Fig. 3).

In the last case, we showed if only accelerometer outputs are used for modal states estimation, then it is equivalnet to the first case that is with the displacement sensors feedback .

The conclusion of three cases studied is , for a light damped space structure , a set of rate signals must be generated to ease the burden of the observer for estimation of a dependable set of modal states. Without any rate feedback signals the observer gains tend to be large in realizing large negative real parts of the observer eigen-values. High observer gain is not desirable because it amplifies measurement noises and also model errors. If accleromaters are only sensors to be installed on the structure , then these signals can be integrated to obtain rate signals. The design of an observer with only position or only acceleration feedback is difficult , the convergency of the the estimates to the true states are poor for some states. The design and performance analysis of each observer studied are presented in reference [2   ].

CASE 1   POSITION MEASUREMENT
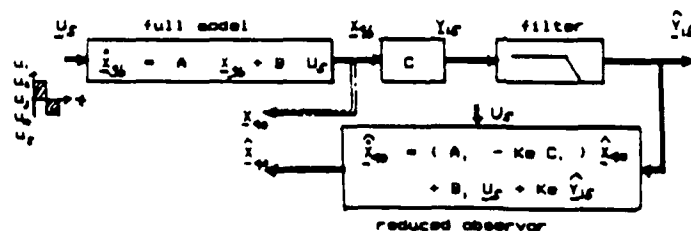
Fig. 2

CASE 2   POSITION AND VELOCITY MEASUREMENTS
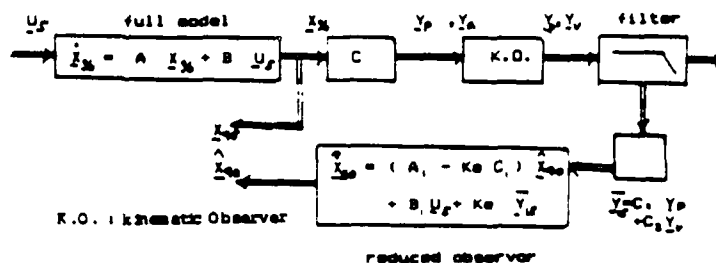
Fig. 3

VI. INDEPENDENT MODAL SPACE CONTROL SYSTEM

A design technique, independent modal control (IMSC) has been applied as a method of generating control laws of future large flexible spacecraft [3]. The main advantage of the IMSC method is that the control law can be generated without regard to the locations of actuators. But this does not imply the actuator locations are immaterial. An IMSC vibration control system is desgined for the ASTREX test article with the first 20 modal states and the 20 actuators listed in Table 2 . The final control law [presented in ref. 2] takes the form

$$U_{20}(t) = \phi^{-1}(p) (D* - D_0) \dot{x}_{20} \qquad (6)$$

where ϕ and D are given in Eq.2 , D* is the desired closed-loop damping of the structure and $\dot{x}_{20}$ is the estimated modal state rate signals. If we set D* = α D , here α is a scalar value, then the control input energy require for the active damping will be proportional to ;

$$U_{20}(t) = (\alpha - 1) \phi^{-1} D_0 \dot{x}_{20} \qquad (7)$$

A vibration control system with α = 16 is studied. Figs. 5 a-b show some of the typical responses of the IMSC system (the ASTREX test article model with 48 modes). In this simulation the external disturbances are four thrusters forces (880 N each loacated at node points 1 , 4 , 64 , 67 . See Fig. 4) . The active suppression of the vibration is impressive, but the input energy required for control is extremely large for any practical implementation (see Figs 6 a-b). High input energy

level is attribute to the fact many elements in $\phi^{-1}(p)$ matrix are large, so even for small α value in Eq. 7 , the magnitude of the $U_{20}(t)$ will be very large. This fact simply points out that for the ASTREX test article the IMSC vibration control system may not be a pratical system for implementation.
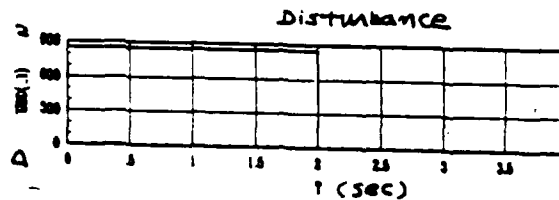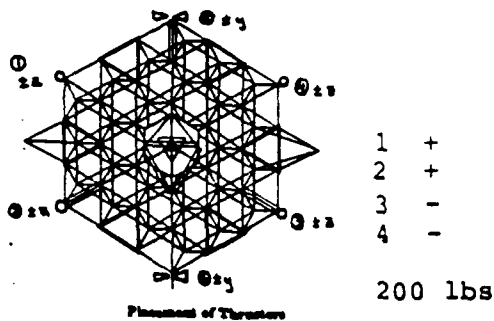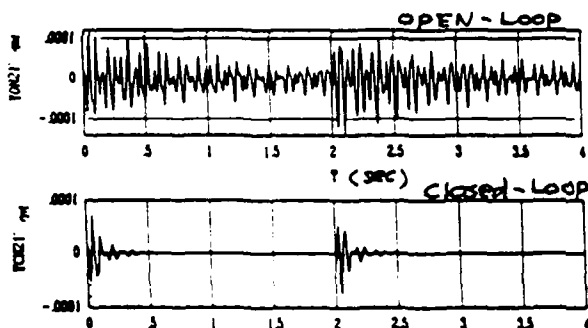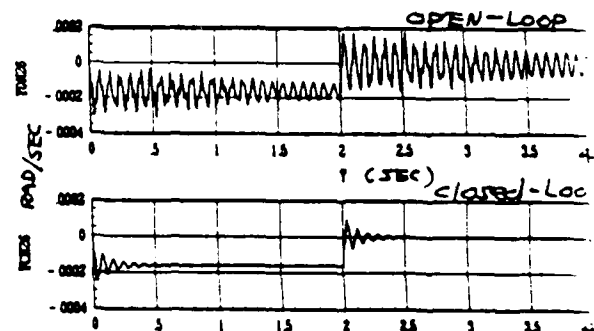

1 +
2 +
3 -
4 -

200 lbs

Fig. 4 Thruster locations and signal size

Figs 5 a-b   Open and Closed Loop Systems Responses
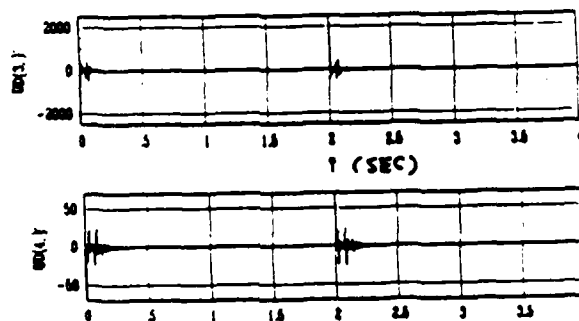
Actuator command (N-m)
U₂ : ND# 206 R1
U4 : ND# 200 R1

Fig. 6 Actuator Commands

VII. LINEAR QUADRATIC REGULATOR

The linear quadratic regulator (LQR) design method is applied for active vibration control of the ASTREX test article. A state feedback controller is designed based on a reduced-order model (the first 20 modes) . The block diagram of the control system is shown in Fig. 7 . The dynamics of the structure is approximated by 48 modes , and the plant state dynamic equation is a 96-order system. The plant distrubances D_4 (t) are four thruster forces which are used for slewing control of the test article(see Fig. 4).

Consider a reduced order model in the modal domain

$$\dot{X}_{40} = A \ X_{40} + B_1 U_{15} + B_2 D_4 \qquad (8)$$

here the 15 actuator locations are specified in Table 2 . (the first 15). The modal states $X_{40} = [\ x_{20} \ \dot{x}_{20} \ ]^T$ are assumed to be available from the state observer. The performance index to be minimized is defined as

$$(9)$$
$$\min J = \int_0^\infty (\ x_{20}^T \ R_{xx} \ X_{20} + \dot{x}_{20}^T R_{xx} \ \dot{x}_{20} + U_{15}^T R_{uu} U_{15}) \ dt$$

The control law is generated by a linear combination of the all estimated states as $U_{15}(t) = - (K_1 \ x_{20} + K_2 \ \dot{x}_{20})$.

For a given set of the weighting matrices in the performance index the feedback gain matrices $[K_1 , K_2]$ can be determined from solving the standard steady state Riccati equations. A try and cut iterative approach is often required to arrive at the best set of the weighting matrices.

Figs 9 a-b shows some results of the LQR vibration control system. Some of the actuator commands are shown in Figs 10 a-b-c.

The disturbance signals D_4 (t) are shown in Figs 8 (note
the size of the disturbance signals for this case is about 1/2 of
those D_4 (t) used in the IMSC control system).

The performance of the LQR control system is reasonable well.
More active damping can be brought into the system with a refined
set of the weighting matrices. When compared this system with the
IMSC system, compare Figs. 10 b-c and Figs 6 , the
combined control effort U_{15}(t) of the LQR system are
significantly less than those of the IMSC system. . This fact
simply says that for the large flexible space structure system
the control with a group effort (a team effort) requires much
less energy than the system in which an individual input is used
for control of each mode.

For a large flexible space structure where the natural
frequencies ω_i of the elastic modes are relatively large, but the
damping factor ζ_i associated with each mode is very small, a
control system which can provide active damping into the system
is therefore needed. In such a system the time constant of each
mode; $\tau_i = (1/ \zeta_i \omega_i)$, can be reduced by actively
increaseing ζ_i value. A control system with just rate
feedback ; U_{15}(t) $= - K_2 \dot{x}_{20}$, may be suffice to reduce
the time constant of each structure mode. It is observed in the
simulation study that the rate feedback alone can provide good
damping into the system. The control system with the just the
rate feedback is shown in Fig. 7 (use the same K_2 gain
matrix of the full state feedback system). Table 1
compares the eigen-values of the open-loop system, the full state

feedback system, and the rate feedback control system . The rate
feedback control system can be considered as the most practical
control system for space application , because the on-board
computational time for generating the control law may be reduced
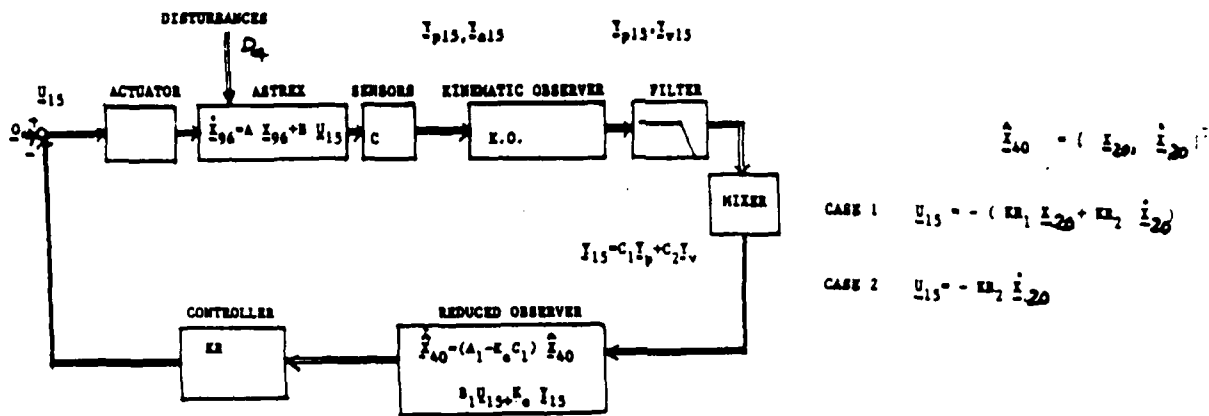by a significant amount. (see Fig. 11 for control performance of this system)
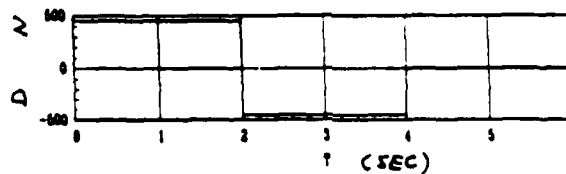

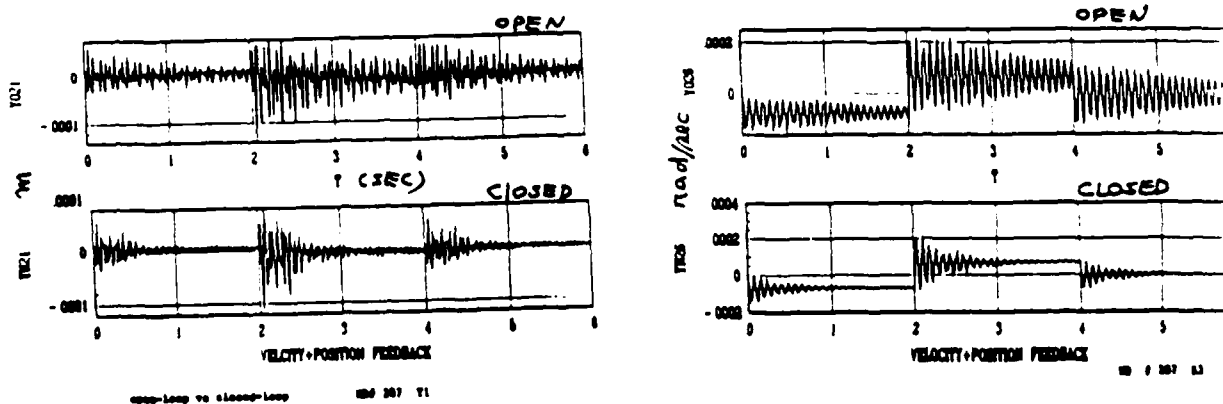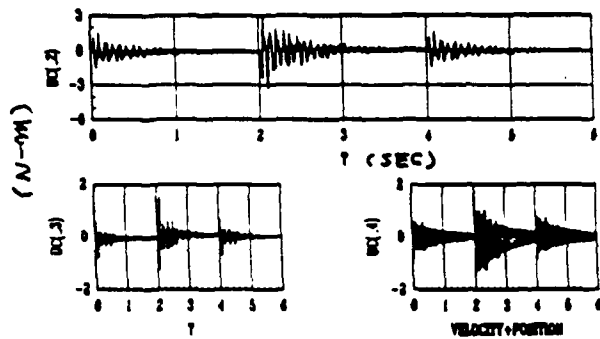Fig. 7 LQR Vibration Control System

Fig. 8   Disturbance

Fig. 9 a-b   Opne and Closed Loop System Responses

Fig. 10 Closed-Loop Actuator Commands

U_2 : ND#31 R1 N-M
U_3 : ND#206 R1
U_4 : ND#208 R1

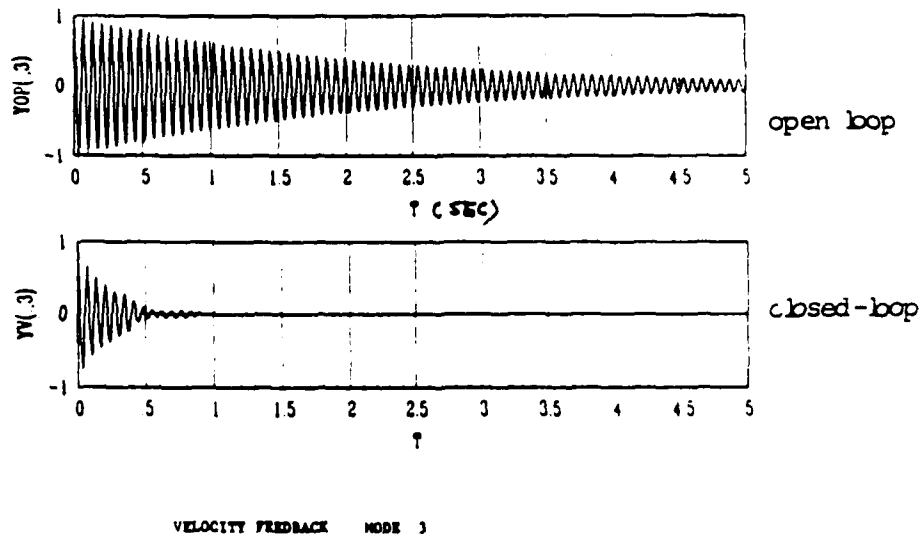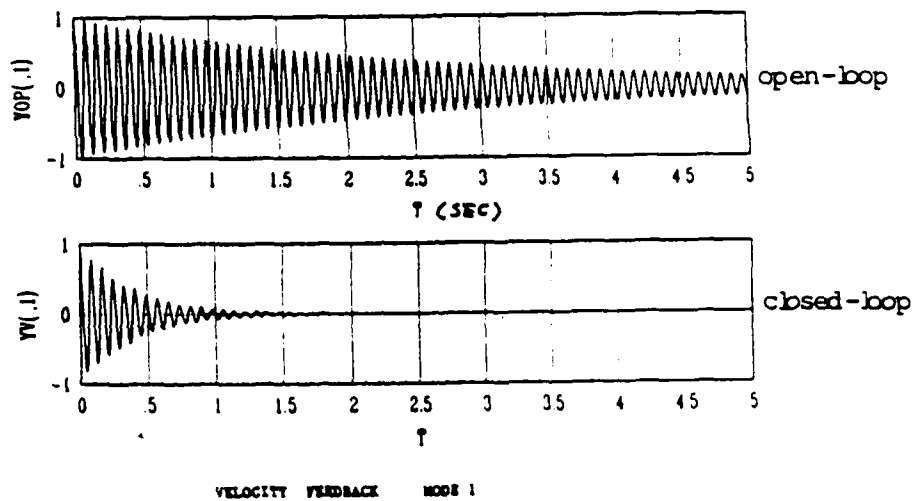VELOCITY FEEDBACK   MODE 1

VELOCITY FEEDBACK   MODE 3

Fig. 11   Rate-Feedback Control System

VIII. RECOMMENDATIONS

The preliminary study on hardware placement and evaluation of actuator enegey level require for controlling of each mode has been completed. On the selection of a minimum set of actuators and sensors a work is still needed. A study is needed to evaluate the number of hardwares vs the control performance. Mostlikely a set of accelerometers will be placed on the ASTREX test article for vibration measurement. Rate signal must be generated from these sensor outputs to ease the observer effort for quick convergency of the estimated states to the true states. The observer design for this case should be investigated.

A systematic approach must be developed on the selection of a critical set of structure modes which forms a reduced model for a controller design.

The discrete domain analysis of the LQR vibration control system must be performed. Since the ASTREX system will be monitored and controlled by a digital computer . The samping time effect on the control system quality must be investigated. A fine -pointing control system is working well. A complete performance evaluation of the combined vibration and fine-pointing control system is recommended. The performance of the fine-pointing control system is presented in the reference [2].

research possible (the Air Force Command and the Air Force
Office of Scientific Research, Mr. W. Roe of the Astronautics
Laboratory. and the staff of Universal Energy Systems).

It was a honor and a joy for me to participate in the
development of the large space research facility ASTREX at
the Astronautics Laboratory , Edwards AFB. I wish to thank
Dr. Alok Das for his guidance and encouragement .
Capt. G. Norris has provided me detail information on ASTREX
which helped me in designing the control systems, thank to
Graig. To Mr. Weid Schlaege I would like to extend many
thanks in helping me to start on the computing facility at the
Laboratory ,and he provided me the ASTREX finite elements
models, and many beautiful animated ASTREX slides and a video,
and also a computer tape containing all my summer results. All
these will provide great eduactional values to the university
campus. To Joel L Berg , I appreiciate his generosity for
allowing me to study his collection of literatures on space
structure dynamics and controls.

REFERENCES

1. G.A. Norris, Initial Operational Capability of the ASTREX
   Larege Sapce Structures Testbed. Third NASA/DOD CSI
   Conference. San Diago.Jan-Feb, 1989.

2. J.C. Wang , Synthesis of An Active Vibration Control Systems
   and A Fine-Pointing Control System. San Jose State University.

3. L. Metrovitch, Modeling and Control of Distributed Structure,
   VPI and State University.

1989 USAF-UES SUMMER FACULTY RESEARCH PROGRAM

GRADUATE STUDENT RESEARCH PROGRAM

Sponsored by the

AIR FORCE OFFICE OF SCIENTIFIC RESEARCH

Conducted by the

Universal Energy Systems, Inc.

<u>FINAL REPORT</u>

Dynamic Mechanical Response of Carbon/Carbon Composites by
Vibrating Reed Measurements

Prepared by: Phillip G. Wapner, Ph.D.

Academic Rank: Associate Professor

Department and   Mechanical Engineering and Energy Processes

University: Southern Illinois University at Carbondale

Research Location: ASTRONAUTICS LABORATORY/VSSC
                    Edwards AFB, CA 93523

USAF Researcher: Dr. Peter B. Pollock

Date: 26 Sept 89

Contract No: F49620-88-C-0053

Dynamic Mechanical Response of Carbon/Carbon
Composites by Vibrating Reed Measurements

by

Phillip G. Wapner

ABSTRACT

A vibrating-reed apparatus was designed and constructed which
measures the damping capacity of carbon/carbon composites as a function
of temperature; i.e., their ability to dissipate acoustic energy in the
frequency range of 200 to 500 cps between 25°C and 750°C. Typical reed
dimensions are 5 cm x 1 cm x 0.1 cm (L x W x D), and the measurement is
performed by determining the half-peak-height bandwidth of the reed at
its fundamental vibration frequency.

Three specimens of carbon/carbon composites were examined: (a)
pitch matrix; (b) CVD matrix (low density); and (c) CVD matrix (high
density). Damping of specimen (b) was, on average, five times higher
than (a) and (c). Moreover, all three specimens displayed distinctive
shapes of their temperature-versus-damping capacity curves.
Microphotographs of all three specimens seem to indicate that matrix
bonds between fiber bundles, rather than within bundles themselves,
causes the high damping of specimen (b).

Acknowledgements

I wish to thank the Air Force Systems Command and the Air Force Office
of Scientific Research for sponsorship of this research. Universal
Energy Systems also needs to be mentioned for their help and timely
assistance in the administration and direction of this program.

My awareness and appreciation of the caliber of research being carried
out at USAF's Astronautics Laboratory, Edwards AFB, increased
considerably this summer. This was in large part due to the efforts of
two persons who worked closely with me and helped coordinate my
research: Jim Wanchek, the lab director; and Peter Pollock, one of his
researchers. I am indebted to them, and Wayne Roe, my Focal Point at
USAL, for a very worthwhile as well as enjoyable summer. In addition,
modelmakers Ernie Butler, Wayne Killingsworth, and Neil Vaughn were
indispensable during actual construction of my research apparatus.

Lab manager Technical Sargent Walter Hamm also needs to be mentioned
here. His low-keyed but effective management style solved all my day-
to-day problems with ease. He is a credit to the United State Air
Force.

Back at my home base in Carbondale, Illinois, I want to thank Dr. Pawel
Tlomak for his help in designing the apparatus and in preparing
specimens for, and actually taking optical reflectance microphotographs
of carbon/carbon composites I studied during the summer. This was done
after I returned home and was critical to our understanding of why
damping response can vary so widely in carbon/carbon composites.

I INTRODUCTION

Carbon/carbon (c/c) composites are one of the new high-performance materials being developed for aerospace applications. Light and strong with exceptional stiffness that is retained at high temperatures, they may prove to be the only materials capable of handling many defense and aerospace projects. Unfortunately, their engineering properties are not well known; and are, in fact, still being developed and improved.

The Astronautics Laboratory at Edwards Air Force Base is deeply committed to measuring the physical properties of c/c composites (as well as other high-performance materials) and characterizing their response to a variety of environments that might be encountered in aerospace applications. To this end, they have assembled a group of researchers and technicians, and the necessary test equipment, at their Composites Laboratory (VSSC). These personnel are extremely interested in any technique which will help predict and understand the physical properties of these materials, especially c/c composites.

Southern Illinois University at Carbondale has a long tradition of research in coal-related investigations including new technologies such as liquefaction and gasification, as well as older techniques such as simple beneficiation. This program rather naturally evolved to include research on materials made from coal. Five years ago, the Materials Technology Center (MTC) was created on campus, and its head, Dr. Maurice Wright, quickly established the study of structural carbons (including c/c composites) as one of its main research directives. Today, the Center receives over a million dollars annually from a variety of industrial and governmental sources. My own MTC-related research

involves the production of carbon fibers from pitch, and the non-destructive testing (NDE) of c/c composites by vibrating reed measurements. I have constructed a melt-spinning apparatus and use it to spin fibers from mesophase pitch; and I have constructed a low-temperature (less than 500°C) vibrating reed apparatus to study c/c composites. It is this latter project that prompted my summer faculty fellowship at the Astronautics Laboratory.

II OBJECTIVES OF THE RESEARCH EFFORT:

The ability to accurately measure damping capacity, Ψ, of solid specimens at high temperatures is severely limited by two constraints; First, the entire specimen must be at a uniform temperature, otherwise Ψ versus temperature becomes virtually impossible to evaluate; and second, the motion of the specimen must be accurately detected while at these elevated temperatures. Above 300°C, this becomes quite difficult to do. Insulation on wires melts, and the large coefficient of thermal expansion of metals loosens clamping devices holding specimens. Thus, a successful vibrating reed (or other dynamic mechanical apparatus for measuring damping capacity, such as a torsional pendulum) must be able to firmly grasp a specimen throughout its operating temperature range, and simultaneously accurately measure the specimen's amplitude of vibration as a function of frequency. Of course, the amplitude-measuring system must not physically hinder free specimen motion, so direct contact is probably not feasible. At Southern Illinois University at Carbondale, Dr. Pawel Tlomak and I designed and built a vibrating reed apparatus capable of operating between 25°C and roughly

500°C. It was used to study the effect of oxidation on the damping capacity of a pitch-matrix c/c composite.[1]

The first objective of my summer research project at USAL/VSSC was to improve the design of this apparatus, and then construct it so data could be gathered reliably between 25°C and 750°C.

The second objective was to then use this instrument to gather data on specimens of c/c composites manufactured by at least two different techniques in order to determine what differences, if any occur, in their dynamic mechanical response; i.e., damping capacity versus temperature profiles.

A third, less well-defined goal was to attempt to explain any differences that occur in objective two by alternative characterization techniques. This was deliberately left somewhat vague since it was not known beforehand what, if any, alternative characterization technique might correlate with differences, if any, observed in dynamic mechanical response.

III DESIGN AND CONSTRUCTION OF VIBRATING REED APPARATUS

    (A) DRIVING HEAD ASSEMBLY

Figures 1, 2, and 3 are drawings of the major support items in the driving head, and Figure 4 provides a vertical view of the unit. The driving speaker is a long-throw 4" Woofer (Radio Shack model 40-1022) rated at 10 watts. It is mounted horizontally on the base plate. A 1/4" diameter stainless steel tube epoxied to the speaker cone extends downward through the base plate and extension plate. Nylon bushings

guide it ensuring free vertical motion; but no lateral motion. In this way, mechanical oscillations are smoothly transferred to the reed specimen holder, which attaches to the end of the 1/4" diameter stainless steel speaker tube.

A six-volt low-rpm gear motor (Edwards Scientific model J36,116) positions an electrode vertically above the reed specimen through a gear drive. The electrode is a high-temperature capacitance-type probe connected to a Mechanical Technology, Inc. amplifier (model AS-1021-SAI).

This device senses the capacitance change due to reed vibration relative to a stationary electrode, and converts it to a zero-to-ten volt signal proportional to that displacement. Measurement accuracy is on the order of tens of micro-inches.

The speaker is driven by a Hewlett-Packard frequency synthesizer (model HP3325B) amplified by a Sansui amplifier (model R-303). A standard laboratory DMM and oscilloscope are used to monitor output signals from the MTI amplifier. Figure 5a is a photograph of the apparatus without the plastic dome used to keep a vacuum. A quartz tube 15" long and 2 1/2" diameter fits onto the bottom of the base plate, and then a tube furnace is brought up around the quartz tube to provide temperature control.

(B) SPECIMEN HOLDER

In order to insure constant clamping pressure on the reed specimens, a device was designed which is passive in the hot zone; i.e., pressure is applied by mechanical means from outside the furnace. This is

accomplished by a spring-loaded plunger fed down through a stainless steel specimen holder tube. At the bottom of the tube, the specimen is clamped between jaws compressed by the plunger. A hoop-shaped structure at the bottom of the specimen tube holds the jaws in place. Figure 5b shows the electrode and specimen holder configuration. Figure 5c is a view of just the specimen holder (assembled), and 5d is an exploded view. When the specimen holder is screw-mounted to the speaker tube, the spring used to compress the jaws via the plunger stays at room temperature. Thus, even if differential thermal expansion takes place, a uniform pressure is maintained on the specimen. Many more descriptive drawings are available to anyone interested.

IV EXPERIMENTAL DATA

Three specimens of c/c composites were ultimately selected for study: Specimen A is a pitch-matrix sample obtained from a rocket engine exit cone; Specimen B is a CVD-matrix sample from HITCO; and Specimen C is a CVD-matrix sample of NOVOTEX, also from an exit cone. All three specimens were cut to rough shape with a diamond band saw, and then ground and polished. Final grit size was 0.3 micron (diamond dust). Final specimen dimensions were all very similar, typically measuring 2 1/4" x 3/8" x 0.040" (L x W x D). Specimen lengths free of the clamp were all roughly 1 3/4".

The data are presented in Figure 6. As can be seen from this figure, Specimen B, the HITCO sample, oftentimes had a damping capacity more than an order-of-magnitude higher than Specimens A and C.

Reproducibility on all three curves was excellent below 500°C (± 5 percent). Between 500° and 700°, Reproducibility decreased almost linearly to ± 25% due to background-noise level increases in the output signal from the MTI amplifier. Above approximately 750°C data-taking became virtually impossible due to this background noise. Oscilloscope scans identified it to be essentially "white" in nature, i.e., many frequencies superimposed one upon another. According to MTI, this is probably due to thermal excitation of free electrons in the measuring probe and/or breakdown of its ceramic insulation.

Since the noise is white in nature whereas reed vibrations are monotonic, selective signal filtration ought to reduce the signal-to-noise ratio, extending the data-taking temperatures considerably. No attempt was made to do this since the summer was over by this point. Upon return to Southern Illinois University, all three specimens were submitted for examination by optical reflectance microscopy (ORM), transmission electron microscopy (TEM) and x-ray diffraction (XRD). At the time of writing of this final report, only ORD results are available. The most pertinent of these are provided in Figures 7, 8, and 9, and will be discussed in the next section.

V DISCUSSION OF RESULTS

It is well known that exposure to severe environments such as radiation or high-temperature oxygen, damages polymers and composite materials[1-6]. Furthermore, this damage can be identified by its effect upon damping capacity. It increases due to the presence of defects which act as energy sinks. The same effect has been observed in composites with imperfect bonding. it is this latter effect that seems to explain the

much larger damping capacity of Specimen B. Looking at Specimen A (see Figure 7a and 7b), one observes tightly packed fiber bundles (good intra-bundle bonding) which are themselves tightly bonded together (good inter-bundle bonding) with a matrix having few voids. The lower magnification is useful for observing inter-bundle bonding, while higher magnification is useful for intra-bundle bonding.

Looking next at Specimen B (Figure 8a and 8b), one observes good intra-bundle bonding, but rather poor inter-bundle cementing together. Moreover, the matrix between bundles is full of voids. Evidently, the CVD process employed with this specimen did not adequately densify the composite structure. It has a low matrix density.

Specimen C (see Figure 9a and 9b) is much more like Specimen A in its intra-bundle and inter-bundle bonding, and its damping capacity-versus-temperature profile is very similar. Interestingly, its structure is quite different. Specimen A is a regular 2D weave while Specimen C is a more-or-less random 3D weave. Evidently, matrix properties are more influential on damping capacity than weave geometry.

Specimen C has high matrix density relative to Specimen B. its CVD process appears to have been more successful at densifying the composite.

VI RECOMMENDATIONS

a. The use of damping capacity measurements at elevated temperatures as an aid in the evaluation and understanding of internal structures of c/c composites is still in its infancy. This research, as well as that of others, indicates it has the potential to be a very

useful tool, if properly applied. Certainly, this summer's project shows considerable promise to this end. Conceivably, damping capacity measurements could be used as a quantitative measure of densification of c/c composites during manufacture, and perhaps as an NDE technique for predicting failure of existing c/c composite structures due to debonding.

b. Certainly, a great deal of additional work needs to be carried out in this area before this promise can be delivered. I will be applying for a mini-grant to initiate this work. The research will continue this summer's work plan, extending the data base to include a much larger number of specimens. Hopefully, industry support can be obtained in the procurement of specimens. The research will also be extended to include studies of modified c/c composites; i.e., to determine what happens to damping capacity after oxidation, or delamination due to excess mechanical loading. This, again, has the potential for significant NDE application.

c. One final recommendation that might prove fruitful would be to extend the useful temperature range of this apparatus to 2000°C, or even higher. The present limit on temperature is primarily due to materials of construction, stainless steel; and, to a lesser extent, the amplitude measuring device. Both can be modified without too much difficulty to reach the higher temperatures. Tantalum and/or ceramics can easily withstand 2500°C, and a laser motion-detector is currently available commercially which is capable of measuring reed motion with adequate accuracy. The payoffs are admittedly unknown. No one has carried out damping capacity measurements on c/c composites at these temperatures to my knowledge. However, phase changes do occur at these temperatures

(graphitization), and thus basic kinetic rate data might be measurable with this technique.

REFERENCES

1. Tlomak, P. and Wapner, P.G. (1989), "Vibrating Reed Studies of Carbon/Carbon Composites," Restricted Session, presented at the 13th Annual Conference on Composite Materials and Structures, Cocoa Beach, Florida, January 18-20.

2. Memory, J.D., Fornes, R.E., and Gilbert, R.D. (1988), "Radiation Effects on Graphite Fiber Reinforced Composites," J. Reinf. Plastics and Composites, 7, 33-65.

3. Hartwig, G. (1987), "Radiation Damage to Polymers and Fibre Composites," NTIS, April 1987, File Number DE87703681.

4. Reed, S.M., Herakovich, C.T., and Sykes, G.F. (1986), "Effects of Space Radiation on a chemically modified graphite-epoxy composite material. Interim report, NASA-TM-89232, October 1986.

5. Kishore, N.N., Ghosh, A., and Agarval, B.D. (1982), "Damping Characteristics of Fiber Composites with Imperfect Bonding," J. Reinf. Plastics and Composites, 1, 41-81.

6. DiCarlo, J.A. and Maisel, J.E. (1979), "High Temperature Dynamic Modulus and Damping of Aluminum and Titanium Matrix Composites," in "Advanced Fibers and Composites for Elevated Temperatures," Ahmad, I. and Noton, B.R. eds., The Metallurgical Society of AIME, 55-79.
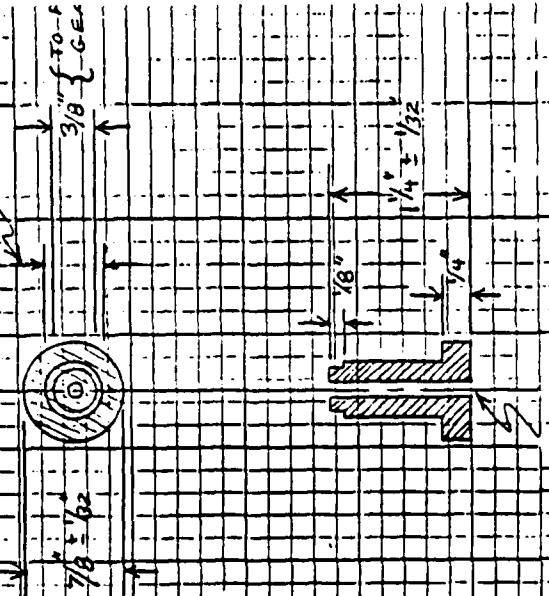
Figure - 2

Figure - 1
31-13

PHIL WARNER 6/9/89

PART "A"

BASE PLATE FOR VIB. REED APP.

MAT'L OF CONSTRUCTION: 1/2" THICK BRASS
(NEED 1)

3/16" DIA.

1/2" DIA., EQUALLY SPACED FROM CENTER

3/16" DIA. EQUALLY SPACED FROM CENTER

1 1/2 ± 1/64

1/2 ± 1/64

3 1/16 ± 1/64

9/16 = 3"

NOTE: 1/2" DIA. HOLE ARE TO MATCH AS CLOSELY AS POSSIBLE THE 1/2" DIA. HOLES IN PART "B", SAME WITH 3/16" HOLES.

SCALE: 2" |——→

PHIL WARNER 6/9/89

PART "B"

EXTENSION PLATE FOR VIB. REED APP.

MAT'L OF CONSTRUCTION: 1/2" THICK BRASS
(NEED 1)

3/16" DIA.

1/2" DIA.

1/2" DIA.

3/16" DIA.

1 1/4 ± 1/64

1/2 ± 1/64

13/16" DIA

3/16 ± 1/64

2 1/16 ± 1/64
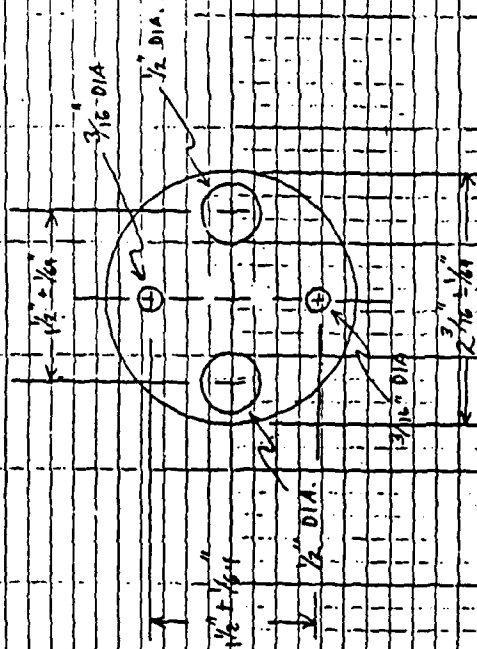
NOTE: 1/2" DIA. = 3/16" DIA. HOLES ARE T' MATCH AS CLOSELY AS POSSIBLE - SIMILAR HOLE ON PART "A"

SCALE: 1" |——→

PHIL WAPNER
6/19/89

PART "F"

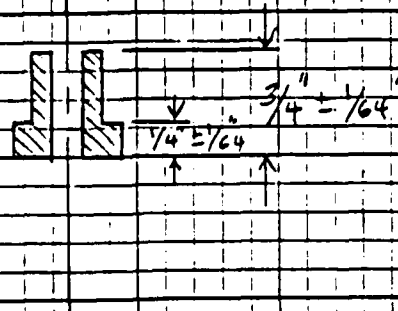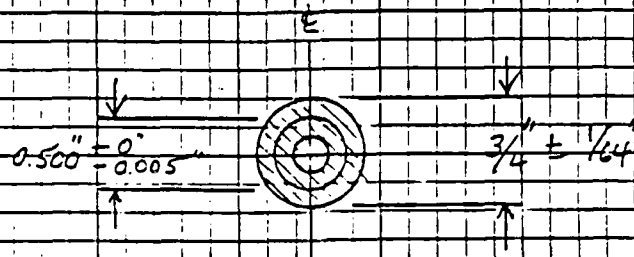FRICTION BUSHING FOR VIB REED APP

MAT'L OF CONSTRUCTION: FIBERGLASS REINFORCED
TEFLON OR NYLON

(NEED 6)

0.500" +0"/-0.005"   3/4" ± 1/64"

3/4" ± 1/64"
1/4" ± 1/64

SCALE:

Figure - 3

TOP VIEW OF VIB REED APPARATUS

PHILLIP WAPNER
6/9/89

SPEAKER

REED SPECIMEN HOLDER PORT

ELECTRODE DRIVE GEAR
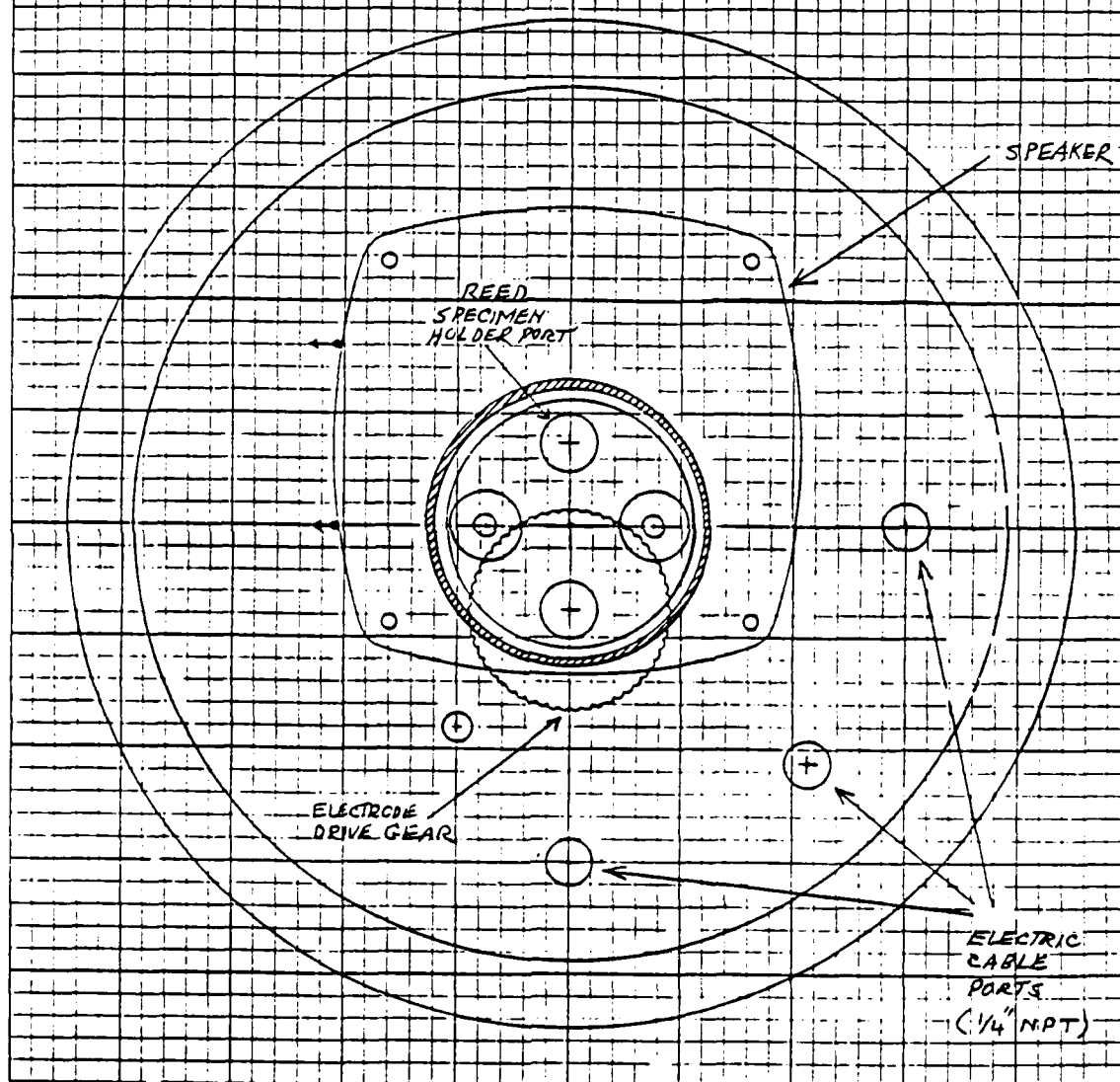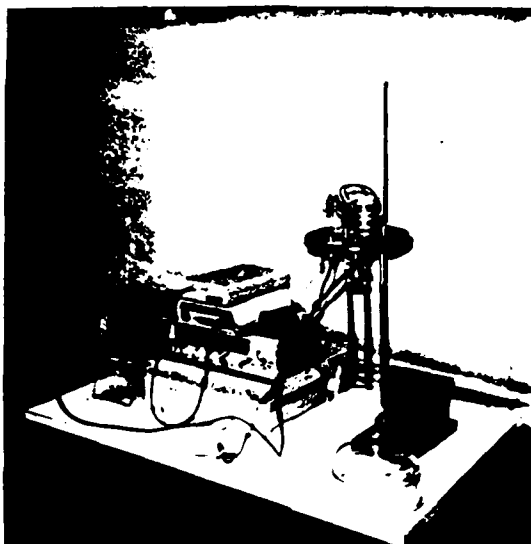
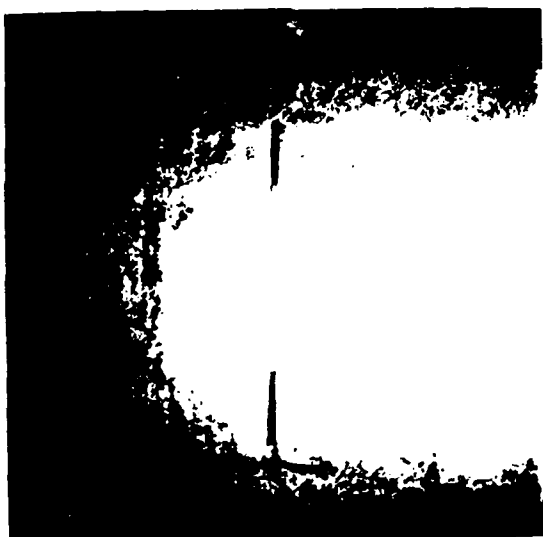ELECTRIC CABLE PORTS (1/4" N.P.T)

Figure - 4

31-16

A.

B.

C.

D.

Figure 5 Vibrating Reed Approach

Damping Capacity vs Temperature
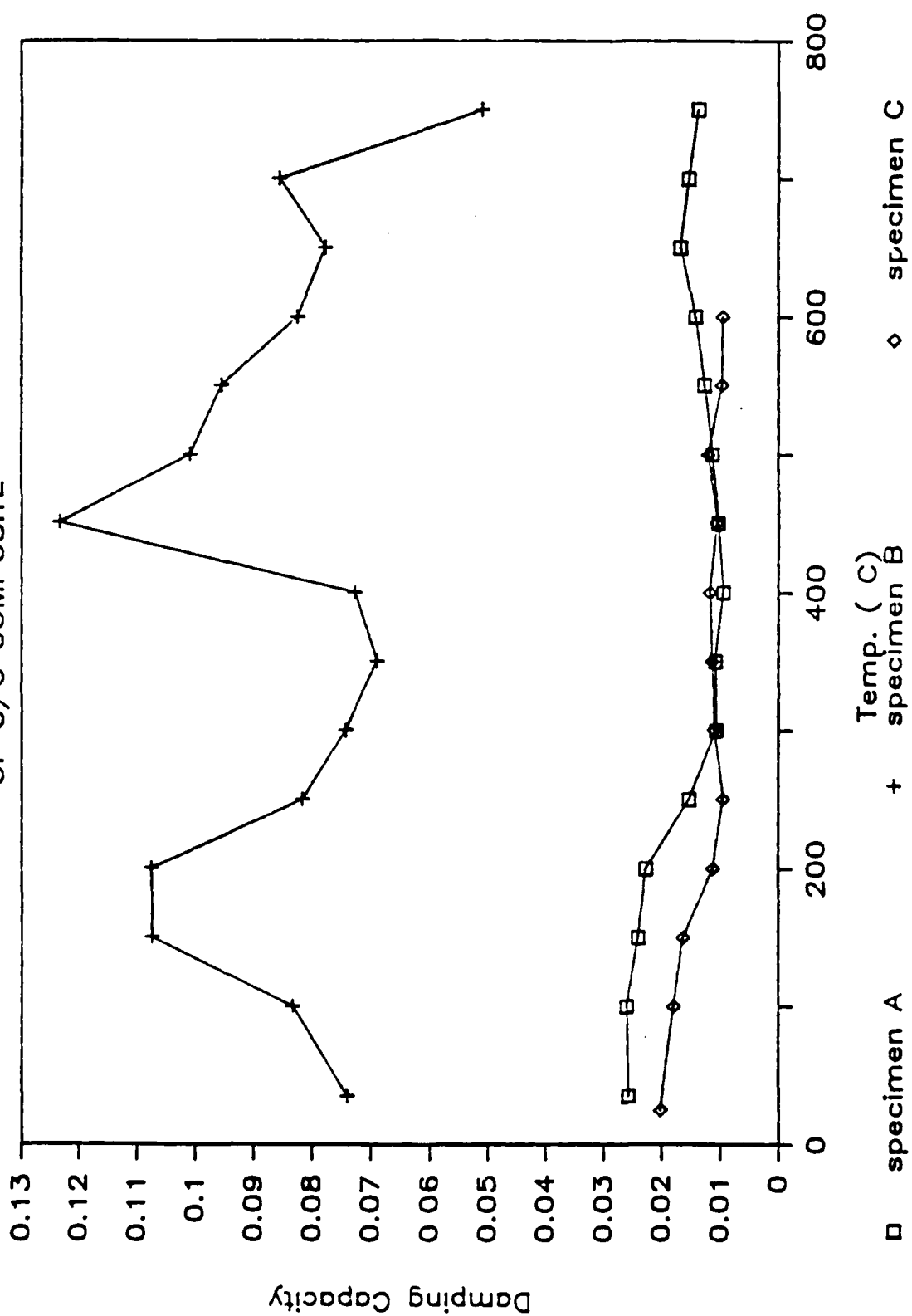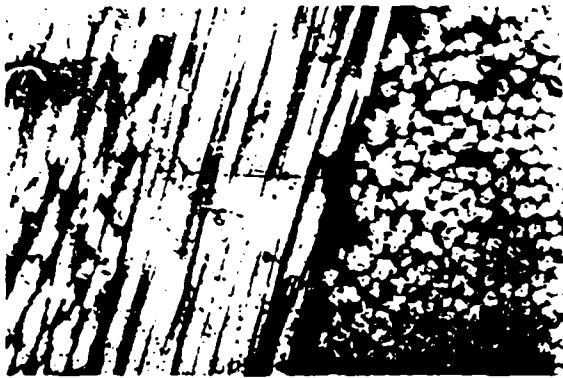OF C/C COMPOSITE

Figure - 6

(a) 50 X Magnification

(a) 50 X Magnification

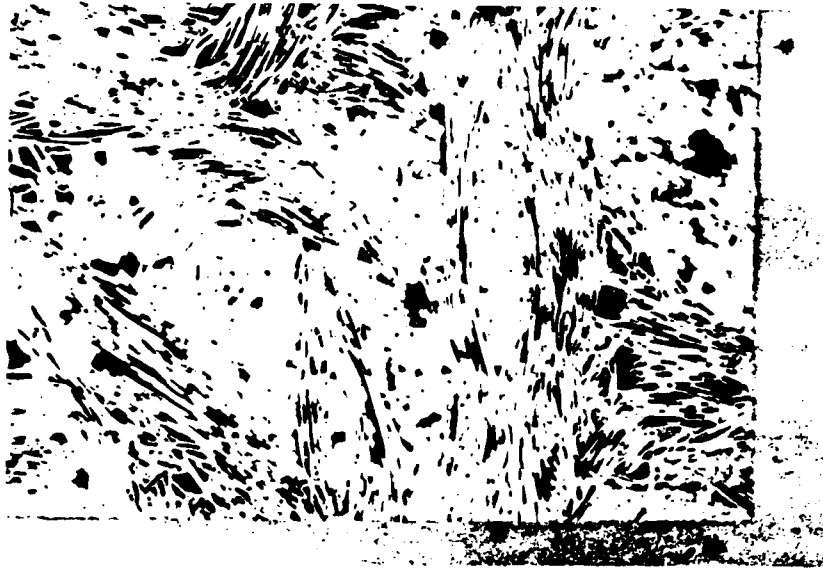(b) 400 X Magnification

(b) 400 X Magnification

Figure 7: Pitch-Matrix C/C Composite
(Specimen 4)

Figure 8: CVD-Matrix C/C Composite
(Specimen 1)

(a) 50 X Magnification

(b) 400 X Magnification

Figure 9: CVD-Matrix c/c Composite
(Specimen C)

1989 USAF-UES SUMMER FACULTY RESEARCH PROGRAM

GRADUATE STUDENT RESEARCH PROGRAM

SPONSORED BY THE

AIR FORCE OFFICE OF SCIENTIFIC RESEARCH

CONDUCTED BY

UNIVERSAL ENERGY SYSTEMS, INC.

FINAL REPORT

Carrier Free Radar

Prepared by: Beryl L. Barber, Assistant Professor

                      Electronic Engineering Department

                      Oregon Institute of Technology

                      and Graduate Graduate Engineers

                      Keith Carroll - New Mexico State

                      Douglas Pederson - U C L A

                      George Ramlow - U C L A

Research Location: ESD/Hanscom AFB and RADC/Griffiss AFB

USAF Researchers: Lt. Col James D. Taylor, USAF

                      Al Dahlgren, ESD

CARRIER FREE RADAR

BY

BERYL L. BARBER

AND

KEITH CARROLL, DOUGLAS PEDERSON, GEORGE RAMLOW

Investigation is made into the short pulse radar. Many problems are covered and a look at definitions discussed. Solutions to some of the problems are offered. These investigations were confirmed experimentally.

ACKNOWLEDGMENTS

WE WISH TO THANK The Electronic System Division and the Air Force OFFICE OF SCIENTIFIC RESEARCH for the sponsorship of this research. we would also like to mention Universal Energy Systems for their concern and help in various administrative areas.

Special thanks should be given to many people at RADC: Bobby Gray who provided working space and materials to construct various special components and for his advice and consul in the high power field, Mike Wicks and Dave Mokry who gave of their time and knowledge in short pulse generation and measurement, Mike Little and Carl Thomas who helped with obtaining equipment and computer assistance, Frank Welker for his wealth of knowledge in short pulses, Anthony Lattanzio and Anthony LoVaglio who helped in many ways. We would also like to thank Ed Hjort who provided the facility for RF testing.

We would not have been able to accomplish most of the work without the excellent cooperation of the people of RADC/OCTP-OCTS.

I. INTRODUCTION

Carrier Free Radar may be defined as a radar in which only the information bandwidth of RF is transmitted. It is commonly considered to be "impulse radar" and most often the pulse is generated using a "spark gap". Other definitions might include any system based upon a time domain concept. This is in contrast to a conventional radar in which pulse timing is used on a modulated carrier.

Many advantages are offered in the short pulse concept but these advantages create problems which must be solved before the short pulse or Carrier Free Radar can become a reality.

This paper covers some of these problems and offers possible solutions in most cases.

II. OBJECTIVE

The objective of this effort was to effectively "see" a target using short pulse techniques. This we were unable to do using any presently available equipment. Much was

accomplished, however, and we believe fully that at this time the technology is available to design and construct such equipments.

III. The Short Pulse

Let us first examine certain basic fundamentals of the short pulse. The short pulse by definition means that a very short time elapses in one cycle; that is that a single 2-nanosecond pulse results in a frequency of that pulse of five hundred megahertz. If the pulse were a true sine wave it would require a system bandwith of at least one gigahertz. If the pulse is a square wave the harmonic content would be very high and the required bandwidth would be at least five gigahertz to take advantage of the harmonic content.

If we return to the one five-hundred-megahertz sine-wave and a bandwidth of one gigahertz, then the information energy would be totally contained in that single sine wave; but the noise of interference would be the total integrated noise of the entire gigahertz passband.

This condition can be greatly improved by lengthening the pulse but this then becomes a conventional pulse. The wide bandwidth requirement reduces as the pulse energy is

allowed to build with time. i.e., several cycles. The best definition is in the single cycle operation where actual time domain measurements may be made.

Looking at the "best of worlds" it appears that ideally we should have a rather low frequency high harmonic energy pulse. Even better would be a combination of many low frequency pulses together, all containing high harmonics. Due to the non-linearity this would result in many cross products which is defined as non-sinusodial pulses.

The bandwidth requirement of the short pulse results in a receiver bandwidth which at least theoretically starts at zero frequency. This allows interference from all of the low frequency generators such as radio stations, television stations, C-B radios, telephones, communications and industrial radiation. These must be filtered out with a resultant decrease in information bandwidth.

IV. The Spark Gap Pulse

Let us examine the action of the spark gap current. Some sort of capacitor or storage is used to store the energy prior to initiation of the arc. The energy in the capacitor may be expressed as $p = \frac{1}{2} C U^2$ where C is the

capacity in farads and v is the voltage to which it is charged. As the arc initiates the generated signal will be driving some inductance. The impedance in the arc will be on the order of milliohms while the frequency may be expressed in time as $dt = -\frac{L}{v} di$. As the resistance in the arc is very small and the current high, the time of the transmitted pulse will be a function of L which is mainly the driving point impedance. "v" is the charge voltage but it decreases rapidly with time which increases the time of the transmitted pulse. Note that the resultant frequency is mostly related to the driving point impedance but the energy in the pulse is independent of that impedance. This means that the energy in the pulse is dissipated but not necessarily transmitted.

Looking at the arc, the current starts slowly (due to parasitic inductance), then increases rapidly, and then slows at the current peak. After the peak it decreases slowly as the driving voltage decreases until the arc is extinguished. Little energy is contained in the final decay process.

As the current began its increase, a large amount of energy was released resulting in low frequency generation. Due to the arc characteristics the frequency swept from some low frequency to a high frequency and then back to some

low frequency with the major part of the energy being produced (converted) in the low frequency range. (Our measurements appeared to contain most energy in the two hundred to three hundred megahertz range with usable energy in the one gigahertz range.)

Many designs of spark gap generators have been made using shorted stubs to enhance the pulse and create a single sine wave. This works well but is a filter in which the single frequency is transmitted and the remaining energy is dissipated in the arc junction.

V. Tests

Many measurements were made on the test range. In order to obtain some sort of reference the transmitter was located at approximately three hundred meters from the receiver and at the waveform observed. The following equipment was used:

Transmitter	IKOR IMP100
Transmitter Antenna	12' wideband blade
Transmitter Feed	12" RG 9/U
Receiver	HP 54111D
Receiver Antenna	4' wideband blade
Receiver Feed	3' RG 9/U
Receiver Filter	Chebyshev Band Reject

The location was on a bare dirt road with trees and heavy brush on both sides. The open lane was approximately twenty feet wide.

First tests were unusable because of television transmitter interference, and suitable band reject filters were designed and constructed. These were lumped constant filters but later filters were constructed using microstrip techniques.

Final tests show the IKOR generator to provide a single cycle with approximately five cycles of ringing, at approximately 280 megahertz, with a repetition rate of two kilohertz. In this generator the two kilohertz repetition rate signal is used as a carrier in order to make measurements.

The system was then set up as a conventional radar but with the transmitter located approximately fifty meters in front of the receiver. This was necessary to provide for transmitter triggering of the receiver without undue saturation. An aluminum covered box of a cubic foot was used as a corner reflector target. Numerous moving target measurements were made but a stationary target could not be resolved. We believe this is primarily a problem of the receiver and not a deficiency in the short pulse idea.

Tests were then made through approximately twenty yards of dense brush and were made both in calm air conditions and in windy conditions. Little effect was found due to the wind and the foliage appears as a dielectric, that is, the foliage appears longer than it actually is.

In detecting, using a single cycle pulse, the resolution works against us using the oscilloscope as a receiver. We are observing in the time domain and due to the transmitter level we could not detect the reflected signal. In summation, movement can be detected while fixed targets cannot.

VI. Possible Solutions

The oscilloscope is essentially a DC amplifier. One improvement that might be made is to pass the received signal through a high pass filter and eliminate those frequencies below approximately one hundred megahertz. This will effect the overall resolution but eliminating the low frequencies would be a good trade-off.
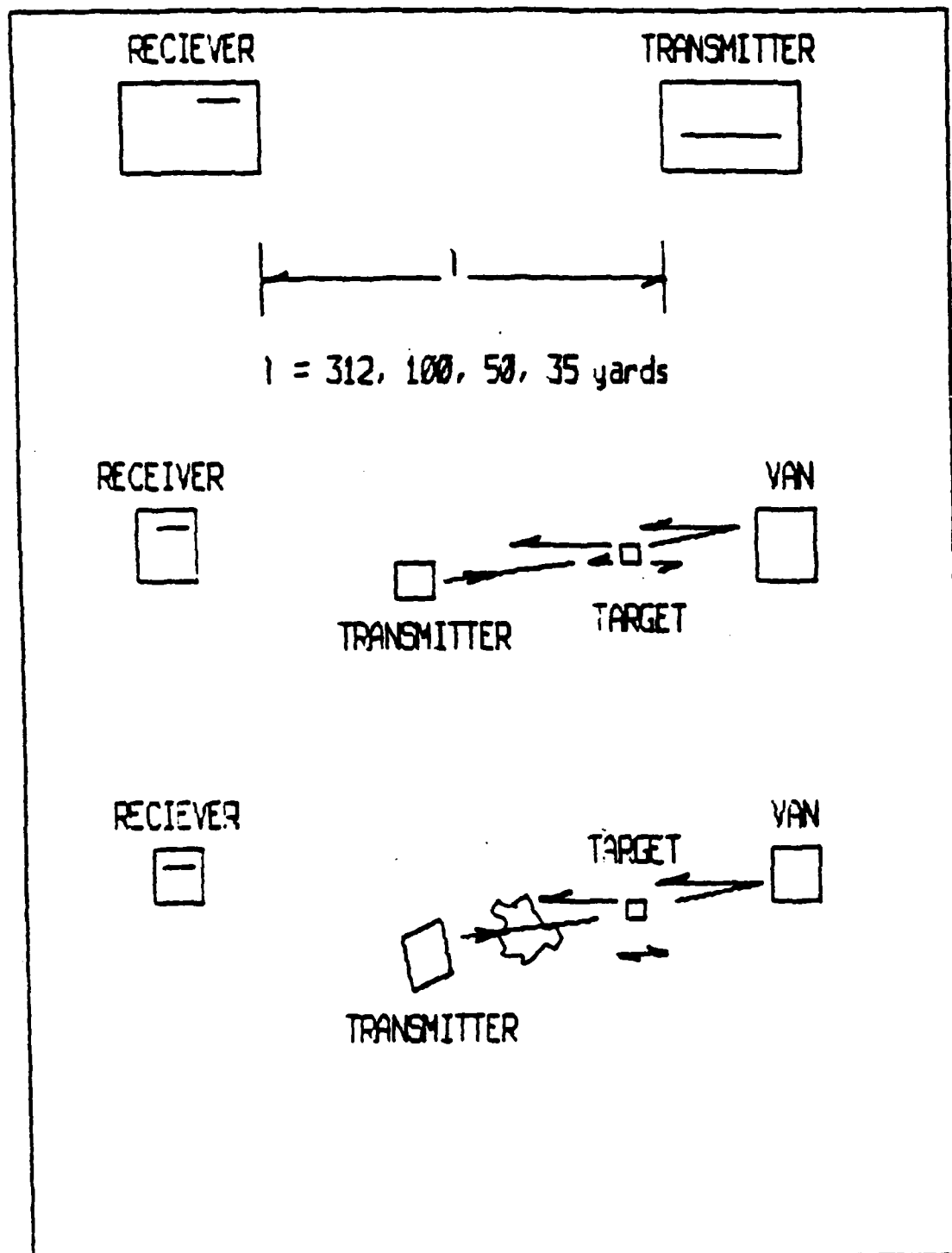
The transmit/receive will always be a problem but can be alleviated with a high dynamic range receiver and an input limiter - quite possibly a dual diode limiter.

Receiver gating will be a must and one of the major problems here is physical timing. Better control of the transmitter pulse is needed to reduce jitter. A problem with gating is the bandwidth and response time of the gate. Here we have the some problem as that of passing a single gigahertz cycle.

The best solution, at this time appears to be in an up-converting receiver where the frequency versus bandwith ratios are better and more easily processed. A multiple IF would be used with different bandwidths. This could then be processed using digital techniques combined with analog references.
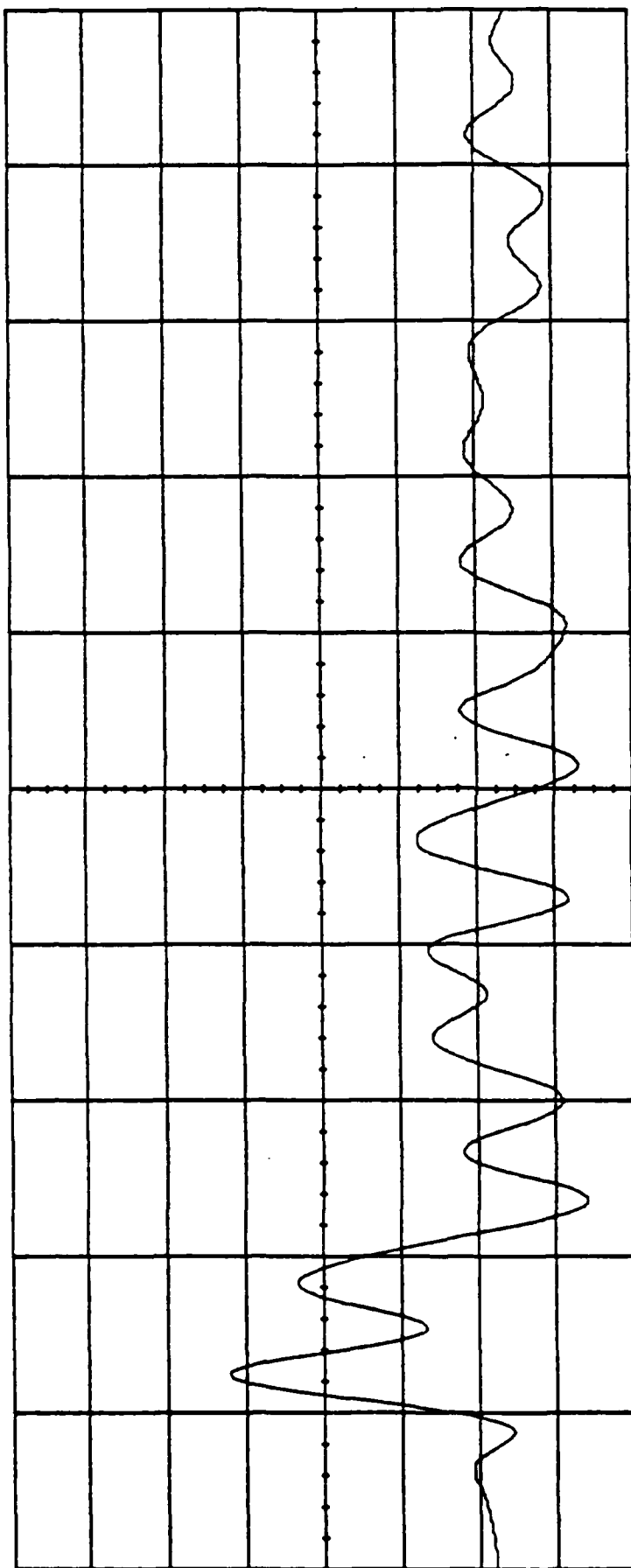
VII. Conclusion

We believe that there is technology available to build a short pulse radar with good definition. There is however, no test equipment, at this time, capable of testing the radar. The short pulse radar concept offers many advantages and efforts should continue. It appears that the major effort should be in the timing of the transmitter and in the receiver.

RECIEVER   TRANSMITTER

l = 312, 100, 50, 35 yards

RECEIVER   VAN

TRANSMITTER   TARGET

RECIEVER   VAN

TARGET

TRANSMITTER

-6.360 ns   18.640 ns   43.640 ns

Ch. 1   = 10.00 mVolts/div   Offset   = 29.60 mVolts
Timebase   = 5.00 ns/div   Delay   = -6.360 ns

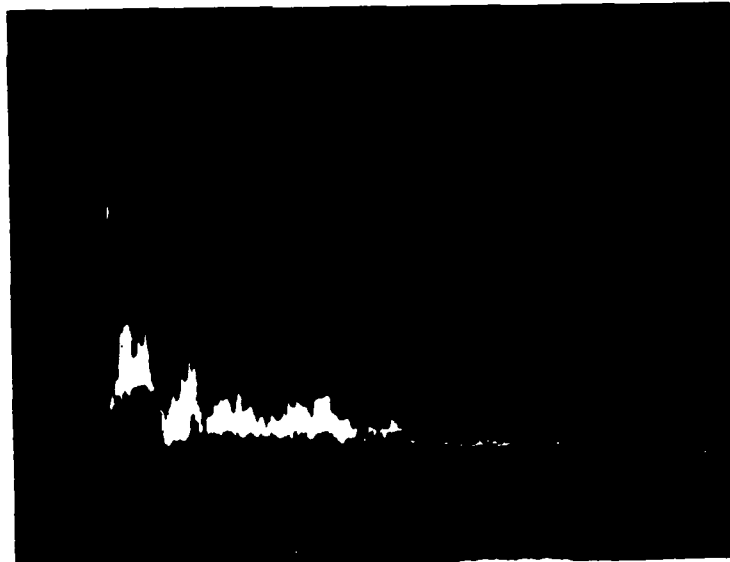Signal received on HP54111D from IKOR IMP100, 12'¢1' Blade at 312 yds

32-13

```
Ch. 1       =   50.00 mVolts/div
Timebase    =    2.00 ns/div
Channel 1 Parameters
Fall Time   =    1.160 ns
P-P Volts   =  231.0 mVolts
Start       =  195.240 ns
Vmarker1    =   56.81 mVolts

Rise Time   =  990 ps
Preshoot    =  31.25 mVolts
Avg Volts   =  74.05 mVolts
Stop        =  195.240 ns
Vmarker2    =  256.8 mVolts

Offset      =  199.0 mVolts
Delay       =    5.240 ns
+Width      =    1.790 ns
Overshoot   =    0.000 Volts
Delta T     =  0.00000 s
Delta V     =  200.0 mVolts
```

-4.760 ns   5.240 ns   15.240 ns

Lab Data: IKOR IMP10D, 6-Bit Resolution pulse through 950 MHz High Pass
filter as seen on HP 54111D

5 pulses

Ch. 1	=	49.00	mVolts/div
Timebase	=	2.00	ns/div
Memory 5			
Timebase	=	1.000	Volts/div
Timebase	=	50.0	ns/div
Channel 1 Parameters			
Rise Time	=	840	ps
Fall Time	=	70	ps
P-P Volts	=	372.4	mVolts
Dutycycle	=	79.10	%
Start	=	-180	ps
Vmarker1	=	-1.960	mVolts

Freq.	=	1.80972	GHz
+Width	=	440	ps
Preshoot	=	114.8	mVolts
Avg Volts	=	168.4	mVolts
Stop	=	370	ps
Vmarker2	=	254.8	mVolts

Offset	=	65.00	mVolts
Delay	=	6.200	ns
Offset	=	0.000	Volts
Delay	=	0.00000	s
Period	=	550	ps
-Width	=	120	ps
Overshoot	=	0.000	Volts
RMS Volts	=	182.8	mVolts
Delta T	=	550	ps
Delta V	=	256.7	mVolts

Lab Data: IKOR IMP100 Integrated pulse through 950 MHz High pass
filter as seen on HP 54111D

10 second integration

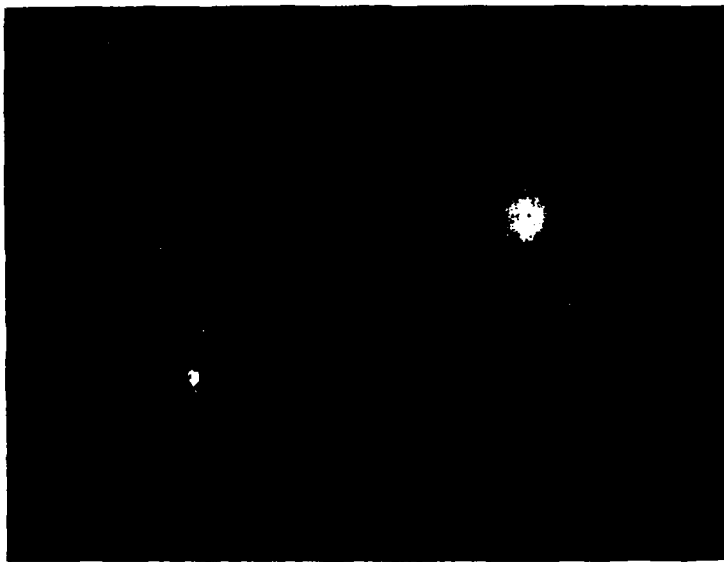# Spectrum Analyzer Display (HP)

Received Signal – Transmitter OFF

Received Signal – OIT 1

PRF = 10 Hz

Spectrum Analyzer Display (HP)

Received Signal — Transmitter OFF

Received Signal — IKOR IMP 100 on

PRF = 2KHz

HP 54111D   Display

Taken of one foot corner reflector
at 312 feet
USING   OIT   PULSER

RADAR

BIBLIOGRAPHY

Halliday, David and Resnick, Robert. Physics for Students
of Science and Engineering. New York: John Wiley & Sons,
1962.

Lee, S. W. and Lo, Y. T., Antenna Handbook: Theory,
Applications, and Design, Pub. Van Nostrand Reinhold Co.,
New York.

Network Analysis with Applications
William D. Stanley, 1985 Reston Publishing Co.

Microwave Filters, Impedance Matching Networks, and
Coupling Structures.
G. Matthaei/L. Young/EMT. Jones, 1980 Artech House Inc.

The Microwave Engineers' Handbook
1964, Published by William Bazzy

Preliminary Results of the Transient Response of Broadband
Antennas by K. Stiefvater, P. vanEtten and B. DiTano
Technical Report RADC-TR-69-203, June 1969

1989 USAF-UES SUMMER FACULTY RESEARCH PROGRAM

GRADUATE STUDENT RESEARCH PROGRAM

Sponsored by the

AIR FORCE OFFICE OF SCIENTIFIC RESEARCH

Conducted by the

Universal Energy Systems, Inc.

FINAL REPORT

Detection Performance for Over Resolved Targets with Varying Energy Level in Cells

Prepared by:	Ajit K. Choudhury, ph.D
Academic Rank	Associate Professor
Department and	Electrical Engineering Department
University	Howard University, Washington, D.C. 20059
Research Location:	RADC/OCTS, Griffiss AFB, Rome, NY.
USAF Researcher:	Al Dahlgren
Date;	September 12, 1989
Contract No:	F49620-88-c-0053

DETECTION PERFORMANCE FOR OVER RESOLVED TARGETS WITH VARYING ENERGY LEVEL IN CELLS

by

Ajit K. Choudhury

ABSTRACT

Ultra wide band radar will soon become a useful tool for detecting small and fast moving objects such as cruise missiles. In ultra wide band radar very short pulses of very high energy are transmitted periodically. Since the pulses are very short the targets are completely resolved into several subscatterers and these subscatterers occupy the different resolution cells spanning the target and as a consequence the target is over resolved. In this research report we study the detedtion performance of over resolved targets with varying energy levels in the different resolution cells for several scatterers.

ACKNOWLEGEMENTS

DETECTION PERFORMANCE FOR OVER RESOLVED TARGETS WITH VARYING ENERGY LEVEL IN CELLS

AJIT K . CHOUDHURY

DEPARTMENT OF ELECTRICAL ENGINEERING

HOWARD UNIVERSITY. WASHINGTON. D.C. 20059

I. INTRODUCTION

Detection probabilities of different scatterers (targets) namely (a) constant amplitude, (b) Rayleigh and (c) dominant plus Rayleigh targets are well known and documented starting with Woodward [1], Swerling[2] and Marcum[3,4].For these scatterers plots showing detection probabiliity versus signal—to—noise for different values of false alarm probabiltiy and the number of pulses integrated have been documented. Various researchers over the years have studied the detection performance of over resolved targets. The recent research report (RADC—TR—84—61) of Vincent C. Vannicola, Kenneth G. Hillman and William L. Simkins[5] is a comprehensive one.In that researach work it is assumed that all cells spanning the target possess equal energy.In this research report we study the detection performance for over resolved targets having different energy levels in different resolution cells. Also the detection threshold and false alarm setting are being generalised. The target is declared present if energy levels of at least k out of M resolution cells exceed the threshold where k is any number between 1 and 25% of M . False alarm occurs when the target is absent and noise in the resolution cells excced the threshold. A false alarm may be declared if noise in at least n out of the M resolution cells

exceeds the threshold. n is a variable integer at our choice lying between 1 and 25% of M . n and k may be equal. The work of P.K.Hughes II [6] may be mentioned as one which deals with high resolution radar and resolution cells having varying energy levels.

Let us make the connection between ultra wide band radar and over resolved targets. Ultra wide band radar, under the sponsorship of USAF has been making progress in the last several years. Soon ultra wide band radar will become a reality. In ultra wide band radar short pulses of one or two nanoseconds duration and of very high energy are periodically transmitted .The back scatterers from the targets are received at the receiving antennas.Since the pulse lengths are very short the target is resolved into several subscatterers and these these subscatterers occupy different resolution cells in the radar screen. So in the ultra wide band radar more resolution cells are illumined by the target and M, the number of resolution cells illumined by the targets could be of the order of hundred. A picture of ultra wide band radar target scattereing is presented at the end of the research report. .

My background and interest is in the area of estimation , detection and signal processing. The above research problem is of interest to me. I can contribute additional insights to the above problem, which will be valuable in the near future when ultra wide band radar becomes a reality. Documentation of detection performance for over resolved targets as a function of the resolution index (M), signal−to−noise ratio will play an important role in signal processing to detect targets illumined by short pulses of ultra wide band radar. It is well known from the above studies [5] that the detection performance for over resolved targets deteriorates as the number of over resolved cells increases. Therefore , for over resolved targets we need better signal processing techniques.

II. OBJECTIVES OF THE RESEARCH EFFORT:

Over the past several years USAF has been developing technology to make ultra wide band radar a dependable device to detect aand track cruise missiles and other fast moving projectiles. Technology is still in its infancy. One of the difficulties of ultra wide band radar is the generation of short pulses of one or two nanoseconds long. There may be a connection between the switching devices of EMP (electromagnetic pulse simulator) and the switching devices for the generation of short pulses of ultra wide band radar. With this fact in view preparation of an overview on EMP (electromagnetic pulse)simulator was assigned to me.

My objective and goal during the summer ten week period is to do research on the detection performances for over resolved targets with varying energy levels in the resolution cells and to prepare an overview on the EMP simulator.

III DETECTION PERFORMANCE FOR OVER RESOLVED TARGETS WITH VARYING ENERGY LEVELS IN CELLS

In this section we briefly describe the method. Let the energy levels in the resolution cells be divided into r levels of quantization. r is equal to 1,2, 4,8,16,32 etc. depending on the level of quntization . Let M_1, M_2, M_3, ..., M_r be the number of resolution cells having signal energy levels E_1, E_2, E_3,

E_4, ..., E_r respectively. Then the folling relationships holds

$$M_1 (E_1)+M_2 (E_2)+ ...... + M_r (E_r) = E \qquad (1)$$

$$M_1 + M_2 + ... + M_r = M \qquad (2)$$

where E is the total energy comprising of all the resolution cells and

M is the resolution index. Let PDM_1, PDM_2, PDM_3, ..., PDM_r be the

probabilities of a single threshold crossings out of M_1, M_2, M_3, ..., M_r

subscatterers having energy levels E_1, E_2, E_3, ... E_r respectively. Let us

assume that the receiver declares that the target is present when at least k out of

M cells crosses the threshold. k is a number lying between 1 and 25% of M.

The computation of PDM_1, PDM_2, ... PDM_r depends on the scatterer

model, waveform shapes, M_i, threshold model, signal-to-noise ratio, and

the number of pulses considered. Expressions of PDM_i under such conditions

are available in [6]. Threshold setting is obtained from false alarm constraint.

A false alarm occurs when noise in at least n out of M resolution cells exceed

the threshold. The probability of detection of the targets can be expressed as

complex function of PDM_i, false alarm setting. This has been calculated but is

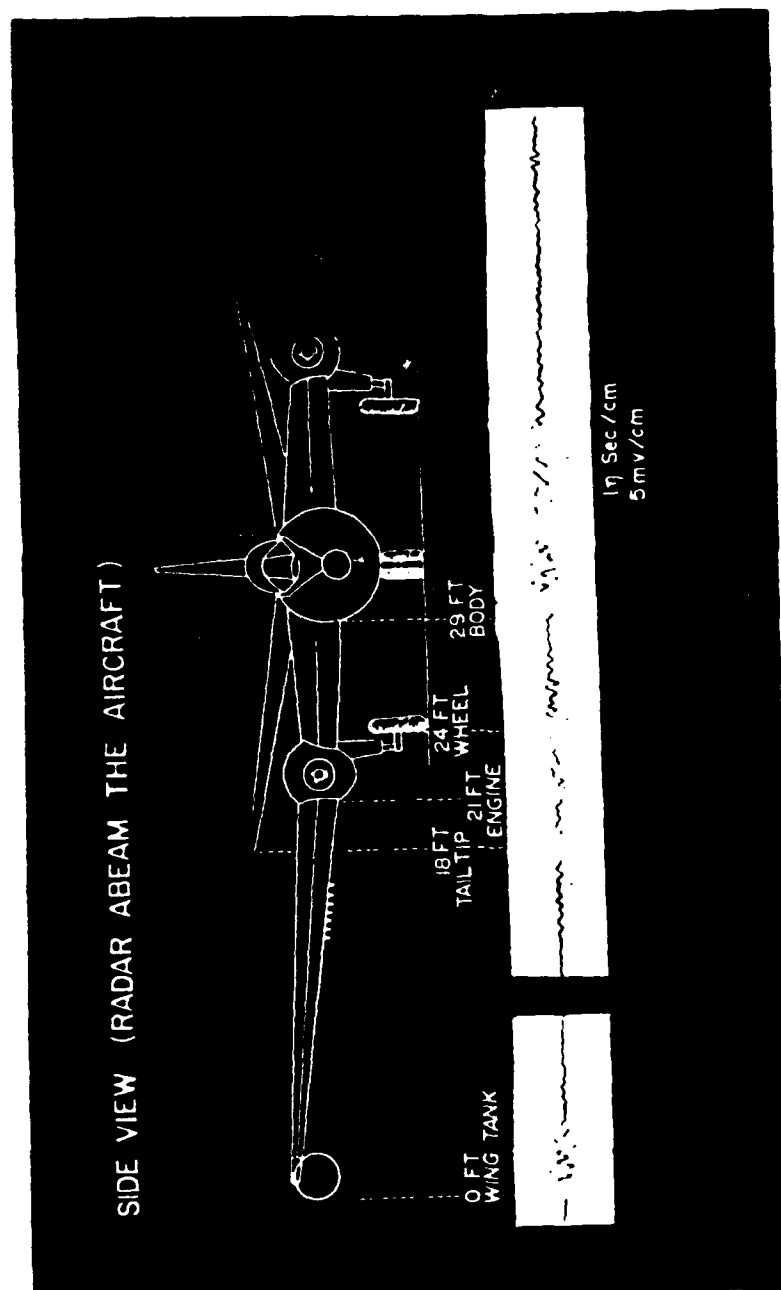not presented here for lack of space.

VI RECOMMENDATIONS:

With the advent of ultra wide band radar the study of detection performance of over resolved targets has a special place. Short pulses of the ultra wide band radar resolve targets into subscatterers and all the resolution cells are illumined and we have the case of an over resolved target. Preliminary studies indicate that the detection performance deteriorates as the number of illumined cells increase. Hence we need sophisticated signal processing techniques to detect over resolved targets. In ten weeks I have just formulated the research problem. More research is needed in the following two areas :

(a) In depth study of detection performance for over resolved targets having vaarying energy levels in the cells.
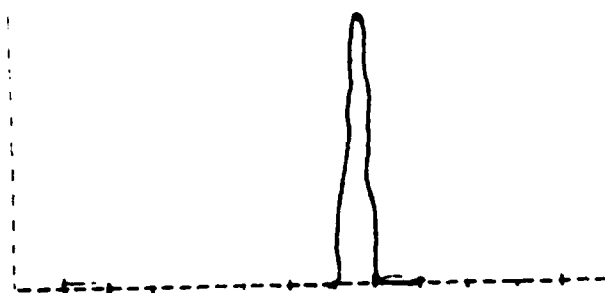
(b) Developement of sophisticated signal processing techniques to detect over resolved target

B 57 RESPONSE TO L-BAND MONOCYCLE
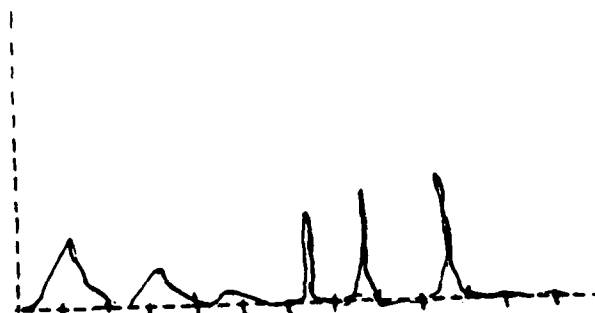
SIDE VIEW (RADAR ABEAM THE AIRCRAFT)

29 FT BODY
24 FT WHEEL
21 FT ENGINE
18 FT TAIL TIP
0 FT WING TANK

17 Sec/cm
5 mv/cm

Courtesy of RADC

REGULARLY RESOLVED AND OVER RESOLVED TARGETS

Regularly Resolved Case

Over Resolved Case

RECEIVER FOR CONSTANT AMPLITUDE INCOHERENT
PULSE TRAIN

pulse train

⊓⊔⊓⊔⊓⊔ ... ⊓⊔

Single pulse matched filter	Envelope detector	Pulse Train sampler

$\ln I_0 (r_i \sqrt{R_p})$	video integration	Threshold comparison

Signal present

Signal absent
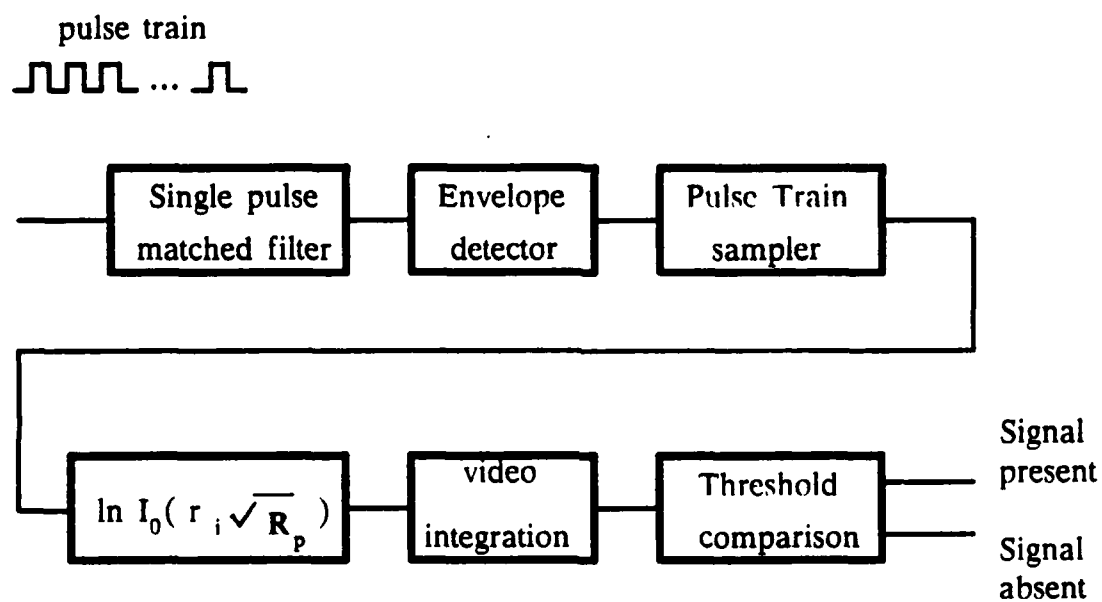
Optimum detection receiver for a constant amplitude incoherent pulse train

The graph shows curves labeled M=1, M=2, M=5, M=10 plotting 100 × Prob of ovedion (y-axis) against S/N in DB (x-axis).

y-axis: 100 × Prob of ovedion, labeled y, scale from 1 to 100

x-axis: S/N in DB, labeled X, from -20.000 to 30.000

bfa = .01

N = # of pulses incoherently integrated = 1
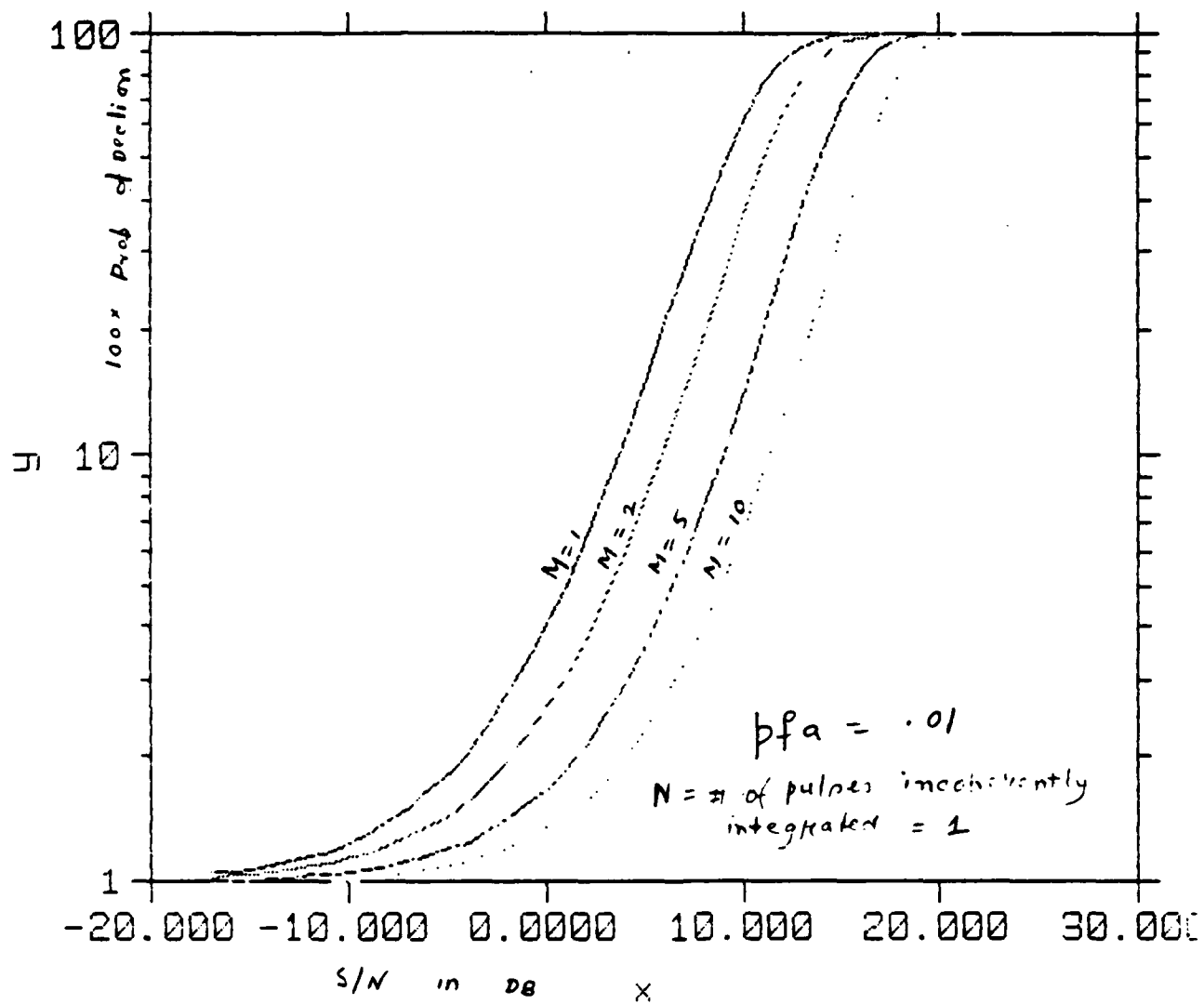
:1, 2, 5, 10, bfa = .01

REFERENCES

[1]   Woodward , P.M., " Probability and Information Theory with Applications to Radar," McGraw-Hill , New York, 1953.

[2]   Swerling, P., " Probability of detection for Fluctuating Targets," Rand Research Memo RM-1217, March 1954. Also reissued in IRE Trans. on Infor. Theory, vol. IT -6, no. 2, pp 59-144.

[3]   Marcum, J.I., " A Statistical Theory of Target Detection by Pulsed Radar, " Rand Research Memo. RM-754, December 1947.
Also reissued in IRE Trans. on Inf.Theory, vol. IT-6, no. 2 , pp. 59-144.

[4]   Marcum, J.I., " A Statistaical Theory of Target Detection by Pulsed Radar (Mathematical Appendix), " Rand Research Memo RM -753, July 1948. Also reissued in IRE Trans. on Infor. Theory, vol. IT-6 no.2, pp. 145-267, April 1960.

[5]   Vincent C. Vannicola, Kenneth G. Hillman and William L. Simkins., " Detection Performance for over Resolved Targets , " RADC-TR-84-61, In-house Report , September 1984.

[6]   DiFranco, J.V. , and Rubin, W.L.. " Radar Detection , " Prentice-

Hall, Inc., Englewood Cliffs, New Jersey, 1968.

[7]   Hughes II,b P.K.,   " A High—Resolution Radar Detection Strategy,"

IEEE Trans . on Aerosp. and Electron . System.. vol. AES—19, no.5, pp.

663—667, September 1983.

[8]   Pachares J. ,   " A Table of Bias Levels Useful in Radar Detection

Problems, " IRE Trans. on Info. Theory, vol. IT—4. pp.38—45, March 1958.

1989 USAF-UES SUMMER FACULTY RESEARCH PROGRAM/

GRADUATE STUDENT RESEARCH PROGRAM

Sponsored by the

AIR FORCE OFFICE OF SCIENTIFIC RESEARCH

Conducted by the

Universal Energy Systems, Inc.

FINAL REPORT

Analysis of Testability Concepts and its
Application to RSIP

Prepared by: Dr. S. Natarajan
                       Bradley K. Herman

Academic Rank: Associate Professor
                       Graduate Student

Department and   Electrical Engineering Department

 University: Tennessee Technological University

Research Location: ESD/TCWU
                       Hanscom AFB, MA

USAF Researcher: Major Ken Howes

Date: 18 Aug 89

Contract No: F49620-88-C-0053

Analysis of Testability Concepts and its

Application to RSIP

by

Dr. S. Natarajan
and
Bradley K. Herman

ABSTRACT

Testability is becoming an increasingly important design consideration as systems continue to become more complex. In order to be effective, testability must be considered at the earliest possible point in the design phase. This will allow changes to be made to the design when it is still feasible to do so. The incorporation of testability must be done in a systematic manner to be effective. Verification of inherent testability must be done with the proper CAD testability analysis tool and the results should be applied back to the design to improve inherent testability.

Acknowledgements

I. INTRODUCTION:

The Radar System Improvement Program (RSIP) for the AWACS aircraft is currently being implemented in the USAF. In this program, the issues related to enhancing both built-in and off-line testing are being addressed early in the acquisition phase. This inclusion of testability concepts has the goal of eliminating interim contractor support (ICS) and thus reducing the life-cycle cost (LCC) of the system. In addition to reducing the LCC of the system, the incorporation of testability in the design phase also increases the reliability, maintainability, and availability of the system. The main focus of our research was to analyze the concepts of testability and also issues related to the testing of modern electronic circuits. Based on this study, we were expected to make recommendations as to how testability can be applied effectively to RSIP.

Our research interests are in the areas of design, analysis, and testing of electronic circuits. The first author has published several papers in the areas of electronic circuits, computer-aided-design and analysis cf electronic circuits, and measurement and instrumentation

(testing). The second author has designed and built several instrumentation systems for a research group at Tennessee Technological University. Our assignment to this project resulted from design for testability and testing being well within our interests.

II. OBJECTIVES OF THE RESEARCH EFFORT:

The USAF is currently involved in improving certain electronic systems in the AWACS aircraft to improve its radar capabilities. This project is called the Radar System Improvement Program (RSIP). In order to improve the reliability, maintainability, and availability (RM&A) and reduce the life-cycle cost (LCC) of the system, Electronic Systems Division (ESD) at Hanscom AFB has decided to incorporate testability early in the design process of the new system. Therefore our original objectives were to identify the testability concepts and how they should be applied to RSIP.

ESD is also in the process of acquiring test program sets (TPSs) for depot maintenance. The prime contractor for the system and the TPSs is Westinghouse Electric Corporation (WEC) and the repair depot for the AWACS radar

system is Warner Robins Air Logistics Center (WRALC).
During the course of our research on the concepts of
testability, two objectives were added to include WEC and
WRALC. The additional objectives were:

1. Identify the needs of WRALC to maintain TPSs

2. Study the proposal by WEC for its adequacy in
   addressing testability and TPS development.

Finally, we made specific recommendations as to how the
testability concepts should be applied to RSIP.

III. METHOD OF APPROACH AND A BRIEF SUMMARY OF OUR
     RESEARCH:

Our research started with a literature search on
testability and it continued along with the information
gathering on TPS development. We first traveled to Tinker
AFB in Oklahoma City to learn about the AWACS system. To
gather information on testability, testing, and TPS
development we traveled to the Illinois Institute of
Technology Research Institute (IITRI) at Rome, NY, WRALC
near Macon, GA, and WEC in Hunt Valley, MD. We also
studied the proposal submitted by WEC t gather information
on their methodologies of applying testability to RSIP and

developing TPSs. The results of our research and our analysis were put in the form of a research report and it has been submitted to Major Ken Howes, ESD/TCWU, our technical point of contact. A brief summary of this report is as follows:

Testability addresses the issues involved in achieving the inherent ability in a circuit card assembly (CCA) through its design characteristics to be testable so that the desirable levels of fault detection and fault isolation can be achieved in an accurate, timely, and cost-effective manner. The incorporation of testability is most effective during the design phase and it is called design for testability (DFT). The incorporation of DFT improves the reliability, maintainability, and availability (RM&A) and reduces the life-cycle cost of the particular system.

The test effectiveness, though it is related to testability, is an entirely different concept and it is measured in terms of fault detection and fault isolation (FD/FI) levels. The test effectiveness depends on the following:

1. (inherent) testability

2. test strategy

3. automatic test equipment (ATE)

4. test program sets (TPSs).

The development of a good and efficient set of TPSs for a given ATE (ATE has already been selected as the Teradyne L293 for RSIP) depends on the inherent testability and test strategy. A high level of FD/FI cannot be achieved without the first two. The major risks were identified of not incorporating DFT and the analysis of DFT in the CCAs. They are:

* poor quality CCAs in terms of RM&A

* unreasonable increase in the time and cost of generating test patterns

* resulting test time and cost (during the maintenance phase) may be excessive

* most importantly, the desired level of test effectiveness in terms of FD/FI levels may not be met making the development of TPSs nearly impossible.

After having established that the risks are high, we used MIL-STD-2165 to identify the steps as to how testability should be applied to RSIP.

1. Develop testability program plan

2. Develop sufficient, achievable, and affordable testability goals for both built-in (on-line) and depot (off-line) testing

3. Integrate testability concepts into the design

    process

4. Regular evaluation of the extent to which testability

    requirements are being met

5. Review of the testability program.

There are several CAD tools available for testability

analysis (TA). No definitive recommendation can be given

at this point as to the exact tool that can be used.

Further research is necessary to compare these tools to

arrive at such a conclusion.

The second part of the report identifies and justifies

the requirements of WRALC for proper maintenance of the

TPSs after they are delivered by WEC. In addition to the

list of traditional requirements requested by WRALC, it was

identified that WRALC personnel would require the

following:

* an identical CAD system to be used for TPS maintenance

    as that used by WEC for TPS development

* a testability analysis tool.

WRALC has neither the new tools nor the training to use

them properly at this time. The tools and training are

necessary for them to be able to maintain the TPSs

effectively.

The third part of the report provides an analysis of the proposal for incorporating testability and TPS development submitted by WEC. This analysis identifies the strengths and weaknesses of the proposal in applying testability to RSIP and in the development of TPSs. Some of the important conclusions of this analysis are:

1. The technical details of the incorporation of DFT are not discussed in the proposal.

2. WEC should address the issue of DFT through a program directive that should provide clear guidelines and targets for incorporating testability. It should also provide the methods and tools to be used in testability analysis (TA) and the method for incorporating the results of TA.

3. Since test engineers are not part of the design team, WEC needs to train design and/or TPS engineers in DFT and TA.

4. If the above point is not addressed well in advance, it will defeat the purpose of incorporating DFT.

5. The inclusion of TPS engineers from WRALC as part of the design team is good for both WEC and WRALC. This will provide continuity between the development phase

and the maintenance phase of the TPSs. But WRALC TPS engineers should have a commitment to remain at WEC throughout the development process and also to return to WRALC to make use of the knowledge gained at WEC.

6. WEC has identified the tool to measure the test effectiveness of digital circuits only. It has not identified the CAD tool for TA. Furthermore, it has not identified the fault simulator for analog and hybrid circuits.

7. The WEC proposal does not follow the systematic method of addressing the issues related to testability and such an unplanned approach will most likely lead to complications resulting in poor testability and thus ineffective TPSs.

The last part of the report was to arrive at the conclusions and recommendations based on our independent research for the goodness of the program over its life-cycle. These recommendations are given in the next section.

IV. RECOMMENDATIONS:

The information we gathered from our discussions with personnel at the various installations dealt mainly with TPS development. This indicated that most people are willing to try and solve the testing problems from a software standpoint. Our independent research of published literature and DOD documents indicates that the testing solution lies in a correct hardware design that should be designed for testability and then only a good and efficient set of TPSs can be developed. At the present time, it is our conclusion that without the proper verification of inherent testability, the USAF has no way of knowing whether the program is getting its money's worth for including testability.

For a successful incorporation of testability in RSIP, the following specific recommendations are suggested for the benefit of the program over its life-cycle:

1. The focus for achieving fault detection and fault isolation (FD/FI) levels seems to be from a purely software standpoint.

-The majority of people we talked to were set in the
false idea that writing software for TPSs could
overcome all hardware design limitations.

-The hardware design concepts that we stressed in
this paper must be fully and seriously addressed.

2. Quick-Fault by Mentor Graphics is not a testability
analysis (TA) tool.

-Many TA tools are available including the
following: LOGMOD/STAT, STAMP, DTA, CAFIT, ACE,
and IN-ATE. No evaluation has been done at this
time. Further research is necessary to identify
the correct tool.

-Once a TA tool is chosen, WRALC personnel need to
be trained as soon as possible on its use.

3. Persons with expertise should be called upon to do
evaluations of the results Westinghouse Electric
Corporation (WEC) presents from the TA tool.

-If WRALC personnel are sufficiently trained at this
point they should do the evaluations.

-Otherwise it is recommended that an independent
third party with expertise in testability analysis
do the evaluations.

4. Quick-Fault only measures test effectiveness of digital
circuits.

-A fault simulator for analog and hybrid circuits should be identified.

-If none are found, extensive circuit simulation results must be presented to verify FD/FI levels.

5.   The unquestioned grouping of possibly detected faults and detected faults in the fault simulator output is incorrect.

-Possibly detected faults are highly circuit dependent and cannot always be considered detected.

-Any reference to such a grouping in the SOW should be removed.

-Possibly detected faults should be reclassified either manually or automatically as either detected or undetected using proper engineering judgment. Such a reclassification should be independently evaluated.

6.   Continuity between WEC TPS development and WRALC TPS maintenance can be enhanced by two things:

-The inclusion of WRALC personnel with the WEC design team should definitely be implemented.

-The establishment of an identical CAD system at WRALC to do TPS maintenance.

Further research into various testability analysis (TA) tools needs to be done if the use of inadequate tools and delays are to be avoided in the future. Since new tools are being introduced on a regular basis, a standardized method of evaluation needs to be developed. Most in-depth TA tool studies have been done at either the IC level or the system level. Since most analysis for military systems needs to be at the card level, research must be focused in this direction. RSIP would provide a wide variety of cards (digital, analog, and hybrid) for performing a TA tool study. RSIP will also be using VLSI and VHSIC ICs that any new TA tool should be able to deal with. The major areas that we feel need to be looked at in TA tools are the method of determining figures-of-merit and providing test strategy. Some other criteria that we would like to look into for TA tools are:

-schematic capture

-hierarchal levels

-feedback collapsing and removal

-useful for digital, analog, and hybrid

-providing test vectors

-fault detection and isolation levels

-etc.

REFERENCES

Nagle, H.T., S.C. Roy, C.F. Hawkins, M.G. McNamer, R.R. Fritzemeier, "Design for Testability and Built-In Self Test: A Review," IEEE Transactions on Industrial Electronics, pp. 129-140, May 1989.

Byron, J., L. Deight, G. Stratton, "RADC Testability Notebook," RADC-TR-82-189, June 1982.

Private Communication at WRALC with Dean DeMeyer.

Joint Service, "Joint Service Built-in Test Design Guide," AFLCP 800-39, 19 March 1981.

Fritzemeier, R.R., H.T. Nagle, C.F. Hawkins, "Fundamentals of Testability - A Tutorial," IEEE Transactions on Industrial Electronics, pp. 117-128, May 1989.

Robach, C., S. Guibert, "Testability Measures: A Review," Computer Systems Science and Engineering, pp. 117-126, July 1988.

Brglez, F., D. Bryan, J. Calhoun, G. Kedem, R. Lisanke, "Automated Synthesis for Testability," IEEE Transactions on Industrial Electronics, pp. 263-277, May 1989.

MIL-STD-2165, "Testability Program for Electronic Systems and Equipment," 26 Jan 1985.

Goldstein, L.H., "Controllability/Observability Analysis of Digital Circuits," IEEE Transactions on Circuits and Systems, Vol. CAS-26, No. 9, pp. 685-693, Sept. 1979.

LOGMOD/STAT, Detex Systems, Inc., Villa Park, CA.

STAMP, Arinc Research Corp., Annapolis, MD.

McNamer, M.G., S.C. Roy, H.T. Nagle, "Statistical Fault Sampling," IEEE Transactions on Industrial Electronics, pp. 141-150, May 1989.

Seth, S., V. Agrawal, H. Farhat, "A Theory of Testability with Application to Fault Coverage Analysis," Proceedings 1st European Test Conference, Paris, pp. 139-143, April 1989.

Arnold, R.S., "Software Restructuring," Proceedings of the IEEE, Vol. 77, No. 4, pp. 607-617, April 1989.

WEC Proposal, "Organic Depot," Technical Volume II, Annex A.

1989 USAF-AES SUMMER FACULTY RESEARCH PROGRAM

GRADUATE STUDENT RESEARCH PROGRAM

Sponsored by the

AIR FORCE OFFICE OF SCIENTIFIC RESEARCH

Conducted by the

Universal Systems, Inc. ·

PROPOSED INNOVATIVE SEMI-HARD AIRCRAFT SHELTER

Prepared by: Jon B. Anderson, Ph. D.

Academic Rank: Assistant Professor

Department and   Department of Technology

University: Texas Tech University, Lubbock, Texas

Research Location: USAFESC/RDCS
                      Tyndall AFB
                      Florida   32403

USAF RESEARCHER: LT   James M. Underwood, USN

Date: 11 Aug   89

Contract No. ·   F49620-88-C-0053

Project No.   210

PROPOSED INNOVATIVE SEMI-HARD AIRCRAFT SHELTER

by

Jon B. Anderson, Ph. D.

ABSTRACT

Aircraft shelters at forward bases must meet the criteria of
ease and speed of construction, transportability of
components, modular components and aircraft protection.
Meeting these needs is the object of this proposed
structure. The structure has two forms of protection,
protective elements that are manufactured on site and the
ability to resist loadings by changes in geometry as well as
material deformations.

Acknowledgements

Many people deserve thanks for their encouragement and
positive attitude during my effort. My effort focal point,
LT James M. Underwood, USN, deserves special thanks for time
spent and input provided which made this a rewarding and
productive experience. Thanks to William S. Strickland,
Chief RDCS, for taking time from his full schedule to lend
his expertise to difficult segments of the work. Capt Diane
Miller, and Capt Richard Reid, USAF provided assistance in
their areas of expertise which was greatly appreciated.

Proposed Innovative Semi-Hard Aircraft Shelter

for

USAFESC/RDCS, Tyndall AFB, FL

by

Jon Anderson, Ph. D.

Texas Tech University

Lubbock, TX

79409

August 2, 1989

Introduction. Aircraft shelters at forward bases must meet
the criteria of simplicity, ease and speed of construction,
transportability of components, modular components and
aircraft protection. Meeting these needs is the object of
this proposed structure. The structure has two forms of
protection, protective elements that are manufactured on
site and the ability to resist dynamic loadings by changes
in geometry as well as material deformations.

Objectives. Principal objective for this report is to
propose a new concept for an aircraft shelter, primarily for
forward bases, for consideration by AFESC .DCS to determine
if the system can be used effectively as a protective
structure.

Description of Proposed Shelter System. This protective
structure falls in the rapidly constructed, semihardened
category and is intended for fighter type aircraft at
forward basing areas.

Principal advantages of the system include ease of
construction, transportability, reduction of heavy equipment
usage, modular components, and variable protection levels.

A typical construction sequence would begin with an
excavation. A modular truss system is then erected. AM-2
runway mats are placed on the floor and ramps of the
shelter. Next the protective layer, which also forms the
roof and walls, is placed. As a final step the excavated
soil is used to cover the structure leaving the entrance
and exit ramps open. The simplicity of construction is very
evident and is explained in further detail next.

Excavation is performed by a bulldozer that scrapes the

trench to a desired
depth. Depth of
protective structure
floor depends on its
usage and amount of
soil cover desired
for protection. As
a minimum it is
suggested that the
roof be placed at
the level of the
natural ground.
This minimum depth
inhibits the entry
of ground burst

Figure 1

secondary missiles at damaging velocities. In the rare
event that the natural soil is not suitable for bulldozer
excavation, explosives are used to loosen the ground for
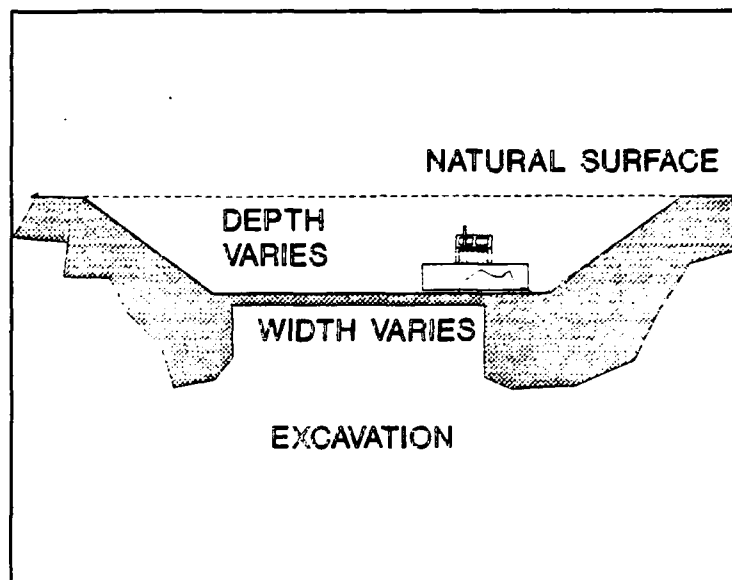excavation (See Figure 1).

Tiebacks are drilled, cables place and concreted. These are
ordinary tiebacks used for excavation retaining walls in
building construction. The modular truss system is placed,
attached to cable stiffeners, and erected (See Figure 2).

Stability cables are threaded through eyelets on the ends of
the trusses, set to approximately the proper length and
secured on each side of the thread hole using bolted cable
stops. Cables are attached to all tiebacks except for the
two upper on one end of the shelter. Remaining cable stays
(except for ground level) at the shelter end are used to
erect the structure using the heavy equipment.

Cables should be strung in continuous lengths as shown in

Figure 3, to avoid
straight lines.
Exceptions are the
ground level cables
and transverse
tensioning cables.
See Figure 3.

Protective roof and
wall elements are
now placed by crane
over the truss
system. These
elements consist of
steel pipe filled

Figure 2

with concrete. Pipes can be varied by length and diameter
as required by the perceived threat. When greater
protection is desired the number of protective element
layers are increased to provide the level of protection
wanted. As in the "rock rubble" concept, if protective
level is based on the number of calibers of the weapon, the
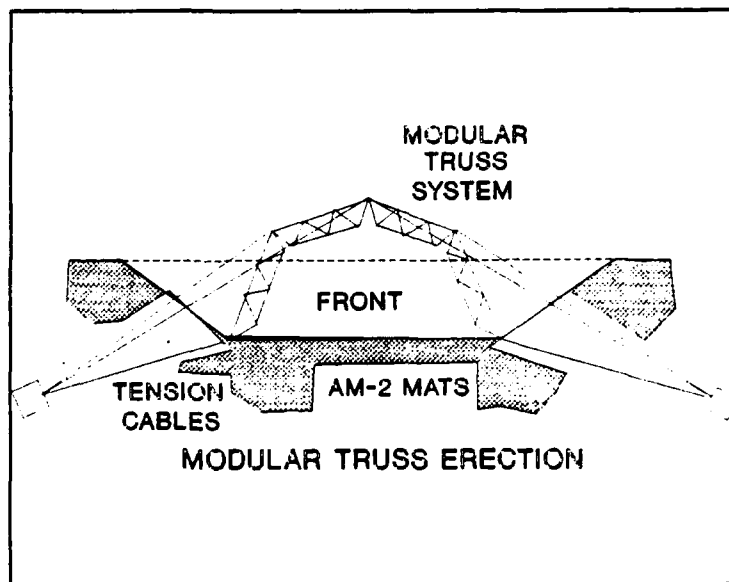diameter of the pipe can be increased accordingly. See
Figure 4.

Pipe lengths are standard mill lengths. Total length of
individual pipes may vary with producing mill but final
length is not critical. Pipes are stacked against trusses
end to end . Pipes are not necessarily connected to trusses
or to each other. As an assembly convenience, pipes would
be spot welded to trusses to maintain a specific stacking
order during placement and backfill. Length of pipes should
be three between-truss distances. A few pipes near the

entrance to the shelter may need to be welded end to end to retain the soil past the entrance until the natural slope of soil on the sides of the ramp meets the supported embankment slope.

TOP VIEW OF SHELTER
EXAMPLES OF CONTINUOUS CABLE PATHS ON SHELTER
Figure 3

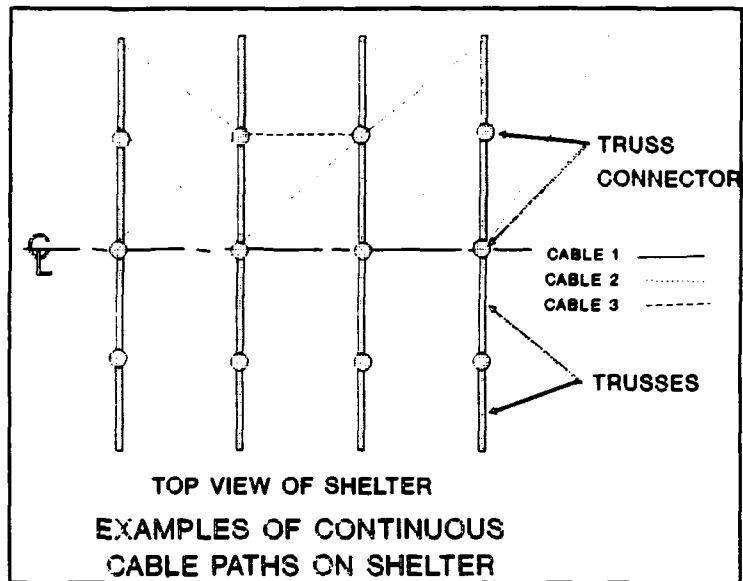An impermeable/coarse drain/permeable media covering over the protective elements is desirable but not absolutely necessary.

Backfill and embankments over the protective elements (and drain layer if included) complete the shelter. See Figure 5.

Because of the construction method a secondary advantage to the shelter would be when natural vegetation of the area is allowed to grow over the embankment and through the AM-2 mats, the shelter would be difficult to identify visually from higher altitudes.

Rationale for Proposed Shelter System. Primarily, the unique feature of the proposed protective structure is its adaptability to different perceived threats. Concrete and steel thicknesses can be increased by placing more layers of concrete filled pipe on the truss system. Soil cover can be increased by burying the structure to a greater depth. The

optimum solution can
be obtained through
various
configurations of
soil cover and steel
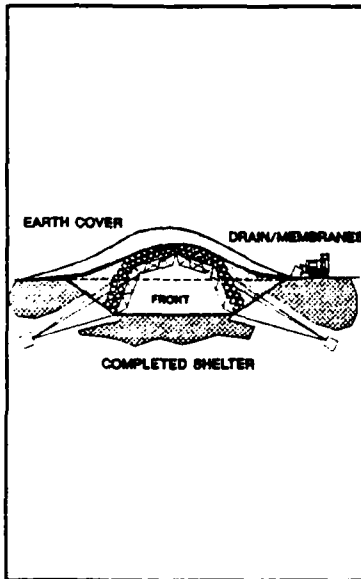pipe quantities in
response to
perceived threat.

MODULAR
TRUSS
SYSTEM

FRONT

TENSION
CABLES

AM-2 MATS

PIPE PLACEMENT

Figure 4

EARTH COVER
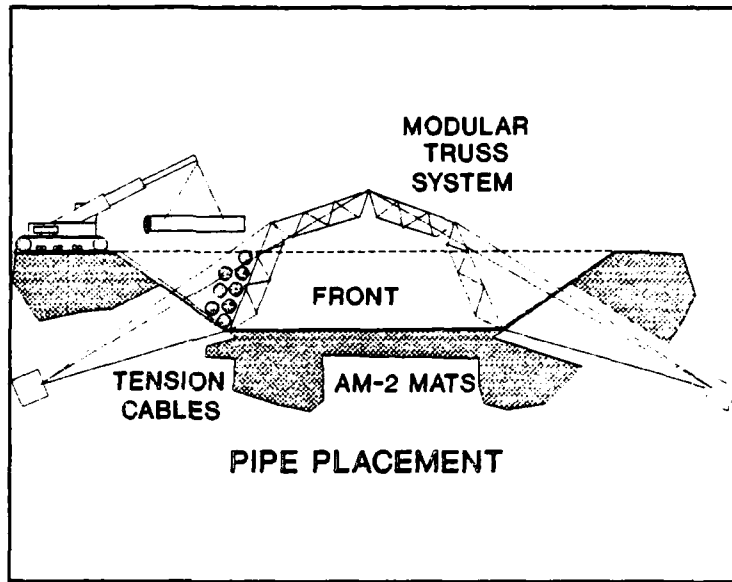
DRAIN/MEMBRANE

FRONT

COMPLETED SHELTER

Figure 5

Ease of construction is another
practical aspect of this structure.
Minimal heavy equipment is required. A
bulldozer, medium capacity crane, and
tieback setting equipment (usually
attached to the crane) are all that is
required. Smaller equipment items
includes such items as cable tensioners and wrenches. A
rock drill for setting explosives in difficult soils may
occasionally be needed.

Transportation requirements of components are reasonable.
Steel pipe, cement, cable and modular truss elements are the
only transported elements. Other items, water and aggregate
for example, will probably be available near the site.

At this point in development the shelters response to
various threats is not known but engineering experience

indicates that tension restrained structures may provide
additional survivability due to their ability to relieve
stress by changes in geometry in addition to material
deformation.

Limitations on Scope of Investigation. Proposed shelters
are intended for forward bases and as such are essentially
earth covered tubes with both ends open and ramp access to
the surface for the aircraft. Based on this assessment,
items such as blast doors and nuclear or chemical resistance
are not considered.

Feasibility of Proposed Construction Method. All materials
and construction techniques mentioned are currently
available and continuously in use in the US construction
industry. Standardization of components will make the
system efficient and effective. Trusses will be made from
standard pipe sizes and cables are common sizes.
Standardization and minimum number of components will
eliminate shelters that can not be erected due to the lack
of a single specialized part. For example, additional
forces due to deeper burial can be resisted by merely
reducing the spacing of the standardized trusses.
Simplicity is also achieved in the fact that only 5
components, steel pipe, modular trusses, cable, cement and
AM-2 mats, need to be transported. Transportability of
these items are within the range of delivery systems
currently available. Transportable components of a single
shelter weigh in the range of 150,000 to 200,000 lbs and
could be transported by 5, C-130H type aircraft.

Construction Procedures Based on Vulnerability Assessment.
Considerations for placement of the proposed protective
structure include, but are not limited to, type of attack

expected, weapons types used, importance of facility and soil type in the area of construction.

Some examples would be placement for ground burst, air burst and penetrator type weapons.

A typical placement response could be to make the shelter longer. This limits the number of appropriate angles necessary for an air burst to send damaging secondary missiles into the structure. A direct hit is discounted.

Penetration type weapons ca.. penetrate certain soil types for distances greater than a hundred feet. Placement, in this case,
would consist of increasing the number of concrete filled pipe used to form the roof and walls of the shelter. This increases the thickness of concrete and steel protecting the shelter from penetration and the subsequent blast. Diameter of pipes can also be varied based upon caliber of expected penetrators as in the "rock rubble" concept.

Defense against guided weapons can only be effected by placement of the individual shelters in random directions. This type of attack requires specific ranges of attack paths for each shelter. Once the base is alerted to the attack, these individual attacks can be countered with ground and air defenses.

Placement possibilities are not limited to the above. Commanders in the field can construct a shelter system placed according to their individual needs.

Proposed shelter system can incorporate many of the protective systems now under study during its construction.

Systems such as deflection grids, rock rubble, reinforced earth and layered systems that combine different resistance components can be easily placed during installation of the shelter. Burster slabs can be approximated by placing smaller square or rectangular slabs of such dimensions that they conform to the curvature of the embankment.

Recommendations. Reviewers of this document have expressed an interest in the concept and have suggested that testing be done to determine the level of protection provided by the protective elements suggested in this document. A proposed test plan is attached in Appendix A. Once testing has indicated an acceptable protection level, the shelter concept should be developed in terms of structural design, construction methods and survivability to a range of weapons.

Appendix A

Test Plan for Protective Elements Used in
Proposed Innovative Protective Aircraft Shelter

by
Jon Anderson, Ph.D.
Texas Tech University
Lubbock, Texas
79409

Objectives of this test series are to determine the level of protection provided by the proposed innovative semi-hard aircraft shelter protective elements in terms of penetration resistance and deflection of penetrator and to gather the type of data that will aid in development of an analytical method to predict the behavior of the protective elements when subjected to a penetrator type weapon.

Equipment required, other than the test facility, is a pipe holding rack, photographic equipment including a high speed camera, methods to measure projectile velocity and a 155 mm howitzer to accelerate projectiles.

Data collected during the test includes, but is not limited to, the following:

a. Striking velocity of projectile.

b. Striking point of projectile.

c. Rotation of ends of each pipe during penetration, including initial and final rotational location of each pipe.

d. Path of projectile through the pipe layers.

e. Location of projectile at completion of travel.

f. In long span pipe tests the permanent flexural distortion of each pipe.

g. Location of points where pipe shell has been penetrated including photographs of damage.

h. Condition of projectile at completion of travel.

Testing will be divided into three phases. Each phase
consisting of a specific configuration of protective
elements and number of shots.

Phase 1. Phase one uses short concrete filled pipes of
three to five diameters between support points. This
configuration will minimize the response parameters of
longitudinal rotation and flexural response of the concrete
filled pipes. Short pipe series will consist of twenty
shots. Shot configurations in the short pipe series will be

> a. five shots loose stacking (See Figure 6), shot path
> perpendicular to target face in both the horizontal and
> vertical plane (See Figure 7). Penetrator is set to
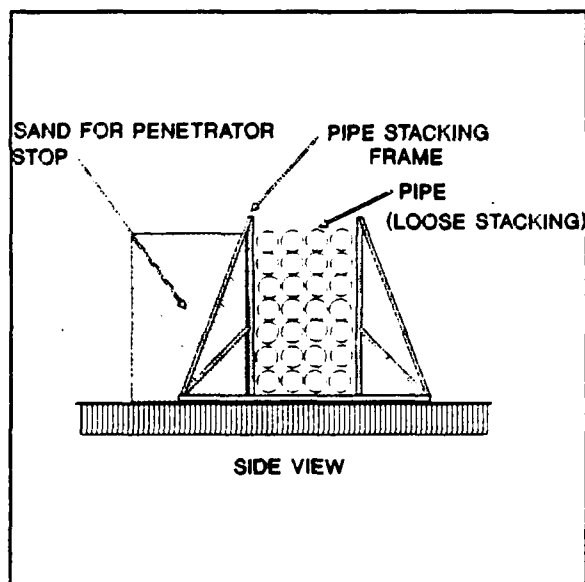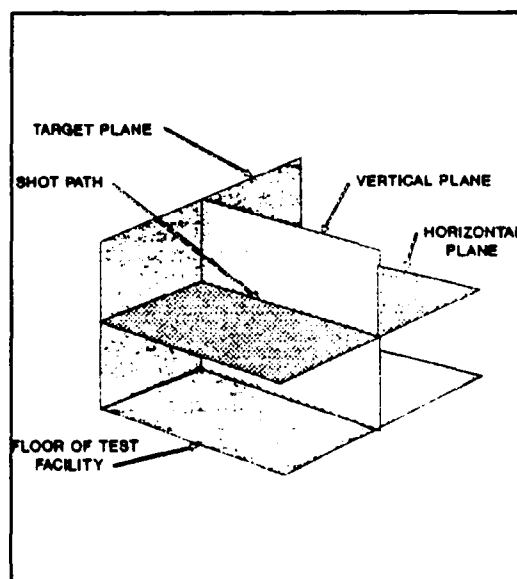> strike between pipes (See Figure 8).

Figure 6

Figure 7

> b. five shots loose
> stacking, shot path
> perpendicular to target face
> in both the horizontal and

vertical plane. Penetrator is set to strike a single pipe
at its tangent to the vertical(See Figure 10).

c. five shots dense stacking (See Figure 9), shot path
perpendicular to target face in both the horizontal and
vertical plane. Penetrator striking the face at any
location on the vertical face of the pipe stack.

d. five shots dense stacking in the elevated position on
the stacking frame (See Figure 11), shot path
perpendicular to the target face in the horizontal
direction and at an appropriate angle in the vertical
plane with penetrator striking any point in the pipe
stack.

Horizontal plane angle shots are not recommended for the
short pipe series.

Pending a successful outcome of the phase 1 program, phase 2
is initiated.

Phase 2. Phase two uses long (compared to diameter)
concrete filled pipes, perhaps 20 ft or longer, supported at
intervals proportional to those expected on the proposed
semi-hardened aircraft shelter. In this configuration
bending effects will be evaluated in the data acquisition.
Additionally, shot paths at an angle to the horizontal
plane will be performed. Long pipe series will consist of
thirty five shots. Shot configurations in the long pipe
series will be:

a. five shots loose stacking, shot path perpendicular to
target in both horizontal and vertical planes with
penetrator striking between pipes.

b. five shots loose stacking, shot path perpendicular to target plane in both horizontal and vertical direction with penetrator striking a single pipe at its tangent to the vertical.
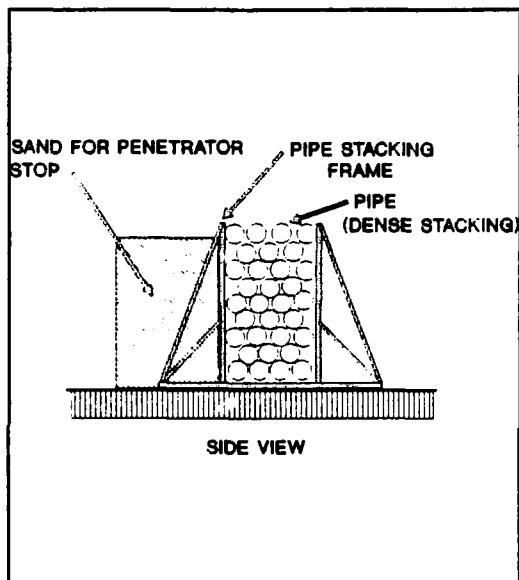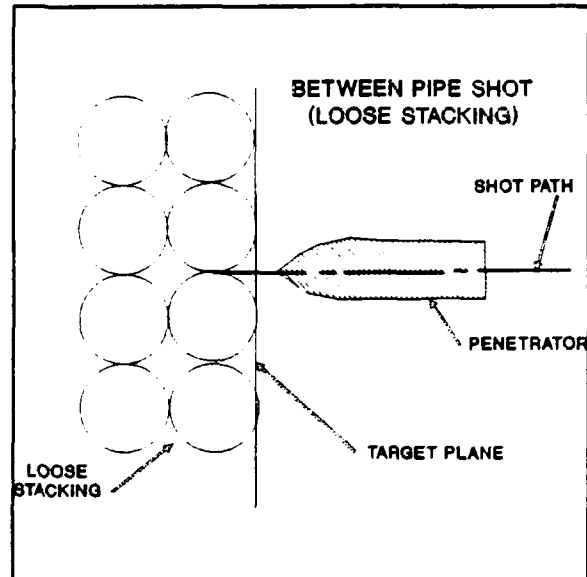

Figure 8

Figure 9

c. five shots dense packing, shot path perpendicular to target plane in both horizontal and vertical planes with penetrator striking any location on the target face.

d. five shots dense stacking in the elevated position on the stacking frame with shot path perpendicular in the horizontal plane and at an appropriate angle in the vertical plane. Penetrator can strike any point in the pipe stack.

f. five shots loose stacking, shot path perpendicular to the target plane in the vertical plane and at an appropriate angle in the horizontal plane with the

penetrator striking a
single pipe at its
tangent to the vertical.

Figure 11

Figure 10

e. five shots loose
stacking, shot path
perpendicular to the target
plane in the vertical plane
and at an appropriate angle
in the horizontal plane
with   penetrator striking
between pipes.
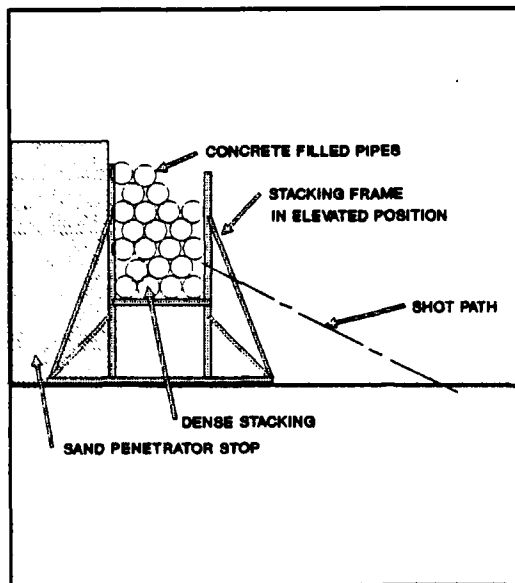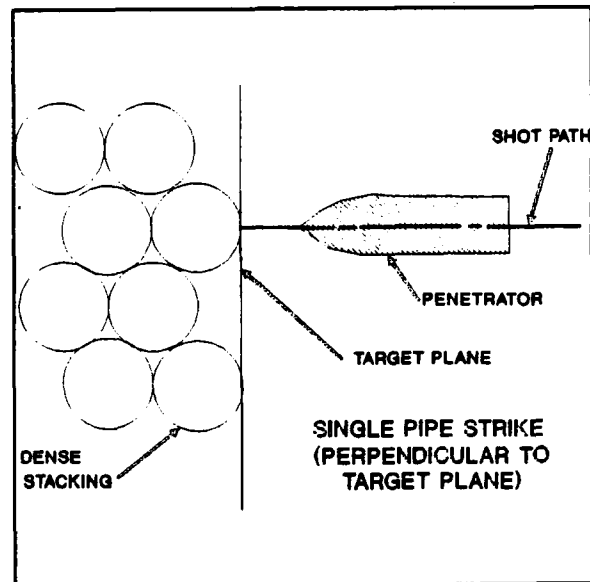
g. five shots dense stacking, shot path perpendicular to
the target plane in the vertical plane and at an
appropriate angle in the horizontal plane and at an
appropriate angle in the horizontal plane with the
penetrator striking any location on the vertical target
face of the stack.

With acceptable data produced by phase two, phase three will
be initiated.

Phase 3. Phase three will provide data for the resistance of the protective element system as it would be placed in the field. As an economy measure, readily available pen web steel joists can be used in place of the modular trusses. Test configuration will be similar to the long pipe series except trusses and cable stays will replace the pipe stacking frame (See Figure 12). Phase three will consist of ten shots. Shot configuration in phase three will consist of:

a. five shots loose stacking with five feet of locally available soil placed in front of the pipe stack to simulate the backfill over the shelter. Shot path will be in a direction chosen from the results of phase one and two. Penetrator strike point will be at any location relative to the target face.

b. five shots dense packing with five feet of locally available soil placed in front of the pipe stack to simulate the backfill over the shelter (See figure 12). Shot path will be in a direction chosen from the results of phase one and two. Penetrator strike point will be at any location relative to the target face.

Completion of the test series consists of data reduction and photographs taken of each deformed or penetrated pipe section.
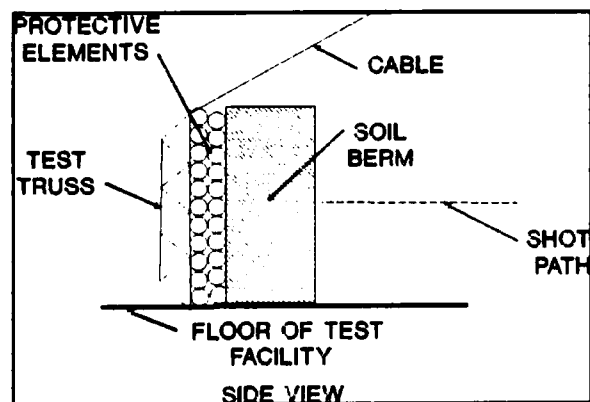
Figure 12

1989 USAF-UES SUMMER FACULTY RESEARCH PROGRAM

Sponsored by the

AIR FORCE OFFICE OF SCIENTIFIC RESEARCH

Conducted by the

Universal Energy Systems, Inc.

FINAL REPORT

JP-8 IGNITABILITY

Prepared by: William W. Bannister, PhD

Academic Rank: Professor

Department and   Chemistry

University: University of Lowell
                      Lowell, MA   01854

Research Location: AFESC/RDCF
                      Tyndall AFB, FL   32403-6001

USAF Researcher: Mr. Joseph Walker

Date: 25 September 1989

Contract No.:   F49620-88-C-0053

JP-8 IGNITABILITY

William W. Bannister

Abstract

A <u>reversed</u> relationship exists between molecular weight and ignition temperatures: up to a point, volatile higher molecular weight fuels have <u>lower</u> IT's and are more easily ignited by hot surfaces. Moreover, fuels which would be anticipated to be most subject to free radical effects are actually most resistant to hot surface ignition: free radical effects appear unimportant among factors influencing ignition temperature, and ionic effects, induced by thermoelectric (and, perhaps in some instances, oxyionic hot surface) effects, seem to be most important. For higher members of the alkane family this trend may reverse, resulting in minimum IT's for the C - C alkanes. Branched chain alkanes, arenes and olefins also have higher IT's than analogous straight chain alkanes. Important parameters in governing IT's of fuel components include: (1) the effect of molecular weight on the velocity of the fuel molecule near the hot surface; (2) the effect of rigidity of the fuel molecule on its ability to recoil from the hot surface; and (3) the effect of specific heat of the molecule with regard to ability for dissipation of heat energy within the molecule.

ACKNOWLEDGMENTS

JP-8 IGNITABILITY

WILLIAM W. BANNISTER

DEPARTMENT OF CHEMISTRY

UNIVERSITY OF LOWELL

LOWELL, MA 01854

AFESC/RDC SCIENTIFIC COLLEAGUE: JOSEPH WALKER

AFESC FOCAL POINT: PERRY SULLIVAN

INTRODUCTION

An Ionic Mechanism for Spontaneous Ignition

Ignition initiates by contact of fuel with a flame, or with a hot surface. For ignition by flame contact, the flash point is the important fuel characteristic.[1] Flash points are a function of fuel volatility. Therefore, low molecular weight (and thus low boiling point and low flash point) fuels generally are regarded as having greater flammability. Hot surface ignitions (characterized by spontaneous ignition temperature [IT] values[1]) may be even more important, however, particularly for ignitions in catastrophic situations (gunfire, crashes, fuel spills on hot engines, and other instances of aviation interest) in which open flames may not be initially present. The objectives of this project are to examine mechanisms which

may be involved in ignition processes, and to study improved techniques for measuring IT values for short duration exposures of fuels with hot surfaces.

Although it is conventionally accepted that fire reactions proceed through high energy propagating free radical mechanisms, there are very serious anomalies with regard to ignition phenomenon which have occasioned our group to conclude that the earliest initiation stages may be of an ionic, rather than free radical nature. As can be seen in Figure 1, arenes and olefins, which should be most susceptible to free radical formation,[6] are actually most resistant to hot surface ignition. Moreover, contrary to the order of reactivities shown in Figure 1, branched chain alkanes and cycloalkanes undergo free radical reactions more readily than straight chain alkanes;[6] and cyclopentanes are more reactive to free radical reactions than is the case for cyclohexanes.[7] On the other hand, there is much better agreement with carbanion formation proclivities for these species[6] - particularly since it has been shown that initial oxidative

Fig. 1. Spontaneous IT's of Typical Hydrocarbons[2-5]

attack on aliphatic hydrocarbons occurs most readily at primary C-H bonds, with secondary C-H bonds favored over tertiary C-H bonds.[8] This is precisely in the same order of stabilizing substituent effects for carbanions.[6]

In addition to the evidence cited above, regarding electronic contributions by the functionality of the fuel family to an anionic initiation mechanism for hot surface ignitions, there are also important considerations based on polarizing influences which may be exerted by the ambient atmosphere over the hot surface, and by the nature of the hot surface itself.

Thus, Finnerty's group at Aberdeen Proving Ground studied mixtures of propane with from 8.7% to 95.6% Halons 1301, 233 and 1011, and with hydrogen bromide (all of these normally being regarded as highly efficient flame extinguishing agents).[9] "Surprisingly, it was discovered that [the halons, and especially hydrogen bromide], instead of inhibiting the ignition of propane, actually act as ignition promoters!" [Emphasis added.] Although this was not considered in the Aberdeen report, halons, and especially hydrogen bromide are highly polar species which would serve to appreciably polarize the ambient air in the vicinity of the hot surface, thereby facilitating ionic ignition initiation processes.

It becomes interesting at this juncture to speculate about the possible polarizing influence which could also be exerted by water, in the form of water or water-based extinguishing agents, as entrained water in contaminated fuel, or as high humidity air conditions. In addition to anecdotal accounts this author has heard from highly skilled fire fighting experts, regarding anomalously difficult extinguishments in such conditions, paragraph III.(b)2. of Appendix A of the NFPA Standard 407 Fire Code states: "The amount of water ... entrained in the fuel due to water contamination is not particularly significant from a fire hazard viewpoint except that the amount of water increases the static generation hazard of the fuel."[1(b)] It may then be necessary to add to the NFPA statement a further caution, that increased fire hazards could arise from increased hot surface ignition propensities due to polarizing influences of water, in addition to increased static electrical charge generation effects.

Very importantly, as noted in Figure 2, there are large variations (often more than 100° C) in IT values which can be attributed only to the nature of the hot surface. The thermoelectric power effect is the only parameter which seems to correlate well with ignition temperature trends.

Fig. 2. Ignition Temperature Trends,[1,3,10] Emissivities,[11] and Thermoelectric Power Effects [S][12] of Surfaces

	Spontaneous Ignition Temperatures	Emissivity (ca. 300° C)	Integrated Thermoelectric Power [S] [from ca. 200° to ca. 500° C] volts
Quartz	Lowest	0.94	Oxyionic Surface
Gold		0.02	+ 0.5
Titanium	(steadily	0.6	+ 0.4
Iron *	increasing	0.8	+ 0.2
Zinc	values)	0.05	+ 0.2 (?)
Aluminum		0.15	- 0.5
Platinum	Highest	0.08	- 2.3

Figure 3 illustrates both the positive and negative types of thermoelectric power [S] effects. If a temperature gradiant is operational, with the cooler portion of the hot body at the surface, the negative power effect metals (e.g., aluminum or platinum) are polarized so that a small but significant drift of electron density occurs toward the cooler surface, with a corresponding accumulation of negative charge at the surface. For positive thermopower metals (e.g., gold or titanium) the opposite effect is noted, with a small but .significant positive charge accumulation at the surface.

Figure 3. Thermoelectric power effects or metals.[12]
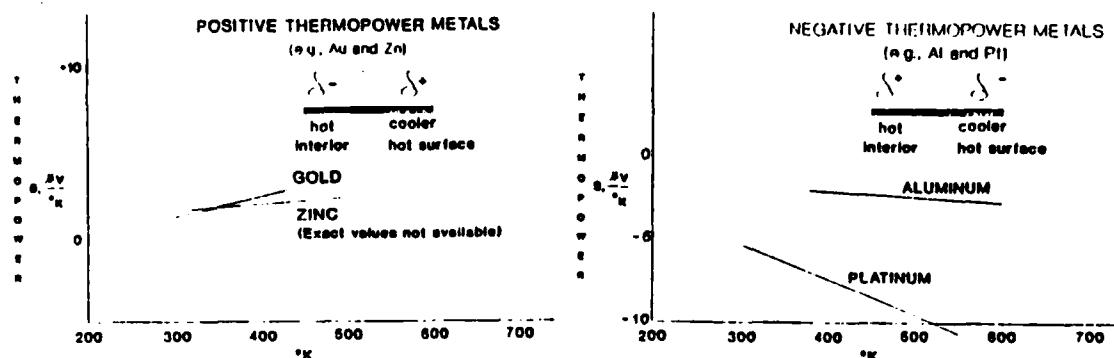
As shown in Figure 4, one result of this polarization would be an anticipated repulsion of pi bonded species (such as in oxygen, and in arenes and olefins) by negative thermopower metals. Thus, for negative type metals (which, as seen in Figure 3 are indeed characterized by having the higher ignition temperatures), more thermal energy (higher IT values) would be required to activate oxygen molecules which would not be adsorbed as tightly as would be the case for positive type metals, which would exert an attractive force for the oxygen with correspondingly lowered IT requirements. Oxyanionic surfaces such as quartz or glass also could facilitate thermal polarization of oxygen molecules by virtue of strong attractive forces between the negative dipole of the oxygen molecule and the strongly positively charged nature of the silicon moiety of the quartz matrix (or the cationic species in other oxyanionic materials).[13]

Fig. 4.   Repulsion of Pi Bonds by Negatively Charged Groups

Solomons, T. W. G., "Organic Chemistry", 4h ed., J. W. Wiley & Sons, Inc., New York, 1988, p. 227

negative thermopower metal
(hot surface, hotter interior)
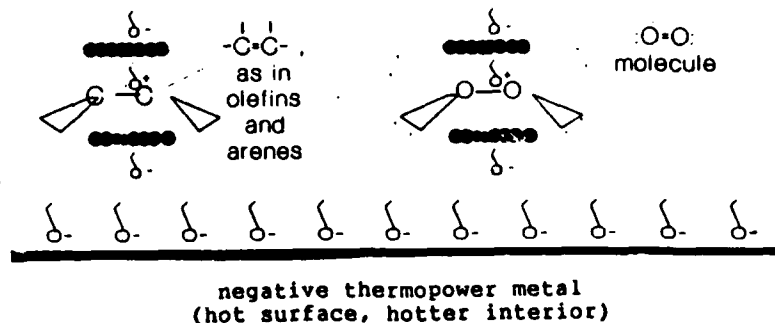
Thus, existing evidence seems to implicate a thermal polarization of oxygen molecules (induced by polarizing effects of the hot surface), as presented in Figure 5. The high gas phase Bronsted basicity[6] of the negative dipole of the excited oxygen molecule could be expected to provoke proton abstraction from the thermally exicted fuel molecule, to form a carbanion/hydroperoxy cation pair.* A rapid single electron transfer can then be anticipated to generate the highly energetic propagating free radical systems which are the basis for conventional free radical theories of combustion; and stabilizing or destabilizing influences in such free radical propagation systems would remain entirely operational from this stage on.   (Other

---

* Dr. Homer Carhart of Naval Research Labs has suggested that hydrogen bonding between a polarized hydrocarbon molecule and an incipent hydroperoxy cation may be operational in this mechanism.

carbanionic intermediacies in single electron transfers for free radical formations have also been recently reported.[14])

Fig. 5. Hot Surface Ignition Facilitated by Positive
Thermopower Metals (and by Oxyanionic Surfaces)
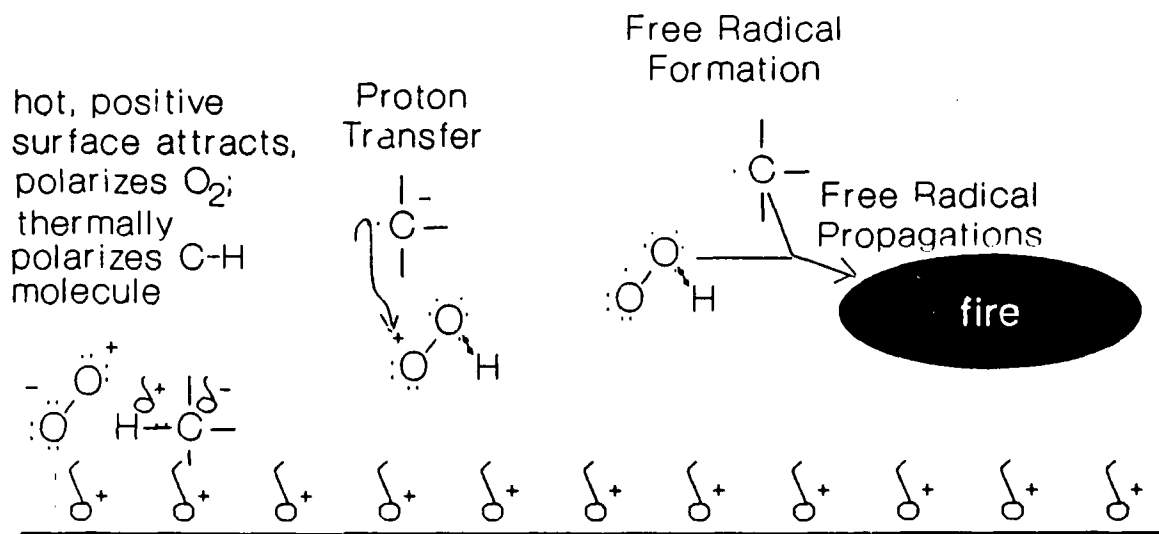
As indicated previously, negative thermopower metal surfaces would function in a similar mechanistic pathway, except that the oxygen molecule tends to be repelled by the partial negative charge character of the surface, requiring higher IT's to achieve adequate thermal polarization.

Correlations of Spontaneous Ignition Temperatures with Molecular Structures of Flammable Compounds

As can be seen in Figure 1, there is a <u>decrease</u> in IT values with increasing molecular weight for all classes of hydrocarbon fuels, from C_4 through C_{10}, using conventional ASTM procedures for IT determinations.[15] For alkanes and olefins the upward trend continues very dramatically for the lower molecular weight species, through methane and ethylene.[1,5] This reverse trend is least noticeable for branched chain alkanes.

Precise data is not available, particularly for the higher molecular weight species. In accordance with the ASTM procedures,[15] fuel is directed onto a hot surfacem with heating for up to ten minutes, the IT being the lowest temperature at which ignition occurs. Since decomposition often occurs during heating, the IT may not be characteristic of the original material, but rather of its decomposition products.[16] Many variables affect IT, so measurements are poorly reproducible.[1]

As shown in Figure 6, for IT values for alkanes from methane to hexadecane, there are actually two types of curves which have been observed by different groups, apparently utilizing somewhat different procedures which

have resulted in both lower and upper projected tracks of IT values for the higher alkanes. The number of data points available in the literature for alkanes above C_8 is much lower than exists for C_{1-8}, due to the increasing unreliability of the ASTM procedures with increasing molecular weight. The lower projected track of IT values in Figure 6 is an asymptotic sweep along a $200°$ isotherm for alkanes beyond C_8. This track may be due to pyrolytic decompositions (which typically become important above $200°$, particularly for the ten minute heating protocol of the existing ASTM procedure). A large alkane thus has sufficient time to crack to smaller hexanes, heptanes and octanes; and the actually determined IT value is the $240°$ IT value of these smaller species rather than that of the original larger molecular weight alkane.

A very poorly defined upper projected track may also exist in Figure 6, based on several anomalously high IT values for C_{14-20}. Although this is speculative at this point, these high values may be based on shorter combustion times which would thus require higher temperatures for such ignitions.

Obviously, either track could actually pertain. Values for the lower track curve have significance for those situations involving long term storage of fuels in areas in

Fig. 6. Correlations of Ignition Temperatures for n-Alkanes
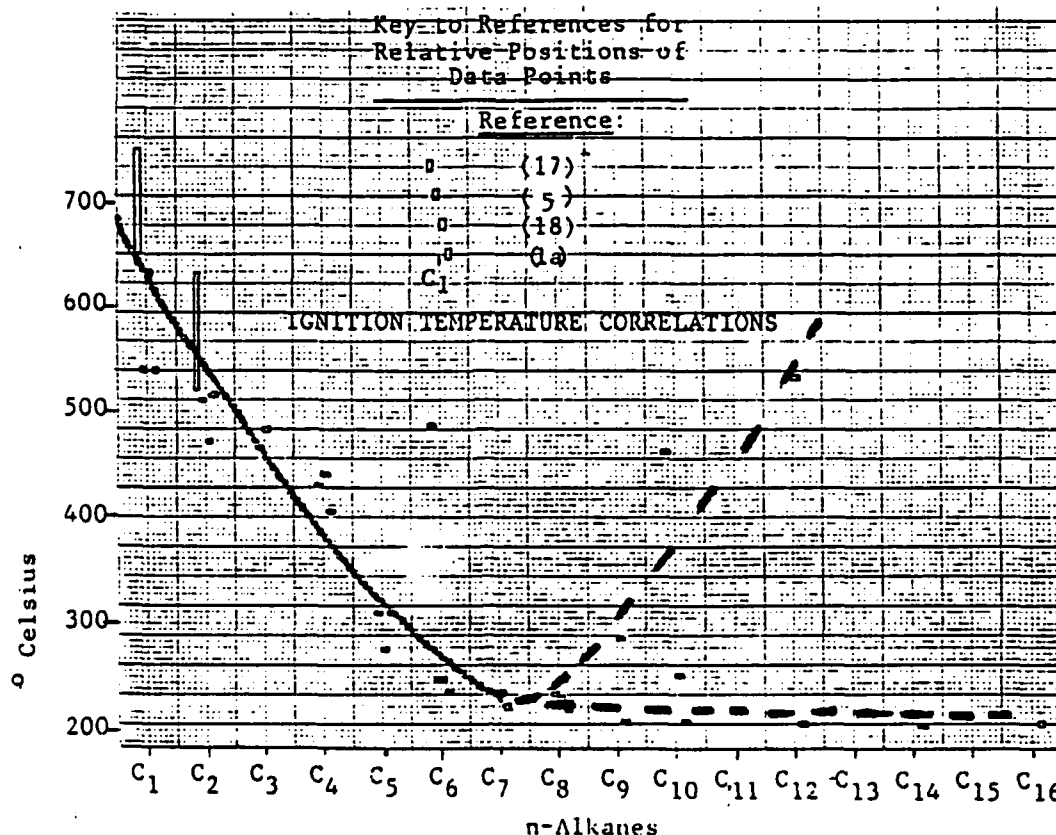
which possibilities for prolonged contact with hot surfaces may be a consideration. A particular need exists, however, for development of new techniques and equipment for determination of IT values which would relate to short term or instantaneous contacts of fuels with hot surfaces (as in situations involving crashes or gunfire), for which currently available data is insufficient and good values are unattainable with existing equipment and techniques.

Fuel characteristics which have been identified as having possible impact on the ignition temperatures are discussed below, and are illustrated in Figure 7.

Fig. 7. Molecular Characteristics Affecting Ignition Temperatures

Typical JP-8 component (A):   Typical JP-4 component (B):

dodecane   heptane

$CH_3\text{-}CH_2\text{-}CH_2\text{-}CH_2\text{-}CH_2\text{-}CH_2\text{-}CH_2\text{-}CH_2\text{-}CH_2\text{-}CH_2\text{-}CH_2\text{-}CH_3$ $CH_3\text{-}CH_2\text{-}CH_2\text{-}CH_2\text{-}CH_2\text{-}CH_2\text{-}CH_3$

(slow movement of massive molecule)   (smaller, rapid movement)

HOT SURFACE

[(1), (2), (3) ... (8), (9) above indicate positions of molecules A and B at same time intervals, relative to hot surface area.]

Molecular velocity at temperature (T, °K) is inversely proportional to the molecular weight (M); smaller molecules have greater speed.

$$\text{Average velocity} = 14,600\,(T/M)^{\frac{1}{2}} \text{ cm/sec}$$

The slow moving heavy molecule A (above) is therefore near the hot surface longer than the lighter and faster B, and A has more time available to absorb energy from the hot radiating surface.

The larger molecule A has more mobile C-C bonds and therefore more rotational degrees of freedom than the smaller B. Thus, A will tend to be "mushier" with less elastic recoil on impact with the hot surface than the smaller, more rigid B which can bounce away more readily. Again, molecule A will have more time to energize than B.

To offset this, and although the larger molecule has greater surface area enabling it to absorb more heat than the smaller molecule, the large molecule's volume is increased even more than is the surface area (by comparison with the smaller molecule). Absorbed heat is then dissipated more through the large molecule, which accordingly is cooler than the small molecule. This effect is more pronounced with increased molecular weights (and volumes). In this case A (dodecane) needs more heat (with a higher ignition temperature) to energize it to its decomposition point than does B (heptane). For smaller molecules (e.g., comparing hexane [C_6] and propane [C_3]), this offsetting factor of increased molecular specific heats is not as important as the molecular speed and rigidity effects: in such cases the heavier molecule has the lower ignition temperature.

1. <u>Molecular weight effects on speed and inertia for heavier molecules.</u> These effects increase residence time in the vicinity of a hot surface, with increased time for energy transfer.

2. <u>Molecular rigidity.</u> Rigid molecules have reduced rotational degrees of freedom within the molecular structures. This would significantly decrease "floppiness" of the molecule in its impact with a hot surface, allowing the more rigid structure to rebound readily and rapidly with correspondingly reduced residence times in the vicinity of the hot surface, and considerably reduced energy transfer from the surface to the fuel molecule.

3. <u>Specific molecular heat.</u> For smaller molecules relative speed and relative rigidity are important. For lower alkanes, each addition of a methylene unit imparts a significant increase in molecular weight and in internal degrees of rotational freedom. Thus, in going from ethane to propane, there is a 17% decrease in speed at 500°C, whereas decane is only 5% slower than nonane at this temperature. Internal rotational degrees of freedom are even more considerably enhanced for propane, which is very flexible compared with very rigid ethane; but decane and nonane have very little difference in

"mushiness" due to this effect. Thus, decreased speed and rigidity arising from increased molecular weight are much less important for the higher alkanes.

Moreover, higher alkanes begin to enjoy the benefit of increased "molecular specific heat". When lower alkanes such as propane are energized by radiational heat, all atoms of the small molecule are fairly equally irradiated. For larger molecules, some atoms will be in the shadow of others. The hotter surface atoms can then transfer some of their increased energies to the cooler internal atoms. Thus, a higher ignition temperature will be required to attain decomposition energies for a molecule large enough to provide shadowing by some of its atoms to other neighboring atoms.

EXPERIMENTAL

In the first phase of this project we have designed and are almost completed with the construction of an apparatus diagrammed in Figure 8, using gold and platinum coated glass tubes. (As can be noted in Figure 3, these two metals represent extremes in positive and negative thermoelectric effects.)

Fig. 7. Molecular Characteristics Affecting Ignition
Temperatures

Typical JP-3 component (A):   Typical JP-4 component (B):
dodecane   heptane

$CH_3-CH_2-CH_2-CH_2-CH_2-CH_2-CH_2-CH_2-CH_2-CH_2-CH_2-CH_3$ $CH_3-CH_2-CH_2-CH_2-CH_2-CH_2-CH_3$

(slow movement of massive molecule)   (smaller, rapid movement)

HOT SURFACE

[(1), (2), (3) ... (8), (9) above indicate positions of molecules A
and B at same time intervals, relative to hot surface area.]

Molecular velocity at temperature (T, °K) is inversely proportional
to the molecular weight (M); smaller molecules have greater speed.

Average velocity $= 14,600(T/M)^{\frac{1}{2}}$ cm/sec

The slow moving heavy molecule A (above) is therefore near the hot
surface longer than the lighter and faster B, and A has more time
available to absorb energy from the hot radiating surface.

The larger molecule A has more mobile C-C bonds and therefore more
rotational degrees of freedom than the smaller B. Thus, A will
tend to be "mushier" with less elastic recoil on impact with the hot
surface than the smaller, more rigid B which can bounce away more
readily. Again, molecule A will have more time to energize than B.

To offset this, and although the larger molecule has greater surface
area enabling it to absorb more heat than the smaller molecule, the
large molecule's volume is increased even more than is the surface
area (by comparison with the smaller molecule). Absorbed heat is
then dissipated more through the large molecule, which accordingly
is cooler than the small molecule. This effect is more pronounced
with increased molecular weights (and volumes). In this case
A (dodecane) needs more heat (with a higher ignition temperature)
to energize it to its decomposition point than does B (heptane).
For smaller molecules (e.g., comparing hexane [C_6] and propane
[C_3]), this offsetting factor of increased molecular specific heats
is not as important as the molecular speed and rigidity effects: in
such cases the heavier molecule has the lower ignition temperature.

Fig. 8. Combustion Tube Assembly

1. sample line 1/16" OD stainless tubing

2. thermocouple well

3. thermocouple

4. finger, aurinized pyrex

5. casing (internal surface aurinized or gold coated)

6. gold capillary 1/16" OD ID .010"

7. elbow fitting 90°

8. copper mesh electrode, with electrical lead

9. syringe for fuel injection

10. septum seal

11. controlled humidity air line, with valve

REFERENCES

1.(a) "Fire Hazard Properties, Flammable Liquids, Gases &
       Volatile Solids", Nat'l Fire Prot. Assn. Boston 1960.

  (b) NFPA Standard 407 Fire Code, Nat'l Fire Prot. Assn.,
       Boston, MA.

2. Swarts, D.E.; Frank, C.E. Natl. Adv. Comm. Aeronaut.,
   Tech. Notes #3384, 1955; Chem. Abstr. 1955, 49, 14446e.

3. Jackson, J. L. Ind. Eng. Chem. 1951, 43, 2869.

4. Miller, R. Symp. #6, Major Aircraft Fires (Proc.), Fire
   Res. Station, Boreham Wood, Herts, UK, Dec. 1966, 54-65.

5. McCracken, D. J. "Hydrocarbon Combustion & Physical
   Properties", BRL-1496; Ballistic Res. Labs, Aberdeen
   Proving Ground, MD (1970).

6. March, J. "Adv. Organic Chemistry", 3rd ed., McGraw-
   Hill Book Co., New York, 1985, pp. 142-9; 152-3; 163-6.

7. Brown, H.C.; Borkowski. J.Am.Chem.Soc. 1952, 74, 1894;
   Brown, H.C.; Brewster, J. H.; Schechter, H. ibid. 1954,
   76, 467.

8. Frank, C.E.; Blackham, A.U. Natl. Adv. Comm. Aeronaut.,
   Tech. Notes # 3384, 1955; Chem. Abstr. 1955, 49, 14446e.

9. Finnerty, A. E. "The Physical and Chemical Mechanisms Behind
   Fire-Safe Fuels", BRL-1947, Ballistic Res. Labs,
   Abderdeen Proving Ground, MD (1976).

10. Myronuk, D. J. "Dynamic Hot Surface Ignition of
    Aircraft Fuels and Hydraulic Fluids", AFAPL-TR-79-2095,
    Aero Propulsion Labs, Wright Aeronautical Labs,
    Wright-Patterson AFB, OH (1980).

11. Weast, R., "Handbook of Chemistry & Physics", 58th ed.,
    CRC Press, Inc., Boca Raton, FL, 1978, E229-230.

12. Blatt, F.J.; Schroeder, P.; Greig, D. "Thermoelectric
    Power of Metals", Plenum Press, New York, 1976,
    pp. 5, 29, 91, 149.

13.(a) Cho, P. "Catalytic Ignition and Heat Release of
       Fuel/Air Mixtures". Dissertation Abst., 45/07-B, p.
       2279 Ann Arbor, MI, 1985; 162 pp.

   (b) Mehandru, S.P.; Anderson, A.B. "Adsorption of O_2,
       SO_2 and SO_3 on Nickel Oxide", NASA Report NAS
       1.26:176072; NTIS No. N85-32175/0/HDO

14. Barton, D.J.R.; Jones, D.W. J. Chem. Soc. 1965, 3563.

15. "Autoignition Temperature of Liquid Chemicals", ASTM
    Designation E 659 - 78 (Reapproved 1984).

16. Affens, W. A.; Johnson, J. E.; Carhart, H. E. J. Chem.
    Eng. Data 1961, 6, 613-619 (and references therein).

17. Lange, N.A. "Handbook of Chemistry", 9th ed., Handbook
    Publishing Co., Sandusky, OH, 1956, p. 824.

18. Perry, R. H. "Chemical Engineering Handbook", 3rd ed.,
    McGraw-Hill Book Co., New York, 1950, pp. 1584-1585.

1989 USAF-UES SUMMER FACULTY RESEARCH PROGRAM

GRADUATE STUDENT RESEARCH PROGRAM

Sponsored by the

AIR FORCE OFFICE OF SCIENTIFIC RESEARCH

Conducted by the

Universal Energy Systems, Inc.

FINAL REPORT

Effect of Jet Aircraft Noise on
Domestic Goats

Prepared by:	Emerson L. Besch, Ph.D.
Academic Rank:	Professor
Department and	Department of Physiological Sciences
University:	University of Florida
Research Location:	AFESC/RDVS
	Tyndall AFB
	Panama City, FL 32403-6001
USAF Researcher:	Joan Scott, Ph.D.
Date:	08 SEP 89
Contract No:	F49620-88-C-0053

Effect of Jet Aircraft Noise on Domestic Goats

by

Emerson L. Besch

ABSTRACT

Noise from low-level jet aircraft is a common occurrence at Air Force installations but numerous complaints have been received about the effect of this stressor on domestic animals and wildlife. In an attempt to evaluate the physiological consequences of jet aircraft noise, domestic goats were housed in two locations on Tyndall AFB: one site was near an active runway but the other was in a more remote area of the base. Although attempts were made to control all variables, factors such as location of the animal sites on base, weather conditions, proximity of goats to predator animals, aircraft operations, flight patterns, and noise intensities all were beyond the control of the investigators. But, general signs, behavioral responses, hematological and blood chemistry changes, and blood hormone assays were performed in both groups. Pen and shelter size and design, availability to feed and water, and husbandry practices were the same among both groups. Although not all data have been analyzed to date, some preliminary conclusions can be made. 1) Both groups displayed a stressor effect of the transport to the base sites; 2) The animals housed at the remote site did not appear to adjust to their surroundings as readily as those housed near the runway site; 3) There were detectable differences in nutrition between the two groups of goats that are thought to be related to the natural flora at the sites; 4) There is some evidence to suggest that the goats near the runway were affected by the noise of the jet aircraft; 5) Future research is needed for which protocol development and variables to be controlled are suggested. Results of hormone assays will be made available in an addendum report.

Acknowledgements

I wish to thank the Air Force Systems Command and Air Force Office of Scientific Research for funding and Universal Energy Systems, Incorporated, for administering the Summer Faculty Research Program. The opportunity to conduct field type studies dealing with a serious environmental problem on a military installation was an adventure that provided knowledge and experiences that otherwise would not have been available to me.

Many individuals were responsible for making my stay at Tyndall AFB (TAFB) productive, enriching, and rewarding. In particular, I wish to thank Dr. Joan Scott for providing the stimulus that led to initiation, the persistence that led to approval, and the assistance that led to successful completion of the project. I also wish to offer special thanks to Mr. Jon D. Zern, Graduate Student Researcher, for his friendship, "can do" attitude, adventuresome spirit, significant and substantive assistance, and unrelenting efforts. Others who were especially helpful include Captain Janice F. Gaska, USAF, Chief, Clinical Laboratory Services, and the Clinical Laboratory Personnel of the TAFB Hospital for completing all hematological and clinical chemistry tests; SGT Delwin C. Lovell, USA, Veterinary Specialist for assistance in collecting data and providing health care to the animals; Mr. Robert N. Bates, Chief, Natural Resources, TAFB, and his staff for constructing the goat pens and enclosures; Captain Steven Tobias, VC, USA, Base Veterinarian for providing goat health care and professional advice as Chairman of the Animal Care and Use Committee (ACUC); LTC Warren P. Humphreys, USAF, JA, for furnishing legal assistance regarding acquisition of the goats and serving on the ACUC; and LTC Neil J. Lamb, USAF, BSC, for furnishing advice and serving on the ACUC. Thanks also are offered to Major Paul Kirch, USAF, Major Michael M. Thompson, USAF, Captain Michael L. Davenport, USAF, MSGT Anderson Edwards, TSGT Jim B. Whitcomb, USAF, Janet L. Davis, Neill Hunter, Dorothy J. Miller, and Perry H. Sullivan, Jr., most of whom are attached to the AFESC. Thanks also go to many others too numerous to name. And, last but not least, a special "Thank You" to Mr. Holton R. Harders, Parker, Florida, for the generous "loan" of the goats used in this study.

I.   INTRODUCTION:

Noise is defined as unwanted sound which originates from many sources including aircraft, surface transportation, and industrial and construction sites (Anonymous, 1987).   While many sources (e.g., fans, pumps, motors) contain pure-tone components, sound from jet aircraft exhaust is termed random noise because it contains all frequencies.   Although only about 25% of the population in the U.S. is seriously disturbed by aircraft noise compared to traffic noise, this stressor, in and around airports and air bases, tends to be more localized than surface transportation noise.   Nonetheless, because of geographic location of many military bases, flight operations (e.g., takeoffs, landings, subsonic flights) continue over some urbanized and rural areas where populations of domestic animals and wildlife are exposed to noises of high intensity (Bond, 1971).

Noise may result in auditory damage (e.g., hearing loss, nerve damage), non-auditory effects (e.g., release of thyroid hormones, behavioral changes), or behavioral modifications (e.g., locate young, mate, avoidance) in animals. In some cases, the response depends more upon how the sound is interpreted by the animal rather than the intensity of the signal.   For example, some sounds even when weak are not considered meaningful because they do not contain information calling for attention or action whereas meaningful sounds (e.g., warning signals) cause the organism to react accordingly (Borg, 1979).

In the 1960-70s, the focus of many noise studies was on occasional booms which did not appear to have much effect on an animal's behavior, except for the startle response (Bell, 1972).   All domestic species studied (e.g., cattle, sheep, horses, pigs, poultry)   appear to physiologically adapt to sonic booms (Casady and Lehmann, 1967; Espmark et al, 1974; Ewbank, 1977; Shotton, 1982) and subsonic flight noise (Bond, et al, 1963; Cottereau, 1979) with no loss of productivity.   In general, behavioral reactions appear to be minimal except for the avian species.   For the latter, animals may 'scatter' or 'crowd' (Ewbank, 1977) or tend to exhibit an 'alert' reaction and 'movement' away from the source of the sound (Bond, 1971).   Sonic booms cause a 'startle' response in cattle and sheep but this decreases as the duration of exposure increases; sheep

appear to be more disturbed by sonic booms when they are standing compared to lying (Espmark et al, 1974).

The National Environmental Policy Act (NEPAct) of 1969 requires the U.S. Air Force (USAF) to evaluate the impact of all actions--including noise pollution--that significantly affect the quality of the ambient environment. This is accomplished through the preparation of Environmental Impact Statements (EIS) which are basic planning and management documents. An EIS must include assessment of potentially adverse ecological impacts of noise and sonic booms on domestic animals and wildlife.

But, the USAF must continue to conduct flight operations in current aircraft and in assigned airspaces over private and public land in fulfillment of its National defense mission. The advantages of those activities include acquiring basic flight skills, improving mobilization readiness, and meeting mission requirements. Perhaps the numerous complaints about aircraft noise constitute the major disadvantage.

To deal with those complaints, assessments of potentially adverse physiological effects of noise and sonic booms on domestic animal productivity are needed. Peak noise levels obviously are related to many factors including aircraft type, location of measuring devices, altitude of the aircraft, and atmospheric conditions. Preliminary information from Tyndall AFB (TAFB) suggests that it is ideally suited for conducting research trials on the effect of low-level jet aircraft noise on animals. The research proposed here offers an opportunity to obtain data on the effects of noise on the physiology of a domestic species with a wildlife analog.

II.   OBJECTIVES OF THE RESEARCH EFFORT:

Jet aircraft noise research can be approached in at least two ways: 1) in the laboratory, or 2) in the field. Research conducted in the laboratory must include simulation of the noise stressor and methods of assessing the physiological consequences of exposure to that stressor. Further, the size of laboratory facilities usually limits the size of the animal--and therefore the number of animals--that can be simultaneously studied. Field research on the

other hand, has the advantage of bringing the investigator and animals to the location of the stressor to be investigated.

Although the latter approach provides a cost-effective way of obtaining information on the effects of noise on animals, it also involves considerable problems. In fact, after becoming aware of the opportunity to conduct noise studies on domestic animals at TAFB, I was uncertain whether such a study was feasible. That is, considering the short period of time available (10-wk) for the study, the apparent lack of qualified personnel to assist in project implementation, the apparent lack of appropriate and needed clinical laboratory resources, the nonavailability of animals or animal facilities at TAFB, the inability to control all variables (e.g., weather, noise intensities, feed and water intake), and the potential logistical problems, it was uncertain whether project protocols could be developed or useful data obtained. After two pre-Summer trips to TAFB, I was impressed with the "can do" attitude of Air Force Engineering and Services Center (AFESC) and other personnel (Refer to Acknowledgement Section) who agreed to provide assistance.

As a consequence, I became convinced that the project would furnish meaningful data. So a plan of action and timelines were developed which formed the basis of the study to evaluate physiological responses of goats exposed to low-level jet aircraft noise. The main objectives were to acquire information that would be valuable in assessing and predicting jet aircraft noise effects on livestock. At the very least, it was felt that the obtained information could form the basis for follow-up experiments in which improved control of variables and more refined or sensitive measurement techniques would be utilized.

In selecting the two sites for housing goats at TAFB, noise contour maps (Figure 1) were utilized. They revealed that 24-hr time-averaged noise levels range from 65-85 dB depending upon several factors including the direction of take-off or landing, the type of aircraft, aircraft engine power levels, proximity of sampling site to the runway, and the altitude of the aircraft. Peak noise values were higher and measurements from individual aircraft overflights reveal intensities of up to 125 dB(A) for about 10-20 sec at the Northwest end of the runway (site "A" in Figure 2) and about 65 dB near the TAFB Natural Resources (site "B" in Figure 2).

The research plan provided for locating the goats at the two TAFB sites for about 5 wk of the total Summer Faculty Research Program. Because of prior conflicts in the Summer Fellow's schedule, his 10 wk period at TAFB overlapped that of the Graduate Student Researcher (Figure 3). As a consequence, the project lasted about 13 wk. In the early part of the project period, much effort was directed to acquiring budget approval, developing purchase orders and letters of justification, solving logistical problems, purchasing supplies, constructing goat pens and shelters, arranging for sample analyses. Later on, additional time was expended analyzing data, formatting results, writing reports, and obtaining additional samples after the animals were returned to their owner (Refer also to Section IV, Objective B, below and Zern, 1989).

The goat was chosen as the animal model because it is:

A.   An ubiquitous domestic animal.

B.   Easily managed and maintained.

C   Readily available.

D.   Comparatively inexpensive.

E.   A ruminant.

F.   Ideally suited as a wildlife analog.

The goats were obtained from a local (i.e., Parker, Florida) source so transport to the TAFB sites would not involve long distances. Those animals were relatively tame (i.e., accustomed to social contact with humans) and transport and handling were not thought to constitute serious stressors. But, blood and other parameters were evaluated in some animals to determine the effect of transport. Attempts also were made to provide feed and hay of the same brand and quantity as provided by the goat owner (Harris, 1987). Feed and water were available ad libitum.

Measurements were selected to optimize the detection of physiological changes resulting from exposure to noise. Customary husbandry practices were followed (Zern, 1989) and no invasive procedures other than venipuncture were utilized. All measurements were the same for both experimental and control groups.

Measurements included:

A.   GENERAL SIGNS: Heart rate, respiratory frequency, body weight.

B.   BEHAVIORIAL MANIFESTATIONS: Avoidance, startle.

C.   HEMATOLOGY: Differential white cell counts, packed cell volumes.

D.   CLINICAL CHEMISTRY: Plasma proteins, cholesterol, triglycerides.

E.   PLASMA HORMONES: Adrenal cortex (e.g., cortisol) and thyroid (t_3 and t_4) hormones.

Baseline data were collected on 20 goats for 14 da preceding their being transported to the two TAFB locations (6 animals at each site and 8 returned to "home" base) after pen and shelter construction (McGowan, 1986) was completed. Respiratory frequency, heart rate, body weights, and the general appearance of each animal were recorded on each day blood samples were collected. To mitigate the potential effects of animal manipulations, attempts were made to expose the goats to regular and periodic petting and handling. In addition to a shelter, stall, and a feeder, the amount of exercise and social space per animal were similar to what was in their usual surroundings so that the effect of a confinement stressor was minimized. The standard clinical chemistry profile (Chemical Analyzer, IL Model 761) was performed on all serum samples. Because of their morphology, red and white blood cells could not be machine counted and manual techniques were not available. White blood cell differential counts and packed cell volumes were manually completed.

III.   OBJECTIVE A: GENERAL SIGNS

Heart rate and respiratory frequency data are summarized in Table 1. Although there was no significant difference in baseline heart rates between the two groups of TAFB goats, the Group 1 animals (i.e., located at the Runway site) displayed a decreasing heart rate over time which is consistent with their behavior (i.e., they adjusted quickly to their new environment, displayed a friendly, social response to the investigators, and were easily managed). Group 2 goats, on the other hand, never seemed to adjust (during the entire 5 wk period) to their new environment and displayed apprehensiveness, proved difficult to manage, and exhibited uneasiness at the sight of people (i.e., response was more pronounced when several individuals were present

compared to only one person being present). Respiratory frequency (Table 1) doubled on the first day after being transported to the Tyndall sites for Group 1 and Group 2 goats but stayed relatively constant for those in Harders' yard ("Home" base). The body weight regression coefficient for Group 1 goats (a = 0.067) was not appreciably different from that of Group 2 goats (a = 0.053).

Table 1. Heart rates and respiratory frequencies (Mean $\pm$ S.E.) for goats.

Location	Measurement	Baseline	Noise Exposure Period		
			+ 1da	+7da	+32 da
Runway (Group No. 1):					
	Heart Rate (bpm)	136.2 $\pm$ 8.6	141.7 $\pm$ 11.9	115.0 $\pm$ 8.8*	116.7 $\pm$ 6.7*
	Resp. Freq. (bpm)	39.5 $\pm$ 1.8	75.8 $\pm$ 13.5**	39.2 $\pm$ 1.5	31.7 $\pm$ 1.8*
Natural Resources (Group No. 2):					
	Heart Rate (bpm)	140.3 $\pm$ 5.6	131.7 $\pm$ 10.1	153.3 $\pm$ 18.0	138.3 $\pm$ 17.0
	Resp. Freq. (bpm)	41.8 $\pm$ 2.3	74.2 $\pm$ 17.5**	36.7 $\pm$ 3.3	31.7 $\pm$ 2.1**
Harders' Yard:					
	Heart Rate (bpm)	142.2 $\pm$ 7.6	121.4 $\pm$ 6.7*	112.8 $\pm$ 3.6*	111.4 $\pm$ 5.1*
	Resp. Freq. (bpm)	37.6 $\pm$ 1.6	45.7 $\pm$ 4.1**	36.4 $\pm$ 2.4	35.7 $\pm$ 3.7

* $P < 0.02$ ** $P < 0.05$

IV.   OBJECTIVE B: BEHAVIORAL MANIFESTATIONS

Behavioral and physiological adjustments to environmental stressors can provide information on the well-being of animals (Dantzer and Mormede, 1983). Utilizing human-reared (HR) and dam-reared (DR) goats exposed to 5-min encounters with other goats or a stationary person, Lyons and Price (1987) observed no consistent relationship between heart rates and changes in behavior. Further, they report that the significant difference between HR and DR goats in vocal rates during encounters with other goats was not accompanied by group differences in heart rates.

Although the general locations of the TAFB sites (i.e., one "near" a runway with the associated high noise intensities and one remote from the runway) were specified by the research protocol (Figure 2), the specific locations were beyond the control of the Summer Fellow. As a result, the

ambiance of the sites, except for the noise intensities, was similar but not equivalent (Zern, 1989).

The differences in observed behavior between the two groups of goats are thought to be related at least partly to the site differences (Figure 2). That is, the Group 1 (Runway) site was open, grassy, and in full view of the roadway, vehicular traffic, noise and people--not unlike the goats' previous "home." Conversely, the Group 2 (Natural Resources) site was isolated in a woodsy area, quiet, and contained no easily recognized "markers." The pen and shelter were situated in a cleared area of the woods but contained low brush and plants but no grass.

Other potential explanations of the differences in goat behavior--particularly those in Group 2--were investigated with no conclusive result: 1) The goats in this group may have responded to the actions of the "dominant" personality who may have been the only animal in the group who was unable to adjust to the new environment (Plausible, but since the animals were grouped randomly why did not Group 1 also contain a "troublemaker"?); 2) The nearby radar installation may have transmitted at frequencies that adversely affected the goats (Unlikely because of the transmission frequency and angle of horizontal scan); 3) A nearby height finder may have provided an averse stimulus (The height finder presents a hazard, but the proximity to the goat pens precludes any effect); 4) It was alleged that guard dogs were housed/trained nearby and their odors (dependent upon the prevailing wind direction) may have caused the goats to be apprehensive (An investigation revealed that the guard dogs actually were housed/trained on the opposite side of TAFB); 5) The combat arms training site and skeet range are both within about 100-150 yd from the goat pen (The sound of periodic, but regular, gunfire may have contributed to the apprehensiveness of the goats); 6) The Group 2 site may have been inadvertently located near a track or trail of some wildlife predator species (e.g., coyote) endemic to the Panama City, Florida, area.

Regarding jet aircraft noise, only Group 1 goats displayed behavioral changes. For a few days following their placement at the Runway Site, some animals displayed moderate reactions (e.g., startle while standing, interruption of walking) following takeoff of the F15 aircraft. Within a few

days (i.e., a week or less), the animals appeared to be oblivious to all aircraft noise. That is, until the "Copper Flag" went up on 6 August. Coincident with that event, the Northeast runway (on direct line over the Group 1 pen area) was opened, and on 7 August aircraft activity was increased, takeoffs were directly over the pen, and planes flew at all times of the day and night. Resultant peak noise intensities of up to 120 dB(A) for about 10-20 sec were recorded (compared to previous peak intensities of about 95 dB(A) for up to 13 sec). The latter were obtained from planes operating from the Southwest runway only (Figure 3) for 4 wk of the 5 wk experimental period as the Northeast was closed (an event unbeknown to the Summer Fellow at the time the pens were constructed). An extra blood sample was collected--2 da after the Copper Flag was hoisted--in order to detect changes, if any, in the hematology or serum chemistry (See also Section V, Objective C, below).

V.   OBJECTIVE C: HEMATOLOGY

According to Selye (1936), a stressor response results from exposure to any condition or situation for which the animal is unaccustomed or non-adapted. The characteristic response involves cardiovascular and metabolic changes or the "fight or flight" reactions described by Cannon (1929). Mechanisms which enable an animal to respond to adverse environmental situations (i.e., stressors) are dependent upon interactions between endocrine and nervous systems (Stephens, 1980). Stressor stimuli initially involve the hypothalamus where the autonomic nervous system is stimulated to cause 1) release of norepinephrine at sympathetic nerve endings, and 2) release of epinephrine and norepinephrine from the adrenal medulla.

As the result of being exposed to a stressor, the adenohypophyseal-adrenocortical response causes eosinopenia (Swenson, 1984) as well as relative neutrophilia and lymphopenia (Besch et al, 1967). As is evident from the data contained in Table 2, the Group 1 goats displayed a nonsignificant eosinopenia and a highly significant lymphopenia ($p < 0.02$) and neutrophilia ($p < 0.005$) within one day after being placed in the pens located at the Northwest end of the runway (site "A" in Figure 2). Similar neutrophilia and lymphopenia--but no eosinopenia--were observed in Group 2 goats near Natural Resources (site "B" in Figure 2).

Within 7 da the values for all three types of cells were within baseline values except for Group 2 neutrophils. This continued until day +32 when the "Copper Flag" went up and the Northeast runway was reopened. As a consequence, nonsignificant changes in lymphocytes and neutrophils were detected in Group 1 goats (Table 2). These are thought to be the result of the increased flight activity directly over the Group 1 goat pens where noise intensities of up to 100-120 dB(A) for about 20 sec duration were measured (See also Section IV, Objective B, above).

Table 2. Changes in relative white blood cell percentages (Mean ± SE) in two groups of goats.

Location	Cell Type (%)	Baseline Data	+ 1 da	+3 da	+7 da	+32 da
				Noise Exposure Period		
Lymphocytes						
Runway (Group No. 1)		63.0 ± 3.2	48.3 ± 4.63	51.8 ± 6.84	56.0 ± 6.5	65.2 ± 1.8
Natural Resources (Grp Np. 2)		59.6 ± 2.9	52.2 ± 2.72	53.5 ± 5.75	57.2 ± 3.3	58.7 ± 1.8
Neutrophils						
Runway		25.8 ± 1.7	45.0 ± 4.81	38.3 ± 5.12	32.0 ± 3.0	29.0 ± 1.5
Natural Resources		29.4 ± 1.4	37.8 ± 1.83	36.7 ± 3.14	36.0 ± 3.34	30.3 ± 1.9
Eosinophils						
Runway		4.1 ± 0.7	3.6 ± 0.7	2.4 ± 1.1	2.6 ± 1.2	2.5 ± 0.6
Natural Resources		4.5 ± 1.0	4.6 ± 1.3	3.6 ± 1.4	4.8 ± 1.3	8.3 ± 2.1

[1] $P < 0.005$ [2] $P < 0.01$ [3] $P < 0.02$ [4] $P < 0.05$ [5] $P > 0.05$

VI.   OBJECTIVE D: CLINICAL CHEMISTRY

In all, 23 different chemical substances were measured in each of about 300 blood serum samples. These included glucose, blood urea nitrogen (BUN), alkaline phosphatase, cholesterol, sodium, potassium, total proteins, and albumin:globulin ratios. In the short period of time since the collection of the last blood sample, it has not been possible to analyze all of the data. However, based on preliminary calculations, some comments are possible.

For example, cholesterol and triglycerides were significantly reduced in Group 1 goats (Table 3) which may indicate that their nutritional state or thyroid activity was different compared to Group 2 animals. Differences in

triglyceride and cholesterol levels between the two groups may be due to different flora at the two sites. Serum sodium was significantly elevated in both groups immediately after arriving at TAFB but stayed elevated in Group 2 (but not Group 1) animals which may have resulted from either water deficit or increased adrenal cortical activity. The latter may be confirmed when the RIA data are available (Refer to Section VII, Objective E, below). Also, alkaline phosphatase levels tended to remain at relatively constant levels in Group 1 but decreased in Group 2 animals for the 5 wk experimental period.

Table 3. Selected blood serum clinical chemistry data (Mean $\pm$ S.E.) from goats.

			Noise Exposure Period		
Location	Measurement	Baseline	+ 1da	+ 7da	+ 32da
Runway (Group No. 1):					
	Sodium (mEq/L)	146.3 $\pm$ 0.8	151.3 $\pm$ 0.6*	146.8 $\pm$ 0.5	147.7 $\pm$ 0.4
	Potassium (mEq/L)	4.6 $\pm$ 0.1	4.4 $\pm$ 0.2	3.9 $\pm$ 0.1**	3.8 $\pm$ 0.1**
	Triglycer. (mg/dL)	28.2 $\pm$ 3.8	21.5 $\pm$ 1.8***	20.7 $\pm$ 1.1***	20.8 $\pm$ 2.6***
	Cholesterol (mg/dL)	106.3 $\pm$ 3.5	106.0 $\pm$ 6.6	94.8 $\pm$ 9.6	75.7 $\pm$ 7.1**
	Alk. Phosphat. (U/L)	352.5 $\pm$ 26.6	352.0 $\pm$ 15.1	282.0 $\pm$ 26.0	337.0 $\pm$ 38.0
Natural Resources (Group No. 2):					
	Sodium (mEq.L)	146.0 $\pm$ 0.5	151.0 $\pm$ 0.9*	149.0 $\pm$ 0.9*	149.0 $\pm$ 0.5***
	Potassium (mEq/L)	4.4 $\pm$ 0.1	4.4 $\pm$ 0.1	3.9 $\pm$ 0.1*	3.8 $\pm$ 0.1**
	Triglycer. (mg/dL)	24.8 $\pm$ 3.0	28.2 $\pm$ 2.8	31.7 $\pm$ 2.5	24.2 $\pm$ 1.5
	Cholesterol (mg/dL)	103.7 $\pm$ 9.1	109.7 $\pm$ 11.6	105.7 $\pm$ 24.3	93.5 $\pm$ 5.2
	Alk. Phosphat. (U/L)	302.5 $\pm$ 26.1	320.7 $\pm$ 21.3	253.2 $\pm$ 21.3	212.0 $\pm$ 18.6**

* P < 0.005   ** P < 0.02   *** P < 0.05

VII.   OBJECTIVE E: HORMONAL RESPONSES

Should exposure to stressors persist, an animal attempts to adapt physiologically by secreting corticotrophin-releasing hormone (CRH) from the hypothalamus. CRH stimulates the anterior hypophysis to secrete adrenocorticotrophic hormone (ACTH) which, in turn, stimulates the adrenal cortex to secrete corticosteroids into the blood stream. Fluctuations in responses of the adrenal medulla and cortex, hypophysis, and hypothalamus have been used to describe the interactions between animals and adverse environments (Stephens, 1980).

Noise intensities similar to those of jet aircraft have been shown to alter milk production in cows (Kovalcik and Scottnik, 1971) and goats (Sugawara et al, 1979). Further, because of the relative lymphopenia, neutrophilia, and eosinopenia displayed by Group 1 goats (Refer to Section V, Objective C, above) exposed to jet aircraft noise, it is reasonable to assume that plasma levels of cortisol, t3, and t4 hormones also would be elevated (Falconer and Hetzel, 1964). Accordingly, plasma samples were collected and frozen for subsequent radioimmunoassay (RIA) for adrenal cortex (e.g., cortisol and corticosterone) and thyroid gland (t3 and t4) hormones. Unfortunately, the capability to perform the RIAs was not available at TAFB and a contract had to be negotiated with the University of Florida for these analyses the results of which are not expected to be available until late September or early October, 1989.[1]

VIII. RECOMMENDATIONS:

A.   PLAN FOLLOWUP EXPERIMENTS: In particular, more information is needed from other domestic species (e.g., bovine, equine) in which the causal relationship between the noise stressor and the animal are quantified.   Also, some attempt should be made to develop additional information on the effect of isolation or social deprivation on the behavior and physiology of goats.

B.   DEVELOP RESEARCH ALTERNATIVES: Rather than replicate the type of experiment described herein (i.e., bringing the animals to the source of the stressor), future studies should systematically expose animals to directed overflights (i.e., bring the aircraft to the animals).   In that scenario, it is envisioned that the animals would be housed in standard animal facilities so that physical variables could be properly controlled and other factors including feed intake, water intake, and feed utilization could be measured.

C.   PROVIDE DATA ANALYSES ASSISTANCE: Although personal computers and printers were available at AFESC to analyze data or prepare reports, no biostatistics capability was available to the Summer Fellow.   As a consequence,

---

[1]   Radioimmunoassay data for blood plasma levels of adrenal cortex and thyroid gland hormones will be forwarded to Universal Energy Systems at a later date as an addendum to this report.

the final report contains only those calculations that could be accomplished with available PC software. Also, inability to complete the radioimmunoassays locally together with the inordinate amount of time to process purchase orders caused delays in obtaining and analyzing data.

D. **EVOLVE ANIMAL RESEARCH CAPABILITY:** If animal experimentation on site is an objective of the host laboratory, the capability to support and conduct such research should be available to the Summer Fellow.. It is very difficult to prepare a research protocol, develop and obtain approval of the research budget, solve all logistic problems, obtain approval on all purchase orders, design and construct animal pens and shelters, improvise laboratory support, and still have time left--from the 10 wk tenure--to fulfill the research objectives, analyze the data, and prepare a final report!

E. **CONTINUE THE PROGRAM:** Notwithstanding all of those difficulties, the Summer Faculty and Graduate Student Research Programs are excellent mechanisms to deal with issues that can be managed in a 10 wk period. The experiences are interesting, rewarding, and enriching. The opportunity to participate in problem solving activities, share in the cross-fertilization of ideas, partake in potential networking, and contribute to information generation all are worthwhile consequences of the program.

IX. **REFERENCES:**

1. Anonymous. "Acoustic Noise," In: McGraw-Hill Encyclopedia of Science and Technology. Vol. I, 6th Ed. New York, McGraw-Hill Book Company, 1987, pp 70-78.

2. Bell, W. B., "Animal responses to sonic booms," J Acoust Soc Amer, 1972, Vol. 51, 758-765, 1972.

3. Besch, E. L., A. H. Smith, R. R. Burton, and S. J. Sluka, "Physiological limitations of animal restraint," Aerospace Med, 1967, Vol. 38(11), pp. 1139-1134.

4. Bond, J., "Noise--Its effect on the physiology and behavior of animals," Agric Sci Rev, 1971, Vol. 9(4), pp. 1-10.

5.   Bond, J., C. F. Winchester, L. E. Campbell and J. C. Webb, USDA Tech Bull No. 1280. Washington, DC, U. S. Department of Agriculture, 1963, 17p.

6.   Borg, E., "Physiological aspects of the effects of sound on man and animals," Acta Otolaryngol Suppl, 1979, Vol. 360, pp. 80-85.

7.   Cannon, W. B., Bodily Change in Pain, Hunger, Fear and Rage: An Account of Recent Research into the Function of Emotional Excitement, 2nd Ed., New York, Appleton, 1929.

8.   Casady, R. B., R. P. Lehmann, "Response of farm animals to sonic booms," Studies at Edwards Air Force Base, California, 6-30 June 1966. Interim Report, Beltsville, MD:, US Department of Agriculture, 1967, 8 p.

9.   Cottereau, P., "Effect of sonic boom from aircraft on wildlife and animal husbandry," In: Effects of Noise on Wildlife. J. L. Fletcher and R. G. Busnel, eds., New York, Academic Press, 1978, pp 63-79.

10.   Dantzer, R., P. Mormede, "Stress in farm animals: a need for reevaluation," J Anim Sci. 1983, Vol. 57, pp. 6-18.

11.   Espmark, Y, L. Falt, and B. Falt, "Behavioral responses in cattle and sheep exposed to sonic booms and low-altitude subsonic flights," Vet Rec, 1974, Vol. 94(6), pp. 106-113.

12.   Ewbank, R., "The effects of sonic booms on farm animals," Vet Annual, 1977, Vol. 17, pp. 296-306.

13.   Falconer, I. R., B. S. Hetzel. "Effect of emotional stress and TSH on thyroid vein hormone level in sheep with exteriorized thyroids," Endocrinol, 1964, Vol. 75(1), pp. 42-48.

14.   Harris, B., Jr. "Feeding and Management of Dairy Goats." Circular 761. Gainesville, FL, Florida Cooperative Extension Service, Institute of Food and Agricultural Sciences, University of Florida, 1987, 10 p.

15.   Kovalcik, K., J. Scottnik., "The effect of noise on milk efficiency of cows," Zivocisna vyroba (Praha), 1971, Vol. 16(10-11):, pp. 795-804.

16.   Lyons, D, M,, E. O. Price, "Relationship between heart rates and behavior of goats in encounters with people," Appl Anim Behav Sci, 1987, Vol. 18, pp. 363-369.

17.   McGowan, C. A., "Raising a small flock of goats for meat and milk: Management practices, housing, and facilities," Circular 644.   Florida Cooperative Extension Service, Institute of Food and Agricultural Sciences, University of Florida, Gainesville, FL 32610, 1986, 12 p.

18.   Selye, H., "A syndrome produced by diverse nocuous agents," Nature, 1936, Vol. 138, p. 32.

19.   Shotton, L. R., "Response of wildlife and farm animals to low-level military jet overflight," Reporter, 1982, Vol. II(6), pp. 161-164.

20.   Stephens, D. B., "Stress and its measurement in domestic animals: a review of behavioral and physiological studies under field and laboratory situations," Advances in Vet Sci Comp Med, 1980, Vol. 24, pp. 179-210.

21.   Sugawara, H., F. Aoyagi, and K. Abe, "Studies on the electroencephalogram in ruminants.   X.   Effects of the noise on the electroencephalogram and lactation in goats," J. Fac Agricul, Iwate Univ (Japan), 1979, Vol. 14(4), pp. 319-339.

22.   Swenson, M. J., "Blood Circulation and the Cardiovascular System," In: Dukes' Physiology of Domestic Animals, 10th Ed., Ithaca, NY, Cornell Univ Press, 1984, pp. 15-40.

23.   Zern, J. D. Final Report on 1989 Graduate Student Research Program to Universal Energy Systems, Inc., Dayton, OH, 14 AUG 89.
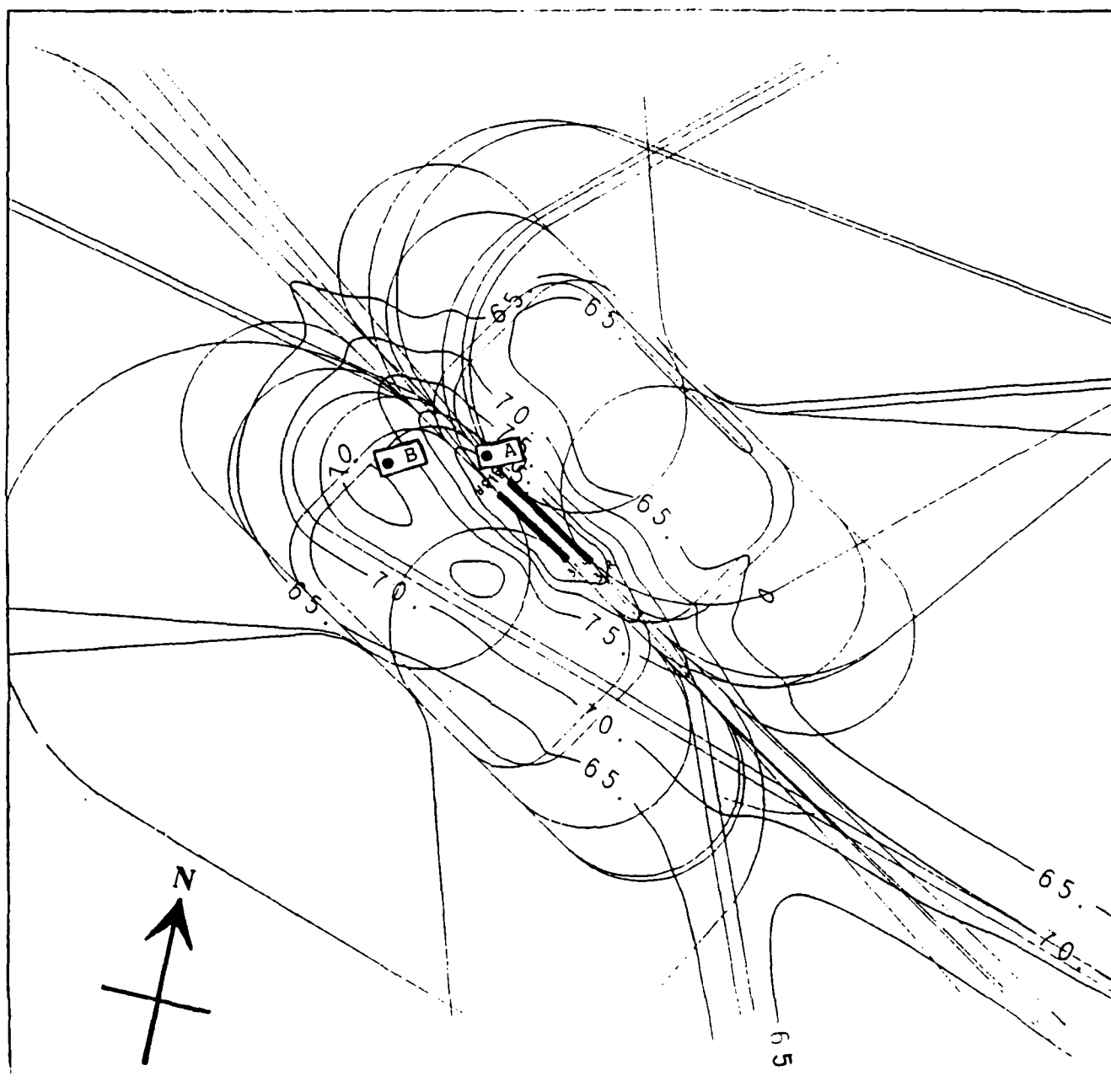
Figure 1. Noise countour map of area surrounding Tyndall AFB runways. Group 1 animals were at site "A" and Group 2 animals at site "B".

Figure 2. Grid map showing the location of the two goat pen areas and
aircraft runways at Tyndall AFB. Location A is the Runway
(Group 1 animals) site and B is the Natural Resources (Group 2
animals) site.

1989 SUMMER FACULTY RESEARCH PROGRAM
USAF ENGINEERING AND SERVICES CENTER
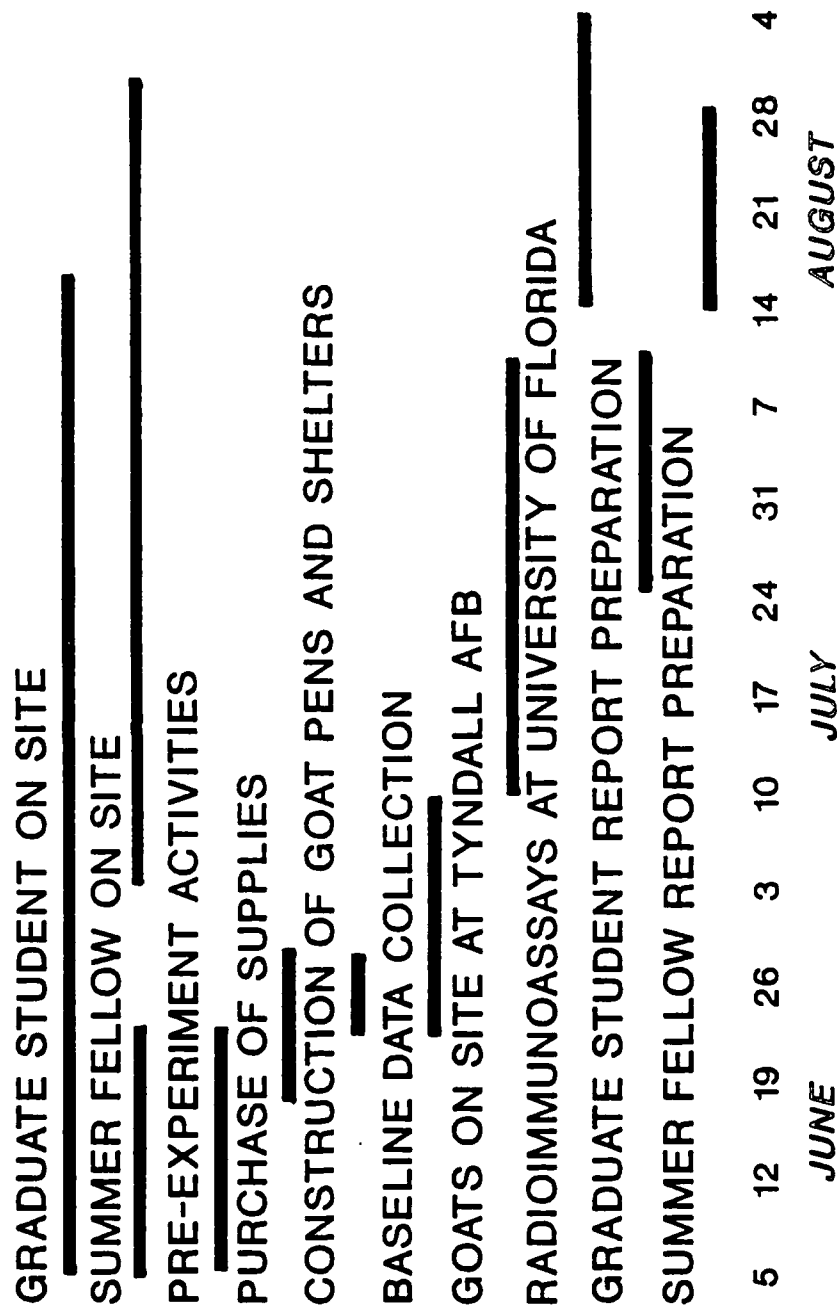### TYNDALL AFB FL 32403-6001

PLAN OF ACTION AND TIMELINES

GRADUATE STUDENT ON SITE

SUMMER FELLOW ON SITE

PRE-EXPERIMENT ACTIVITIES

PURCHASE OF SUPPLIES

CONSTRUCTION OF GOAT PENS AND SHELTERS

BASELINE DATA COLLECTION

GOATS ON SITE AT TYNDALL AFB

RADIOIMMUNOASSAYS AT UNIVERSITY OF FLORIDA

GRADUATE STUDENT REPORT PREPARATION

SUMMER FELLOW REPORT PREPARATION

5	12	19	26	3	10	17	24	31	7	14	21	28	4
JUNE				*JULY*						*AUGUST*			

Figure 3. Plan of action and timelines for activities related to the Tyndall AFB goat project.

1989 USAF-UES Summer Faculty Research Program

Sponsored by the

AIR FORCE OFFICE OF SCIENTIFIC RESEARCH

Conducted by the

Universal Energy Systems, Inc.

An Algorithmic System for Subjective Comparisons

Prepared by: Anthony Jack Carlisle

Academic Rank: Assistant Professor

Department and   Department of Mathematics and
    University   Computer Science
                            Huntingdon College, Montgomery, AL

Research Location: Engineering and Services Center
                            Tyndall AFB, FL 32403-6001

USAF Researcher: Mr. Perry Sullivan, Effort Focal Point

Date: May 12, 1989

Contract No: F49620-88-C-0053

<u>An Algorithmic System for Subjective Comparisons</u>

by

Anthony Jack Carlisle

<u>ABSTRACT</u>

Specific segments of human-machine natural language interfacing are investigated. Indefinite and ill-defines natural languages phrases concerning quantitative and qualitative measures are parsed and the constituents interpreted as fuzzy language distributions. The components are then mathematically recombined to produce a small range of possible intended values. Similarly, the inverse is also addressed, i.e., matching fuzzy distributions to natural language descriptions. Various techniques are investigated for attempting to fit distributions into the most appropriate phrasings. A methodology for constructing and maintaining a dictionary of such phrases is discussed and demonstrated.

ACKNOWLEDGMENTS

I wish to express my appreciation to the Air Force Systems Command and the Air Force Office of Scientific Research for their sponsorship of this program, and to Universal Energy Systems for their management of this endeavor.

I would also like to thank Perry Sullivan for his guidance and encouragement, Capt. Charles Manzione and his staff for the friendly and most cooperative working environment, and especially Ed   Alexander for his advice, encouragement, and hospitality, and for making space in his crowded office for still another desk.

I. INTRODUCTION:

Computers are discrete, unambiguous mechanisms. Unfortunately, human communication is normally imprecise, ambiguous, and highly context oriented. As work in robotics and teachable machines progresses, an need will grow for a methodology to interface the human with the machine. The most general, and natural, of these possible interfaces is language. The question, then, is whether to force humans to use precise, unambiguous language, or to construct machines to interpret natural language.

In the Armed Services, the tenure of normal enlisted personnel is relatively brief, and thus speed of training in any field is important. Any increase in the flexibility of the machine will result in a decrease in the training time of the operator. As a consequence, language-intelligent systems will be of real value to the Services.

My research has been in automated natural language translation, specifically in translating between the virtually unambiguous and highly regular Esperanto and the highly ambiguous and irregular English. Within this field, I have concentrated on context-defined indefinite or ill-defined phrases, and more lately on the interpretation of such phrases as fuzzy expressions. My interest in applying neural networks to the computation of such expressions led to my request for assignment at the Air Force Engineering and Services Center.

II. OBJECTIVES OF THE RESEARCH EFFORT:

The long range objective of this research is to development a system for mechanically interpreting verbal commands in natural phrasings for directing semi-intelligent automated equipment. As a intermediate goal and focus for the investigation of qualitative and quantitative natural language expressions, a system for using natural language phrases to compare competing items was formulated and submitted. This model consists of several phases, the first of which is the development and implementation of a phrase dictionary maintenance program. The initial objective of this limited research period was the completion of this first phase.

Initially, the model was to be constructed using the neural network software available at the AFESC Field Operations site. However, the availability of and familiarity with other Artificial Intelligence software resulted in a shift to more deterministic tools. The work thus far has been done in Prolog and "C" on an Apple Macintosh II, and any further research will likely stay with the same platform.

III. OVERVIEW OF THE FUZZY PHRASE DICTIONARY PROJECT:

The purpose of the dictionary is to provide a standard interpretation for key phrases and modifiers for the subsequent phases of the project. Since the ultimate purpose of a qualitative or quantitative phrase is to voice some sort of measure, the dictionary essentially maps natural language phrases to values. However, since natural language is imprecise and ambiguous, the values incorporated into the dictionary can be either discrete numbers, number ranges, "fuzzy" distributions, or mathematical expressions to modify such values. For example, the dictionary entry dozen maps precisely to the value 12, whereas dozens is an imprecise value, and is represented by the fuzzy distribution in figure 1.

16 18 20 22 24 26 28 30 32 34 36 38 40 42 44 46 48
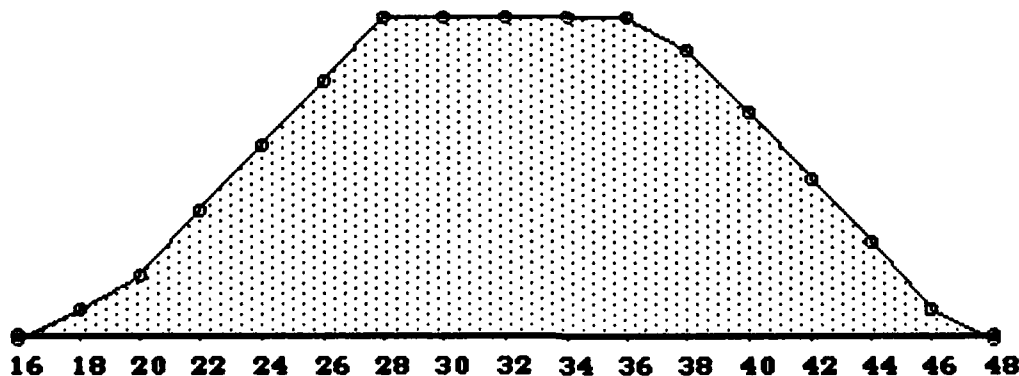
Figure 1. "dozens"

The dictionary software must examine a natural language phrase and identify each defined component, and, for items not yet defined, allow for their entry and definition in any of the acceptable formats (discrete, range, numeric distribution, or mathematical expression).

IV. BRIEF TUTORIAL ON FUZZY DISTRIBUTIONS:

In order to understand the expression analysis methodology, it is first necessary to have at least a cursory grasp of fuzzy numbers and fuzzy expressions. This report segment is an overview of the pertinent terms and concepts.

The key concept in fuzzy mathematics is the idea of degree of membership in a set. If we assign complete membership in a term a value of one, then we can say that number that is perfectly defined in a term plots as 1, and any number perfectly absent in the definition of the term plots as zero. For example, a plot for dozen, a precise value of 12, would be as show in figure 2. Note that "12" has complete membership in dozen and all other values have absolutely no membership in the term.
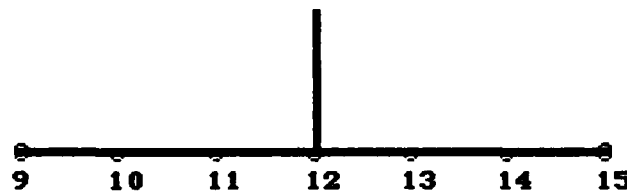
Figure 2. "dozen"

Now let us consider a less precisely defined term. A classic example of a fuzzy modifier is few. Most people define few as "three or more", thus declaring three to have complete membership in few. A question arises, however, when dealing with other values: is two sometimes a few? How about four, or five, or six? What about ten, twenty, or one hundred? Obviously, when we say " a few dollars", some of these values are more likely than others. It is the "possibility" that a value is intended by the term that defines it membership, usually rated on the scale of zero to one. Note that "possibility" does not equate to "probability", a word which implies the ability to accurately measure a value. Fuzzy membership is as ill-defined as the term being defined.

Once we have defined the distribution for few, then what is the distribution for very few? The word very is a modifier, attenuating the distribution of few to accent the higher membership values and reduce the lesser membership values. Figure 3 gives a graphic interpretation of few and very few.
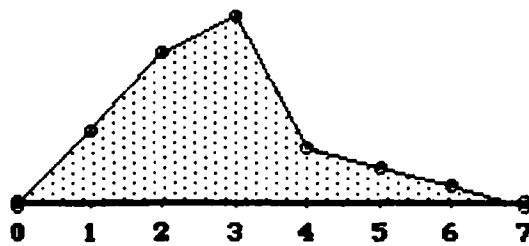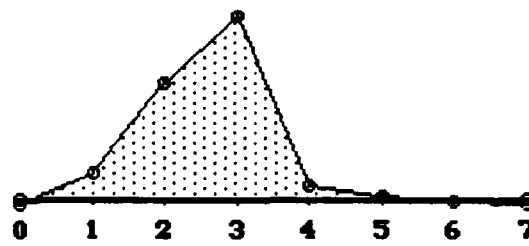
Figure 3.a "few"   Figure 3.b "very few"

Modifiers can act in several ways. For example, some modifiers are simple multiplications of the primary term, some modifiers are simple expressions, and some modifiers are complex expressions.

Simple multipliers, such as four dozen or twice as far, are relatively easy to implement - the fuzzy distribution equated to the term is multiplied by the constant equated to the modifier. This results in a simple shift in the baseline, but no change in the shape of the distribution.

Simple expressions fall into six basic forms[3]: complementation, normalization, concentration, dilation, and fuzzification. Complementation (not) is a straightforward inverse of the primary distribution. For example, the figure below (Figure 4) demonstrates low and not(low).
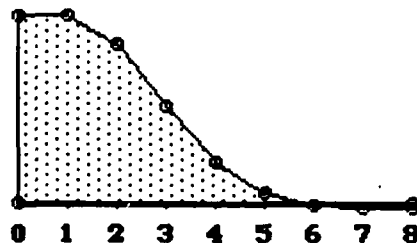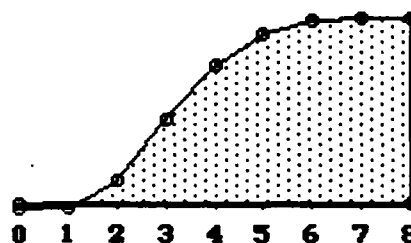
Figure 4.a "low"   Figure 4.b "not(low)"

Normalization is likewise a straightforward process, simply proportionally extending each value along the distribution until the largest of the values equals 1. This operation is typically used on the results of other operations to guarantee uniformity in distributions.

Concentration and dilation "intensify" and "fuzzify", respectively. The previous example, very few, was a concentration of few. Similarly, dilation increases the imprecision of a distribution, as in about a dozen. Graphic examples of both follow in Figure 5.
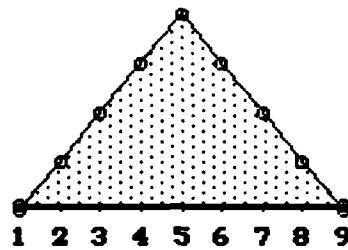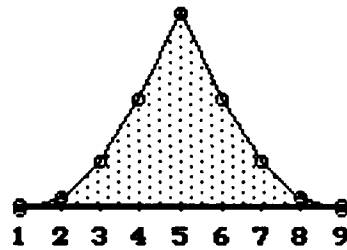
Figure 5.a X
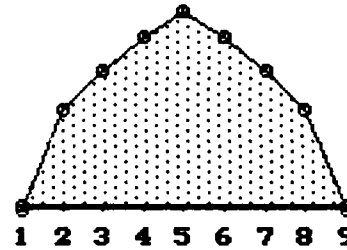

Figure 5.b CON(X)   Figure 5.c DIL(X)

Intensification is increases the contrast between values with membership of more than half in the distribution and those with less than half membership. It is very much like a combination of concentration and dilation. Fuzzification is generally used to convert a discrete value to a fuzzy distribution ("blur"). Both functions are demonstrated below.
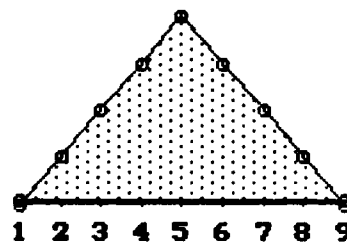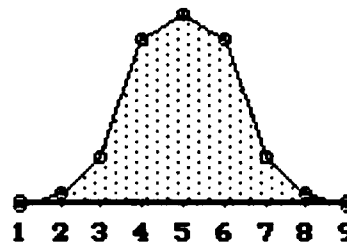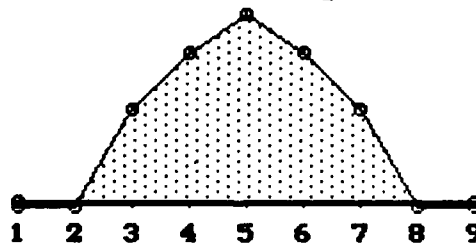

Figure 6.a X   Figure 6.b INT(X)

Figure 7 FUZ(5)
Fuzzification of "5"

Complex fuzzy expressions are formed of the above functions with along with fuzzy union and intersection. For example, the expression "slightly tall" can be computed by the fuzzy complex expression NORM("tall" AND NOT("very"("tall"))). Figure 7 show the result of these operations.
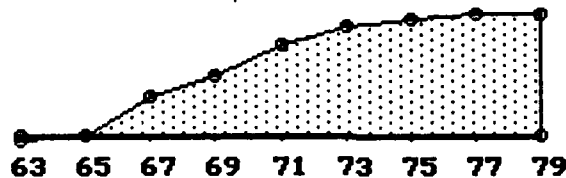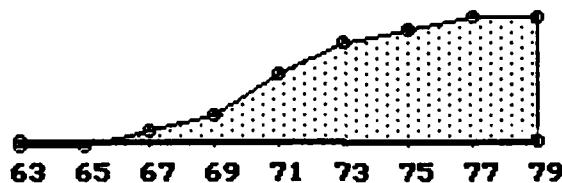
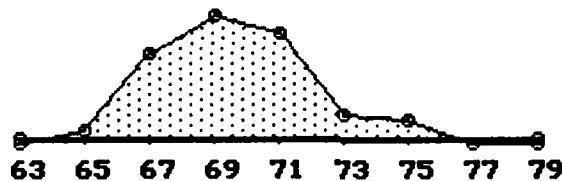Figure 8.a "tall" (in inches)

Figure 8.b "very tall"

Figure 8.c "slightly tall"

Fuzzy distributions are stored as lists of pairs, membership value and set point. Such a list for the distribution above would appear as:

slightly tall -> 0/63, .05/65, .75/67, 1/69, .9/71, .5/73, .4/75, 0/77, 0/79

V. THE NATURAL LANGUAGE PARSER:

The first step in evaluating any expression in natural language is to identify the constituents as to their functional part of speech. The parser implemented for this project is (partially) shown below in production rule format. Those sections labeled Dictionary are where the dictionary program supplies the appropriate definition.

sentence-> compound phrase | simple phrase

compound phrase-> conjunctive phrase | range phrase

simple phrase->relational phrase | hedged primary

conjunctive phrase->relational phrase AND relational phrase

range phrase->hedged primary TO hedged primary

relational phrase->composite relation THAN hedged primary

composite relation->relation hedge relation relation

relation hedge->Dictionary (such as slightly or much)

relation->Dictionary (such as lower)

hedged primary->hedge primary primary | fuzzy number

hedge->Dictionary (such as more or less or very)

primary->Dictionary (such as low or high)

fuzzy number->fuzzifier number

fuzzifier->Dictionary

(parser modifier from Schmucker[3])

The program accepts the input natural language expression, then attempts to parse the expression using the grammar above. If the parse is successful, the parser returns an expression made up of the appropriate fuzzy functions and terms. If the parse is unsuccessful, the offending words are isolated and the user executing the program must either supply definitions or alternate phrasing.

As an example of the parser's function, consider the expression "rather important". Since important and rather are both represented in the dictionary, the parser returns NORM("important" AND NOT(VERY("important"))). Note that a pointer to the dictionary's fuzzy distribution for important is actually returned in the places marked "important" above.

VI. THE FUZZY EXPRESSION PARSER:

The second step in analyzing the natural language expression is to compute the results of the

38-10

fuzzy function based expression. The parser used here is a two-part stack oriented process that converts the expression to postfix notation, then computes the result. Both parts make use of the same stack space to conserve space.

The example used above would be rearranged by the first step to "important" VERY NOT "important" AND NORM, then popped from the stack and computed. Such parsers are quite common and will not be further documented here.

VII. THE USER INTERFACE:

The user interface is a significant part of the dictionary maintenance program. This version works exclusively on the Apple Macintosh® platform, although a Microsoft Windows® version is quite conceivable.

The primary communication between the user and the program occurs in a highly structured programming device call a dialog box, as shown in Figure 9, with an example definition. The user supplies the expression, and, if the expression parses from the existing dictionary components, the dialog box displays both the computational expression and the distribution (graphically and numerically). The user may alter the expression in the input box, the definition box, or either of the distribution boxes (alterations to the graph are done with the standard mouse), and may specify that the expression be added to the dictionary, removed from the dictionary, or the changes ignored.

If the entered expression is not able to be parsed, the program displays the undefined portions and asks the user to supply definitions. The user may enter a definition as a fuzzy expression or a numeric list, (the fields other than the entered one are updated as the data is entered) and the user may alter the definition using any of the fields. Finally, the user can either add the definition to the dictionary or discard the work. (The remove button is dimmed and disabled during data entry and is only valid when searching and/or altering the dictionary entries.)
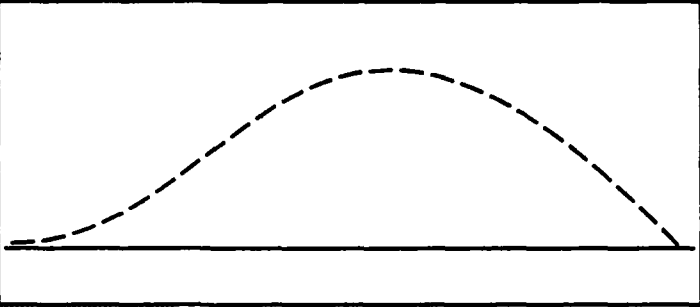
Enter Expression: more or less valuable

Definition: FUZ(*valuable*)

Distribution:

✓ Definition Found!

Fuzzy Expression Dictionary Maintenance System

0/1,.1/2,.15/3,.2/4,.3/5,.5/6,.8/7,.86/9,.95/10,
1/11,.95/12,.85/13,.7/14,.55/14,.3/15,0/16

| Add/Replace | Remove | Cancel |

Figure 9. The User Dialog Box

VIII. TESTING THE DEFINITIONS:

To test the "reasonableness" of the definitions, a fuzzy "spreadsheet" was constructed. This matrix allowed definitions and weights to be entered as subjective expressions, then a weighted average is computed and the results ranked and interpreted as a natural language phrase. The spreadsheet was then tested using various product evaluations from Consumer Reports. Ten evaluations were performed, and in all ten tests, the spreadsheet rankings agreed with Consumer Reports' rankings within major groupings. An example of such a spreadsheet is given in figure 10. The example is a comparison of Waxed Dental Floss[12], chosen for this report because of its brevity. Other comparisons run included Miniature LCD TV Sets[13], Bathroom Scales[11], Compact 35mm Cameras[7], Built-in Refrigerators[6], Aluminum Foil and Freezer Wrap[10], Garage-door

Openers[4], Telephones[9], Compact-disc Players[8], and Hand Vacuum Cleaners[5].

	Brooks	Butler Shred-res.	Butler Waxed	CVS	Duane Reade	Johnson & Johnson	Woolworth
Cost per Month	Average	Above Average	Very High	Low	Low	High	Average
Thinness	Above Average	Below Average	Very High	Below Average	Low	Below Average	Very Low
Resist. to Shredding	Average	Excellent	Poor	Good	Good	Good	Good
Resist. to Breaking	Average	Below Average	Poor	Average	Average	Average	Above Average
Results	Below Average Choice	Best Choice	Poor Choice	Average Choice	Average Choice	Below Average Choice	Good Choice

Figure 10. "Waxed Dental Floss" (screen image, reduced for printing)

Verifying the spreadsheet results indicates that the expressions used in the dictionary are valid. The "results" column of the spreadsheet is generated by matching the weighted averages to a selected set of natural language phrases. The "best fit" was chosen using a least squares comparison to the phrase set. This method is reasonably fast (for small phrase sets), but the output is naturally quite limited. Several methods for interpreting the result distribution directly to natural language modifiers and primaries were generally unsuccessful. The reason is quite obvious in hindsight: an ill-defined (fuzzy) value divided by another such number results in an even less precise result. In a nutshell, then, A•B=C does not mean that C/B=A for fuzzy distributions, and an exact, or even near, decomposition into modifiers and primaries is not feasible[1,2].

IX. Recommendations:

The primary recommendation for this project is that further Air Force sponsored research on this topic be discontinued. While the Dictionary Maintenance Program is operational, the "spreadsheet" above is simply a testing device, less than fully developed. Although this particular application of the dictionary has considerable practical application and should be continued further, and other applications of fuzzy analysis of natural language may arise as the robotics

research blooms, the utility of this program to the Air Force now and in the immediate future suggests that further development at Air Force expense is not justifiable. As a result, the remainder of this project should be pursued by private research.

REFERENCES

1. Kandel, Abraham, Fuzzy Mathematical Techniques with Applications, Reading, Massachusetts, Addison-Wesley Publishing Company, 1986.

2. Kaufmann, Arnold, and Gupta, Madan M., Introduction to Fuzzy Arithmetic: Theory and Applications, New York, New York, Van Nostrand Reinhold Company, 1984.

3. Schmucker, Kurt J., Fuzzy Sets, Natural Language Computations, and Risk Analysis, Rockville, Maryland, Computer Science Press, 1984.

4. Consumer Union, "Garage-door Openers", Consumer Reports, Vol. 53, No. 10, October, 1988, pp. 644-648.

5. Consumer Union, "Hand-held Vacuum Cleaners", Consumer Reports, Vol. 53, No. 10, October, 1988, pp. 619-622.

6. Consumer Union, "Build-in Refrigerators", Consumer Reports, Vol. 53, No. 11, November, 1988, pp. 716-719.

7. Consumer Union, "Compact 35mm Cameras", Consumer Reports, Vol. 53, No. 11, November, 1988, pp. 703-709.

8. Consumer Union, "CD Players", Consumer Reports, Vol. 54, No. 1, January, 1989, pp. 27-32.

9. Consumer Union, "Telephones", Consumer Reports, Vol. 54, No. 1, January, 1989, pp. 40-45.

10. Consumer Union, "Food Wraps", Consumer Reports, Vol. 54, No. 2, February, 1989, pp. 120-123.

11.   Consumer Union, "Bathroom Scales", <u>Consumer Reports</u>, Vol. 54, No. 7, July, 1989, pp. 461-466.

12.   Consumer Union, "New Ways to Save Your Teeth?", <u>Consumer Reports</u>, Vol. 54, No. 8, August, 1989, pp.504-510.

13.   Consumer Union, "The Big Picture in Tiny TV", <u>Consumer Reports</u>, Vol. 54, No. 8, August, 1989, pp.524-527.

1989 USAF-UES SUMMER FACULTY RESEARCH PROGRAM/

GRADUATE STUDENT RESEARCH PROGRAM

Sponsored by the

AIR FORCE OFFICE OF SCIENTIFIC RESEARCH

Conducted by the

Universal Energy Systems, Inc.

FINAL REPORT

THE STUDY OF ALKALI-ENHANCED CEMENTS AND CONCRETES

Prepared by:	Derald Chriss
Academic Rank:	Assistant Professor
Department and	Department of Chemistry
University:	Southern University
Research Location:	Air Force Engineering and Services Center Air Base Operating Surfaces (RDCP) Tyndall AFB, FL.
USAF Researcher:	Patricia C. Suggs
Date:	25 September 1989
Contract No:	F49620-88-C-0053

The Study of Alkali Enhanced Cements and Concretes

by

Derald Chriss

ABSTRACT

A study of the effects of alkali hydroxides on cements and mortars has been undertaken. The alkali hydroxides used in this study were LiOH and NaOH. The cements used were Ground Granulated Slag Cement, Portland Cement, a mixture of the above mentioned cements, and a High Alumina Slag Cement. The mortars consisted of the above mentioned cements in combination with sands and clays, with the alkali hydroxides added in variable amounts.

The results indicate that the major role of the alkali hydroxides is to increase the long term compressive strengths of the specimens prepared. In some instances, the alkali hydroxides helped to increase the setting times of the mortars. The results also indicate that specimens containing clay contents of 10 to 15% yield the most promising clay samples, whereas the sand samples prepared yielded no conclusive results with respect to the optimal percentage.

ACKNOWLEDGEMENTS

Sincere appreciation is expressed to the Air Force Systems Command and the Air Force Office of Scientific Research for sponsoring this work. Universal Energy Systems, Inc. should also be commended for the flawless administrational aspect of this project. Thanks also are extended to the Air Force Engineering and Services Center.

In addition, I would like to thank Patricia C. Suggs for her valuable assistance in this project. Thanks also are extended to MSgt. Al Wackowski, Perry Sullivan, Dean Hitzelberger, and David Timian for their assistance.

Finally, I would like to thank my wife, Sharon, for her patience and assistance during this summer period.

I. INTRODUCTION

Alkali metal hydroxides have been reported as set accelerators for cements and concretes[1,2]. Although the ultimate compressive strengths of specimens prepared with these hydroxides are comparable to those without[3], the early setting times and good early strengths of alkali hydroxide cement and concrete specimens further adds to the ability to use fine sands and sandy loams as well as coarse aggregates.

The Air Base Operating Surfaces Branch (RDCP) of the Air Force Engineering and Services Center at Tyndall AFB, has been interested in aircraft runway construction and rapid runway repairs and it was felt that alkali hydroxides may be of great importance in these areas. In addition, the need to limit the amount of carry-in materials for construction of aircraft runways is of particular concern. For this reason, the use of clays, sand, sandy loams, and other types of soils as filler materials is of interest.

My past experience in analytical methods of analysis, contributed to my being selected by RDCP, as a researcher in this area. It was hoped that micro-analytical test methods could be developed during this summer research period, however time did not permit this to occur.

II. OBJECTIVES OF THE RESEARCH EFFORT

The objectives of this research project were to attempt to (a) increase the compressive strengths of cementitious materials available (b) decrease the times required for setting of these cementitious materials (c) decrease the water:cement ratios of mortar specimens (d) develop concretes using fine aggregates such as sand and clay, and (e) study the role and affects of alkali metal hydroxides on the above mentioned mixtures.

One of the original objectives was to develop a cementitious material using a combination of lime, alumina (glassified), and sand (in an unglassified mixture). Although much time was spent addressing this objective, we were unsuccesful in developing a suitable combination.

The above objectives arose from the fact that the Air Force has a great need to develop improved ways of constructing and or repairing runways rapidly and with a minimum of carry-in materials.

III. EXPERIMENTAL

The specimens prepared and tested consisted of cements, cement mixtures, and mortars utilizing sands and clays.

Alkali Hydroxides

The alkali hydroxides used in this investigation were lithium hydroxide (LiOH), and sodium hydroxide (NaOH). For each specimen containing LiOH, the desired amount of LiOH was measured, using a platform balance, then dissolved (using a magnetic stirrer) in a portion of the water required.

For those specimens containing NaOH, the desired amounts of NaOH were obtained by adding the required volumes of a 10 molar NaOH solution.

Cements

The cements used in this investigation were Portland Cement (PC) Type I (Ideal Cement Company, Denver, CO.) and Ground Granulated Slag Cement (SC) (Blue Circle Atlantic, Atlanta, GA.). In addition to the above cements, mixtures of the PC and SC were used as well as a High Alumina Slag Cement (HASC) prepared in the laboratory by mixing alumina type A-14 (Alcoa

Industrial Chemicals Division, Bauxite, AR.) and the SC mentioned above. The HASC was comprised of 62% SC and 38% alumina, which accounts for a total alumina percentage of 45%.

Two inch cube specimens of these cements were prepared for testing according to ASTM C109 specifications.

Clay Mortars

The clay used in the preparation of mortars contained small amounts of granite, sand and water (approximately 14% by mass). Large chunks of clay were first broken into smaller pieces by hand and by the use of a #8 molecular sieve, to obtain flakes of the clay. These flakes were then mixed with either water, LiOH or NaOH solution (approximately 30 seconds with stirring). This short time was used to minimize the loss of plasticity of the clay.

To these initial clay-solvent mixtures were added, alternately and with stirring, small quantities of cement and remaining aqueous component until all components were combined. The mortar mixes were poured into 2 inch cube molds (24 hours) then removed and allowed to air cure until tested. The percentages of clay component ranged from 10 to 30%.

Sand Mortars

The sand mortars were prepared using a silica sand and an F-grade sand (both obtained from Ottawa Sand Company). The desired amounts of sand were measured using a platform balance then mixed with the desired amounts of cement. Afterwards small portions of these mixtures were added to the aqueous component, with mixing, until all components were combined. The percentages of sand ranged up to 76%.

IV. TESTING METHODS

The measurements of compressive strengths were obtained using a Marshall Stability Tester (Soiltest, Model # 1211-AJ) and a Material Test System (MTS Corporation Model # 800). The mortars and procedures were in accordance with ASTM Method C109-84.

The time of setting measurements were made using the Vicat Needle test method in accordance with ASTM method C191-82.

V. RESULTS AND DISCUSSION

The majority of the specimens tested were mortars with sand
as the major component. Specimens using clay (small
percentages) were also prepared. A listing of the components
of each specimen along with the water:cement ratios may be
found in Table I. As indicated earlier, the attempts to
produce a suitable cementitious material from an unglassified
lime, alumina, and sand (CAS) mixture were unsuccesful.
Figure I, however, indicates the composition of the CAS
specimens and compares them to those of ordinary SC and PC,
as well as those compositions used by MacDowell[4].

On the basis of early compressive strength test results (1-7
days), it is clear that our clay and sand mortars are much
weaker than those specimens of the SC, PC, and SC-PC mixtures
with water only (which are used a references). Of our
mortars, however, those specimens which exhibited early
strengths were those prepared with the SC-PC mixture as the
binding material.

CLAY SAMPLES

Samples composed of a 5Ø:5Ø SC-PC mixture with 12% clay
(w/c=Ø.4Ø) exhibited 3 day strengths of 3,Ø23 psi (G6) and

TABLE I: SPECIMEN COMPOSITION

ID	% Slag	% Sand	% Clay	% LiOH	% NaOH	% P.C.	w/c H2O
B1	99	-	-	0.13	-		0.30
B2	100	-	-	-	-	-	0.34
B3	99	-	-	0.12	-	-	0.30
B4	CAS						
C1	25	73	-	2.0	-	-	0.12
C2	25	75	-	-	-	-	0.11
C3	CAS						
D1 #	26	73	-	1.0	-	-	0.25
D2	27	73	-	-	-	-	0.25
D3	26	73	-	1.0	-	-	0.25
D4	26	73	-	1.0	-	-	0.13
E1	25	-	75	-	-	-	0.45
E2 *	25	73	-	2.0	-	-	0.11
E3 #	26	73	-	1.0	-	-	0.11
E4 #	27	73	-	-	-	-	0.11
E5 *	27	73	-	1.0	-	-	0.13
E6	25	75	-	-	3.7	-	0.32
E7	25	75	-	3.7	-	-	0.32
F1	CAS						
F2 #*	25	75	-	-	-	-	0.20
F3	94	-	-	6.0	-	-	0.39
F4 *	93	-	-	-	7.0	-	0.39
F5	CAS						
F6	CAS						
F7	CAS						
F8	88	-	12	-	-	-	0.40
F9	82	-	12	6.0	-	-	0.34
F10 *	100	-	-	-	-	-	0.40
F11	81	-	19	-	-	-	0.41
G1	24	70	-	-	-	-	0.40
G2	-	75	-	-	-	25	0.23
G3	12	73	-	3.0	-	12	0.19
G4	12	73	-	-	3.0	12	0.19
G5	44	-	12	-	-	44	0.40
G6	41	-	13	5.0	-	41	0.36
G7	41	-	13	-	5.0	41	0.36
G8 #*	41	-	13	-	5.0	41	0.36
G9	32	-	30	-	5.0	33	0.35
H1	70	-	30	-	-	-	0.41
H2 #	38	-	19	-	5.0	38	0.41
H3	50	-	-	-	-	50	0.35
H4 #	-	-	-	-	-	100	0.35

* HASC (high alumina slag cement)
\# TOS (time of setting measurements taken)
CAS (lime-alumina-sand)

FIGURE 1: CAS Compositions

SC=Slag
PC=Portland
MC=MacDowell
● =Our Samples

SiO₂

Al₂O₃
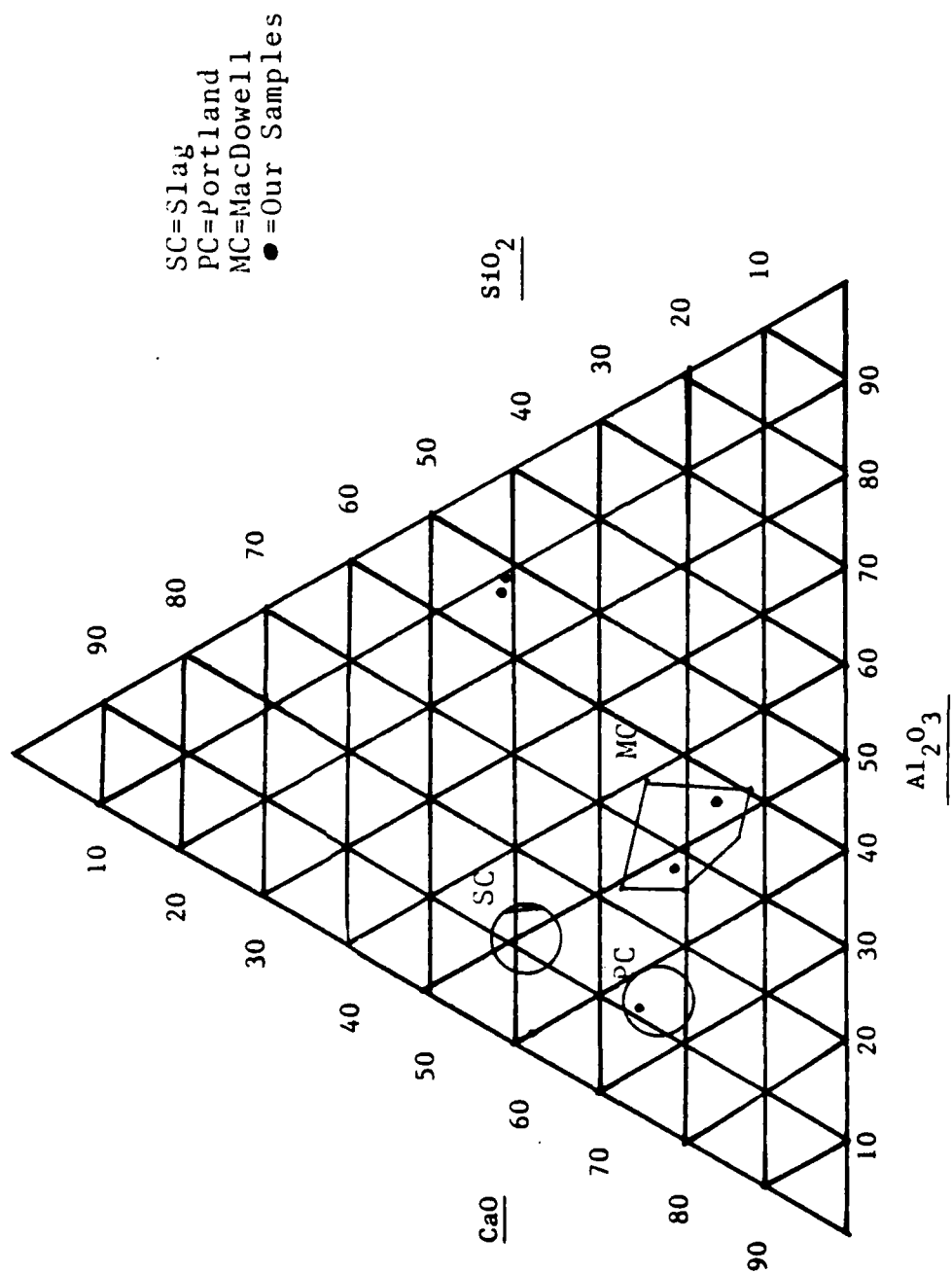
CaO

2,063 psi (G7), compared to 5,000 psi for the cement:water only specimens. The 20% clay sample (H2), gave a 4 day strength test of 2,000 psi and 30% clay sample (G9) gave a 7 day strength test of 1,800 psi.

Those specimens using slag cement only as the binding material along with clay, yielded 7 day strengths of 1,531 (F8), 2,141 (F9), and 1,256 psi (F11) respectively. The lower strength of the F11 specimen is attributed to the higher percentage of clay (19% to 12%). Sample E1 (75% clay), yielded a 7 day compressive strength test of 1,041 psi.

Long term studies indicate that the clay samples range from a compressive strength value of about 4,000 to 5,000 psi for F8 and F9 (21 days) to about 2,000 to 3,500 psi for F11 (28 days). For those specimens with the SC-PC mixture, the values ranged upwards to 6,000 to 7,000 psi for G6 (28 days). These results indicate that the compressive strengths increase proportionally, with respect to time, with those samples containing 10 to 15% clay yielding the highest strengths short and long term.

SAND SAMPLES

Of the sand samples, those specimens with the smaller w/c
ratios yielded the higher compressive strengths (G4 yielding
the highest at 28 days). The E series of sand mortars (E2-
E7) yielded much weaker specimens (attributed to using w/c
ratios which were to low). The results also indicate that the
function of the alkali hydroxides is to increase the long term
compressive strengths rather than the short term strengths.

Another factor in compressive strength results for sand
specimens, is the type of sand used. Those specimens with the
higher short and long term compressive strengths were those
which were prepared using silica sand as opposed to other
types of sand. Not much variation was observed with respect
to the sand samples, since all specimens were prepared using
sand percentages of about 75% in accordance with the work of
Kutti and Malinowski[5], and Glukhovskii[6]. Undoubtedly, more
experimental data must be obtained for sand samples.
Variation of sand percentages is essential to determining the
optimal sand percentages.

VI. RECOMMENDATIONS

It is recommended that the center pursue the work with the glassified lime, alumina, and sand mixture. The work done during the summer rules out the use of this combination in an unglassified mixture.

Secondly, it is recommended that the center experiment more with the combination of cement and clay mortars. It is felt that adjusting the ratio of cement, clay, and water may produce specimens of reasonable strength.

Much more experimentation is necessary with respect to the use of superplasticizer. It has been documented[6] that superplasticizers reduce the water to cement ratios required for thorough mixing. Results of some work done this summer, indicates that lowering the w:c ratio may increase the strength of certain specimens. The use of a superplasticizer will be very useful in this respect.

Finally, it is recommended that time of setting measurements be made of those samples which may be prepared in the future. The short summer period just did not allow time for conclusive results with respect to these measurements.

REFERENCES

1. Novinson, T. and Crahan, J., ACI Materials Journal, Tit. no. 85-M2, Jan-Feb 1988, p. 12

2. Boldyrev, S. and Tumenez, A., "In the USSR: Progress in Production of Binders and Concretes", Pit & Quarry; Sept, 1984, p. 68

3. Committee Report "Ground Granulated Blast-Furnace Slag as a Cementitious Constituent in Concrete", ACI Materials Journal, Tit. no. 84-M34, p. 327

4. MacDowell, J.F., United States Patent, Pat. No. 4,605,443, Aug 12, 1986

5. Kutti, T., Malinowski, R. and Srebnik, M., Silicates Industriels, 1982-6, p. 149

6. Glukhovskii, I.A., and Pashkov, I. A., Gidrotekhnicheskoe Stroitel'stvo, No. 2, pp. 14-16, February, 1967

1989 USAF-UES SUMMER FACULTY RESEARCH PROGRAM/
GRADUATE STUDENT RESEARCH PROGRAM

Sponsored by the
AIR FORCE OFFICE OF SCIENTIFIC RESEARCH
Conducted by the
Universal Energy Systems, Inc.
FINAL REPORT

PREDICTION OF THE CAPILLARY PRESSURE-SATURATION RELATIONSHIPS FOR AQUIFERS CONTAMINATED WITH JET FUELS

Prepared by:	Dr. Avery H. Demond
Academic Rank:	Assistant Professor
Department and	Civil Engineering
University:	University of Massachusetts
Research Location:	AFESC/RDVW
	Tyndall AFB, FL 32403
USAF Researcher:	Mr. Jack Milligan
Date:	August 30, 1989
Contract No.:	F49620-88-C-0053

PREDICTION OF THE CAPILLARY PRESSURE-SATURATION RELATIONSHIPS FOR AQUIFERS CONTAMINATED WITH JET FUELS

by

Dr. Avery H. Demond

ABSTRACT

Many correlations exist to relate the depth of aviation fuel in a monitoring well to the thickness of the fuel layer in an aquifer. Unfortunately, many of these correlations require knowledge of the capillary pressure relationships, information which may be difficult to obtain. The purpose of this project was to develop a technique to predict the relevant capillary pressure-saturation relationships from easily measured physico-chemical parameters of a jet fuel spill site. The technique proposed here is composed of three steps: estimating the air-water capillary pressure from grain-size data, estimating the interfacial tensions of air-JP4 and JP4-water from surface tension and density data, and then combining this information to yield the capillary pressure relationships for air-JP4 and JP4-water using Leverett's function. This technique can yield reasonably accurate results for clean JP-4 in Tyndall sand. Modifications may have to be made to make the technique applicable to aviation spills in other soil materials.

ACKNOWLEDGEMENTS

I thank the Air Force Systems Command, Air Force Office of Scientific Research, Universal Energy Systems and the Air Force Engineering and Services Center for their sponsorship and administration of this research.

Certain individuals should be mentioned by name for their contributions to making this research possible: Mr. Jack Milligan, Lt. Col. Tom Lubozynski, Dr. Daniel Stone, and Mr. Perry Sullivan.

I. INTRODUCTION

The Air Force has identified spills of jet fuels, such as JP-4, as a major source of groundwater contamination on bases across the nation. Owing to the low aqueous solubility of jet fuel in water, this contaminant persists as a separate liquid phase and is transported as such in groundwater. The clean-up of jet fuel spill sites is hampered by the lack of information and understanding of multiphase flow processes.

The monitoring of spills at bases such as Eglin AFB (FL) has demonstrated that the correspondence between the depth of jet fuel in a observation well is not straightforwardly related to the thickness of the layer in the aquifer. Consequently, one of the current research missions of the Air Force Engineering and Services Center, Environics Division, (Tyndall AFB, FL) is to develop better methods to predict the thickness of the layer of jet fuel in an aquifer from the depth of jet fuel in a monitoring well.

My research interests are in the general area of contaminant migration in the subsurface. In particular, I am interested in organic contaminants, moving as a separate liquid phase. In the past, I have conducted research in the measurement and estimation of parameters necessary for the description of the movement of compounds such as n-dodecane and o-xylene in the subsurface. The expertise developed from this prior research contributed to my being assigned to the Environics Division of the Air Force Engineering and Services Center.

II. OBJECTIVE OF THE RESEARCH EFFORT

Despite its importance in calculating the quantity of recoverable jet fuel, there is no generally accepted method for the estimation of thickness of the fuel layer in an aquifer from the depth of fuel in an observation well. Many of the suggested methods for relating the depth of fuel in a monitoring well to that in an aquifer (including the one developed last summer by another faculty member on the Summer Faculty Research Program, Dr. Deanna Durnford [Colorado State University]) require parameters describing the capillary pressure-saturation relationships of the system (Blake and Hall, 1984; Schiegg, 1984; Durnford, 1988). Unfortunately, determining these relationships in a laboratory can be time consuming and tedious, and many laboratories are not properly equipped to make these

measurements. The need for data that may not be readily obtainable limits the usefulness of these equations.

With this problem in mind, the objective of this project was to develop a technique so that the required data may be estimated. Such a technique would aid in the estimation of the recoverable fuel at a spill site without resorting to expensive laboratory measurements.

III. BACKGROUND

In response to the observation that the depth of the fuel in a monitoring well is not a direct indication of the thickness of the fuel layer, many correlations have been developed to relate these two quantities. A characteristic that many of these correlations have in common is that they depend on knowing the capillary pressure-saturation relationships for the various liquid pairs at the site.

The dependence of capillary pressure on saturation is an important relationship in many processes, including soil water movement and oil reservoir behavior. This relationship gives capillary pressure, P_c, defined as the pressure difference between the wetting and the nonwetting phases:

$$P_c = P_{nw} - P_w \qquad [1]$$

where P = pressure and the subscripts, c, nw and w = capillary, nonwetting and
wetting, respectively,

as a function of saturation of the wetting phase, S_w, defined as the ratio of the volume of voids filled with the wetting phase to the total volume of void space of the porous medium:

$$S_w = V_w/V_t \qquad [2]$$

where V = volume of voids and, the subscripts, w and
t = wetting and total, respectively.

To measure such a relationship, a pressure cell is often utilized. This technique involves placing a sample of the porous medium initially saturated with the wetting phase (e.g. water) in contact with a porous plate also saturated with that phase. Pressure is applied to a second phase and the amount of the wetting phase discharged at each pressure is measured. The porous plate acts as a semi-permeable barrier: the wetting phase can pass through the plate, but the nonwetting phase cannot if the plate's pores are sufficiently small. The other face of the pressure plate is in contact with the wetting phase at a known pressure. The capillary pressure inside the cell can be regulated either by applying a pressure to the nonwetting phase on one side of the pressure plate, or by lowering the pressure of the wetting phase on the other side. When a sample has reached an apparent equilibrium at a given capillary pressure, its saturation can be determined by weighing the sample or by measuring the effluent volume. Since the time to reach equilibrium may be quite long depending on the soil sample and properties of the pressure plate, the generation of a complete capillary pressure-saturation relationship may take on the order of weeks.

Since there are three relevant liquid pairs at a fuel spill site, three capillary curves must be measured:

wetting phase	nonwetting phase
water	JP-4
water	air
JP-4	air

The measurement of these three capillary pressure curves may take a considerable amount of time. On top of that, many labs are not equipped with pressure cells or precision pressure regulators which are used in making these measurements. Consequently, it is useful to investigate methods for estimating these relationships from simpler physico-chemical parameters so that the methods for predicting fuel thickness can be used easily.

IV. RESULTS AND DISCUSSION

Based on preliminary research, a general strategy for obtaining the objective of developing a technique to predict the necessary capillary pressure-saturation relationships was devised:

1) estimate the air-water capillary pressure-saturation relationship,

2) estimate the interfacial tension between air-JP4 and between water-JP4, and then

3) use this information to estimate the air-JP4 and water-JP4 capillary pressure-saturation relationships.

The following sections describe the methods for each step in turn.

1) Estimation of the Air-Water Capillary Pressure-Saturation Relationship

The methods available in the soil science literature for the estimation of the air-water capillary pressure-saturation relationship can be loosely classified into two groups: those based on grain-size distributions and those based on pore-size distributions. Although the methods based on pore-size distributions are better developed, they require data obtained by mercury porosimetry or other sophisticated techniques. Since the data needed in methods based on grain size distributions can be obtained primarily by sieving, these methods were examined more closely here.

A method that appeared to be simple, yet yield accurate results for Tyndall sand was a method developed by Arya and Paris (1981) based on the similar shapes of capillary pressure-saturation curves and grain size distribution curves. Using Eqns. [3] and [4]

$$\theta_{vi} = \sum_{j=1}^{i} V_{vj} \rho_b \qquad [3]$$

where θ_{vi} = moisture content of ith particle-size range
$= \phi S_{wi}$, where ϕ is the porosity,
$V_{vj} = (W_i/\rho_b)e$,

and W_i = mass fraction in ith particle size range,
ρ_b = bulk density of sand, and
e = void ratio = $\phi/(1-\phi)$;

$$P_{ci} = \frac{2\gamma \cos\alpha}{\rho_w g r_i} \qquad [4]$$

where γ = interfacial tension,

α = contact angle,

ρ_w = density of water,

g = gravitational acceleration constant,

$r_i = R_i [4en_i^{(1-\beta)}/6)]^{1/2}$

and R_i = mean particle radius of ith particle size range,

$n_i = 3W_i/4\pi R_i^3 \rho_b$,

β = empirical parameter, usually ranging from 1.35 - 1.40.

the air-water capillary pressure-saturation relationship (P_c vs. S_w) can be obtained knowing R_i, the mean particle radius of ith particle size range, W_i, the mass fraction in the ith particle size range, and ρ_b, the bulk density of the soil. This information can be readily obtained from the weight of a field sample and a simple sieve analysis. Figure 1 shows the grain-size distribution measured for Tyndall sand. Figure 2 shows a comparison between the predicted capillary pressure-saturation relationship obtained with the data from Figure 1 (taking β as equal to 1.1), and the measured relationship for Tyndall sand. As this comparison shows, the method estimates the initial portions of the curve well. At lower saturations, however, the model does not perform as well. Since the model is based on the grain-size distribution curve which tends to zero at small particle diameters, the model predicts a residual saturation equal to zero. Since most of the correlations relating the depth of fuel in a well to that in an aquifer only need information from the initial portions of the curve, the method's inability to predict the residual saturation accurately does not preclude its usefulness in this context.

2a)   Estimation of the Surface Tension for Air-JP4

Reid et al. (1987) suggest a variety of methods for estimating the surface tension of mixtures. Only certain methods are suitable, however, considering that JP-4 is a complex mixture, made up of nearly 100 identified components none of which comprises more than 4% by weight. The method selected was a modified version of the Macleod-Sugden correlation (Macleod, 1923; Sugden, 1924; Reid et al., 1987):

$$\sigma_m^{1/4} = \rho_{L_m} \sum_{i=1}^{n} x_i \sigma_i^{1/4} / \rho_{L_i} \qquad [5]$$

where σ_m = surface tension of the mixture $\left(\dfrac{dynes}{cm}\right)$

ρ_{L_m} = density of the mixture in terms of moles $\left(\dfrac{g\text{-}moles}{cm^3}\right)$

x_i = mole fraction of the ith component (-)

σ_i = surface tension of ith component $\left(\dfrac{dynes}{cm}\right)$ and

ρ_{L_i} = density of ith component in term of moles $\left(\dfrac{g\text{-}moles}{cm^3}\right)$

This method requires the values of surface tension, densities and molecular weights for the components. These data can be obtained from the following sources:

property	source
surface tension	Jasper, 1972
density	Weast, 1987
molecular weight	Weast, 1987

In calculating the surface tension of the mixture, only those components which comprised more than 2/3% of the mixture by weight were included. It was found that including additional components below that percentage did not significantly alter the calculated value for surface tension.

Table I shows a comparison between the calculated and measured values of the surface tension of JP-4.

Table I.

Comparison of Calculated and Measured Surface Tensions for JP-4 (dynes/cm at 20°C)

literature (est.)	25[a]
measured (clean)	25[b]
estimated	23
measured (from field site)	27[b]

Sources of values: a: Sittig, 1985; b: Durnford, 1988.

This comparison shows that the value calculated using the modified Macleod-Sugden method is close to the measured value. Part of the success of the method in this circumstance is undoubtably due to the fact that the dominant components for JP-4 are similar in nature. The mixture is dominated by linear and branched ?   .₃ whose individual surface tensions range from 16.05 dynes/cm (n-pentane) tᴄ .ᴜ3 (n-butylcyclohexane), with smaller quantities of aromatic hydrocarbons such as o-xylene (29.02 dynes/cm) and 1,2,4-trimethyl benzene (29.71 dynes/cm). The similarity of the components makes it plausible that the components would contribute to the surface tension of the mixture in proportion to their mole fraction, as the modified Macleod-Sugden method assumes.

Table I also suggests that the surface tension of the mixture is not highly affected by contamination. The values of surface tension for clean JP-4 and for JP-4 withdrawn from a sampling well at a spill site on Tyndall AFB are close.

2b)   Estimation of the Interfacial Tension for JP4-Water

Reliable methods for the calculation of interfacial tension between a complex mixture, such as JP-4, and another liquid phase do not exist. Most of the methods developed for the calculation of interfacial tension are for pure phases only (Antonov, 1907; Donahue and Bartell, 1952; Girifalco and Good, 1957; Fowkes, 1963). Fu and co-workers (Fu et al., 1986) recently developed a method that is capable of handling up to quartenary systems (two liquid phases, two solutes), provided that adequate solubility data is available.

In the absence of a better alternative, it was decided to treat JP-4 as a "pure" hydrocarbon with characteristics equivalent to that of the mixture. Then, using the Girifalco-Good-Fowkes equation (Girifalco and Good, 1957; Fowkes, 1963):

$$\gamma_{H_2O/ORG} = \gamma_{H_2O} + \gamma_{ORG} - 2(\gamma_{H_2O}^d \gamma_{ORG}^d)^{1/2} \qquad [6]$$

where $\gamma_{H_2O/ORG}$ = interfacial tension between the aqueous and organic liquids,

γ_{H_2O} = surface tension of aqueous phase,

γ_{ORG} = surface tension of organic phase, and

γ^d = dispersion component of surface tension;

and the values of: γ_{H_2O} = 72.75 dynes/cm (Vargaftik et al., 1983),

$\gamma_{H_2O}{}^d$ = 21.8 dynes/cm (Fowkes, 1964)

$\gamma_{ORG} = \gamma_{ORG}{}^d$ = 23 dynes/cm;

an estimate of the interfacial tension could be obtained.

Table II show a comparison of measured and calculated values for JP-4.

<div align="center">

Table II.

Comparison of Measured and Calculated Interfacial Tensions for JP-4-Water
(dynes/cm at 20°C)

</div>

literature (est.)	50[a]
estimated	51
measured (contaminated)	38[b]
	18[c]
	5[b]

Sources: a: Sittig, 1985; b: Durnford, 1988; c: measured in this study using a du Nuoy tensiometer following ASTM D971-82 (ASTM 1988) on JP-4 extracted from well T-9.

This comparison shows good agreement between the calculated and reported values for clean JP-4. Although not intended for use with mixtures, the ability of the Girifalco-Good-Fowkes equation to give a reasonable estimate in this case rests on the observation discussed above that the dominant components of JP-4 are similar. Most of the identified components have high aqueous interfacial tensions. The linear alkanes from C_5 to C_{16} have interfacial tensions that range from 49.0 to 53.3 dynes/cm (Johnson and Dettre, 1966), so a predicted value of 51 dynes/cm is reasonable for this hydrocarbon mixture.

The comparison of calculated and measured values (Table II) shows that the interfacial tension between JP-4 and water is significantly altered by contamination. In fact, the difference seen in the results given in Tables I and II suggests that the interfacial tension is much more susceptible to contamination effects than surface tension is. A similar

observation has been made by others who have noted that interfacial tension is a much more sensitive indicator of contamination than surface tension (Good, 1979).

Since the values in Table II show that the interfacial tension for clean JP-4 is not an appropriate value for in the field, the question arises of how to estimate the interfacial tension between contaminated JP-4 and water. Unfortunately, there is no method for the prediction of the effect of the contaminant on interfacial tension unless the identity and the concentration of the contaminant are known. The susceptibility of interfacial tension to contamination effects means that to obtain a reasonably accurate value for the JP-4-water interfacial tension in the field, one must measure it. Furthermore, the range of values reported in Table II suggests that the value varies with the conditions at a particular well. Thus, a series of measurements may be needed to characterize the conditions at a particular spill site.

The technique I recommend to measure interfacial tension is using a du Nouy tensiometer (such as that sold by CSC Scientific, Fairfax, VA) and following ASTM standard #D971-82 (ASTM, 1988). With this method, interfacial tension can be measured quickly (within minutes assuming that the instrument is calibrated) and accurately enough for routine use. The instrument can be used in the field as well, provided that a level, stable surface is available. In addition, the same instrument can be used to measure surface tension.

3) Estimation of Capillary Pressure Relationships for Air-JP4 and Water-JP4 Systems

The drainage capillary pressure relationships for immiscible organic compounds in unconsolidated sands have been predicted reasonably successfully using Leverett's function (Leverett, 1941) (Lenhard and Parker, 1987; Demond, 1988):

$$J(S_w) = P_{c_1}/\gamma_1 \, (k_1/\phi_1)^{1/2} = P_{c_2}/\gamma_2 \, (k_2/\phi_2)^{1/2} \qquad [7]$$

where $J(S_w)$ = Leverett function and S_w is the saturation of the wetting phase,
P_c = capillary pressure,
γ = interfacial tension,
k = permeability,

ϕ = porosity, and

subscripts 1 and 2 refer to systems 1 and 2 respectively.

In this application, the porous medium is the same in the JP-4-water and air-JP-4 systems as in the air-water system. Thus, the porosities and the permeabilities are the same:

$$k_1 = k_2$$
$$\phi_1 = \phi_2$$

and Leverett's function yields:

$$P_{c_2} = P_{c_1} \left(\frac{\gamma_2}{\gamma_1} \right) \text{ at a given } S_w \qquad [8]$$

Applying Eqn. 8 to the two systems for which we wish to estimate the capillary pressure relationships, air-JP-4 and JP-4-water, gives:

$$P_{c[AIR-JP4]} = P_{c[AIR-WATER]} \left(\gamma_{[AIR-JP4]} / \gamma_{[AIR-WATER]} \right) = P_{c[AIR-WATER]} (23/72.75)$$

and

$$P_{c[JP4-WATER]} = P_{c[AIR-WATER]} \left(\gamma_{[JP4-WATER]} / \gamma_{[AIR-WATER]} \right) = P_{c[AIR-WATER]} (51/72.75)$$

respectively, at a given value of saturation of the wetting phase.

A comparison of the predicted and measured capillary pressure curves for an 0.8 mm sand is shown in Figure 3. Figure 3b shows excellent agreement between the measured and predicted curves for the system of air-JP4. The agreement is considerably poorer for the JP4-water system (Figure 3c). This discrepancy between predicted and measured relationships probably stems from an inaccurate value for the interfacial tension between this sample of JP-4 and water. Although the JP-4 used in the measurements was not from a field site, it appears that it was subjected to contamination. Problems have been reported in the past in obtaining an accurate value for interfacial tension of such highly hydrophobic compounds, due to the tendency of whatever impurities are present to concentrate at the organic-water interface (Johnson and Dettre, 1966). The discrepancy seen in Figure 3c

stresses the importance of measuring the interfacial tension between the particular sample of JP-4 and water in order to obtain an accurate estimate of the capillary pressure-saturation relationship for that specific system.

V. RECOMMENDATIONS

The three-step method described above represents a means for obtaining information necessary in the use of many correlations relating the depth of jet fuel in a monitoring well and the thickness of the free fuel layer in an aquifer. Using this method, the desired information about capillary pressure-saturation relationships can be generated within hours, rather than within the weeks that are required for the laboratory measurement of these relationships. This technique was developed with the characteristics of jet fuel and Tyndall sand in mind. If the technique is to be applied to other sites where different soil materials or different contaminants are present, certain limitations should be recognized:

1) Estimation of the air-water capillary pressure relationship from grain-size data: Depending on the type of soil present, the value of the empirical parameter, β, in Arya and Paris's (1981) method will change. Arya and Paris give suitable values for β for a range of soils from sandy loam to silty clay. However, the simplicity of the model precludes its suitability for soils that are poorly sorted, that show a high degree of aggregation or that exhibit marked volume changes upon wetting and drying. In these circumstances, other more complex models, will have to used or the air-water capillary pressure relationship will have to be measured.

2) Estimation of the surface tension of air-JP4 and interfacial tension of JP-4-water: The modified Macleod-Sugden method for the prediction of surface tension assumes that each constituent contributes to the mixture's surface tension in proportion to its mole fraction. With respect to Jp-4, this assumption seems reasonable, given the fact that the dominant components of JP-4 are similar. If the mixture whose surface tension is unknown contains a variety of significantly different components, such as alcohols and alkanes, other methods recommended in Reid et al. (1987) may be more suitable.

For estimating the interfacial tension between water and a pure organic liquid, either Donahue and Bartell's method (1952) or Fu et al.'s method (1986) yield reasonable results. In addition, Fu et al.'s method can be used for systems of up to four constituents. Apparently, there are no recommended methods for measuring the aqueous-organic

interfacial tension for systems made up of more than four constituents. The method used here, the Girifalco-Good-Fowkes equation, is, in reality, applicable to pure phases only. It was used here under the assumption that the interaction of JP-4 and water was similar to that of a pure hydrocarbon and water and consequently, it is not generally applicable to other mixtures.

The clean compound values for surface tension and interfacial tension may not reflect values in the field. Although, in this study, the surface tensions for clean JP-4 and field JP-4 were similar, the value of interfacial tension ranged from 5 - 50 dynes/cm. Such a large range in interfacial tension values will result in a large range of possible capillary pressure relationships. No method exists that can account for all the factors that may alter the JP-4-water interfacial tension; consequently, this parameter must be measured. Since both interfacial tension and surface tension can be measured readily with a du Nouy tensiometer using a single sample, it is recommended that both parameters be measured.

3) Estimation of air-JP4 and JP-4-water capillary pressure relationships:
The method recommended here, Leverett's method, yields the best results in clean, well-sorted unconsclidated soils. It is particularly poorly suited for soils that may exhibit swelling and shrinkage as the ambient fluid changes. In addition, Demond (1988) noted that the method gives increasingly inaccurate results as the interfacial tension between the organic liquid and aqueous phase decreases. As the interfacial tension decreases, the capillary pressures predicted by Leverett's method become smaller than the measured values. Thus, the predicted capillary pressure relationships for the JP4-water system will be more accurate if the interfacial tension is 50 dynes/cm than if it is 5 dynes/cm.

This project focused on the prediction of capillary pressure relationships. To fully describe the multiphase flow of jet fuel in aquifers, additional parameters are needed and these, too, may have to be estimated. How the error produced through the use of estimated values affects the final predictions of jet fuel migration in an aquifer is unknown. The evaluation of the effect of error in property estimation on predictions of the movement of jet fuels is the subject of my research initiation (mini-grant) proposal.

REFERENCES

American Society of Testing and Materials, 1988. Annual Book of ASTM Standards. American Society of Testing and Materials, Philadelphia, PA.

Antonov, G.N., 1907. J. Russ. Phys. Chem. Soc. 93:342.

Arya, L.M., and J.F. Paris, 1981. Soil Sci. Soc. Amer. J. 45 : 1023-1030.

Blake, S.B., and R.A. Hall, 1984. Fourth National Symposium and Exposition on Aquifer Restoration and Groundwater Monitoring, Columbus, OH.

Demond, A.H., 1988. Capillarity in Two-Phase Flow of Organic Contaminants in Groundwater. Ph.D. dissertation. Department of Civil Engineering, Stanford University.

Donahue, D.J., and F.E. Bartell, 1952. J. Phys. Chem. 56:480-484.

Durnford, D., 1988. Petroleum Thickness in Groundwater, Final Report to AFESC, Tyndall AFB, Panama City, FL.

Fowkes, F.M., 1963. J. Phys. Chem. 67 : 2538-2541.

Fowkes, F.M., 1964. Ind. Eng. Chem. 56(12):40-52.

Fu, J., B. Li, and Z. Wang, 1986. Chem. Eng. Sci. 41(10):2673-2679.

Girifalco, L.A., and R.J. Good, 1957. J. Phys. Chem. 61 : 904-909.

Good, R.J., 1979. In: Surface and Colloid Science, Vol. 11. Plenum Press, NY, pp.1-29.

Jasper, J.J., 1972. J. Phys. Chem. Ref. Data 1: 841.

Johnson, R.E., Jr., and R.H. Dettre, 1966. J. Colloid Interf. Sci. 21:610-622.

Lenhard, R.J., and J.C. Parker, 1987. J. Contaminant Hydrology 1:407-424.

Leverett, M.C., 1941. Trans. AIME 142 : 152-169.

Macleod, D.B., 1923. Trans. Faraday Soc. 19 : 38.

Reid, R.C., J.M. Prausnitz, and B.E. Poling, 1987. The Properties of Gases and Liquids, 4th ed. McGraw-Hill, New York.

Schiegg, H.O., 1984. Wat. Sci. Tech. 17 : 467-476.

Sittig, M., 1985. Handbook of Toxic and Hazardous Chemicals and Carcinogens, 2nd ed. Noyes Publications, Park Ridge, NJ.

Sugden, S., 1924. J. Chem. Soc. 1924 : 32.

Vargaftik, N.B., B.N. Volkov, and L.D. Voljak, 1983. J. Phys. Chem. Ref. Data 12(3):817-820.

Weast, R.C., M.J. Astle, and W.H. Beyer, eds., 1986. CRC Handbook of Chemistry and Physics, 67th ed. CRC Press, Boca Raton, FL.

Figure 1. GRAIN SIZE DISTRIBUTION OF TYNDALL SAND
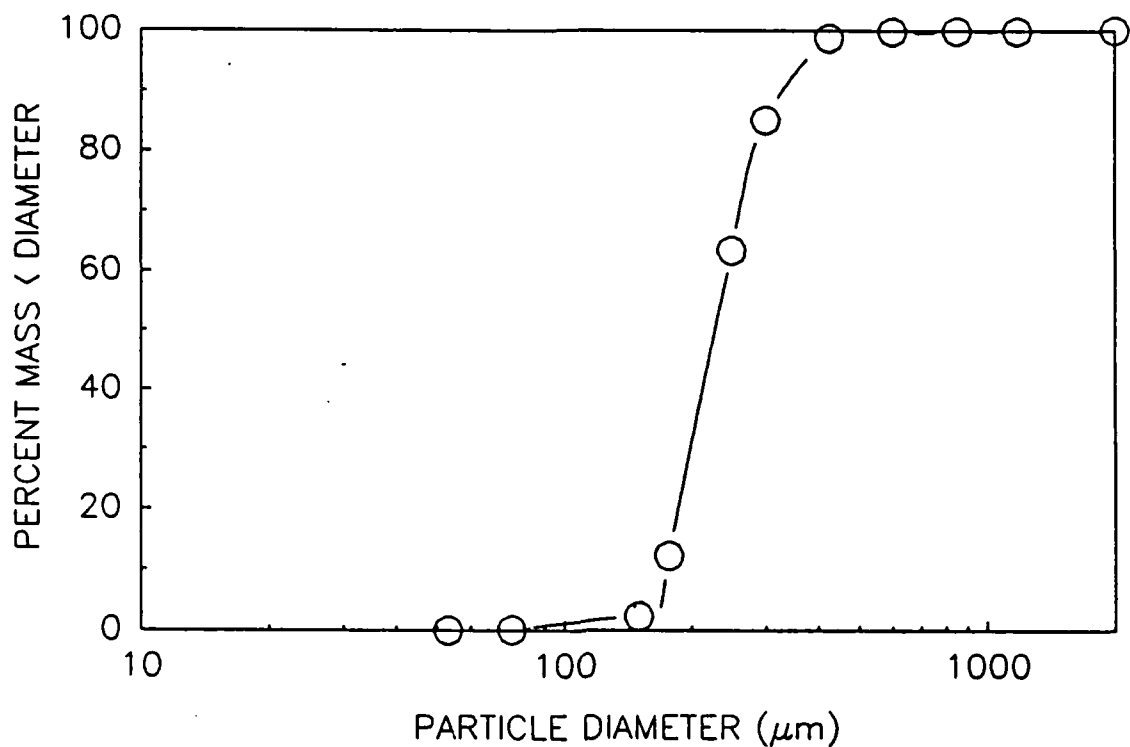
Figure 2. MEASURED AND PREDICTED CAPILLARY PRESSURE—
SATURATION RELATIONSHIPS FOR AIR—WATER IN TYNDALL SAND

Figure 3.
CAPILLARY PRESSURE – SATURATION RELATIONSHIPS IN 0.8mm SAND
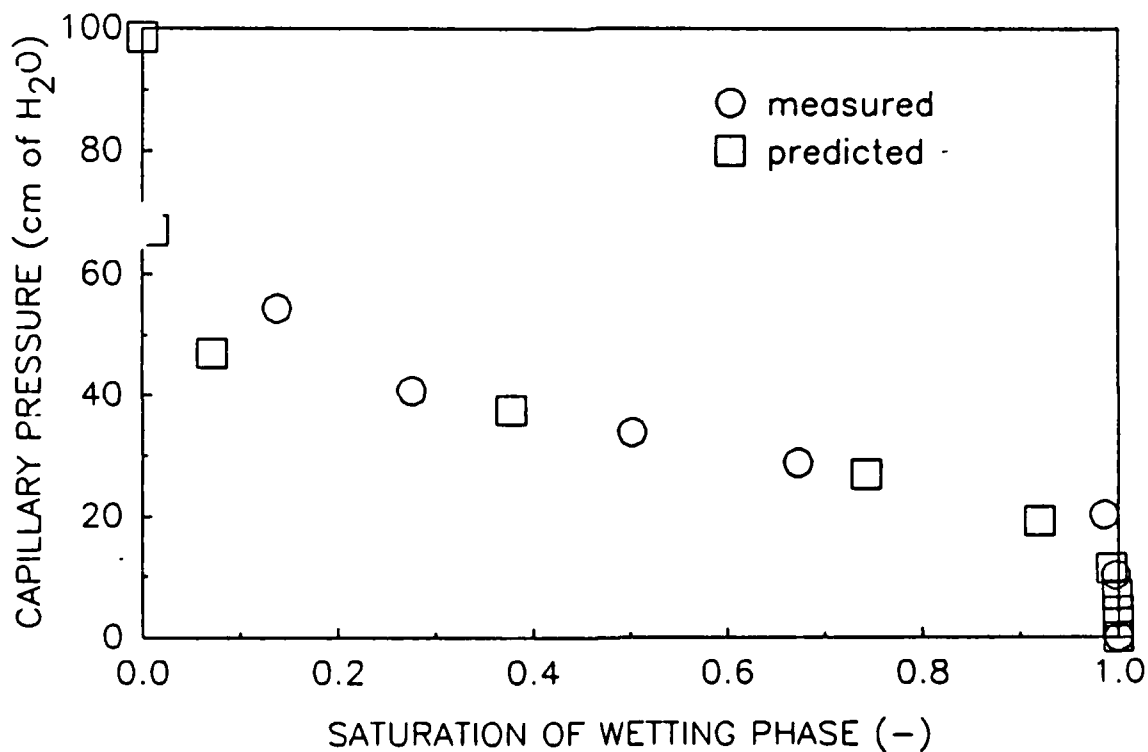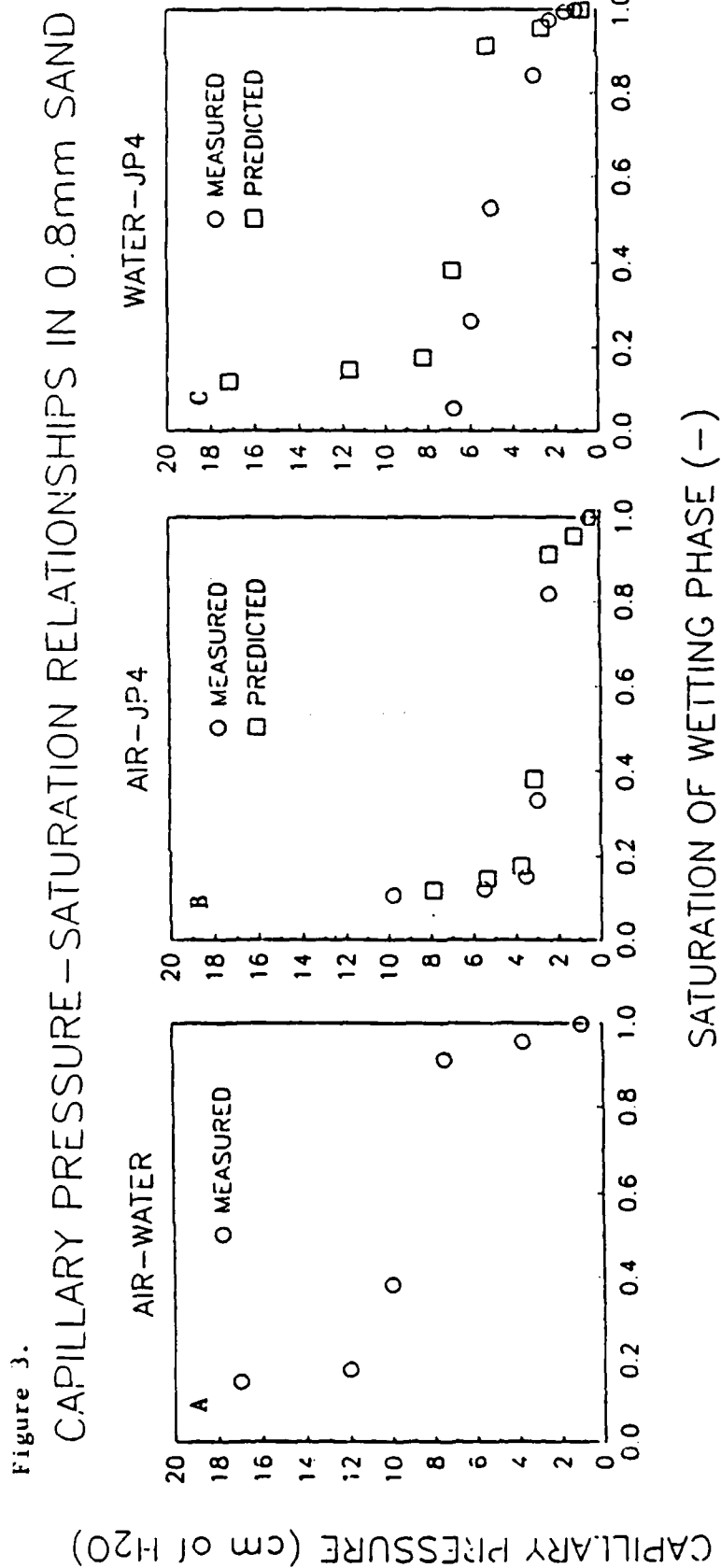
Source of data: Durnford, 1988

1989 USAF-UES SUMMER FACULTY RESEARCH PROGRAM

GRADUATE STUDENT RESEARCH PROGRAM

Sponsored by the

AIR FORCE OFFICE OF SCIENTIFIC RESEARCH

Conducted by the

Universal Energy Systems, Inc.

CONTAMINANT FLUX REDUCTION THROUGH
IN SITU SOLUBILITY MODIFICATION

Prepared by: Kirk Hatfield, Ph.D. and Joseph Ziegler

Academic Rank: Assistant Professor,   Graduate Student

Department and   Civil Engineering

   University   University of Florida

Research Location: Engineering and Services Center
                      Tyndall AFB FL 32403-6001

USAF Researcher: Thomas B. Stauffer, Ph.D.

Date: 24 Jul 89

Contract No: F49620-88-C-0053

CONTAMINATE FLUX REDUCTION

THOUGH IN SITU SOLUBILITY

MODIFICATION

by
Kirk Hatfield and
Joseph Ziegler

ABSTRACT

Research was conducted to develop and test a bench-scale in situ groundwater pollutant partition system. A zone was created within a sand box aquifer where the porous medium had been treated with a decane/mineral oil solution to induce partitioning into the organic phase. Hydrophobic groundwater pollutants were intercepted within the partition zone as they migrated from the source. Contaminate flux reductions of 85 to 99.9 percent were observed in the laboratory. Chemical partition experiments indicate small systems (of 1 meter in length) could remove hydrophobic contaminates under natural hydraulic gradients for 5 to 8 years.

ACKNOWLEDGMENTS

I would like to acknowledge the efforts of those who facilitated the completion of this work. Special gratitude is extended to Drs. Tom Stauffer and David Burris for their guidance, insight, and enthusiasm which were instrumental in the development and execution of this research. Mike Henley should know that his exceptional technical assistance carried us through to the end. Mr Jack Milligan (LBJ) I thank for the borrowed books and equipment. Tom Griffin should be recognized for patience and timely suggestions while we worked feverishly to construct the needed equipment. TSGT Jim Whitcomb efficiently provided everything and anything that was requested. A warm thanks is felt for Linda Colvin, Bonnie Castillo, and Lynda Walsh, all of whom cheerfully provided typing assistance. Finally, I wish to express my appreciation to the Air Force Systems Command, the Air Force Office of Scientific Research, and the Air Force Engineering and Services Center for sponsoring this research.

ACKNOWLEDGMENTS

I would like to thank the Air Force Systems Command and the Air Force Office of Scientific Research for sponsorship of this research. I would also like to thank all the people at the Air Force Engineering and Services Center, Tyndall AFB, Florida. Dr. Tom Stauffer and Dr. Dave Burris provided me with valuable information in the laboratory. Thom Griffen, who is in charge of fabrications, assisted greatly with the construction of experimental apparatus. The head of supply, TSgt Jim Whitcomb, managed to get everything I needed. Mike Henley saved me a considerable amount of time by automating the gas chromatograph instrument. Finally, I would like to thank Dr. Kirk Hatfield, the summer faculty fellow with whom I worked. He made my ten weeks very rewarding and enjoyable. The whole experience was exciting to me.

I.   INTRODUCTION:

Groundwater pollution has posed a serious threat to the long-term availability of the nation's most common form of potable water. The Engineering and Services Laboratory at Tyndall AFB has been conducting research necessary to understanding groundwater contamination as well as finding solutions to protect and restore existing supplies. Hydrophobic contaminants like those found in jet fuels, sorb onto porous media containing appreciable levels of organic carbon. This phenomena has led the Engineering and Services Laboratory to consider if in situ solubility modification can be used to reduce pollutant fluxes. Solubility modification could be achieved through chemical partition system; a zone within the aquifer where the organic content of the porous medium has been increased to enhance the partition'¬g of dissolved hydrophobic pollutants from the aqueous phase into an immobilized organic phase. The partition system would intercept pollutants as they flow from the source, leaving the downgradient water quality preserved.

This research will pursue studies that develop bench-scale in situ partition systems and then examine contaminant flux reductions. My research interests have been in modeling of groundwater pollutant fate and transport. The assignment to the Engineering and Services Laboratory at Tyndall AFB is consistent with my research experience and my interest in the physical and chemical processes affecting the design and performance of an in situ partition system.

II.   OBJECTIVES OF THE RESEARCH EFFORT:

As a 1989 Summer Faculty Research Fellow, my initial objectives were to identify candidate materials for the immobilized phase in the partition zone and determine how the partition zone could be created in situ. Initial experimental efforts quickly identified a decane/ mineral oil solution as a suitable organic phase for the partition zone; consequently, we amended our research objectives to the following:

> 1) examine strategies of constructing a partit'on zone
>   in situ, and,
>
> 2) investigate potential contaminant reductions produced by a
>   partition system at the bench scale.

To meet these objectives, a series of column, tank, and chemical partition experiments were performed.

III. <u>COLUMN EXPERIMENTS</u>:

<u>Materials and Methods</u>.

The purpose of these experiments was to investigate subsurface injection strategies that would develop the partition zone in situ. Four borosilicate glass columns (450 mm long and 50 mm I.D.) with threaded polypropylene end fittings were packed with a coarse sand. A sieve analysis on the sand produced an effective grain size of 0.7 mm and a uniformity coefficient of 2.1. The porosity and bulk density were respectively 0.40 and 1.63 and were determined from displacement experiments conducted with the sand packed in graduated cylinders. Tygon tubing connected the base fittings of each column to a common constant head tank. A mean water level was established overnight; producing a capillary fringe that averaged 1.9 cm. Into each column, 8 ml of JP-4 was injected just above the capillary fringe. The JP-4 was spiked with Uvitex OB, a lipophilic dye that fluoresces blue under ultraviolet light. Within 24 hours, the water table was twice fluctuated 4.5 cm above and below the mean level.

We next proceeded to inject the organic phase selected for the partition zone (20 percent decane/80 percent light mineral oil). The phase was spiked with Fluorescent Yellow 131SC, a lipophilic dye that allows observation of phase movement under UV light. In each column, 24.0 ml was injected. For the first column, injection occurred immediately above the capillary fringe with the water table depressed 6.5 cm below the mean. This placed the organic phase in an unsaturated zone beneath an area contaminated with surrogate fuel, but above the water table. In the second and third columns, the organic phase was injected beneath the water table, but below the zone contaminated with JP-4. During the injections, the water table elevations for the second and third columns were at the high and low levels, respectively. The fourth column was selected to serve as the control. During the 12 hours following the decane/mineral oil injection, water tables in each column were fluctuated through one cycle of 4.5 cm above and below the mean water level.

Results.

Figure 1. illustrates the distribution of JP-4 and organic phase in column one and the distribution of JP-4 in the control. Under a UV light, it was evident that fluctuating the water table spread the JP-4 from a high located above the capillary fringe of the high water table to a low corresponding to the top of the capillary fringe of the low water table. The highest levels of jet fuel appeared to accumulate on the top of the prevailing capillary fringe. Test column No. 1 shows distinct layers of jet fuel and decane/mineral oil. Results from columns two and three indicate predictable layers of the jet fuel and the decane/mineral oil did not develop when injection of the organic phase occurred below the capillary fringe of the prevailing water table.

From these column experiments, we determined that the partition zone to be most easily constructed in situ when injection of the organic phase occurred in the unsaturated zone above the capillary fringe and not beneath the water table. This is consistent with the findings of Schwille and Pankow (1988), who found increased lateral spreading of an organic phase as the infiltrating phase reached the capillary fringe. The material spreading occurs because less pressure is needed to overcome the interfacial tension between the organic phase and air than the organic phase and water.

IV. COARSE SAND TANK EXPERIMENTS:

Materials and Methods.

Flow-through tank experiments were designed and conducted to elucidate practical concerns associated with in situ construction of the partition zones and to demonstrate the reductions in contaminant fluxes from a simulated jet fuel spill. Two plexiglass tanks were constructed with inside dimensions of 83.5 cm length, 46.5 cm height, and 3.0 cm width. One tank served as a control while the other functioned as the test. Figure 2. shows the general tank configuration. Water enters chamber A through a constant head reservoir, then exits chamber B through a stopcock. The two chambers were hand packed with the same coarse sand used in the column experiments. Chamber A received a direct injection of surrogate jet fuel, while, chamber B was monitored for changes in water quality; note in figure 2. the numbered sampling ports in chamber B.
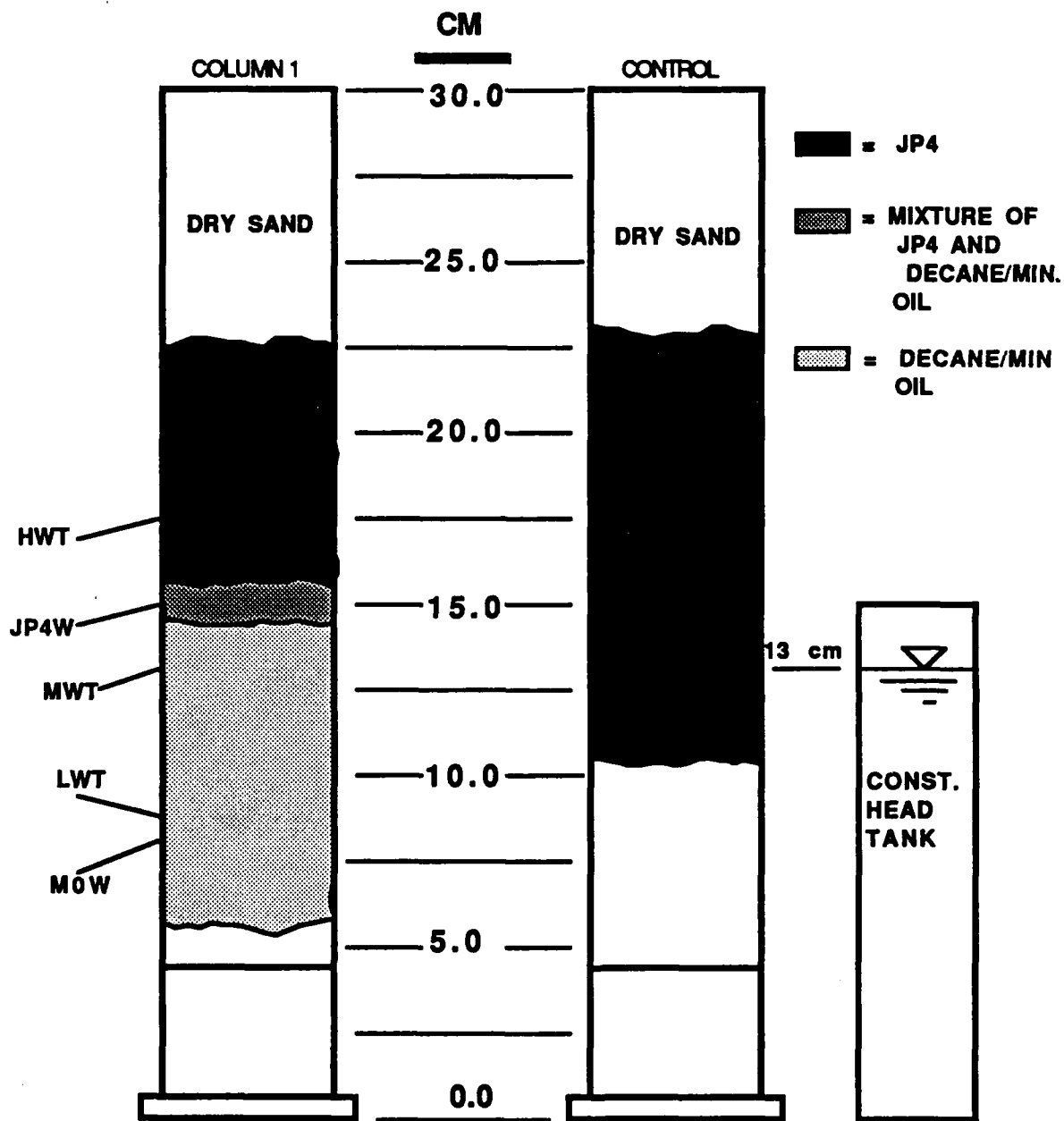
Figure 1. Comparison of JP-4 and Decane/mineral oil distributions in the test column Number 1 and in the control column. HWT (high water table), JP-4W (elevation of JP-4 injection), MWT (mean water table), LWT (low water table), and MOW (elevation of decane/mineral oil injection).
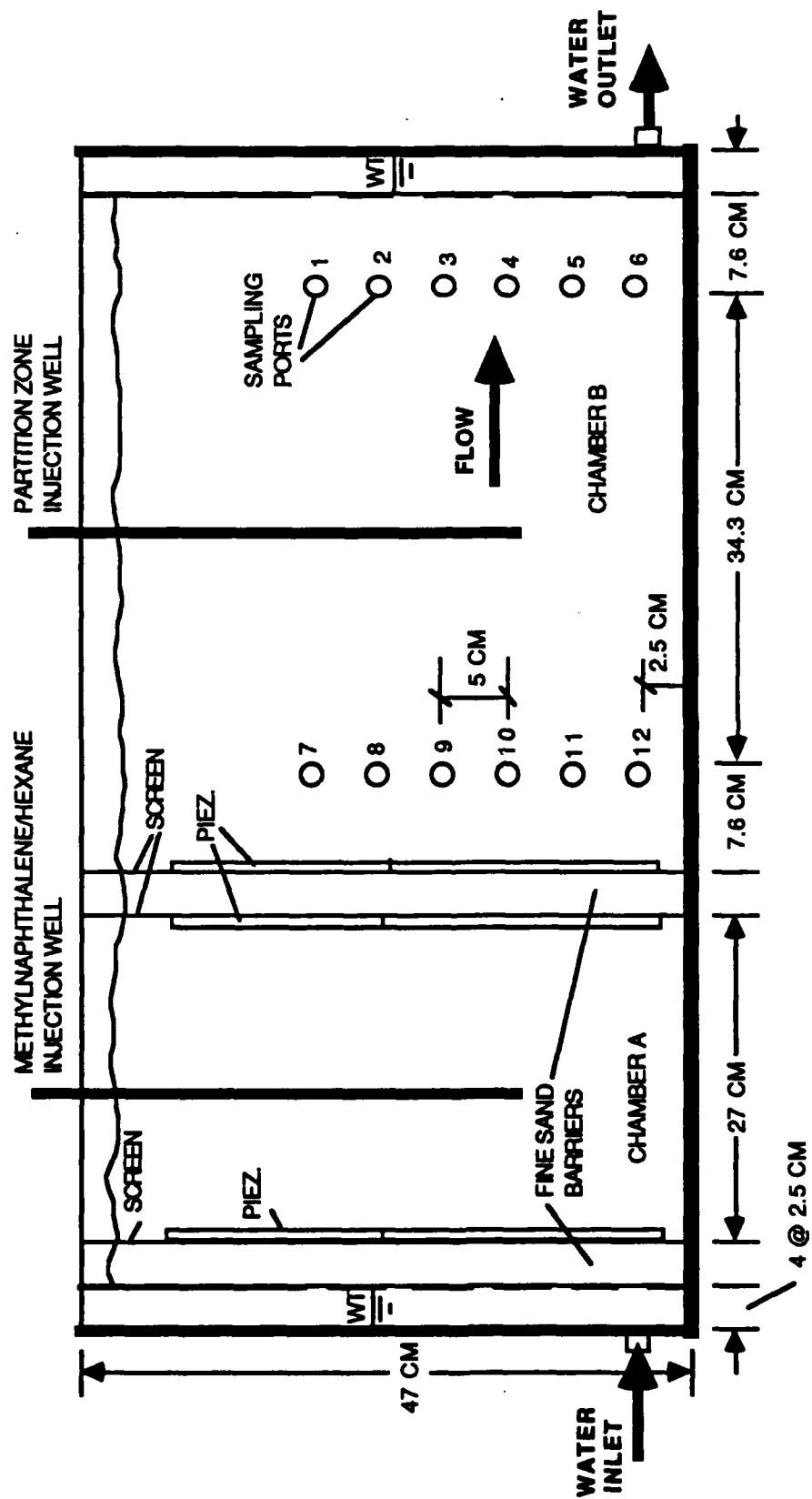
Figure 2. Configuration of the flow-through tank.

1-Methylnaphthalene/hexane (23/77 v/v and s.g. 0.74) was used in the experiments as an equally dense surrogate for JP-4. A surrogate was used because the chemical partitioning of a single constitute (i.e., methylnaphthalene) is easier to follow than the multiple components of JP-4. Methylnaphthalene is relatively insoluble and nonvolatile; therefore, experimental concentrations of methyl-naphthalene should reflect representative contaminant levels down-gradient from weathered or vented fuel spills.

Both tanks were saturated to a mean flow depth of 20.0 cm and allowed to equilibrate overnight. The experiment began with the 30 ml subsurface injection of the methylnaphthalene/hexane solution inside chamber A of each tank. Injection occurred at 21.9 cm (on top of the capillary fringe), and then the water table was adjusted through 11.0 cm to 29.0 cm and back to 20 cm.

Efforts were then directed at creating a horizontal partition zone in chamber A of the test tank; the zone would rest between an area contaminated with surrogate fuel and the moving groundwater flow field. The water table was lowered to 7.0 cm when 90.0 ml of the decane/mineral oil (20/80 v/v) was injected at 8.9 cm (beneath the surrogate fuel, but above the capillary fringe of the depressed water table). Finally, water levels in both tanks were returned to 20.0 cm.

At frequent intervals, flow measurements were taken while 6.0 – 9.0 ml water samples were collected from ports in chamber B of both the control and test tanks. Sample analyses were performed on a Varian 3700 gas chromatograph. The samples were initially shaken with a 0.5 ml hexane extracting solution containing an internal standard of ca. 20.0 mg/l naphthalene, and then concentrations of methylnaphthalene were determined from a 1.0 ul splitless injection of the extract onto 30 m SPB-5 column with flame ionization detection. The temperature of the column was 150 °C. Split flow was resumed 0.5 minute after injection.

After 48 hours, preparations were made to create vertical partition curtain between sampling ports in chamber B of both tanks. First, the water table was lowered in each tank to 7 cm. Next, 40.0 ml of decane/mineral oil was injected above the capillary fringe (8.9 cm) of both the control and test tanks. The water table was twice adjusted

between mean (20 cm) and low (11 cm) water table elevations before sampling resumed at mean flow depth.

After an additional 48 hours, the water table was raised to 29 cm. Sampling continued for another 100 hours before both tanks were sealed and placed in a -65 $^\circ$C freezer until frozen. Later, both tanks were sacrificed to obtain soil samples that were analyzed for total organic carbon (TOC), total methylnaphthalene, and volatile solids. A LECO 112 carbon determinator was used to obtain raw sample TOCs. Total methylnaphthalene levels were determined using the procedure developed for the water samples, except that 3.0 ml of hexane extract (instead of 0.5 ml) was shaken with 1.3 - 3.0 g of soil (instead of water). Volatile solids were determined following the procedure outlined in Standard Methods for the Examination of Water and Wastewater (APHA, AWWA, and WPCF, 1985).

<u>Results</u>.

The injection of surrogate fuel or decane/mineral oil generally formed a layer 1 to 4 cm thick above the capillary fringe. Fluctuating the water table smeared the phases from the capillary fringe of the high water table to the top of the capillary fringe of the low water table. In the test tank where both decane/mineral oil and surrogate fuel were injected in chamber A, multiple smear zones developed with decane/ mineral oil on the bottom, a transition zone of both organic phases above that, and finally, an upper layer of methylnaphthalene/ hexane.

The natural bulk organic content of the sand was found to be 0.3 mg/cm^3. Soil analyses determined the mass of decane/mineral oil per unit volume of coarse sand to range 9.2 to 38.8 mg/cm^3 in the vertical partition zones. Methylnaphthalene varied 0.05 to 8.38 mg/cm^3 in the spill zones. The observed distributions for both organic phases are illustrated in figure 3. for the test tank.

A total of 77 and 70 pore volumes of water were eluted through the control and test tanks, respectively; a pore volume was defined as the void volume in the saturated flow zone between the columns of sampling ports. Pore velocities averaged 3.27 m/day for the control and 4.17 m/day for the test. The average hydraulic conductivity of 1.23 cm/s was estimated from multiple measurements of flow and water levels.
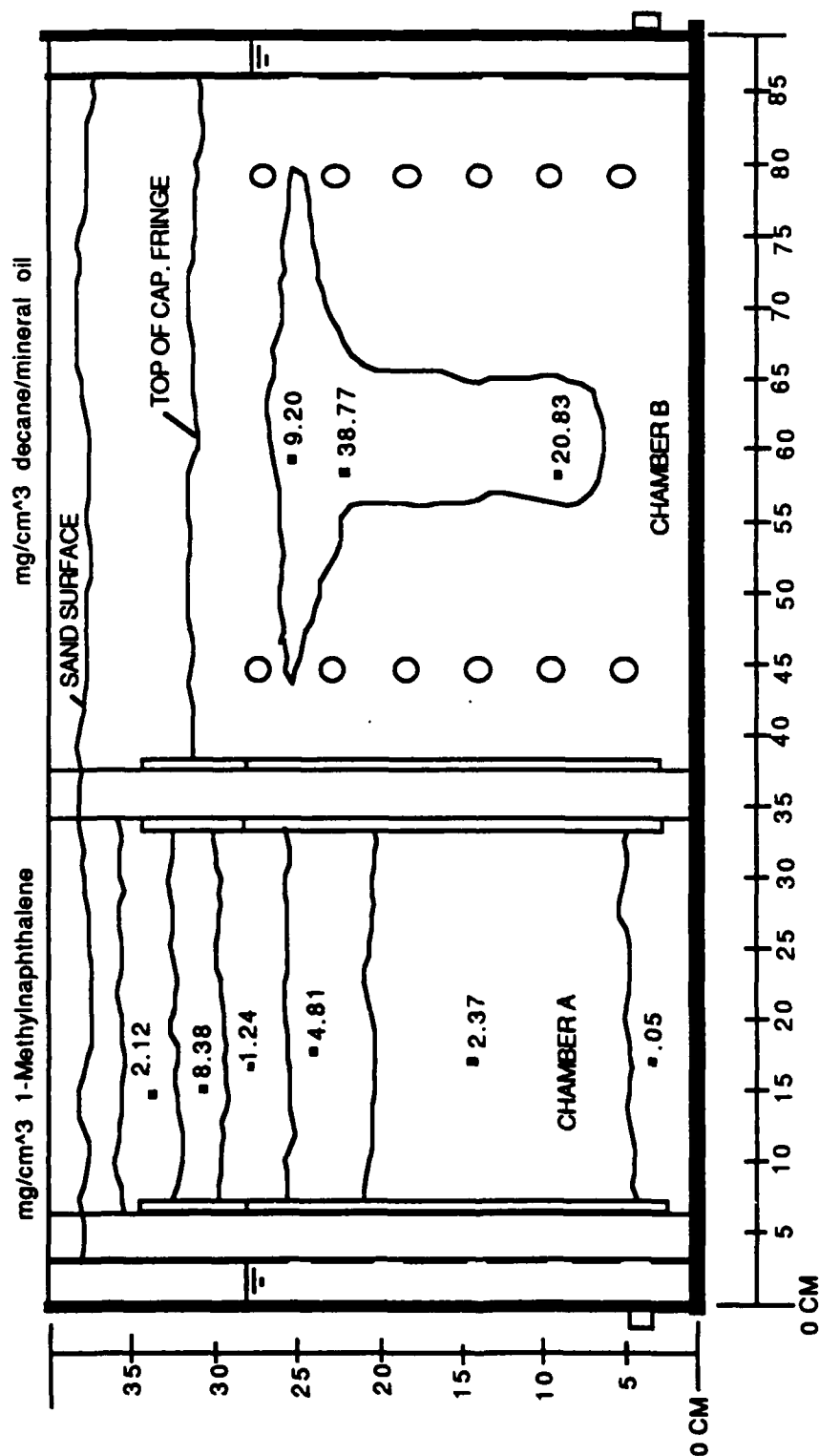
Figure 3. Distribution of 1-Methylnaphthalene and decane/mineral oil in the test tank of the coarse sand flow-through tank experiment

Dissolved methylnaphthalene concentrations were generally highest in ports situated near the water table. Figure 4. depicts typical concentrations from ports 4 and 10 of the test tank (see figure 2. for clarification). Concentrations in the test tank, prior to the installation of the vertical partition curtain, were about half that of the control because of the horizontal partition zone in chamber A of the test tank. After the vertical partition curtains were created, it was evident in both the control and test tanks that methylnaphthalene concentrations dropped 86 to 95 percent between ports of equal elevation (i.e., 9-3, and 10-4). Raising the water table submerged ports 7, 1, 8, and 2. Reductions continued to be high except between ports 7 and 1, where the partition zone did not completely intersect the flow path. The high flux reductions raised concerns that water was not flowing through the partition zone; however, an injection of an anionic red food coloring into the test tank at ports 7 through 12, showed that parallel flow was occurring throughout the partition zone.

Results indicate the vertical partition configuration is much more effective than the horizontal. However, the effectiveness of a given system depends on the distribution of decane/mineral oil in space and if the partition zone adequately intercepts contaminated groundwater flow.

V.   FINE SAND TANK EXPERIMENTS:

Materials and Methods.

Flow-through tank experiments were also performed with a fine sand. A sieve analysis on the sand determined the effective size and uniformity coefficient to be 0.24 and 1.67, respectively. The porosity was 0.37 and the bulk density 1.57. These tank experiments were conducted in the same general manner as the experiments with the coarse sand. However, several differences should be noted. First, the amount of surrogate fuel injected in chamber A of each tank was limited to 15.0 ml. Second, these experiments focused on the contaminant flux reductions produced from a vertical partition zone in chamber B of the test tank; no decane/mineral oil was injected into the control tank. Third, limitations on the tank dimensions required direct injection of both the surrogate fuel and the decane/mineral oil within the capillary fringe. The surrogate fuel was injected at 16.0 cm and the
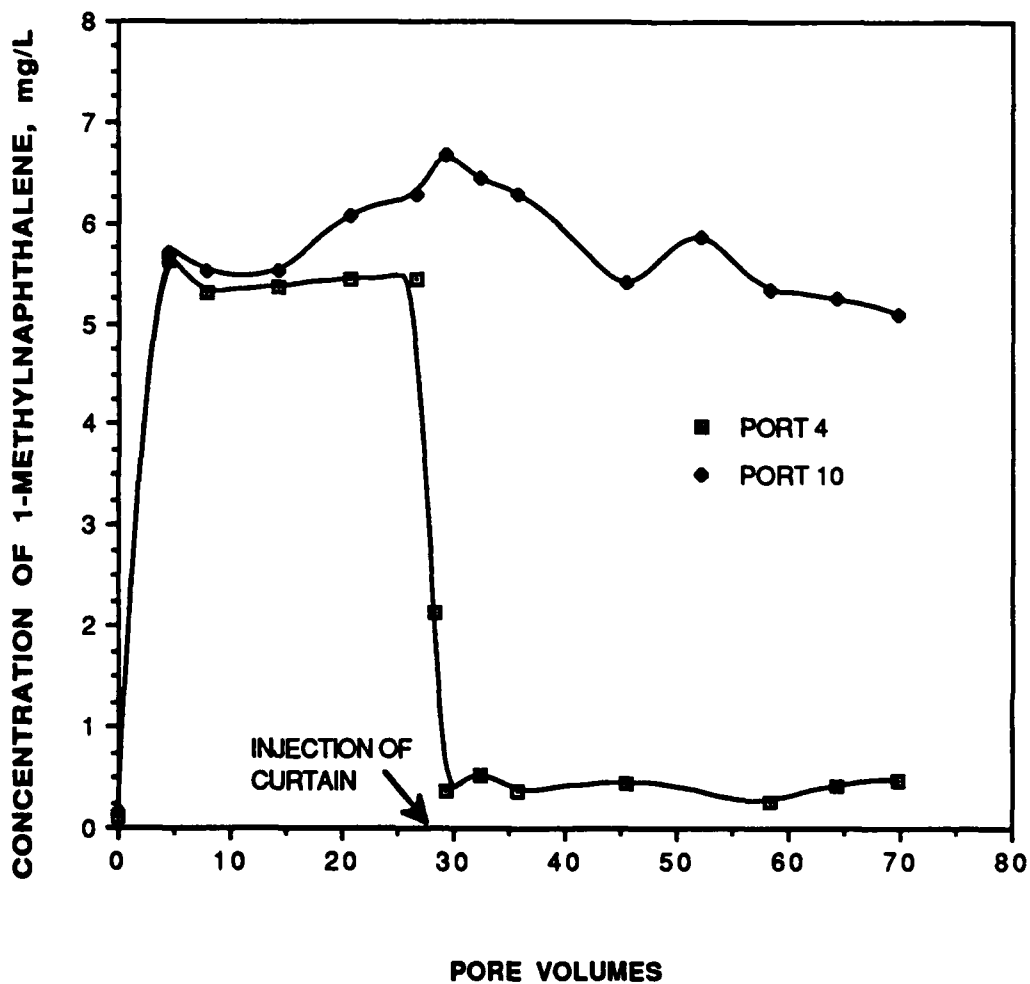
Figure 4. From the coarse sand flow-through tank experiments: concentrations of 1-Methylnaphthalene on opposite sides of the partition curtain versus pore volumes.
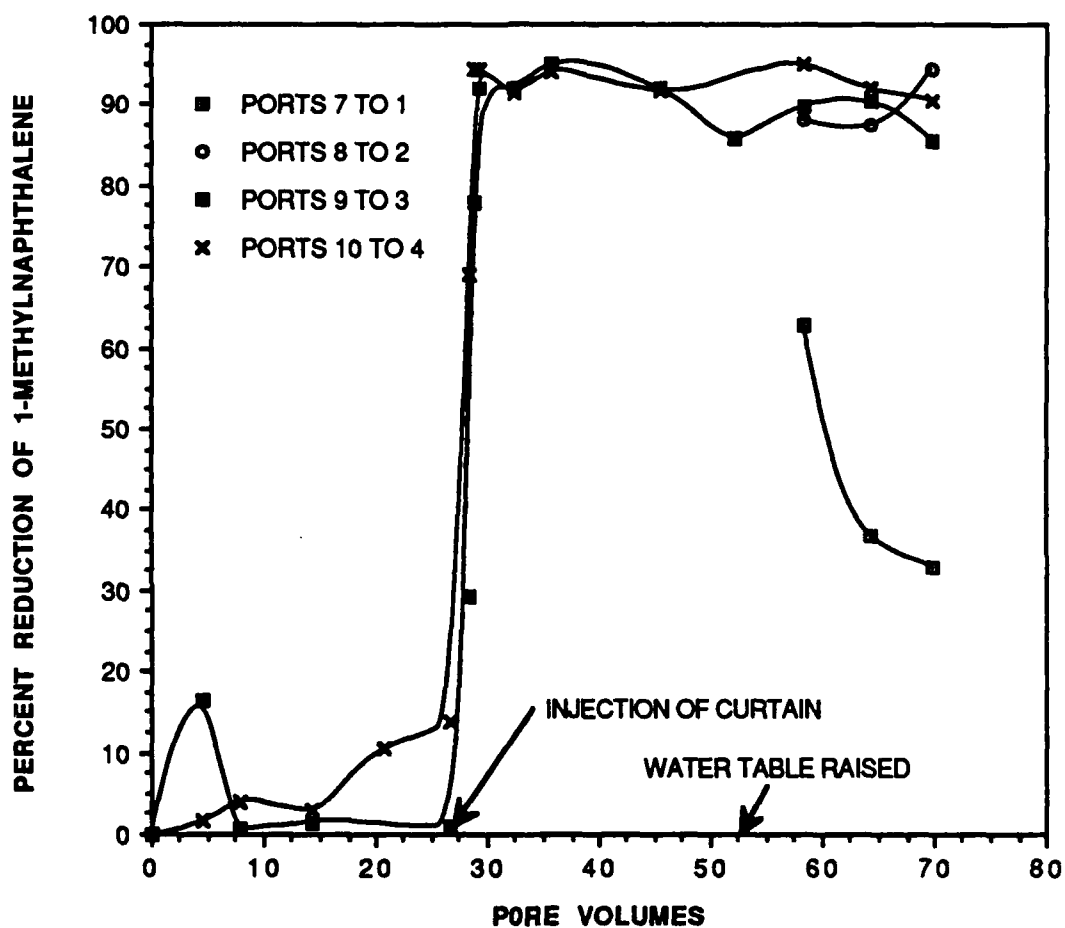
Figure 5. From the coarse sand flow-through tank experiments: reductions of 1-methylnaphthalene across the partition curtain versus pore volumes.

decane/mineral oil was injected at multiple elevations ranging from 10.0 to 20 cm. All injections occurred with the water table depress to 4.0 cm. Fourth, the decane/mineral oil was 66.7 percent decane and 33.3 percent mineral oil by volume. Finally, the decane/mineral oil injections occurred twice; in the beginning (31.5 ml) and then 72 hours later (85 ml). Water samples were collected at frequent intervals for 148 hours until the tanks were sealed and frozen. Methods of soil analysis were as previously described.

Results.

For these experiments, the methylnaphthalene/hexane and the decane/mineral oil were both injected the capillary fringe. Consequently, less lateral spreading of the phases occurred than with the coarse sand. The vertical partition zone in the test tank looked similar to the one depicted in figure 3. The natural bulk organic content of the fine sand was 0.32 mg/cm^3. Measured levels of methylnaphthalene per unit volume of sand were 0.003 to 18.02 mg/cm^3 for the test tank; therefore, the organic phase filled less than 11.0 percent of the available pore volume.

A total of 63 pore volumes of water were eluted through the control while 57 pore volumes passed through the test tank. Estimated pore velocities were 3.25 and 3.59 m/day for the test and control, respectively. The hydraulic conductivity of the sand was found to be 0.04 cm/sec.

Typical concentrations of methylnaphthalene from the upper ports of the test tank are shown in figure 6. The concentrations in port 8 (upgradient from the vertical partition zone) were comparable to the control The initial injection of decane/mineral oil produced flux reductions between ports 8 and 2 that were no greater than 30 percent (see figure 7). After additional decane/mineral oil was added (the second injection), observed reductions increased in the upper three ports to levels of 98.4 to 99.9 percent. The lower three sets of ports had essentially no measurable levels of methylnaphthalene. Parallel flow paths through the partition zone were verified when an anionic green food coloring was injected into the test tank at ports 7 through 12.

Higher flux reductions were observed with the fine sand than with the coarse. Clearly, different decane/mineral oil solutions with
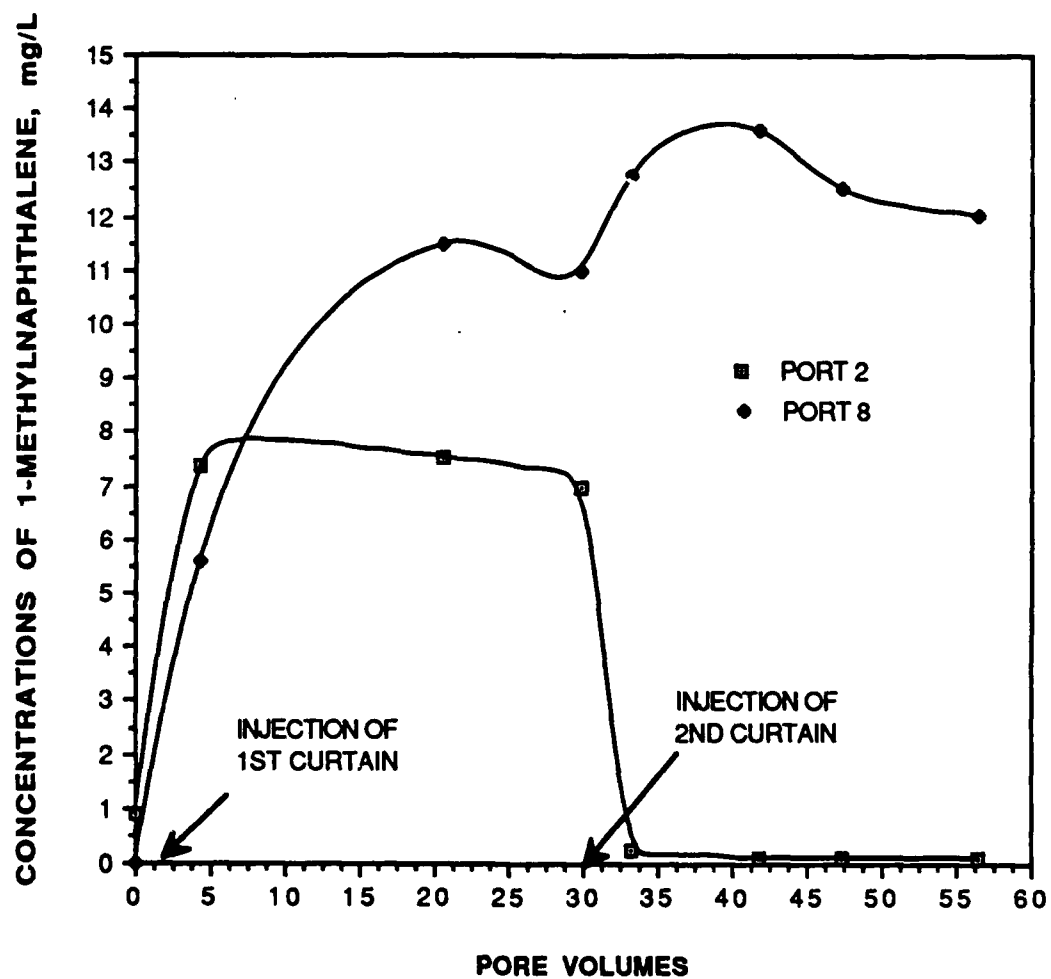
Figure 6. From the fine sand flow-through tank experiment: concentration of 1-methylnappthalene on opposite sides of the partition curtain versus pore volumes.
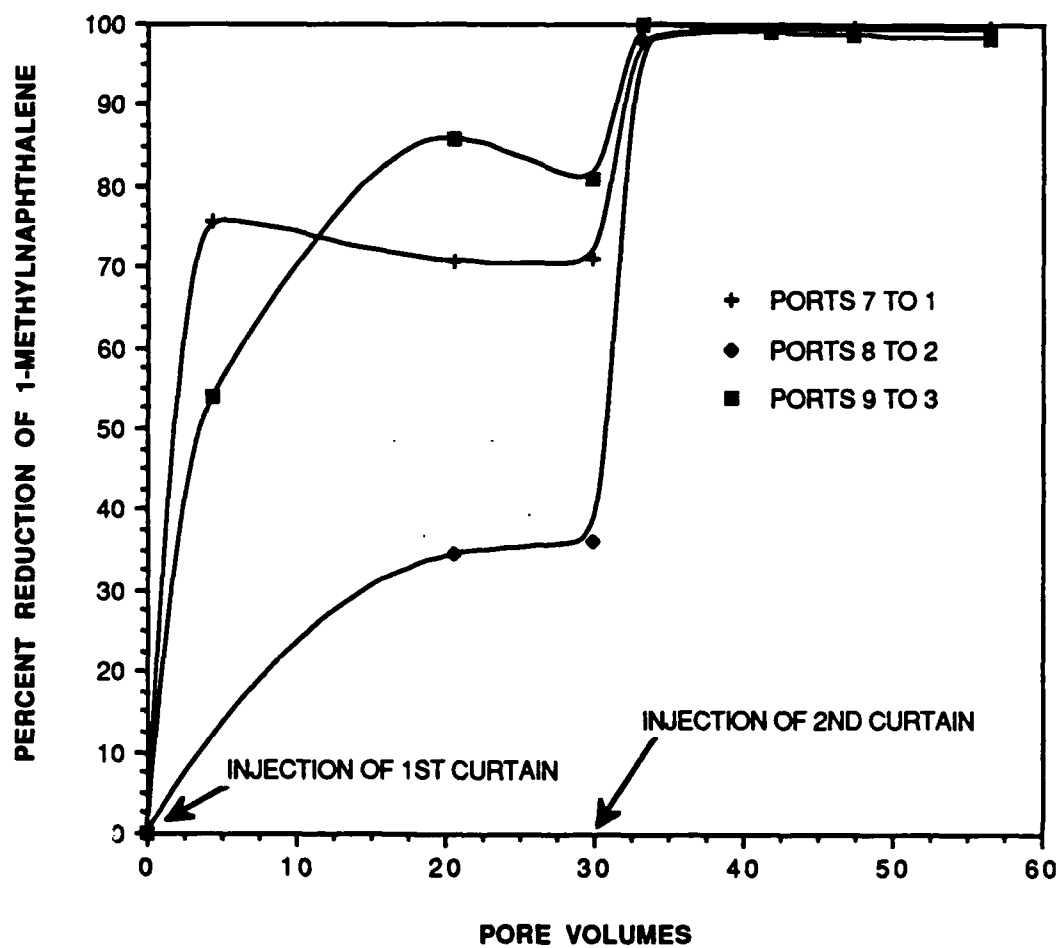
Figure 7. From the fine sand flow-through tank experiments: reductions of 1-methylnaphthalene across the partition curtain versus pore volumes.

different partition coefficients were used between experiments. The next section presents results indicating a larger partition coefficient for the decane/mineral oil solution used with the fine sand. In addition, a large volume of decane/mineral oil was added to the fine sand system.

VI.   CHEMICAL PARTITION EXPERIMENTS:

Methods and Materials.

These experiments were designed to determine the equilibrium partitioning of methylnaphthalene between water and the decane/mineral oil. Two solutions were made. Solution A was 49.5 ml of decane/mineral oil (20/80 v/v; s.g. 0.8213) and 0.5 ml methylnaphthalene (s.g. 1.024). Solution B was 49.5 ml decane/mineral oil (66.7/33.3 v/v; s.g. 0.7732) and 0.5 ml methylnaphthalene. Two saturation flasks were prepared with 250.0 ml of distilled water and a small magnetic stir bar. Into one flask went 5.0 ml of solution A and into the other flask went 5.0 ml of solution B. After 72 hours, water samples (6-7 ml) were withdrawn and the concentration of dissolve methylnaphthalene determined in the same manner as with the water samples from the tank experiments.

Results.

The methylnaphthalene concentrations in water from the flask spiked with solution A were determined to be 1.3 mg/l, while the water equilibrated with solution B had 1.2 mg/l. From these concentrations, partition coefficients K were calculated where

$$K = \frac{[mg\ methylnaphthalene/mg\ decane/mineral\ oil]}{[mg\ methylnaphthalene/mg\ water]}$$

The partitioning between water and the 20 percent decane/80 percent mineral oil was 9650. Increasing the decane fraction in the organic phase to 66.7 percent increased the partition coefficient to 11100.

The equilibrium partition coefficients for two decane/mineral phases can be used to obtain estimates of the time duration to 100 percent breakthrough for the associated partition systems studied in the fine and coarse sands. Assuming a partition zone 1 meter thick and a groundwater flow of 0.3 m/day, the time to breakthrough for the coarse sand system would be 5.1 years and 8.5 years for the fine sand system. The estimates were made using the average of observed values for the mass of decane/mineral oil per bulk volume of sand (23.0 mg/cm^3 for the coarse and 31.0 mg/cm^3 for the fine).

VII. RECOMMENDATIONS:

This research effort has demonstrated that in situ solubility modification can lead to significant reductions in contaminant fluxes in porous media. The operation of the partition system is passive with contaminant removal occurring as local groundwater gradients force flow through the partition zone. Small partition systems, on the order of 1 meter in length, can potentially delay downgradient groundwater contamination for upwards of 5 to 8 years.

Further work is needed to make these systems viable in the field. First, we need to develop the capability of predicting the subsurface movement of the organic phase used to create the partition zone. Research on multiphase flow is needed which will provide the capacity to predict the shape of the partition zone and distribution of the organic phase in the porous media. This research will also reveal changes in the flow field that should occur when the partition zone is installed. Second, we need to better understand the chemistry behind the chemical partitioning. Developing our understanding through column breakthrough experiments will provide the necessary data to predict the performance and longevity of partition systems. Combining results of research suggested above will lead to systematic design of partition systems and the prediction of performance.

REFERENCES

1. APHA, AWWA, and WPCF, Standard Methods for Examination of Water and Wastewater, 16th Edition, American Public Health Association, Washington, DC 20005, 1985, pp. 97-98.

2. Schwille, F. and J.F. Pankow, Dense Chlorinated Solvents in Porous and Fractured Media: Model Experiments, Lewis Publishers, Chelsea, Michigan, 1988, p. 7.

1989 USAF-UES SUMMER FACULTY RESEARCH PROGRAM/
GRADUATE STUDENT RESEARCH PROGRAM

Sponsored by the
AIR FORCE OFFICE OF SCIENTIFIC RESEARCH
Conducted by the
Universal Energy Systems, Inc.
FINAL REPORT

AN FT-IR SPECTROSCOPIC INVESTIGATION OF SURFACTANT ADSORPTION
AT THE MINERAL-WATER INTERFACE

Prepared by:	Dr. Kim F. Hayes
Academic Rank:	Assistant Professor
Department and	Civil Engineering
University:	University of Michigan
Research Location:	AFESC/RDVS
	Tyndall AFB, FL 32403
USAF Researcher:	Dr. Dan A. Stone
Date:	September 20, 1989
Contract No.:	F49620-88-C-0053

AN FT-IR SPECTROSCOPIC INVESTIGATION OF SURFACTANT ADSORPTION AT THE MINERAL-WATER INTERFACE

by

Dr. Kim F. Hayes

ABSTRACT

An ATR (Attenuated Internal Reflection) FT-IR (Fourier Transform Infrared) spectroscopic study of the adsorption of propionic acid at the γ-Al_2O_3-water interface has been conducted. The main objective of this effort was to demonstrate the feasibility of using ATR FTIR spectroscopy to investigate the structure and orientation of surfactants adsorbed at mineral-water interfaces. The results of the study indicate that the FT-IR method has sufficient sensitivity to detect IR bands of sorbed surfactants. Further work is required before the spectral features that were observed can be fully interpreted. It is postulated that a surface complex was formed between the carboxylic acid functional group of propionic acid and a surface aluminol group. The need for FTIR spectroscopic studies of surfactant-mineral interactions and the application of surfactants to spill sites as a means of spill containment and remediation is discussed.

ACKNOWLEDGEMENTS

I thank the Air Force Systems Command, Air Force Office of Scientific Research, Universal Energy Systems and the Air Force Engineering and Services Center for their sponsorship and administration of this research.

Certain individuals should be mentioned by name for their contributions to making this research possible. In particular, I am indebted to Dr. Dan A. Stone for sharing his expertise, equipment, and time, and to Dr. Terence T. Tipton and Sgt. Jim Whitcomb for helping with my day to day research needs. Special thanks also to Mr. Perry Sullivan for overseeing the administration of my summer visit and to Drs. Thomas Stauffer and David Burris for stimulating discussions about future research needs of the Air Force.

FT-IR SPECTROSCOPIC STUDY OF SURFACTANT ADSORPTION AT THE MINERAL OXIDE/WATER INTERFACE

I. INTRODUCTION

Containment and cleanup of groundwater contaminated by jet fuel spills at US Air Force bases is an area of growing concern. One way to control pollutant migration or to remove contaminants from spill sites is to introduce surfactants (surface active agents) into groundwater aquifers. These agents can change the chemical properties of the interfacial regions between the fuel, water, and aquifer solids and change the mobility of water-soluble and insoluble portions of spilled fuel. A better understanding of the chemical interaction of surfactants with aquifer material is required before we can effectively apply this method to the remediation of contaminated sites.

The Environics Division of the Air Force Engineering and Services Center at Tyndall AFB (Florida) is responsible for Air Force Environmental Quality Research and Development Programs. In-house research is conducted in atmospheric and groundwater chemistry, microbial degradation, and groundwater and industrial waste treatment. Specialized equipment includes computer-controlled Fourier Transform Infrared (FT-IR) Spectrometers equiped with Horizontal Flat-Plate Crystals for chemical studies of surfactant adsorption at mineral-water interfaces. The facilities and on-going research efforts at Tyndall AFB are ideally suited for conducting studies of surfactant adsorption effects on surface chemical properties of aquifer material, and how changes in aquifer properties caused by surfactant adsorption might influence efforts to contain and cleanup jet fuel spills.

My research focuses on the effects of changes in interfacial properties on contaminant transport and transformation processes of aqueous systems. In recent work, I have conducted spectroscopic studies to determine the structure and composition of toxic, inorganic, metal ions at mineral-water interfaces and how metal ion sorption affects interfacial properties (Hayes, 1987; Hayes et al., 1988)). A natural extension of this work is to investigate, spectroscopically, how organic solutes, such as surfactants, change the chemical properties of the interfacial regions, and hence, organic contaminant transport. My previous spectroscopic work and current interest in containment and cleanup of aquifers

contaminated by hazardous organic compounds, such as jet fuels, contributed to my assignment to the Environics Division at Tyndall AFB.

II. OBJECTIVE OF THE RESEARCH EFFORT

To date there have been few spectroscopic investigations of surfactant sorption at mineral-water interfaces. Few studies have been conducted because of the lack of sensitivity of most spectroscopic methods to detect relatively small concentrations of surfactant (typically much less than 0.1 mole %) in the presence of relatively large concentrations of water or solid. One promising method is ATR (Attenuated Total Reflection) FT-IR (Fourier Transform Infrared) spectroscopy (Harrick, 1985; Mirabella and Harrick, 1985; Griffiths and de Haseth, 1986). In general, infrared (IR) spectroscopy can be used to identify the structure and orientation of molecules. Shifts in the IR vibrational energy of chemical functional groups, like $-CH_2$, $-OH$, $-COOH$, reflect changes in these groups' local coordination structure. The magnitude and direction of chemical shifts of molecular vibrational modes are used to infer local structure at the interface.

IR studies with water present have been problematic because water absorbs strongly in the mid-range IR region (4000 to 250 cm^{-1}), thus masking many of the vibrational modes of organic functional groups. The introduction of attenuated total reflection (ATR) cells (Harrick, 1967) overcame this difficulty by providing a means of focusing the pathlength of light on the interfacial region. This method provides an enhancement of the signal coming from an adsorbed species near the ATR plate relative to water. With the advent of computer-controlled, rapid-scanning FT-IR spectrometers, several thousand spectral scans can be performed on a single sample. Background spectra of water similarly collected can be accurately subtracted from signals coming from dilute solutes. The result is that previously hard-to-detect spectral features of sorbed molecules can now be enhanced sufficiently to make in-situ (i.e., in the presence of water) studies of sorbed molecules possible. Recent studies have shown that ATR-FT-IR can be employed successfully in aqueous systems to probe the structure and composition of inorganic and organic acids sorbed at water-mineral interfaces. (Tejedor-Tejedor and Anderson, 1986; Yost, 1986; Zeltner et al., 1986; Leppinen et al., 1988). In non-aqueous systems, others have shown that the structural orientation of surfactants can be determined (Kimura et al., 1986; Allara and Nuzzo et al., 1985; Ganguly and Mohan, 1988).

The main objective of my work performed during the Summer Faculty Research Program

appointment was to establish the feasibility of using FT-IR spectroscopy to investigate the structure and orientation of surfactant molecules sorbed at mineral/water interface. This information is needed to develop a quantitative theory relating surface chemical property changes to surfactant adsorption and mineral surface wettability. This type of information, in turn, is needed to select the appropriate surfactant for groundwater containment or remediation.

III. EXPERIMENTAL SETUP, RESULTS AND DISCUSSION.

Experimental Systems and Conditions. The system to be studied in this project was chosen to be representative of that found at organic contamination spill sites, but simple enough so that the relevant chemical properties could be manipulated in a known and characterizable way. The range of conditions (pH, ionic strength, or surfactant concentration) considered were either those expected at contamination sites or those needed to affect significant changes in the properties measured (e.g., amount sorbed). Since the goal of the summer project was to test the feasibility of the ATR-FT-IR method, in this preliminary study, optimal system conditions and constituents were chosen. These included choosing a surfactant with relatively well known IR and simple solution spectra, an electrolyte which would not mask the important IR region for surfactant functional groups (e.g., $1000 \, cm^{-1}$ to $2000 \, cm^{-1}$), a sorbent to which the chosen surfactant would sorb strongly, and a pH range where maximum surfactant sorption would occur.

In this study, the oxide mineral, γ-Al_2O_3, was used. The aluminol (Al-OH) groups on the surface of alumina have properties representative of the amphoteric surface sites of soil material, and hence provide a good model for the type of interactions expected between surfactants and surface sites of minerals found in contaminated aquifers such as sands, aluminosilicate rocks, and clay minerals. Since the most permeable zones of aquifers are the zones of most concern for hazardous material transport in groundwater, interactions with mineral surface sites, as opposed to interlayer clay sites, are the more relevant to study. Previous studies have shown that anionic surfactants like the one chosen for this study sorb relatively strongly to aluminum oxide (Ulrich et al., 1988).

To demonstrate the feasibility of using FT-IR for investigating the interaction of surfactants with mineral surfaces the fatty acid, propionic acid (C_2H_5COOH) was chosen. Propionic acid has a hydrophobic (C_2H_5) and a hydrophilic (-COOH) moiety, a feature common to

many amphipathic surfactants, and sorbs relatively strongly to γ-Al_2O_3. It also has a reasonably simple and well known IR spectrum. These features made it a good choice for this initial study.

Research Approach. The summer research experimental program had two parts: (1) Adsorption Measurements, and (2) FT-IR Spectroscopic Measurements.

Adsorption Measurements. In the adsorption experiments, the quantity of solute sorbed to the solid is typically determined by the loss of solute from the liquid phase. The protocol to be followed in these experiments was as follows. A series of 3.5 ml tubes was assembled. To each tube, the liquid and solid were added first. Then surfactant, appropriate radiotracers (^{14}C labeled propionic acid), background electrolyte (NaCl), and acid (HCl) or base (NaOH) were added in the appropriate amounts. The actual amounts were adjusted so that the total ionic strength and surfactant concentrations were held constant for a range of pH values. The pH was varied by adding different amounts of acid or base to each tube.

Mixing was accomplished by end-over-end rotation of the 3.5 ml reactor tubes. A pH meter equipped with a combination electrode was used to measure the pH in the aqueous phase. The amount of surfactant adsorbed was determined using radiotracers by analyzing the supernatant for radioactivity following solid/liquid separation. Solid/liquid separation was accomplished by centrifugation. To analyze the level of radioactivity, an aliquot of the surpernatant is mixed with a phosphor cocktail and its activity counted with a scintillation counter.

FT-IR Measurements. In this study a Nicolet 740 Series spectrometer with an ATR horizontal flat-plate sampling boat and germanium crystal (transmission from 800 cm^{-1} to 5000 cm^{-1}) was used to collect the FT-IR spectra. The details of the apparatus and measurement technique can be found elsewhere (see, e.g., Yost, 1986).

FT-IR Sample Preparation and Anaylsis. Sorption samples for FT-IR analysis were prepared as discussed above. After 24 hours of equilibration time in the batch reactors, the suspension samples were centrifuged and placed as a wet paste onto the horizontal ATR germanium plate. Spectra were collected for the supernatant and the centrifuged, but wet paste. The final sorption spectrum was obtained by subtracting the supernatant spectrum from the sorption sample spectrum, both of which had been previously corrected against the

empty cell background. Each spectrum was the result of 1000 co-added spectra collected at $4\ cm^{-1}$ resolution.

Results and Discussion. The summer program was divided into three major tasks to accomplish the research ojectives: (1) to perform soprtion studies to determine the solution conditions required for maximum propionic acid (PA) sorption, (2) to obtain the necessary solution and background FT-IR data for spectral analysis, and (3) to obtain a useable spectroscopic signal from ATR FT-IR measurements for propionic acid sorbed to γ-Al_2O_3.

The first portion of the summer effort went into the determination of the appropriate solution conditions where maximum adsorption of propionic sorption occurs at the γ-Al_2O_3-water interface. Adsorption measurements were made over a pH range of 3 to 10, an ionic strength range of 0.1M to 0.001M, and a total propionic acid (PA) concentration range of 10^{-2} M to 10^{-4} M. The pH adsorption behavior for propionic acid adsorption as a function of total PA concentration at an ionic strength of 0.03M (added as NaCl) is shown in Figure 1. As is common for fattty acid adsorption, the maximum sorption occurs near the pK_A, which for PA is 4.9. The adsorption maximum near the pK_A can be attributed to two opposing driving forces: (1) as the pH is lowered, the γ-Al_2O_3 surface is becoming more positively charged and the negatively charged propionate ion is attracted to the surface, and (2) at pH values below the pK_A, propionic acid becomes predominately a neutral species which favors the aqueous phase instead of the positively charged surface. This results in the observed sorption maximum near the pK_A. In the subsequent FT-IR study, the sample with a 10^{-2} M total PA, an ionic strength of 0.03M, and a pH value of 5.1 was used. This sample represented the highest surface coverage obtained from the sorption studies (50 μmoles PA sorbed/gm of sorbent).

Having established the conditions for maximum sorption, the next step was to obtain the appropriate propionic solution spectra which would be needed to interpret any useable spectra obtained from the sorption spectroscopic study. Figures 2 - 4 show the background and baseline corrected solution spectra for propionic acid at pH values of 2.8, 4.1, and 11.3, respectively. Figure 5 shows the spectrum resulting from the addition of 0.2M Al(III) to 0.5M PA at a pH value of 1.8. The main feature to compare among the spectra is the band near $1716\ cm^{-1}$. It appears in all of the spectra except the for the PA solution sample at the pH value of 11.3. This band can be attributed to a COOH stretching band. It shifts to lower frequency of $1540\ cm^{-1}$ when PA (C_2H_5COOH) dissociates to C_2H_5COO- (PA dissociates

at pH values below 4.9). At a pH of 4.1, PA has only partially dissociated and so both bands are observed in this system (Figure 3). At a pH of value of 2.8, PA is completely in the form of RCOOH so no band at $1544 \, cm^{-1}$ is observed (Figure 2). For similar reasons, at a pH of 11.3 only the RCOO- form is present so no band is observed at $1716 \, cm^{-1}$ (Figure 4). The appearance of a band at $1630 \, cm^{-1}$, as a shoulder to the band at $1718 \, cm^{-1}$, in the Al(III)-PA system (Figure 5) suggests that PA is forming a complex with the Al(III) species in solution. Shifts to lower wave numbers are indicative of metal ligand complex formation between carboxylic acid and the aluminum ion (Yost, 1986).

The final task in this study was to obtain a spectrum for PA sorbed onto γ-Al_2O_3. The background and baseline corrected spectrum for PA sorption onto γ-Al_2O_3 at pH of 5 is shown in Figure 6. As can be seen here, a significant band is observed near $1640 \, cm^{-1}$. While it is premature to unequivocably assign this band to a particular IR vibrational mode, it is close to the band ($1630 \, cm^{-1}$) that appeared in the Al(III)-PA system described above which was attributed to the formation of an aluminum carboxylate complex. These preliminary results indicate that ATR FT-IR spectroscopy will likely be very useful for understanding the interactions between surfactant molecules and mineral-water interfaces. A more complete spectroscopic study is certainly warranted.

IV. RECOMMENDATIONS

My summer research project has demonstrated that FT-IR spectroscopy has potential for investigating the structure and composition of surfactant molecules sorbed at the mineral-water interface. Further in-depth studies, based in this initial feasibility study, are needed to provide a molecular level understanding of the interaction between surfactants and surfaces. With this type of information we should eventually be able to engineer surfactant/mineral systems to accomplish objectives important to the needs of the Air Force. In particular, we need to know more about how surfactants interact with the various minerals that are found at jet fuel spill sites so that we can better evaluate this alternate surfactant technology as a means for site remediation. For example, surfactants may be useful for containment of jet fuel spills by increasing the sorption capacity of minerals near a spill site and thereby provide a protective barrier to solute transport way from the site, or they may be added to change the wettability characteristics of minerals so as to enhance the removal of immiscible fuel trapped in the porous minerals at the spill site. We need to know which surfactants will work for a particular site, based on the chemical properties of the surfactant and the minerals.

There simply was not enough time in the short ten-week period to both develop the methodology and to complete a thorough investigation of all surfactant types that might be added to and minerals that may be found at Air Force jet-fuel sites. However, the initial study has indicated that FT-IR work should be continued. In parallel with FTIR studies, a study of the interaction of a range of surfactant types with aquifer materials should be intitiated. This work is needed to better define which types of surfactants/mineral systems are worth investigating at the molecular level, and which systems would be most suitable for jet-fuel, spill-site remediation.

I will be applying to the AFOSR mini grant program with two objectives in mind: (1) to continue FT-IR investigations of surfactant adsorption at mineral/water interfaces, and (2) to initiate a sorption study to look at a suite of surfactant and mineral types for the purposes of determining which systems would be most relevant and suitable for further FT-IR study. For example, in the summer research program, I worked almost exclusively with a straight-chained, anionic surfactant and a simple amphoteric oxide mineral. Future studies should include other minerals that have surface chemical properties representative of other minerals types that might be found in abundance at spill sites, such as quartz and clays. Other surfactant types need to be evaluated as well, including longer-chained anionic and cationic surfactants.
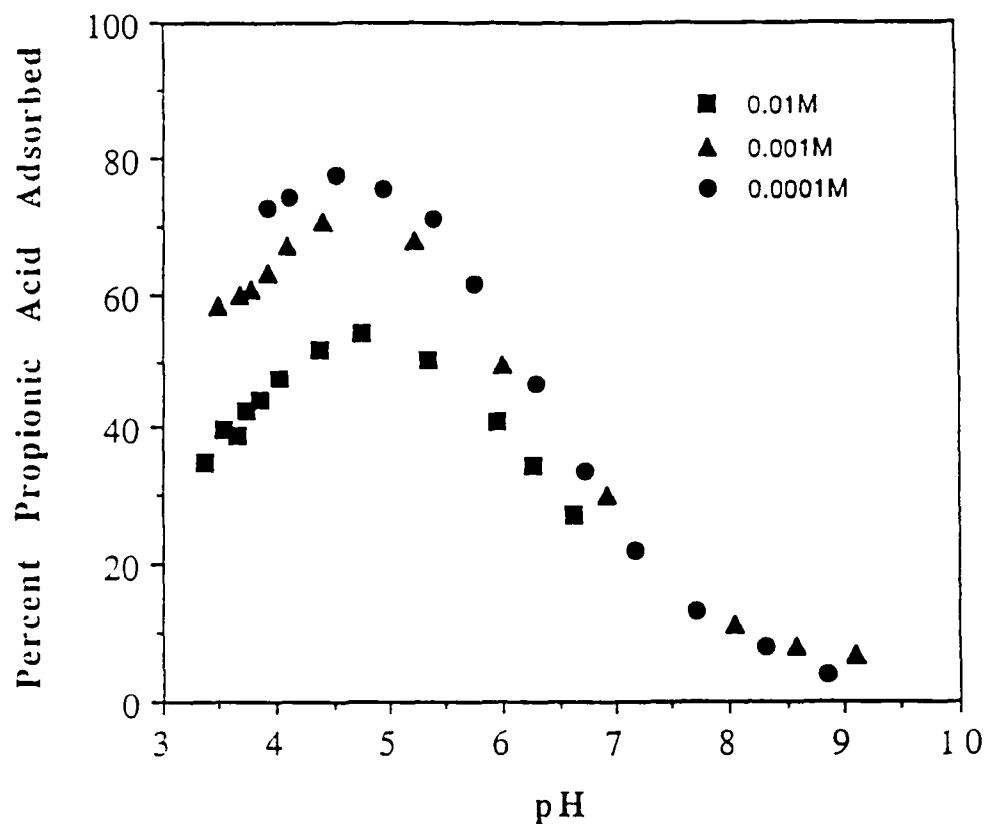
Figure 1. Percent propionic acid (PA) adsorption versus pH as a function of total PA concentration (100g/l γ-Al$_2$O$_3$; I = 0.03M as NaCl).
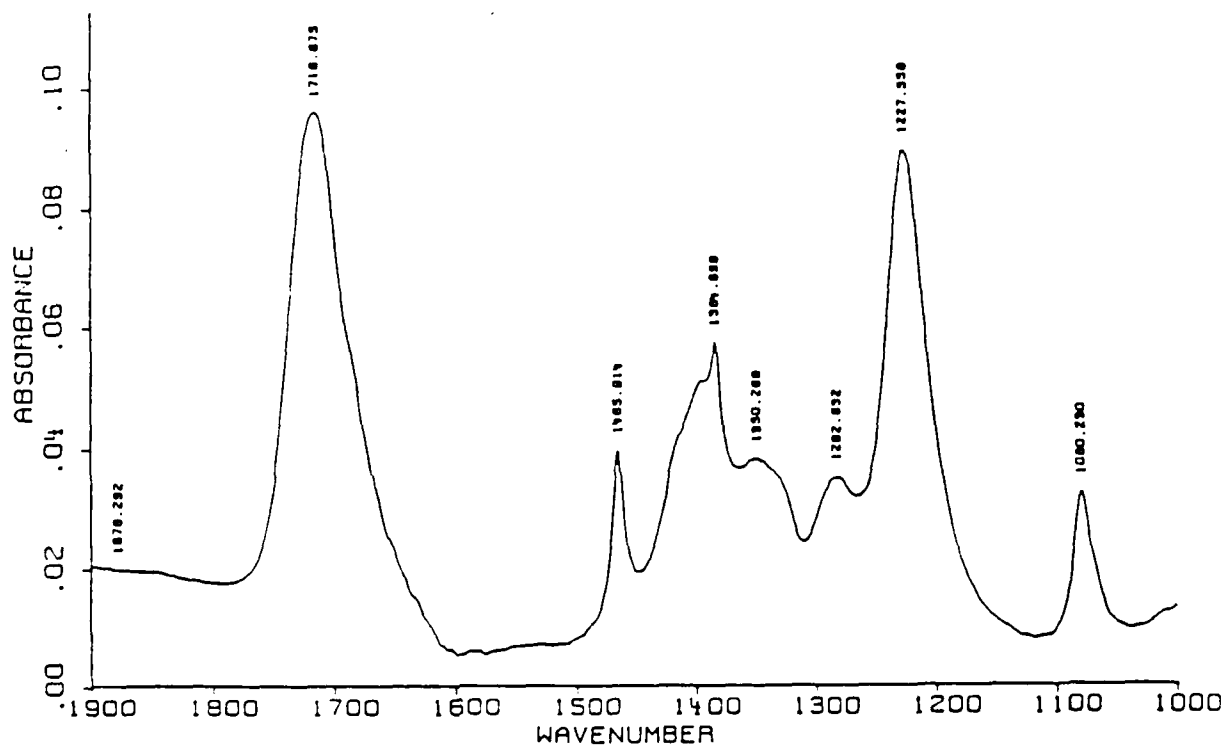
Figure 2. FTIR spectrum of a 0.5M propionic acid solution in 1M NaCl at pH = 2.8.
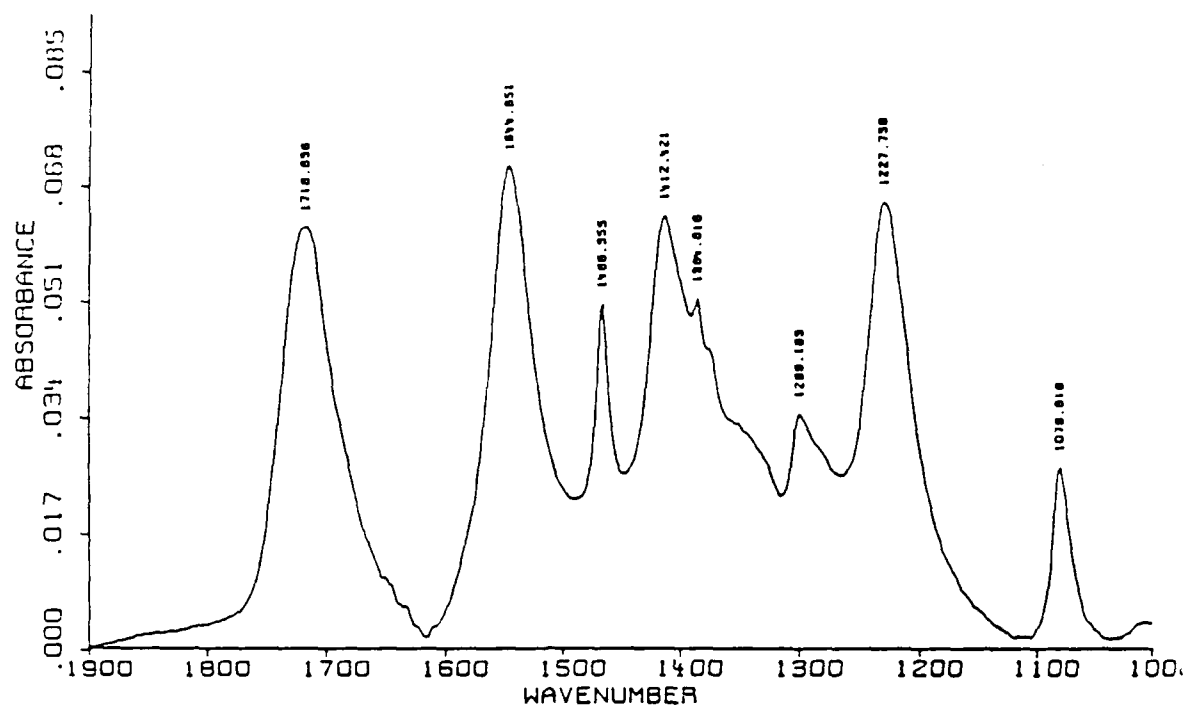
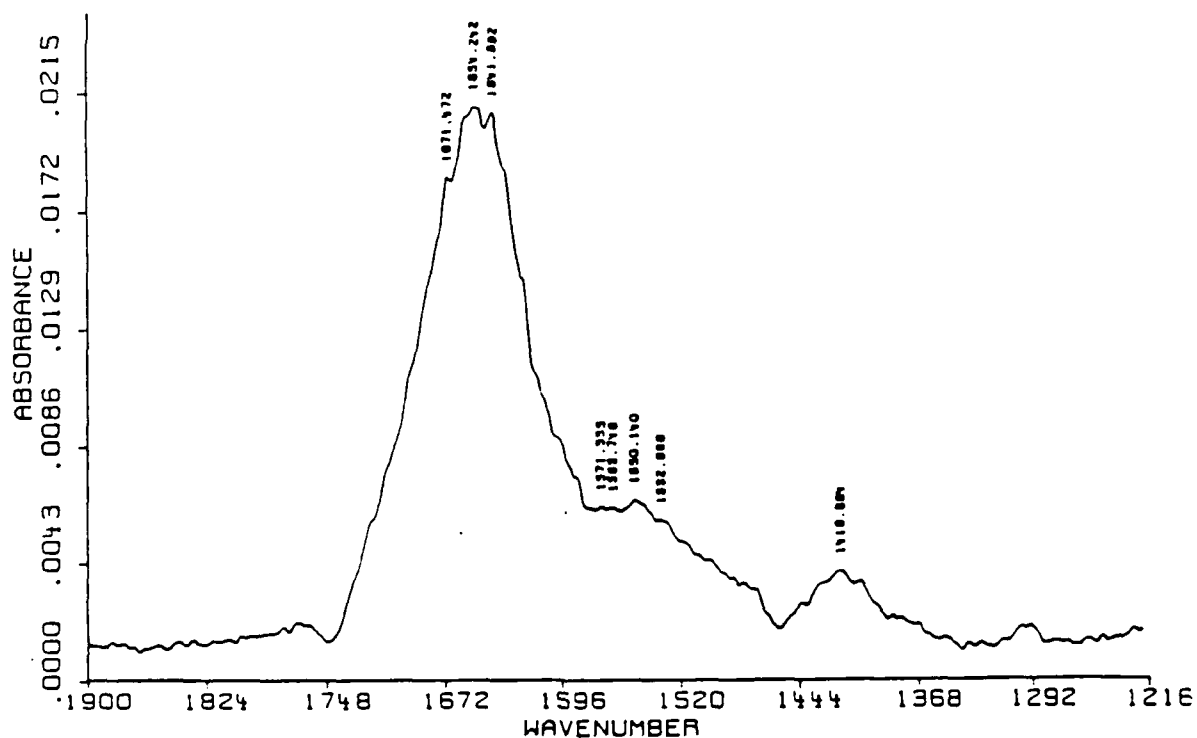Figure 3. FTIR spectrum of a 0.5M propionic acid solution in 1M NaCl at pH = 4.1.
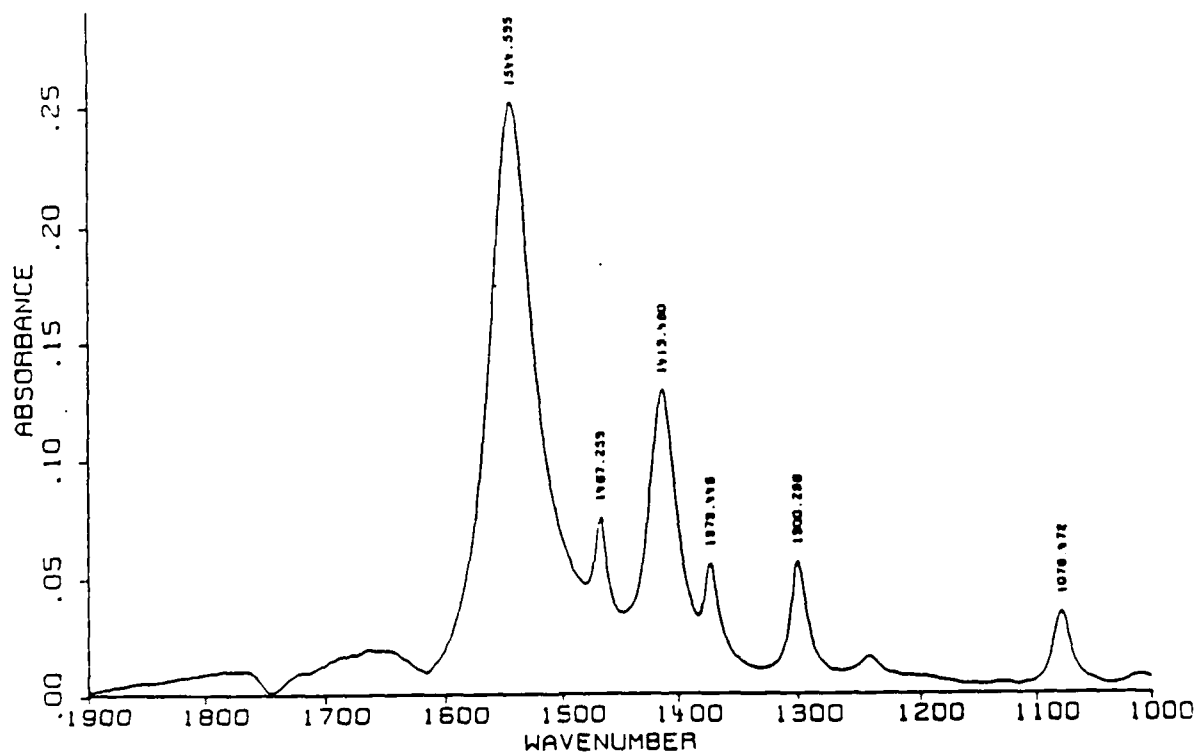
Figure 4. FTIR spectrum of a 0.5M propionic acid solution in 1M NaCl at pH = 11.3.
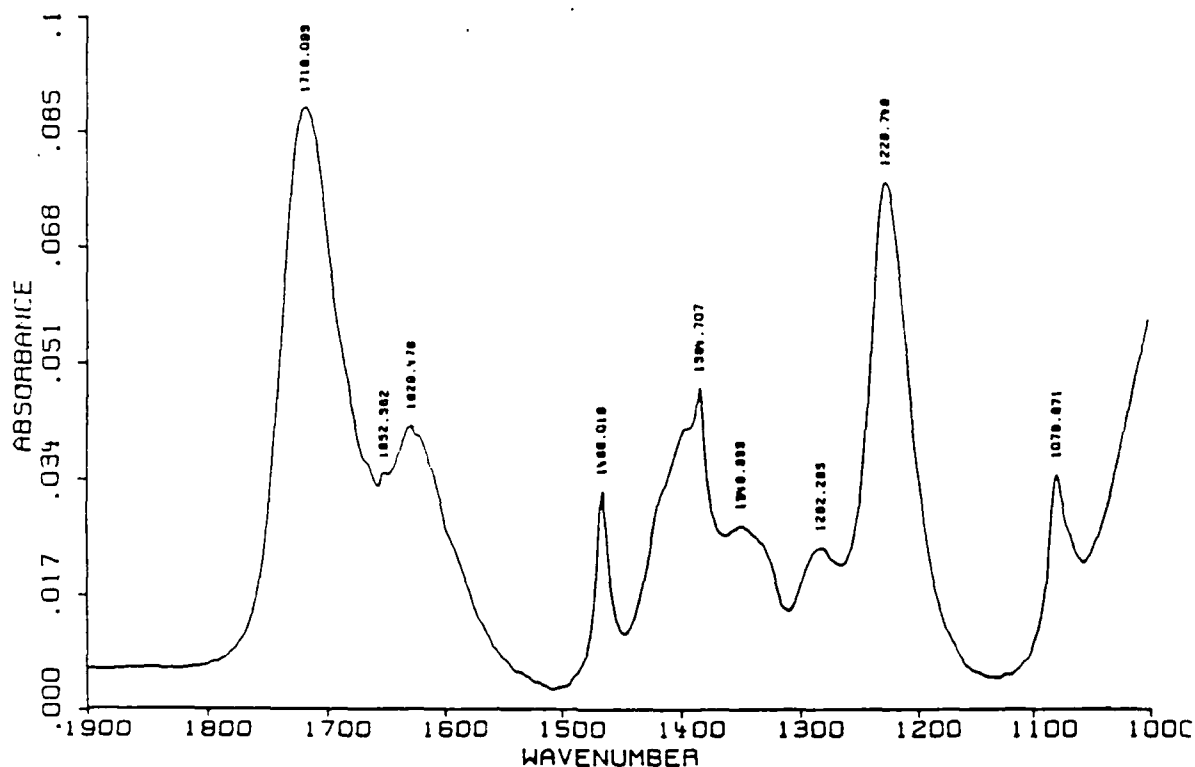
Figure 5. FTIR spectrum of a 0.2M Al(Ⅲ) and 0.5M propionic acid solution in 1M NaCl at pH = 1.8.

Figure 6. FTIR spectrum of propionic acid adsorption onto γ-Al_2O_3 (pH = 5.1; I = 0.03M as NaCl; total PA = 0.01M; 100g/l γ-Al_2O_3; near 50% adsorbed point shown in Figure 1).

REFERENCES

Allara, D.L., and R.G. Nuzzo, "Spontaneously Organized Molecular Assemblies. 2. Quantitative Infrared Spectroscopic Determination of Equilibrium Structures of Solution-Adsorbed n-Alkanoic Acids on an Oxidized Aluminum Surface," Langmuir, 1985, Vol. 1, pp.52- 66.

Ganguly, S. and V.K. Mohan, "FT-IR Spectroscopic Studies on Interactions of Fatty Acids in Solution and on a Salt Surface," Colloids and Surfaces, 1988, Vol. 30, pp. 287-294.

Griffiths, P.R. and J.A. de Haseth, Fourier Transform Infrared Spectrometry, New York, New York, John Wiley and Sons, 1986.

Harrick, N.J., Internal Reflection Spectroscopy, Ossining, New York, Harrick Scientific Corporation, 1985.

Hayes, K.F., "Equilibrium, Spectroscopic, and Kinetic Studies of Ion Adsorption at the Oxide/Aqueous Interface," Ph.D. Dissertation, Dept. of Civil Engineering, Stanford University, Stanford, CA, 1987, 260 pp.

Hayes, K.F., A.L. Roe, G.E. Brown, Jr., K.O. Hodgson, J.O. Leckie, and G.A. Parks, "In Situ X-ray Absorption Study of Surface Complexes: Selenium Oxyanions on α-FeOOH," Science, 1987, Vol. 238, pp.783-786.

Kimura, F., J. Umemura, and T. Takenaka, "FTIR-ATR Studies on Langmuir-Blodgett Films of Stearic Acid with 1-9 Monolayers," Langmuir, 1986, Vol. 2, pp.96-101.

Leppinen, J.O., C.I. Basilio, and R.H. Yoon, "FTIR Study of Thionocarbamate Adsorption on Sulfide Minerals," Colloids and Surfaces, 1988, Vol. 32, pp. 113-125.

Mirabella, F.M. and N.J. Harrick, Internal Reflection Spectroscopy: Review and Supplement, Ossining, New York, Harrick Scientific Corporation, 1985.

Tejedor-Tejedor, M.T., and M.A. Anderson, "In-situ Attenuated Total Reflection Fourier Transform Infrared Studies of the Goethite-Aqueous Solution Interface," Langmuir,

1986, Vol. 2, pp. 203-210.

Ulrich, H.-J., W. Stumm, and B. Cosovic, "Adsorption of Aliphatic Fatty Acids on Aquatic Interfaces. Comparison Between Two Model Surfaces: The Mercury Electrode and δ-Al_2O_3 Colloids," Environ. Sci. Technol., 1988, Vol. 22, pp.37-41.

Yost, E.C., "Adsorption/Desorption and In-situ Bonding Mechanism Studies of Benzoic and Phenolic Compounds with Aqueous-Goethite Suspensions," Ph.D. Dissertation, University of Wisconsin-Madison, 1986, 336 pp.

Zeltner, W.A., E.C. Yost, M.L. Machesky, M.I. Tejedor-Tejedor, and M.A. Anderson, "Characterization of Anion Adsorption on Goethite Using Titration Calorimetry and CIR-FTIR," In: Geochemical Processes at Mineral Surfaces, J.A. Davis and K.F. Hayes, eds. ACS Symposium Series No. 323, American Chemical Society, Washington, D.C., 1986, Chapter 8.

1989 USAF-UES SUMMER FACULTY RESEARCH PROGRAM/

GRADUATE STUDENT RESEARCH PROGRAM

Sponsored by the

AIR FORCE OFFICE OF SCIENTIFIC RESEARCH

Conducted by the

Universal Energy Systems, Inc.

FINAL REPORT

Biodegradation of Jet Fuel JP-8

Prepared by:	Deborah D. Ross, Ph.D.
Academic Rank:	Assistant Professor
Department and	Department of Biological Sciences
University:	Indiana Univ.-Purdue Univ.
Research Location:	USAFESL/RDVW Tyndall AFB Panama City, FL
USAF Researcher:	Jim Spain

Date:	28 July 1989
Contract No:	F49620-88-C-0053

Biodegradation of Jet Fuel JP-8

by Deborah D. Ross

ABSTRACT

The fate of jet fuel JP-8 was studied in water, water/sediment slurries and soil samples using a quiescent flask test system. For each treatment, killed samples were compared to active samples to assess the relative contributions of biodegradation and volatilization in removing JP-8. At appropriate time intervals, flasks were extracted with CS_2 and analyzed by gas chromatography/mass spectrometry.

In water and water/sediment slurries, the major removal process was evaporation. No significant differences were noted between active and sterilized flasks, indicating that biodegradation was not a major factor in removal of JP-8 under these test conditions. When removal in water alone was compared to removal in water/sediment slurries, greater losses were observed in water alone, indicating that the presence of sediment sequesters the jet fuel rendering it less susceptible to volatilization. Removal of JP-8 from active soil samples was greater than removal in sterilized soil samples, indicating that biodegradation was a significant factor in removal of JP-8 from soil. Thus, strategies to enhance biodegradation would be expected to have greatest impact in the soil environnment.

Acknowledgements

I wish to thank the Air Force Office of Scientific Research for spnsorship of this research and Universal Energy Systems for administrative coordination of this program.

Many people within the Environics Division of the Research and Development Directorate contributed to making this summer a valuable and rewarding research experience for me: Dr. Jim Spain for providing me with support and encouragement; Dr. Billy Haigler, Dr. Charles Pettigrew, Dr. Bill Stevens, and Ms. Shirley Nishino of the Microbiology Laboratory for many rewarding discussions and for friendly assistance; and Dr. Howard Mayfield for coordinating the analytical effort without which this resaerch project would not have been possible.

I. INTRODUCTION

Accidental releases of jet fuel are unavoidable consequences of Air Force operations. Knowledge of the environmental transport and fate of jet fuel is therefore essential in contingency planning for emergency response to jet fuel spills.

Upon release to the environment, whether on water or on soil, jet fuels are immediately subjected to physical and biological processes which redistribute and/or remove the fuel from the point of release. Aqueous solubility, evaporation, adsorption and biodegradation are the major processes which will affect the fate and transport of jet fuel. Of these, only evaporation and biodegradability will result in loss of the hydrocarbons from the point of release, and only biodegradation will result in the complete destruction of the hydrocarbons. Information on the biodegradability of the jet feul is therefore essential for an assessment of the environmental fate of spilled fuel. The Microbiology Laboratory within the Environics Divison of the Engineering and Services Laboratory at Tyndall Air Force Base is concerned with the biodegradability of chemicals utilized in Air Force operations.

My research interests have focused on the biodegradability of a variety of environmental chemicals, including aromatic hydrocarbons, pesticides and surfactants. Industrial research experience exposed me to various methodologies for assessing rates of biodegradation in natural microbial assemblages in soil and activated sludge. In addition, I have had experience with the

isolation and study of pure cultures of microorganisms selected to carry out particular biodegradative transformations. This experience was responsible for my assignment to the Microbiology Laboratory of the Engineering and Services Center.

II. OBJECTIVES OF THE RESEARCH EFFORT:

The Air Force has devoted considerable attention to the environmental impact of jet fuels. In a literature review of biodegradation of jet fuels, Carlson (1981) found that, although very little research had been directed to jet fuels per se, a considerable literature existed on the biodegradation of hydrocarbon components of jet fuels. Based on this survey, Carlson concluded that the n-alkane components of jet fuels as well as the low molecular weight aromatic hydrocarbons would be readily biodegradable. Olefins, isoalkanes, cycloalkanes and polynuclear aromatic hydrocarbons are less easily degraded. The actual rate of biodegradation depends on a variety of factors, including number of hydrocarbon-degrading bacteria present, history of prior exposure to hydrocarbons, nutrient availability, temperature and pH.

Biodegradation of the hydrocarbon components of JP-4 was studied by Spain and workers (1983). In these studies, JP-4 as well as a model fuel made up of known quantities of individual hydrocarbons present in JP-4 were added to water and sediments samples from several aquatic environments, and the disappearance of hydrocarbons

was followed over several days. Use of aquatic samples which were killed by the addition of mercuric chloride allowed comparison of biotic and abiotic removal processes.

Results indicated that evaporation was the major removal process for the low molecular weight, volatile hydrocarbons. Addition of sediment to water samples affected the removal of JP-4 components by reducing the rate of volatilization. For most individual hydrocarbons, biodegradation was not as significant for removal as was evaporation. For those hydrocarbons which were susceptible to biodegradation, the extent of biodegradative removal was a function of the water sample.

To further elucidate the role of biodegradation in removal of JP-4, additional studies were conducted by Pritchard and coworkers (1988) using a quiescent bottle system designed to simulate a fuel spill on a quiet body of water. Results again indicated that volatilization was the primary removal process with lower molecular weight hydrocarbons being lost at a more rapid rate than higher molecular weight hydrocarbons.

The primary goal of the present study was to evaluate the processes responsible for the removal of JP-8 from the environment. Due to the results of previous studies which suggested that volatilization was the major process for removal of jet fuels from the environment, the quiescent bottle test was selected as the test method because it would minimize evaporative losses. Since

sediment was seen to influence the fate of JP-4, treatments containing water alone and water plus sediment were included in the experimental design. In addition to bottles receiving JP-8 as test fuel, bottles treated with JP-4 were included to serve as positive controls. Finally, a series of bottles containing soil were included in this study. Fuel spills and leaks from storage tanks mas contaminate the soil as well as the aquatic environment and information on removal from soil would be useful for the assessment of the environmental fate of JP-8.

The second goal of the present study was to evaluate the toxicity of JP-8 to microorganisms. Evidence from previous studies indicating that biodegradation was lower in sediment treatments than in water treatments suggested that either toxicity to biodegradative organisms might be occurring or that adsorption to sediment might render the hydrocarbons less available for biodegradation. A toxicity study was therefore incorporated into the study goals in order to aid in the interpretation of the biodegradation test results.

III. REMOVAL OF JP-8

Methods

The quiescent bottle technique of Spain and Somerville (1985) was used to assess the rate of removal of JP-8 from aqueous environmental samples. For these experiments, water and sediment were collected from a brackish water bayou located on Tyndall Air

Force Base. Water was filtered through a 3.0 um membrane filter and incubated overnight at room temperature with stirring. The sediment slurry was passed through a 1 mm screen and decanted several times to allow sand particles to settle out. The resulting slurry was incubated overnight with stirring and forced aeration (laboratory air).

JP-8 was incubated under four conditions: (1) water alone; (2) sterile water containing 0.05% $HgCl_2$; (3) water supplemented with sediment to give a concentration of 5,000 mg/L (dry weight basis); (4) water supplemented with sediment as in (3), but sterilized with 0.05% $HgCl_2$. The tests were conducted in 150 ml milk dilution bottles containing 25 mls of water or water/sediment slurry. JP-8 at a loading of 250 ul was added to each bottle. Bottles were capped, placed horizontally on a shaker and shaken for 15 min at 150 rpm to achieve an initial interaction between the fuel and the microorganisms. Following this treatment, caps were removed and bottles were incubated in the horizontal position in an undisturbed condition. For each treatment, 15 bottles were prepared. At 0 time, and 5, 10, 21 and 40 days, triplicate bottles were removed for extraction and analysis. Water and sediment not treated with fuel were used for the enumeration of heterotrophic bacteria by the most-probable number (MPN) technique (Koch, 1981).

In order to compare removal of JP-8 with that of JP-4, identical sets of bottles were prepared using JP-4. For these experiments, only six bottles per treatment were used, three for 0 time and

three for final (40 day) analysis.

A soil incubation study was also included. For this study, 25 g (dry weight equivalent) of soil collected from the campus of Chippola Community College, was placed in 150 ml milk dilution bottles. Two sets of bottles were used, one set containing untreated (active) soil and the other receiving soil treated with 2% (wt) $HgCl_2$. Each bottle received 250 ul of JP-8. Twelve bottles were prepared per treatment, and triplicate bottles were removed at 0 time, and 10, 21 and 31 days. Three bottles containing 25 g of soil (dry weight) were weighed and incubated under identical conditions to the JP-8 bottles. These bottles were weighed weekly to calculate weight loss. The corresponding amount of water was added to the JP-8 bottles to maintain a constant moisture level. The heterotrophic bacterial population in untreated soil was estimated by the MPN method refered to previously.

After the appropriate time interval, the remaining fuel was extracted from water and water/sediment slurries by the addition of 2 mL of CS_2 (containing D_{10}-ethylbenzene as an internal standard). Solvent and sample were shaken for 5 min on a wrist action mechanical shaker, then samples were centrifuged for 10 min at 1200 rpm. A 1 mL aliquot of the solvent was transferred to an autosampler vial and analyzed immediately. Soil samples were extracted similarly except that 15 mL of CS_2 (with internal standard) was used.

Extracts were analyzed by high resolution capillary gas chromatography with a Hewlett Packard gas chromatograph equipped with a mass detector. The column was a DB5 capillary column, 30 m long, 0.25 mm i.d. Water and water/sediment samples were injected in the split mode (1:30) while soil samples were injected in the splitless mode. Injector and detector temperatures were 200 C. The temperature program began at 40 C with a 4 min isothermal period followed by 3/min increase to 250 C.

Results

Evaporation was the major removal process occurring in water treatments, removing significant levels of the volatile components of JP-8 by Day 5 (Figure 1). Differences in the distribution of components in the active and killed treatments were slight, indicating that biodegradation was not a significant removal process during the initial exposure period. By day 40, singificant removal of fuel components was apparent. However, no significant differences between the active treatments and the killed treatments were observed, indicating that biodegradation was not altering the composition of JP-8.

In contrast to water, losses of low molecular weight fuel components did not occur in water/sediment slurries (Figure 2). Even after 40 days, distribution of components of JP-8 were no different than they were at day 0 in both active and killed treatments. Thus, biodegradation was not effective in removing
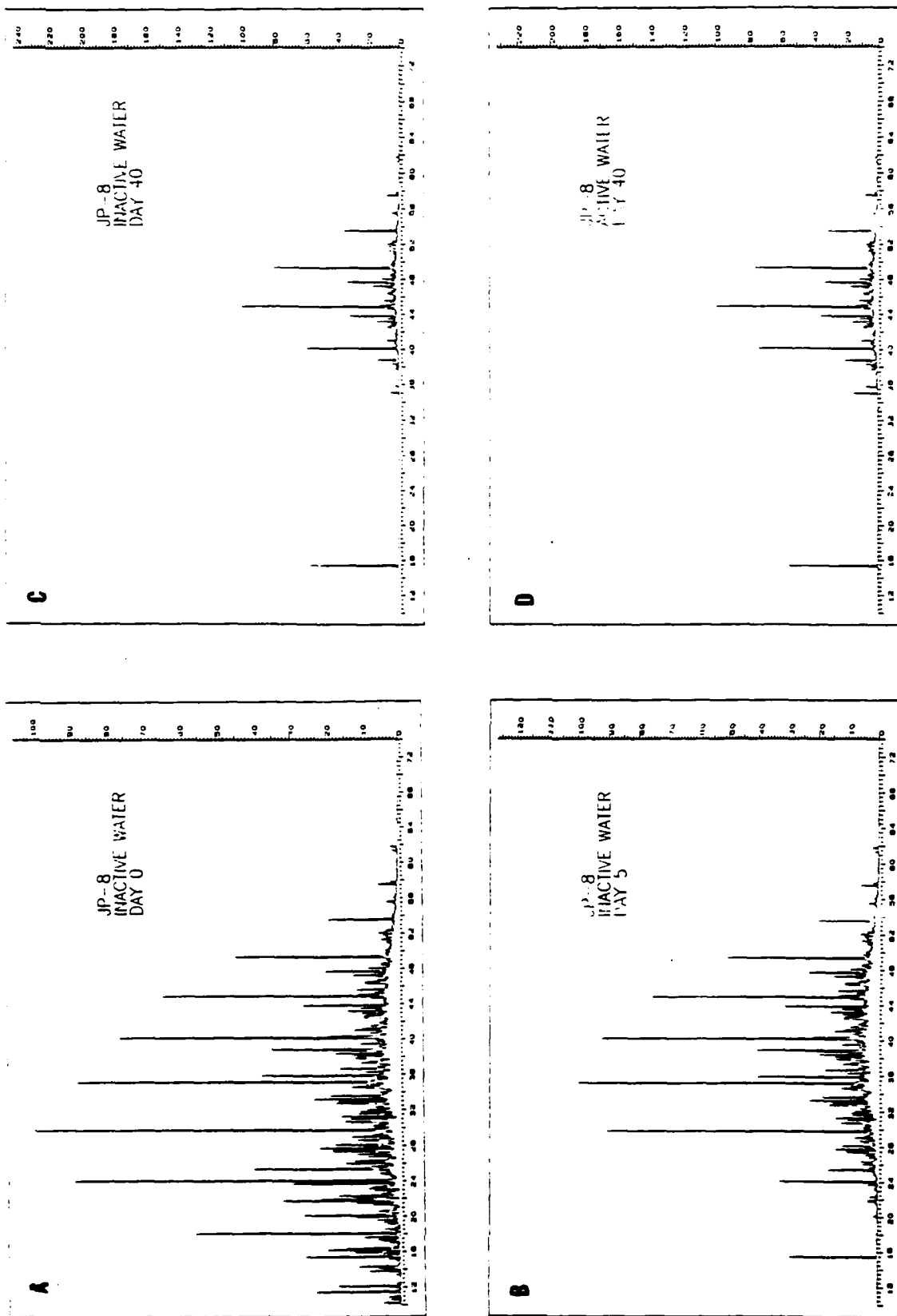
Fig. 1 Removal of JP-8 in water: (A) JP-8 at 0 time;   (B) JP-8 in sterilized treatment at day 5;   (C) JP-8 in sterilized treatment at day 40;   (D) JP-8 in active treatment at day 40
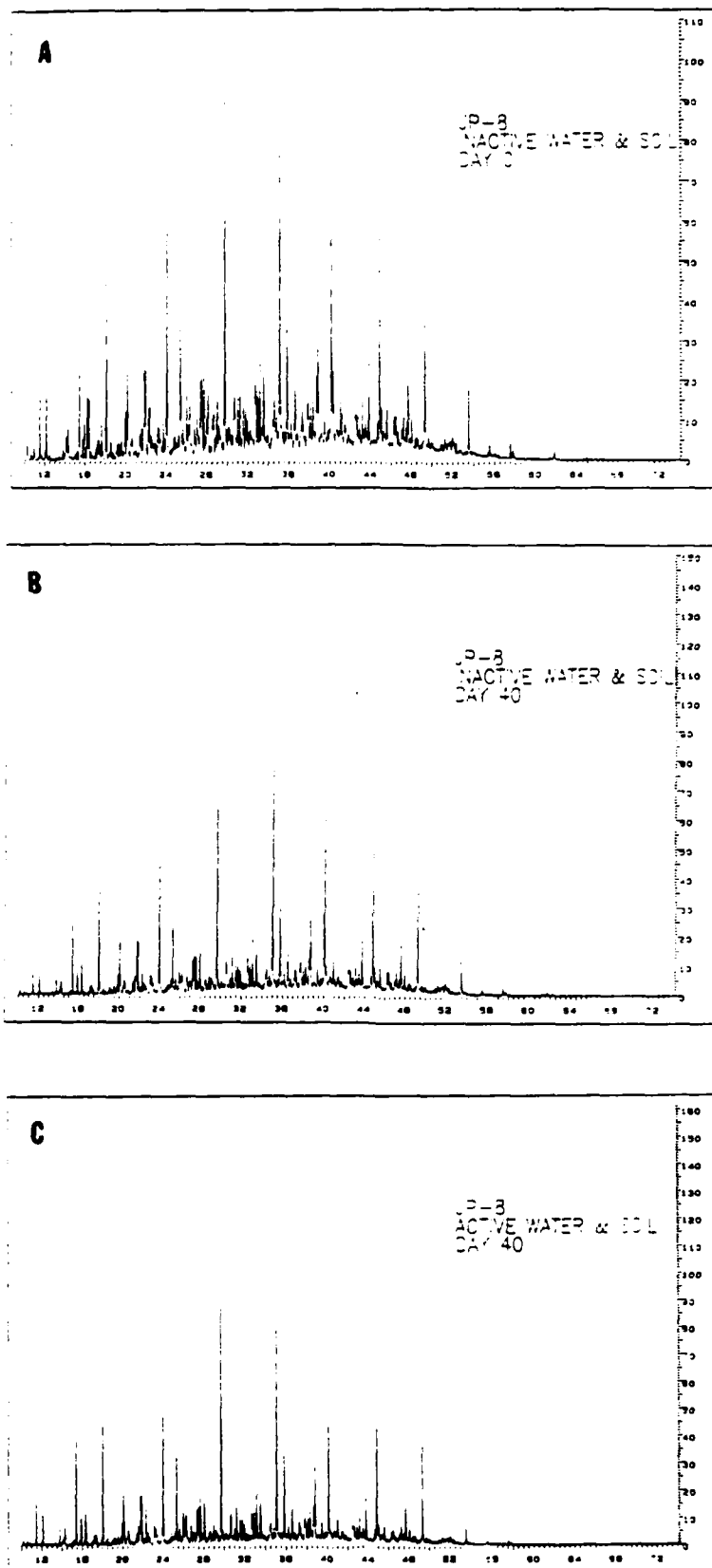
Fig. 2   Removal of JP-8 in water/sediment slurries: (A) JP-8 at
time 0;   (B) JP-8 in sterilized treatment at day 40;   (C) JP-8 in
active treatment at day 40

fuel from water/sediment slurries, and evaporation was significantly retarded in the presence of sediment.

In both active and killed soil treatments, significant loss of JP-8 components had occurred by day 10 (Figure 3); however, removal was greater in the active treatments indicating that biodegradation was a quantitatively significant process in the removal of JP-8 from soil. By day 21, only minor amounts of components of JP-8 remained in the active soil treatments while the greater amounts of the same components remained in the killed treatments. Very little additional removal occurred in both treatments between day 21 and day 31. While evaporation alone will reduce the levels of JP-8 components in soil, biodegradation can remove all but traces of JP-8 components, including components that may be relatively nonsusceptible to evaporation.

IV. TOXICITY OF JP-8 TO MICROORGANISMS

Methods

Because previous results with JP-4 suggested that toxicity to microorganisms could be limiting biodegradation, toxicity studies were undertaken with JP-8 using water and water supplemented with sediment (5,000 mg/L). Water was collected from the same location as for the biodegradation study and filtered through a 3 um diameter membrane filter. It was dispensed into Erlenmeyer flasks which received either no JP-8, or 0.01%, 0.1% or 1% JP-8. All treatments were prepared in triplicate. Flasks were incubated at
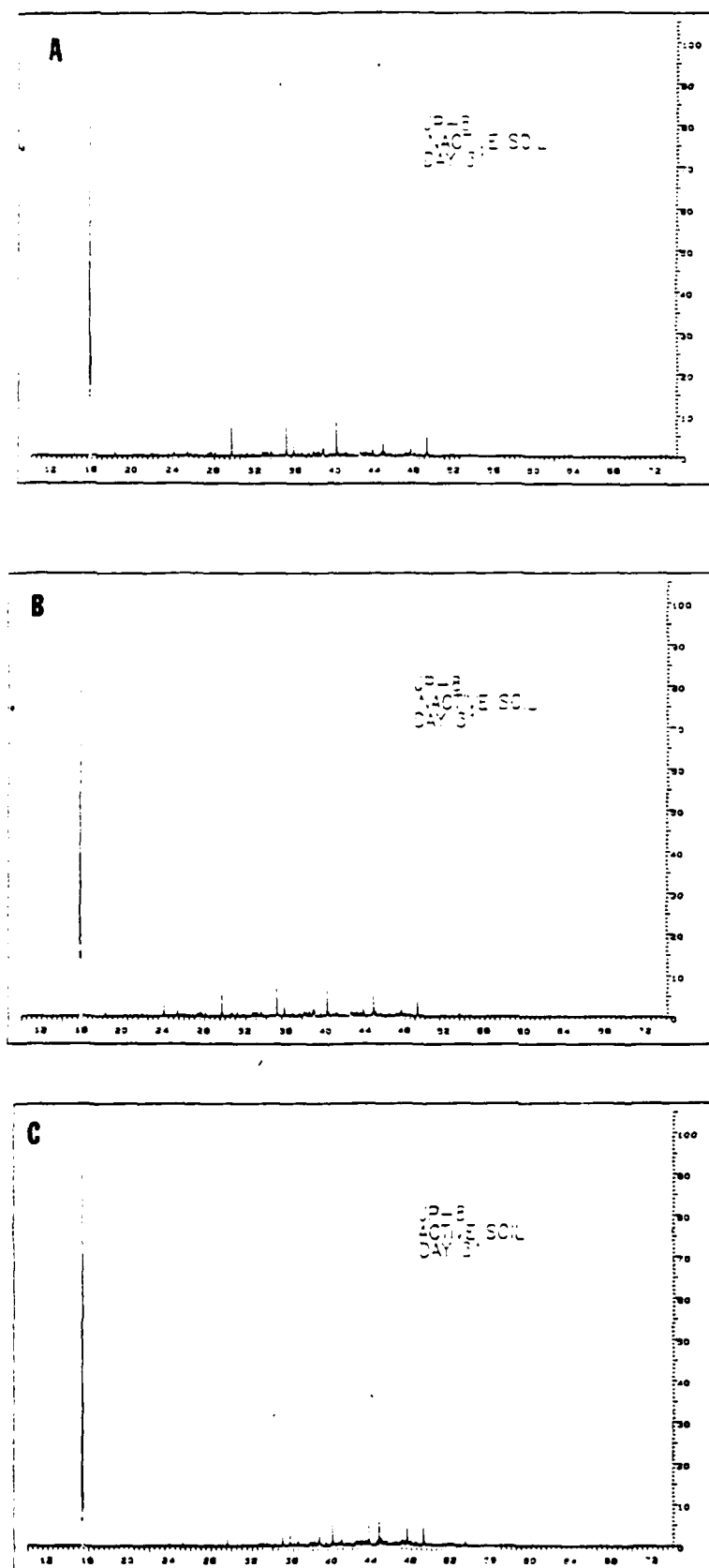
Fig. 3   Removal of JP-8 in soil: (A)   JP-8 at time 0;   (B) JP-8 in sterilized treatment at day 31;   (C)   JP-8 in active treatment at day 31

30 C on a shaker at 200 rpm. Samples were removed at 0, 1, 2 and 4 days and assayed for glucose mineralization and hexadecane mineralization by the method described below. Incubations with water supplemented with sediment were prepared in a similar fashion except that the 0.01% JP-8 treatment was not included. This was done based on the results of a preliminary study which suggested that 0.01% JP-8 had negligible effect on glucose mineralization when compared to the control in a water/sediment slurry.

Glucose mineralization was assessed by measuring the production of $^{14}CO_2$ when ^{14}C-labeled glucose was added to aliquots of the water or water/sediment incubations. Five 5-ml samples were removed from each incubation flask and placed in 60 ml serum vials. Two vials received 0.5 ml 2N H_2SO_4 to serve as killed cell controls. Each vial received uniformly labeled glucose (Pathfinder Laboratories) at a final concentration of 20 ug/L. Flasks were capped with rubber stoppers fitted with center wells containing 0.1 ml of 10N NaOH absorbed onto a filter paper wick. Vials were incubated for 4 hr at 30 C with shaking (200 rpm). At the end of the incubation period, reaction in the active vials was stopped by the addition of 0.5 ml 2N H_2SO_4. Vials were incubated with shaking for an additional hour to ensure complete trapping of CO_2. Wicks were then removed, placed in a scintillation cocktail consisting of 10 ml Ecolume (ICN Biomedicals, Inc., Irvine, CA) and 1 ml methanol, and counted by liquid scintillation counting (Beckman Model LS 9800).

Hexadecane mineralization was assessed by measuring the production of $^{14}CO_2$ when ^{14}C-labeled hexadecane was added to aliquots of the water or water-sediment incubations in a similar manner as glucose mineralization. Labeled hexadecane was added to the vials at a final concentration of 250 ug/L. The hexadecane was dissolved in hexane; hexane was selected as solvent because it did not inhibit glucose mineralization when added to water-sediment slurries. Incubations with labeled hexadecane were conducted for 18 hours.

Results

Results of the toxicity assays with water/sediment slurries are shown in Figure 4A. Addition of JP-8 at concentrations of 0.1% and 1.0% enhanced microbial activity as indicated by an increase in glucose mineralization when compared to the control. This increase in microbial heterotrophic activity did not extend to hydrocarbon degradation. Mineralization of hexadecane was negligible in all water/sediment treatments at all time periods.

In contrast to microbial activity in water/sediment slurries, activity in water alone was inhibited by all concentrations of JP-8 as indicated by a depression of glucose mineralization in comparison to the control (Figure 4B). Over the time period of the experiment, microbial activity in the water treated with 0.01% JP-8 increased to the control level. Microbial activity in the other treatments remained low. Hexadecane mineralization (Figure 4C) was higher in the water treated with 0.01% JP-8 than it was in the control, but by day 4 had decreased to the control level.
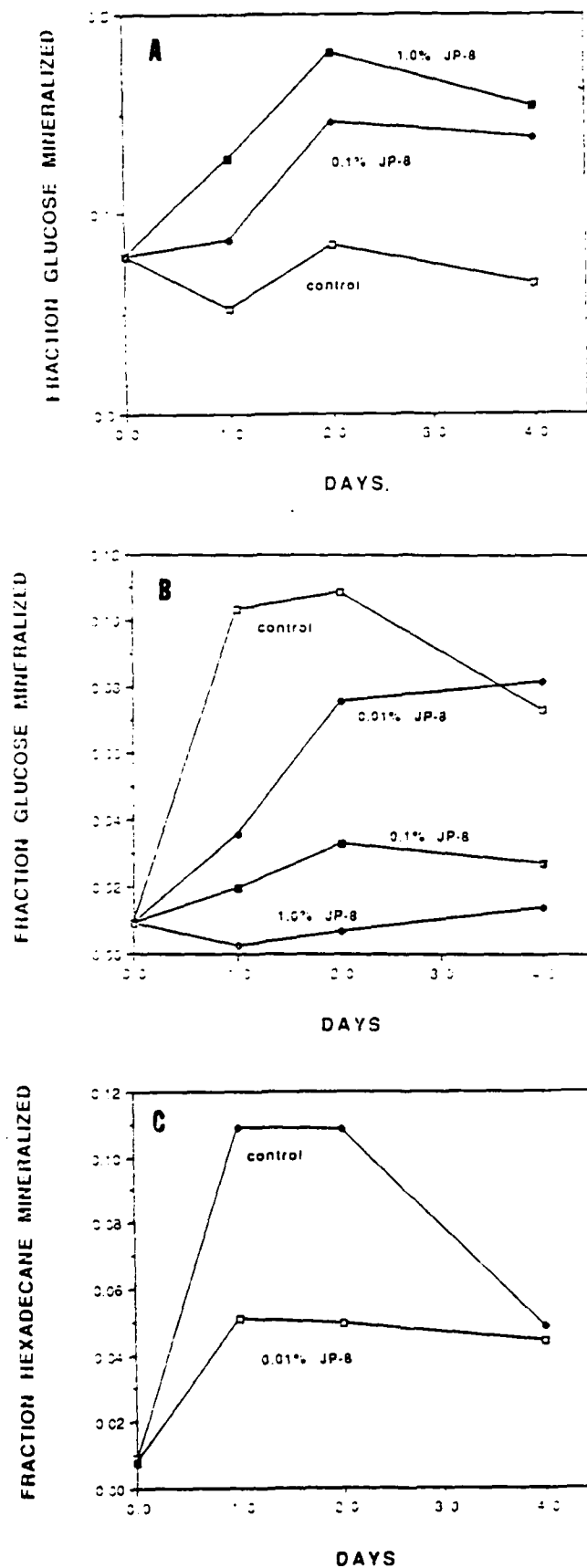
Fig. 4 Toxicity of JP-8 to microorganisms: (A) Toxicity to water/sediment slurries as measured by glucose mineralization; (B) Toxicity to water as measured by glucose mineralization and (C) hexadecane mineralization

Hexadecane mineralization in 0.1% JP-8 treated water was negligible at day 1, and was low but measurable on day 2 (fraction utilized 0.006) and 4 (fraction utilized 0.003). Hexadecane mineralization in the 1.0% JP-8 treatment was negligible at all sampling times.

V. RECOMMENDATIONS:

a. Spills of substantial quantities of JP-8 on water are likely to inhibit biodegradative capabilities of aquatic microorganisms. Remedial actions should concentrate on enhancement of evaporation as a removal process.

b. Care should be taken to avoid mixing sediment with spilled fuel in shallow water because this will inhibit evaporative loss of the fuel.

c. Lack of biodegradation in water/sediment slurries remains unexplained and deserves further attention.

d. Biodegradation is singificant in soil and efforts to maximize biodegradation rates could lead to enhanced fuel removal in spill situations. Attention should be focused on factors which will increase microbial degradation of JP-8 and other Air Force jet fuels.

REFERENCES

Carlson, R. E. 1981. The biological degradation of spilled jet fuels: a literature review. USAF/ESC Report ESL-TR-81-50.

Koch, A. L. 1981. Growth measurements, pp 179-207. In Gerhardt, P. (ed.), Manual of Methods for General Bacteriology. American Society for Microbiology, Washington, D.C.

Pritchard, P. H., T. P. Maziarz, L. H. Mueller, and A. W. Bourquin. 1988. Environmental fate and effects of shale-derived jet fuel. USAF/ESC Report ESL-TR-87-09.

Spain, J. C. and C. C. Somerville. 1985. Fate and toxicity of high density missile fuels RJ-5 and JP-9 in aquatic test systems. Chemosphere 14:239-248.

Spain, J. C., C. C. Somerville, L. C. Butler, T. J. Lee, and A. W. Bourquin. 1983. Degradation of jet fuel hydrocarbons by aquatic microbial communities. USAF/ESC Report ESL-TR-83-26.

1989 USAF-UES SUMMER FACULTY RESEARCH PROGRAM/

GRADUATE STUDENT RESEARCH PROGRAM

Sponsored by the

AIR FORCE OFFICE OF SCIENTIFIC RESEARCH

Conducted by the

Universal Energy Systems, Inc.

FINAL REPORT

FURTHER DEVELOPMENT OF THE AFESC CENTRIFUGE FACILITY

Prepared by: Dr. Teresa Taylor

Academic Rank: Assistant Professor

Department and   The Charles Edward Via, Jr.
                               Department of Civil Engineering
University: Virginia Polytechnic Institute and
                                   State University

Research Location: USAF/AFESC
                               Tyndall AFB
                               Panama City FL 32403

USAF Researcher: Michael R. Purcell

Date: 06 Sept 89

Contract No: F49620-88-C-0053

Further Development of the AFESC Centrifuge Facility

by

Teresa Taylor

ABSTRACT

Through a variety of technical and non-technical subtasks, an effort was made to better prepare the Air Force Engineering Services Center (AFESC) centrifuge facility for use by different researchers. This effort included identification of maintenance and special equipment needs, and assistance in development of an on-site centrifuge library. Research areas of particular military interest were identified, such as blast loading over buried structures. Instrumented pilot tests for assessing the centrifuge capabilities and limitations related to the identified research areas were planned; however, due to lack of appropriate gages and other required support equipment and supplies these tests were not carried out. Several non-instrumented blast tests were successfully conducted, and one non-calibrated instrumented blast test utilizing the newly acquired on-board data acquisition system was conducted.

ACKNOWLEDGEMENTS

I. INTRODUCTION:

My research interests have most recently concentrated in the field of centrifuge modeling. Previous work conducted for the USAF (Fragaszy and Taylor, 1988) involved modeling of projectile penetration into granular soils. This work resulted in familiarization with the AFESC centrifuge facility and provided the major impetus for my return under the auspices of the summer faculty research program.

II. OBJECTIVES OF THE RESEARCH EFFORT:

The major objective of this appointment was to work with the AFESC centrifuge facility to ready it for a variety of research projects of potential military interest. Many of the tasks involved in realizing this objective were largely non-technical, and included developing maintenance recommendations, ascertaining requirements for shielding of critical or easily damaged machine components during testing, analyzing machine performance under different test conditions, and recommending improvements to the facility and support test equipment. Another primarily nontechnical task included providing assistance in categorizing centrifuge literature, which was to be contained on site to provide future researchers with ready access to pertinent literature. More technical tasks involved in realizing the main objective included the following:

--Conduct a variety of pilot blast tests to assess capabilities of the machine and its performance under blast loading. This objective would include theoretical and physical verification of scaling relationships and appropriate ranges for the AFESC centrifuge, and comparison to results obtained by previous researchers (Nielsen, 1983; Bradley, et al., 1984). A technique for conducting blast tests in the centrifuge facility would also be developed, utilizing derivations of methods employed in other blast loading investigations (Schmidt, 1979; Tabatabai, et al., 1988).

--Work with the newly acquired on-board data acquisition system and a variety of instrument gages and test conditions to

44-4

calibrate gages, assess system performance and machine limitations, and develop instrumentation recommendations for different test conditions. This objective would also include composing introductory user-friendly documentation for data acquisition and reduction.

--Develop a projectile velocity measuring device for use in the centrifuge, and conduct 1-g and elevated g calibration tests.

--Work with constructing and calibrating a large scale centrifuge sample preparation device (pluviator), based on prototype pluviator previously developed (Taylor, et al., 1988).

III.   APPROACHES AND RESULTS

The secondary objectives listed in the preceding section outline the planned approach for meeting the main objective of preparing the centrifuge facility for different research projects. The non-technical subtasks were generally accomplished within the research period, and details are provided below.

a.   Maintenance Recommendations

The centrifuge and containment facility were carefully inspected for mechanical and structural problems, and maintenance procedures compared to those provided by the centrifuge manufacturer. Several items were addressed as a result of this inspection:

--The chains in the self-balancing mechanism were observed to be misaligned, causing difficulties with both static and dynamic balancing. The chains were realigned by AFESC Instrumentation personnel.

--Recommendations for strict adherence to the lubrication schedule and lubrication fluids recommended by the manufacturer were made.

--Inspection of the pivot pins for the payload platforms revealed trapped dirt and worn washers, preventing smooth travel of the

platforms. The pivot pins were cleaned, and recommendations made for manufacture of teflon washers to replace the aluminum washers.

b.   Shielding Requirements

A pilot blast test was used to observe the quantity of sand that would be released inside the containment facility from a typical charge at 20 g's. Recommendations were made for a plexiglass shield, attached to the rotor arm, to be located in front of the rotor to protect critical connections and machine parts. An effective mechanism for in-flight shielding of the pivot pins on the payload platform could not easily be developed that would allow for the necessary motion of the pins, yet resist the g-forces to which a shield would be subjected. An interim recommendation was made for inspection of the pins after each blast test, and removal and cleaning as necessary.

c.   Machine Performance

--Tests and calculations were performed to verify that the payload platform, over its entire load range (0 to 300 lbs.), and over its full g-level operating range (1-100), could not reach a vertical position without compensating weights, due to the location of the pivot pins with respect to the line of action of the centrifugal force. A computer program was written to determine the required compensating weights, and a series of calibration tests were performed to verify the results and allow adjustment for machine performance. Results were simplified to allow researchers to choose from either 5 lb., 10 lb. or 15 lb. compensating weights for any g-level and payload. Figure 1 presents the resulting test design chart.

--Recommendations were made to manufacture additional weights for the opposing payload platform to allow more accurate static balancing of the centrifuge prior to testing.
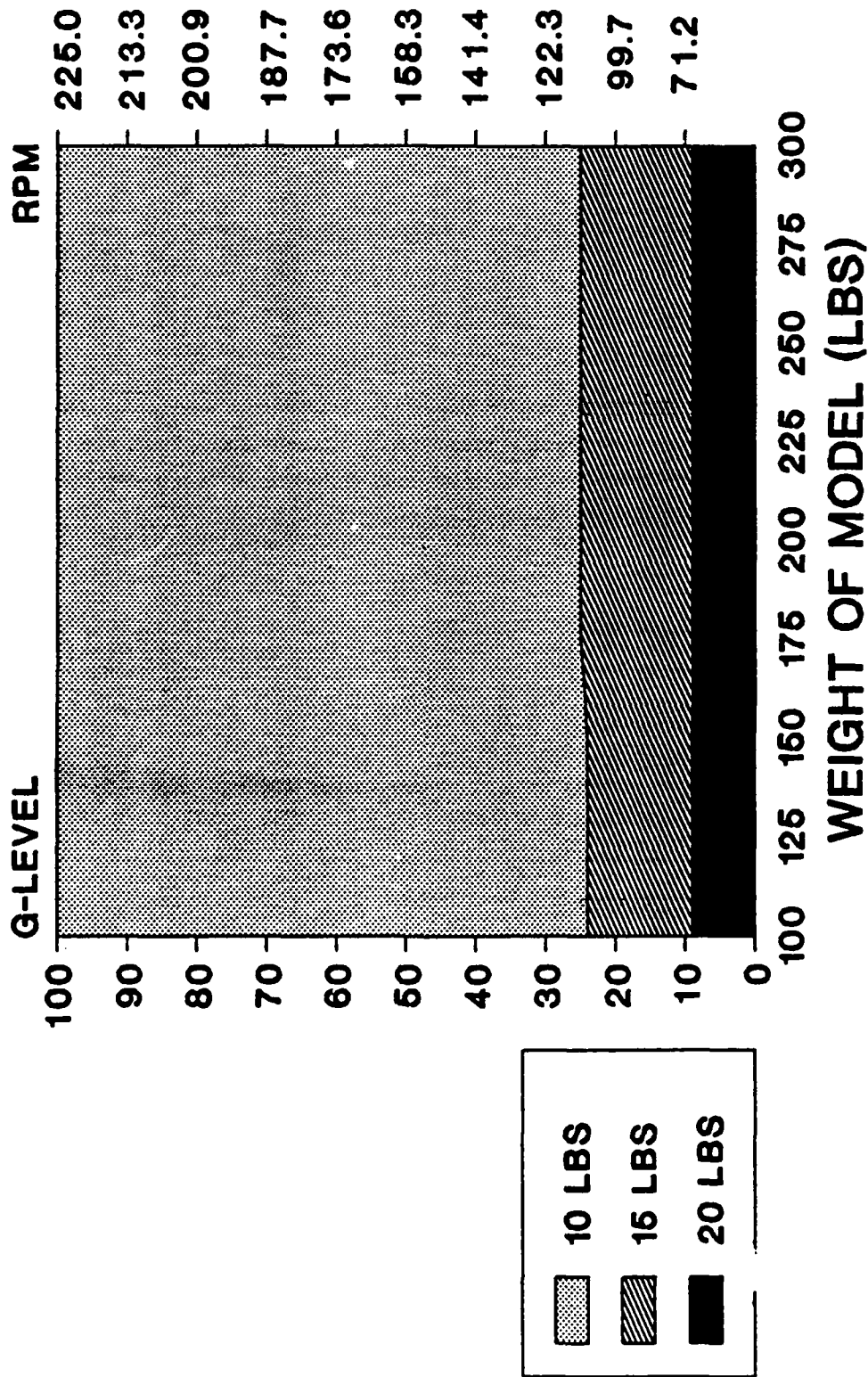
FIGURE 1. Test Design Chart for Platform Verticality

d.   Containment Facility and Support Equipment

--Numbered position locator stripes inside the containment housing were lengthened, and numbers were added at several locations, to allow the stripes to be viewed with the on-board video camera adjusted to different angles.

--A new centrifuge bucket was constructed of 24 in. diameter PVC pipe. This bucket was designed to take advantage of the maximum dimensions of the payload platform and minimize container edge effects.

e.   Centrifuge Literature

--Collected literature was reviewed, abstracts written and keywords identified, to allow the information to be included in the main database of the AFESC library. A comprehensive bibliography was prepared.

The technical subtasks related to the main objective could not be accomplished during the research period. Details concerning this follow:

a.   Blast Tests

Due to the failure of the manufacturer to supply soil gages ordered at the end of 1988, and insufficient quantity of explosives, the pilot blast test program that had been planned could not be conducted. A few 1-g and 20-g non-instrumented blast tests were conducted to study the throw-out of soil, as well as methods of implanting, containing, and triggering the explosive during centrifuge operation. Explosives were selected to model TNT equivalent values for conventional weapons (Lewis, et al., 1988).

b.   On-board Data Acquisition System

--The recently acquired data acquisition system was poorly documented by the manufacturer. This fact, coupled with personnel changes in AFESC Instrumentation, prevented the system from being

ready for research use until the end of the research period. The problem was augmented by the lack of appropriate soil gages.

--A pilot instrumented blast test was conducted at the end of the research period utilizing the data acquisition system and a non-calibrated makeshift pressure gage. A sample graph of the results provided by the system is shown in Figure 2. The initial detonation and blast wave, as well as the reflected wave, appear to be exhibited in this figure. Although the pressure gage could not be precisely calibrated, the approximate magnitudes reported are not unreasonable.

c.   Projectile Velocity Measuring Device

In coordination with AFESC Instrumentation, a projectile velocity measuring device for use on the centrifuge was designed. This device screwed to the barrel of the gun used for firing projectiles. It utilized a series of three sets of infrared-emitting diodes and detectors, in conjunction with a counter circuit that determined the time of travel between the first and second, and the first and third set of diodes. The system was tested under 1-g conditions using falling weights. Because minor repairs to the gun were delayed by nonarrival of parts from the manufacturer, the velocity measuring device was not able to be tested at higher velocities on either the centrifuge or under 1-g conditions.

d.   Sample Preparation Device (Pluviator)

Construction of the pluviator was delayed and did not begin during the research period; thus, calibration tests and development of component parts was not possible.

IV.   RECOMMENDATIONS:

The non-technical subtasks addressed in this effort involved a general investigation of the performance and maintenance of the centrifuge facility. It was clear from this investigation that some changes in
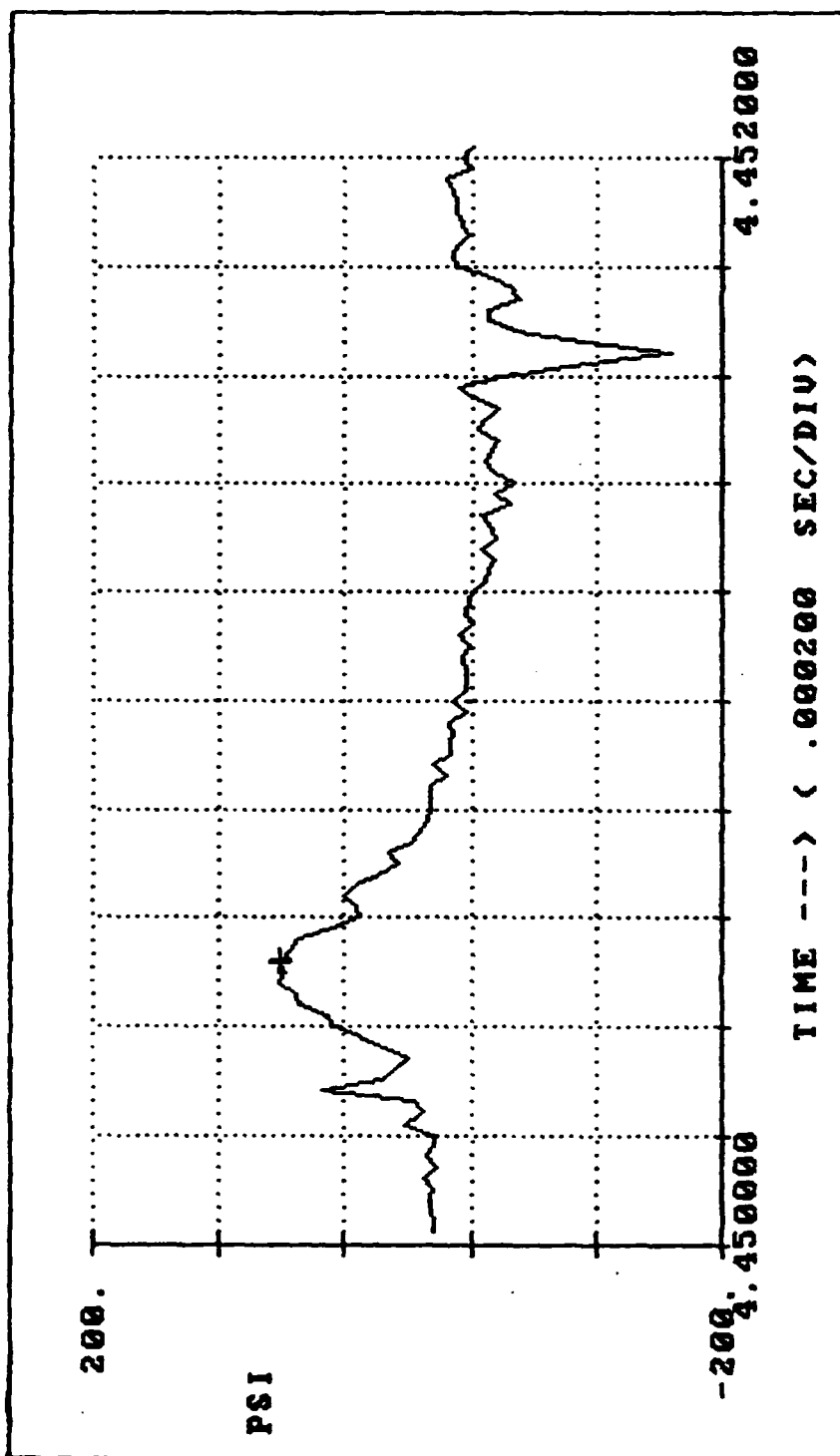
FIGURE 2. Sample Output from On-board Data Acquisition System, Pilot Blast Test

maintenance, particularly in conjunction with blast testing, were necessary. These changes were implemented during the research period. Recommendations were also made requiring manufacture of washers, weights, and shields. Manufacture of these items is being scheduled. Work has also begun on the sample preparation device (pluviator).

The technical subtasks of the research effort, as previously explained, were generally not accomplished. These subtasks are, nevertheless, valid and useful. Their accomplishment would contribute greatly to the successful utilization of the AFESC centrifuge facility.

REFERENCES

Bradley, D. M., Townsend, F. C., Fagundo, F. E. and Davidson, J. L. Centrifugal Scaling Laws for Ground Launch Cruise Missile Shelter. AFESC Report No. ESL-TR-84-07, Tyndall AFB, Fl, April, 1984, 90 pp.

Fragaszy, R. J., and Taylor, T. A. Centrifuge Modeling of Projectile Penetration in Granular Soils. AFESC Report No. ESL-TR-88-76, Tyndall AFB, Fl, 1988, 141 pp.

Lewis, M. J., Friesenhahn, G. J., and Nash, P. T. Breeden Bin Propagation Test Series, Part I. Technical Report SWRI No. 06-2067 prepared for Ogden Air Logistics Center by Southwest Research Institute, 1988.

Nielsen, J. P. The Centrifugal Simulation of Blast Parameters. AFESC Report No. ESL-TR-83-12, Tyndall AFB, Fl, December, 1983, 89 pp.

Schmidt, R. M. Simulation of Large-Scale Explosive Cratering and Ground Shock Using a 600-G Geotechnic Centrifuge. Proc. 6th Int'l Symp on Military Applications of Blast Simulation, Cahors, France, 1979, 35 pp.

Tabatabai, H., Bloomquist, D., McVay, M. C., Gill, J. J. and Townsend, F. C. Centrifugal Modeling of Underground Structures Subjected to Blast Loading. AFESC Report No. ESL-TR-87-62, Tyndall AFB, Fl, March, 1988, 311 pp.

Taylor, T., Meyer, M., and Fragaszy, R. Design of a Soil Pluviator for Centrifuge Sample Preparation. Proc. 25th Symposium of Engineering Geology and Soils Engineering, Coeur d'Alene, Idaho, 1988, pp. 191-199.

1989 USAF-UES SUMMER FACULTY RESEARCH PROGRAM/ GRADUATE RESEARCH PROGRAM

Sponsored by the

AIR FORCE OFFICE OF SCIENTIFIC RESEARCH

Conducted by the

Universal Energy Systems, Inc.

FINAL REPORT

"STATIC AND DYNAMIC BEHAVIOR OF COMPACTED UNSATURATED SANDS"

Prepared by:	George E. Veyera, Ph.D.
Academic Rank:	Assistant Professor
Department and	Department of Civil and Environmental Engineering
University:	University of Rhode Island
Research Location:	USAF Engineering and Services Center HQAFESC/RDCM Tyndall AFB Panama City, FL 32403
USAF Researcher:	Dr. C. Allen Ross
Date:	30 September 89
Contract No.:	F49620-88-0053

"STATIC AND DYNAMIC BEHAVIOR OF COMPACTED UNSATURATED SANDS"

by

George E. Veyera, Ph.D.

Abstract

Laboratory tests were conducted to evaluate the influence of microstructure, compaction moisture content, compaction energy, degree of saturation and boundary conditions on the stress transmission characteristics and compressibility of four cohesionless sands. The four soils tested were Eglin sand, Ottawa 20-30, Base (Tyndall) sand and Ottawa F-58 sand. Soil specimens dynamically compacted to a constant dry density at different initial water contents to achieve varying degrees of saturation. Dynamic uniaxial compression tests were performed using a Split-Hopkinson Pressure Bar (SHPB) device to determine stress transmission and stress wave propagation characteristics. Static uniaxial compression tests were performed using an MTS loading system to evaluate soil skeleton compressibilities. A preliminary analysis of the experimental data indicates that both the dynamic and static behavior of the sands tested is strongly dependent on soil microstructure. Initial capillary pressures during compaction, confinement conditions during compaction and testing, and soil grain characteristics strongly affect the development of soil microstructure. From the test results, the most prominent influences of these parameters on soil behavior were observed at intermediate levels of saturation (from about 20 to 60%). In this range of saturations, results generally indicated that stress transmission and stress wave propagation velocity increased in the soil for dynamic tests, and soil stiffness increased in the static tests.

Acknowledgements

I. INTRODUCTION:

The prediction of ground motions from explosive detonations and their effects on structures requires information about the response of geologic materials to intense transient loadings. Both laboratory and field investigations have provided insight into the stress wave propagation characteristics of soils. Of particular interest is the ability of a soil to transmit applied dynamic stresses. Since soil is a multiphase media, in the general case (eg. solids, water and air), its static and dynamic behavior is very complex. The general nature of stress wave propagation in particulate media such as soils depends on a number of parameters, the interrelationship between which is not fully understood. Soil microstructure is affected by the degree of saturation (moisture condition), soil density, effective stress, applied stress intensity, stress history and the nature of the material itself (e.g. particle size, shape, distribution, mineralogical constituent(s), etc.).

A soil's ability to transmit applied dynamic stresses (energy) is of particular interest to the U.S. Air Force with respect to military structural protection and survivability designs. Typical engineering analyses assume that little or no material property changes occur under dynamic loadings and in addition, analyses do not account for the effects of saturation (moisture conditions) on energy transmission soils. This is primarily due to an incomplete understanding of the behavior of soils under transient loadings and uncertainties about field boundary conditions. Results from U.S Air Force field and laboratory tests with explosive detonations in soils have shown that material property changes do in fact occur and that variations in soil stiffness (or compressibility) significantly affect both dynamic and static stress transmission. However, there are currently no theoretical, empirical or numerical methods available for predicting large amplitude compressive stress wave velocity and stress transmission in unsaturated soils (Ross et al., 1986, 1988). Considering this fact, the research outlined herein was performed as a part of the 1989 Summer Faculty Research Program (SFRP) program to specifically examine the influence of selected parameters on the behavior of statically and dynamically loaded unsaturated granular soils. The research has direct applications to groundshock prediction techniques including stress transmission to structures.

My primary research interests have been in the area of soil dynamics with particular emphasis on the behavior of soils subjected to high intensity dynamic compressive stress loadings such as those from explosive detonations. I am very interested in microstructural analysis of soils with respect to their ability to transmit (or absorb) applied dynamic energy

and static loads. I have previously conducted research for the U.S. AFOSR on blast-induced liquefaction of saturated sand which involved the development of a state-of-the-art experimental laboratory facility. In addition, I have also performed research on the behavior of unsaturated soils with emphasis on the evaluating the engineering and hydraulic flow properties of dynamically compacted moist soil specimens.

II.   RESEARCH OBJECTIVES :

The primary objective of the summer research effort was to study the effects of soil microstructure on the dynamic and static response of granular soils compacted to a constant dry density at varying degrees of saturation. Particular emphasis was directed at examining the influence of saturation (moisture conditions) on soil behavior during compaction and testing. From the test results, a theoretical model that accounts for microstructural effects could then be developed to predict the stress transmission and wave propagation velocity in unsaturated soils. Such a method has direct applications to groundshock prediction techniques including stress transmission to structures. The research is important to the U.S. Air Force since there are currently no theoretical, empirical or numerical methods available for predicting large amplitude compressive stress wave velocity and stress transmission in unsaturated soils (Ross et al., 1986, 1988).

III.   BACKGROUND:

A number of research studies have shown that the compaction of moist sands has a measurable influence on a number of both static and dynamic soil properties which can be attributed to variations in soil microstructure and compressibility. Mulillis et al. (1977) investigated 11 different packing methods and showed that the method of compaction, particularly the initial moisture conditions, strongly influences the cyclic liquefaction behavior of fine sands. Wu et al. (1984) performed resonant column tests on fine sands and observed that capillary pressures in specimens compacted moist at saturations in the range of from 5 to 20% produced a significant increase in the dynamic shearing modulus. Using mercury intrusion porosimetry techniques, Juang and Holtz (1986) were able to characterize the effects of compaction and compaction moisture content by a Pore Size Distribution index. Nimmo and Akstin (1988) found that the permeability of sandy soils was highly dependent upon the compaction method, especially moist compaction. They

attributed the variation in permeability to preferred grain orientations during compaction as a result of moisture being present as opposed to dry packing which should give a random orientation. Recent research by Ross et al. (1986, 1988) and Ross (1989) has demonstrated that compacting moist sands at different degrees of saturation prior to dynamic testing can increase the stress transmission ratio by as much as a factor of two and can also lead to increased wave propagation velocities. Additional research by Charlie and Pierce (1988) to study the influences of capillary stresses on the behavior of the same soils tested by Ross further confirmed and extended those findings. Although these researchers have noted the influence of moisture and compaction on the behavior and properties of cohesionless soils, a clear and concise explanation of the phenomena is not currently available.

Soil behavior is primarily controlled by the fundamental principal of effective stress, σ', which is defined as the difference between the total stress, σ, and the porewater pressure, u. Strictly speaking, the concept only applies to a dry or saturated soil as originally developed. However, most natural and compacted soils exist at intermediate levels of saturation (between 0% and 100%) where capillary pressures exist at air-water interfaces in the soil pores. Therefore, these pressures enter into the effective stress relationship. Charlie and Pierce (1988) developed retention curves for Eglin and Ottawa 20-30 sands and demonstrated that the influence of capillary pressures on effective stresses is negligible, being on the order of about 7 kPa (1 psi) or less. However the influence of these capillary pressures in producing soil microstructure during compaction significantly affects soil behavior both statically and dynamically.

Attempts have been made by several researchers to extend effective stress relationships to unsaturated soils. Bishop and Blight (1963) presented the following expression for the effective stress in a unsaturated soil:

$$\sigma' = (\sigma - u_a) + X(u_a - u_w) \tag{1}$$

where, σ' is the effective stress, σ is the total stress, u_a is the pore air pressure, u_w is the pore water pressure, and X is an empirical parameter related to soil suction. For a dry soil, X=1 and for a saturated soil, X=0. Equation 1 accounts for the influence of soil suction on effective stress through the second term, however compressibility effects are not directly accounted for.

Based on the work of Bishop and Blight (1963), Fredlund (1985) proposed a constitutive relationship for the incremental volumetric strain, $d\varepsilon_v$, in a unsaturated soil:

$$d\varepsilon_v = C_t \, d(\sigma - u_a) + C_w \, d(u_a - u_w) \qquad (2)$$

where, C_t is the soil skeleton compressibility with respect to a change in $(\sigma - u_a)$, and C_w is the soil structure compressibility with respect to a change in capillary pressure, $(u_a - u_w)$.

From elastic theory, it can be shown that the confined, uniaxial stress wave propagation velocity (wave speed), V_c, is given by:

$$V_c = \sqrt{\frac{M}{\rho}} \qquad (3)$$

where, M is the constrained modulus and ρ is the density. For a constant density, Equation 3 indicates that the wave propagation velocity (and correspondingly the stress transmission) is a function of modulus which in turn is a function of stress level and compressibility.

In a unsaturated soil, the compressibility represents the combined effects of the soil skeleton, the pore water and pore air compressibilities. Unsaturated porous media will have continuously varying fluid compressibilities due to the multiphase (e.g. air, water, solid) nature of the bulk material. Since volumetric strain (Equation 2), wave speed and stress transmission are all dependent on compressibility, relationships should exist among these parameters. In addition, soil microstructure is a common element influencing each of these parameters, and the microstructural characterization of unsaturated soils will be a key element in model development.

IV. EXPERIMENTAL INVESTIGATION:

Tests were conducted to evaluate the influence of microstructure, compaction moisture content, compaction energy, degree of saturation and boundary conditions on the stress transmission characteristics and compressibility of four cohesionless sands. The four sands tested were Eglin Base sand (medium to fine, well graded, subangular), Ottawa 20-30 sand (medium, uniform, rounded), (Tyndall) Base sand (fine, uniform, subangular) and Ottawa F-58 sand (fine, uniform, subrounded). The Eglin and Base sands were

obtained from Eglin and Tyndall Air Force Bases, respectively and the Ottawa sands were commercially available. Representative soil samples were obtained from the bulk quantities of each material using standard sample splitting procedures. Specimens were tested in uniaxial, confined compression both dynamically and statically. Dynamic tests were performed using a Split-Hopkinson Pressure Bar (SHPB) device to determine stress transmission and wave speed characteristics. Static tests were performed using an MTS loading system to evaluate soil skeleton compressibility. Figures 1 and 2 show generalized schematics of a typical specimen set up for testing.

Specimens of each sand were dynamically compacted to a constant dry density at varying degrees of saturation (different initial moisture contents) in a stainless steel tube instrumented with resistance wire strain gages prior to testing. The stainless steel tube was 7.62 cm (6 inches) long, 5.41 cm (2.13) inches in diameter, with a 0.159 cm (0.0625 inch thick wall). A Standard Proctor hammer was used to consistently apply a controlled amount of compactive effort to soil specimens. The strain gages were used in an attempt to obtain information on the development of lateral stresses in the soil during testing.

All test specimens were formed using four individually compacted layers of equal weight such that a final length of 10.16 cm (4.0 inches) would be obtained prior to testing using. Four individual 2.54 cm (1 inch) lifts were used. Saturations were varied from near 0% to 80% for each soil. At saturations near 0%, each layer of dry soil was poured directly into the tube and compacted. In preparing moist specimens, the required amount of water for a given degree of saturation (when compacted) was added to the originally dry soil, thoroughly mixed in and then allowed to equilibrate for about 30 minutes before compacting.

Since the specimens ranged in degree of saturation from about 0% (dry) to about 80% , the tests were conducted on unsaturated specimens. With respect to this study, the term "unsaturated" implies that both continuous air and water phases exist in the soil (eg. there are no isolated air or water pockets in the grain matrix). For most soils, this generally occurs at saturations less than about 85% (Corey, 1977).

V.   EXPERIMENTAL RESULTS:

Two series of tests were performed on each sand: a static uniaxial compression test and a dynamic uniaxial compression test. Stress strain curves were developed from the static data and were used to obtain information on variations in specimen stiffness with

saturation and compactive energy. Variations in stress wave propagation velocity and transmission ratio were obtained from the dynamic tests. The results obtained during this study are compared with similar tests previously conducted by Ross (1989).

Figures 3 and 4 show results from the MTS static uniaxial compression tests for variations in stiffness and compactive energy (for a constant dry density) with saturation. The compaction energy used to prepare each specimen and stiffness modulus obtained at the maximum applied static load have been normalized to their respective values at 0% saturation. The Ottawa 20-30 and Base (Tyndall) sands show a stronger dependency on saturation with respect to compactive energy required to achieve a constant dry density than do the other sands tested (Figure 3). Ross's (1989) data for the Eglin and Ottawa 20-30 sands show a greater dependency of stiffness on saturation than the results of this study (Figure 4) which may be due to differences in boundary conditions as discussed below. The Ottawa F-58 and Base (Tyndall) sands also indicate some dependency on saturation.

Figures 5 through 12 show results from the SHPB dynamic uniaxial compression tests as a function of saturation. Figures 5, 7, 9 and 11 show the variation in transmission ratio with saturation and Figures 6, 8, 10 and 12 show the variation in wave speed with saturation for the four soils tested. The transmission ratio and the wave speed results have been normalized to their respective values at 0% saturation. The results of this study show less dependency upon saturation and also lower magnitudes of wave speed and transmission ratio for Eglin and Ottawa 20-30 sands (Figures 5 through 8) as compared with data reported by Ross (1989). It was originally believed that the dependency on saturation from previous studies could be explained by increases in effective stresses due to capillary forces. However, Charlie and Pierce (1988) developed capillary retention curves for for Eglin and Ottawa 20-30 sands which showed that the influence of capillary pressures on effective stresses in these two soils is negligible (on the order of about 7 kPa (1 psi) or less) in comparison with the applied static or dynamic loads. Therefore, other factors must be considered to explain the variations in test results.

The primary difference between the two studies lies in the test boundary conditions. Ross (1989) used a relatively thick-walled specimen container (2.54 cm (1.0 inches)), while in this study, an instrumented thin-walled (0.159 cm (0.0625 inches)) tube was used during compaction and testing. The thin-walled tube was used so that information on lateral stress development could be obtained from externally mounted strain gages. Therefore, the boundary conditions in this study deviated more from a uniaxial strain condition than did the thick-walled tube. The response of the strain gages on the specimen

container during testing showed similar general trends when compared with the measured axial stress-strain behavior. However, due to uncertainties in strain gage calibration when applied to the tube containing soil, the interpretation of these results is not clear and therefore, the results have not been included.

Figures 9 through 12 show results for the Ottawa F-58 and Base (Tyndall) sands which had not been tested prior to this study, therefore no comparisons could be made. However, here appears to be some dependence on saturation as shown in these figures, but the results are based on limited data and further testing of these two soils is required.

VI.   SUMMARY AND CONCLUSIONS:

Laboratory tests were conducted to evaluate the influence of microstructure, compaction moisture content, compaction energy, degree of saturation and boundary conditions on the stress transmission characteristics and compressibility of four cohesionless sands. The four soils tested were Eglin sand, Ottawa 20-30, Base (Tyndall) sand and Ottawa F-58 sand. Specimens of each soil were dynamically compacted using a Standard Proctor hammer to a constant dry density at different initial water contents to achieve varying degrees of saturation. Both dynamic and static uniaxial compression tests were conducted on the compacted specimens. The dynamic tests were performed using a Split-Hopkinson Pressure Bar (SHPB) device to determine stress transmission and stress wave propagation characteristics. The static tests were performed using an MTS loading system to evaluate soil skeleton compressibilities.

A preliminary analysis of the experimental data indicates that both the dynamic and static behavior of the sands tested is strongly dependent on soil microstructure. The degree of saturation (moisture content) during compaction is an important factor affecting the development of microstructure in soils. The most prominent influences on soil behavior were observed at intermediate levels of saturation (from about 20 to 60%). In this range of saturations, the results generally indicated that stress transmission and stress wave propagation velocity increased in the soil for dynamic tests, and soil stiffness increased in the static tests. In addition, the effect of boundary conditions has been shown to be important to the stress transmission characteristics of the soils investigated. The results of this study have extended and confirmed in part the observations of previous research efforts by Charlie and Pierce (1988) and Ross (1989) for Eglin and Ottawa 20-30 sands.

Although the influence of moisture (saturation) and compaction method on the behavior and properties of cohesionless soils has been observed in this study and in previous research, a clear and concise explanation of the phenomena is not currently available. Therefore, more extensive laboratory and field studies are needed. Furthermore, the development of numerical models to account for the dynamic and static characteristics of cohesionless soils is also essential.

VII.   RECOMMENDATIONS:

The research reported herein has provided valuable insight into both the dynamic and static response of unsaturated cohesionless soils. However, the understanding of unsaturated soil behavior to applied loads is very limited at present and further studies are required. The results of such studies are very important to the U.S. Air Force with respect to military structural protection and survivability designs. Based on the results of this research effort, several recommendations can be made:

1) The degree of saturation (moisture content) during compaction is an important factor influencing the development of soil microstructure, which in turn affects the soil's response to both static and dynamic loading. Further experimental studies should be conducted to examine the limiting relationship between the degree of saturation and input energy with respect to soil stiffness and dynamic stress transmission. A detailed microstructural analysis of compacted granular soils at varying degrees of saturation should be performed. Such a study will provide important information about how microstructure develops and will be very useful in developing theoretical models that account for the behavior of compacted unsaturated soils.

2) The results of this study and those reported by Ross (1989) have demonstrated the importance of boundary conditions, indicating that compacting moist sands at different degrees of saturation prior to dynamic testing can increase the stress transmission ratio by as much as a factor of two and can also lead to increased wave propagation velocities. Therefore, boundary effects should be experimentally studied in more detail in both the field and laboratory. In addition, it is essential that such studies be coupled with numerical modeling efforts.

3) A series of fully instrumented, carefully controlled small scale field explosive tests should be conducted in close coordination with further laboratory studies. Test

parameters should include variations in saturation (moisture content), compaction methods, boundary conditions and applied energy. Field instrumentation should provide measurements of input energy, transmitted energy, and soil deformation and stress (both vertically and horizontally) as a minimum. Results will be useful in developing correlations between laboratory and field studies, providing valuable input for model development.

4) The development of horizontal stresses in shock loaded soils, particularly those that are unsaturated, is a very important area requiring further experimental analysis. The understanding of this phenomenon, including the development of these stresses and the controlling factors is quite limited at present, for both static and dynamic loading. As a part of the study reported herein, an initial attempt was made to develop a simple laboratory method for lateral stress measurements in soils. It was found that the method had some shortcomings and limitations. Therefore, further refinements and modifications are required and should also be extended to field applications.

REFERENCES

1. Bishop, A. W. and Blight, G. E. (1963) "Some Aspects of Effective Stress in Unsaturated Soils." Geotechnique, Vol. 13, No. 3, September, pp. 177-179.

2. Charlie, W. A. and Pierce, S. J. (1988) "High Intensity Stress Wave Propagation in Unsaturated Sands." Final Report for the USAF/UES Summer Faculty Research Program, AFOSR Contract Number F49620-87-0004, August.

3. Corey, A. T. (1977) <u>Mechanics of Heterogeneous Media</u>. Water Resources Publication, Ft. Collins, CO.

4. Fredlund, D. G. (1985) "Soil Mechanics Principles that Embrace Unsaturated Soils." Proceedings of the 11th International Conference on Soil Mechanics and Foundation Engineering, ISSMFE, San Francisco, pp. 465-472.

5. Juang, C. H. and Holtz, R. D. (1986) "Fabric, Pore Size Distribution, and Permeability of Sandy Soils." Journal of the Geotechnical Engineering Division, ASCE, Vol. 112, No GT9, September, pp. 855-868.

6. Mulillis, J. P., Seed, H. B., Chan, C. K., Mitchell, J. K. and Arulanandan, K. (1977) "Effects of Sample Preparation on Sand Liquefaction." Journal of the Geotechnical Engineering Division, ASCE, Vol. 103, No GT2, February, pp. 91-108.

7. Nimmo, J. R. and Akstin, K. C. (1988) "Hydraulic Conductivity of a Sandy Soil at Low Water Content After Compaction by Various Methods." Journal of the Soil Science Society of America, Division S-1-Soil Physics, Vol. 52, No. 2, March/April, pp. 303-310.

8. Ross, C. A. (1989) "Split-Hopkinson Pressure Bar Tests." Final Report, ESL-TR-88-2, HQ AFESC/RDCM, Air Force Engineering and Services Center, Tyndall AFB, FL.

9. Ross, C. A., Nash, P. T. and Friesenhahn, C. J. (1986) "Pressure Waves in Soils Using a Split-Hopkinson Pressure Bar." ESL-TR-86-29, USAF Engineering and Services Center, Tyndall AFB, FL, July.

10. Ross, C. A., Thompson, P. Y. and Charlie, W. A. (1988) "Moisture Effects on Wave Propagation in Soils." Abstr. of the 7th ASCE/EMD Specialty Conf., Virginia Polytechnic Inst. and State Univ., Blacksburg, VA, May.

11. Wu, S., Gray, D. H. and Richart, F. E. (1984) "Capillary Effects on Dynamic Modulus of Sands and Silts." Journal of the Geotechnical Engineering Division, ASCE, Vol. 110, No GT9, September, pp. 1188-1202.
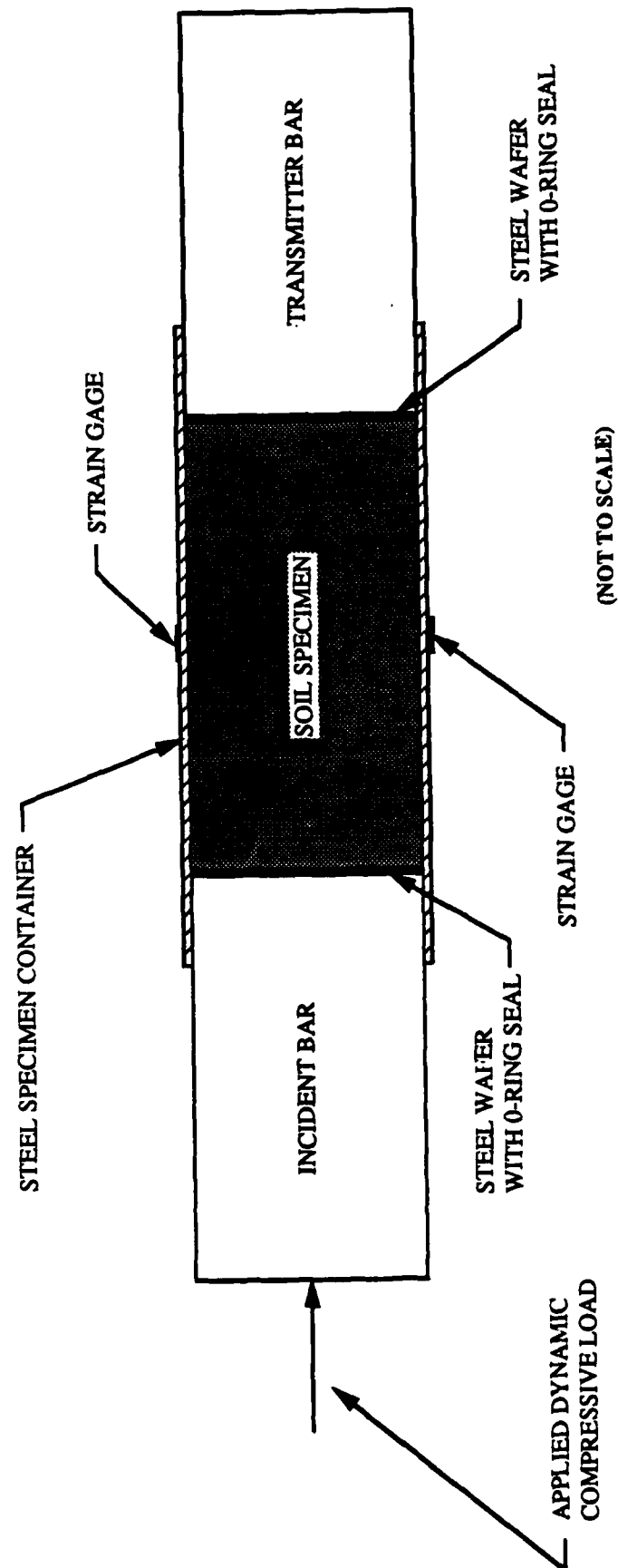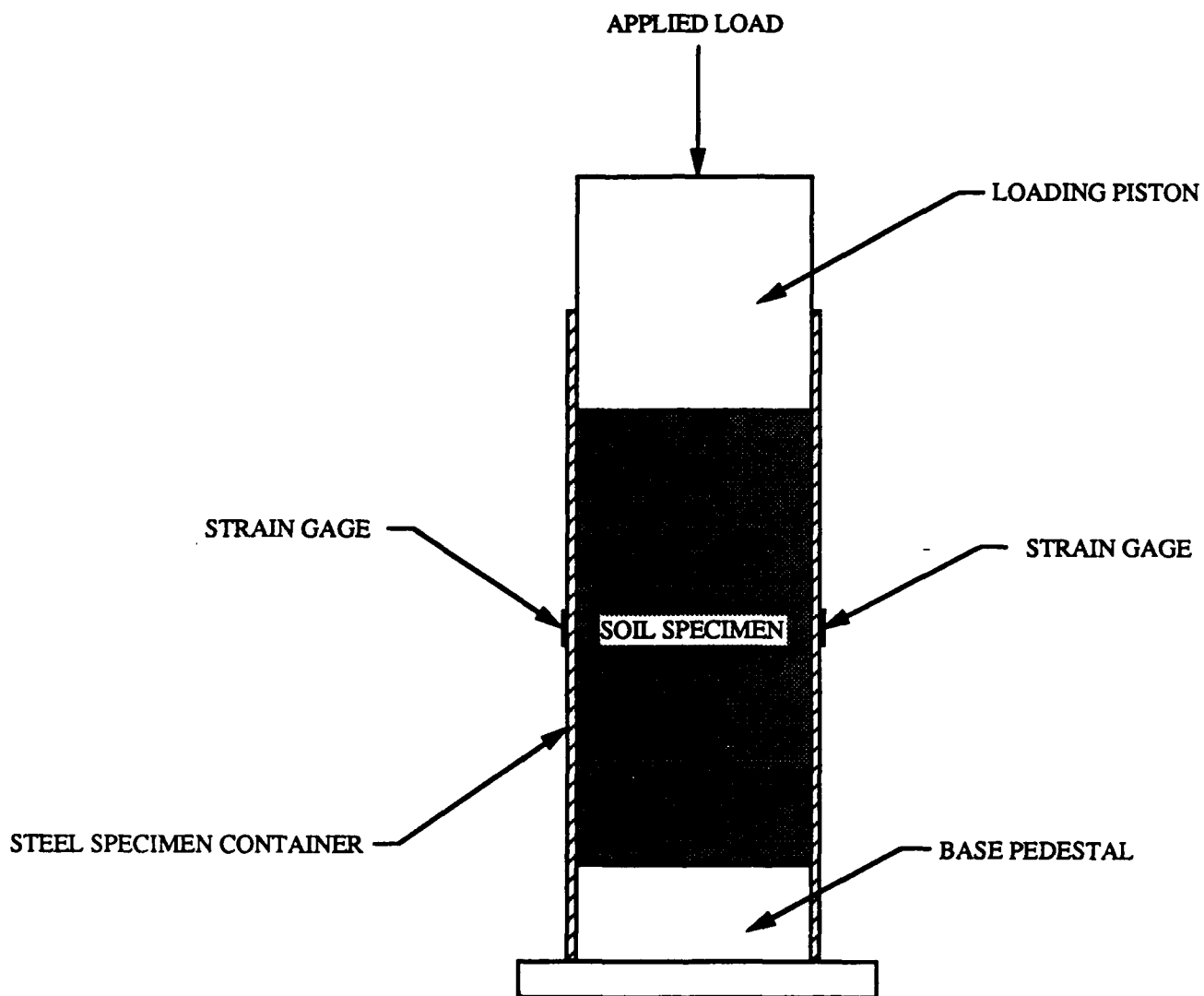
Figure 1. Schematic of Instrumented Soil Specimen Set Up in the Split-Hopkinson Pressure Bar Device.

APPLIED LOAD

LOADING PISTON

STRAIN GAGE

STRAIN GAGE

SOIL SPECIMEN

STEEL SPECIMEN CONTAINER

BASE PEDESTAL

(NOT TO SCALE)

Figure 2. Schematic of Instrumented Soil Specimen Set Up in the MTS Uniaxial Loader.
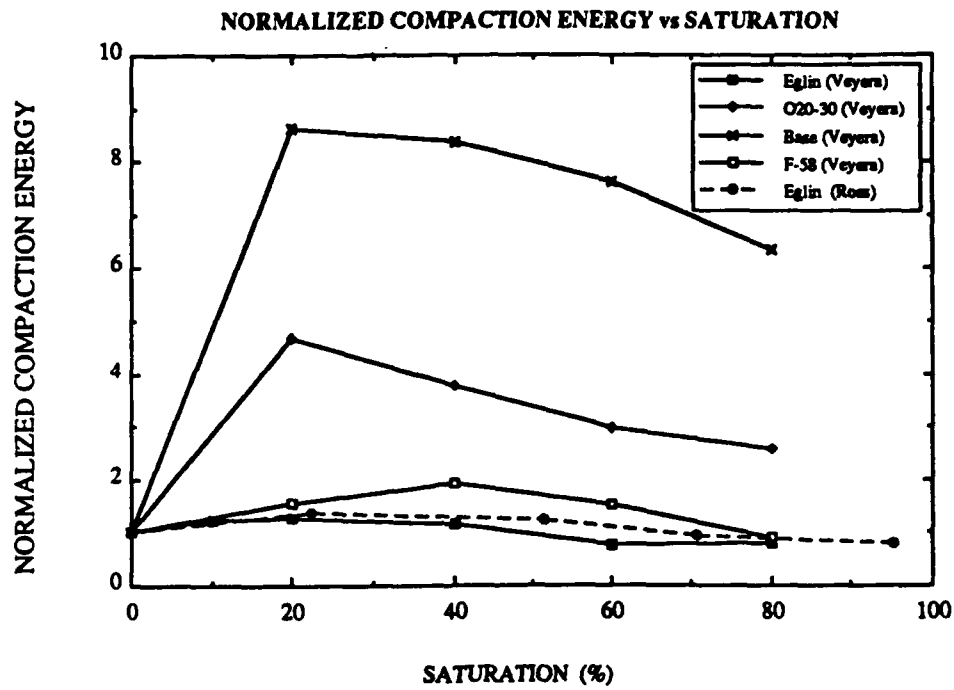
NORMALIZED COMPACTION ENERGY vs SATURATION

Figure 3. Normalized Compaction Energy as a Function of Saturation for Constant Dry Density.

NORMALIZED STIFFNESS MODULUS vs SATURATION
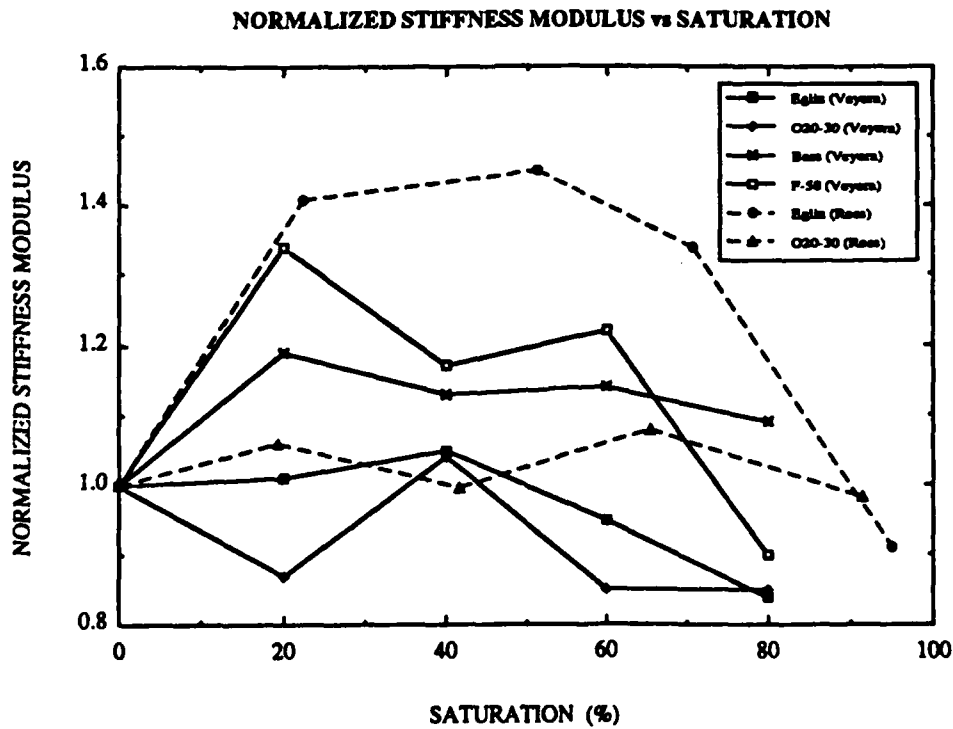
Figure 4. Normalized Stiffness Modulus as a Function of Saturation for Constant Dry Density.
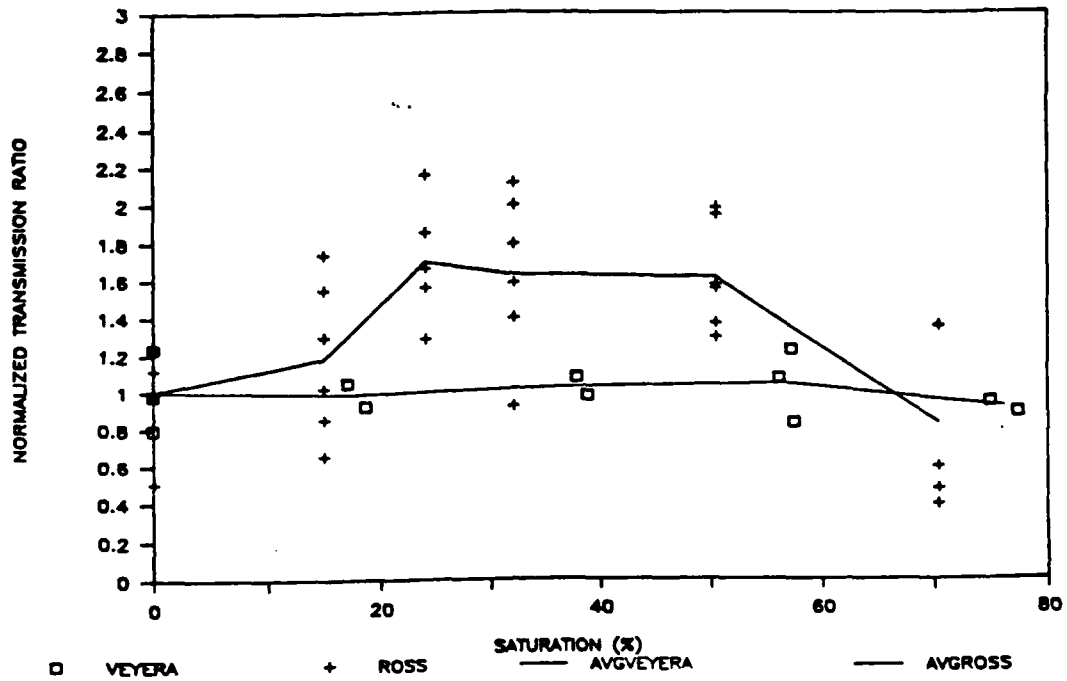
EGLIN SAND
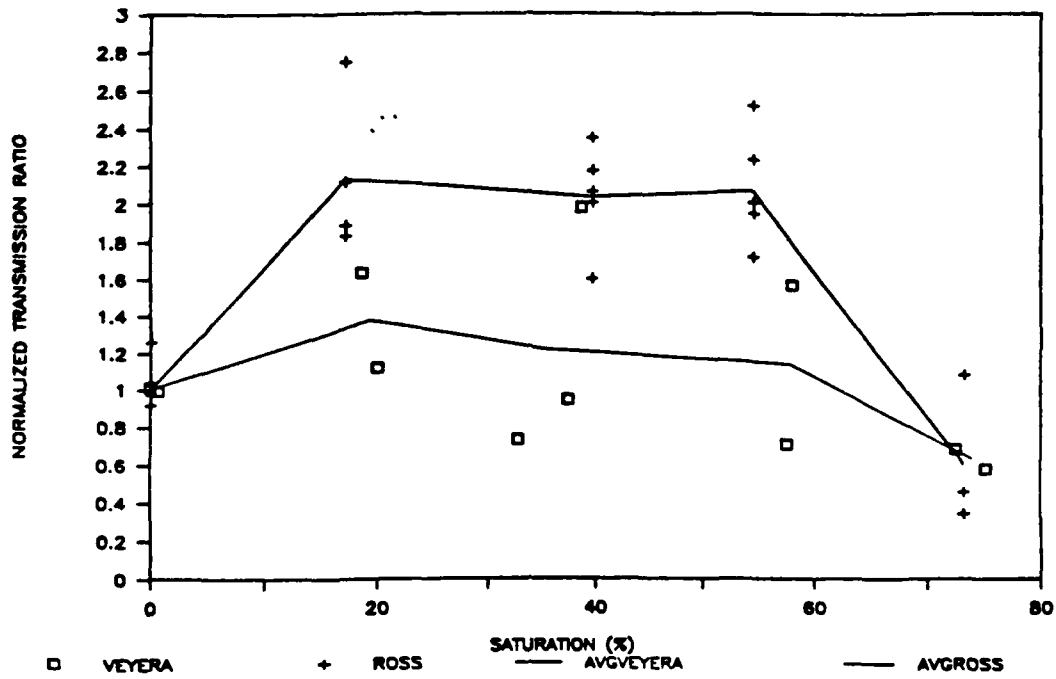
Figure 5.   Normalized Transmission Ratio as a Function of Degree of Saturation for Eglin Base Sand.

EGLIN SAND
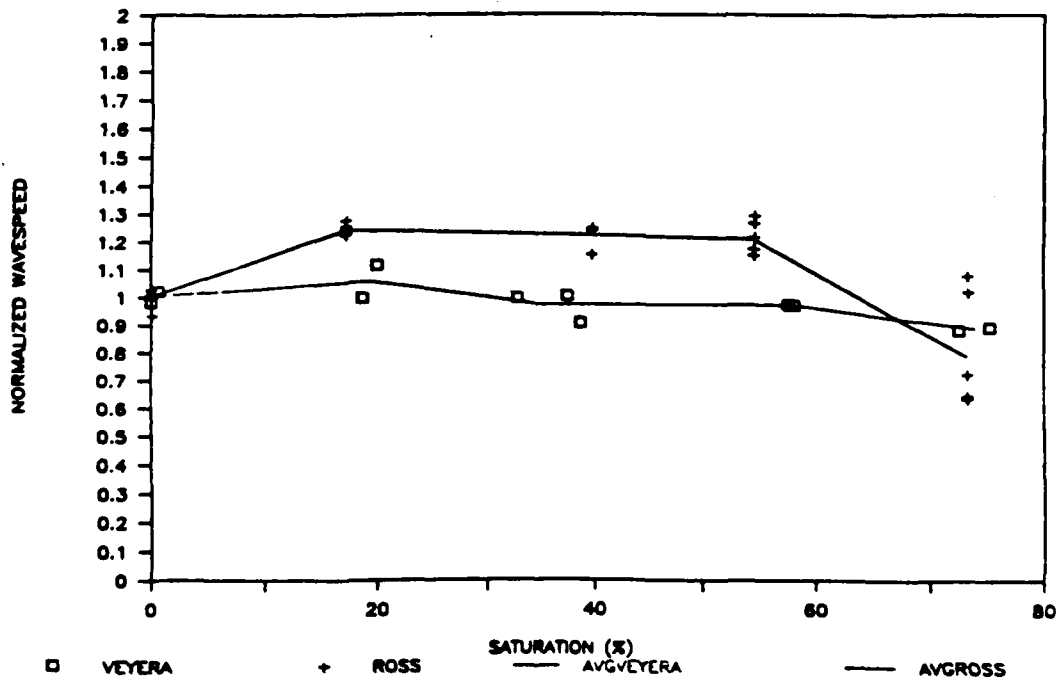
Figure 6.   Normalized Wavespeed as a Function of Degree of Saturation for Eglin Base Sand.

OTTAWA 20—30 SAND

Figure 7. Normalized Transmission Ratio as a Function of Degree of Saturation for Ottawa 20-30 Sand.
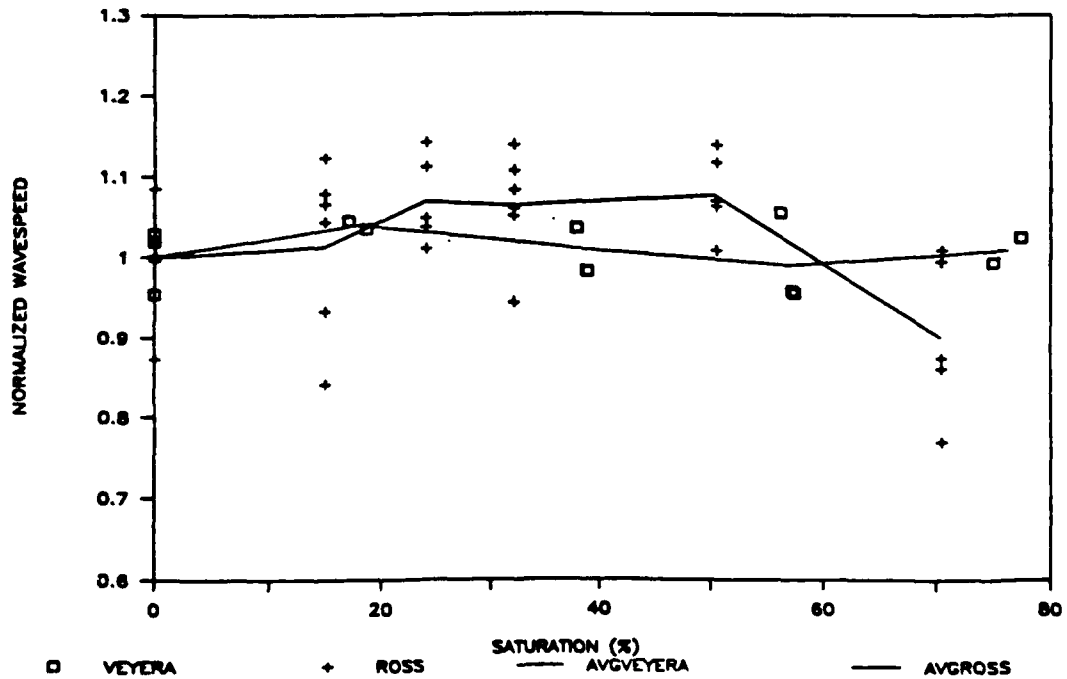
OTTAWA 20—30 SAND

Figure 8. Normalized Wavespeed as a Function of Degree of Saturation for Ottawa 20-30 Sand.
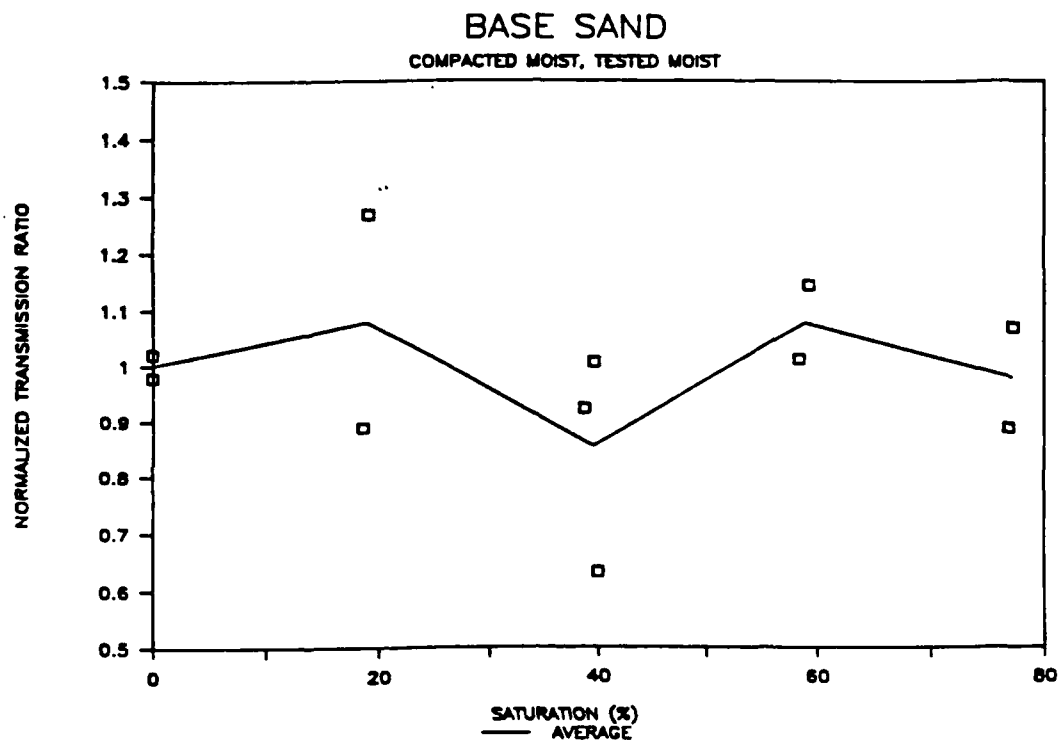
BASE SAND
COMPACTED MOIST, TESTED MOIST

Figure 9.   Normalized Transmission Ratio as a Function of Degree of Saturation for (Tyndall) Base Sand.

BASE SAND
COMPACTED MOIST, TESTED MOIST
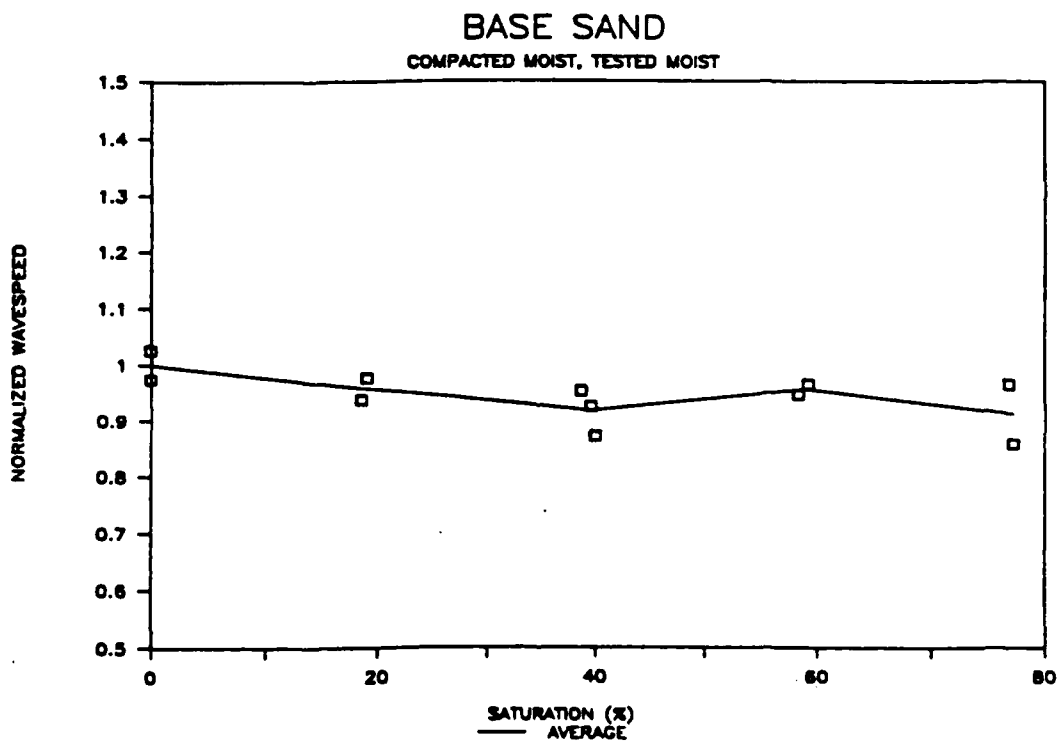
Figure 10.   Normalized Wavespeed as a Function of Degree of Saturation for (Tyndall) Base Sand.

45-19

F-58 SAND
COMPACTED MOIST, TESTED MOIST
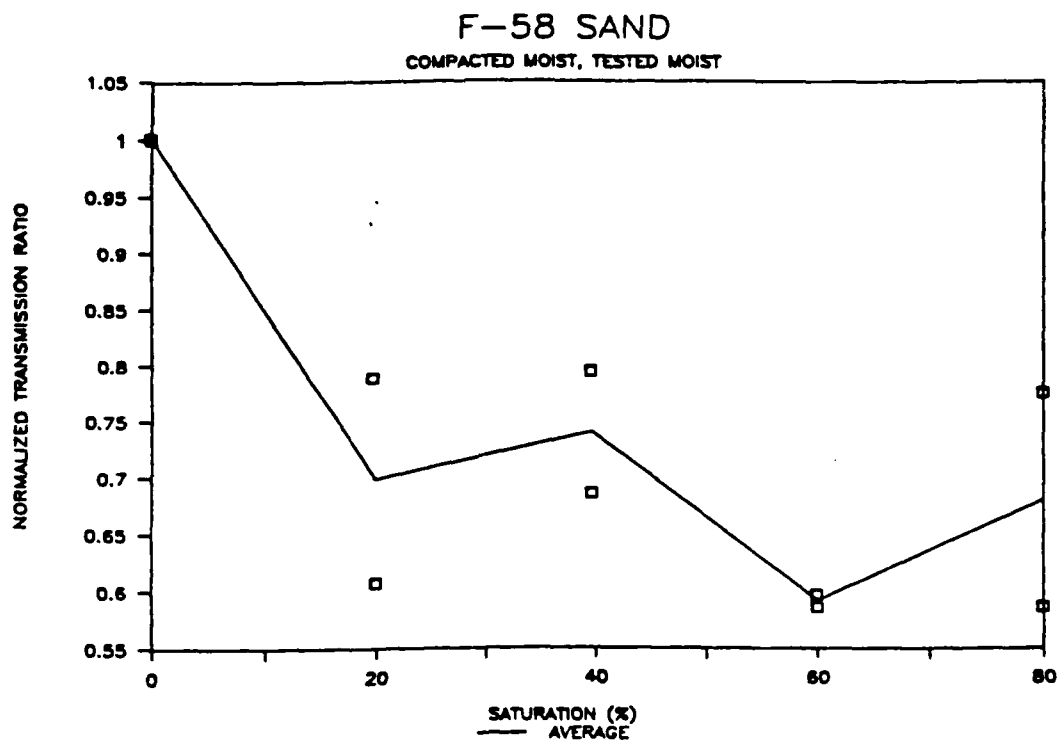
Figure 11.   Normalized Transmission Ratio as a Function of Degree of Saturation for Ottawa F-58 Sand.

F-58 SAND
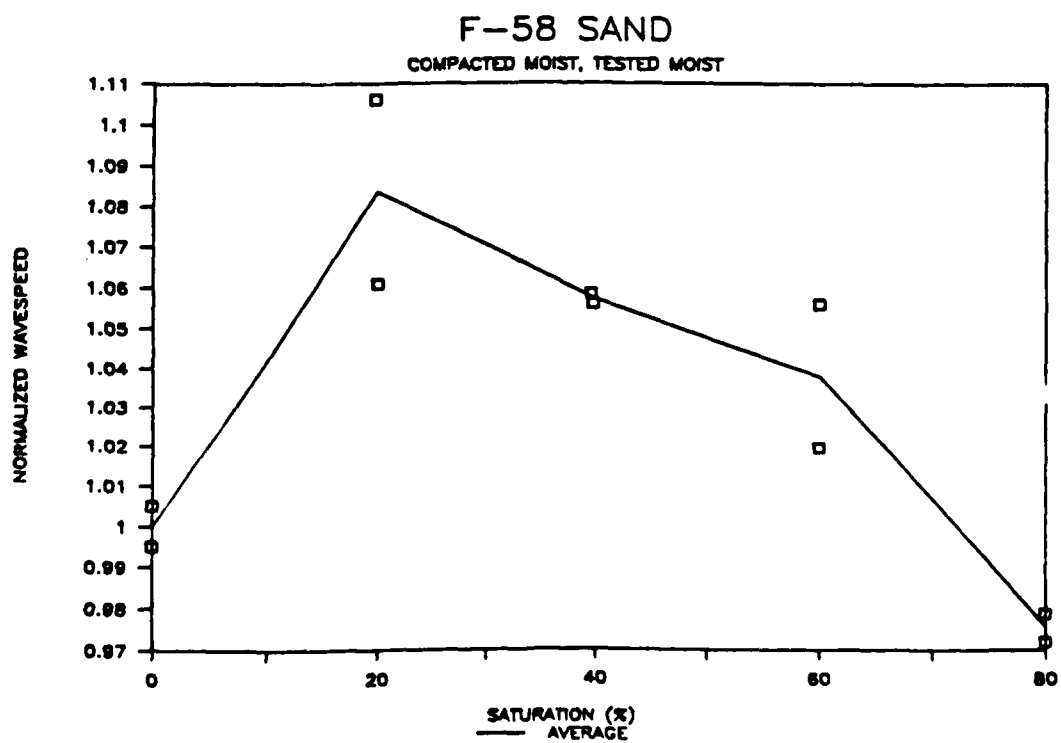## COMPACTED MOIST, TESTED MOIST

Figure 12.   Normalized Wavespeed as a Function of Degree of Saturation for Ottawa F-58 Sand.